Spectroscopy of Rocks and Minerals, and Principles of Spectroscopy

by
Roger N. Clark

U.S. Geological Survey, MS 964
Box 25046 Federal Center
Denver, CO 80225-0046

(303) 236-1332
(303) 236-1371 FAX

http://speclab.cr.usgs.gov

rclark@speclab.cr.usgs.gov

Derived from Chapter 1 in:
Manual of Remote Sensing

John Wiley and Sons, Inc
A. Rencz, Editor
New York
1999

This Web Page last revised June 25, 1999

Contents

1. Introduction

1.1 About This Chapter.

1.2 Absorption and Scattering.

1.3 Spectroscopy Terms.

1.4 Imaging Spectroscopy.

1.5 Atmospheric Transmittance: Windows for Remote Sensing.

2. THE REFLECTION AND ABSORPTION PROCESSES

2.1 Reflection and Absorption..

2.2 Emittance.

2.3 Summary.

3. CAUSES OF ABSORPTION

3.1 Electronic Processes.

3.1.1 Crystal Field Effects.

3.1.2 Charge Transfer Absorptions..

3.1.3 Conduction Bands..

3.1.4 Color Centers..

3.2 Vibrational Processes.

3.2.1 Water and Hydroxyl.

3.2.2 Carbonates.

3.2.3 Other Minerals.

4. SPECTRA OF MISCELLANEOUS MINERALS AND MATERIALS

4.1 Organics.

4.2 Ices.

4.3 Vegetation.

5. THE SENSITIVITY OF ABSORPTION BANDS TO CRYSTAL STRUCTURE AND CHEMISTRY

5.1 Example: Pyroxenes.

5.2 OH Examples.

5.3 Al in Muscovite

5.4 Discussion.

6. THE SCATTERING PROCESS.

6.1 Mixtures.

6.2 Grain Size Effects.

6.3 The Continuum and Band Depth.

6.4 Continuum-Removed Spectral Feature Comparison.

6.5 Other Spectral Variability and Rules.

6.5.1 Viewing Geometry..

6.5.2 Ratioing Spectra.

6.5.3 Iron Oxide, Hydroxide, Sulfate Complexity..

7. QUANTITATIVE UNDERSTANDING: RADIATIVE TRANSFER THEORY.

7.1 "Hapke Theory."

8. SPECTRAL LIBRARIES.

9. CONCLUSIONS AND DISCUSSION.

Acknowledgements

10. References.

---

1. Introduction

1.1 About This Chapter. Spectroscopy is the study of light as a function of wavelength that has been emitted, reflected or scattered from a solid, liquid, or gas. In this chapter I will primarily discuss the spectroscopy of minerals, but the principles apply to any material. No single chapter can cover this topic adequately, and one could argue, not even a single book. Thus, in some ways, this chapter may fall short of expectations, depending on the reader. In this chapter, I have tried to provide an overview of what is already known, some of which may be covered better in other reviews. I have also tried to present some of the practical lessons of spectroscopy, some of which have been in use by spectroscopists as common knowledge, but have not necessarily been previously published in detail. See Adams (1975), Hunt (1977), Farmer (1974), Hunt (1982); Clark and Roush (1984), Clark *et al.* (1990a), Gaffey *et al*. (1993), Salisbury (1993), and references in those papers for more details.

Back to Contents

1.2 Absorption and Scattering. As photons enter a mineral, some are reflected from grain surfaces, some pass through the grain, and some are absorbed. Those photons that are reflected from grain surfaces or refracted through a particle are said to be scattered. Scattered photons may encounter another grain or be scattered away from the surface so they may be detected and measured. Photons may also originate from a surface, a process called emission. All natural surfaces emit photons when they are above absolute zero. Emitted photons are subject to the same physical laws of reflection, refraction, and absorption to which incident photons are bound.

Photons are absorbed in minerals by several processes. The variety of absorption processes and their wavelength dependence allows us to derive information about the chemistry of a mineral from its reflected or emitted light. The human eye is a crude reflectance spectrometer: we can look at a surface and see color. Our eyes and brain are processing the wavelength-dependent scattering of visible-light photons to reveal something about what we are observing, like the red color of hematite or the green color of olivine. A modern spectrometer, however, can measure finer details over a broader wavelength range and with greater precision. Thus, a spectrometer can measure absorptions due to more processes than can be seen with the eye.

Back to Contents

1.3 Spectroscopy Terms. There are 4 general parameters that describe the capability of a spectrometer: 1) spectral range, 2) spectral bandwidth, 3) spectral sampling,

and 4) signal-to-noise ratio (S/N). Spectral range is important to cover enough diagnostic spectral absorptions to solve a desired problem. There are general spectral ranges that are in common use, each to first order controlled by detector technology: a) ultraviolet (UV): 0.001 to 0.4 µm, b) visible: 0.4 to 0.7 µm, c) near-infrared (NIR): 0.7 to 3.0 µm, d) the mid-infrared (MIR): 3.0 to 30 µm, and d) the far infrared (FIR): 30 µm to 1 mm (e.g. see The Photonics Design and Applications Handbook, 1996 and The Handbook of Chemistry and Physics, any recent year). The ~0.4 to 1.0-µm wavelength range is sometimes referred to in the remote sensing literature as the VNIR (visible-near-infrared) and the 1.0 to 2.5-µm range is sometimes referred to as the SWIR (short-wave infrared). It should be noted that these terms are not recognized standard terms in other fields except remote sensing, and because the NIR in VNIR conflicts with the accepted NIR range, the VNIR and SWIR terms probably should be avoided. The mid-infrared covers thermally emitted energy, which for the Earth starts at about 2.5 to 3 µm, peaking near 10 µm, decreasing beyond the peak, with a shape controlled by grey-body emission.

Spectral bandwidth is the width of an individual spectral channel in the spectrometer. The narrower the spectral bandwidth, the narrower the absorption feature the spectrometer will accurately measure, if enough adjacent spectral samples are obtained. Some systems have a few broad channels, not contiguously spaced and, thus, are not considered spectrometers (Figure 1a). Examples include the Landsat Thematic Mapper (TM) system and the MODerate Resolution Imaging Spectroradiometer (MODIS), which can't resolve narrow absorption features. Others, like the NASA JPL Airborne Visual and Infra-Red Imaging Spectrometer (AVIRIS) system have many narrow bandwidths, contiguously spaced (Figure 1b). Figure 1 shows spectra for the mineral alunite that could be obtained by some example broadband and spectrometer systems. Note the loss in subtle spectral detail in the lower resolution systems compared to the laboratory spectrum. Bandwidths and sampling greater than 25 nm rapidly lose the ability to resolve important mineral absorption features. All the spectra in Figure 1b are sampled at half Nyquist (critical sampling) except the Near Infrared Mapping Spectrometer (NIMS), which is at Nyquist sampling. Note, however, that the fine details of the absorption features are lost at the ~25 nm bandpass of NIMS. For example, the shoulder in the 2.2-µm absorption band is lost at 25-nm bandpass. The Visual and Infrared Mapping Spectrometer (VIMS) and NIMS systems measure out to 5 µm, thus can see absorption bands not obtainable by the other systems.

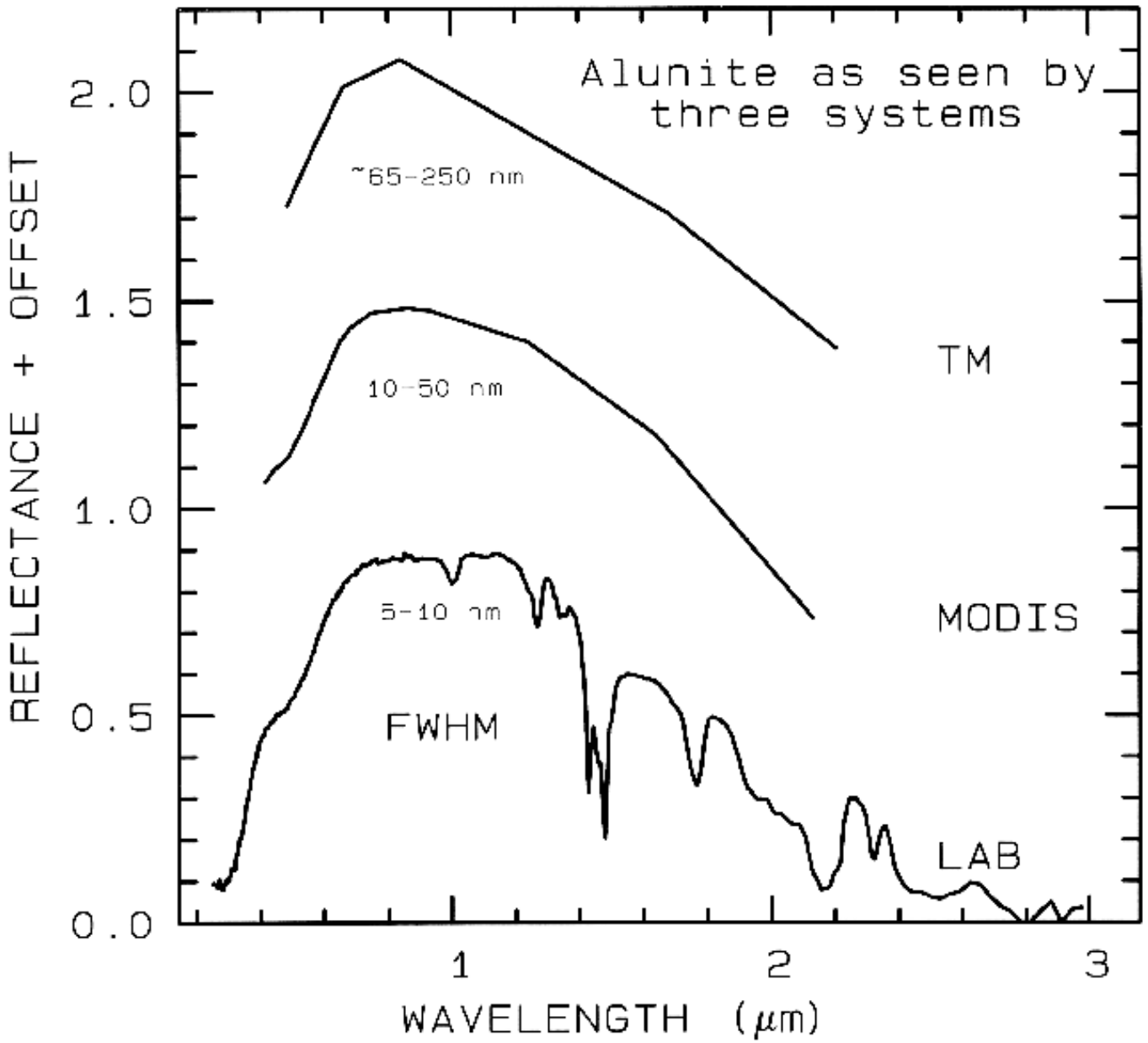

Figure 1a.

Figure 1a: 21k 100dpi gif

Figure 1a: 59k 200dpi gif

Figure 1a: 111k 300dpi gif

Figure 1a. Spectra of the mineral alunite is shown as measured in the laboratory and for broad-band remote sensing instruments (see text). The FWHM is the Full Width at Half Maximum, defined in Figure 2. The alunite is sample HS295.3B from the USGS spectral library (Clark *et al*, 1993b). Each spectrum is offset upward 0.6 units from the one below it for clarity.

Figure 1b.

Figure 1b: 41k 100dpi gif

Figure 1b: 96k 200dpi gif

Figure 1b: 214k 300dpi gif

Figure 1b. Spectra of the mineral alunite is shown as measured in the laboratory and for some imaging spectrometers (see text and Figure 1a). Note: the NIMS and VIMS systems measure to 5 µm. Each spectrum is offset upward 0.3 units from the one below it for clarity.

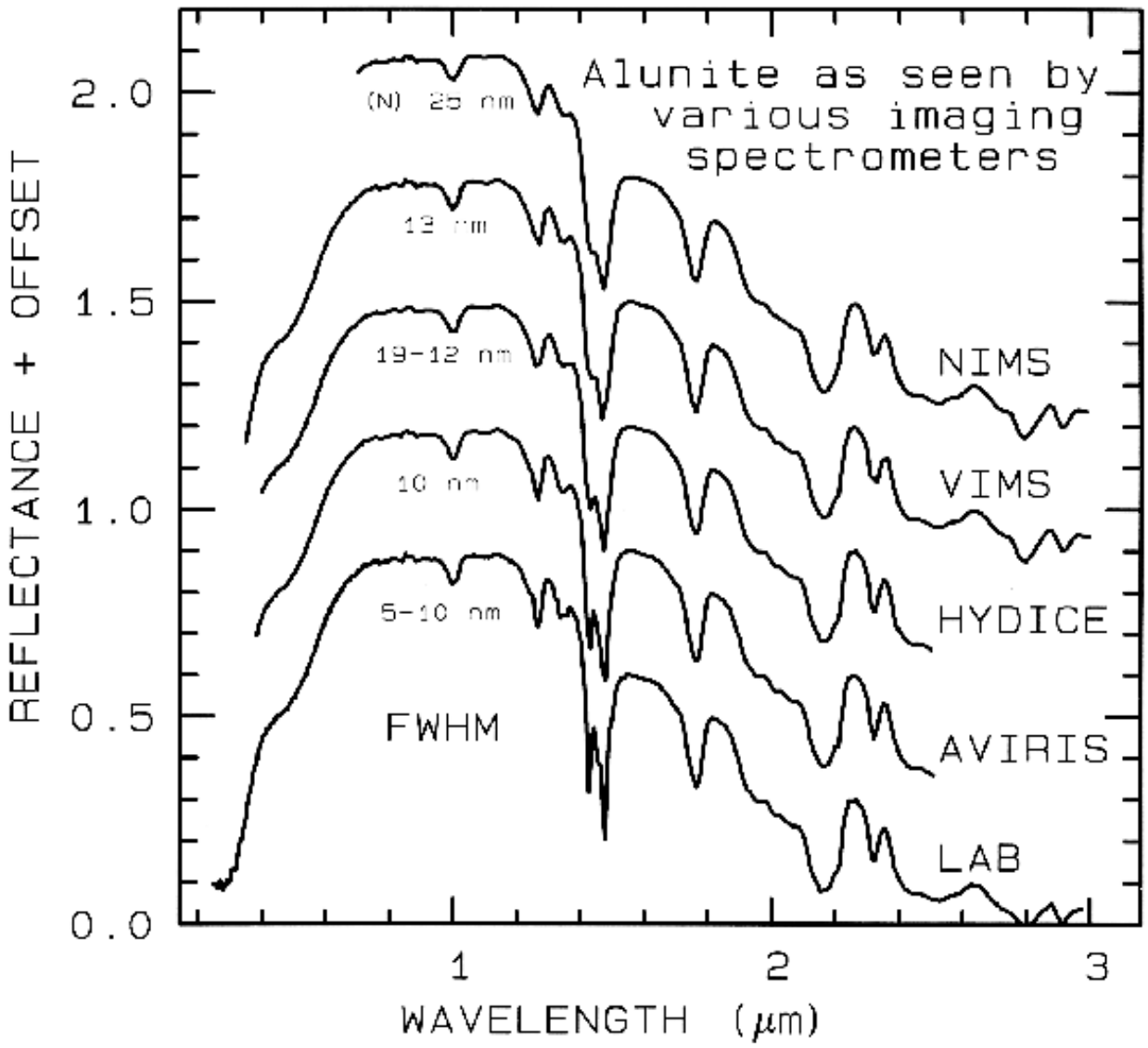

The shape of the bandpass profile is also important. Ideally each spectrometer channel rejects all light except that from within a given narrow wavelength range, but occasionally, due to optical effects too complex to discuss in detail here, light may leak in from out of the bandpass (e.g. scattering within the optical system, or inadequate blocking filters). The most common bandpass in spectrometers is a Gaussian profile. While specific spectrometer designs may have well-defined theoretical bandpass profiles, aberrations in the optical system usually smears the profile closer to a Gaussian shape. The width of the bandpass is usually defined as the width in wavelength at the 50% response level of the function, as shown in Figure 2, called the Full Width at Half Maximum (FWHM).

Figure 2.

Figure 2: 20k 100dpi gif

Figure 2: 36k 200dpi gif

Figure 2: 73k 300dpi gif

Figure 2. A Gaussian profile with a Full Width at Half Maximum (FWHM) of 10 nm is shown. This profile is typical of spectrometers such as AVIRIS which has 224 such profiles spaced at about 10 nm.

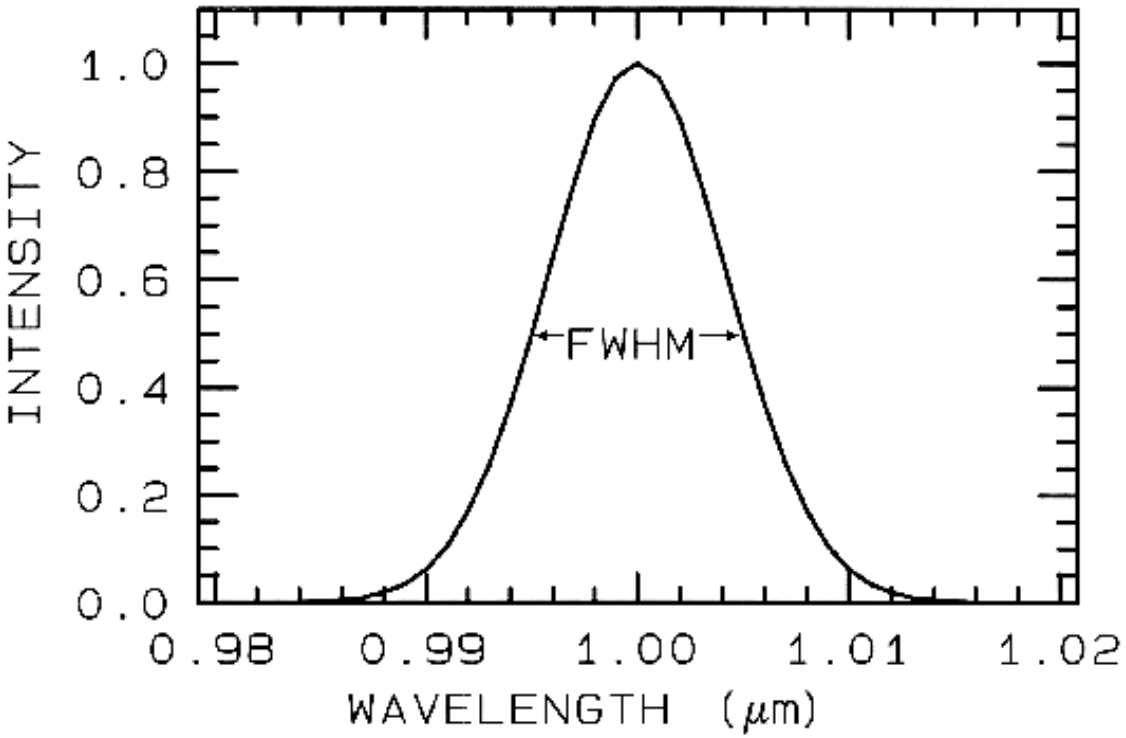

Spectral sampling is the distance in wavelength between the spectral bandpass profiles for each channel in the spectrometer as a function of wavelength. Spectral sampling is often confused with bandpass, with the two lumped together and called resolution. Information theory tells us that to resolve a two spectral features, we must have two samples. Further, in order to not introduce sampling bias, the samples must be close enough together to measure the peak and valley locations. The Nyquist theorem states that the maximum information is obtained by sampling at one-half the FWHM. Spectrometer design, however, sometimes dictates a different sampling, and many modern spectrometers in use (e.g. AVIRIS, VIMS) sample at half-Nyquist: sampling interval approximately equal to the FWHM. Note that the AVIRIS system has a bandpass ~0.01 µm (10 nm), a sampling of ~0.01 µm, and thus has a spectral resolution of ~0.02 µm (20 nm). The NIMS system in Figure 1 can sample at Nyquist (shown), half-Nyquist, and lower.

Finally, a spectrometer must measure the spectrum with enough precision to record details in the spectrum. The signal-to-noise ratio (S/N) required to solve a particular problem will depend on the strength of the spectral features under study. The S/N is dependant on the detector sensitivity, the spectral bandwidth, and intensity of the light reflected or emitted from the surface being measured. A few spectral features are quite strong and a signal to noise of only about 10 will be

adequate to identify them, while others are weak, and a S/N of several hundred (and higher) are often needed (Swayze *et al.*, 1997).

Back to Contents

1.4 Imaging Spectroscopy. Today, spectrometers are in use in the laboratory, in the field, in aircraft (looking both down at the Earth, and up into space), and on satellites. Reflectance and emittance spectroscopy of natural surfaces are sensitive to specific chemical bonds in materials, whether solid, liquid or gas. Spectroscopy has the advantage of being sensitive to both crystalline and amorphous materials, unlike some diagnostic methods, like X-ray diffraction. Spectroscopy's other main advantage is that it can be used up close (e.g. in the laboratory) to far away (e.g. to look down on the Earth, or up at other planets). Spectroscopy's historical disadvantage is that it is too sensitive to small changes in the chemistry and/or structure of a material. The variations in material composition often causes shifts in the position and shape of absorption bands in the spectrum. Thus, with the vast variety of chemistry typically encountered in the real world, spectral signatures can be quite complex and sometimes unintelligible. However, that is now changing with increased knowledge of the natural variation in spectral features and the causes of the shifts. As a result, the previous disadvantage is turning into a huge advantage, allowing us to probe ever more detail about the chemistry of our natural environment.

With the advances in computer and detector technology, the new field of imaging spectroscopy is developing (Goetz *et al.*, 1985, Vane *et al.*, 1993; Green *et a*l., 1990; Mustard and Sunshine, 1997: Chapter 5; Kruse 1997: Chapter 15 and references therein). Imaging spectroscopy is a new technique for obtaining a spectrum in each position of a large array of spatial positions so that any one spectral wavelength can be used to make a recognizable image. The image might be of a rock in the laboratory, a field study site from an aircraft, or a whole planet from a spacecraft or Earth-based telescope. By analyzing the spectral features, and thus specific chemical bonds in materials, one can map where those bonds occur, and thus map materials. Such mapping is best done, in this author's opinion, by spectral feature analysis.

Imaging spectroscopy has many names in the remote sensing community, including imaging spectrometry, hyperspectral, and ultraspectral imaging. Spectroscopy is the study of electromagnetic radiation. Spectrometry is derived from spectro-photometry, the measure of photons as a function of wavelength, a term used for years in astronomy. However, spectrometry is becoming a term used to indicate the measurement of non-light quantities, such as in mass spectrometry (e.g. Ball, 1995). Hyper means excessive, but no imaging spectrometer in use can hardly be considered hyper-spectral, after all, a couple of hundred channels pales in comparison to truly high resolution spectrometer with millions of channels. Ultraspectral is beyond hyperspectral, a lofty goal I do not believe we have reached. Terms like laboratory spectrometer, spectroscopist, reflectance spectroscopy, thermal emission spectroscopy, etc, are in common use. One rarely, if ever sees the converse: spectrometrist, reflectance spectrometry, etc. So it seems prudent to keep the terminology consistent with "imaging spectroscopy."

In this chapter I will introduce you to the factors affecting spectra of natural materials, including scattering and absorption, and the causes of absorption features. I'll also discuss doing quantitative estimates of mixtures, and show example spectra of minerals and other common materials that might be encountered in the natural world.

Back to Contents

1.5 Atmospheric Transmittance: Windows for Remote Sensing. Any effort to measure the spectral properties of a material through a planetary atmosphere, must consider where the atmosphere absorbs. For example, the Earth's atmospheric transmittance is shown in Figure 3. The drop toward the ultraviolet is due to scattering and strong ozone absorption at wavelengths short of 0.35 µm. Ozone also displays an absorption at 9.6 µm. Oxygen absorbs at 0.76 µm in a narrow feature. CO_2 absorbs at 2.01, 2.06, and a weak doublet near 1.6 µm. Water causes most of the rest of the absorption throughout the spectrum and hides additional (weaker) absorptions from other gases. The mid-IR spectrum in Figure 3b shows the effect of doubling CO_2, which in this case is small compared to the absorption due to water. While we will see that the spectral region near 1.4 and 3 µm can be diagnostic of OH-bearing minerals, we can't usually use these wavelengths when remotely measuring spectra through the Earth's atmosphere (it has been done from high elevation observatories during dry weather conditions). However, these spectral regions

can be used in the laboratory where the atmospheric path lengths are thousands of times smaller, or when measuring spectra of other planets from orbiting spacecraft.

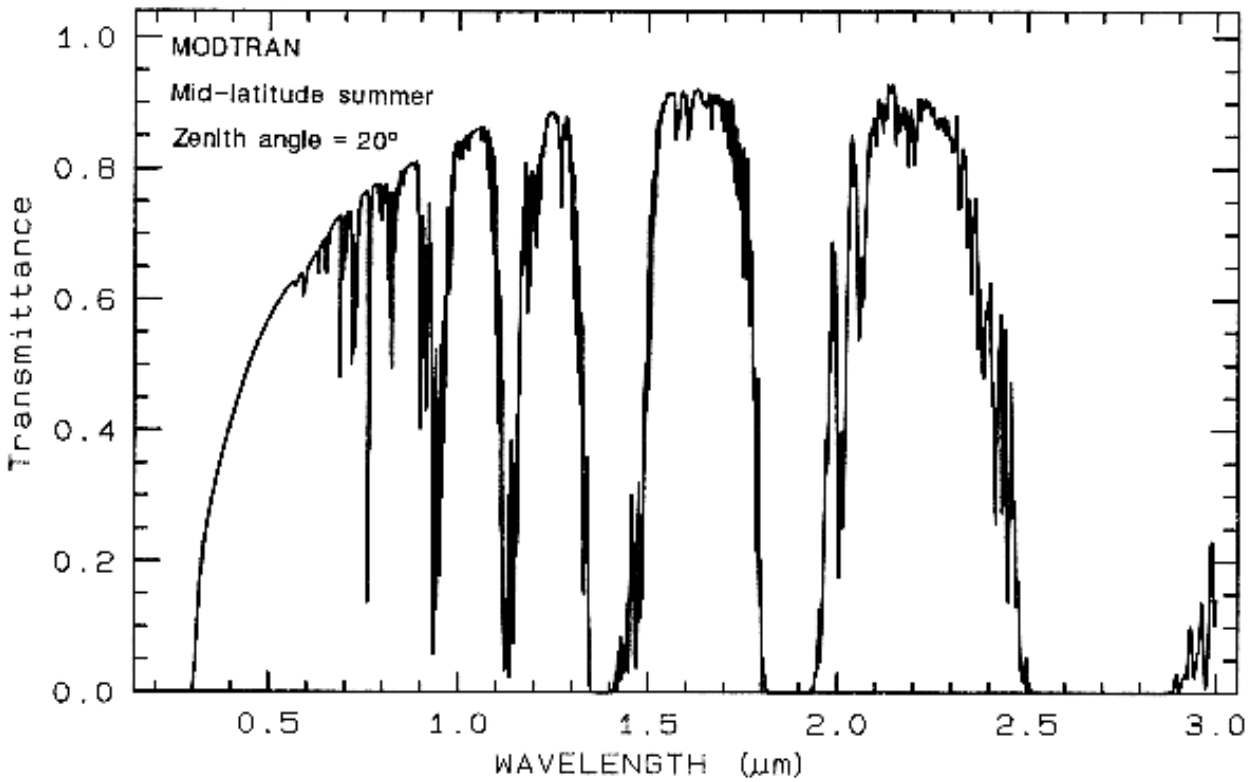

Figure 3a.

Figure 3a: 46k 100dpi gif

Figure 3a: 165k 200dpi gif

Figure 3a: 276k 300dpi gif

Figure 3a. Modtran (Berk *et al*., 1989) modeled atmospheric transmittance, visible to near-infrared. Most of the absorptions are due to water. Oxygen occurs at 0.76 µm, carbon dioxide at 2.0 and 2.06 µm. See text.

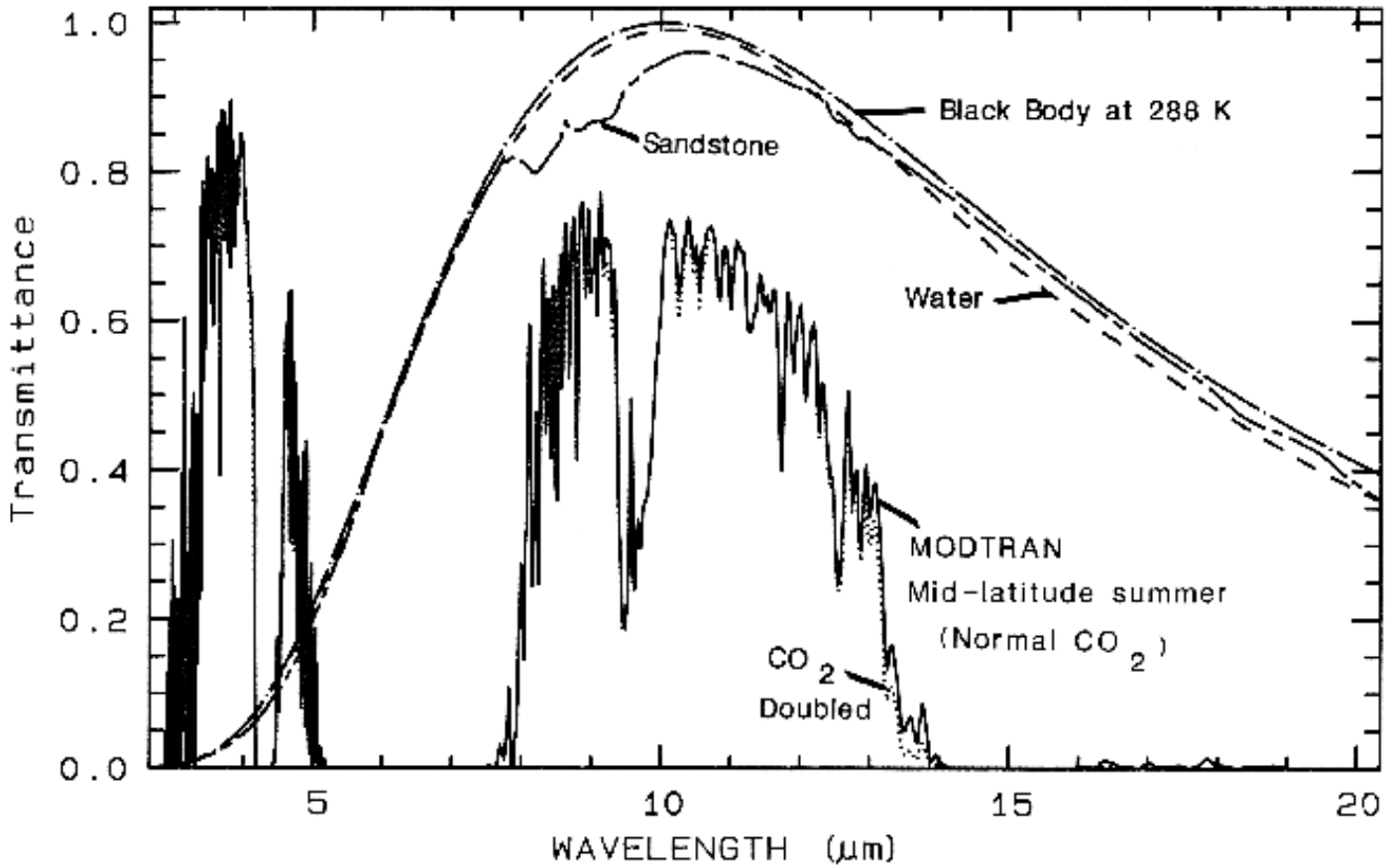

Figure 3b.

Figure 3b: 48k 100dpi gif

Figure 3b: 334k 200dpi gif

Figure 3b: 348k 300dpi gif

Figure 3b. Atmospheric transmittance, mid-infrared is compared to scaled grey-body spectra. Most of the absorption is due to water. Carbon dioxide has a strong 15-µm band, and the dotted line shows the increased absorption due to doubling CO_2. Also shown is the black-body emission at 288 K and the grey-body emission from water and a sandstone scaled to fit on this transmittance scale. The water and sandstone curves were computed from reflectance data using: 1 - reflectance times a black-body at 288 Kelvin.

Back to Contents

2. THE REFLECTION AND ABSORPTION PROCESSES

2.1 Reflection and Absorption.. When a stream of photons encounter a medium with a change in the index of refraction some are reflected and some are refracted into the medium. It is beyond this Chapter to review all the physical laws of reflection and refraction; a good optics or physics book can do that (e.g. Hecht, 1987). However, the basics of reflection should be understood. All materials have a complex index of refraction:

$m = n - jK$ (eqn 1a)

where m is the complex index of refraction, n is the real part of the index, $j = (-1)^{1/2}$, and K is the imaginary part of the index of refraction, sometimes called extinction coefficient.

When photons enter an absorbing medium, they are absorbed according to Beers Law:

$I = I_o e^{-kx}$, (eqn 1b)

where I is the observed intensity, I_o is the original light intensity, k is an absorption coefficient and x is the distance traveled through the medium.

The absorption coefficient is related to the complex index of refraction by the equation:

$k = 4K/\lambda$, (eqn 1c)

where *Lambda* is the wavelength of light. Example index of refraction, n, and extinction coefficient, K are shown in Figure 4a for quartz. The reflection of light, R, normally incident onto a plane surface is described by the Fresnel equation:

$R = [(n - 1)^2 + K^2] / [(n + 1)^2 + K^2]$. (eqn 1d)

At angles other than normal, the reflectance is a complex trigonometric function involving the polarization direction of the incident beam and is left to the reader to study in standard optics or physics text books. The reflection from quartz grains as measured on a laboratory spectrometer is shown in Figure 4b. While the spectrum is of a particulate surface, first surface reflection dominates all wavelengths, and so is similar to the spectrum of a slab of quartz.

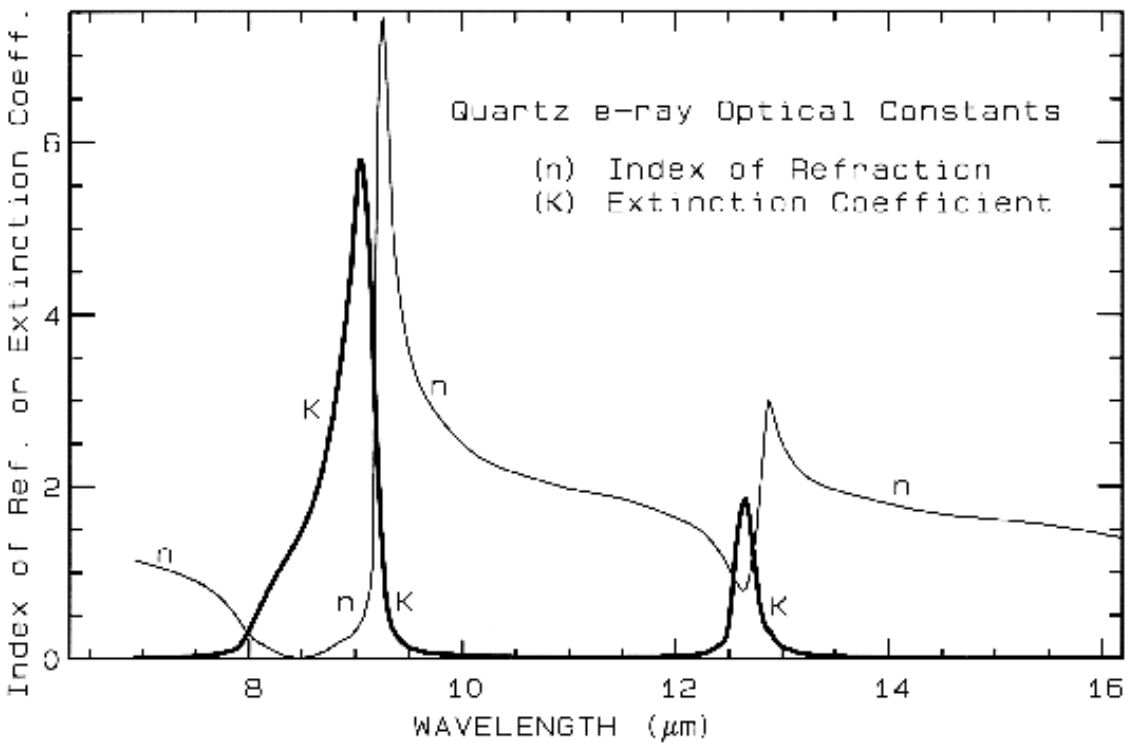

Figure 4a.

Figure 4a: 31k 100dpi gif

Figure 4a: 91k 200dpi gif

Figure 4a: 250k 300dpi gif

Figure 4a. Optical constants of quartz, SiO_2, from Spitzer and Klienman, 1960.

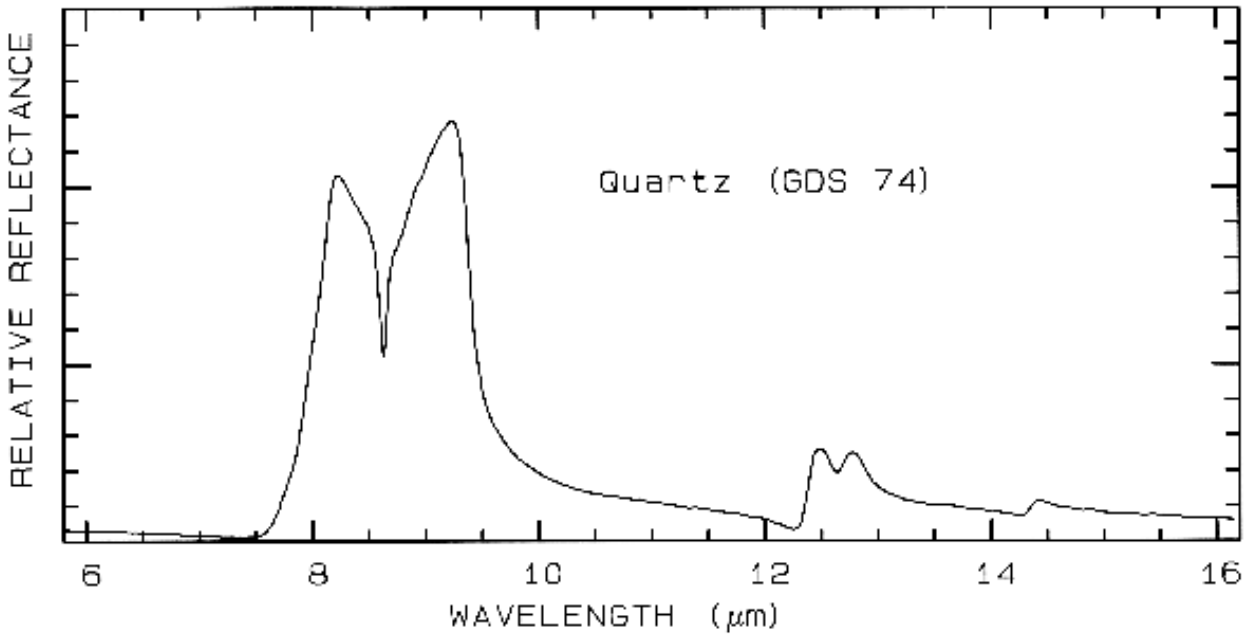

Figure 4b.

Figure 4b: 20k 100dpi gif

Figure 4b: 36k 200dpi gif

Figure 4b: 73k 300dpi gif

Figure 4b. Relative reflectance of powdered quartz.

The absorption coefficient is traditionally expressed in units of cm^{-1} and x in cm. Equations 1a-d hold for a single wavelength. At other wavelengths, the absorption coefficient and index of refraction are different, and the observed reflected intensity varies. The absorption coefficient as a function of wavelength is a fundamental parameter describing the interaction of photons with a material. So is the index of refraction, but it generally varies less than the absorption coefficient as a function of wavelength, especially at visible and near-infrared wavelengths. At fundamental absorption bands, both n and K vary strongly with wavelength, as seen in Figure 4a, though K still varies over more orders of magnitude than n.

The complex index of refraction in Figure 4a shows important properties of materials. As one moves to longer wavelengths (left to right in Figure 4a), the index of refraction decreases to a minimum just before a sharp rise (e.g. at 8.5 and 12.6 µm in Figure 4a). The minimum is often near or even below n = 1. The wavelength where n = 1 is called the Christensen frequency and usually results in a minimum in reflected light because of the small (to zero) difference in the index of refraction compared to the surrounding medium (e.g. air or vacuum). The location of the observed reflectance minimum is also controlled by the extinction coefficient according to equation 1d. Note that the Christensen frequency sometimes occurs at a wavelength shorter than the maximum in the extinction coefficient (e.g. Figure 4a). This

maximum is called the restrahlen band: the location of fundamental vibrational stretching modes in the near and mid-infrared. The combination of n and K at these wavelengths often results in high reflectance. See Hapke (1993) for more details.

Back to Contents

2.2 Emittance. At mid-infrared wavelengths, materials normally receive thermally-emitted photons. In the laboratory, one can shine enough light on a sample to ignore emitted photons and measure reflectance, but that can't be done in typical remote sensing situations. Measuring emitted energy in the laboratory is not easy because all materials emit energy unless cooled to very low temperatures. Trying to measure thermal emission at room temperatures would be like trying to take a picture with a camera with transparent walls and light bulbs turned on inside the camera! However, Kirchofs Law (e.g. Nicodemus, 1965) states:

E = 1 - R (eqn 1e)

where E is emissivity. Several studies have been conducted to show that the rule generally holds (e.g. see Salisbury, 1993 and references therein). While some discrepancies have been found, they may be due to the difficulty of measuring emittance or due to temperature gradients in the samples (e.g. Henderson *et al*., 1996 and references therein). Considering that and the fact that one rarely measures all the light reflected or emitted (usually a directional measurement is made), the law is basically true except in the most rigorous studies where absolute levels and band strengths are critical to the science. In practical terms, small changes in grain size result in spectral changes that are usually larger than the discrepancies in the law.

Back to Contents

2.3 Summary. The complex interaction of light with matter involves reflection and refraction from index of refraction boundaries, a process we call scattering, and absorption by the medium as light passes through the medium. The amount of scattering versus absorption controls the amount of photons we receive from a surface.

Back to Contents

3. CAUSES OF ABSORPTION

What causes absorption bands in the spectra of materials? There are two general processes: electronic and vibrational. Burns (1993) examines the details of electronic processes, and Farmer (1974) covers vibrational. These two books are significant works providing the fundamentals as well as practical information. A shorter introduction to the causes of absorption bands in minerals is given by Hunt (1977, 1982) and Gaffey *et al*. (1993) for the visible and near-infrared.

Back to Contents

3.1 Electronic Processes.

Isolated atoms and ions have discrete energy states. Absorption of photons of a specific wavelength causes a change from one energy state to a higher one. Emission of a photon occurs as a result of a change in an energy state to a lower one. When a photon is absorbed it is usually not emitted at the same wavelength. For example, it can cause heating of the material, resulting in grey-body emission at longer wavelengths.

In a solid, electrons may be shared between individual atoms. The energy level of shared electrons may become smeared over a range of values called "energy bands."

However, bound electrons will still have quantized energy states (e.g. see Burns, 1970, 1993).

Back to Contents

3.1.1 Crystal Field Effects. The most common electronic process revealed in the spectra of minerals is due to unfilled electron shells of transition elements (Ni, Cr, Co, Fe, etc.). Iron is the most common transition element in minerals. For all transition elements, d orbitals have identical energies in an isolated ion, but the energy levels split when the atom is located in a crystal field (e.g. see Burns, 1970, 1993). This splitting of the orbital energy states enables an electron to be moved from a lower level into a higher one by absorption of a photon having an energy matching the energy difference between the states. The energy levels are determined by the valence state of the atom (e.g. Fe^{2+}, Fe^{3+}), its coordination number, and the symmetry of the site it occupies. The levels are also influenced by the type of ligands formed, the extent of distortion of the site, and the value of the metal-ligand interatomic distance (e.g. Burns, 1993). The crystal field varies with crystal structure from mineral to mineral, thus the amount of splitting varies and the same ion (like Fe^{2+}) produces obviously different absorptions, making specific mineral identification possible from spectroscopy (Figure 5, 6, and 7).

Figure 5a.

Figure 5a: 19k 100dpi gif

Figure 5a: 70k 200dpi gif

Figure 5a: 128k 300dpi gif

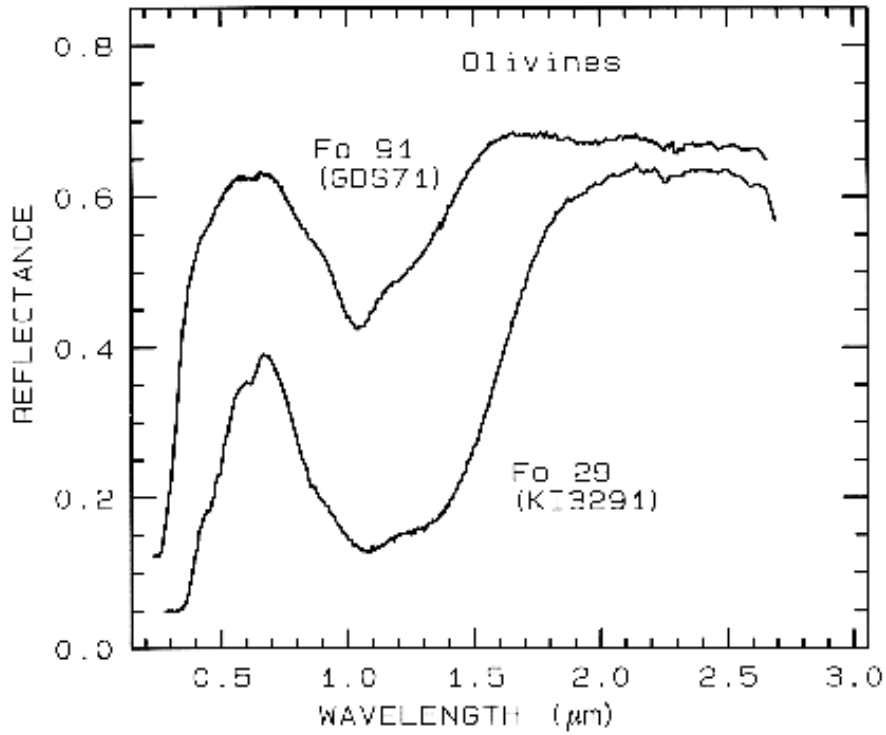

Figure 5a. Reflectance spectra of two olivines showing the change in band position and shape with composition. The 1-µm absorption band is due to a crystal field absorption of Fe^{2+}. "Fo" stands for forsterite (Mg_2SiO_4) in the forsterite-fayalite ($Fe_2^{2+}SiO_4$) olivine solid solution series. The Fo 29 sample (KI3291 from King and Ridley, 1987) has an FeO content of 53.65%, while the Fo 91 sample (GDS 71; labeled Twin Sisters Peak in King and Ridley, 1987) has an FeO content of 7.93%. The mean grain size is 30 and 25 µm respectively. The 1-µm band position varies from about 1.08 µm at Fo 10 to 1.05 µm at Fo 90 (King and Ridley, 1987).

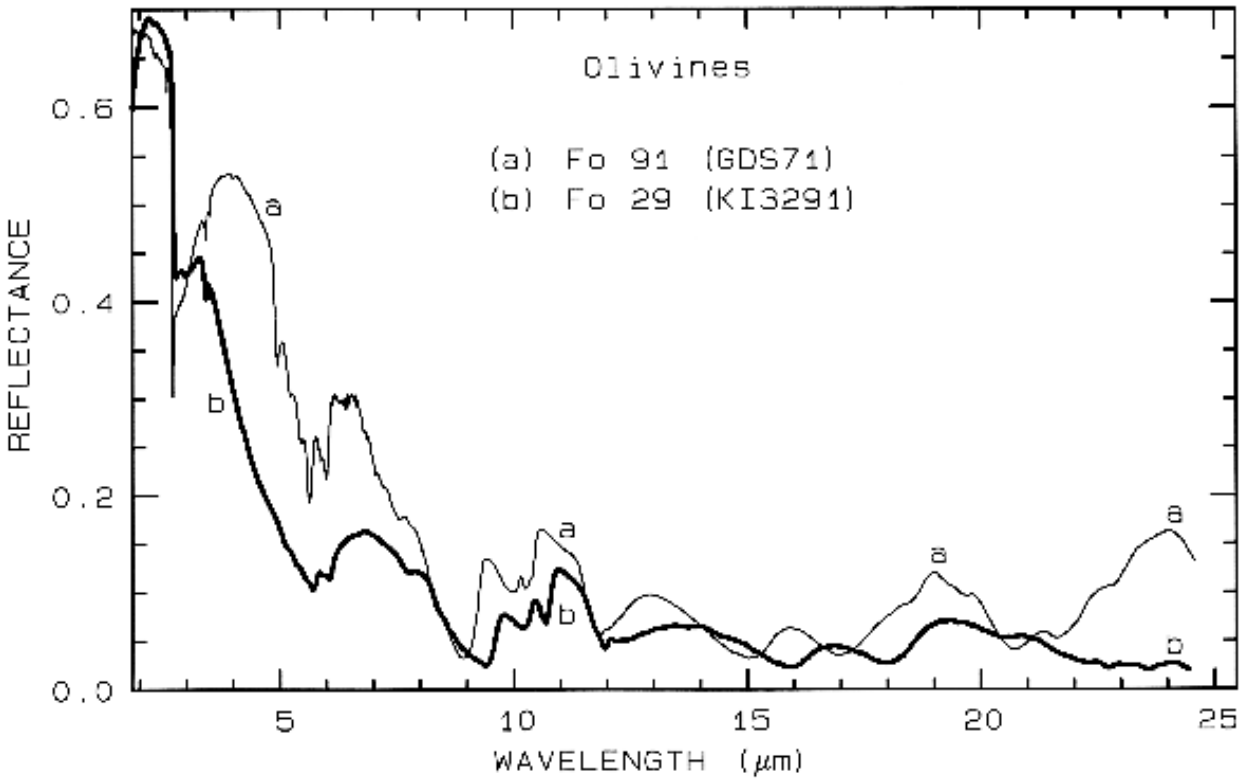

Figure 5b.

Figure 5b: 27k 100dpi gif

Figure 5b: 81k 200dpi gif

Figure 5b: 167k 300dpi gif

Figure 5b. Same as for Figure 5a but for mid-infrared wavelengths. Note the shifts in the spectral features due to the change in composition. See text for discussion of vibrational absorption bands.

Figure 6a.

Figure 6a: 22k 100dpi gif

Figure 6a: 81k 200dpi gif

Figure 6a: 132k 300dpi gif

Figure 6a. Reflectance spectra of two pyroxenes showing the change in Fe^{2+} -absorption band position and shape with composition (from Clark *et al.*, 1993b). Diopside, sample NMNH18685, is $CaMgSi_2O_6$, but some Fe^{2+} substitutes for Mg. Bronzite, sample HS9.3B, is $(Mg,Fe)SiO_3$ with mostly Mg. The 1-µm versus the 2-µm band position of a pyroxene describes the pyroxene composition, Figure 6c. The diopside spectrum is offset 0.2 units upward.

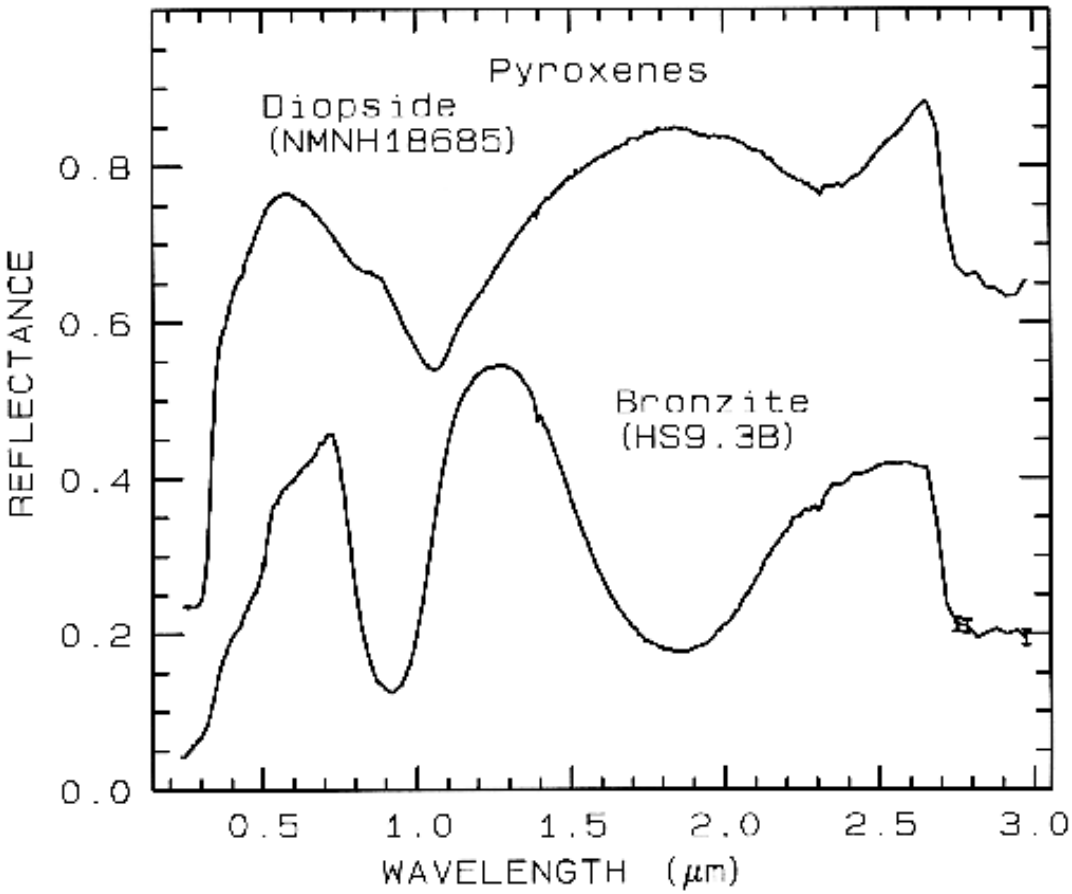

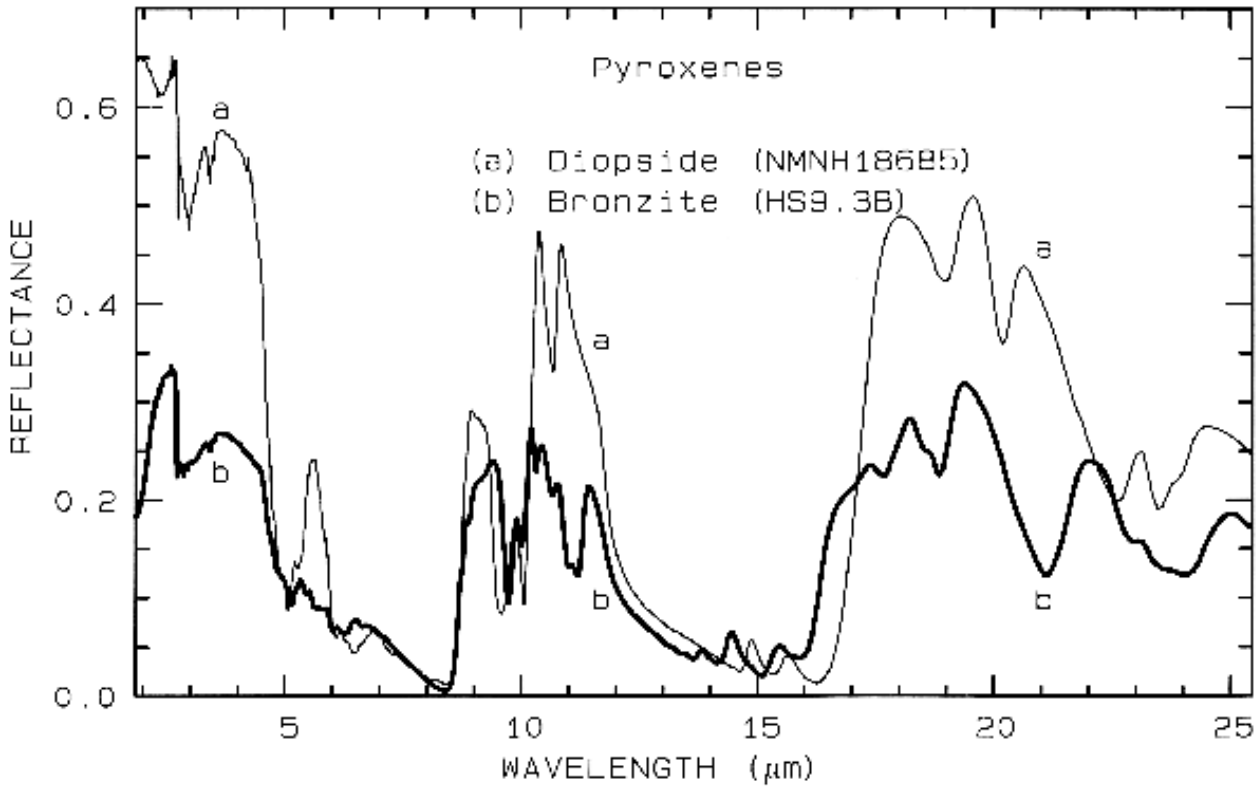

Figure 6b.

Figure 6b: 34k 100dpi gif

Figure 6b: 93k 200dpi gif

Figure 6b: 174k 300dpi gif

Figure 6b. Same as for Figure 6a, but for mid-infrared wavelengths. Note the shifts in the spectral features due to the change in composition.

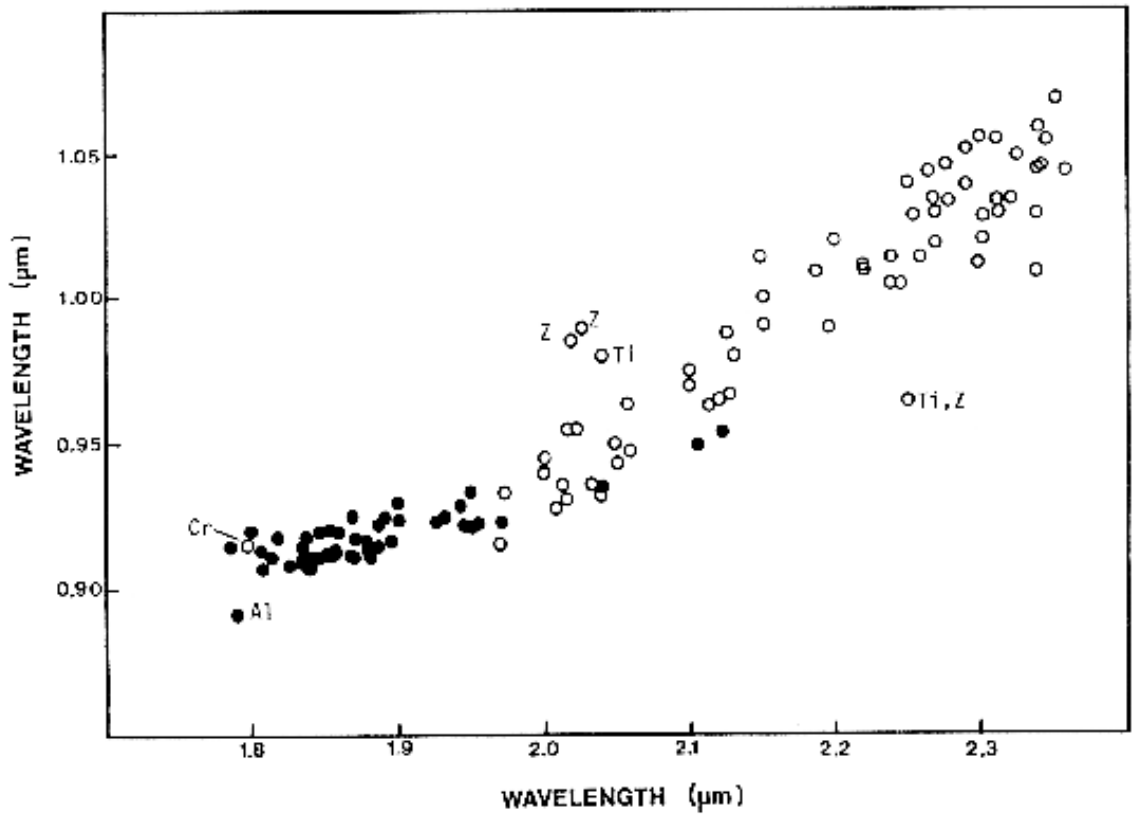

Figure 6c.

Figure 6c: 14k 100dpi gif

Figure 6c: 40k 200dpi gif

Figure 6c: 106k 300dpi gif

Figure 6c. Pyroxene 1-µm versus 2-µm absorption band position as a function of composition, as adapted from Adams (1974) by Cloutis and Gaffey (1991). Open circles have > 11% wollastonite (Wo), and solid symbols < 11 % Wo. Samples with zoned or exolved phases are marked by "Z." Other samples not following the "normal" trend include those with >1% TiO_2 (Ti), > 1% Cr_2O_3 (Cr), or >4% Al_2O_3. From Cloutis and Gaffey (1991).

Figure 7a.

Figure 7a: 20k 100dpi gif

Figure 7a: 53k 200dpi gif

Figure 7a: 123k 300dpi gif

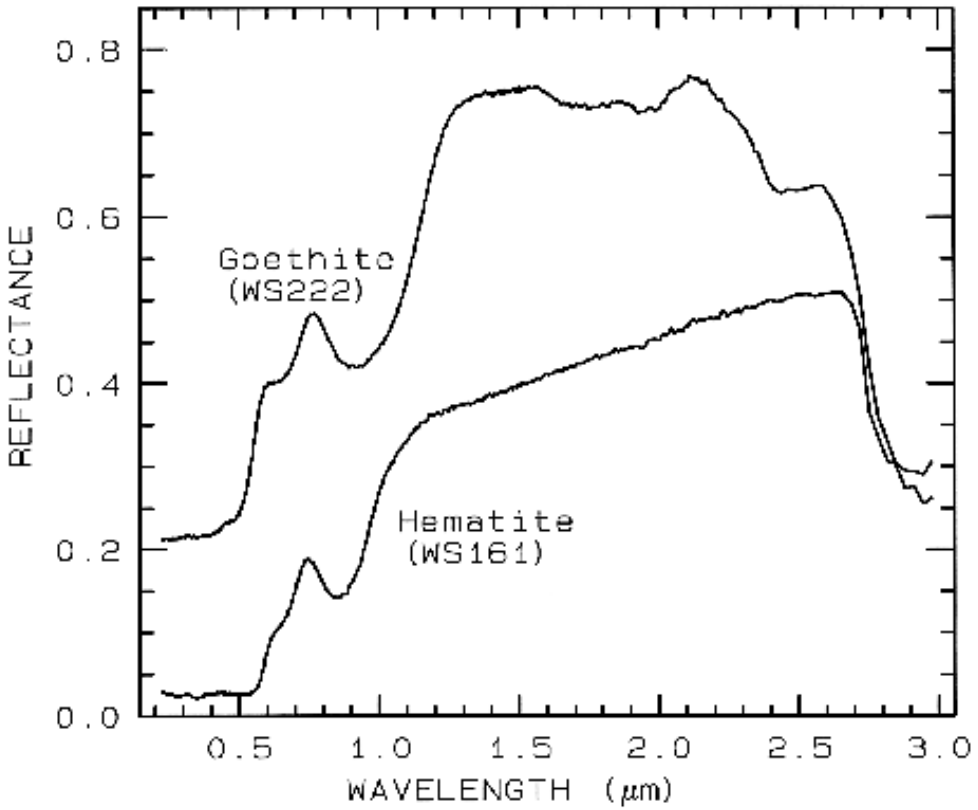

Figure 7a. Reflectance spectra of the iron oxide hematite (Fe_2O_3) and iron hydroxide goethite (FeOOH, from Clark *et al.*, 1993b). The intense charge-transfer band in the UV (< 0.4 μm) is "saturated" in reflectance, so only first surface (specular) reflection is seen in these spectra. The 0.9-μm and 0.86-μm absorption features are due to Laporte-forbidden transitions (e.g. Morris *et al,* 1985; Sherman, 1990 and references therein). The absorption at 2.7-3 μm is due to trace water in the samples., and in the case of goethite, the OH. The goethite spectrum is offset upward 0.2 units.

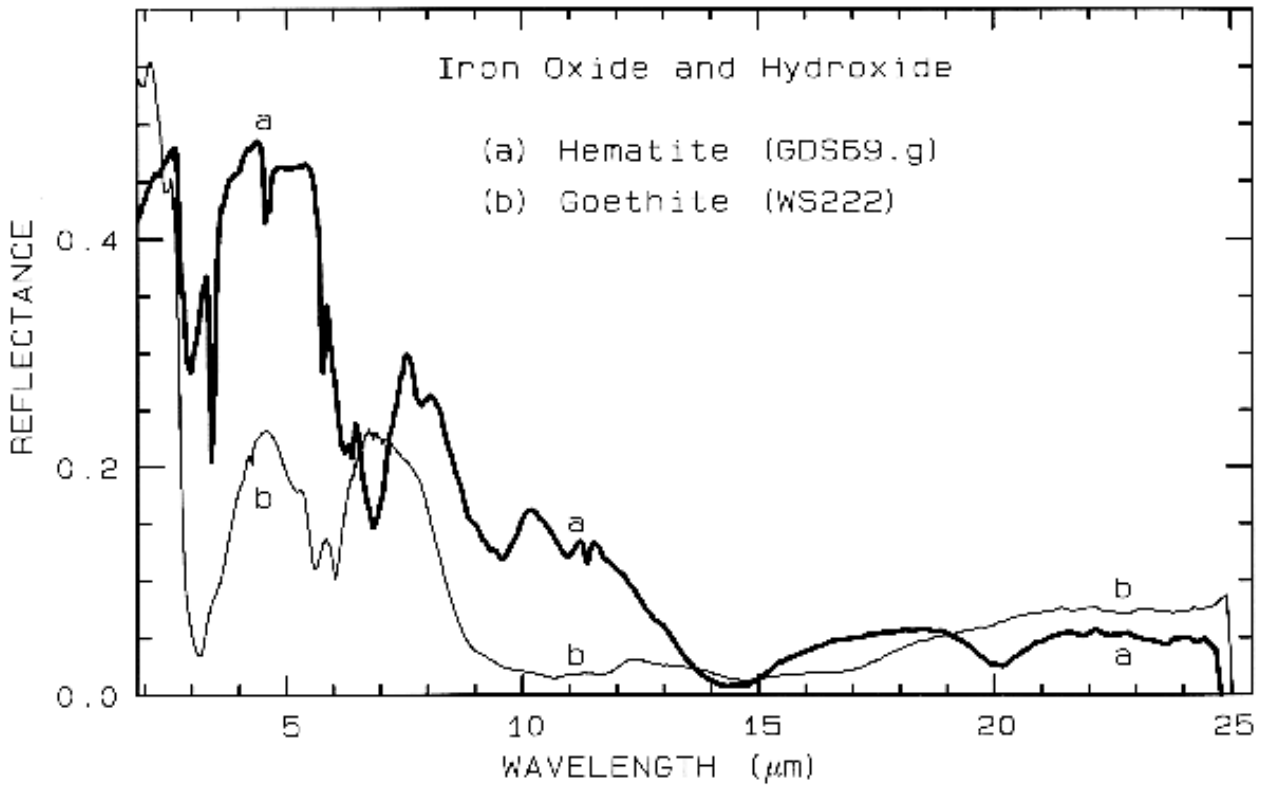

Figure 7b.

Figure 7b: 29k 100dpi gif

Figure 7b: 101k 200dpi gif

Figure 7b: 185k 300dpi gif

Figure 7b. Same as for Figure 7a, but for mid-infrared wavelengths, and no offsets.

Example Fe^{2+} absorptions are shown in Figure 5a (olivines), and Figure 6a (pyroxenes). Note the shift in band position and shape between the different compositions. Example Fe^{3+} absorptions are shown in goethite (FeOOH) and hematite (Fe_2O_3) in Figure 7a. Compositional changes also shift vibrational absorptions, discussed below, and as seen in Figures 5b, 6b, and 7b. The compositional shifts of the electronic absorptions have been studied by Adams (1974, 1975) and Cloutis and Gaffey (1991) for pyroxenes and are shown in Figure 6c, and by King and Ridley (1987) for olivines.

The unfilled shells of rare earth ions involve deep-lying electrons which are well shielded from surrounding crystal fields so the energy levels remain largely unchanged. Thus, absorption bands due to rare earth elements are not diagnostic of mineralogy but to the presence of the ions in the mineral (Figure 8).

Figure 8a.

Figure 8a: 31k 100dpi gif

Figure 8a: 87k 200dpi gif

Figure 8a: 195k 300dpi gif

Figure 8a. Reflectance spectra of rare-earth oxides. These absorptions are due to crystal-field transitions involving deep-lying electrons of the rare-earth element and do not shift when the rare-earth ion is in another mineral. Each spectrum is offset by 1.0 units for clarity. Spectra from Clark *et al.* (1993b).

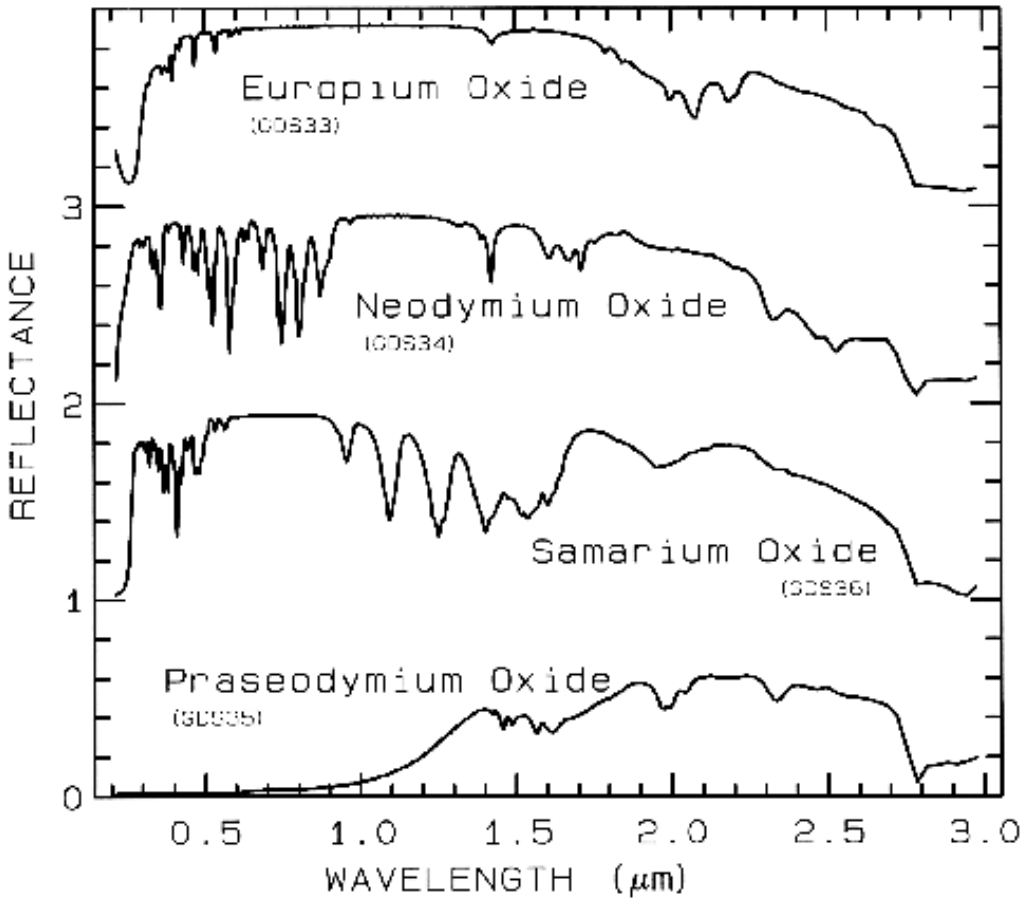

Figure 8b.

Figure 8b: 25k 100dpi gif

Figure 8b: 75k 200dpi gif

Figure 8b: 142k 300dpi gif

Figure 8b. Same as Figure 8a, except showing absorptions in the visible region. Spectra are offset 1.0 units for clarity. Spectral resolution is about 1 nm, critically sampled.

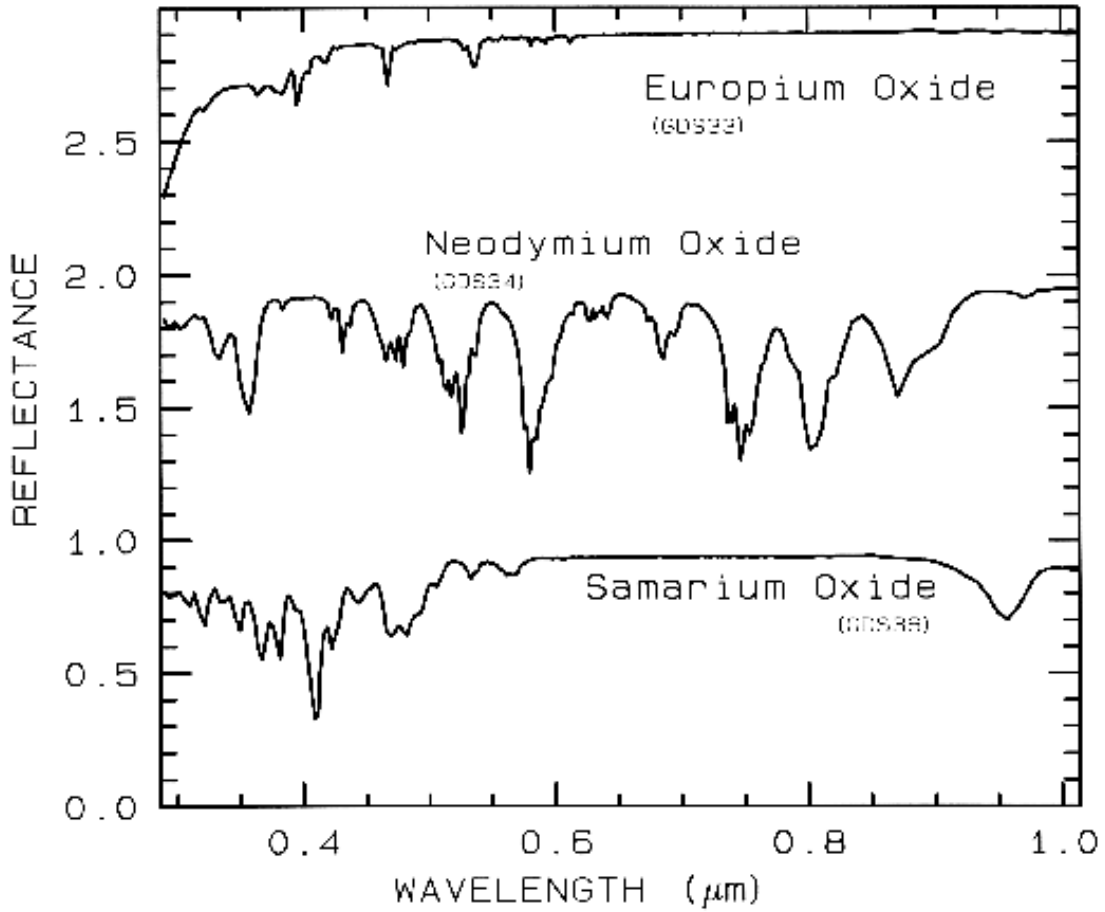

Back to Contents

3.1.2 Charge Transfer Absorptions.. Absorption bands can also be caused by charge transfers, or inter-element transitions where the absorption of a photon causes an electron to move between ions or between ions and ligands. The transition can also occur between the same metal in different valence states, such as between Fe^{2+} and Fe^{3+}. In general, absorption bands caused by charge transfers are diagnostic of mineralogy. Their strengths are typically hundreds to thousands of times stronger than crystal field transitions. The band centers usually occur in the ultraviolet with the wings of the absorption extending into the visible. Charge transfer absorptions are the main cause of the red color of iron oxides and hydroxides (Figure 7a). Morris *et al.* (1985) studied the details of sub-micron iron oxides where it was found that the absorption bands rapidly decrease in intensity. This occurs because of the increased surface to volume ratio at small grain size results in a greater proportion of grain boundaries where crystal field effects are different, resulting in lower magnetic coupling and reduced absorption strength. Other iron oxides probably show similar effects. Reflectance spectra of iron oxides have such strong absorption bands that the shape changes significantly with grain size. This will be discussed later in this chapter and is also illustrated in Figure 27. Small shifts in absorption band position are also observed due to substitution of other elements, like aluminum for iron in hematite (e.g. Morris *et al.*, 1985 and references therein) but more work needs to be done to fully understand the effects.

Back to Contents

3.1.3 Conduction Bands.. In some minerals, there are two energy levels in which electrons may reside: a higher level called the "conduction band," where electrons move freely throughout the lattice, and a lower energy region called the "valence band," where electrons are attached to individual atoms. The difference between the energy levels is called the band gap. The band gap is typically small or non-existent in metals, and very large in dielectrics. In semiconductors, the band gap corresponds to the energy of visible to near-infrared wavelength photons and the spectrum in these cases is approximately a step function. The yellow color of sulfur is caused by such a band gap. The minerals cinnabar (HgS) and Sulfur (S) have spectra showing the band gap in the visible (Figure 9).

Figure 9.

Figure 9: 19k 100dpi gif

Figure 9: 63k 200dpi gif

Figure 9: 110k 300dpi gif

Figure 9. Reflectance spectra of Sulfur, S, (top) and cinnabar, HgS, (bottom) showing conduction bands in the visible (from Clark *et al*., 1993b).

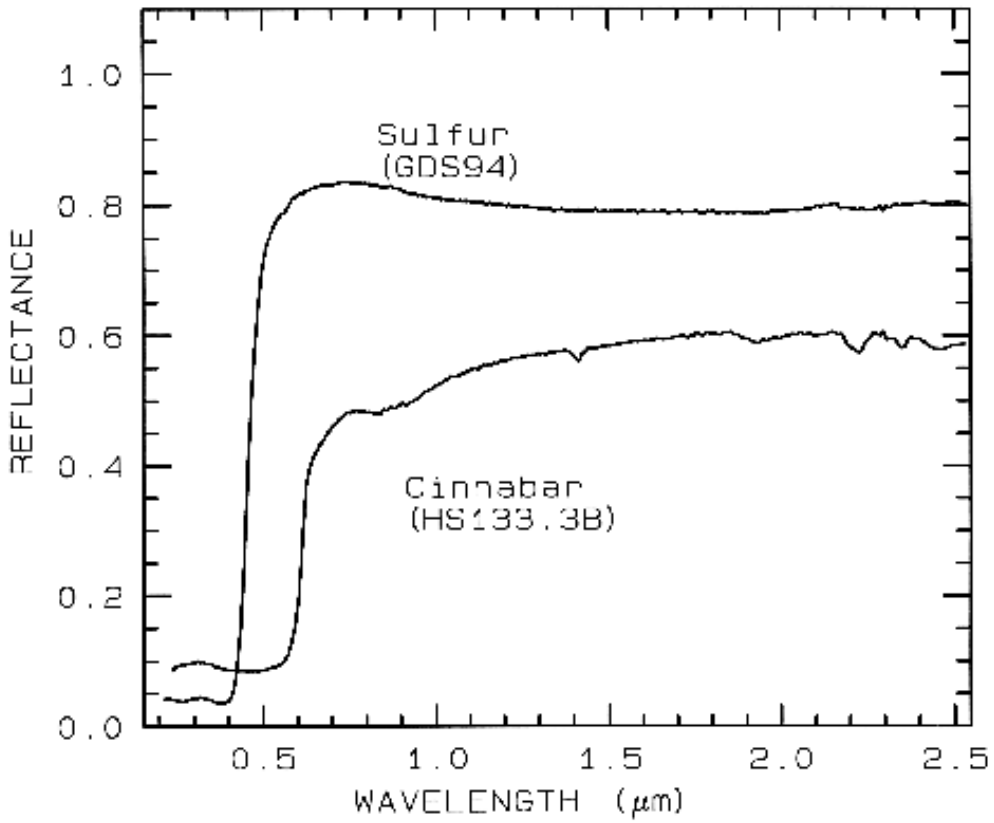

Back to Contents

3.1.4 Color Centers.. A few minerals show color due to absorption by "color centers." A color center is caused by irradiation (e.g. by solar UV radiation) of an imperfect crystal. Crystals in nature have lattice defects that disturb the periodicity of the crystal. For example, defects might be caused by impurities. These defects can produce discrete energy levels and electrons can become bound to them. The movement of an electron into the defect requires photon energy. The yellow, purple and blue colors of fluorite are caused by color centers. See Hunt (1977) and references therein for more details.

More detailed discussions of electronic processes can be found in the review paper by Hunt (1977), Gaffey *et al*. (1993) and the book by Burns (1993). A summary diagram of the causes of absorption bands is shown in Figure 13.

Back to Contents

3.2 Vibrational Processes.

The bonds in a molecule or crystal lattice are like springs with attached weights: the whole system can vibrate. The frequency of vibration depends on the strength of each spring (the bond in a molecule) and their masses (the mass of each element in a molecule). For a molecule with N atoms, there are 3N-6 normal modes of vibrations called fundamentals. Each vibration can also occur at roughly multiples of the original fundamental frequency. The additional vibrations are called overtones when they involve multiples of a single fundamental mode, and combinations when they involve different modes of vibrations.

A vibrational absorption will be seen in the infrared spectrum only if the molecule responsible shows a dipole moment (it is said to be infrared active). A symmetric molecule, like N_2 is not normally infrared active unless it is distorted (for example, when under high pressure). Vibrations from two or more modes can occur at the same frequency, and because they can't be distinguished, are said to be degenerate. An isolated molecule with degenerate modes may show the modes at slightly different frequencies in a crystal because of the non-symmetric influences of the crystal field.

A free molecule can rotate and move translationally, but even in a solid partial rotation and slight translation can occur. These motions are called lattice modes and typically occur at very low energies (longer mid-infrared wavelengths), beyond about 20 µm.

Traditionally, the frequencies of fundamental vibrations are labeled with the greek letter nu (ν) and a subscript (Herzberg, 1945). If a molecule has vibration fundamentals ν_1, ν_2, ν_3, then it can have overtones at approximately $2\nu_1$, $3\nu_1$, $2\nu_2$ and combinations at approximately $\nu_1+\nu_2$, $\nu_2+\nu_3$, $\nu_1+\nu_2+\nu_3$, and so on. These examples used summations of modes, but subtractions are also possible (e.g. $\nu_1+\nu_3-\nu_2$). Each higher overtone or combination is typically 30 to 100 times weaker than the last. Consequently, the spectrum of a mineral can be quite complex. In reflectance spectroscopy, these weak absorptions can be measured easily and diagnostic information routinely gained from 2nd and 3rd overtones and combinations (e.g. Figures 5b, 6b, 7b, 10, 11, 12).

Figure 10a.

Figure 10a: 124k 100dpi gif

Figure 10a: 173k 200dpi gif

Figure 10a: 332k 300dpi gif

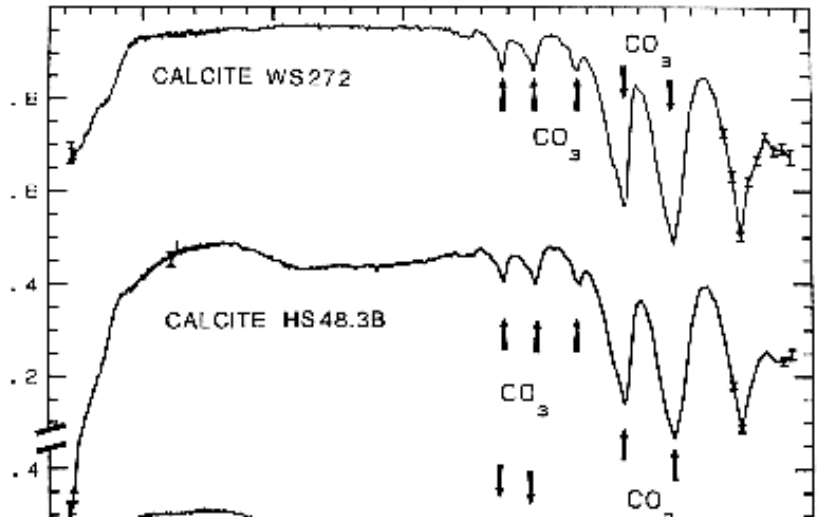

Figure 10a. Reflectance spectra of calcite, dolomite, beryl, gypsum, alunite, rectorite, and jarosite showing vibrational bands due to OH, CO_3 and H_2O, from Clark *et al.*, 1990a).

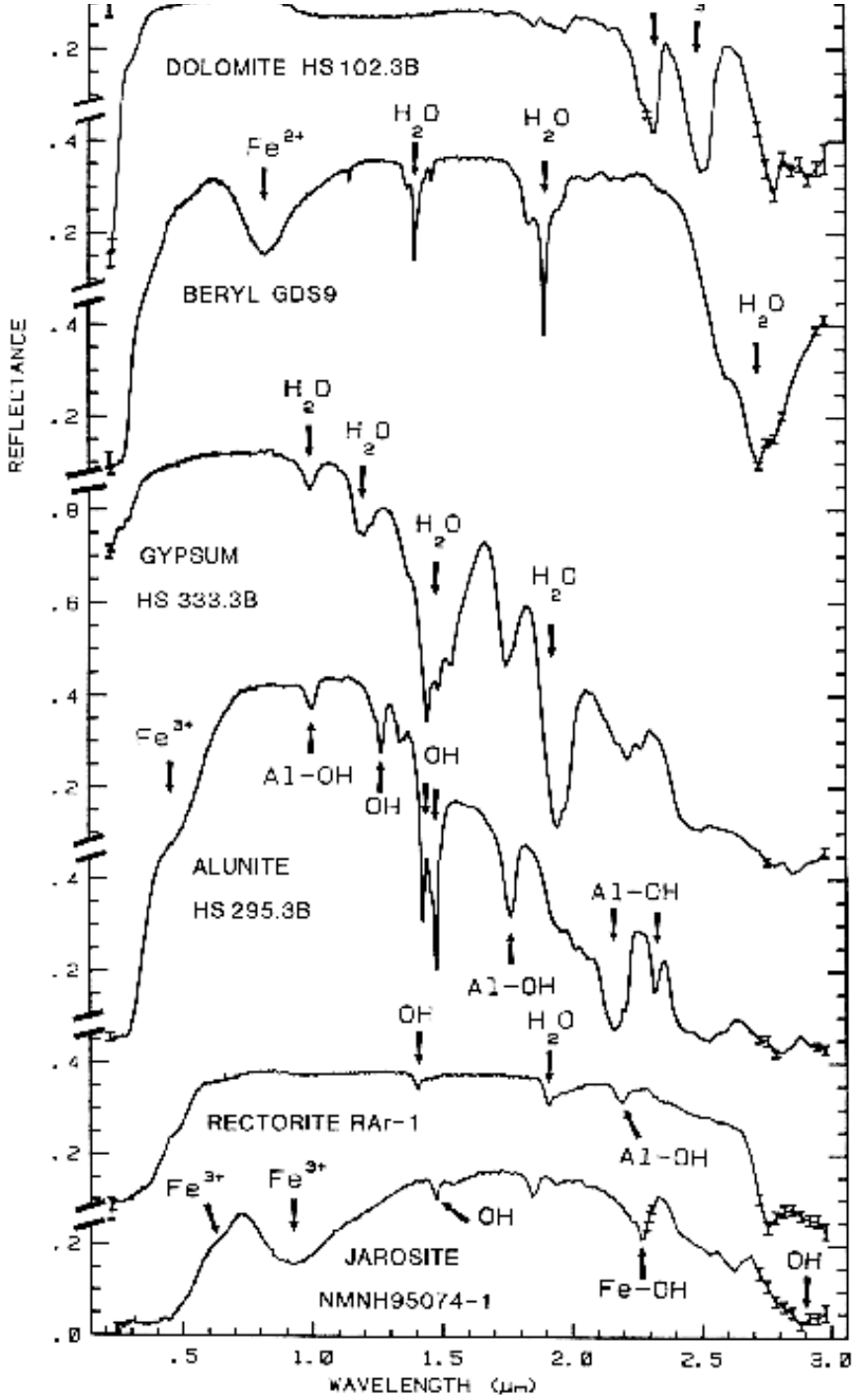
DOLOMITE HS102.3B
Fe2+
H2O
H2O
BERYL GDS9
H2O
H2O
H2O
GYPSUM
HS 333.3B
H2O
H2O
Fe3+
Al-OH
OH
OH
ALUNITE
HS 295.3B
Al-OH
Al-OH
OH
H2O
RECTORITE RAr-1
Al-OH
Fe3+
Fe3+
OH
JAROSITE
NMNH95074-1
Fe-OH
OH
REFLECTANCE
.5
1.0
1.5
2.0
2.5
3.0
WAVELENGTH (μm)

Figure 10b.

Figure 10b: 45k 100dpi gif

Figure 10b: 151k 200dpi gif

Figure 10b: 249k 300dpi gif

Figure 10b. Reflectance spectra of phlogopite, biotite, pyrophyllite, muscovite, epidote, and illite showing vibrational bands due to OH and H_2O, from Clark *et al.*, 1990a).

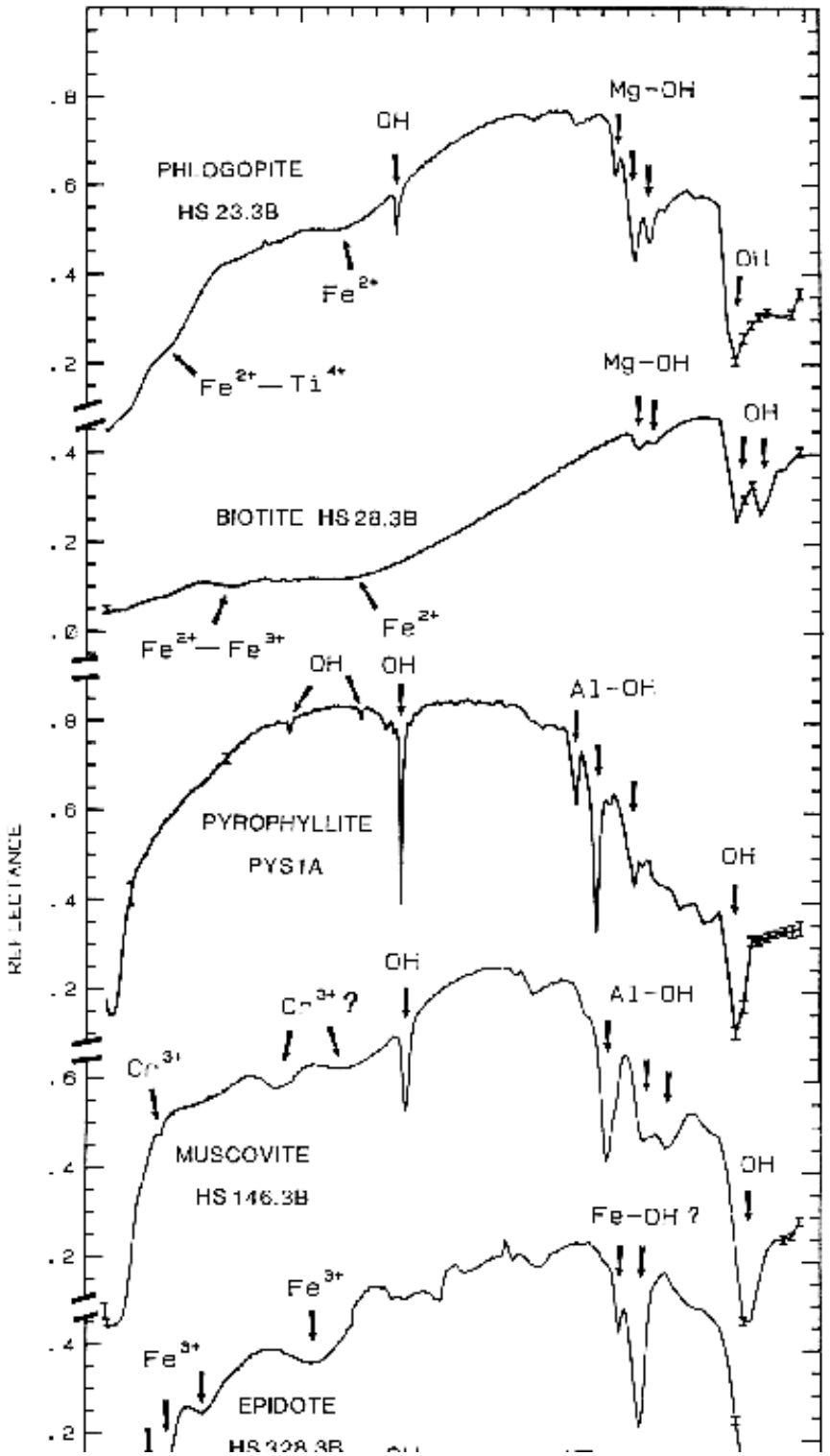

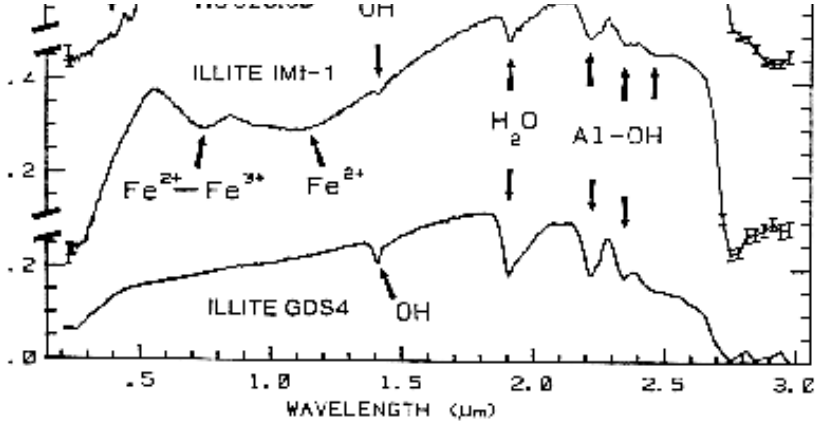

Figure 10c.

Figure 10c: 46k 100dpi gif

Figure 10c: 150k 200dpi gif

Figure 10c: 326k 300dpi gif

Figure 10c. Reflectance spectra of hectorite, halloysite, kaolinite, chrysotile, lizardite, and antigorite showing vibrational bands due to OH (from Clark *et al*., 1990a). Figure 17 shows an expanded view of the 1.4-µm region for chrysotile, lizardite, and antigorite.

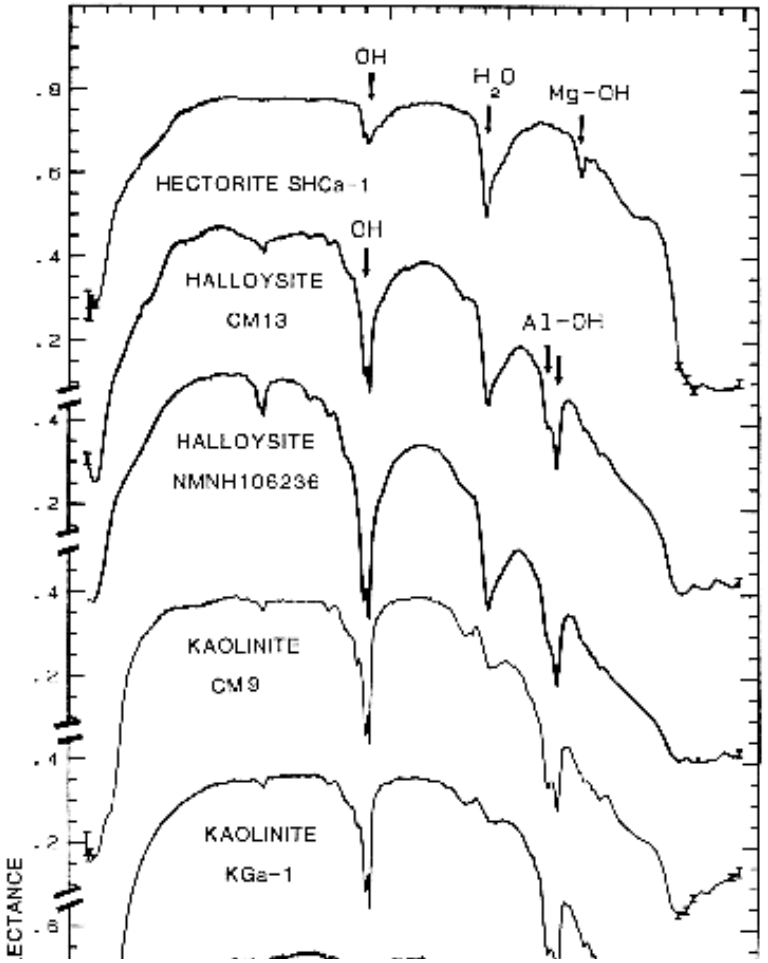

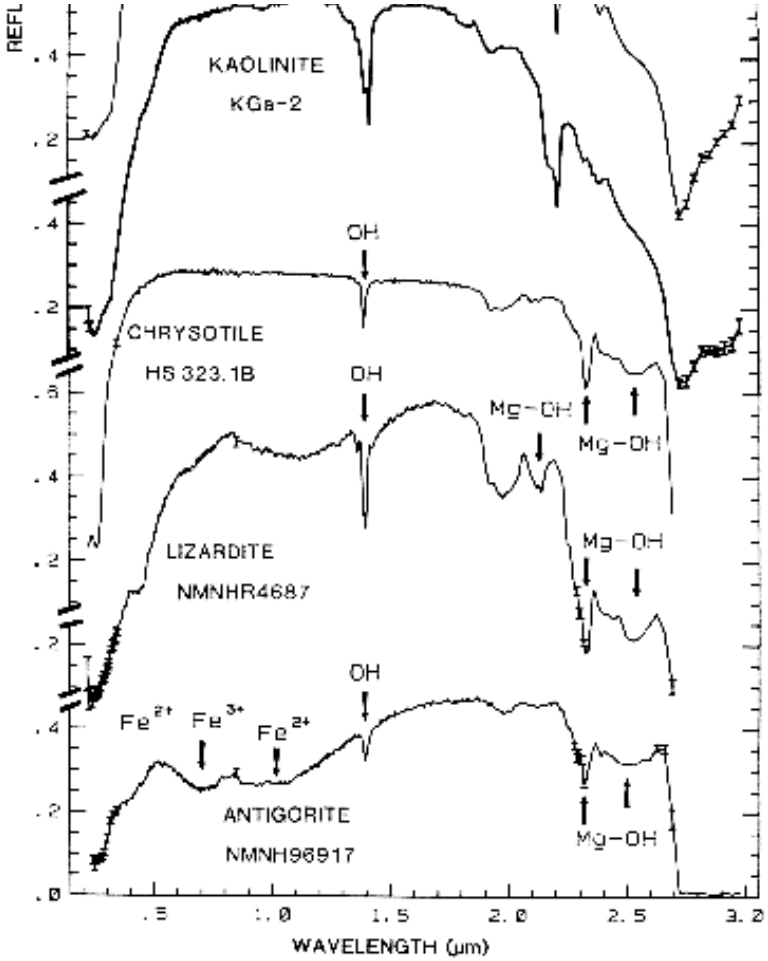
REFL
KAOLINITE
KGa-2
OH
CHRYSOTILE
HS 323.1B
OH
Mg-OH
Mg-OH
LIZARDITE
NMNHR4687
Mg-OH
OH
Fe2+
Fe3+
Fe2+
ANTIGORITE
NMNH96917
Mg-OH
.5
1.0
1.5
2.0
2.5
3.2
WAVELENGTH (μm)

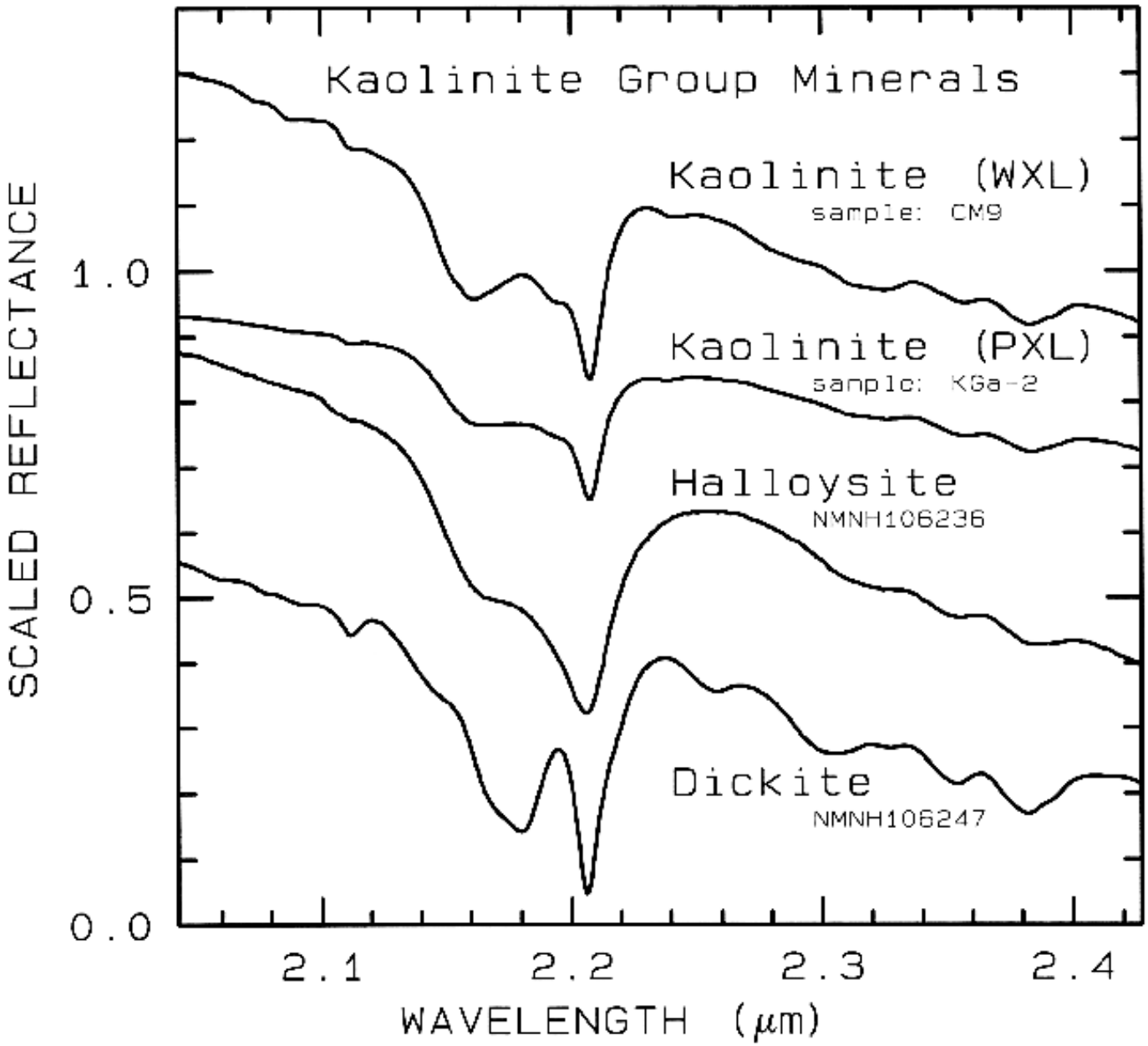

Figure 10d.

Figure 10d: 27k 100dpi gif

Figure 10d: 77k 200dpi gif

Figure 10d: 149k 300dpi gif

Figure 10d. Subtle spectral differences in the kaolinite group minerals near 2.2-µm. Kaolinite CM9 is well crystallized (WXL) while KGa-2 is poorly crystallized (PXL). Spectral bandwidth is 1.9 nm and sampling is 0.95 nm. Each spectrum was scaled to 0.7 at 2.1 µm then offset up or down so that the curves to not overlap. Original reflectances were between 0.5 and 0.8.

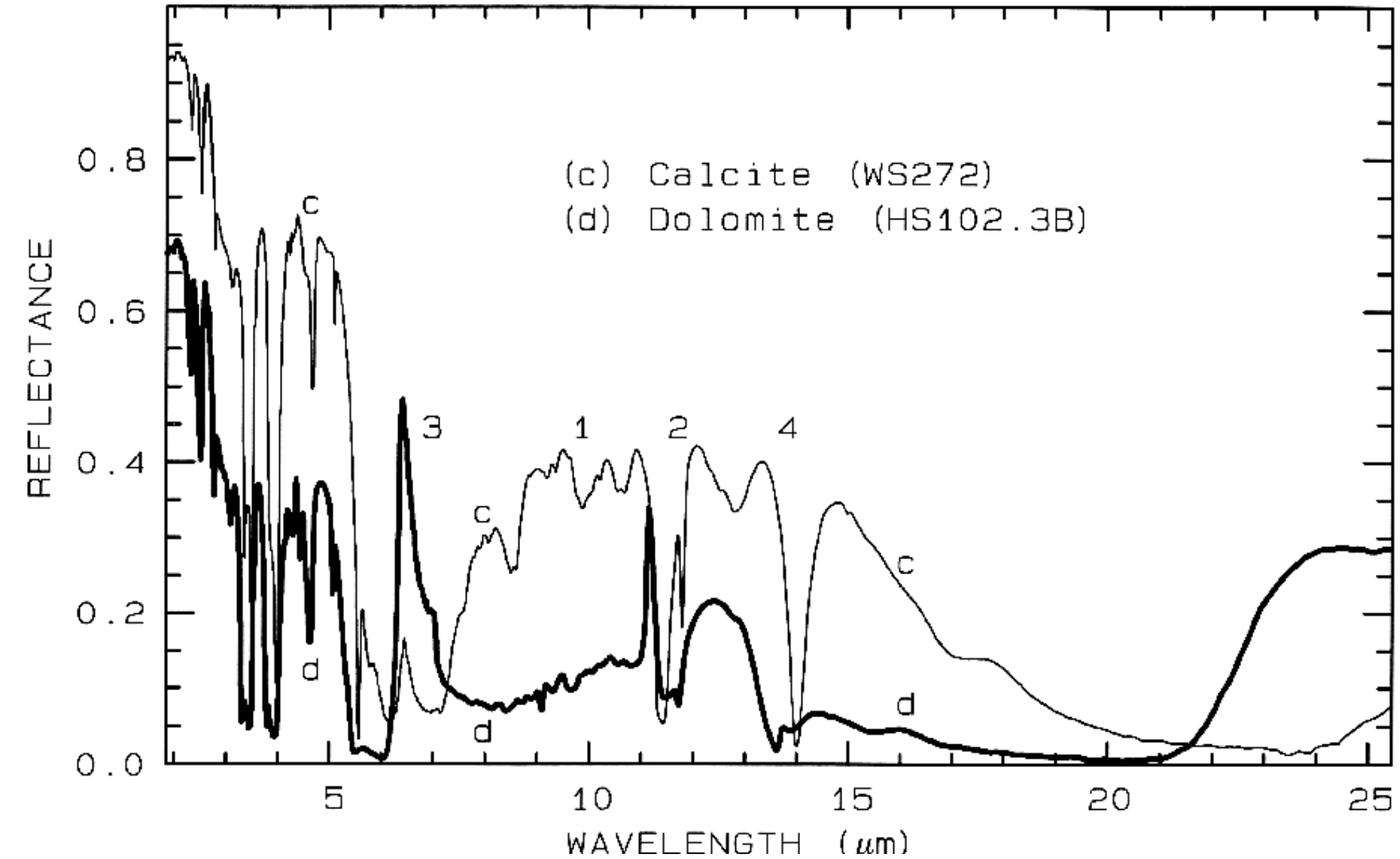

Figure 11,

Figure 11: 41k 100dpi gif

Figure 11: 100k 200dpi gif

Figure 11: 186k 300dpi gif

Figure 11. Comparison of calcite ($CaCO_3$) and dolomite ($CaMg(CO_3)_2$) spectra in the mid-infrared showing small band shifts due to the change in composition between the two minerals. The level change (calcite higher in reflectance than dolomite) is because the calcite has a smaller grain size. The numbers indicate the fundamental stretching positions of v_1 v_2, v_3, and v_4. The v_1 stretch is infrared innactive, but may be weakly present in carbonates. The v_3 fundamental is so strong, only a reflection peak is seen in these spectra.

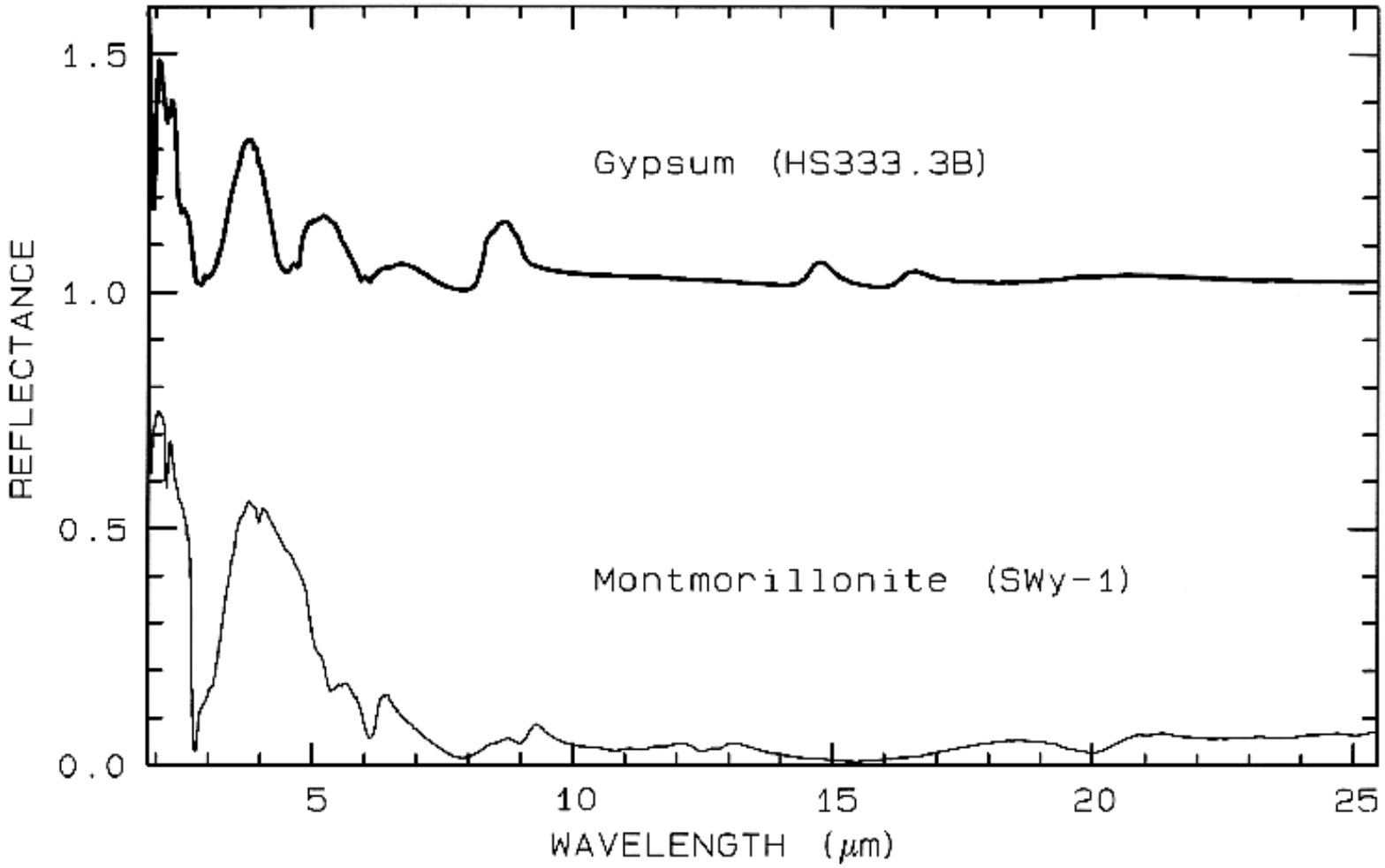

Figure 12.

Figure 12: 22k 100dpi gif

Figure 12: 73k 200dpi gif

Figure 12: 147k 300dpi gif

Figure 12 Mid-IR spectra of gypsum, $CaSO_4 2H_2O$. (top) and montmorillonite, $(Al,Mg)_8(Si_4O_{10})_3(OH)_{10}12H_2O$, (bottom). The gypsum curve is offset upward 1.0 units for clarity. Both samples have very low reflectance because of the water content of the samples. Water is a strong infrared absorber. The montmorillonite also has a small grain size, which also tends to produce low mid-infrared reflectance because of the strong absorption in the mid-infrared.

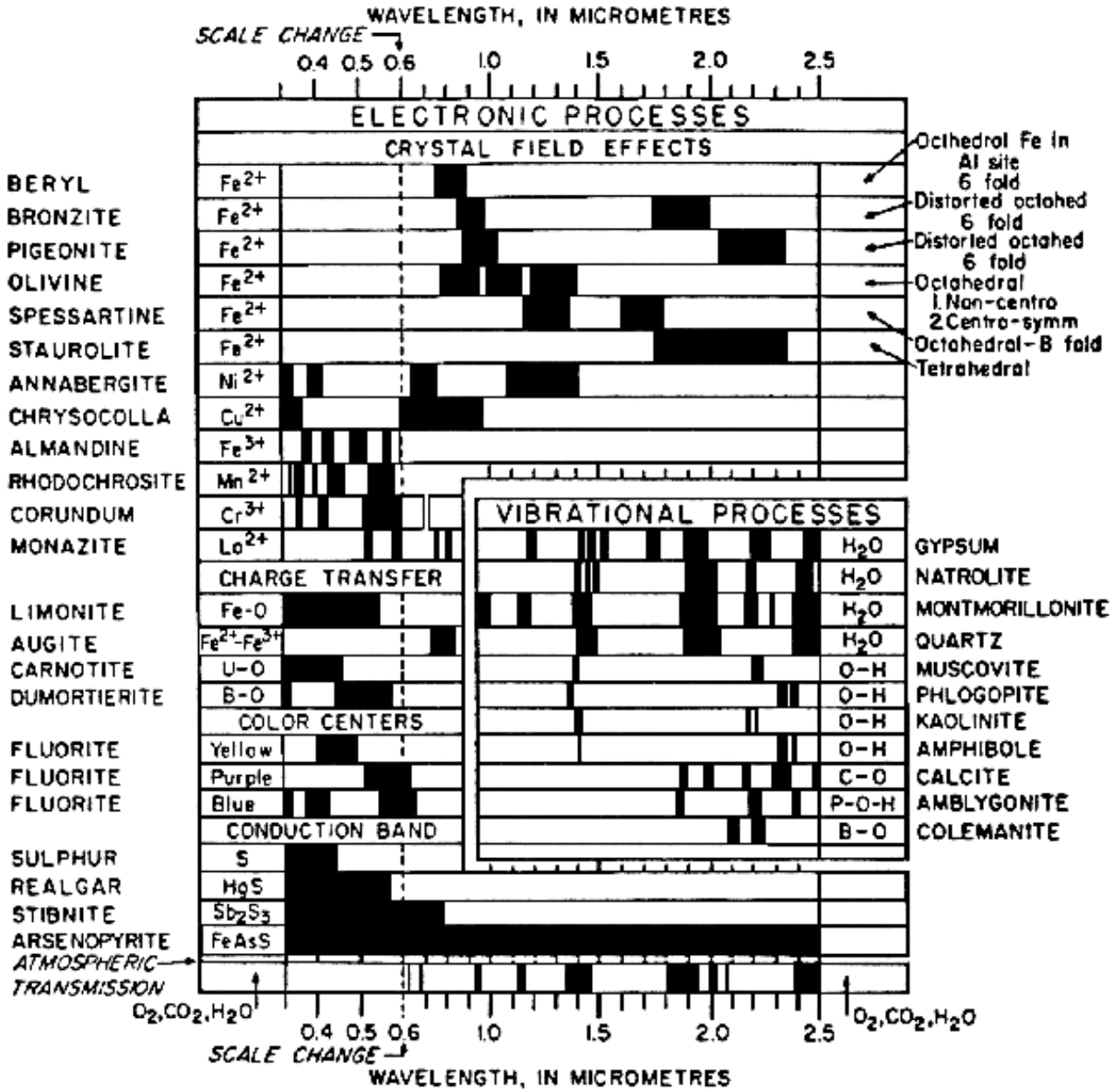

Figure 13a.

Figure 13a: 53k 100dpi gif

Figure 13a: 137k 200dpi gif

Figure 13a: 278k 300dpi gif

Figure 13a. Spectral signature diagram (from Hunt, 1977). The widths of the black bars indicate the relative widths of absorption bands.

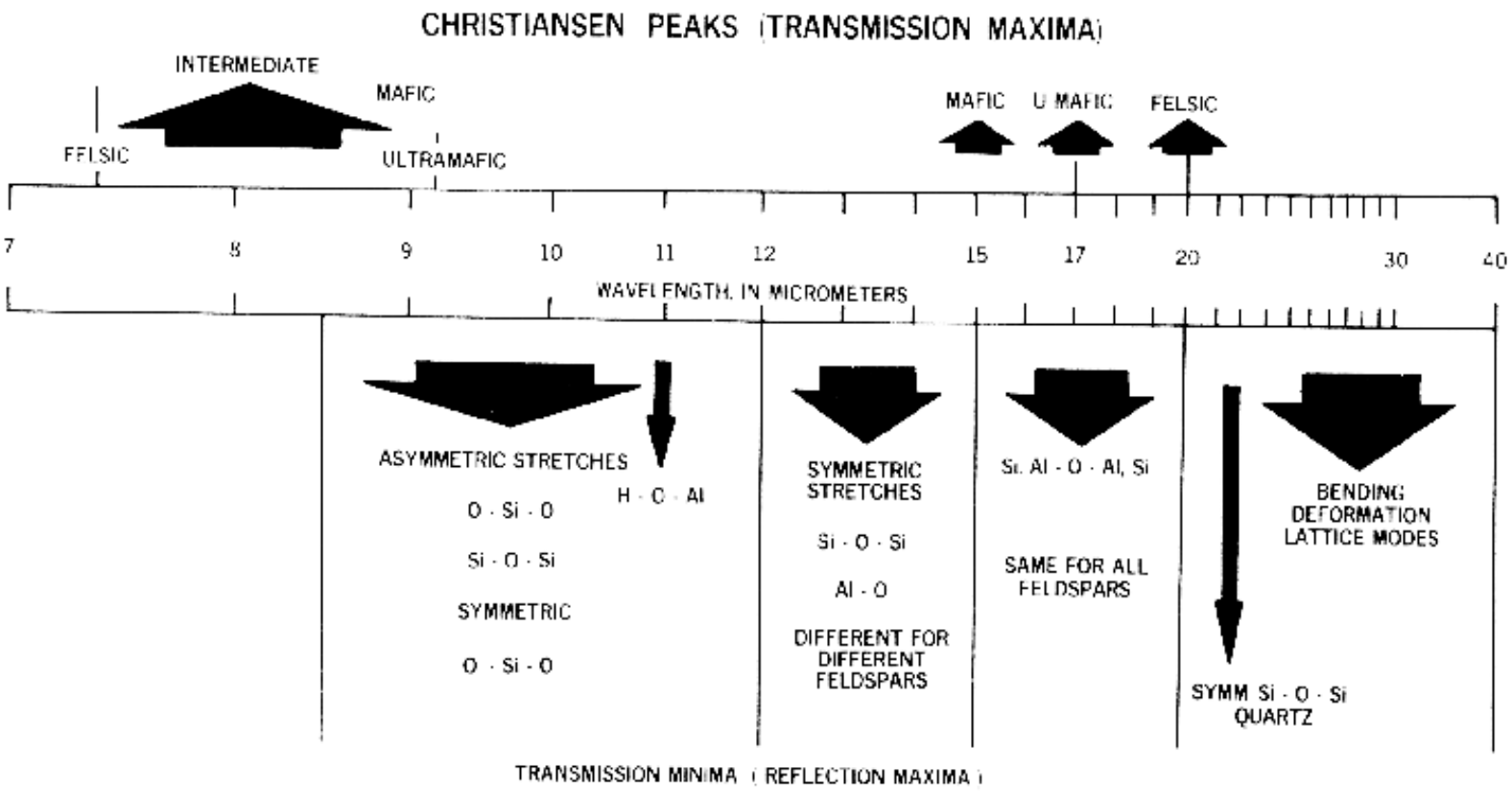

Figure 13b.

Figure 13b: 24k 100dpi gif

Figure 13b: 76k 200dpi gif

Figure 13b: 176k 300dpi gif

Figure 13b. Illustration of the locations and causes of absorptions in mid-infrared spectra of silicates, from Hunt (1982).

Lattice modes are sometimes denoted by v_T and v_R and also couple with other fundamentals, resulting in finer structure seen in some spectra. The causes of vibrational absorptions in mid-IR spectra are summarized in Figure 13b from Hunt (1982).

Mid-infrared reflectance spectra of quartz are shown in Figure 4b. The strong 9-µm Si-O-Si asymmetric stretch fundamental is obvious from the reflection maximum. The O-Si-O bending mode occurs near 25 µm and is the second strongest absorption. The absorption between 12 and 13 µm is the Si-O-Si symmetric stretch fundamental.

Olivine spectra in the mid-infrared are shown in Figure 5b. When Mg is present, a strong absorption appears near 23 µm, perhaps seen in the Fo 91 spectrum. The Si-O-Si asymmetric stretch fundamental occurs near 11 µm, and a weaker symmetric absorption occurs near 12 µm. The absorptions shift with composition as shown in Figure 5b, and discussed in more detail in Farmer (1974, pp. 288-290).

Pyroxene mid-infrared spectra are shown in Figure 6b. The Si-O fundamentals are at similar to other silicates, as indicated in Figure 13b. Grain size effects will be discussed below in section 6.2 and illustrated in Figure 21.

Iron oxide and iron hydroxide mid-infrared spectra are shown in Figure 7b. Because iron is more massive than silicon, Fe-O fundamentals will be at longer wavelengths than Si-O stretching modes. Hematite, Fe_2O_3, has 3 strong stretching modes between 16 and 30 µm. Because iron oxides and hydroxides tend to be fine grained, typically less than the wavelength of mid-infrared photons, and because of the strong absorption in the mid-infrared, iron oxides tend to be dark in reflectance showing few features beyond about 12 µm. The hematite in Figure 7b has a small amount of water as evidenced by the 3-µm absorption, and a moderate amount of organics as seen by the C-H stretch fundamental near 3.4 µm. The goethite, FeOOH, having hydroxyl has a strong 3-µm absorption. The olivines (Figure 5) and pyroxenes (Figure 6) also show small amounts of water in the sample as seen by the 3-µm absorptions in their spectra.

Back to Contents

3.2.1 Water and Hydroxyl. Water and OH (hydroxyl) produce particularly diagnostic absorptions in minerals. The water molecule (H_2O) has N=3, so there are 3N-6=3 fundamental vibrations. In the isolated molecule (vapor phase) they occur at 2.738 µm (v_1, symmetric OH stretch), 6.270 µm (v_2, H-O-H bend), and 2.663 µm (v_3, asymmetric OH stretch). In liquid water, the frequencies shift due to hydrogen bonding: v_1=3.106 µm, v_2=6.079 µm, and v_3=2.903 µm.

The overtones of water are seen in reflectance spectra of H_2O-bearing minerals (Figure 10). The first overtones of the OH stretches occur at about 1.4 µm and the combinations of the H-O-H bend with the OH stretches are found near 1.9 µm. Thus, a mineral whose spectrum has a 1.9-µm absorption band contains water (e.g. hectorite and halloysite in Figure 10c), but a spectrum that has a 1.4-µm band but no 1.9-µm band indicates that only hydroxyl is present (e.g. kaolinite in Figure 10c has only a small amount of water because of the weak 1.9-µm absorption but a large amount of OH). The hydroxyl ion has only one stretching mode and its wavelength position is dependent on the ion to which it is attached. In spectra of OH-bearing minerals, the absorption is typically near 2.7 to 2.8 µm, but can occur anywhere in the range from about 2.67 µm to 3.45 µm (e.g. see Clark *et al*., 1990 and references therein). The OH commonly occurs in multiple crystallographic sites of a specific mineral and is typically attached to metal ions. Thus, there may be more than one OH feature. The metal-OH bend occurs near 10 µm (usually superimposed on the stronger Si-O fundamental in silicates). The combination metal-OH bend plus OH stretch occurs near 2.2 to 2.3 µm and is very diagnostic of mineralogy (e.g. see Clark *et al*., 1990 and references therein).

Back to Contents

3.2.2 Carbonates. Carbonates also show diagnostic vibrational absorption bands (Figure 10a, 11). The observed absorptions are due to the planar CO_3^{-2} ion. There are

four vibrational modes in the free CO_3^{-2} ion: the symmetric stretch, v_1: 1063 cm^{-1} (9.407 µm); the out-of-plane bend, v_2: 879 cm^{-1} (11.4 µm); the asymmetric stretch, v_3: 1415 cm^{-1} (7.067 µm); and the in-plane bend, v_4: 680 cm^{-1} (14.7 µm). The v_1 band is not infrared active in minerals. There are actually six modes in the CO_3^{-2} ion, but 2 are degenerate with the v_3 and $_4$ modes. In carbonate minerals, the v_3 and v_4 bands often appear as a doublet. The doubling has been explained in terms of the lifting of the degeneracy (e.g. see White, 1974) due to mineral structure and anion site.

Combination and overtone bands of the CO_3 fundamentals occur in the near IR. The two strongest are $v_1 + 2v_3$ at 2.50-2.55µm (4000-3900 cm^{-1}), and $3v_3$ at 2.30-2.35 µm (4350-4250 cm^{-1}; e.g. Figure 10a). Three weaker bands occur near 2.12-2.16 µm ($v_1 + 2v_3 + v_4$ or $3v_1 + 2v_4$; 4720-4630 cm^{-1}), 1.97-2.00 µm ($2v_1 + 2v_3$; 5080-5000 cm^{-1}), and 1.85-1.87 µm ($v_1 + 3v_3$; 5400-5350 cm^{-1}; e.g. Figure 10a) (e.g. Hunt and Salisbury, 1971). The band positions in carbonates vary with composition (Hunt and Salisbury, 1971; Gaffey, 1986, Gaffey *et al.*, 1993). An example of such a band shift is seen in Figures 10a, 11 and, in more detail, Figure 24a showing the shift in absorption position from calcite to dolomite.

Back to Contents

3.2.3 Other Minerals. Phosphates, borates, arsenates, and vanadates also have diagnostic vibrational spectra. Space precludes inclusion of spectra here. See Hunt *et al.*, (1972), and Clark *et al.*, (1993b) for visual to near-infrared spectra. In general, the primary absorptions (e.g. P-O stretch) occurs at mid-infrared wavelengths. However, many of these minerals contain OH or H_20 and have absorptions in the near-infrared.

In the mid-infrared, minerals with H_2O, or those that are fine grained, like clays, have very low reflectance, and show only weak spectral structure (e.g. Figure 12). Therefore, in emittance, spectral features will also be weak and thus difficult to detect. Grain size effects will be discussed further below.

Typical spectra of minerals with vibrational bands are shown in Figure 4b, 5b, 6b, 7b, and 10. See Hunt and Salisbury (1970), Hunt and Salisbury (1971), Hunt *et al.* (1971a,b, 1972, 1973), Hunt (1979), Farmer (1974), Gaffey (1986, 1987), Gaffey *et al.*, 1993, Clark *et al.* (1990a), King and Clark (1989a), Swayze and Clark (1990), Mustard (1992) and Salisbury (1993), for more details. A summary of absorption band positions and causes is shown in Figure 13a, b.

Back to Contents

4. SPECTRA OF MISCELLANEOUS MINERALS AND MATERIALS

4.1 Organics.

Organic materials are found all over the Earth, and in the solar system. Organics can be important compounds in some environmental problems. The C-H stretch fundamental occurs near 3.4 µm, (e.g. Figure 14a) the first overtone is near 1.7 µm, and a combination band near 2.3 µm (Figure 14b). The combinations near 2.3 µm can sometimes be confused with OH and carbonate absorptions in minerals (e.g. Figure 10), especially at low spectral resolution. Further discussions and references can be found in Chapter XX of the Manual of Remote Sensing.

Figure 14a.

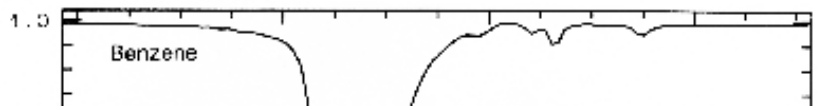

Figure 14a: 49k 100dpi gif

Figure 14a: 127k 200dpi gif

Figure 14a: 1020k 300dpi gif

Figure 14a. Transmittance spectra of organics and mixtures showing the complex absorptions in the CH-stretch fundamental spectral region.

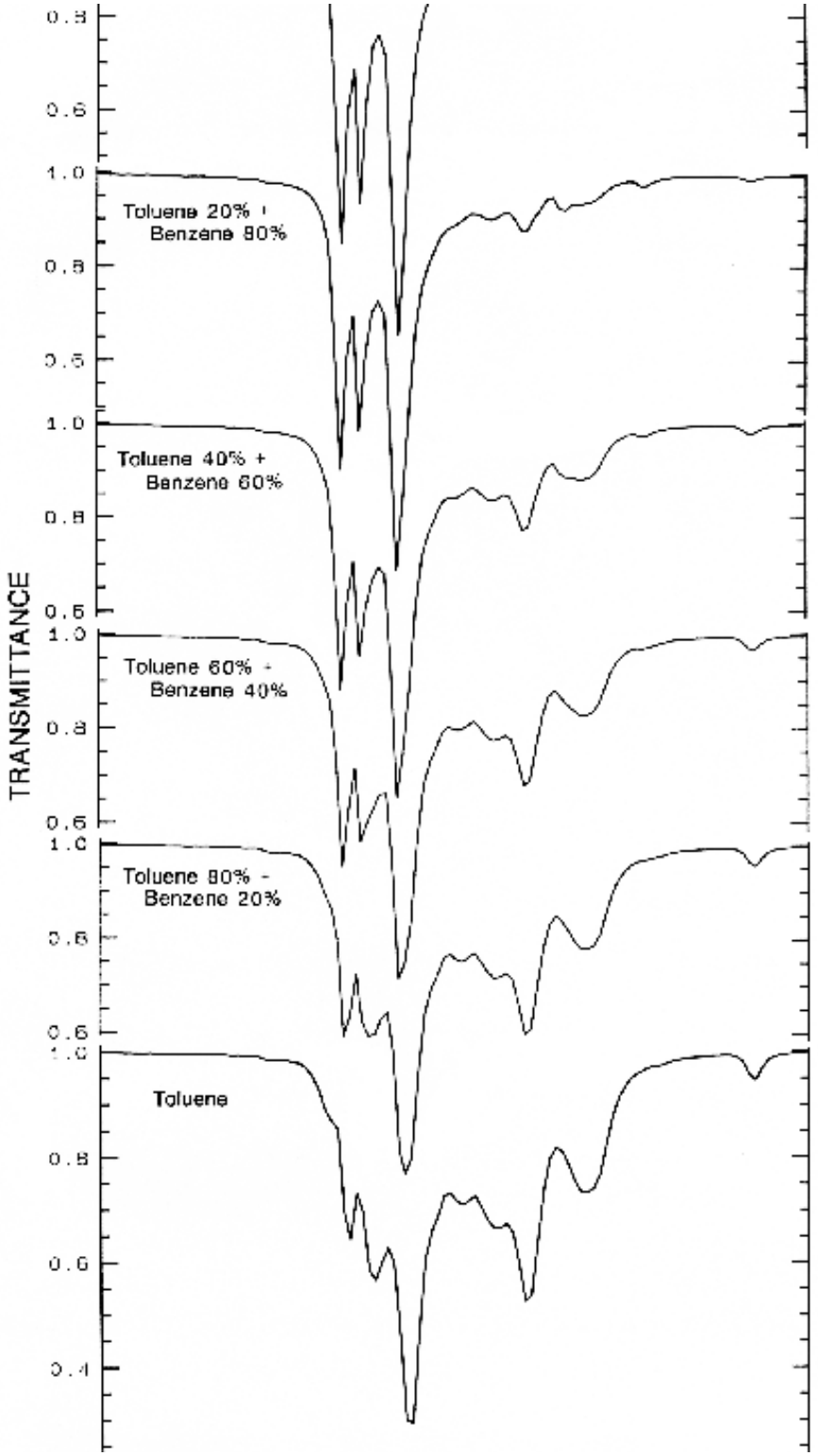

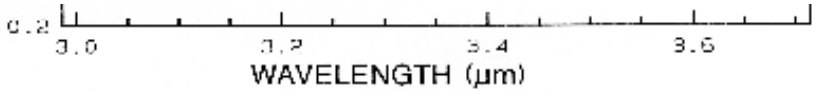

Figure 14b.

Figure 14b: 74k 100dpi gif

Figure 14b: 113k 200dpi gif

Figure 14b: 358k 300dpi gif

Figure 14b. Reflectance spectra of montmorillonite, and montmorillonite mixed with super unleaded gasoline, benzene, toluene, and trichlorethylene. Montmorillonite has an absorption feature at 2.2 μm, whereas the organics have a CH combination band near 2.3 μm. The first overtone of the CH stretch can be seen at 1.7 microns, and the second overtone near 1.15 μm. From King and Clark (1989b).

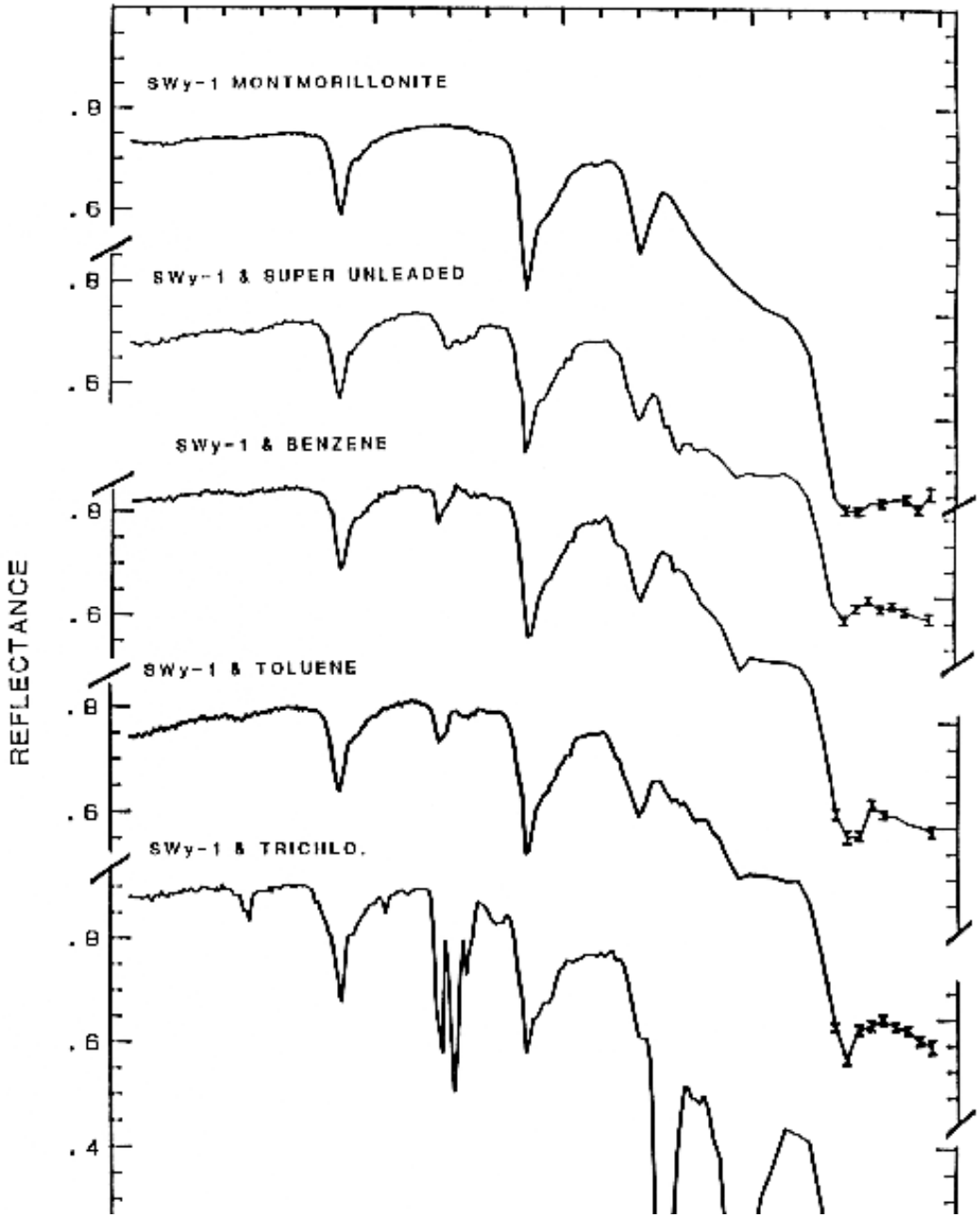

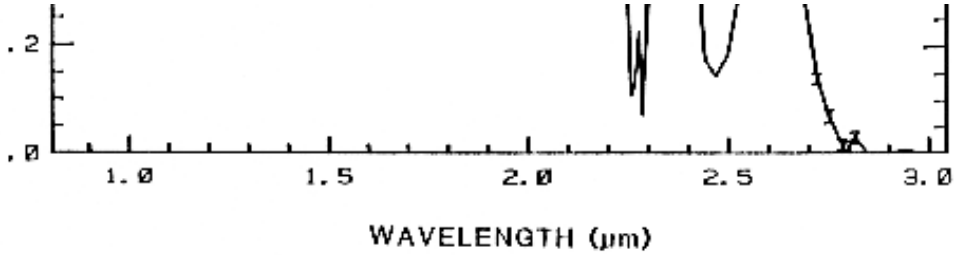

Back to Contents

4.2 Ices.

Just like water in minerals shows diagnostic absorption bands, ice (crystalline H_2O) which is formally a mineral, also shows strong absorption bands. In the planetary literature it is referred as water ice, so as not to confuse it with other ices. Spectra of solid H_2O, CO_2, and CH_4 are shown in Figure 15. The spectral features in Figure 15 are all due to vibrational combinations and overtones, whose fundamentals have previously been discussed in general. Note the H_2O spectra show broad absorptions compared to the others. The reason is that while ice is normally a hexagonal structure, the hydrogen bonds are orientationally disordered (e.g. Hobbs, 1974), and the disorder broadens the absorptions. There are many ices in the solar system (e.g. see reviews by Clark *et al.*, 1986, and Cruikshank *et al.*, 1985).

Ice, being ubiquitous in the solar system is found mixed with other minerals, on the Earth, as well as elsewhere in the solar system (e.g. Clark *et al.*, 1986). The spectral properties if ice and ice-mineral mixtures have been studied by Clark (1981a, b), Clark and Lucey (1984), Lucey and Clark (1985) and references therein.

Figure 15.

Figure 15: 40k 100dpi gif

Figure 15: 96k 200dpi gif

Figure 15: 236k 300dpi gif

Figure 15. Reflectance spectra of solid carbon dioxide, CO_2, methane, CH_4, and water, H_2O, from Clark *et al.* (1986).

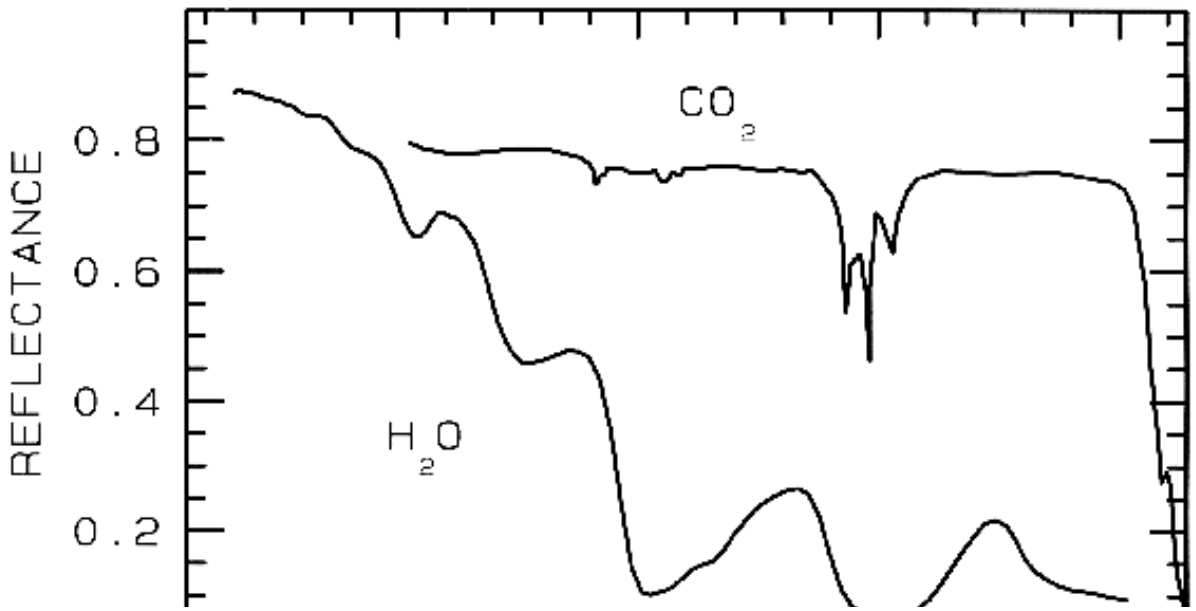

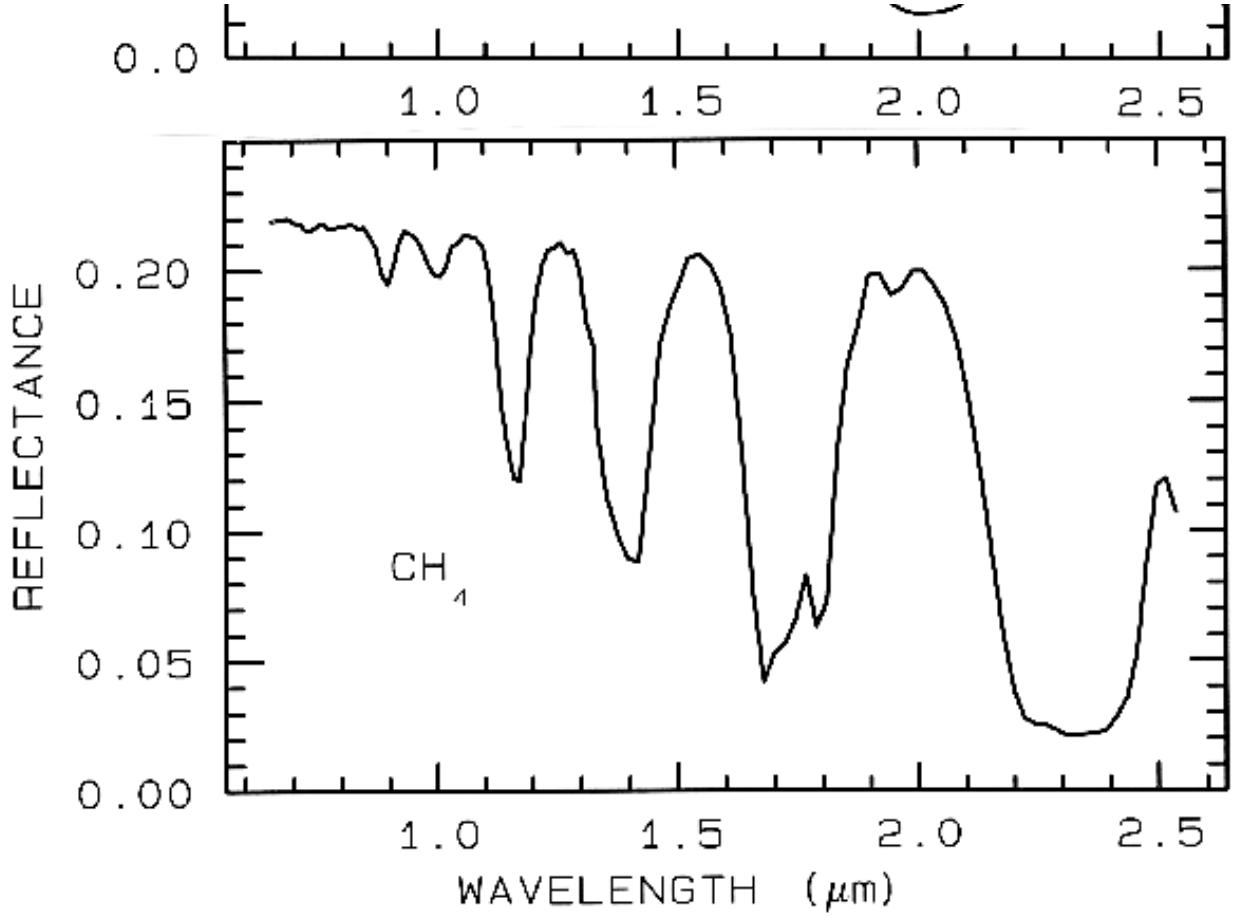

Back to Contents

4.3 Vegetation.

Spectra of vegetation come in two general forms: green and wet (photosynthetic), and dry non-photosynthetic but there is a seemingly continuous range between these two end members. The spectra of these two forms are compared to a soil spectrum in Figure 16. Because all plants are made of the same basic components, their spectra appear generally similar. However, in the spectral analysis section we will see methods for distinguishing subtle spectral details. The near-infrared spectra of green vegetation are dominated by liquid water vibrational absorptions. The water bands are shifted to slightly shorter wavelengths than in liquid water, due to hydrogen bonding. The absorption in the visible is due to chlorophyll, and is discussed in more detail in Chapter XX of Manual of Remote Sensing. The dry non-photosynthetic vegetation spectrum shows absorptions due to cellulose, lignin, and nitrogen. Some of these absorptions can be confused with mineral absorptions, unless a careful spectral analysis is done.

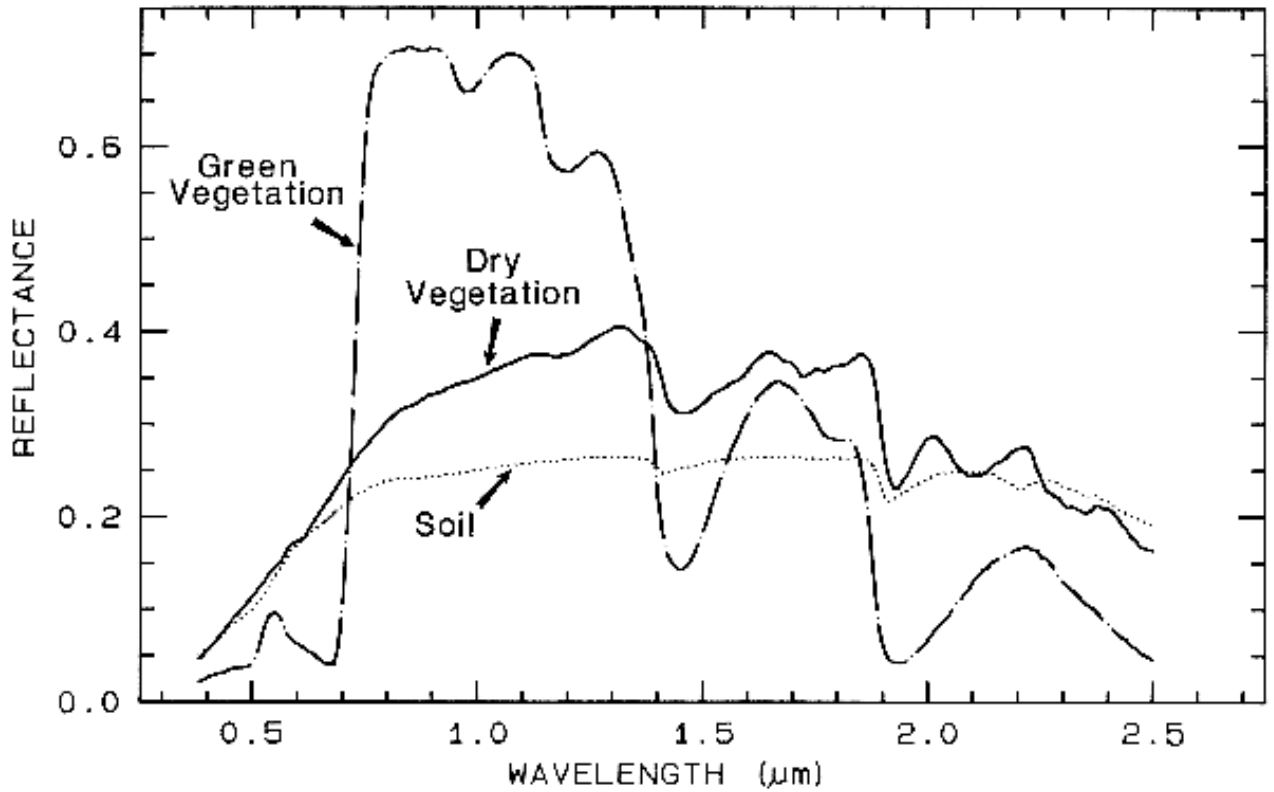

Figure 16.

Figure 16: 25k 100dpi gif

Figure 16: 82k 200dpi gif

Figure 16: 168k 300dpi gif

Figure 16. Reflectance spectra of photosynthetic (green) vegetation, non-photosynthetic (dry) vegetation, and a soil. The green vegetation has absorptions short of 1 μm due to chlorophyll. Those at wavelengths greater than 0.9 μm are dominated by liquid water. The dry vegetation shows absorptions dominated by cellulose, but also lignin and nitrogen. These absorptions must also be present in the green vegetation, but can be detected only weakly in the presence the stronger water bands. The soil spectrum shows a weak signature at 2.2 μm due to montmorillonite.

Back to Contents

5. THE SENSITIVITY OF ABSORPTION BANDS TO CRYSTAL STRUCTURE AND CHEMISTRY

Reflectance spectroscopy shows a wealth of information about mineralogy. Why, then, is spectroscopy not a more widely used technique? In many cases spectroscopy is very sensitive to subtle changes in crystal structure or chemistry. This has resulted in confusion in the past over cause and effect. More recently, this sensitivity has been recognized as a powerful means of studying the structure and composition of minerals. Additional problems occur with reflectance spectra due to scattering and will be discussed below.

Because spectroscopy is sensitive to so many processes, the spectra can be very complex and there is still much to learn. However, it is because of this sensitivity that spectroscopy has great potential as a diagnostic tool. In fact for some materials, spectroscopy is an excellent tool not only for detecting certain chemistries, but also at abundance levels unmatched by other tools. For example, each layer of a layered silicate absorbs radiation almost independently from its neighbors. The absorption of photons does not depend on the longer range crystallographic order as is required to give distinctive X-ray diffraction patterns. Thus, many processes, for example clay dehydroxylation, are detectable with spectroscopy before other methods (e.g. see Farmer, 1974, page 355). Spectroscopy is more sensitive to the presence of clays, iron oxides, iron hydroxides, quartz, and other minerals with strong absorption bands at levels significantly lower than other methods such as X-ray diffraction (e.g. Farmer, 1974, see page 355). Here, a few examples of the possibilities will be shown.

Back to Contents

5.1 Example: Pyroxenes. The iron bands near 1 and 2 µm shift with pyroxene composition as shown in Figure 6a, c. This series has been calibrated by Adams (1975), Cloutis *et al.* (1986), and Cloutis and Gaffey (1991). The olivine 1-µm band also shifts with composition (Figure 5a), although more subtly than with pyroxenes, and the shift has been calibrated by King and Ridley (1987). Note also the shifts, seen as positions of absorption minima and reflectance maxima, in the mid-infrared with different compositions in Figures 5b and 6b.

Back to Contents

5.2 OH Examples. The sharper OH-related absorption bands allow smaller band shifts to be measured. These bands can be so sensitive that it is possible to distinguish between the isochemical end-members of the Mg-rich serpentine group, chrysotile, antigorite, and lizardite (King and Clark, 1989a, and Figure 17). The Fe:Fe+Mg ratio can be estimated from reflectance spectra of minerals with brucite-like structure (Clark *et al*., 1990a, Mustard, 1992, and Figure 17). Mustard (1992) calibrated changes in the 1.4-µm and 2.3-µm absorptions in the tremolite-actinolite solid solution series; example spectra of the 1.4-µm absorptions are shown in Figure 17.

Figure 17.

Figure 17: 54k 100dpi gif

Figure 17: 244k 200dpi gif

Figure 17: 384k 300dpi gif

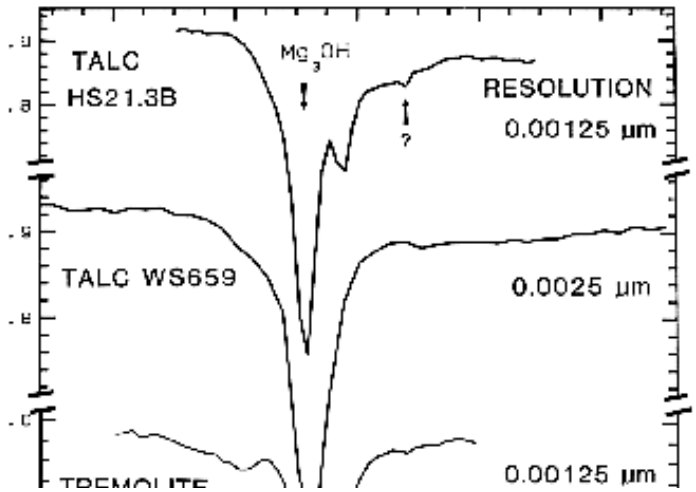

Figure 17. High spectral resolution reflectance spectra of the first overtone of OH in talc, tremolite, actinolite, crysotile, lizardite, and antigorite. The three sharp absorption bands in talc, tremolite and actinolite are caused by Mg and Fe ions associated with the hydroxyls, causing small band shifts. The Fe:Fe+Mg ratio can be estimated. In chrysotile, lizardite and antigorite, the absorptions change with small structural differences even though the composition is constant (from Clark *et al*., 1990a).

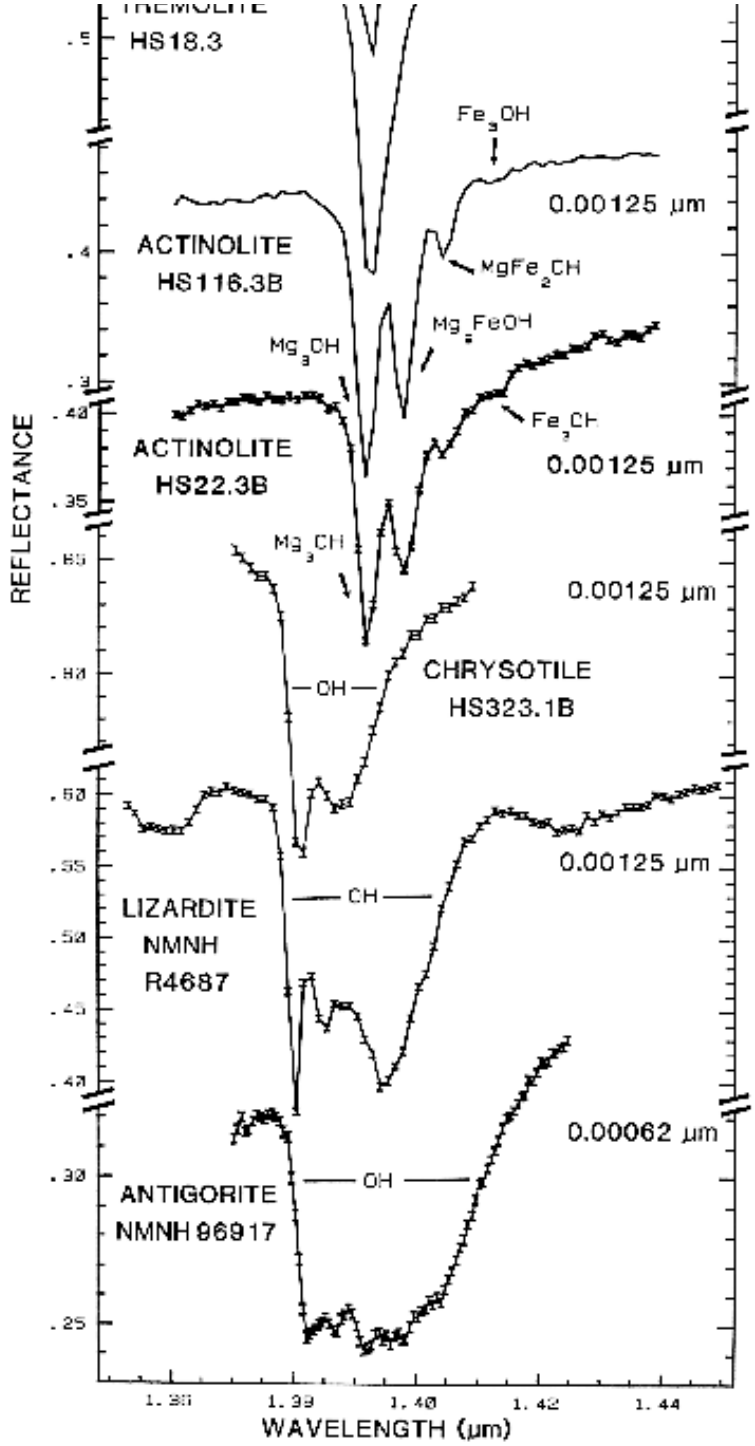
HS18.3
Fe3OH
0.00125 µm
ACTINOLITE
HS116.3B
MgFe2OH
Mg3FeOH
Mg3OH
Fe3OH
ACTINOLITE
HS22.3B
0.00125 µm
Mg3OH
0.00125 µm
OH
CHRYSOTILE
HS323.1B
0.00125 µm
CH
LIZARDITE
NMNH
R4687
0.00062 µm
OH
ANTIGORITE
NMNH 96917
REFLECTANCE
.5
.4
.45
.40
.35
.85
.80
.60
.55
.50
.45
.40
.30
.25
1.38
1.39
1.40
1.42
1.44
WAVELENGTH (µm)

The structure of the 2.2-µm Al-OH band has been shown to be diagnostic of disorder in kaolinite-dickite mixtures (Crowley *et al*., 1988) and the degree of kaolinite crystallinity (Clark *et al*., 1990a), which is illustrated in Figures 10c, d.

The strong and sharp OH features have proven particularly diagnostic of clay mineralogy, perhaps better than with X-ray diffraction (XRD) analysis (like any method, spectroscopy has advantages in some areas and XRD in others). For example, it appears easy to distinguish kaolinite from halloysite with spectroscopy (e.g. Clark *et al*., 1990a), as shown in Figures 10c, d. Montmorillonite is easily distinguished from illite or muscovite (e.g. Clark *et al*., 1990a) whereas XRD analysis combines them into the general term smectites.

Back to Contents

5.3 Al in Muscovite. More recently, subtle shifts have been found in muscovite series with aluminum composition. (e.g. Post and Noble, 1993; Duke, 1995; Swayze, 1997). As elements substitute for aluminum in the crystal structure, the crystal becomes slightly distorted relative to no substitutions. This causes slight changes in Al-O-H bond lengths and thus shifts absorption band position. Example shifts with composition are shown in Figure 18. In this case, the shift of the 2.2-µm absorption appears continuous with composition, compared to the growth of specific absorptions as in the tremolite-actinolite series shown in Figure 17. It is likely that all muscovite-group minerals show similar behavior, and illites may also.

Figure 18.

Figure 18: 26k 100dpi gif

Figure 18: 89k 200dpi gif

Figure 18: 202k 300dpi gif

Figure 18. Reflectance spectra of muscovite showing band shifts due to changing aluminum composition, from Swayze (1997).

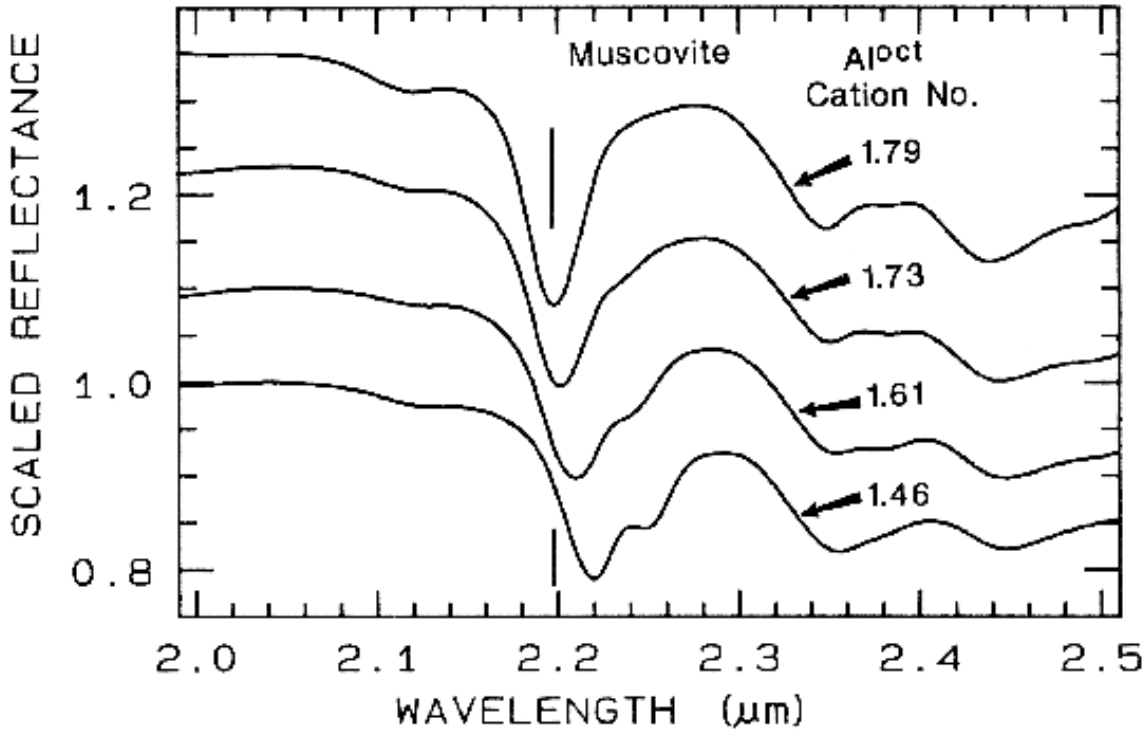

Back to Contents

5.4 Discussion. Reflectance spectroscopy can be used without sample preparation, and it is non-destructive. This makes mapping of exposed minerals from aircraft possible, including detailed clay mineralogy (e.g. Clark *et al*., 1993a). Visual and near-infrared spectroscopy, on the other hand, is insensitive to some minerals which do not have absorptions in this wavelength region. For example, quartz has no diagnostic spectral features in the visible and near-infrared; in fact it is used as optical components in many telescopes and prisms. Quartz must be detected at its fundamental Si-O stretching region near 10 μm., as shown in Figure 4b.

Now that we have explored the causes of absorption features in minerals, we will explore how those features get modified.

Back to Contents

6. THE SCATTERING PROCESS.

Scattering is the process that makes reflectance spectroscopy possible: photons enter a surface, are scattered one or more times, and while some are absorbed, others are scattered from the surface so that we may see and detect them. Scattering can also be thought of as scrambling information. The information is made more complex, and because scattering is a non-linear process, recovery of quantitative information is more difficult.

Consider the simple Beers Law in equation 1b. In transmission, light passes through a slab of material. There is little or no scattering (none in the ideal case; but there are always internal reflections from the surfaces of the medium). Analysis is relatively simple. Reflectance of a particulate surface, however, is much more complex and the optical path of photons is a random walk. At each grain the photons encounter, a certain percentage are absorbed. If the grain is bright, like a quartz grain at visible wavelengths, most photons are scattered and the random walk process can go on for hundreds of encounters. If the grains are dark, like magnetite, the majority of photons will be absorbed at each encounter and essentially all photons will be absorbed in only a few encounters. The random walk process, scattering and the mean depth of photon penetration are discussed in Clark and Roush (1984).

The random walk process of photons scattering in a particulate surface also enhances weak features not normally seen in transmittance, further increasing reflectance spectroscopy as a diagnostic tool. Consider two absorption bands of different strengths, such as a fundamental and an overtone. The stronger absorption will penetrate less into the surface, encountering fewer grains because the photons are absorbed. At the wavelengths of the weaker absorption, less photons are absorbed with each encounter with a grain, so the random walk process goes further, increasing the average photon path length. The greater path length will result in more absorption, thus strengthening the weak absorption in a reflectance spectrum.

Back to Contents

6.1 Mixtures.

The real world (and for that matter, the universe) is a complex mixture of materials, at just about any scale we view it. In general, there are 4 types of mixtures:

1) *Linear Mixture*. The materials in the field of view are optically separated so there is no multiple scattering between components. The combined signal is simply the sum of the fractional area times the spectrum of each component. This is also called areal mixture.

2) *Intimate Mixture*. An intimate mixture occurs when different materials are in intimate contact in a scattering surface, such as the mineral grains in a soil or rock.

Depending on the optical properties of each component, the resulting signal is a highly non-linear combination of the end-member spectra.

3) *Coatings*. Coatings occur when one material coats another. Each coating is a scattering/transmitting layer whose optical thickness varies with material properties and wavelength.

4) *Molecular Mixtures*. Molecular mixtures occur on a molecular level, such as two liquids, or a liquid and a solid mixed together. Examples: water adsorbed onto a mineral; gasoline spilled onto a soil. The close contact of the mixture components can cause band shifts in the adsorbate, such as the interlayer water in montmorillonite, or the water in plants.

An example mixture comparison is shown in Figure 19 for alunite and jarosite. Note in the intimate mixture how the jarosite dominates and the 0.4 to 1.3-µm region. The reason is because in an intimate mixture, the darker material dominates because photons are absorbed when they encounter a dark grain. In the areal mixture, the brighter material dominates.

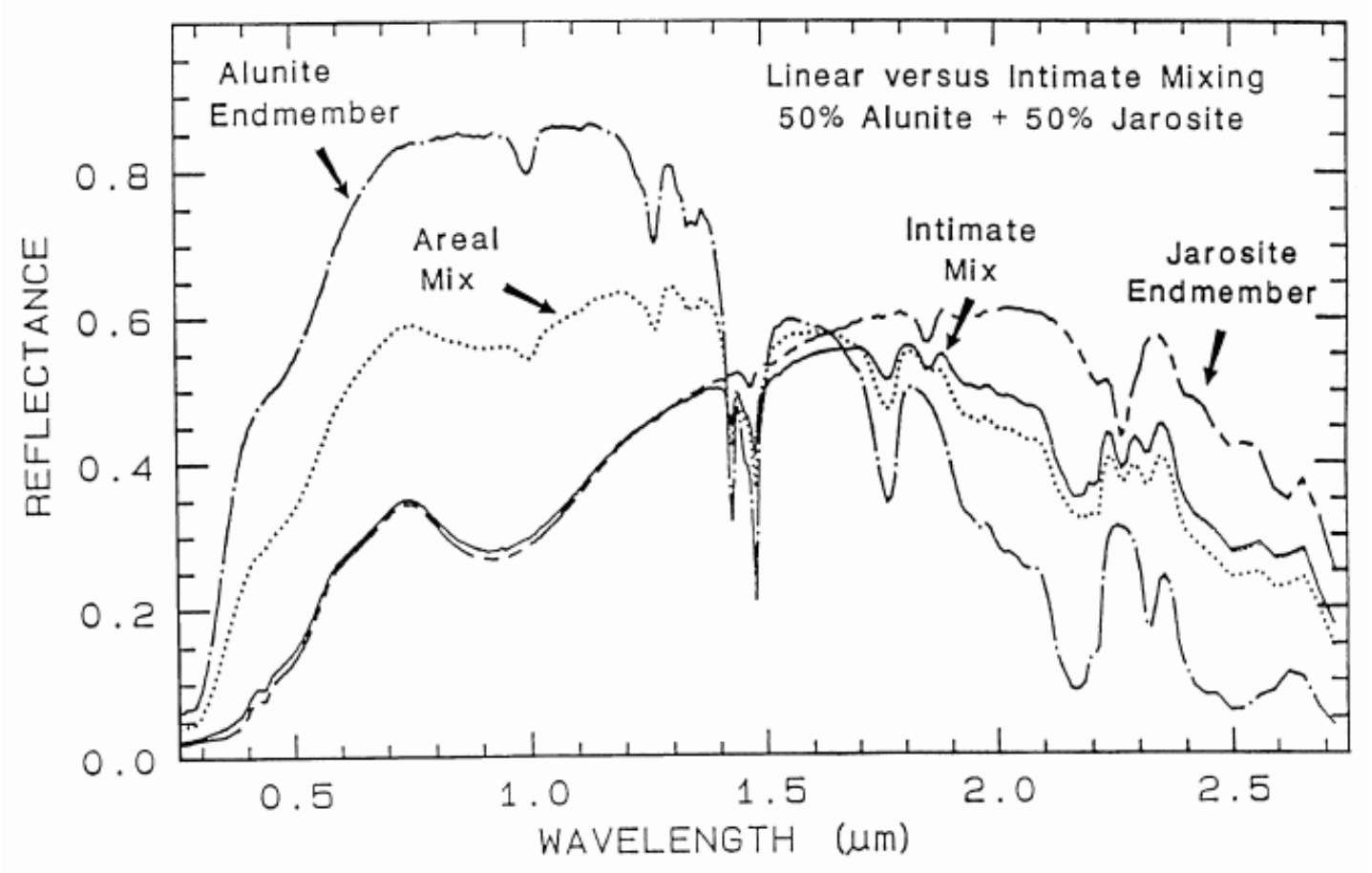

Figure 19.

Figure 19: 36k 100dpi gif

Figure 19: 171k 200dpi gif

Figure 19: 220k 300dpi gif

Figure caption foes here

Figure 19. Reflectance spectra of alunite, jarosite and mixtures of the two. Two mixture types are shown: intimate and areal. In the intimate mixture, the darker of the two spectral components tends to dominate, and in and areal mixture, the brighter component dominates. The areal mixture is a strictly linear combination and was computed from the end-members, whereas the intimate mixture is non-linear and the spectrum of the physical mixture was measured in the laboratory. The jarosite dominates the 0.3-1.4 µm wavelength region in the intimate mixture because of the strong absorption in jarosite at those wavelengths and because the jarosite is finer grained than the alunite and tends to coat the larger alunite grains.

In a mixture of light and dark grains (e.g. quartz and magnetite) the photons have such a high probability of encountering a dark grain that a few percent of dark grains can drastically reduce the reflectance, much more than their weight fraction. The effect is illustrated in Figure 20 with spectra of samples having various proportions of charcoal grains mixed with montmorillonite.

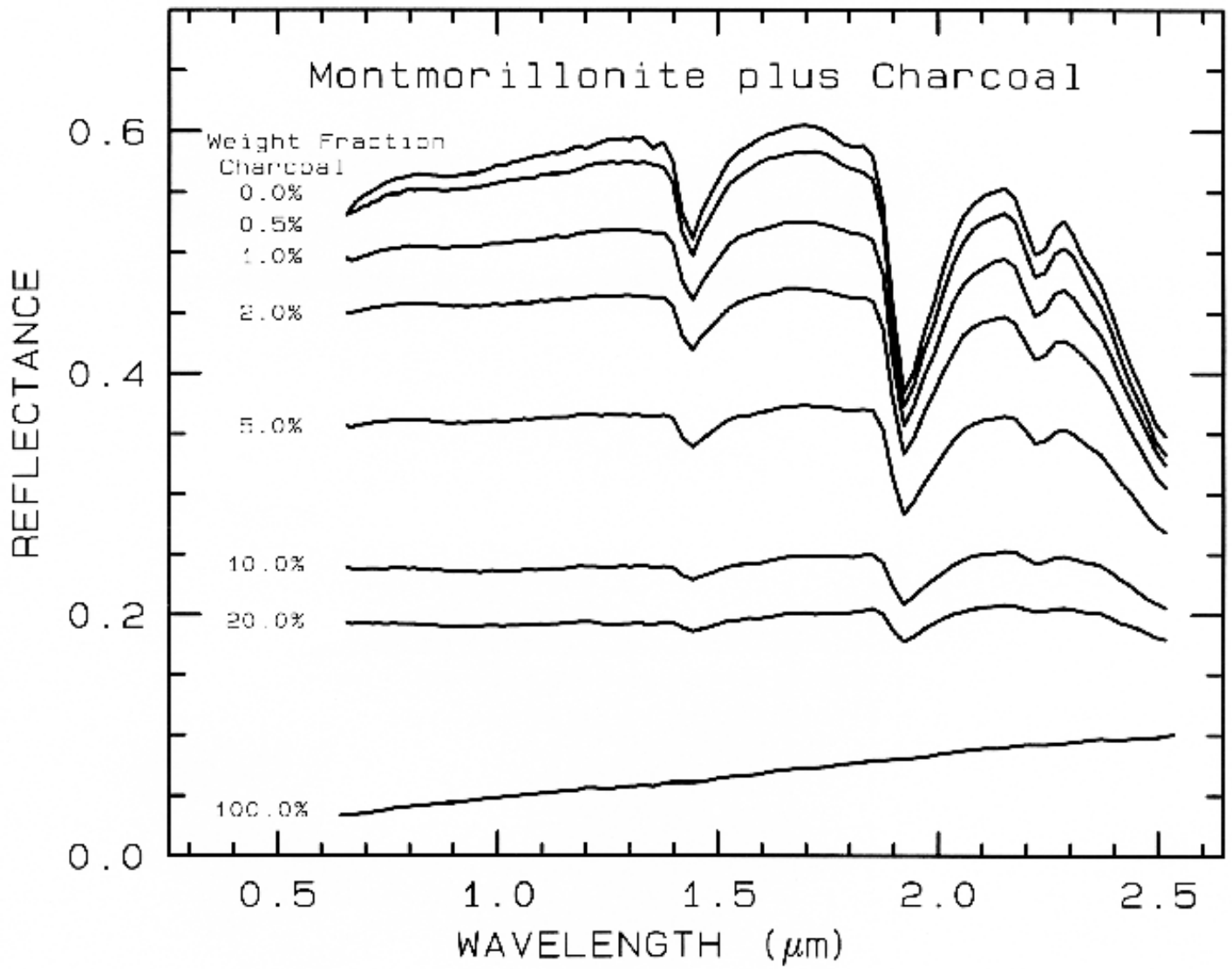

Figure 20.

Figure 20: 56k 100dpi gif

Figure 20: 136k 200dpi gif

Figure 20: 696k 300dpi gif

Figure 20. Reflectance spectra of intimate mixtures of montmorillonite and charcoal illustrates the non-linear aspect of reflectance spectra of mixtures, from Clark (1983). The darkest substance dominates at a given wavelength.

Back to Contents

6.2 Grain Size Effects.

The amount of light scattered and absorbed by a grain is dependent on grain size (e.g. Hapke, 1993; Clark and Roush, 1984; and Figures 21 and 22). A larger grain has a greater internal path where photons may be absorbed according to Beers Law. It is the reflection from the surfaces and internal imperfections that control scattering. In a smaller grain there are proportionally more surface reflections compared to internal photon path lengths, or in other words, the surface-to-volume ratio is a function of grain size. If multiple scattering dominates, as is usually the case in the visible and near- infrared, the reflectance decreases as the grain size increases, as shown in the pyroxene visible to near-infrared spectra in Figure 21a. However, in the mid-infrared, where absorption coefficients are much higher and the index of refraction varies strongly at the Christensen frequencies, first surface reflection is a larger or even dominant component of the scattered signal. In these cases, the grain size effects are much more complex, even reversing trends commonly seen at shorter wavelengths (e.g. Figure 21b).

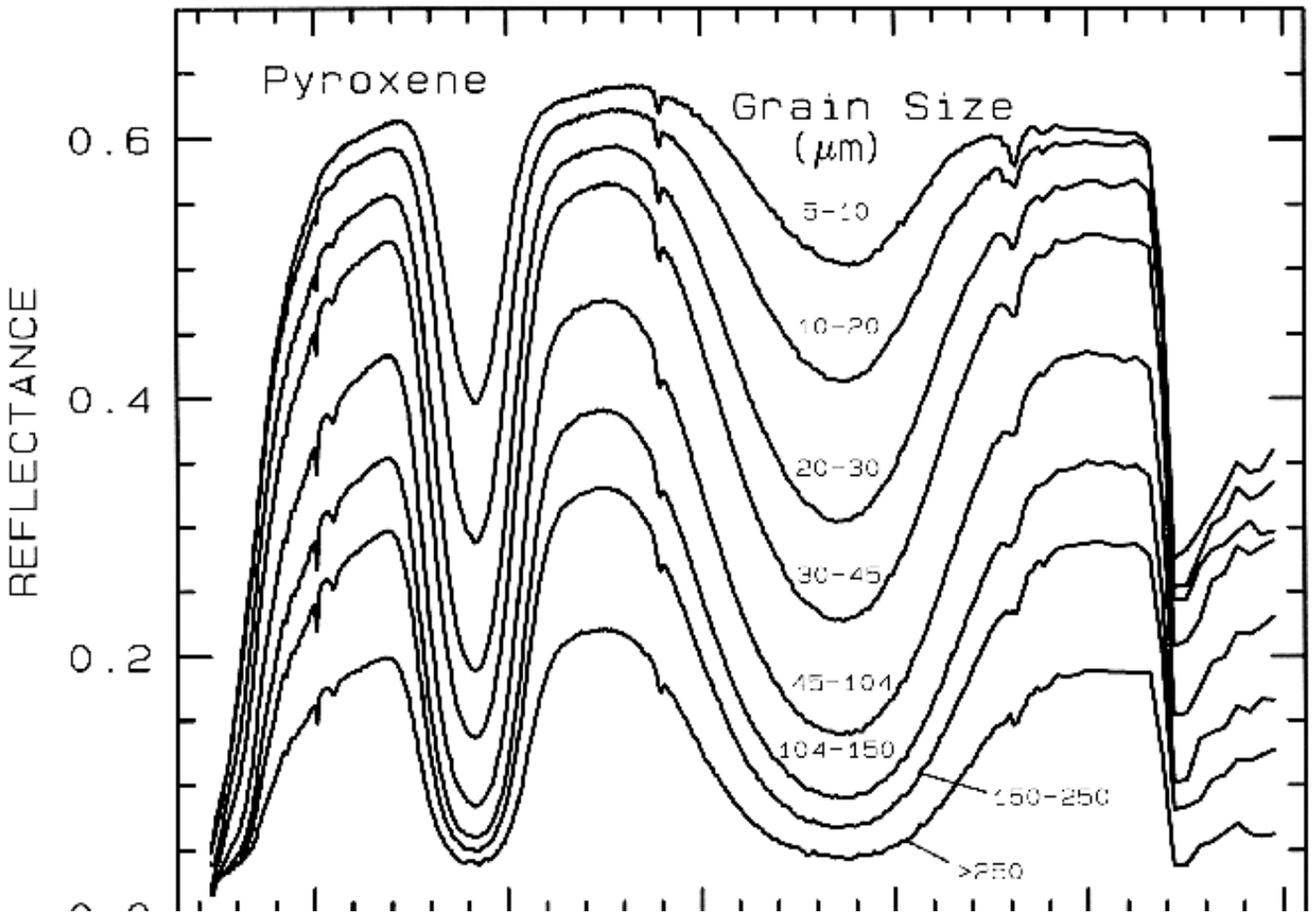

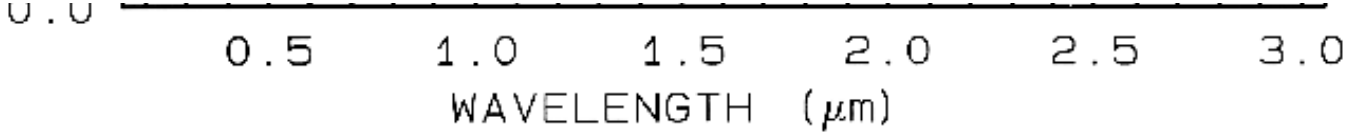

Figure 21a.

Figure 21a: 98k 100dpi gif

Figure 21a: 154k 200dpi gif

Figure 21a: 333k 300dpi gif

Figure 21a. Reflectance Spectra of pyroxene as a function of grain size. As the grain size becomes larger, more light is absorbed and the reflectance drops (from Clark *et al.*, 1993b).

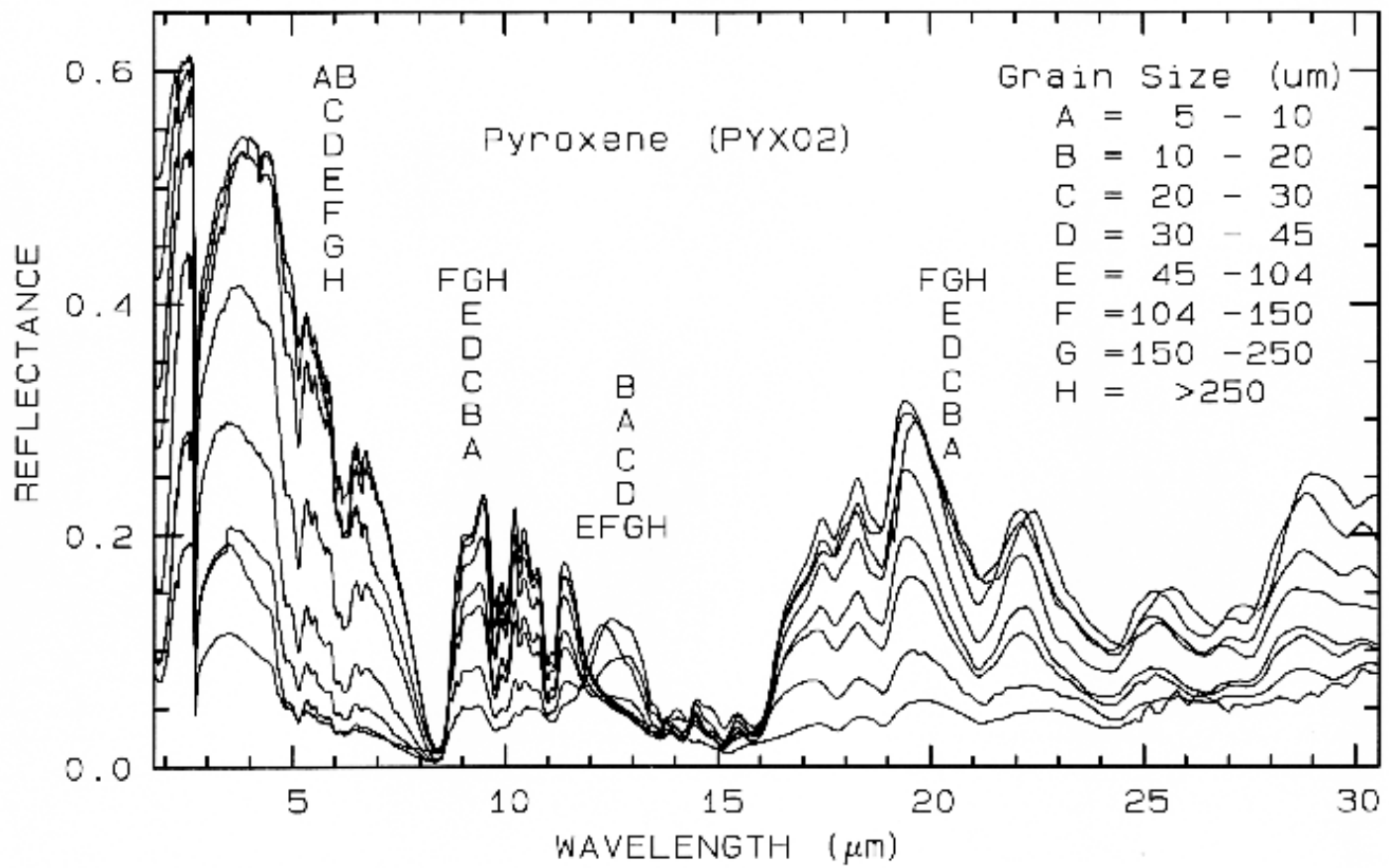

Figure 21b.

Figure 21b: 147k 100dpi gif

Figure 21b: 200k 200dpi gif

Figure 21b: 1022k 300dpi gif

Figure 21b. Same series as in Figure 21a, but for the mid-IR. The position of letter identifiers indicates the relative position of the spectra at the various wavelengths. Note the reversal in the trends at some wavelengths and not others. Grain size effects on the shapes of spectral features in the mid-IR can be quite large.

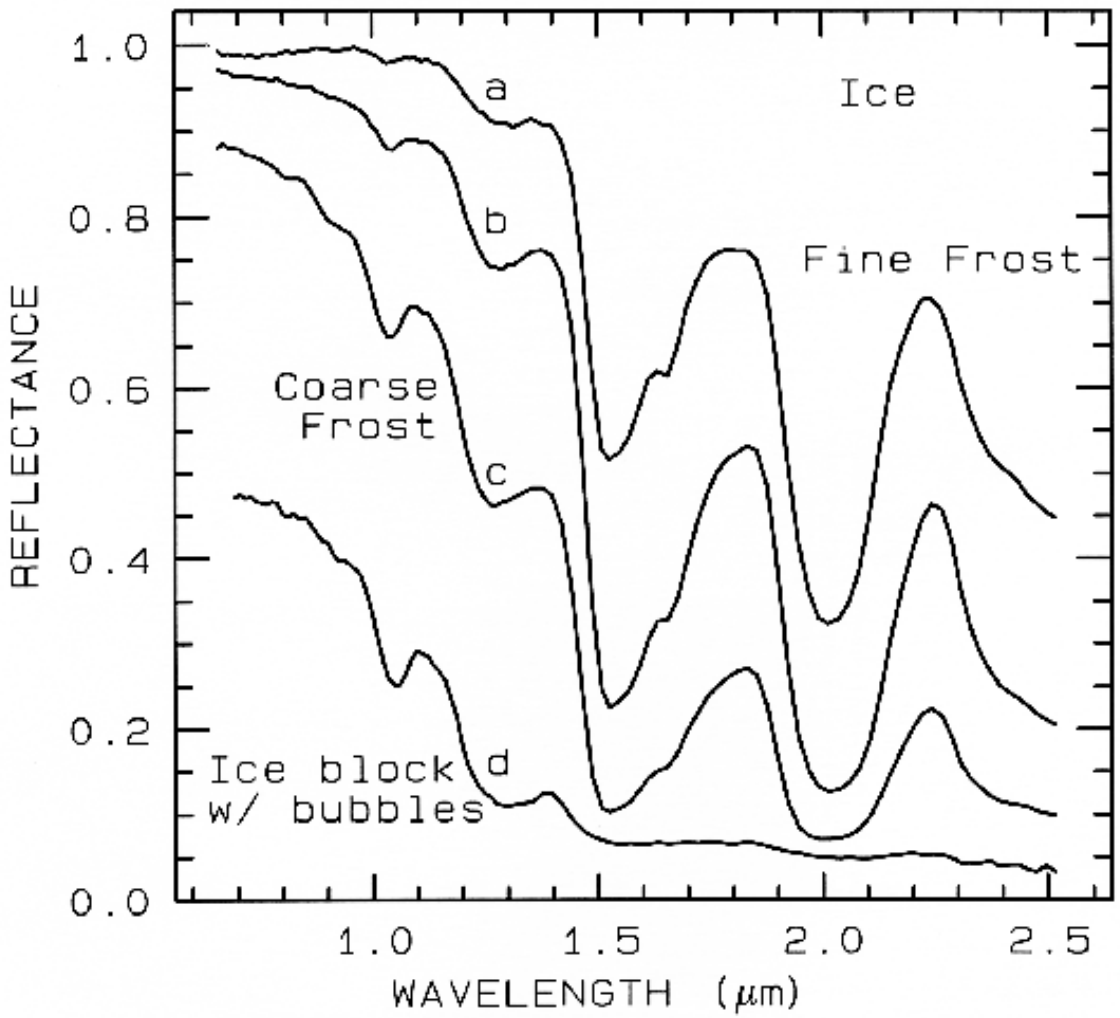

Figure 22a.

Figure 22a: 77k 100dpi gif

Figure 22a: 345k 200dpi gif

Figure 22a: 555k 300dpi gif

Figure 22a. The near-infrared spectral reflectance of A) a fine grained (~50 µm) water frost, B) medium grained (~200 µm) frost, C) coarse grained (400-2000 µm) frost and D) an ice block containing abundant microbubbles. The larger the effective grain size, the greater the mean photon path that photons travel in the ice, and the deeper the absorptions become. Curve D is very low in reflectance because of the large path length in ice. The ice temperatures for these spectra are 112-140 K. From Clark *et al*. (1986).

Figure 22b.

Figure 22b: 90k 100dpi gif

Figure 22b: 106k 200dpi gif

Figure 22b: 227k 300dpi gif

Figure 22b. A series of reflectance spectra of melting snow. The top curve (a) is at 0º C and has only a small amount of liquid water, whereas the lowest spectrum (j) is of a puddle of about 3 cm of water on top of the snow. Note in the top spectrum, there is no 1.65-µm band as in the ice spectra in figure 22a because of the higher temperature.. The 1.65-µm feature is temperature dependent and decreases in strength with increasing temperature (see Clark, 1981a and references therein). Note the increasing absorption at about 0.75 µm and in the short side of the 1-µm ice band, as more liquid water forms. The liquid water becomes spectrally detectable at about spectrum e, when the UV absorption increases. Spectra from Clark, King and Swayze, in preparation.

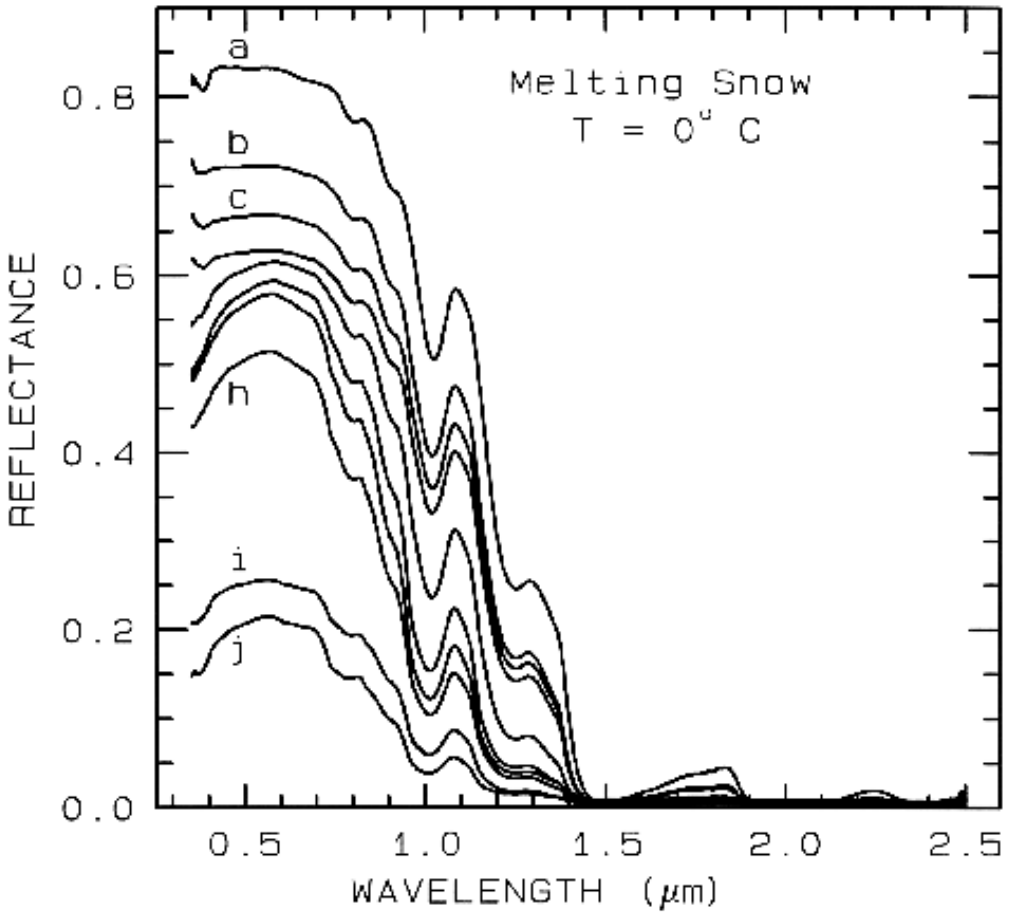

Back to Contents

6.3 The Continuum and Band Depth.

Absorptions in a spectrum have two components: continuum and individual features. The continuum is the "background absorption" onto which other absorption features are superimposed (e.g. see Clark and Roush, 1984). It may be due to the wing of a larger absorption feature. For example, in the pyroxene spectra in Figure 21a, the weak feature at 2.3 µm is due to a trace amount of tremolite in the sample and the absorption is superimposed on the broader 2-µm pyroxene band. The broader pyroxene absorption is the continuum to the narrow 2.3-µm feature. The pyroxene 1.0-µm band is superimposed on the wing of a stronger absorption centered in the ultraviolet.

The depth of an absorption band, D, is usually defined relative to the continuum, R_c:

$D = 1 - R_b / R_c$ (2)

where R_b is the reflectance at the band bottom, and R_c is the reflectance of the continuum at the same wavelength as R_b (Clark and Roush, 1984).

The depth of an absorption is related to the abundance of the absorber and the grain size of the material. Consider a particulate surface with two minerals, one whose spectrum has an absorption band. As the abundance of the second mineral is increased, the band depth, D, of the absorption in the first mineral will decrease. Next consider the visual and near-infrared reflectance spectrum of a pure powdered mineral. As the grain size is increased from a small value, the absorption-band depth, D, will first increase, reach a maximum, and then decrease. This can be seen with the pyroxene spectra in Figure 21a and more so in the ice spectra in Figure 22. If the particle size were made larger and larger, the reflectance spectrum would eventually consist only of first surface reflection, like at most wavelengths beyond 1.45 µm in the ice spectra in Figure 22. The reflectance can never go to zero because of this reflection, unless the index of refraction of the material is 1.0. These concepts, called "band saturation" are explored further in Clark and Lucey (1984) and Lucey and Clark (1985).

A sloping continuum causes an apparent shift in the reflectance minimum, as shown in Figure 23. Continuaa can be thought of as an additive effect of optical constants, but in reflectance spectra, scattering and Beers Law make the effects non-linearly multiplicative (see Clark and Roush, 1984 for more details). So the continuum should be removed by division, whether you are working in reflectance or emittance. The continuum should be removed by subtraction only when working with absorption coefficients. In a spectrum with a sloping continuum, correction removes the effect of shifts in the local reflectance minimum (Figure 23). Note your perception of spectrum E versus A in Figure 23. The spectral features do not appear to be the same, but if you remove the continuum, it is obvious they are the same (Figure 23, top).

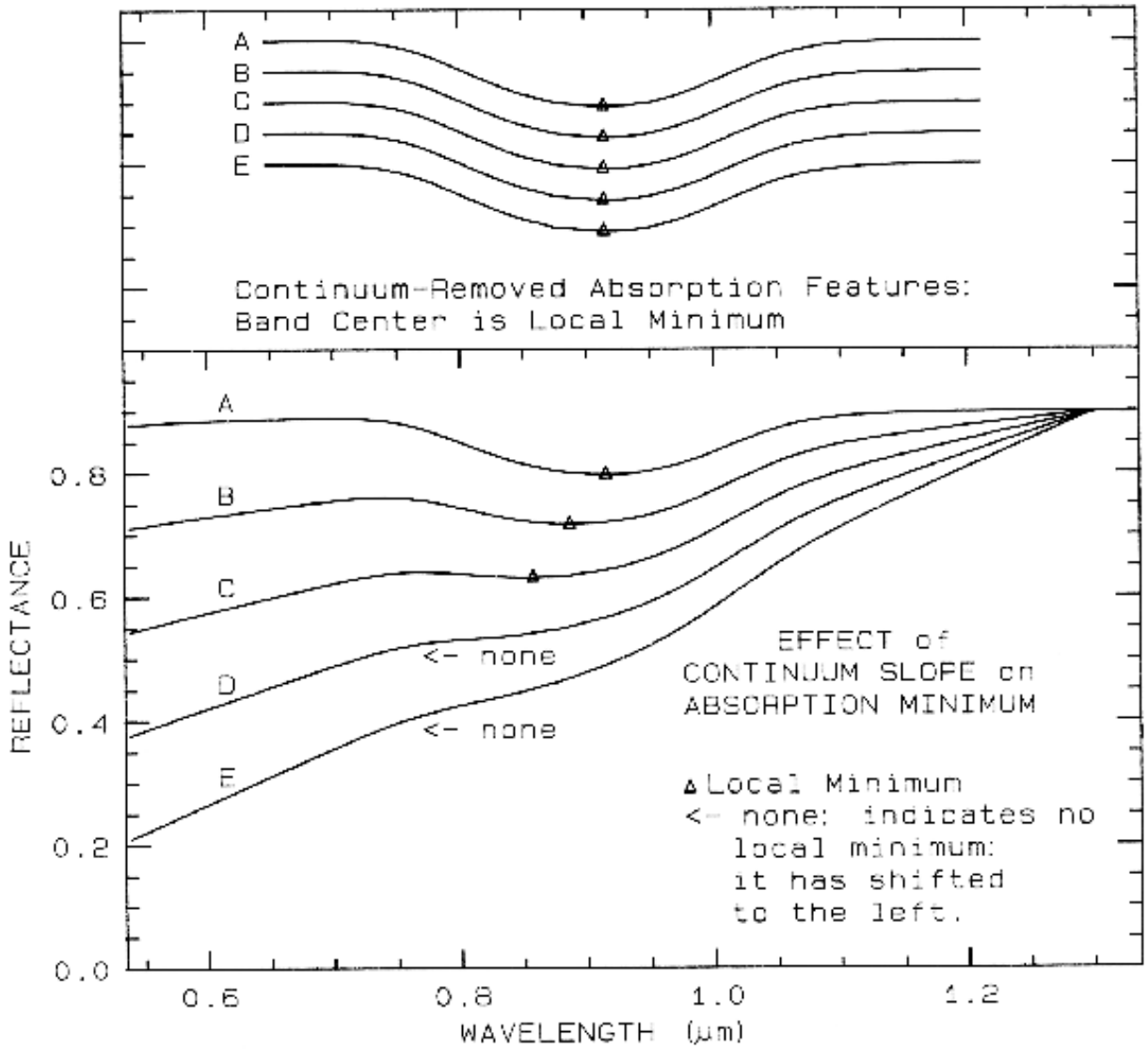

Figure 23.

Figure 23: 38k 100dpi gif

Figure 23: 527k 200dpi gif

Figure 23: 287k 300dpi gif

Figure 23. Illustration of continua and continuum removal. In the lower set of curves, the local minimum in the curve shifts to shorter wavelengths with increasing slope. removal of the continuum by division isolates the spectral features so they may be compared (top). The top set of curves are offset for clarity. In the continuum-

removed spectra, we can see there is no real shift in the absorption-band center.

Back to Contents

6.4 Continuum-Removed Spectral Feature Comparison.

The continuum-removal process isolates spectral features and puts them on a level playing field so they may be intercompared. Continuum removal and feature comparison, is in this author's opinion, the key to successful spectral identification. For example, compare the spectra of calcite ($CaCO_3$) and dolomite ($CaMg(CO_3)_2$) in Figure 10a. If we isolate the spectral features, remove the continuum, and scale the band depth (or band area) to be equal, we can see subtle band shifts and shapes (Figure 24a). Now compare a harder case: halloysite and kaolinite (Figure 10c). You might note that halloysite has a different absorption feature at 1.9 µm. However, if you were obtaining the spectrum through the Earth's atmosphere, you would have virtually no data in that wavelength region because atmospheric water absorbs too much of the signal. The diagnostic feature is the 2.2-µm band. The continua removed 2.2-µm features for halloysite and kaolinite are shown in Figure 24b, where we can see significant differences between the spectra of the two minerals.

Figure 24a.

Figure 24a: 20k 100dpi gif

Figure 24a: 65k 200dpi gif

Figure 24a: 128k 300dpi gif

Figure 24a. Comparison of calcite and dolomite continuum-removed features. The dolomite absorption occurs at a shorter wavelength than the calcite absorption.

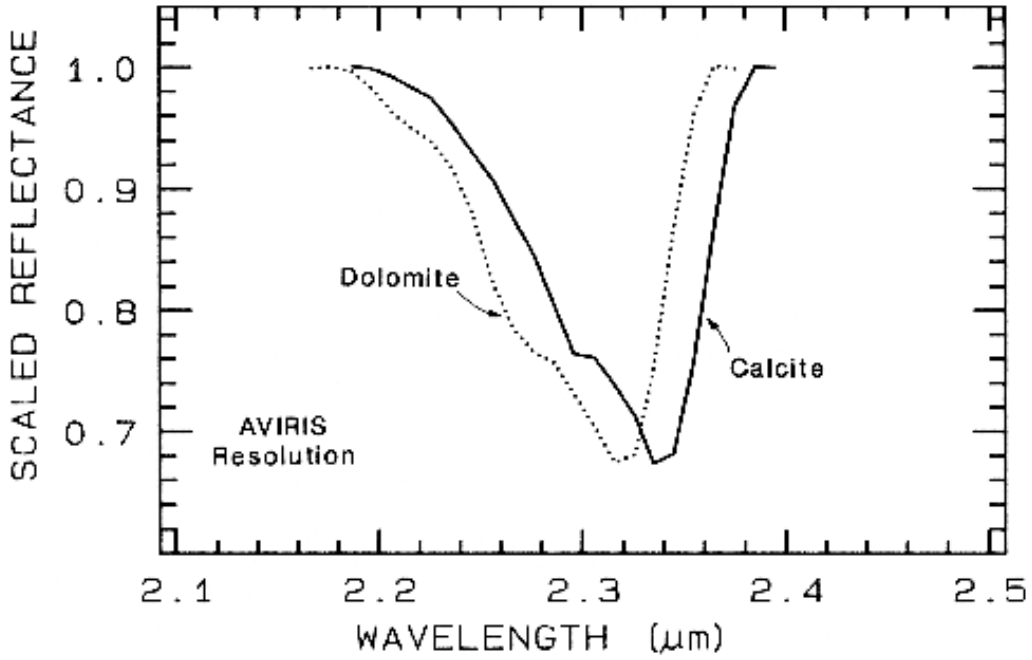

Figure 24b.

Figure 40b: 20k 100dpi gif

Figure 24b: 72k 200dpi gif

Figure 24b: 169k 300dpi gif

Figure 24b. Comparison of kaolinite and halloysite spectral features. Both mineral spectra have the same band position at 2.2 µm. However, the kaolinite spectrum shows a stronger feature at 2.16 µm than in the halloysite spectrum.

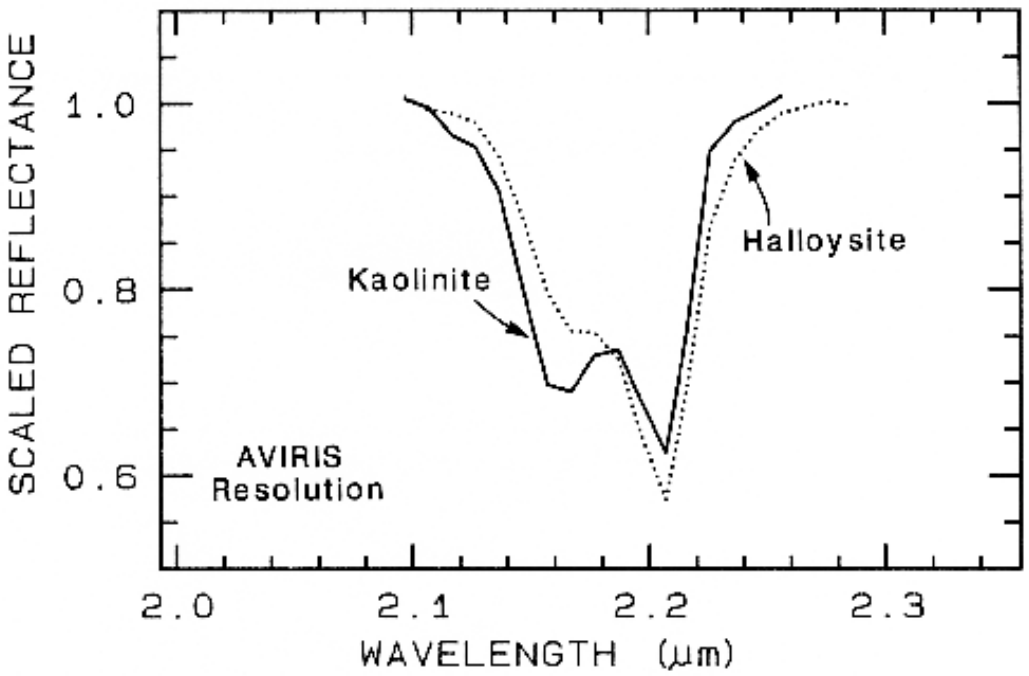

One of the most challenging spectral features to distinguish between are those in spectra of various plant species. Figure 25a shows four plant spectra (the spectra are offset for clarity). The overall shapes are quite similar. If we remove the continuum according to Figure 25b, we see the detailed chlorophyll absorption spectral variations for these as well as other plants in Figure 25c. Shape matching algorithms, like that presented in Clark *et al*. (1990b), can distinguish between these spectra and accurately compare them to spectral libraries (e.g. see Clark *et al*., 1993b, Mustard and Sunshine, Chapter 6).

Figure 25a.

Figure 25a: 35k 100dpi gif

Figure 25a: 120k 200dpi gif

Figure 25a: 391k 300dpi gif

Figure caption foes here

Figure 25a. Reflectance spectra of four types of vegetation. Each curve is offset by 0.05 reflectance unit from the one below. From Clark *et al*. (1995, 1997).

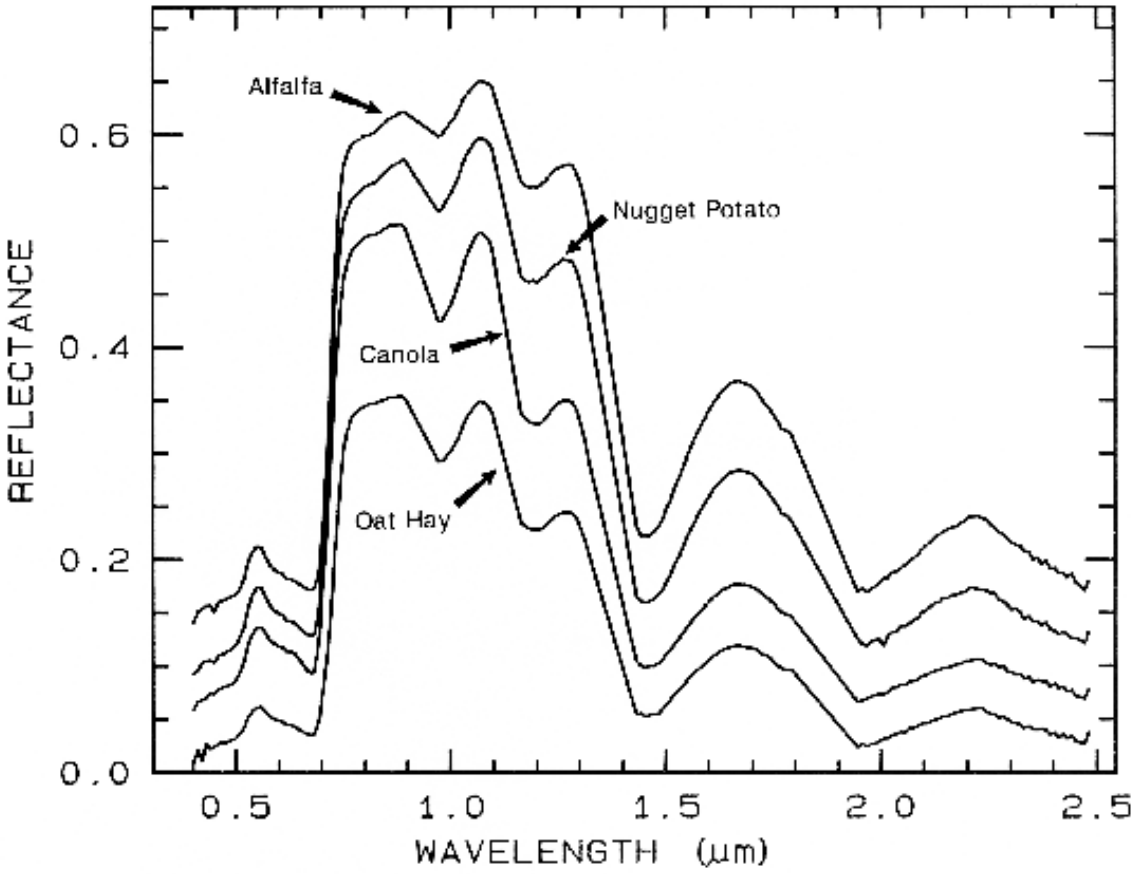

Figure 25b.

Figure 25b: 33k 100dpi gif

Figure 25b: 384k 200dpi gif

Figure 25b: 473k 300dpi gif

Figure 25b. Continuum removal example for a chlorophyll absorption in vegetation.

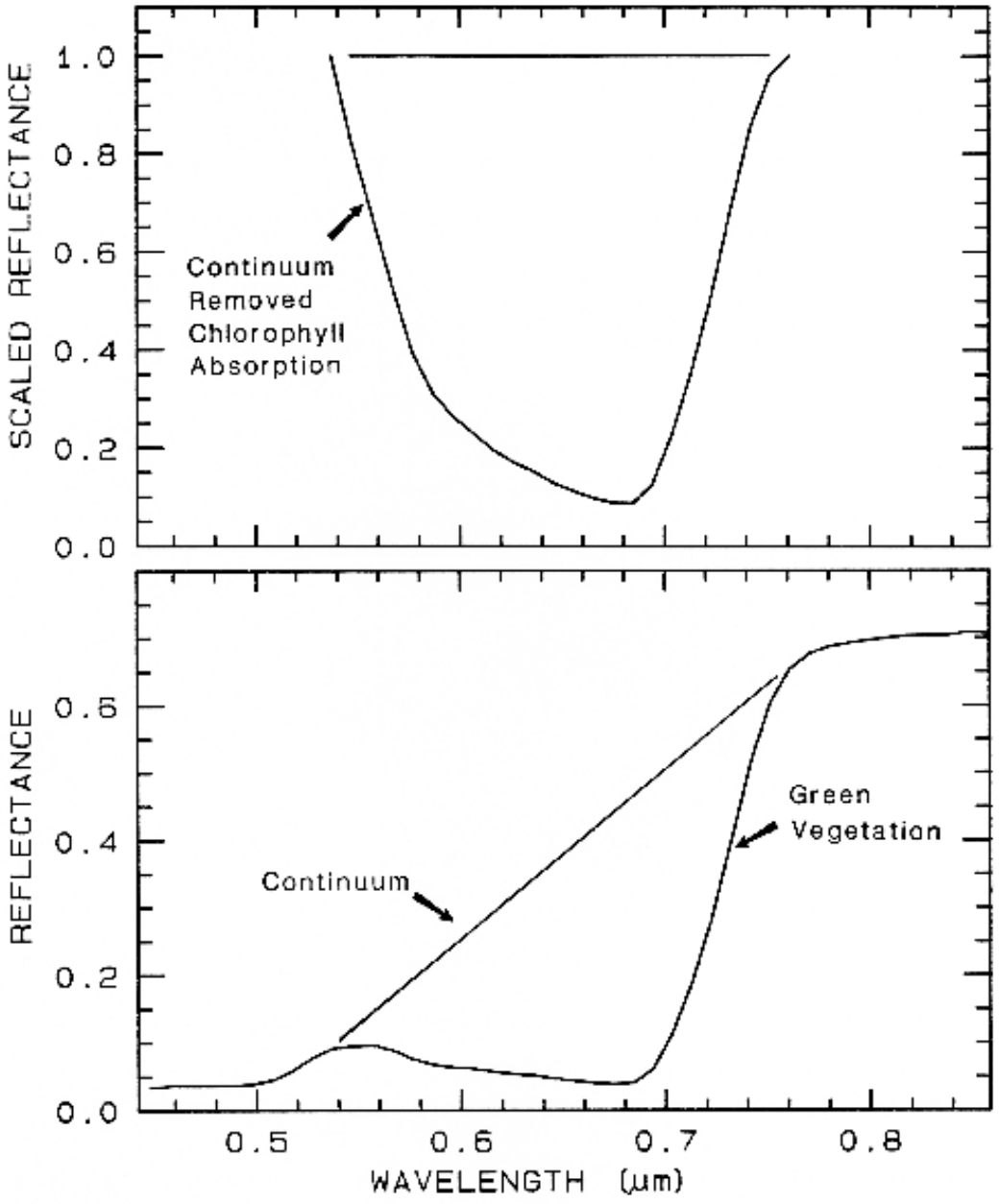

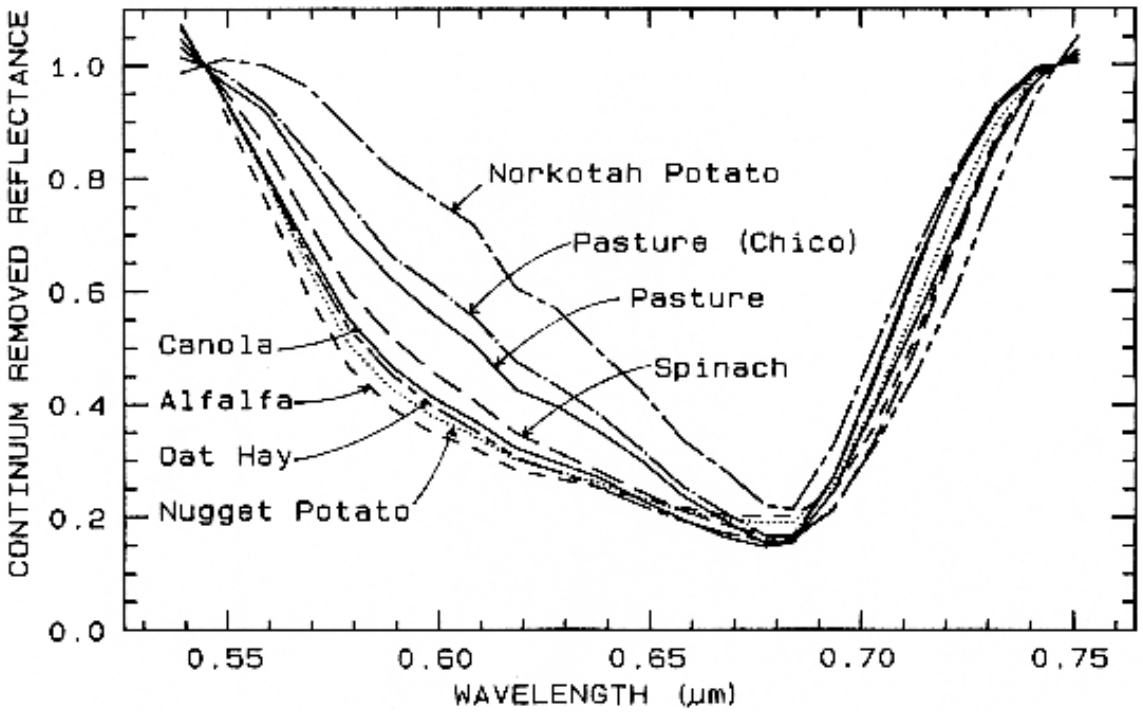

Figure 25c.

Figure 25c: 43k 100dpi gif

Figure 25c: 191k 200dpi gif

Figure 25c: 811k 300dpi gif

Figure 25c. Continuum-removed chlorophyll absorptions for 8 vegetation types (including the 4 from Figure 25a) showing that the continuum removed features can show subtle spectral differences. From Clark *et al.* (1995, 1997).

Back to Contents

6.5 Other Spectral Variability and Rules.

6.5.1 Viewing Geometry. We have seen tremendous variation in the spectral properties of minerals and materials in general, due to composition, grain size, and mixture types. So far viewing geometry has not been discussed. Viewing geometry, including the angle of incidence, angle of reflection, and the phase angle: the angle between the incident light and observer (the angle of reflection), all affect the intensity of light received. Varying the viewing geometry results in changes in shadowing and the proportions of first surface to multiple scattering (e.g. Hapke, 1993; Nelson, 1986; Mustard and Pieters, 1989), which can affect band depths a

small amount except in rare cases (like extreme specular reflection off a mirror or lake surface). While measuring precise light levels are important for things like radiation balance studies, they are of lesser importance in spectral analysis. The following illustrates why.

First, your eye is a crude spectrometer, able to distinguish the spectral properties of materials in a limited wavelength range by the way we interpret color. Pick up any colored object around you. Change the orientation of the local normal on the surface of the object with respect to the angle of incident light, the angle at which you observe it (called the emission or scattering angle), and the angle between the incident and scattered light (the phase angle). As you do this, note any color changes. Unless you chose an unusual material (like a diffraction grating or very shiny object), you will see no significant color change. Plant leaves appear green from any angle, a pile of hematite appears red from any angle. This tells you that the spectral features do not change much with viewing geometry. Your eye/brain combination normalizes intensity variations so that you see the same color, regardless of the actual brightness of the object (the amount of light falling on the surface). The continuum removal does a similar but more sophisticated normalization. The band depth, shape, and position are basically constant with viewing geometry. Band depth will only change with the proportion of specular reflection added to the reflected light. For surfaces (and at wavelengths) where multiple scattering dominates, that change in band depth is minimized.

Back to Contents

6.5.2 Ratioing Spectra. Ratioing two spectra with spectral features can cause spurious features in the ratio (e.g. Clark and King, 1987). However, this ratio can be used to advantage. Consider two spectra, with an absorption edge, such as conduction bands in cinnabar (Figure 9), sulfur, or the chlorophyll-absorption edge in plants at 0.7 μm. If one spectrum is shifted relative to the other and then the two ratioed, the resulting ratio has a residual feature that looks like either an absorption or emission feature (depending on the direction of the shift and which spectrum is the numerator and which is the denominator). An example residual caused by such shifts is shown in Figure 26. This effect has recently been used to determine subtle shifts in the chlorophyll absorption edge in plants (Clark *et al*., 1995, 1997). The intensity of the feature in the reflectance ratio is proportional to the amount of shift between the two spectra, and the shape of the ratio does not change if the shifts are small. Clark *et al*. (1995, 1997) showed that chlorophyll-edge shifts as small as 0.01 times the bandwidth of the spectrometer can be detected. Thus, for the AVIRIS system with 10 nm bandpass and sampling, shifts of 0.1 nm can be readily detected. Such sensitivity indicates the wavelength stability of a spectrometer must be very good for such analyses.

Figure 26.

Figure 26: 66k 100dpi gif

Figure 26: 108k 200dpi gif

Figure 26: 319k 300dpi gif

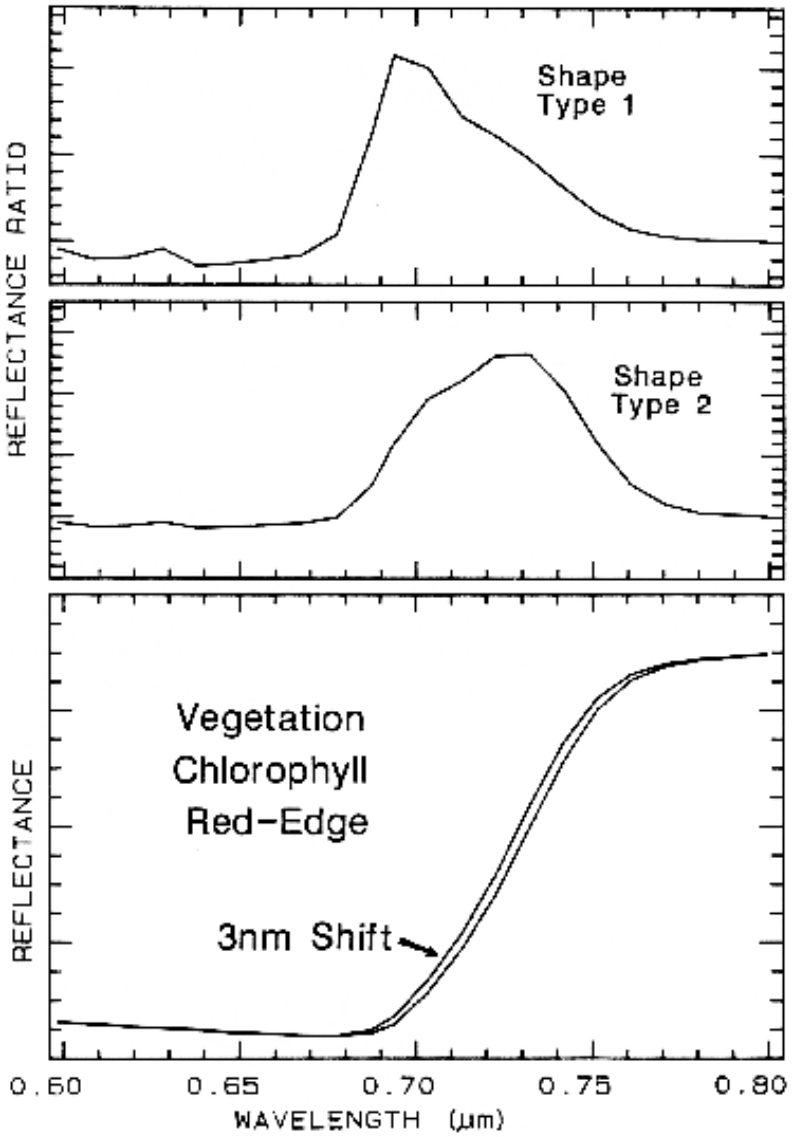

Figure 26. The ratio of two spectra, one slightly shifted from the other results in a spectral feature. The two shapes in this example are from different chlorophyll bands. Shifts as small as 0.01 times the full width at half maximum of the spectrometer system produce 1% features in ratios of strong chlorophyll absorptions. The shape, type 1 profile is from the shifted spectra shown at the bottom of the figure, while the shape, type 2 is from shallower chlorophyll absorptions. From Clark *et al.* (1997).

Back to Contents

6.5.3 Iron Oxide, Hydroxide, Sulfate Complexity. Iron oxides, hydroxides, and sulfates are a special case for remote sensing because they are so ubiquitous. Further, because of the strength of the iron absorptions in the ultraviolet to about 1 µm, at least one if not all are saturated in reflectance. Several hematite reflectance spectra at different grain sizes are shown in Figure 27a. Nanocrystalline hematite (Morris *et al.*, 1985) has such a fine grain size, 25 nm, that the grain surface boundary modifies the electronic transitions, changing and weakening them. The iron absorption at 0.9-µm is reduced in depth, the 0.65-µm band is absent, and the UV absorption is weak. Absorptions in transmittance, as in the thin film case, are 2 times narrower in width (see Clark and Roush, 1984). Larger grain sizes show increased saturation of

the 0.9-µm absorption, broadening and shifting the apparent reflectance minimum to longer wavelengths. The 0.9-µm absorption also shifts position with elements substituted for iron (e.g. see Morris e*t al.*, 1985 and references therein). Continuum removal and scaling the hematite absorption to similar depth shows the wide variety of band shapes and positions that can be found in nature (Figure 27b).

Figure 27a.

Figure 27a: 21k 100dpi gif

Figure 27a: 82k 200dpi gif

Figure 27a: 237k 300dpi gif

Figure 27a. Reflectance spectra of different grain sizes of hematite.

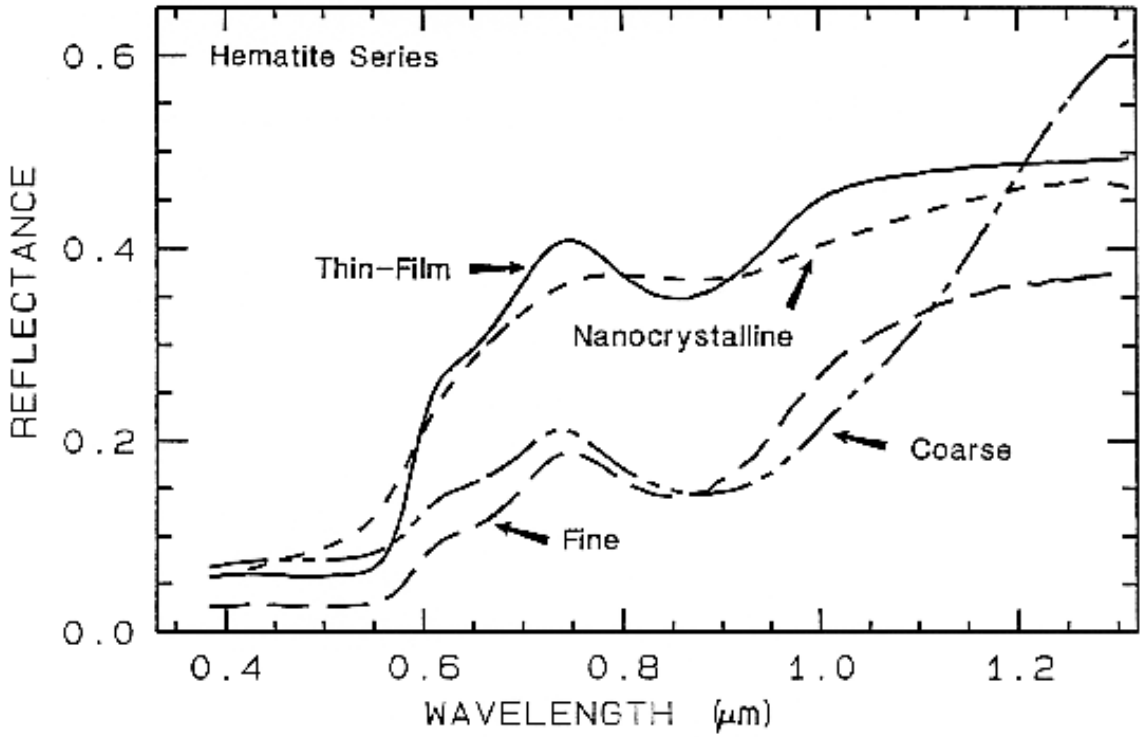

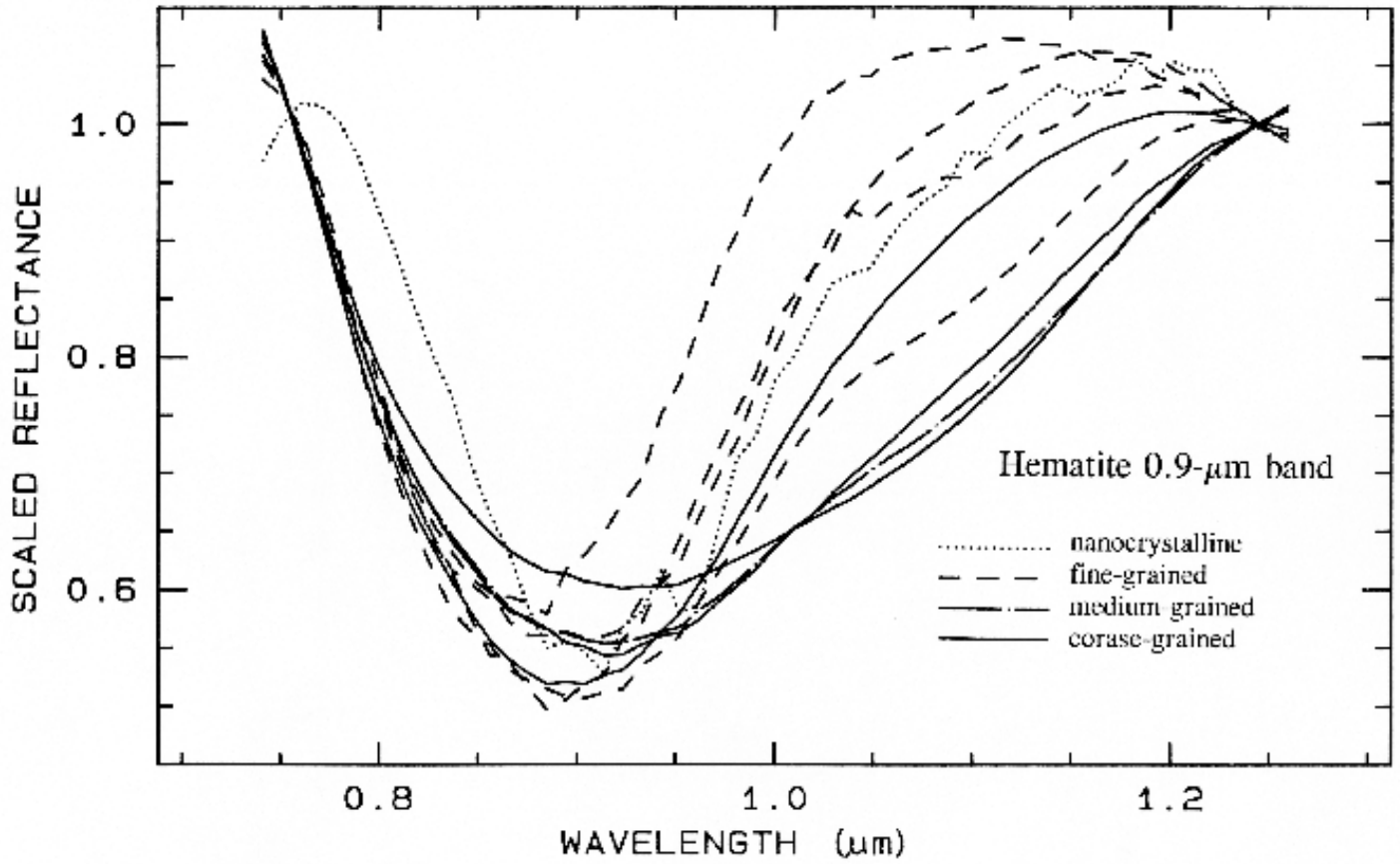

Figure 27b.

Figure 27b: 37k 100dpi gif

Figure 27b: 164k 200dpi gif

Figure 27b: 1213k 300dpi gif

Figure 28a. Spectra of iron oxide, iron hydroxide, and iron sulfate spectra.

There are a whole suite of iron oxides, iron hydroxides, iron sulfates, etc., some only now being discovered, and many amorphous phases, all with similar electronic absorption bands in the visible and near-infrared. A few examples are shown in Figure 28a. Note that hematite has a narrower absorption at a slightly shorter wavelength than goethite. However, a coarse-grained hematite has a broader absorption, approaching the position and width of a fine-grained goethite (or a thin-film goethite).

Jarosite has a narrow absorption near 0.43 µm, but it sometimes appears weak because of the saturated UV absorption. Jarosite, an iron sulfate, has a diagnostic absorption at 2.27 µm due to a combination OH stretch and Fe-OH bend. However, this feature is weaker than the electronic absorptions in the visible and is often masked by clay or alunite (jarosite often occurs in hydrothermal deposits with alunite). The features near 1.475 µm and 1.8 µm are OH related and are commonly seen in sulfate spectra.

Ferrihydrite is an amorphous iron oxide, and its spectrum appears very similar to the orange precipitate, an amorphous iron hydroxide, obtained downstream from the Summitville, Colorado mine (King *et al.*, 1995). However, if we remove the continuum and compare the positions and shapes of the bands (Figure 28b), we can see they are indeed different.

Figure 28a.

Figure 28a: 40k 100dpi gif

Figure 28a: 143k 200dpi gif

Figure 28a: 475k 300dpi gif

Figure 28a. Spectra of iron oxide, iron hydroxide, and iron sulfate spectra.

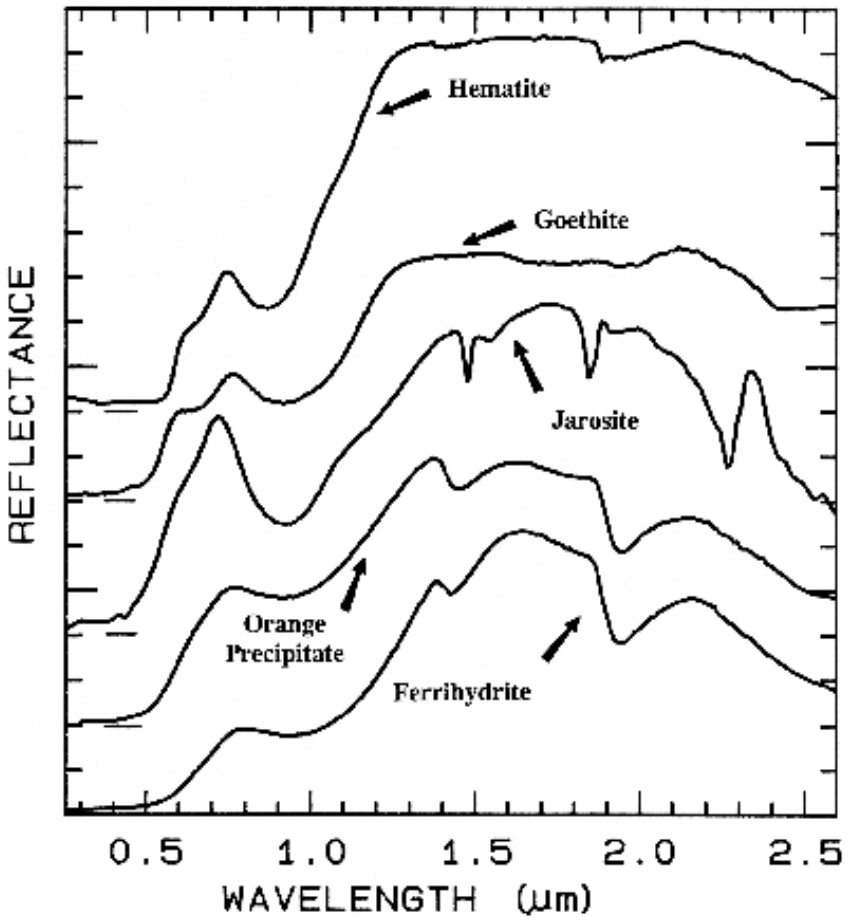

Figure 28b.

Figure 28b: 39k 100dpi gif

Figure 28b: 209k 200dpi gif

Figure 28b: 663k 300dpi gif

Figure 28b. Comparison of the 1-µm continuum-removed-absorption feature of ferrihydrite and an amorphous iron hydroxide (the orange precipitate from Figure 28a). The spectra are offset for clarity. Note the shift in the band center between the two spectra despite the similarities in Figure 28a.

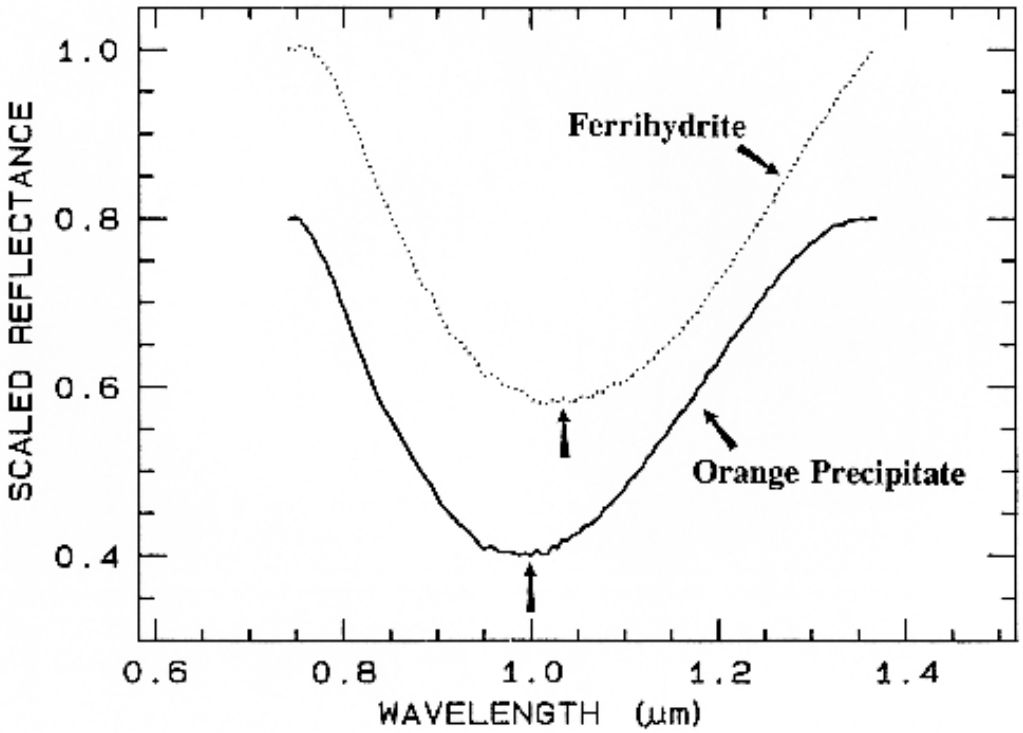

As discussed above, there are many iron-bearing minerals and amorphous materials with similar but distinct absorption bands. How many can be distinguished with reflectance spectroscopy is still a matter of research. An even harder question to answer is how many can be distinguished and not be confused with mixtures of other iron-bearing materials. Detailed spectral analysis, including continuum removal to isolate absorption features can certainly improve the success of distinguishing them.

Iron oxides, hydroxides, and sulfates are additional cases where spectroscopy detects at very low levels because of the strong absorption bands in the visible and ultraviolet. In nature, there appear to be many amorphous iron oxides, hydroxides, etc., with equally intense absorptions. Thus, spectroscopy can not only detect them at levels below other methods (e.g. X-ray diffraction), but in the case of amorphous materials detect them when other methods are not sensitive to their presence when they are major fractions of the sample!

Back to Contents

7. QUANTITATIVE UNDERSTANDING: RADIATIVE TRANSFER THEORY.

There have been many attempts over the years to quantify the scattering process. Kubelka-Munk theory was one of the first and still finds uses today (e.g. Wendlandt and Hecht, 1966; Clark and Roush, 1984). A growing popular method in some industries is log (1/R), where R is reflectance, but this is a less robust attempt at quantifying the scattering process than the decades-old Kubelka-Munk theory (Clark and Roush, 1984). The log (1/R) method is usually combined with computing the derivatives of the log (1/R) spectra and doing a correlation analysis to find particular trends. This has popularly become known as Near-Infrared Reflectance Analysis

(NIRA). Either method has its uses in controlled situations, but there is a modern, more effective alternative. The limitations of these older methods are due to a poor representation of the scattering process and are discussed in Clark and Roush (1984) and Hapke (1993).

Fortunately, in the early 1980's three independent investigations (Hapke, 1981, Gougen, 1981; and Lumme and Bowell, 1982) provided reasonable solutions to the complex radiative transfer problem as applied to particulate surfaces. These theories provide for non-isotropic scattering of light from particles, shadowing between particles, and first surface reflection from grain surfaces, important processes not considered in earlier theories. One theory, that of Hapke (1981, 1993) also provides for mixtures, and because of its relative simplicity compared to the other two, has become the dominant theory used in the planetary and to some degree the terrestrial remote sensing communities.

Back to Contents

7.1 "Hapke Theory." From the optical constants of a mineral, the reflectance (called *radiance factor* by Hapke) can be computed from Hapke's (1981) equation 36:

$r'(w',lambda,\mu,g) = [w'/(4pi)][\mu / (\mu+\mu_o)] \{[1+B(g)]P(g)+H(\mu)H(\mu_o)-1\}$ (eqn 3)

where r' is the reflectance at wavelength , μ_o is the cosine of the angle of incident light, μ is the cosine of the angle of emitted light, g is the phase angle, w' is the average single scattering albedo, B(g) is a backscatter function, P(g) is the average single particle phase function, and H is the Chandrasekhar (1960) H-function for isotropic scatterers. When r' > 0.9 Hapke's approximation of the H-function shows considerable error and equation 3 deviates from measurements (Hapke, 1981). Because of this deviation, a table interpolation subroutine using "exact" values from Chandrasekhar (1960) can be used. The table interpolation is computationally faster than the Hapke approximation and more accurate.

The single scattering albedo is the probability that a photon survives an interaction with a single particle, which includes Fresnel reflection, absorption, scattering, and diffraction due to the presence of an individual grain. Hapke (1981) developed the theory further by deriving a relation between the single scattering albedo, the complex index of refraction, the grain size, and a scattering parameter to describe scattering centers within non-perfect grains. The single scattering albedo of a grain can be found from his equation 24:

$w = S_E + [(1-S_E)(1+S_I)\{r_1 + \exp[-2(k(k+s))^{½} d/3]\}] / [1 -r_1S_I + (r_1 - S_I) \exp[-2(k(k+s))^{½} d/3]]$ (eqn 4)

where S_E and S_I are the external and internal scattering coefficients, respectively, which can be computed from the complex index of refraction (Hapke, 1981, eqn 21), s is a scattering coefficient, d is the particle diameter, k is the absorption coefficient (note Hapke uses instead of k here), and (from Hapke's equation 23):

$r_1 = \{1 - [k/(k+s)]^{½}\} / \{1 + [k/(k+s)]^{½}\}$, (eqn 5a) $= \{1 - [kd/(kd+sd)]^{½}\} / \{1 + [kd/(kd+sd)]^{½}\}$

In a monomineralic surface, w=w'. For a multimineralic surface, w' can be computed from equation 17 of Hapke (1981):

$w' = \{SIGMA_iM_i\ w_i / rho(_i\ d_i)\} / \{SIGMA_i\ (M_i / rho(_i\ d_i)\}$, (eqn 11)

where i refers to the ith component, $SIGMA_i$ is the greek symbol, sigma, for math summation over i components, M_i is the mass fraction, rho_i is the density of the material, d_i the mean grain diameter, and w_i the single scattering albedo of the ith component.

With the Hapke (1981, 1993) reflectance theory, and the optical constants of minerals, reflectance spectra of pure minerals at a single grain size, spectra of a pure mineral with a grain size distribution, and mineral mixtures with varying grain size components can all be computed. Clark and Roush (1984) also showed that a reflectance spectrum can be inverted to determine quantitative information on the abundances and grain sizes of each component. The inversion of reflectance to quantitative abundance has been tested in laboratory mixtures (e.g. Johnson *et al*., 1983, 1992; Clark, 1983, Mustard and Pieters, 1987a, 1989; Shipman and Adams, 1987; Sunshine and Pieters, 1990, 1991; Sunshine *et al*, 1990; Gaffey *et al*., 1993, and references therein). Some quantitative inversion attempts have been undertaken with imaging spectroscopy data (e.g. Mustard and Pieters, 1987b, Li *et al*, 1996, Adams *et al.*, 1993 and references therein).

Back to Contents

8. SPECTRAL LIBRARIES.

The spectra presented in this paper are available on the World Wide Web site:

http://speclab.cr.usgs.gov

as are spectra from the Clark *et al*., (1993b) USGS Digital Spectral Library**.** Other spectral libraries include the mid-infrared work of Salisbury *et al*., (1991). A recently available spectral library web site is the NASA ASTER site (http://asterweb.jpl.nasa.gov), managed by Simon Hook, Jet propulsion Laboratory. This site includes the Salisbury (1991) library and additions since the original publication. As spectral libraries are currently a focus of activity, it is probably best to search the internet and check with the authors referenced in this chapter for the latest information on what is available.

A word of caution with spectral libraries, and spectra obtained from other sources in general: wavelength errors are common except from data obtained on interferometers. This author and colleagues at the USGS have evaluated many spectrometers and other spectral libraries and have found many to have significant wavelength shifts. Other specific libraries and spectrometers are not mentioned here because some may have wavelength shifts and must each be validated. One mineral with a stable absorption feature is a well-crystallized kaolinite, which has a sharp absorption at 2.2086 ± 0.0003 µm, and is commonly found in visible and near-IR libraries. When obtaining spectral library data, confirm that wavelength positions of known features are measured at the correct positions. Absorptions due to rare-earth oxides are often used as wavelength standards in the visible. Mid-IR systems can be checked by interferometer measurements, which is now probably the most common spectrometer in use for this wavelength region.

Also be cautious of spurious spectral features from incomplete reduction to true reflectance. All measurements are made relative to a "white" standard. However, these standards also have spectral features. For example, the common visible and near infrared standards, Halon and Spectralon and derivatives, have significant spectral features in the 2.14-µm region and beyond (e.g. see Clark e*t al.*, 1990a) which must be properly corrected. Mid-infrared standards are more difficult, mainly due to the large wavelength range usually covered. Nash (1986) reviewed some common mid-IR reflectance standards.

Back to Contents

9. CONCLUSIONS AND DISCUSSION.

Reflectance spectroscopy is a rapidly growing science that can be used to derive significant information about mineralogy with little or no sample preparation. It may be used in applications when other methods would be too time consuming or require destruction of precious samples. For example, imaging spectrometers are already acquiring millions of spatially gridded spectra over an area from which mineralogical maps are being made. It is possible to set up real-time monitoring of processes

using spectroscopy, such as monitoring the mineralogy of drill cores at the drilling site. Research is still needed to better understand the subtle changes in absorption features before reflectance spectroscopy will reach its full potential. Good spectral databases documenting all the absorption features are also needed before reflectance spectroscopy can be as widely used a tool as XRD. Spectral databases are now becoming available (e.g. Clark *et al.*, 1993b), and research continues on the spectral properties of minerals, but it will probably take about a decade before general software tools are available to allow reflectance spectroscopy to challenge other analytical methods in the commercial marketplace. For certain classes of minerals, however, spectroscopy is already an excellent tool. Among these classes are clay mineralogy, OH-bearing minerals, iron oxides and hydroxides, carbonates, sulfates, olivines and pyroxenes.

Space limits the contents of any review article covering such a broad topic. Other review articles are Adams (1975), Hunt (1977, 1982), Gaffey *et al*., (1993), Salisbury (1993), and Clark (1995). The Hunt (1982) CRC book chapter in particular presents more spectra, both visible-near-IR and mid-IR, than most other works and seems to be an overlooked but important work.

Back to Contents

Acknowledgements. This work was supported by NASA interagency agreement W15805. Thanks goes to reviewers John Mustard, Gregg Swayze, and Eric Livo, whose comments substantially improved the manuscript.

Back to Contents

10. REFERENCES.

Adams, J.B., 1975, Interpretation of visible and near-infrared diffuse reflectance spectra of pyroxenes and other rock-forming minerals, in *Infrared and Raman Spectroscopy of Lunar and Terrestrial Minerals,* Academic Press, New York, 94-116.

Adams, J.B., 1974, Visible and Near-Infrared Diffuse Reflectance Spectra of Pyroxenes as Applied to Remote Sensing of Solid Objects in the Solar System, *J. Geophys Res.* **79,** 4829-4836.

Adams, J.B., M.O. Smith, and A.R. Gillespie, 1993, Imaging Spectroscopy: Interpretation based on spectral mixture analysis, in *Remote Geochemical Analysis: Elemental and Mineralogical Composition* (C. M. Pieters, and P.A.J. Englert, eds.), Cambridge University Press, Cambridge, 145-166.

Berk, A., L.S. Bernstein, and D.C. Robertson, 1989, "MODTRAN: A moderate resolution model for LOWTRAN 7", Final report, GL-TR-0122, AFGL, Hanscomb AFB, MA, 42 pp.

Burns, R., 1970, *Mineralogical Applications of Crystal Field Theory*, Cambridge University Press, Cambridge, 224p.

Burns, R., 1993, *Mineralogical Applications of Crystal Field Theory, Second Edition*, Cambridge University Press, Cambridge, 551p.

Ball, D.W., 1995, Defining Terms, *Spectroscopy*, **10**, 16-18.

Chandrasekhar, S., *1960, Radiative Transfer*, Dover Publ. Inc., New York, NY, 393p.

Clark, R.N., 1981a, Water Frost and Ice: The Near-Infrared Spectral Reflectance 0.65-2.5 µm, *J. Geophys. Res.*, **86,** 3087-3096.

Clark, R.N., 1981b, The Spectral Reflectance of Water-Mineral Mixtures at Low Temperatures, *J. Geophys. Res.*, **86,** 3074-3086.

Clark, R.N., 1983, Spectral Properties of Mixtures of Montmorillonite and Dark Carbon Grains: Implications for Remote Sensing Minerals Containing Chemically and Physically Adsorbed Water, *J. Geophys. Res.* **88,** 10635- 10644.

Clark, R.N., 1995, Reflectance Spectra, *AGU Handbook of Physical Constants* 12 pages.

Clark, R.N. and T.V.V. King, 1987, Causes of Spurious Features in Spectral Reflectance Data: *Proceedings of the Third Airborne Imaging Spectrometer Data Analysis Workshop,* JPL Publication 87-30, 132-137.

Clark, R.N. and P.G. Lucey, 1984, Spectral Properties of Ice-Particulate Mixtures and Implications for Remote Sensing I: Intimate Mixtures, *J. Geophys. Res.*, **89,** 6341-6348.

Clark, R.N., and Roush, T.L., 1984, Reflectance spectroscopy: Quantitative analysis techniques for remote sensing applications, *J. Geophys. Res.*, **89,** 6329- 6340.

Clark, R.N. and P.G. Lucey, 1984, Spectral Properties of Ice-Particulate Mixtures and Implications for Remote Sensing I: Intimate Mixtures, *J. Geophys. Res.*, **89,** 6341-6348, 1984.

Clark, R.N., F.P. Fanale, and M.J. Gaffey, 1986, Surface Composition of Satellites, in *Satellites* (J. Burns and M.S. Matthews, eds.), Univ. of Arizona Press, Tucson, 437-491.

Clark, R.N., T.V.V. King, M. Klejwa, G. Swayze, and N. Vergo, 1990a, High Spectral Resolution Reflectance Spectroscopy of Minerals, *J. Geophys Res.* **95,** 12653-12680.

Clark, R.N., A.J. Gallagher, and G.A. Swayze, 1990b, Material Absorption Band Depth Mapping of Imaging Spectrometer Data Using a Complete Band Shape Least-Squares Fit with Library Reference Spectra, *Proceedings of the Second Airborne Visible/Infrared Imaging Spectrometer (AVIRIS) Workshop.* JPL Publication 90-54, 176-186.

Clark, R.N., G.A. Swayze, and A. Gallagher, 1993a, Mapping Minerals with Imaging Spectroscopy, *U.S. Geological Survey, Office of Mineral Resources Bulletin 2039,* pp. 141-150.

Clark, R.N., G.A. Swayze, A. Gallagher, T.V.V. King, and W.M. Calvin, 1993b, The U. S. Geological Survey, Digital Spectral Library: Version 1: 0.2 to 3.0 µm, *U.S. Geological Survey, Open File Report 93-592,* 1326 pages.

Clark, R.N., T.V.V. King, C. Ager, and G.A. Swayze, 1995, Initial vegetation species and senescence/stress mapping in the San Luis Valley, Colorado using imaging spectrometer data. *Proceedings: Summitville Forum '95,* H.H. Posey, J.A. Pendelton, and D. Van Zyl Eds., Colorado Geological Survey Special Publication 38, p. 64-69.

Clark, R.N., T.V.V. King, C. Ager, G.A. Swayze, Vegetation Species and Stress Indicator Mapping in the San Luis Valley, Colorado using Imaging Spectrometer

data, Remote Sensing of Environment, submitted, 1997.

Cloutis, E.A., M.J. Gaffey, 1991, Pyroxene Spectroscopy revisited: Spectral-Compositional Correlations and relationships to goetherometry, *J. Geophys Res.*, **96**, 22809-22826.

Cloutis, E.A., M.J. Gaffey, T.L. Jackowski, and K.L. Reed, 1986, Calibrations of Phase Abundance, Composition, and Particle Size Distribution of Olivine-Orthopyroxene mixtures from Reflectance *Spectra, J. Geophys Res*., **91**, 11641-11653.

Crowley, J.K. and Vergo, N., 1988, Near-infrared reflectance spectra of mixtures of kaolin group minerals: use in clay studies, *Clays and Clay Min.*, **36,** 310-316.

Cruikshank, D.P., R.H. Brown, and R.N. Clark, 1985, Methane Ice on Triton and Pluto, in *Ices in the Solar System*, (J. Klinger *et al*., eds.), D. Reidel Publishing Company, 817-827.

Duke, E.F., 1994, Near infrared spectra of muscovite, Tschermak substitution, and metamorphic reaction progress: implications for remote sensing, *Geology*, **22**, p. 621-624.

Farmer, V.C., *1974, The Infra-Red Spectra of Minerals*, (V.C. Farmer, ed.) Mineralogical Society, London, 539pp.

Gaffey, S.J., 1986, Spectral reflectance of carbonate minerals in the visible and near infrared (0.35-2.55 μm): Calcite, aragonite and dolomite, *Am. Mineral.* **71,** 151-162.

Gaffey, S.J., 1987, Spectral reflectance of carbonate minerals in the visible and near infrared (0.35-2.55 μm): Anhydrous carbonate minerals, *J. Geophys. Res.* **92,** 1429-1440.

Gaffey, S.J., L.A. McFadden, D. Nash, and C.M. Pieters, 1993, Ultraviolet, Visible, and Near-infrared Reflectance Spectroscopy: Laboratory spectra of Geologic Materials, in *Remote Geochemical Analysis: Elemental and Mineralogical Composition* (C. M. Pieters, and P.A.J. Englert, eds.), Cambridge University Press, Cambridge, 43-78.

Goetz, A.F.H, G. Vane, J.E. Solomon, and B.N. Rock, 1985, Imaging spectrometry for earth remote sensing, *Science*, **228**, 1147-1153.

Goguen, J.D., 1981, A Theoretical and Experimental Investigation of the Photometric Functions of Particulate Surfaces. Ph.D. Thesis, Cornell Univ., Ithaca.

Green, Robert O., James E. Conel, Veronique Carrere, Carol J. Bruegge, Jack S. Margolis, Michael Rast, and Gordon Hoover, 1990, Determination of the In-Flight Spectral and Radiometric Characteristics of the Airborne Visible/Infrared Imaging Spectrometer (AVIRIS), in *Proceedings of the Second Airborne Visible/Infrared Imaging Spectrometer (AVIRIS) Workshop*, JPL Publication 90-54, pp. 15-22.

Hapke, B., 1981, Bidirectional reflectance spectroscopy 1. Theory, *J. Geophys. Res.* **86,** 3039-3054.

Hapke, B., 1993, *Introduction to the Theory of reflectance and Emittance Spectroscopy*, Cambridge University Press, New York.

Hecht, E., *1987, Optics*, Addison-Wesley Publishing, Reading MA, 676pp.

Henderson, B.G., P.G. Lucey, and B. M. Jakosky, 1996, New laboratory measurements of mid-IR emission spectra of simulated planetary surfaces, *J. Geophys. Res.*, **101**, 14969-14975.

Herzberg, G., 1945, *Molecular spectra and molecular structure, II, Infrared and Raman spectra of polyatomic molecules*, Van Nostrand Reinhold, New York, 632 pp.

Hobbs, P.V., 1974, *Ice Physics*, Clarendon Press, Oxford, 837 pp.

Hunt, G.R., 1977, Spectral signatures of particulate minerals, in the visible and near-infrared, *Geophysics* **42,** 501-513.

Hunt, G.R., 1979, Near-infrared (1.3-2.4 μm) spectra of alteration minerals-Potential for use in remote sensing, *Geophysics* **44,** 1974-1986.

Hunt, G.R., 1982, Spectroscopic properties of rocks and minerals, in *Handbook of Physical properties of rocks, Volume I*, (R. S. Carmichael, ed.) CRC Press, Boca Raton, 295-385.

Hunt, G.R., and Salisbury, J.W., 1970, Visible and near infrared spectra of minerals and rocks. I. Silicate minerals, *Mod. Geology* **1,** 283-300.

Hunt, G.R., and Salisbury, J.W., 1971, Visible and near infrared spectra of minerals and rocks. II. Carbonates, *Mod. Geology* **2,** 23-30.

Hunt, G.R., Salisbury, J.W. and Lenhoff, C.J., 1971a, Visible and near infrared spectra of minerals and rocks. III. Oxides and hydroxides, *Mod. Geology* **2,** 195-205.

Hunt, G.R., Salisbury, J.W. and Lenhoff, C.J., 1971b, Visible and near infrared spectra of minerals and rocks. IV. Sulphides and sulphates, *Mod. Geology* **3,** 1-14.

Hunt, G.R., Salisbury, J.W. and Lenhoff, C.J., 1972, Visible and near infrared spectra of minerals and rocks. V. Halides, arsenates, vanadates, and borates, *Mod. Geology* **3,** 121-132.

Hunt, G.R., Salisbury, J.W. and Lenhoff, C.J., 1973, Visible and near infrared spectra of minerals and rocks. VI. Additional silicates, *Mod. Geology* **4,** 85-106.

Johnson, P., M. Smith, and S. Taylor-George, 1983, A semi-empirical method for analysis of the reflectance spectra of binary mineral mixtures. *J. Geophys. Res.*, **88**, 3557-3561.

Johnson P.M., M.O. Smith, and J.B. Adams, 1992, Simple Algorithms for remote determination of mineral abundances and particle sizes from reflectance spectra, *J. Geophys. Res.*, **97**, 2649-2657.

King, T.V.V. and Clark, R.N., 1989, Spectral characteristics of serpentines and chlorites using high resolution reflectance spectroscopy, *J. Geophys. Res.* **94,** 13997-14008a.

King, T.V.V. and Clark, R.N., 1989b, Reflectance Spectroscopy (0.2 to 20μm) As An Analytical Method For The Detection of Organics In Soils: Proceedings First International Symposium: Field Screening Methods for Hazardous Waste Site Investigations, EPA, p. 485-488.

King, T.V.V. and W.I. Ridley, 1987, Relation of the Spectroscopic Reflectance of Olivine to Mineral Chemistry and Some Remote Sensing Implications, *J. Geophys.*

Res. **92,** 11457-11469.

King, T.V.V., R.N. Clark, C. Ager, and G.A. Swayze, 1995, Remote mineral mapping using AVIRIS data at Summitville, Colorado and the adjacent San Juan Mountains. *Proceedings: Summitville Forum '95,* H.H. Posey, J.A. Pendelton, and D. Van Zyl Eds., Colorado Geological Survey Special Publication 38, p. 59-63.

Kruse, F.A., 1997, Chapter 15: Visible / Infrared Sensors and Case Studies, this volume.

Li, L., J.F. Mustard, and G. He, 1996, Mixing across simple mare-highland contacts: New insights from Clementine UV-VIS data of the Grimaldi basin, *Lunar and Planetary Science XXVII*, 751-752.

Lucey, P.G., and R.N. Clark, 1985, Spectral Properties of Water Ice and Contaminants, in *Ices in the Solar System,* (J. Klinger *et al*., eds.), D. Reidel Publishing Company, 155-168.

Lumme, K. and Bowell, E., 1981, Radiative Transfer in the Surfaces of Atmosphereless Bodies. I. Theory., *Astr. Journ.*, **86,** 1694-1704.

Morris, R.V., H.V. Lauer, C.A. Lawson, E.K. Jr. Gibson, G.A. Nace, and C. Stewart, 1985, Spectral and other physiochemical properties of submicron powders of hematite (-Fe2O3), maghemite (-Fe_2O_3), maghemite (Fe_3O_4), goethite (-FeOOH), and lepidochrosite (-FeOOH), *J. Geophys. Res.* **90,** 3126-3144.

Mustard, J. F., and C. M. Pieters, 1989, Photometeric phase functions of common geologic minerals and applications to quantitative analysis of mineral mixture reflectance spectra, *J. Geophys. Res.* **94**, 13,619-13634.

Mustard, J. F., and C. M. Pieters, 1987, Quantitative abundance estimates from bidirectional reflectance measurements, *Proc. 17th Lunar Planet. Sci. Conf., J. Geophys. Res.*, **92**, E617-E626.

Mustard, J. F., and C. M. Pieters, 1987, Abundance and distribution of serpentinized ultramafic microbreccia in Moses Rock dike: Quantitative application of mapping spectrometer data, *J. Geophys. Res*. **92**, 10,376-10,390.

Mustard, J.F. and J.M. Sunshine, 1997, Chapter 5: Spectral Analysis, this volume.

Mustard, J. F., 1992, Chemical composition of actinolite from reflectance spectra, *American Mineralogist* **77**, 345-358.

Nash, D.B., 1986, Mid-infrared reflectance spectra (2.3-22 μm) of sulfur, gold, FBr, Mgo and halon, *Applied Optics*, **25**, 2427-2433.

Nelson, M.L., 1986, Application of radiative transfer theory to the spectra of mixtures of minerals with anisotropic phase functions, Masters Thesis, University of Hawaii, 71pp.

Nicodemus, F.E., 1965, Directional reflectance and emissivity of an opaque surface. *Applied Optics*, **4**, 767-773.

Post, J.L. and P.N. Noble, 1993. The near-infrared combination band frequencies of dioctahedral smectites, micas, and illites, *Clays and Clay Minerals*. **41**, 639-644.

Salisbury, J.W., L.S. Walter, N. Vergo, and D.M. D'Aria, 1991, Infrared (2.1-25 μm) spectra of minerals, The Johns Hopkins University Press, Baltimore, 267pp.

Salisbury, J.W., 1993, Mid-infrared spectroscopy: Laboratory data, in *Remote Geochemical Analysis: Elemental and Mineralogical Composition* (C. M. Pieters, and P.A.J. Englert, eds.), Cambridge University Press, Cambridge, 79-98.

Sherman, D.M., 1990, Crystal Chemistry, electronic structures and spectra of Fe sites in clay minerals, in *Spectroscopic Characterization of Minerals and their Surfaces* L.M. Coyne, S.W.S. McKeever, and D.F. Drake, eds.) pp. 284-309. American Chemical Society, Washington DC.

Shipman, H. and J.B. Adams, 1987, Detectability of minerals on desert alluvial fans using reflectance spectra, *J. Geophys. Res.*, **92**, 10391-10402.

Spitzer, W.G., and D,A. Kleinman, 1960, Infrared Lattice Bands of Quartz, *Physical Review*, **121**, 1324-1335.

Sunshine, J.M. and C.M. Pieters, 1990, Extraction of compositional information from olivine reflectance spectra: new capability for lunar exploration (abstract), in *Lunar and Planetary Science XXI*, 962-963, Lunar and Planetary Institute, Houston.

Sunshine, J.M. and C.M. Pieters, 1991, Identification of modal abundances in spectra of natural and laboratory pyroxene mixtures: a key component for remote analysis of lunar basalts (abstract), in *Lunar and Planetary Science XXII*, 1361-1362, Lunar and Planetary Instute, Houston.

Sunshine, J.M., C.M. Pieters, and S.R. Pratt, 1990, Deconvolution of mineral absorption bands: an improved approach, *J. Geophys. Res.*, **95**, 6955-6966.

Swayze, G.A. and R.N. Clark, 1990, Infrared Spectra and Crystal Chemistry of Scapolites: Implications for Martian Mineralogy, *J. Geophys. Res.* **95,** 14481-14495.

Swayze, G.A., 1997, The hydrothermal and structural history of the Cuprite Mining District, Southwestern Nevada: an integrated geological and geophysical approach, Ph D. Dissertation, University of Colorado at Boulder, Boulder, Colorado, 430p.

Swayze, G.A., R.N. Clark, A.F.H Goetz, N.S. Gorelick, and T.G. Chrien, 1997, Spectral Identification of surface materials using imaging spectrometer data: evaluating the effects of detector sampling, bandpass, and signal to noise ratio using the U.S.G.S. Tricorder Algorithm, to be submitted to *J Geophys. Res*. in two parts (Part I and Part II).

Wendlandt, W.W., and H.G. Hecht, 1966, *Reflectance Spectroscopy*, Interscience Publisher, New York, 298p.

White, W.B., 1974, The Carbonate minerals, in *The Infrared Spectra of Minerals* (V.C. Farmer, ed.), 227-284, Mineralogical Society, London.

Vane, G., J.E. Duval, and J.B. Wellman, 1993, Imaging spectroscopy of the earth and other solar system bodies, in *Remote Geochemical Analysis: Elemental and Mineralogical Composition* (C. M. Pieters, and P.A.J. Englert, eds.), Cambridge University Press, Cambridge, 121-143.

Back to Contents

Phone email and regular mail addresses of spectroscopy lab personnel for further information.

Speclab Home Page | Speclab Contents/Index

U.S. Geological Survey, a bureau of the U.S. Department of the Interior
This page URL= http://speclab.cr.usgs.gov/PAPERS.refl-mrs/refl4.html
This page is maintained by: Dr. Roger N. Clark rclark@speclab.cr.usgs.gov
Last modified June 25, 1999.

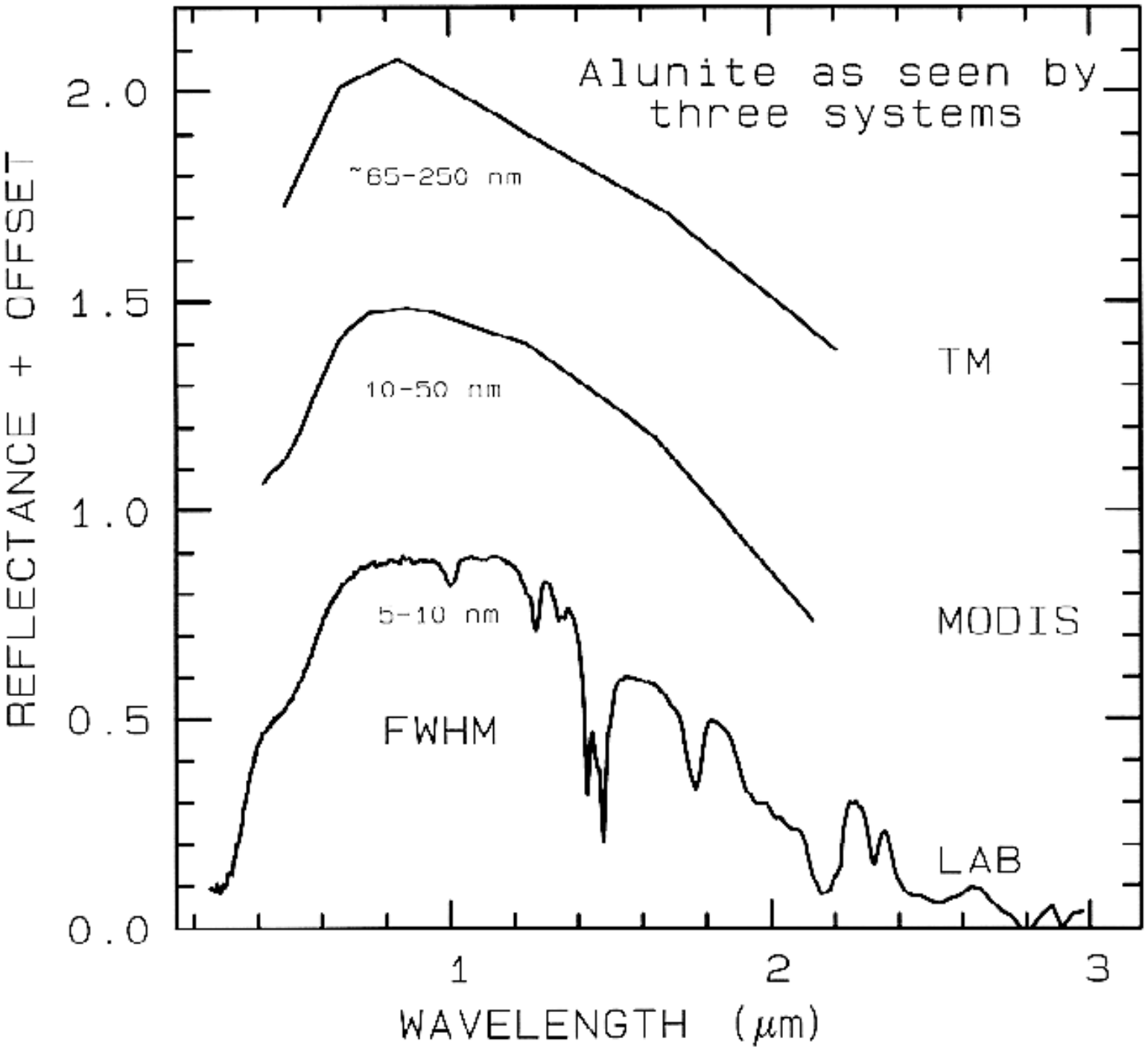
Alunite as seen by three systems
~65-250 nm
TM
10-50 nm
MODIS
5-10 nm
FWHM
LAB
REFLECTANCE + OFFSET
0.0
0.5
1.0
1.5
2.0
1
2
3
WAVELENGTH (μm)

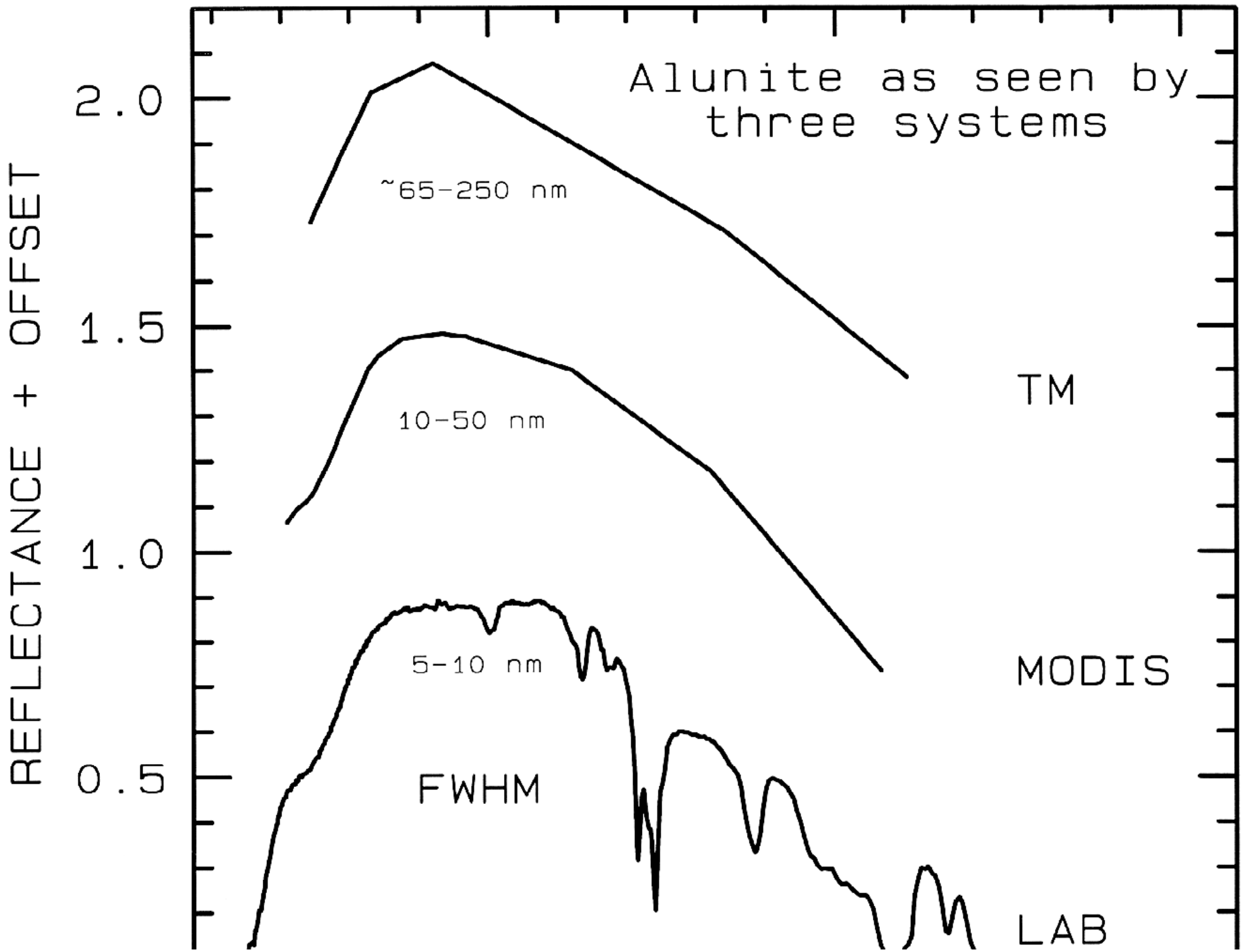
Alunite as seen by three systems
REFLECTANCE + OFFSET
2.0
1.5
1.0
0.5
~65-250 nm
10-50 nm
5-10 nm
FWHM
TM
MODIS
LAB

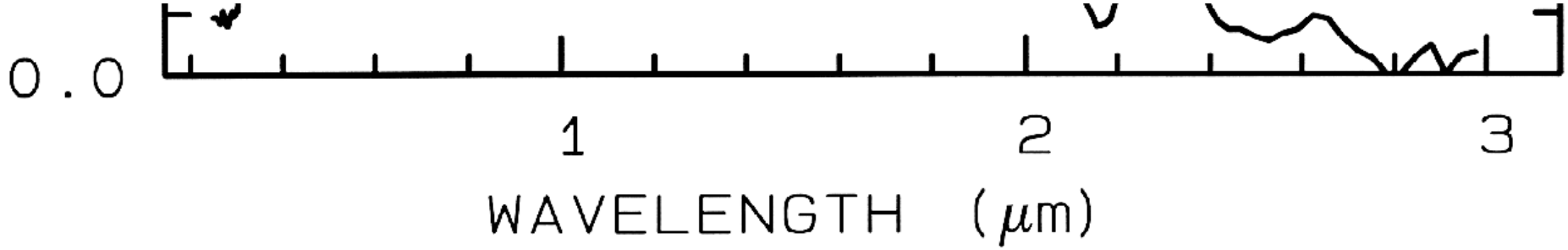
0.0
1
2
3
WAVELENGTH (μm)

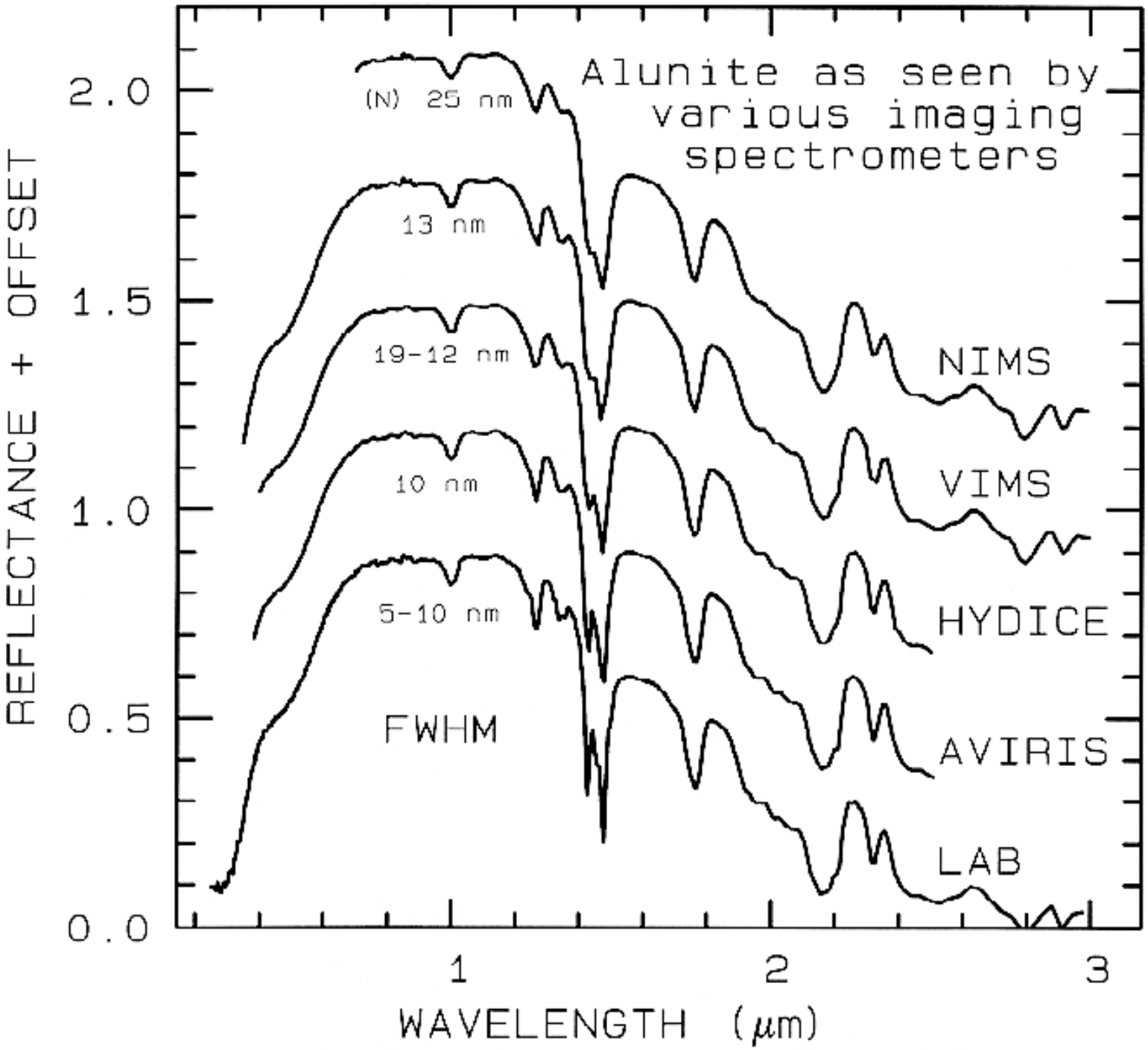
Alunite as seen by various imaging spectrometers
(N) 25 nm
13 nm
19-12 nm
10 nm
5-10 nm
FWHM
NIMS
VIMS
HYDICE
AVIRIS
LAB
REFLECTANCE + OFFSET
0.0
0.5
1.0
1.5
2.0
1
2
3
WAVELENGTH (μm)

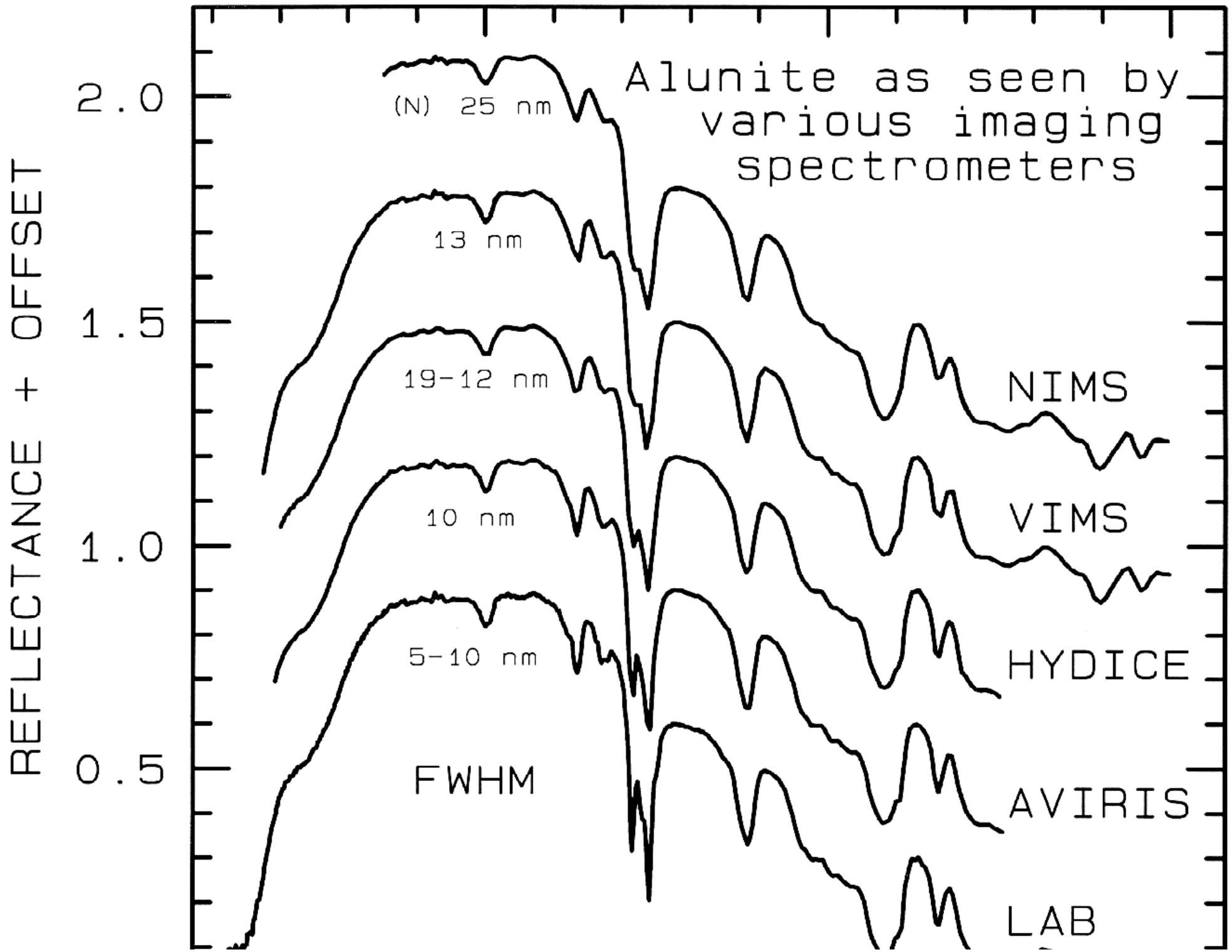
Alunite as seen by various imaging spectrometers
REFLECTANCE + OFFSET
2.0
1.5
1.0
0.5
(N) 25 nm
13 nm
19-12 nm
10 nm
5-10 nm
FWHM
NIMS
VIMS
HYDICE
AVIRIS
LAB


0.0
1
2
3
WAVELENGTH (μm)

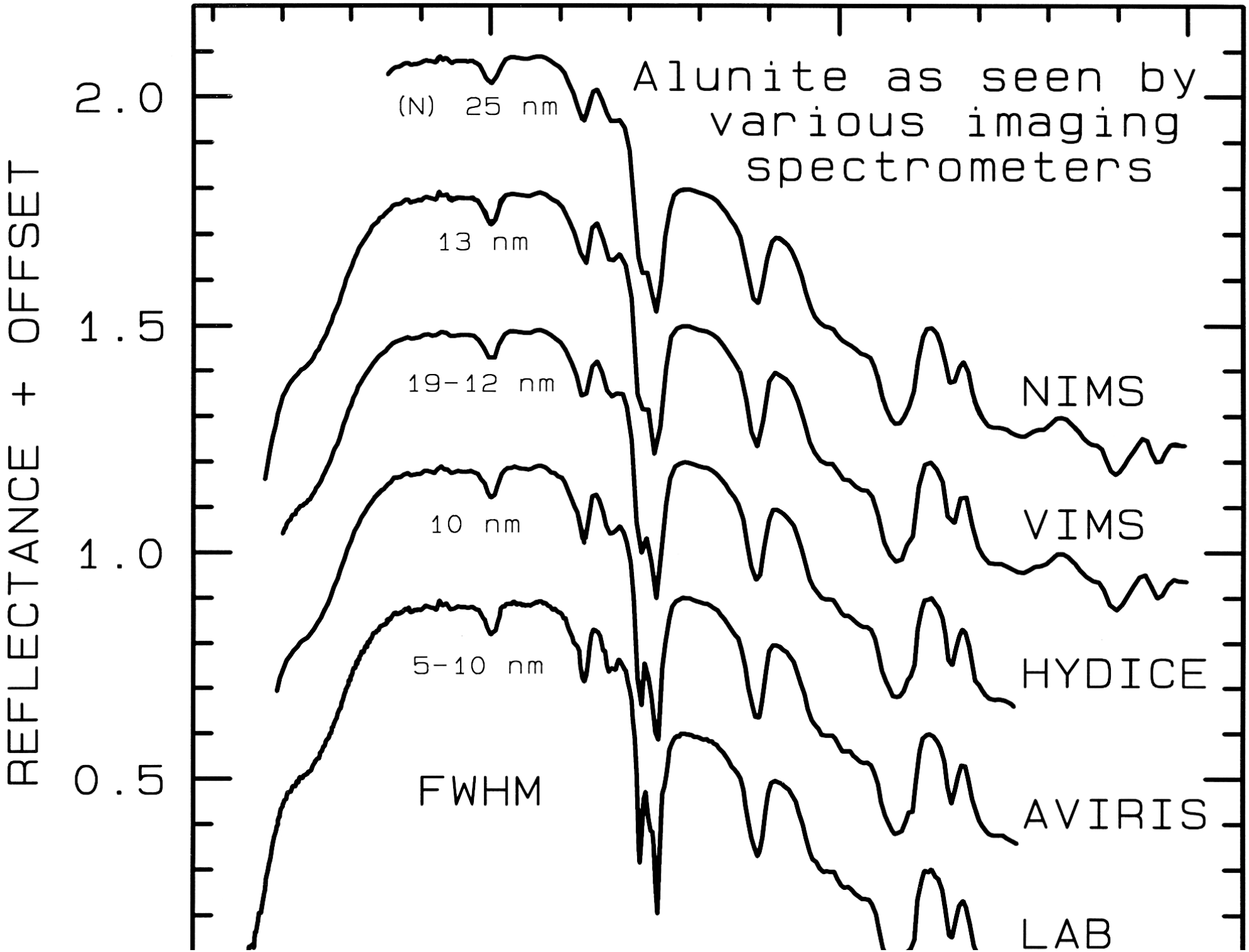
Alunite as seen by various imaging spectrometers
REFLECTANCE + OFFSET
2.0
1.5
1.0
0.5
(N) 25 nm
13 nm
19-12 nm
10 nm
5-10 nm
FWHM
NIMS
VIMS
HYDICE
AVIRIS
LAB

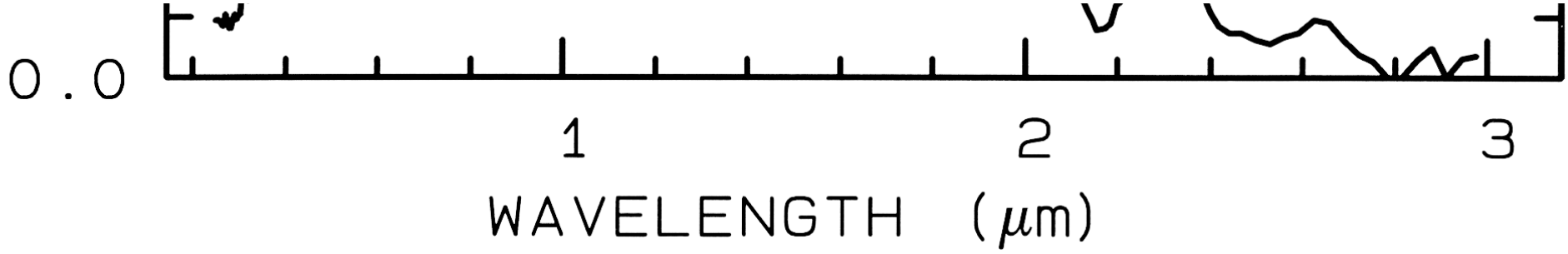
0.0
1
2
3
WAVELENGTH (μm)

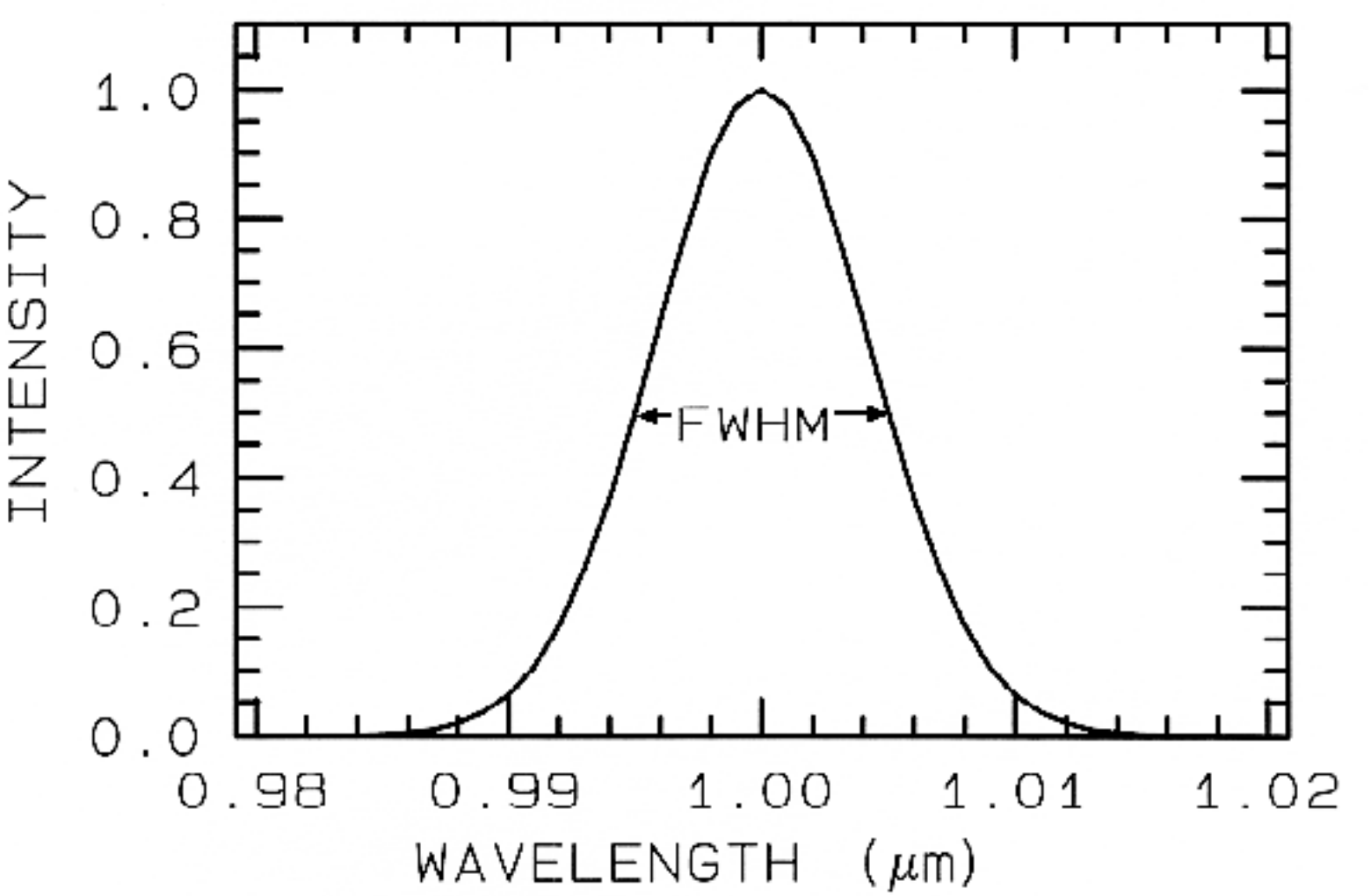
INTENSITY
1.0
0.8
0.6
0.4
0.2
0.0
FWHM
0.98
0.99
1.00
1.01
1.02
WAVELENGTH (μm)

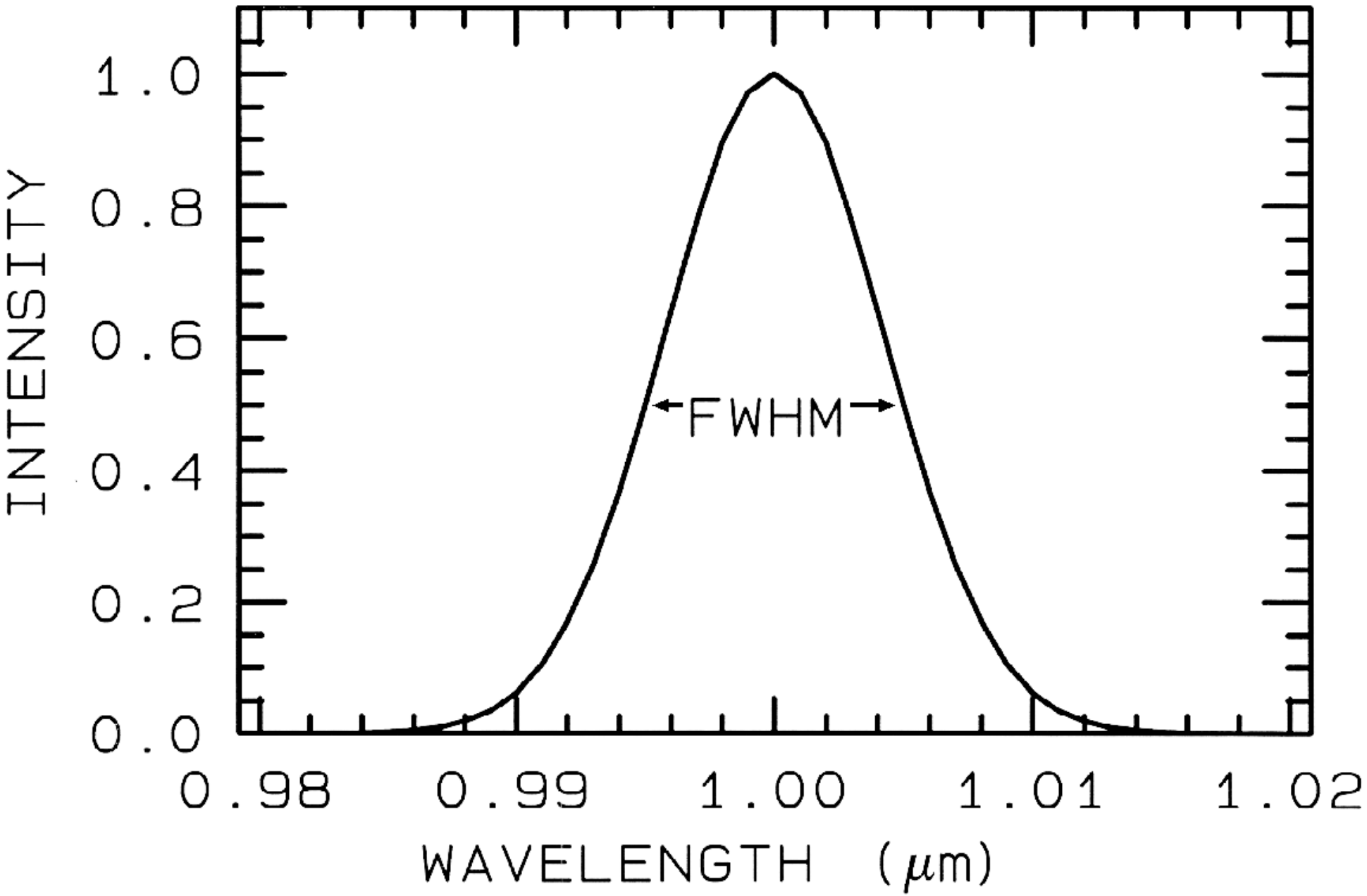
INTENSITY
1.0
0.8
0.6
0.4
0.2
0.0
FWHM
0.98
0.99
1.00
1.01
1.02
WAVELENGTH (μm)

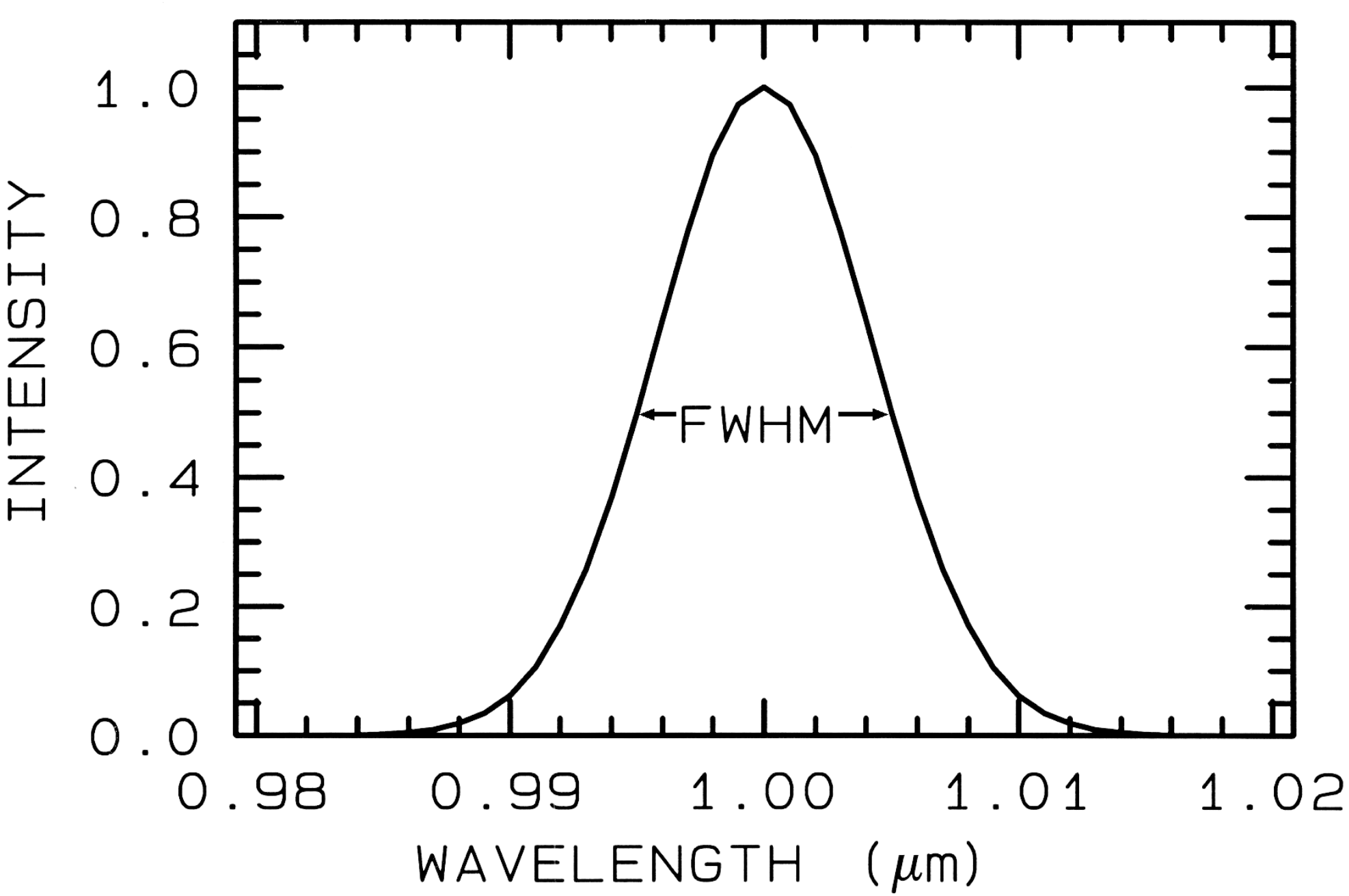
INTENSITY
1.0
0.8
0.6
0.4
0.2
0.0
FWHM
0.98
0.99
1.00
1.01
1.02
WAVELENGTH (μm)

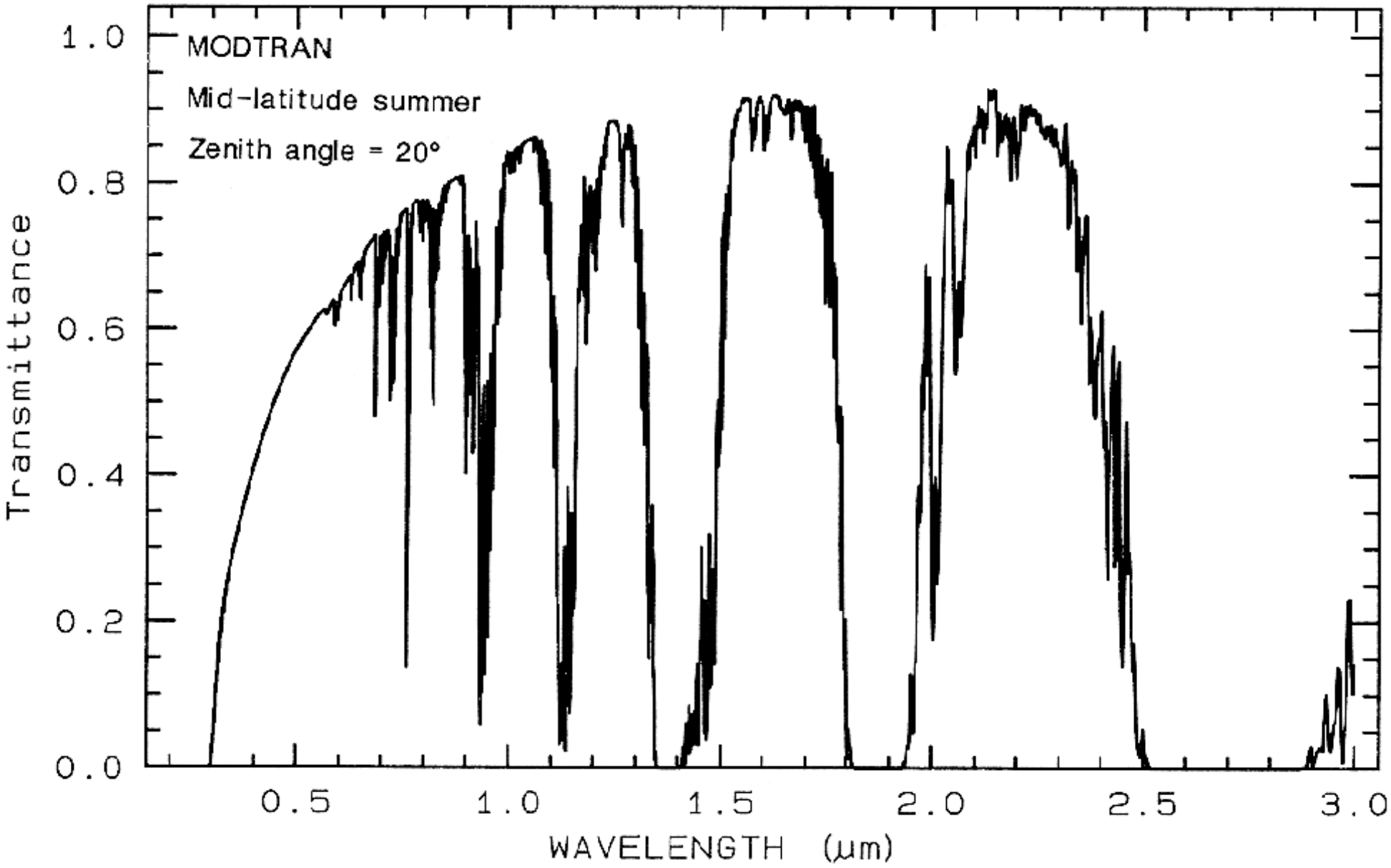
MODTRAN
Mid-latitude summer
Zenith angle = 20°
Transmittance
1.0
0.8
0.6
0.4
0.2
0.0
0.5
1.0
1.5
2.0
2.5
3.0
WAVELENGTH (μm)

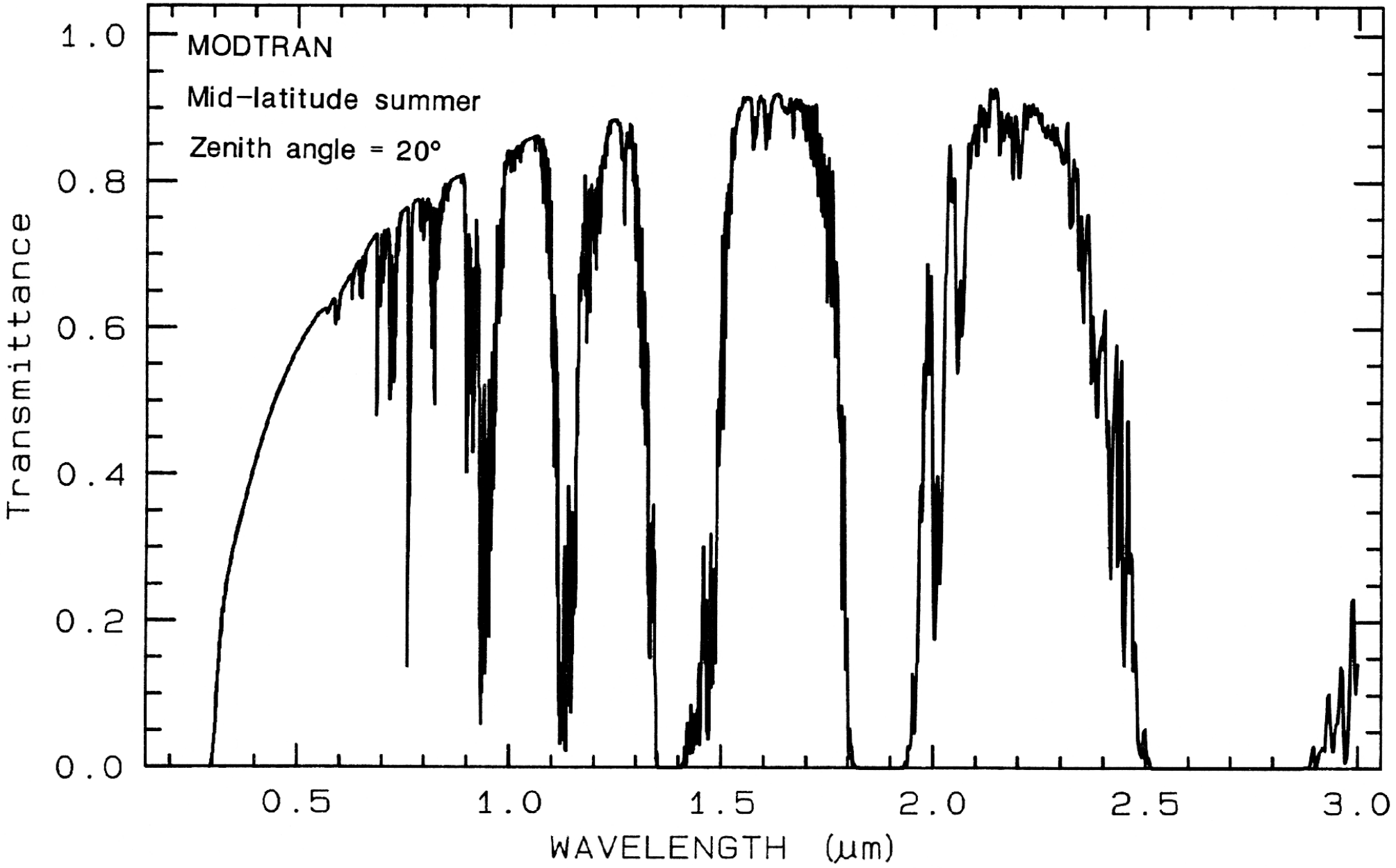
MODTRAN
Mid-latitude summer
Zenith angle = 20°
Transmittance
1.0
0.8
0.6
0.4
0.2
0.0
0.5
1.0
1.5
2.0
2.5
3.0
WAVELENGTH (μm)

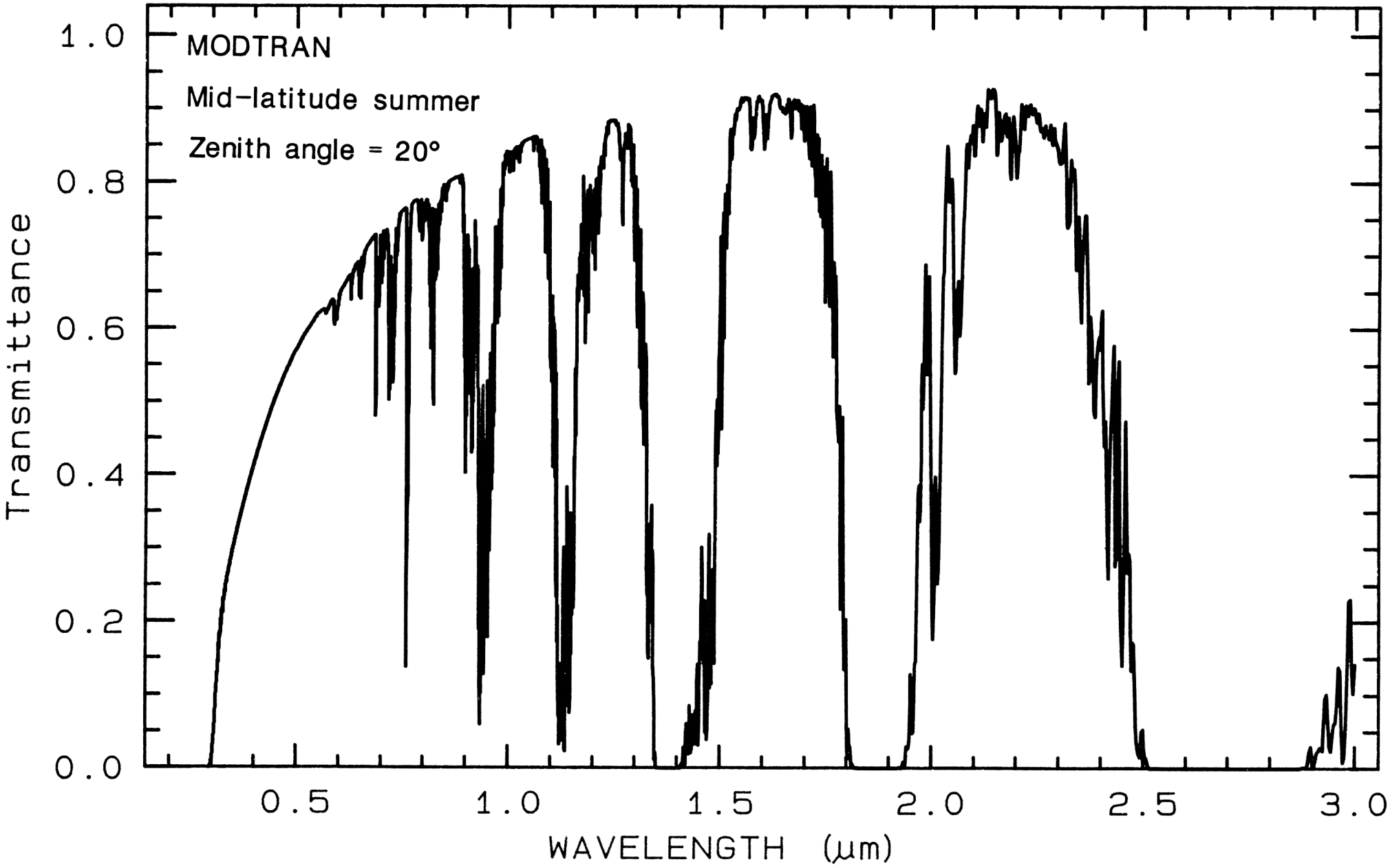
MODTRAN
Mid-latitude summer
Zenith angle = 20°
Transmittance
1.0
0.8
0.6
0.4
0.2
0.0
0.5
1.0
1.5
2.0
2.5
3.0
WAVELENGTH (μm)

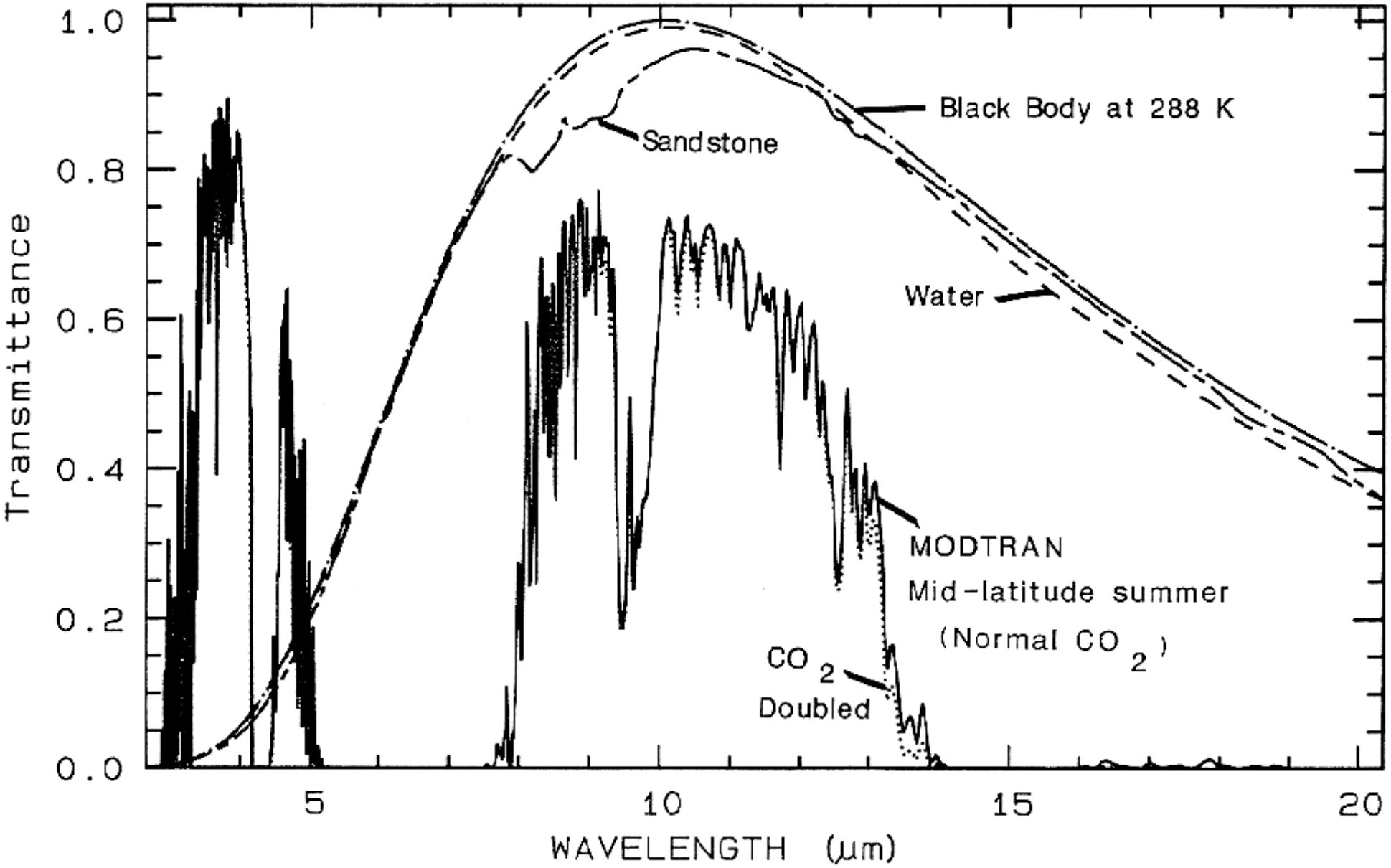
1.0
0.8
0.6
0.4
0.2
0.0
Transmittance
5
10
15
20
WAVELENGTH (μm)
Black Body at 288 K
Sandstone
Water
MODTRAN
Mid-latitude summer
(Normal CO 2)
CO 2
Doubled

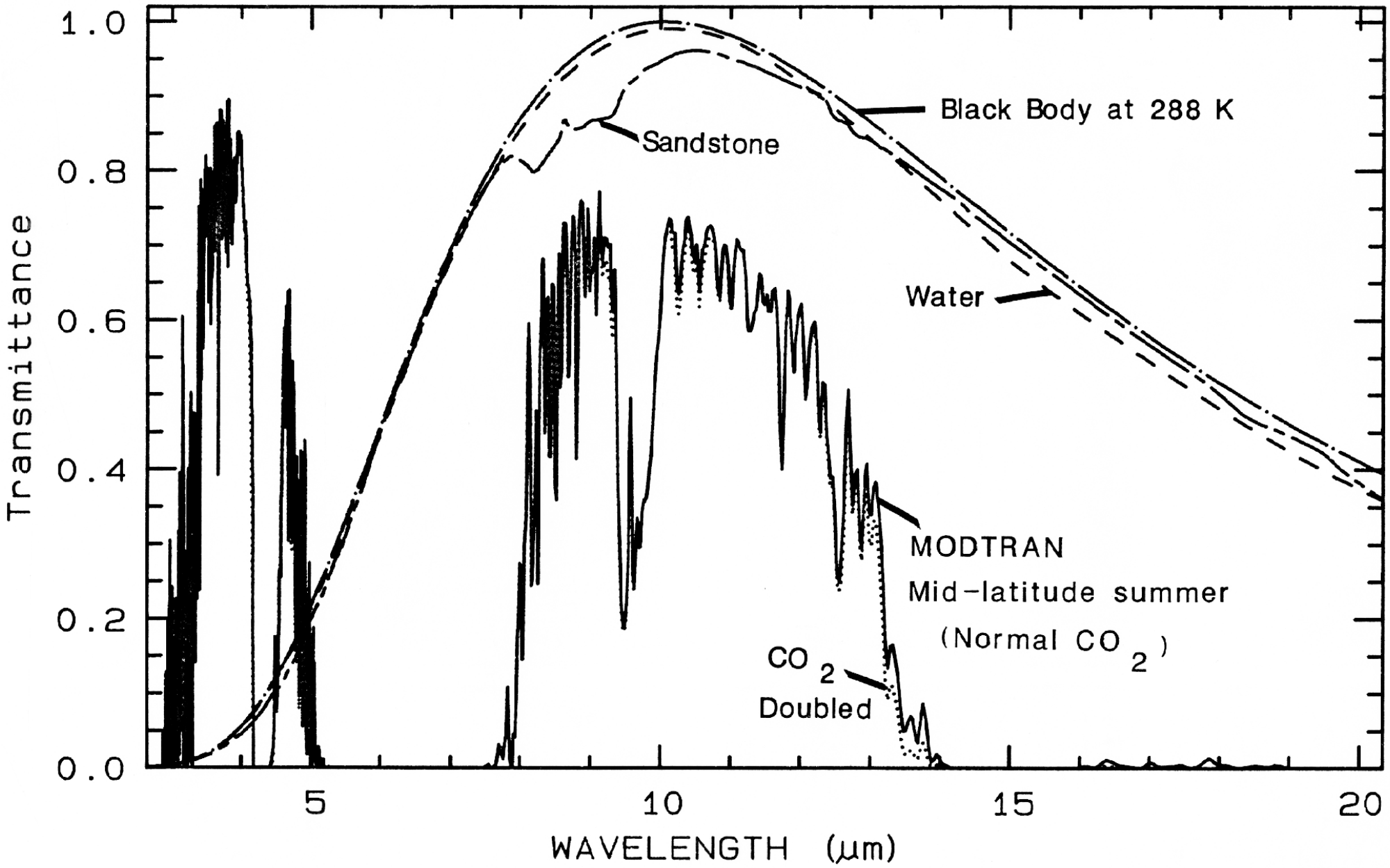
1.0
0.8
0.6
0.4
0.2
0.0
Transmittance
5
10
15
20
WAVELENGTH (μm)
Black Body at 288 K
Sandstone
Water
MODTRAN
Mid-latitude summer
(Normal CO 2)
CO 2
Doubled

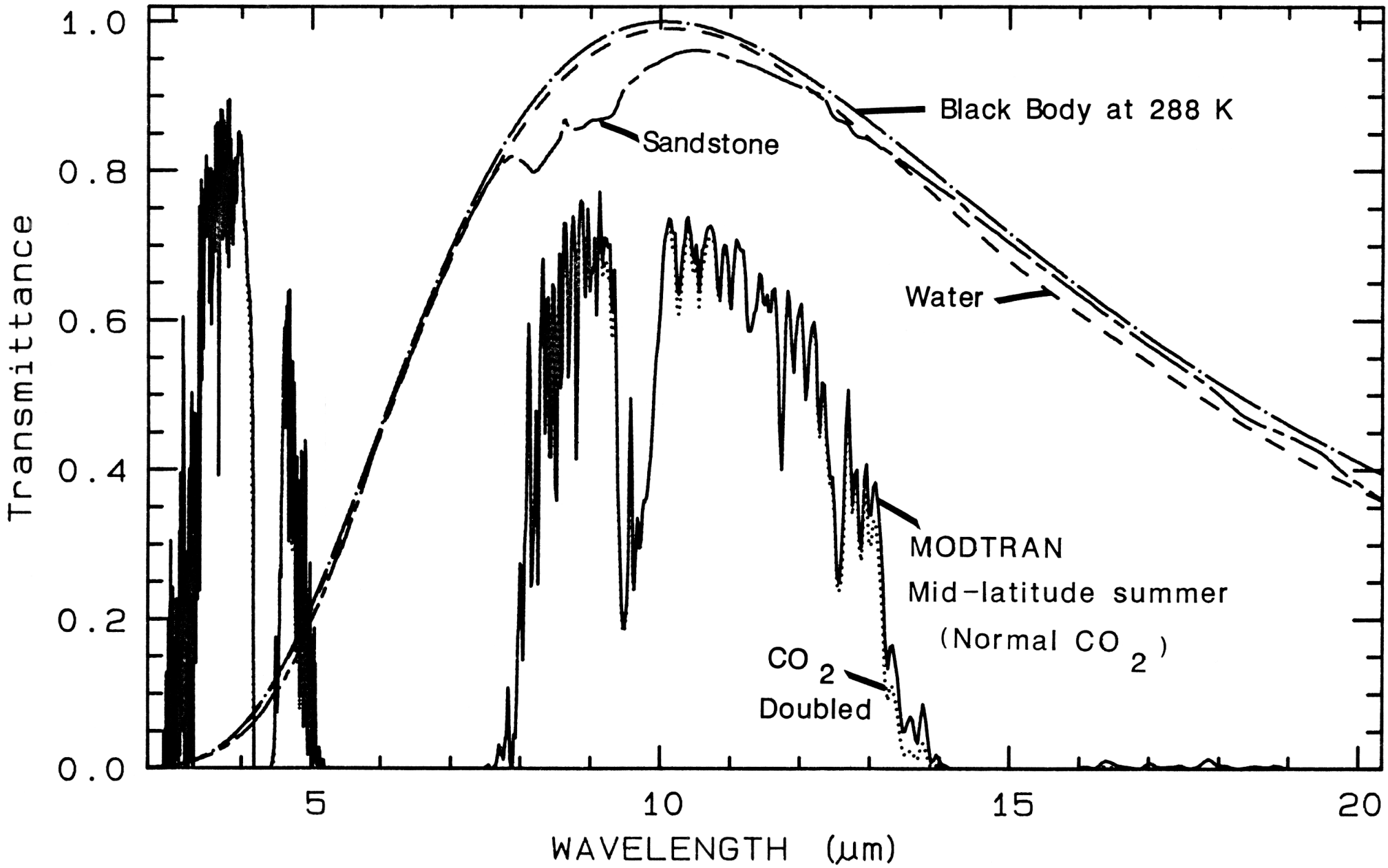
1.0
0.8
0.6
0.4
0.2
0.0
Transmittance
5
10
15
20
WAVELENGTH (μm)
Black Body at 288 K
Sandstone
Water
MODTRAN
Mid-latitude summer
(Normal CO 2)
CO 2
Doubled

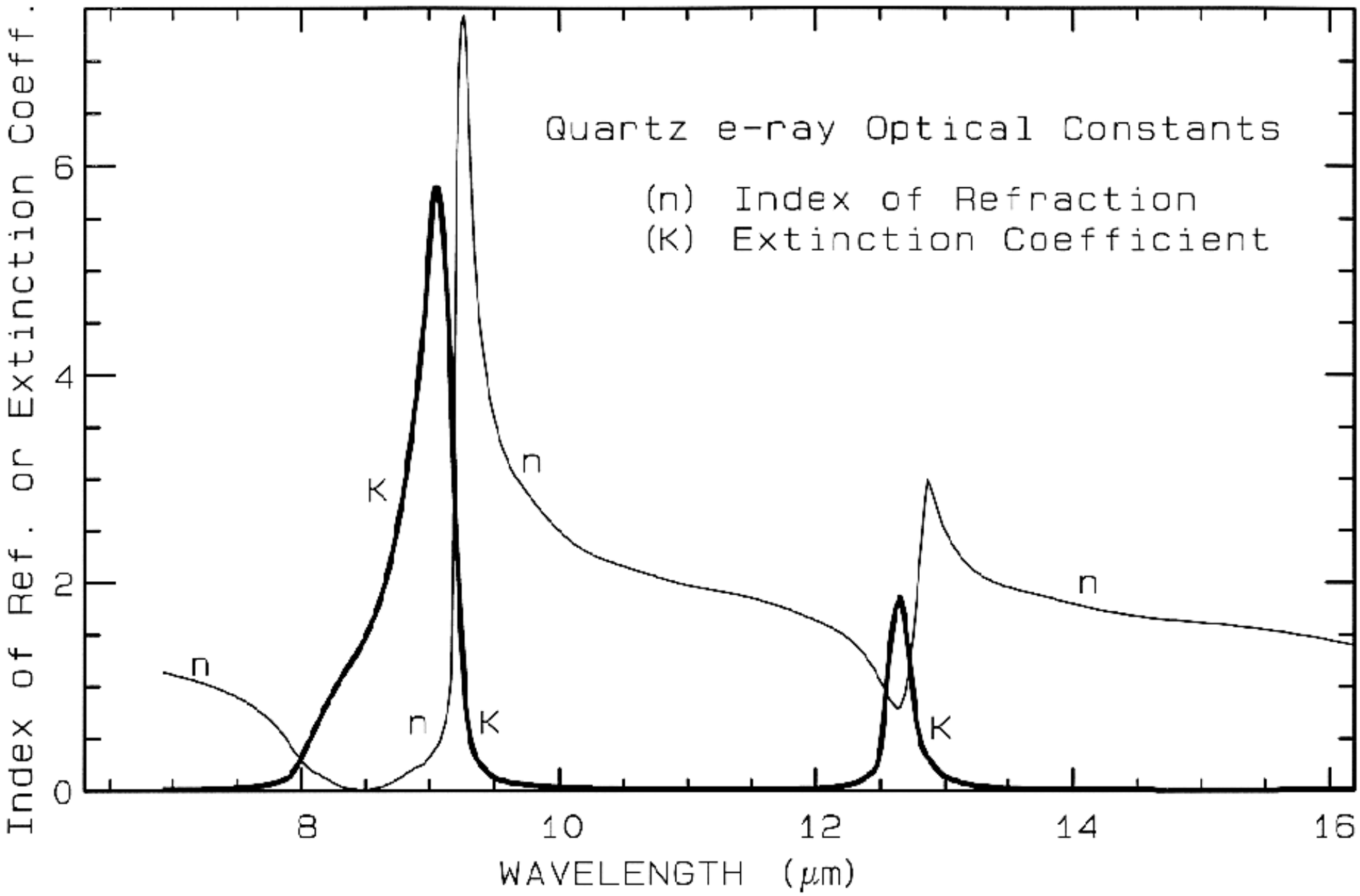
Quartz e-ray Optical Constants
(n) Index of Refraction
(K) Extinction Coefficient
Index of Ref. or Extinction Coeff.
0
2
4
6
8
10
12
14
16
WAVELENGTH (μm)
n
K
n
K
n
K
n

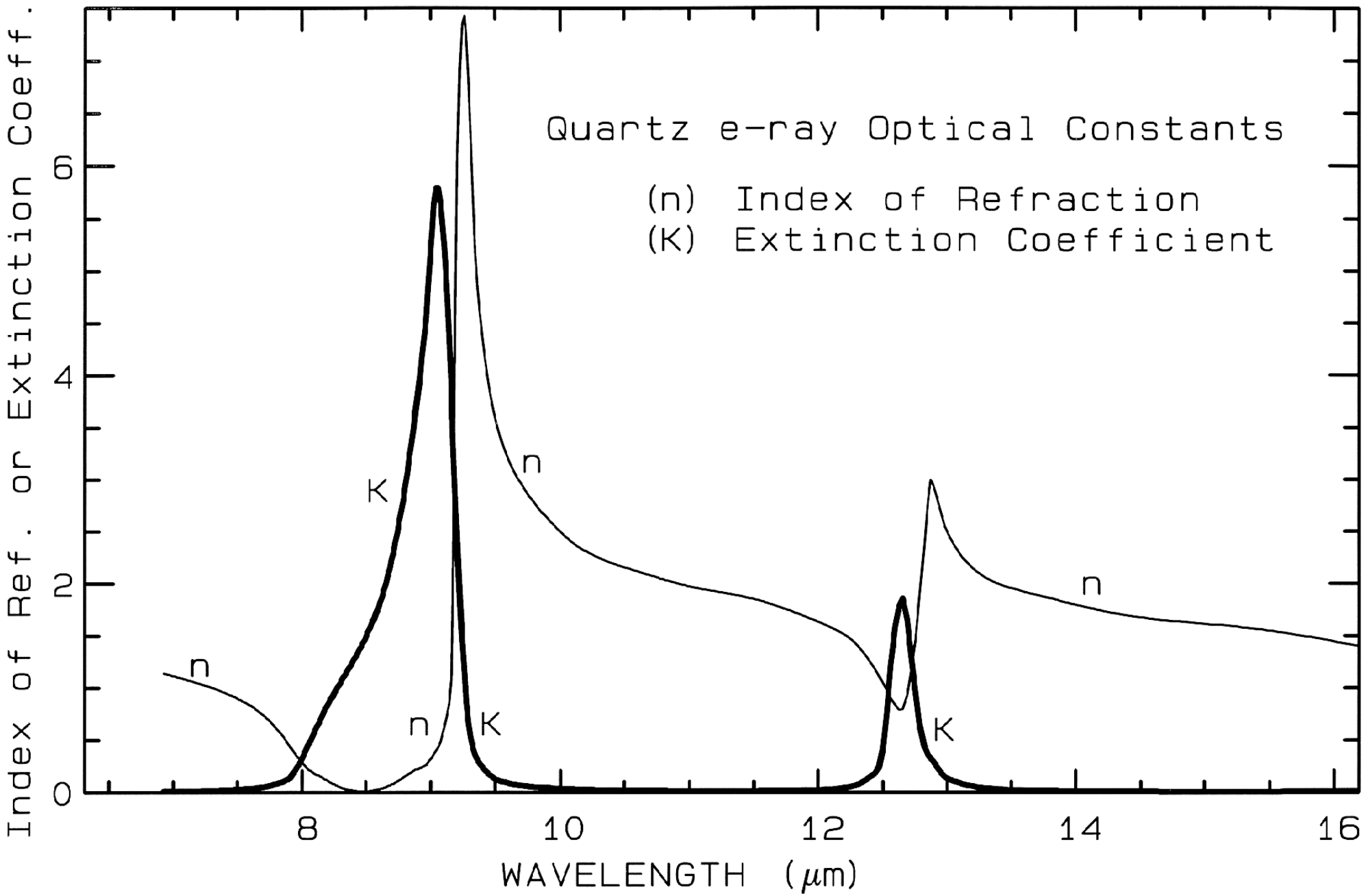
Quartz e-ray Optical Constants
(n) Index of Refraction
(K) Extinction Coefficient
Index of Ref. or Extinction Coeff.
0
2
4
6
8
10
12
14
16
WAVELENGTH (μm)
n
K
n
n
K
n
K

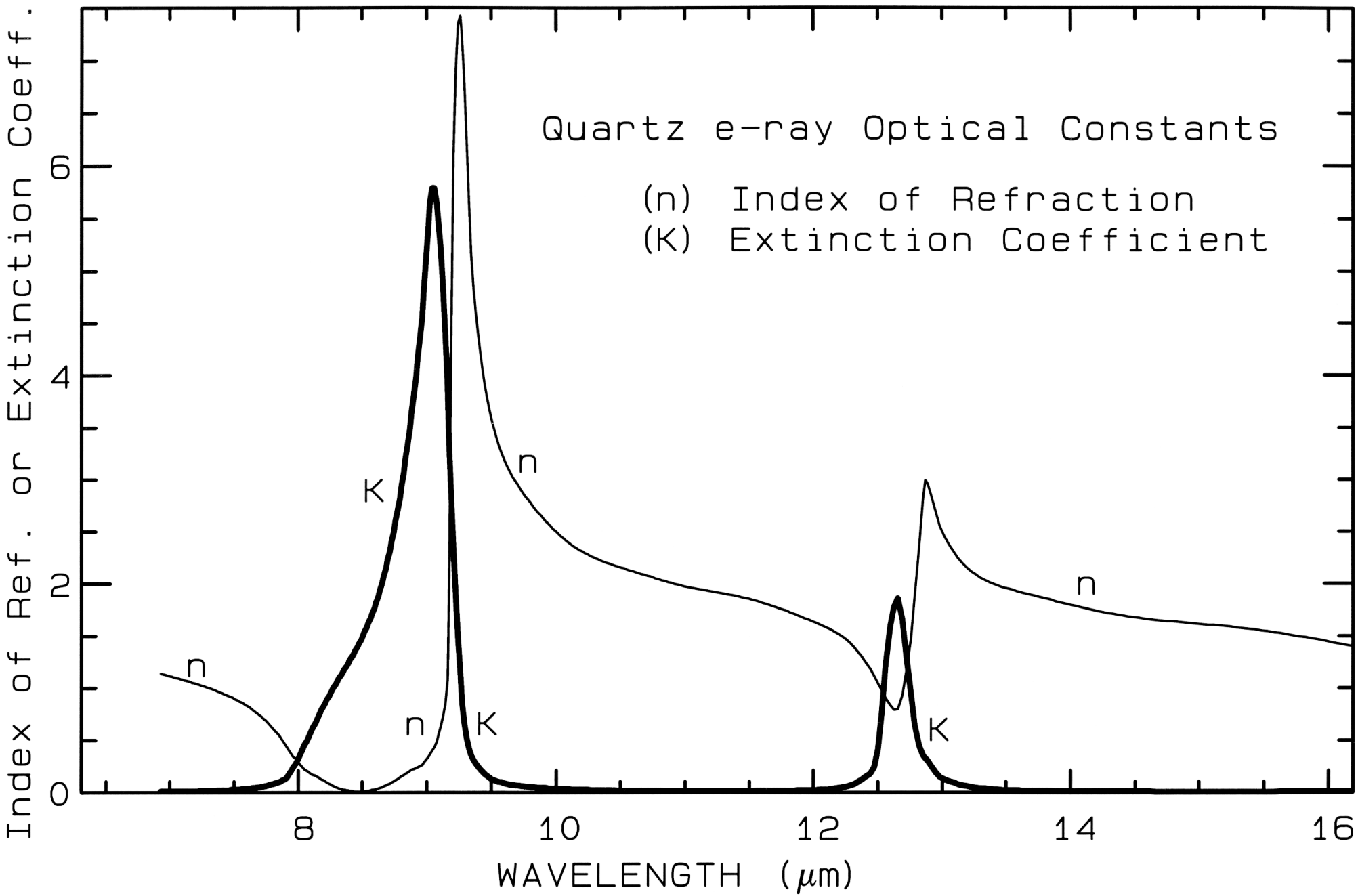
Quartz e-ray Optical Constants
(n) Index of Refraction
(K) Extinction Coefficient
Index of Ref. or Extinction Coeff.
0
2
4
6
8
10
12
14
16
WAVELENGTH (μm)
n
K
n
n
K
n
K

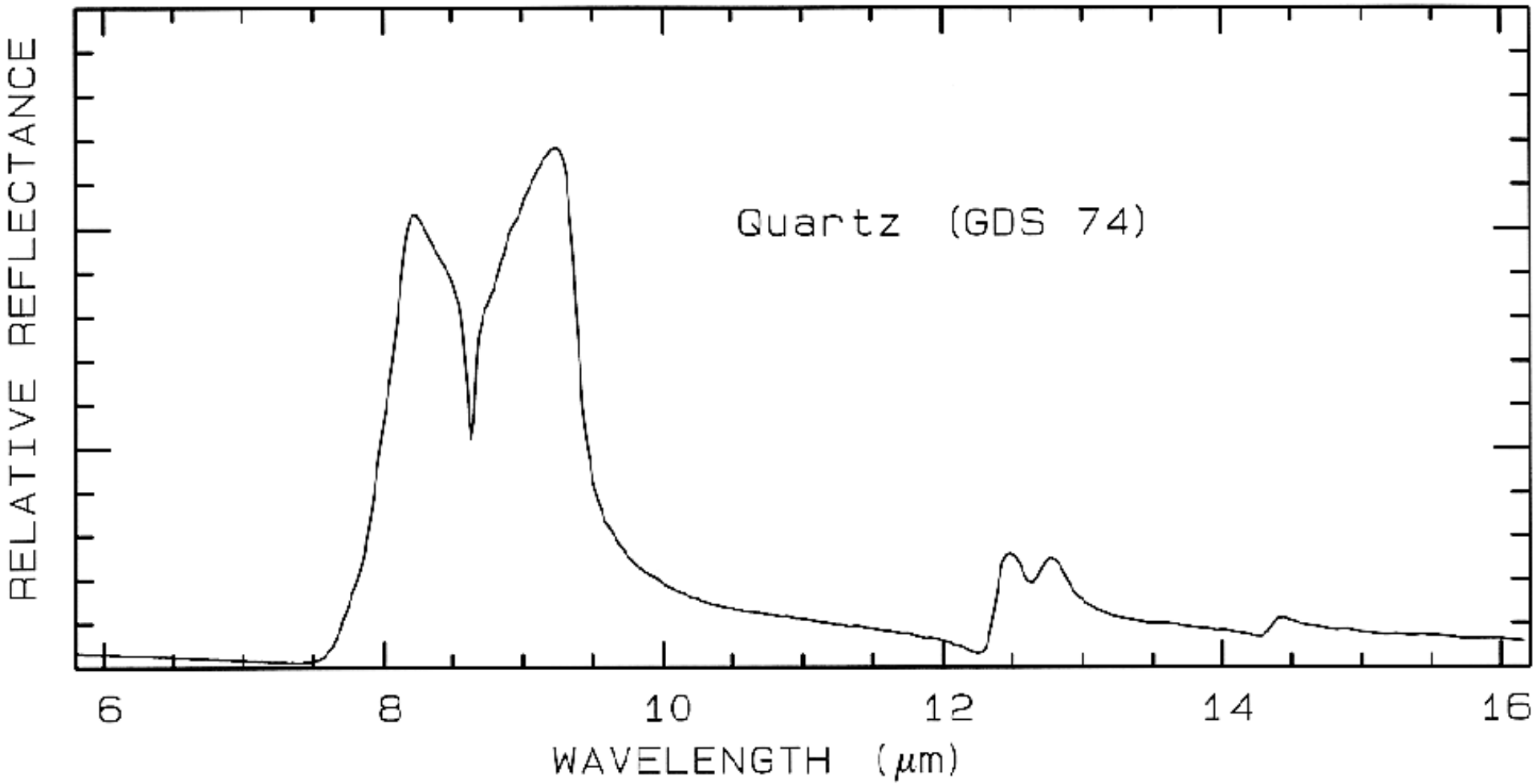
RELATIVE REFLECTANCE
Quartz (GDS 74)
6
8
10
12
14
16
WAVELENGTH (μm)

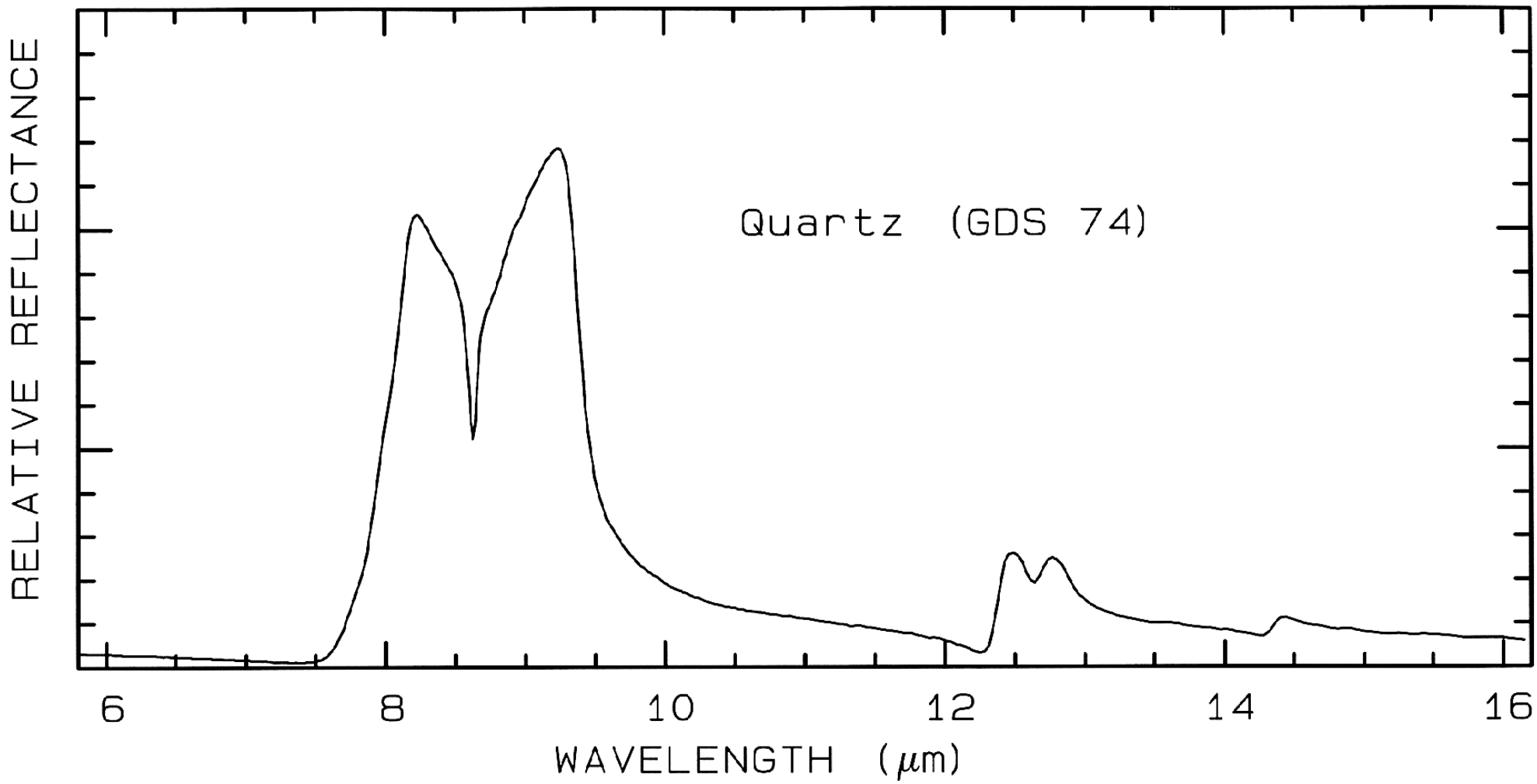
RELATIVE REFLECTANCE
Quartz (GDS 74)
6
8
10
12
14
16
WAVELENGTH (μm)

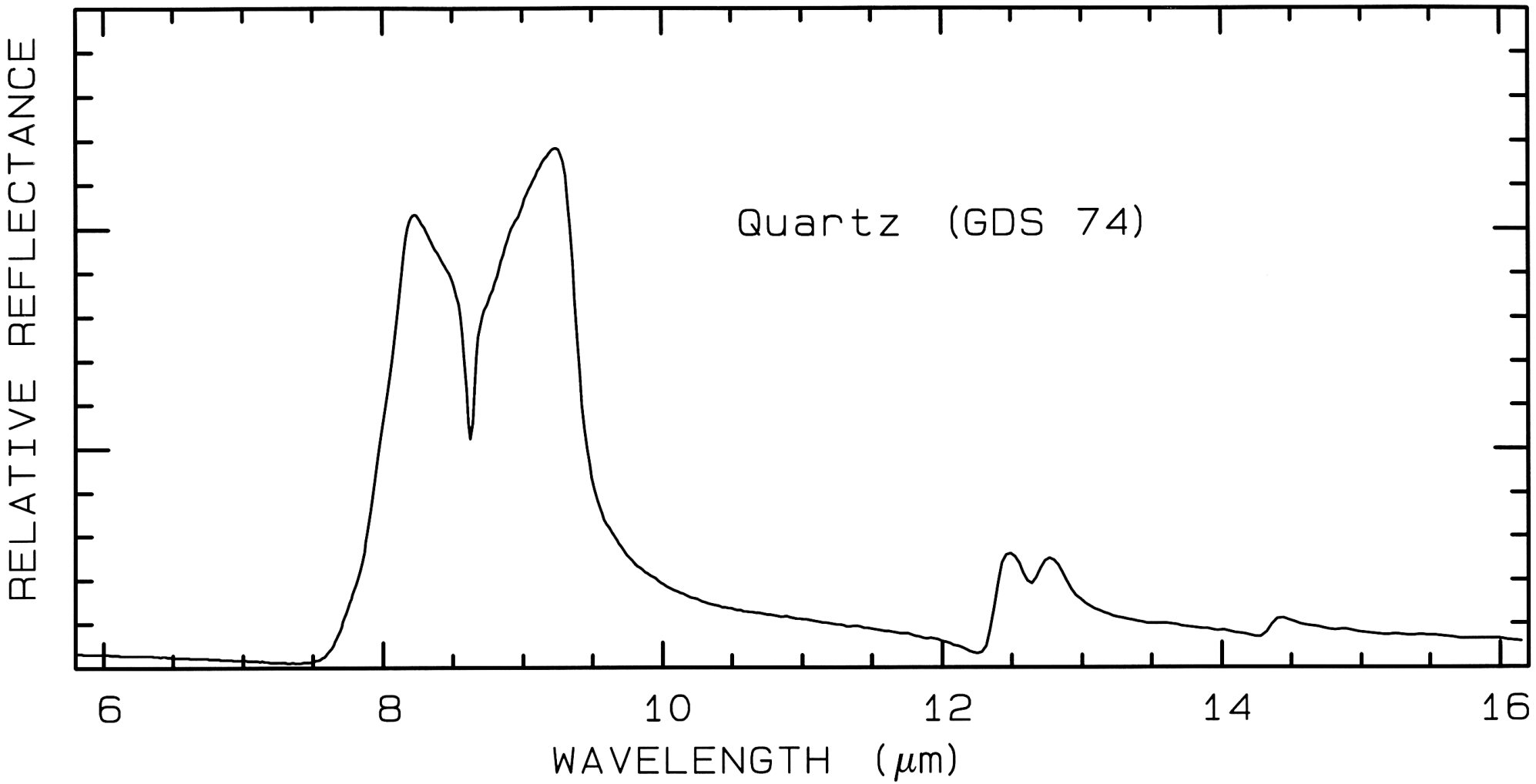
RELATIVE REFLECTANCE
Quartz (GDS 74)
6
8
10
12
14
16
WAVELENGTH (μm)

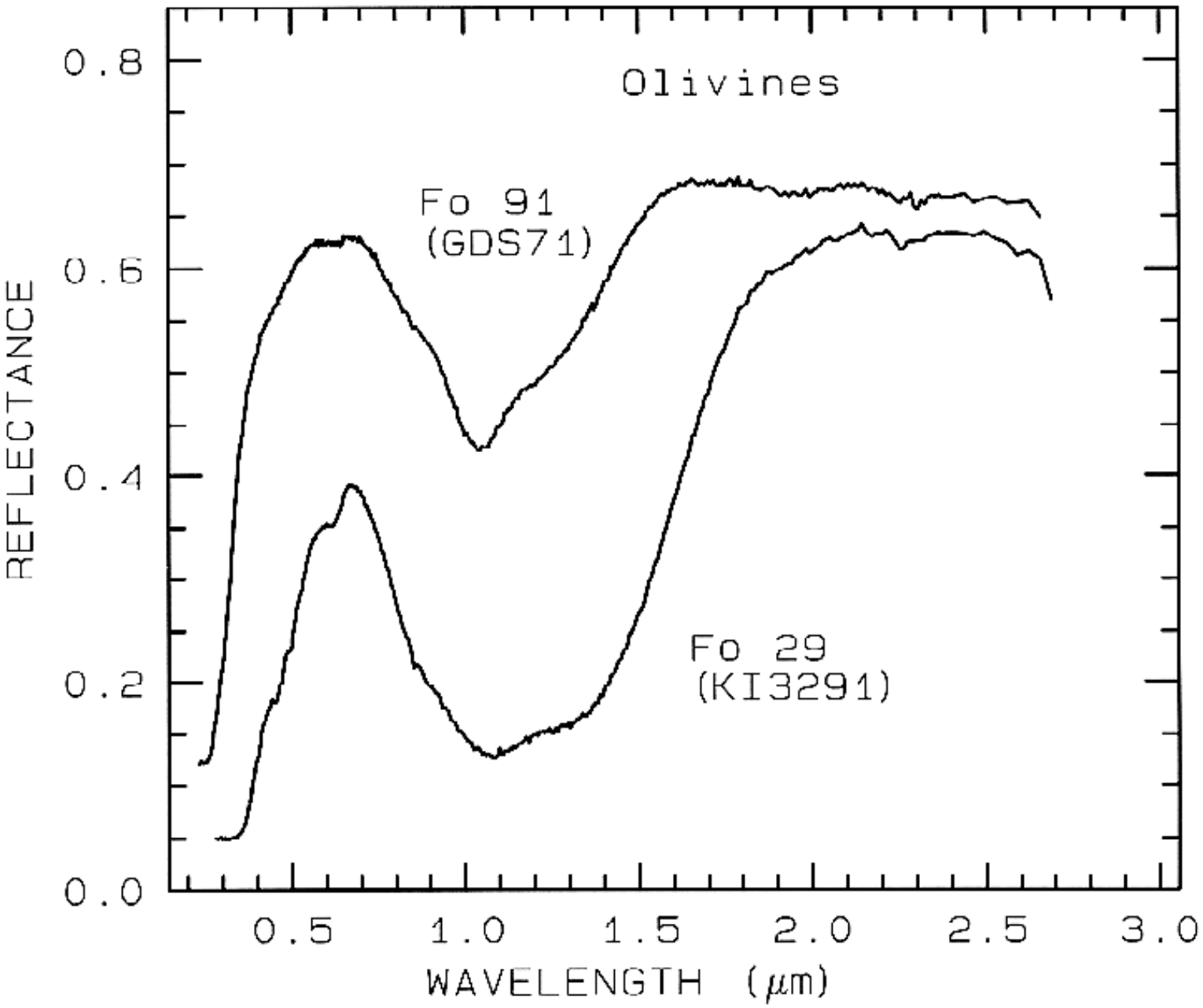
Olivines
Fo 91
(GDS71)
Fo 29
(KI3291)
REFLECTANCE
0.0
0.2
0.4
0.6
0.8
0.5
1.0
1.5
2.0
2.5
3.0
WAVELENGTH (μm)

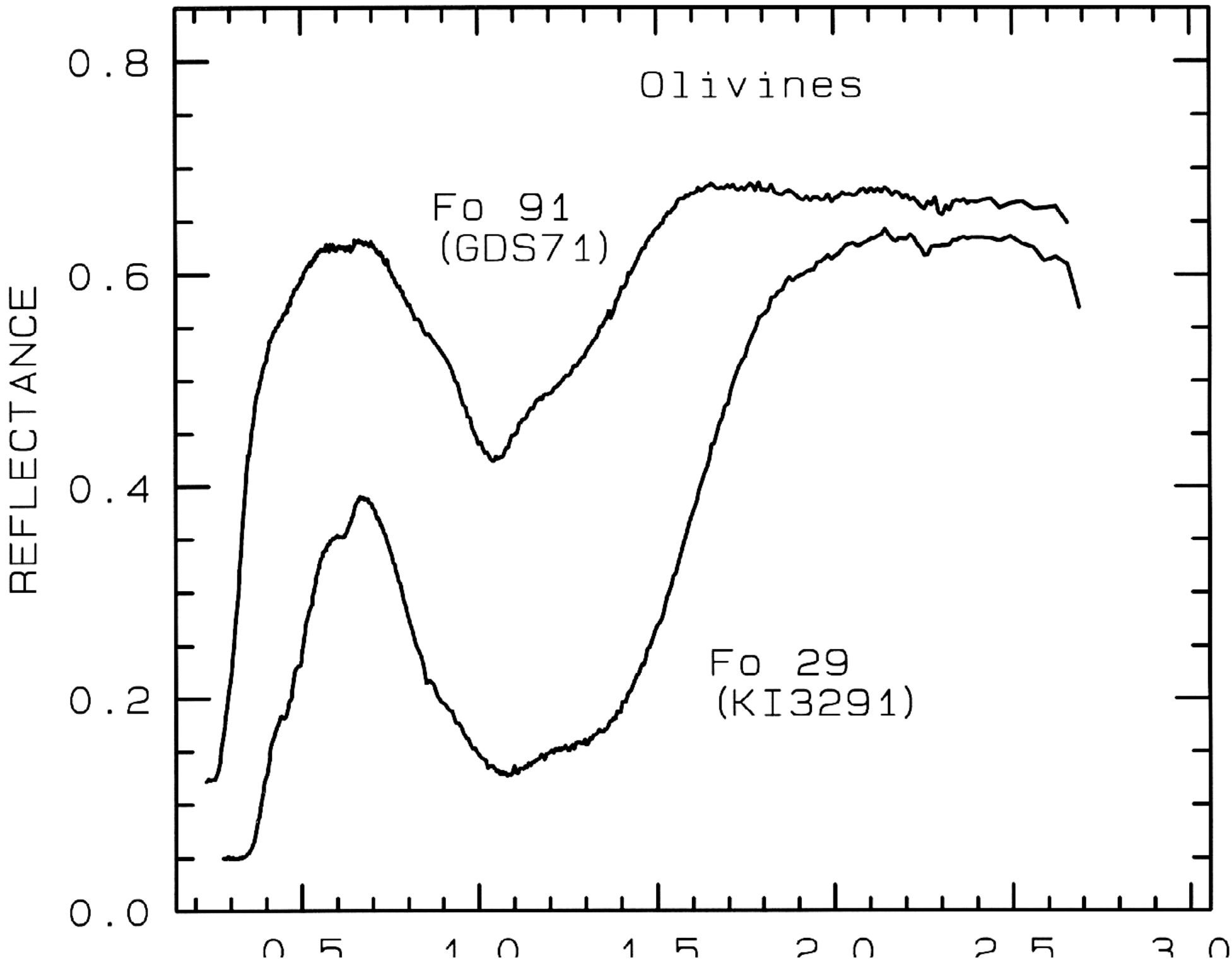
Olivines
Fo 91
(GDS71)
Fo 29
(KI3291)
REFLECTANCE
0.0
0.2
0.4
0.6
0.8
0.5
1.0
1.5
2.0
2.5
3.0

WAVELENGTH (μm)

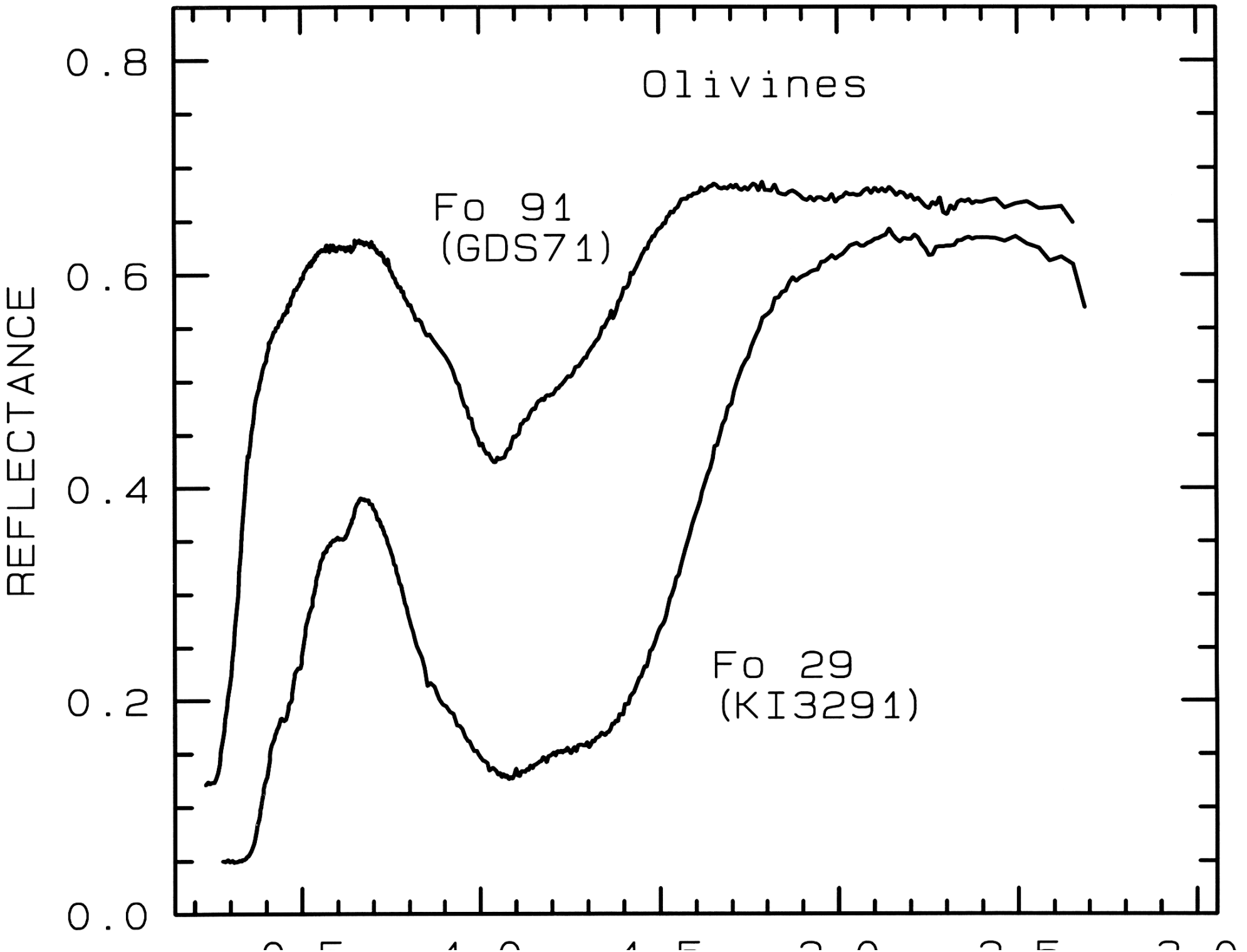
Olivines
Fo 91
(GDS71)
Fo 29
(KI3291)
REFLECTANCE
0.8
0.6
0.4
0.2
0.0

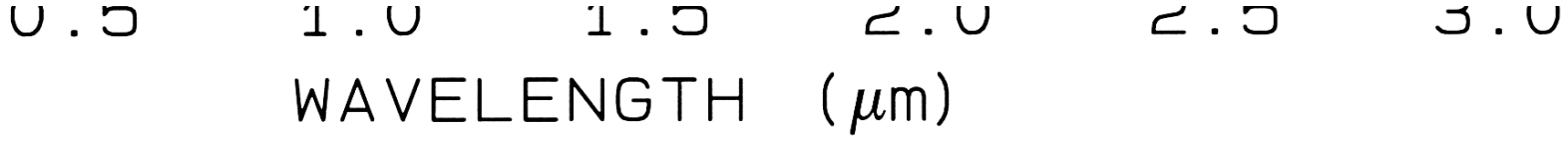
0.5
1.0
1.5
2.0
2.5
3.0
WAVELENGTH (μm)

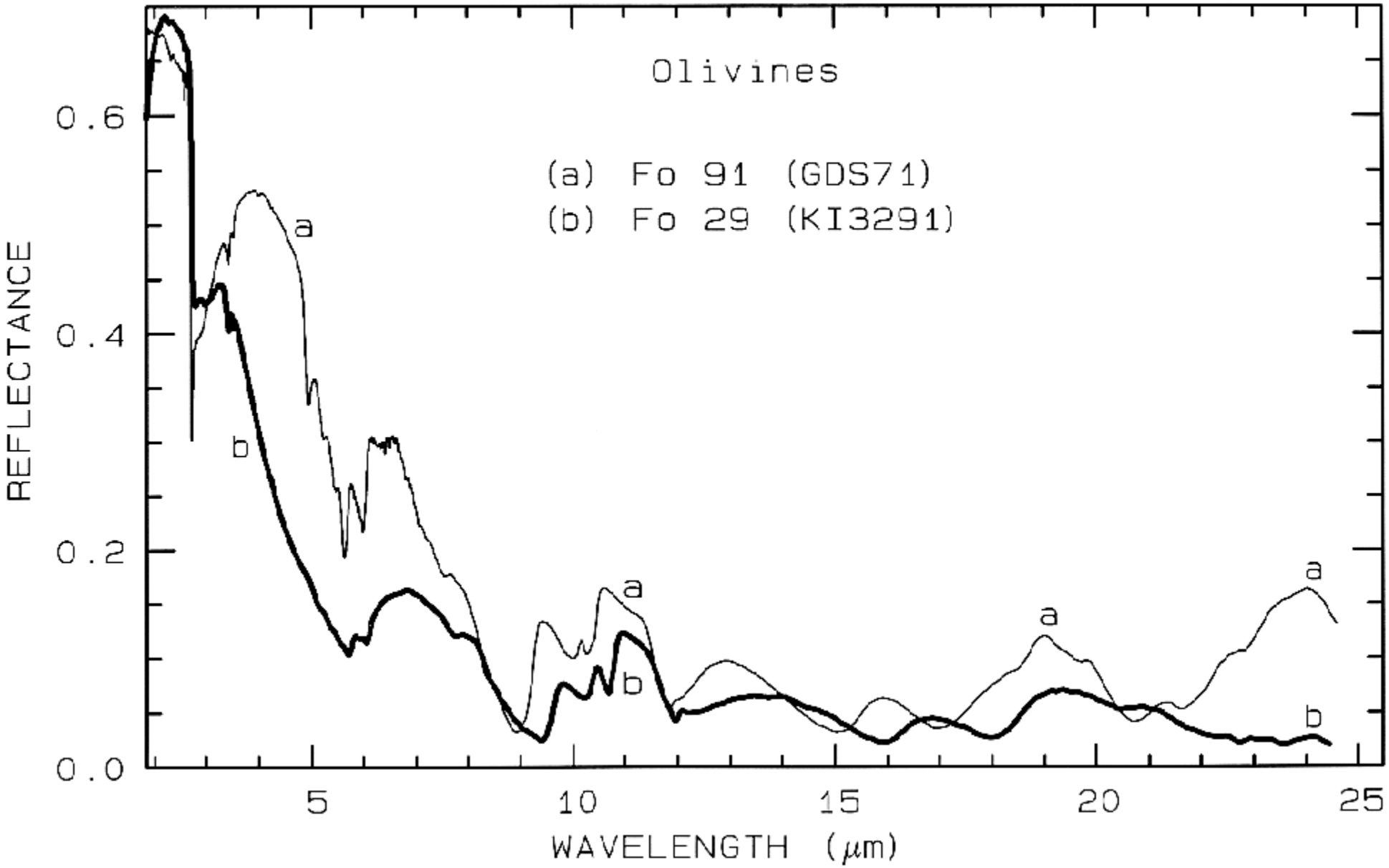
Olivines
(a) Fo 91 (GDS71)
(b) Fo 29 (KI3291)
REFLECTANCE
0.0
0.2
0.4
0.6
5
10
15
20
25
WAVELENGTH (μm)
a
b
a
b
a
b
a
b

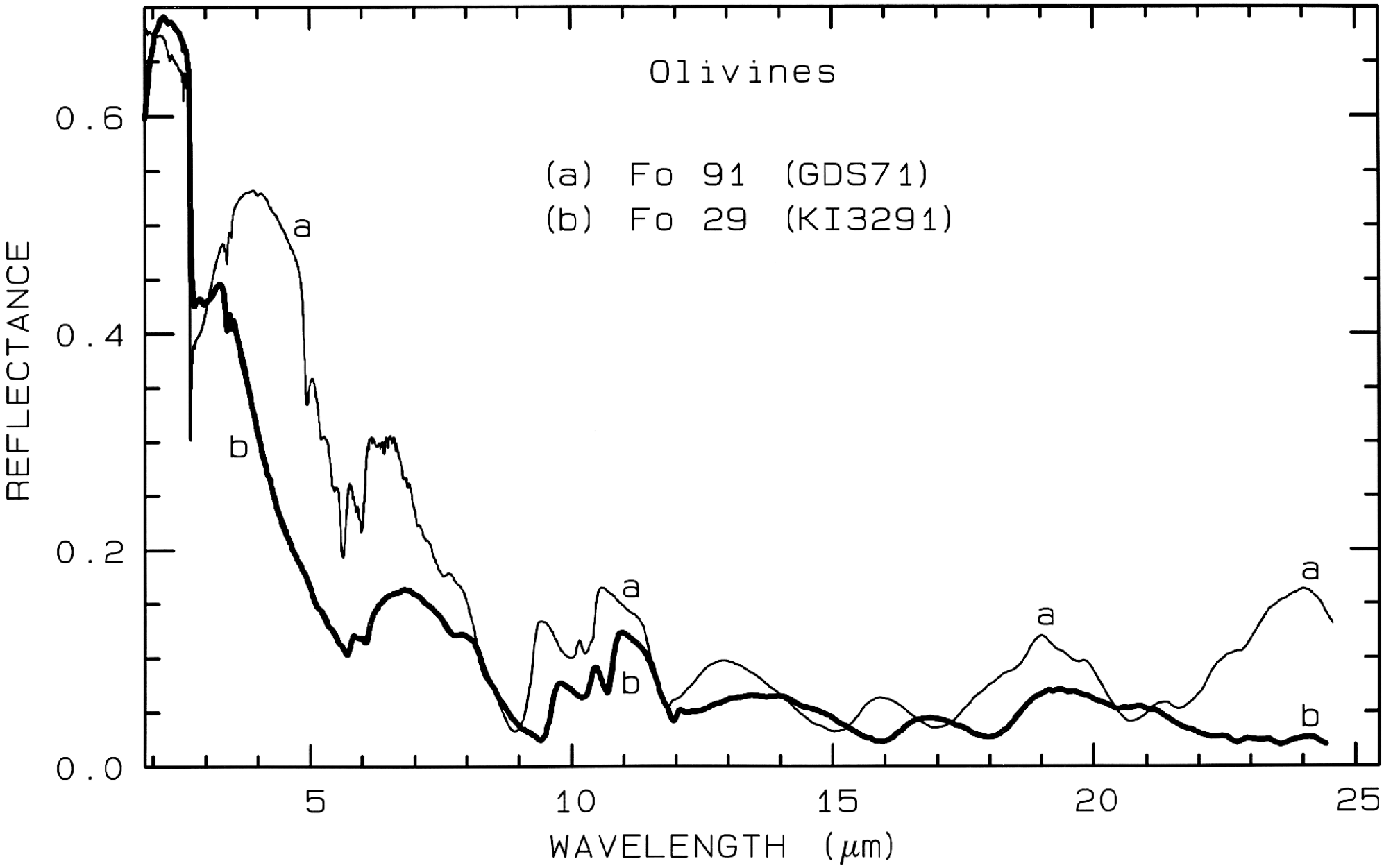
Olivines
(a) Fo 91 (GDS71)
(b) Fo 29 (KI3291)
REFLECTANCE
0.0
0.2
0.4
0.6
5
10
15
20
25
WAVELENGTH (μm)
a
b
a
b
a
b

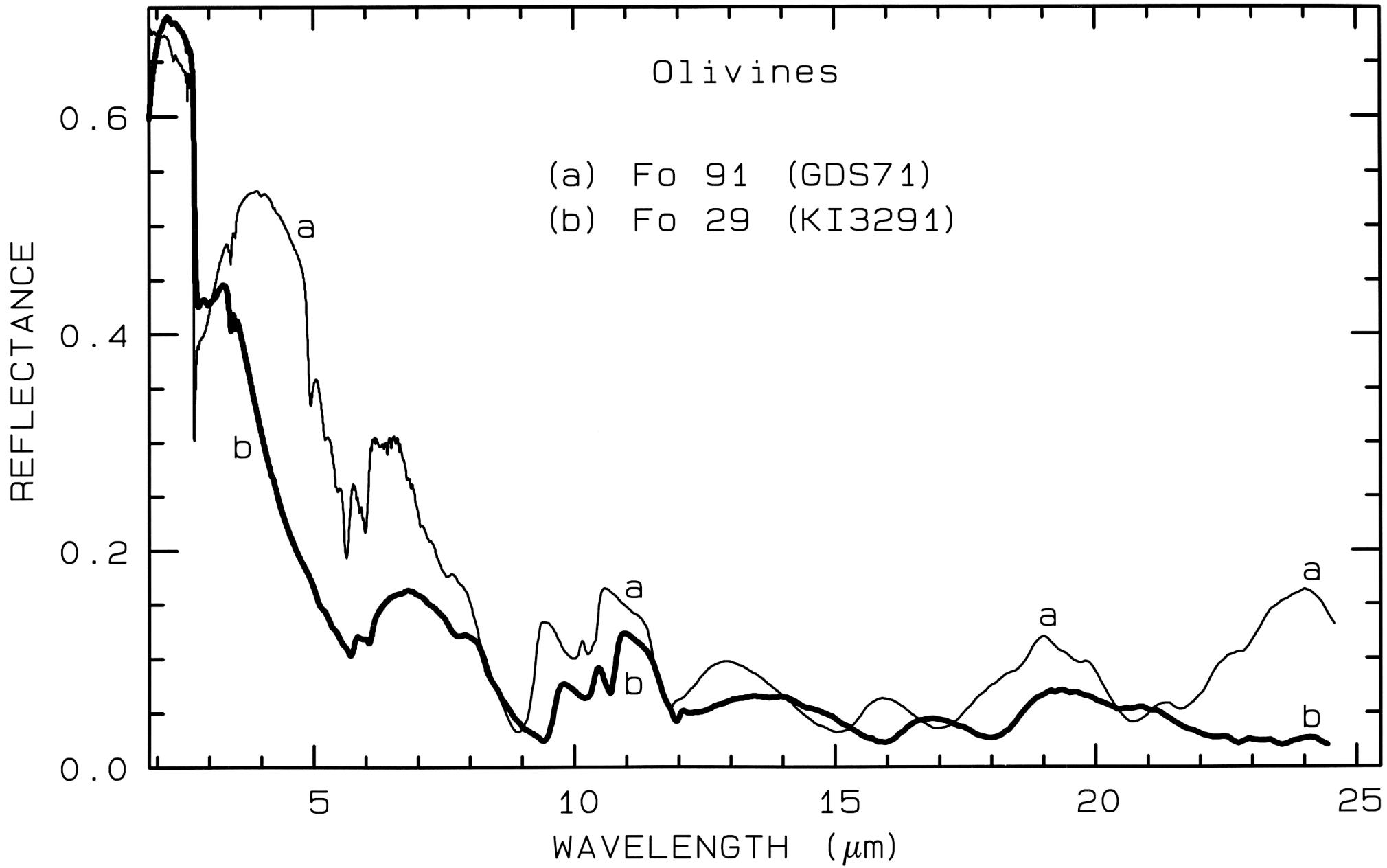
Olivines
(a) Fo 91 (GDS71)
(b) Fo 29 (KI3291)
REFLECTANCE
0.0
0.2
0.4
0.6
5
10
15
20
25
WAVELENGTH (μm)
a
b
a
b
a
b
a
b

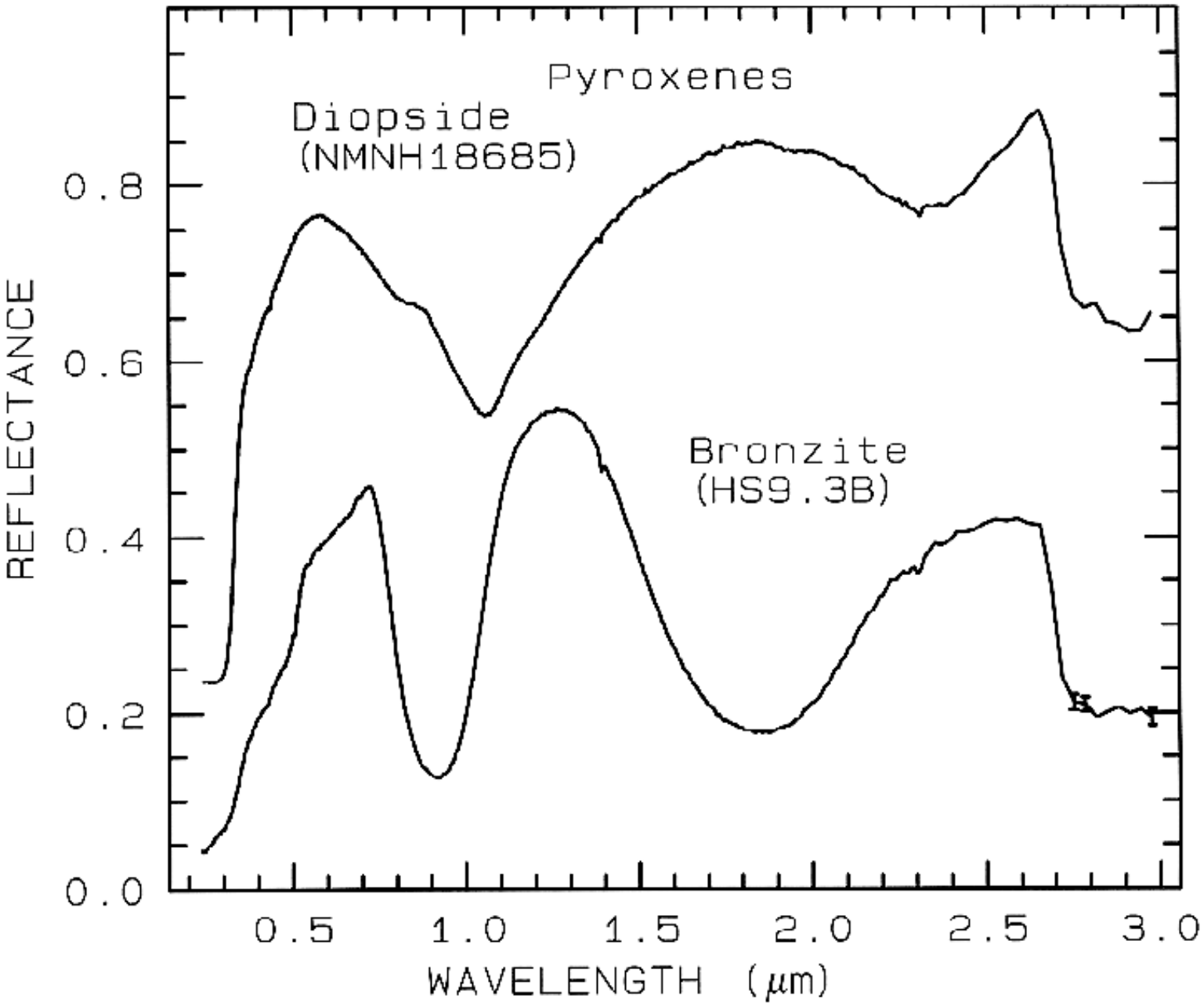
Pyroxenes
Diopside
(NMNH18685)
Bronzite
(HS9.3B)
REFLECTANCE
0.0
0.2
0.4
0.6
0.8
0.5
1.0
1.5
2.0
2.5
3.0
WAVELENGTH (μm)

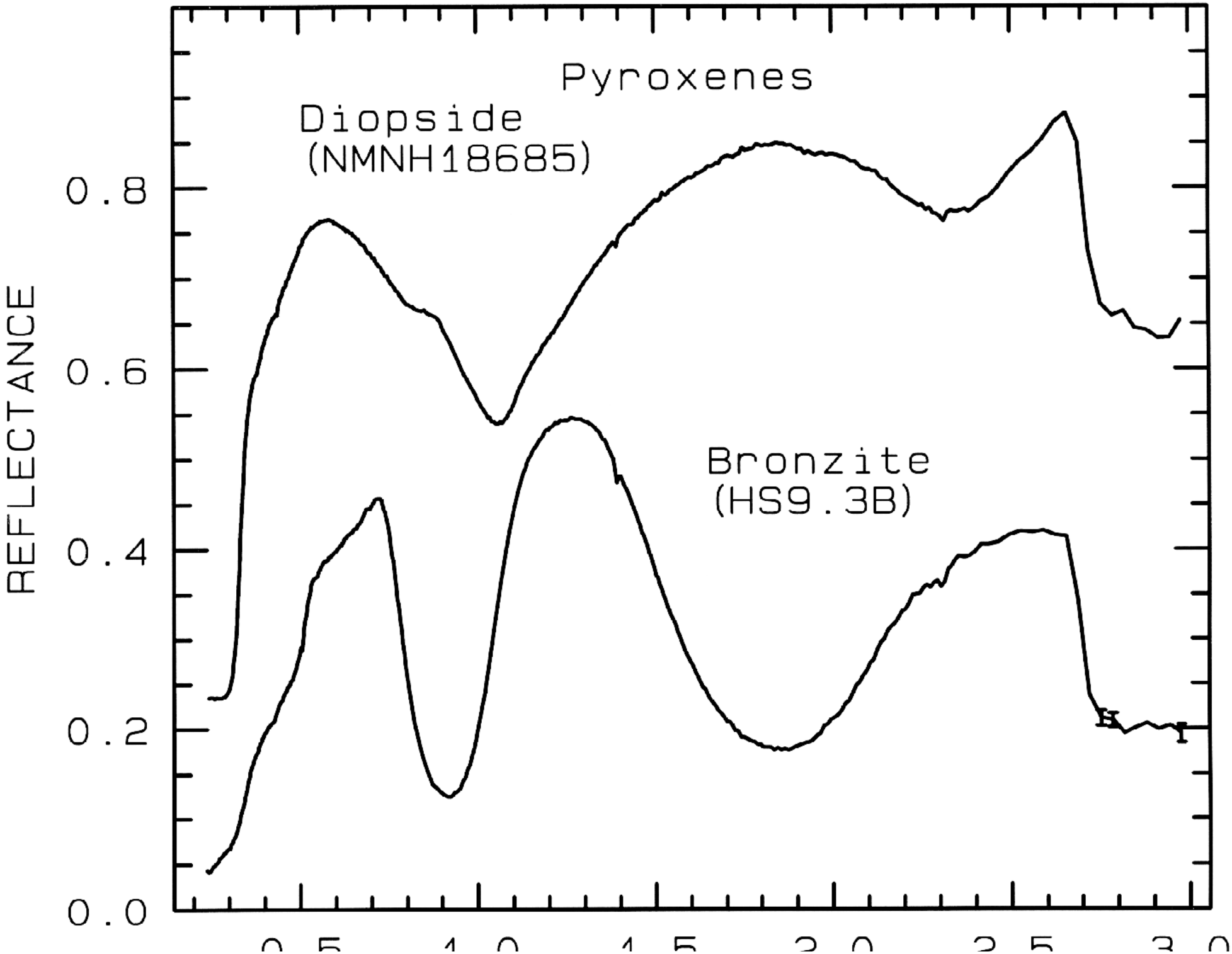
Pyroxenes
Diopside
(NMNH18685)
Bronzite
(HS9.3B)
REFLECTANCE
0.0
0.2
0.4
0.6
0.8
0.5
1.0
1.5
2.0
2.5
3.0

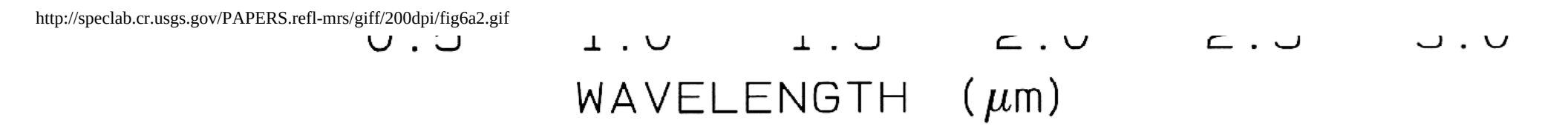
WAVELENGTH (μm)

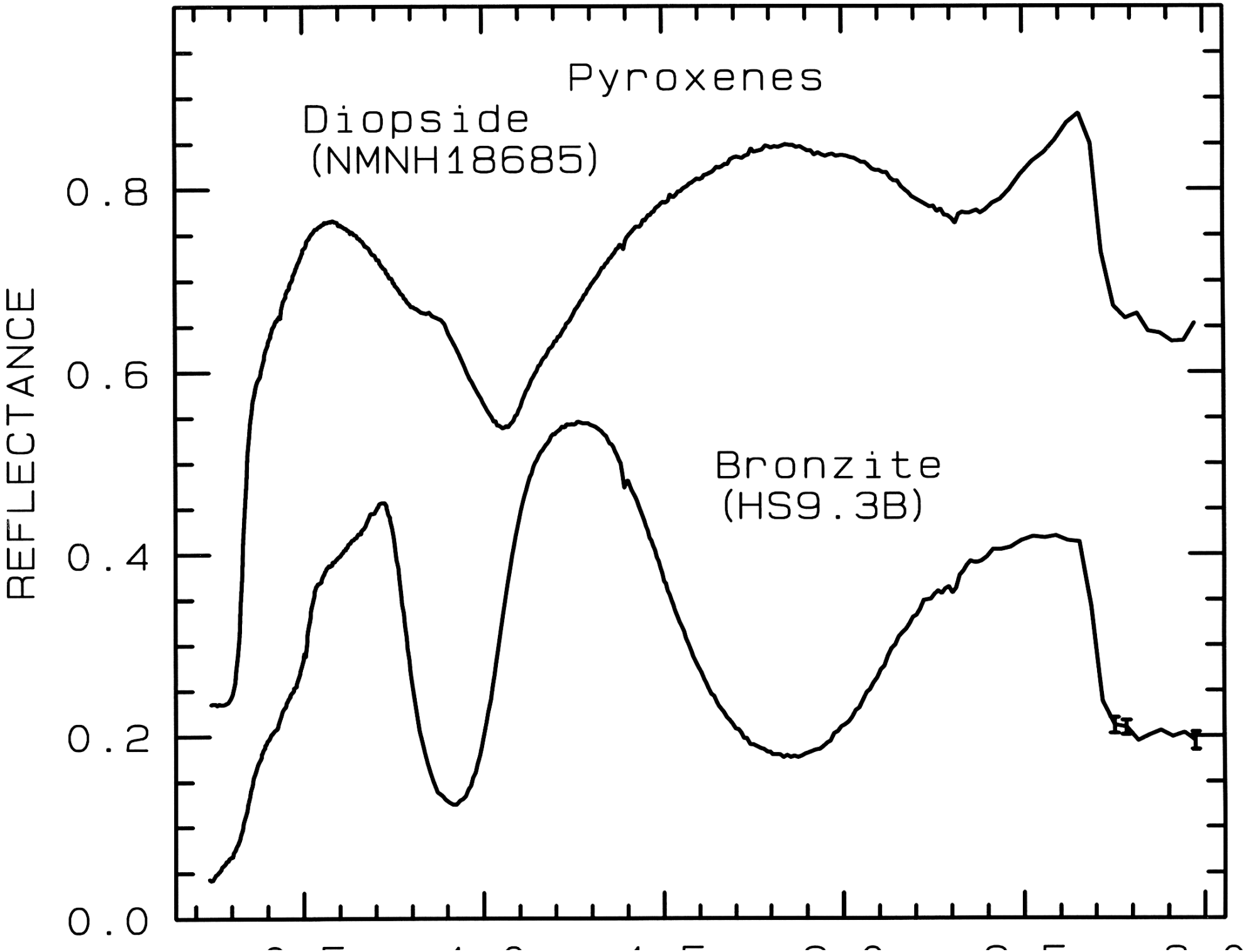
Pyroxenes
Diopside
(NMNH18685)
Bronzite
(HS9.3B)
REFLECTANCE
0.8
0.6
0.4
0.2
0.0

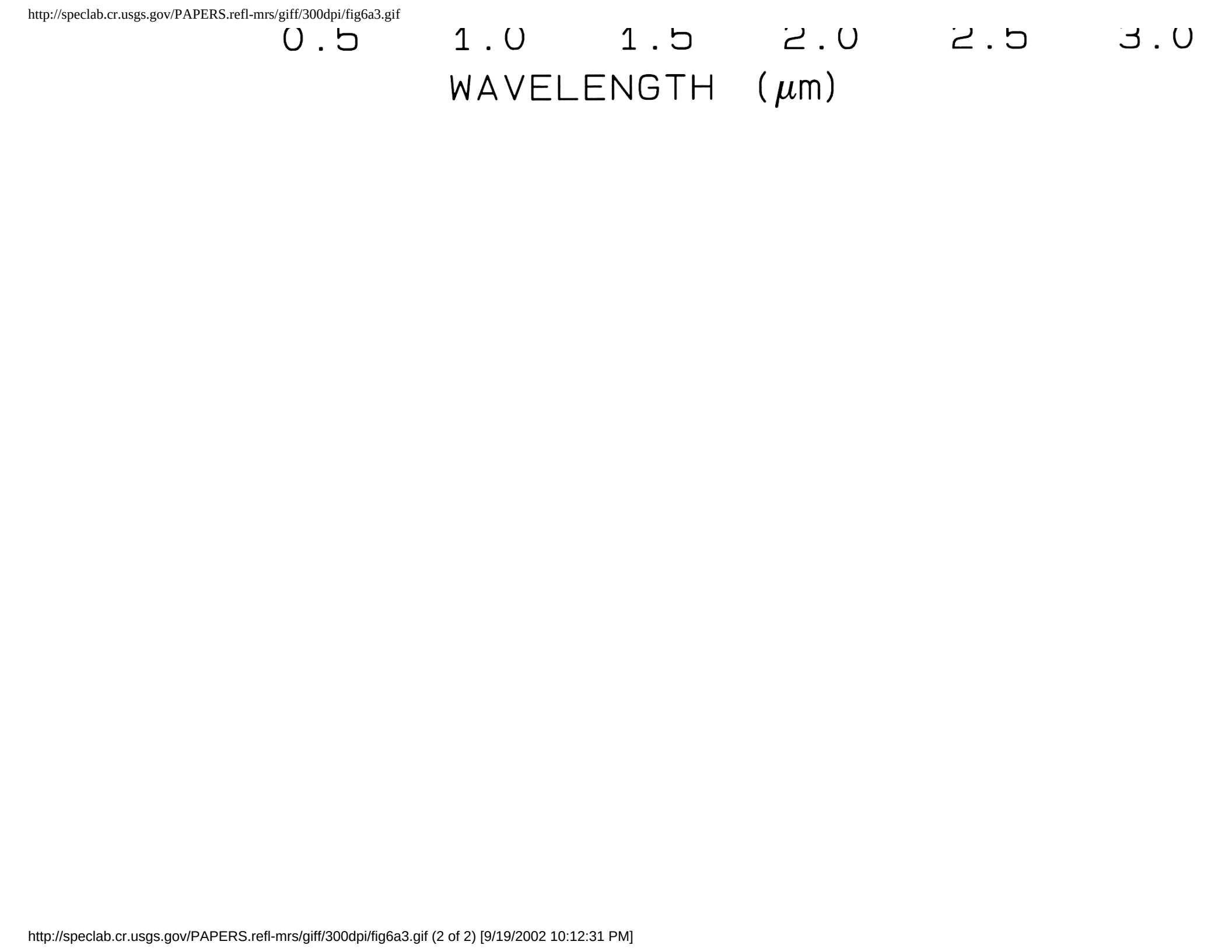
0.5
1.0
1.5
2.0
2.5
3.0
WAVELENGTH (μm)

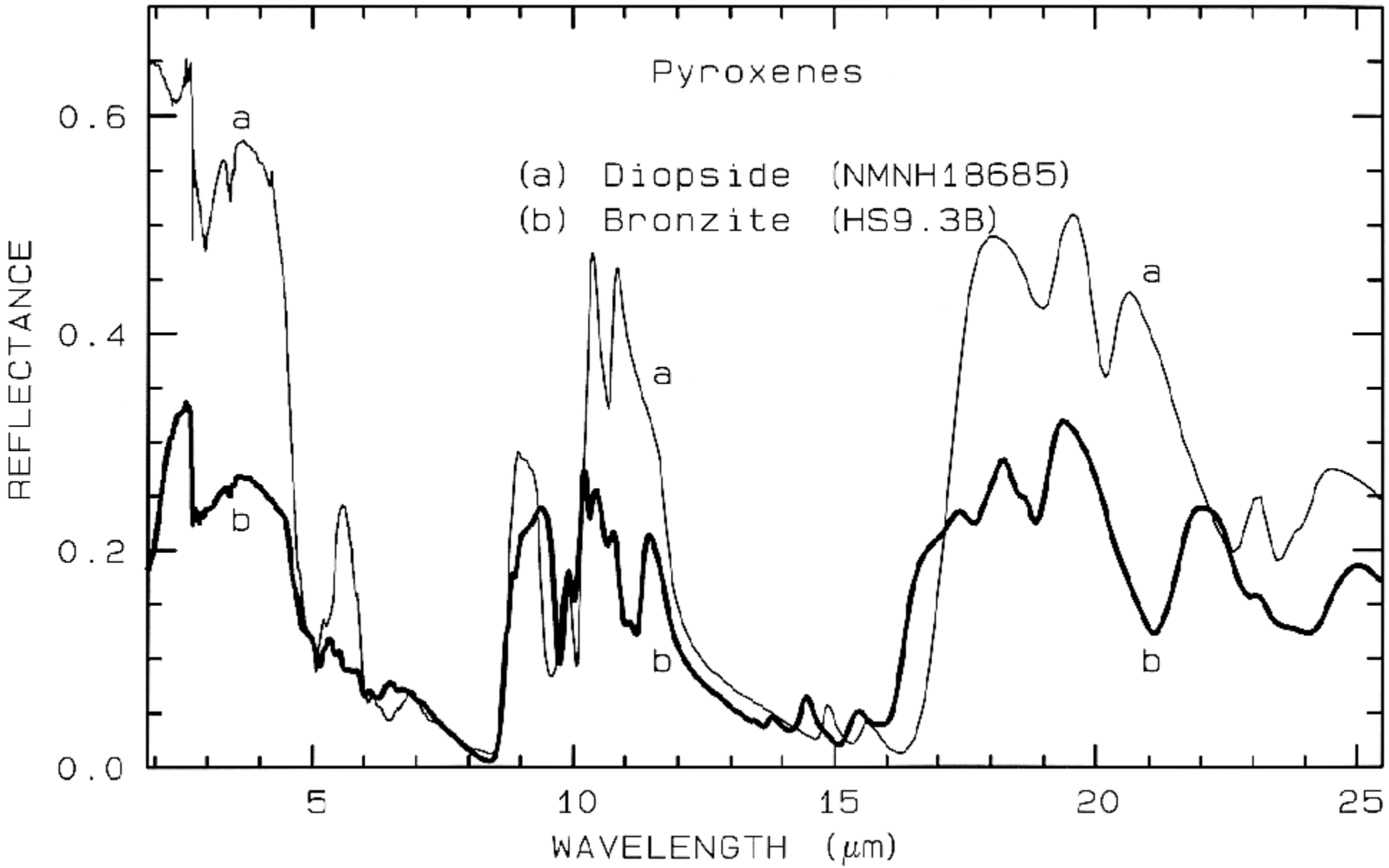
Pyroxenes
(a) Diopside (NMNH18685)
(b) Bronzite (HS9.3B)
REFLECTANCE
0.0
0.2
0.4
0.6
5
10
15
20
25
WAVELENGTH (μm)
a
b
a
b
a
b

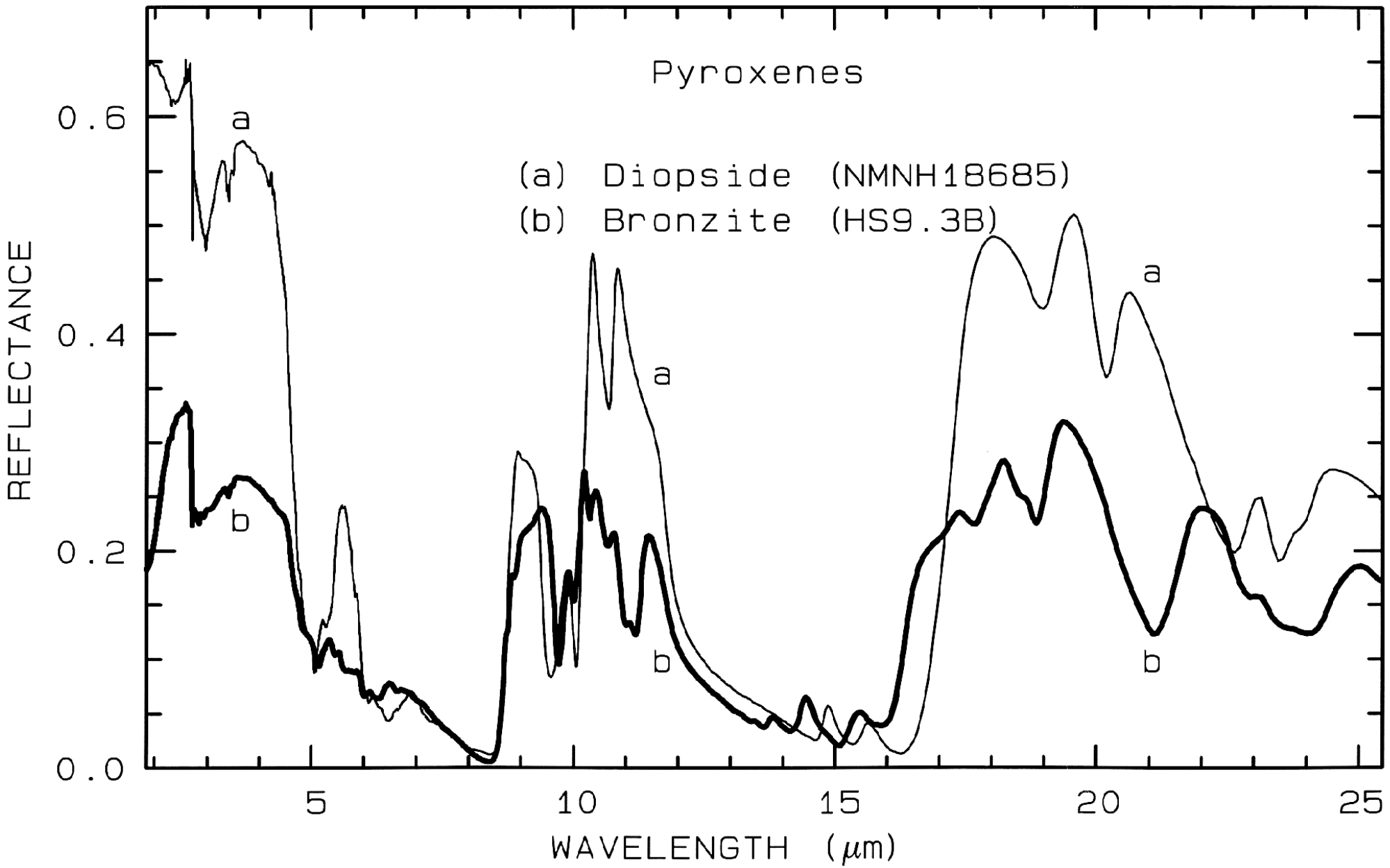
Pyroxenes
(a) Diopside (NMNH18685)
(b) Bronzite (HS9.3B)
REFLECTANCE
0.0
0.2
0.4
0.6
5
10
15
20
25
WAVELENGTH (μm)
a
b
a
b
a
b

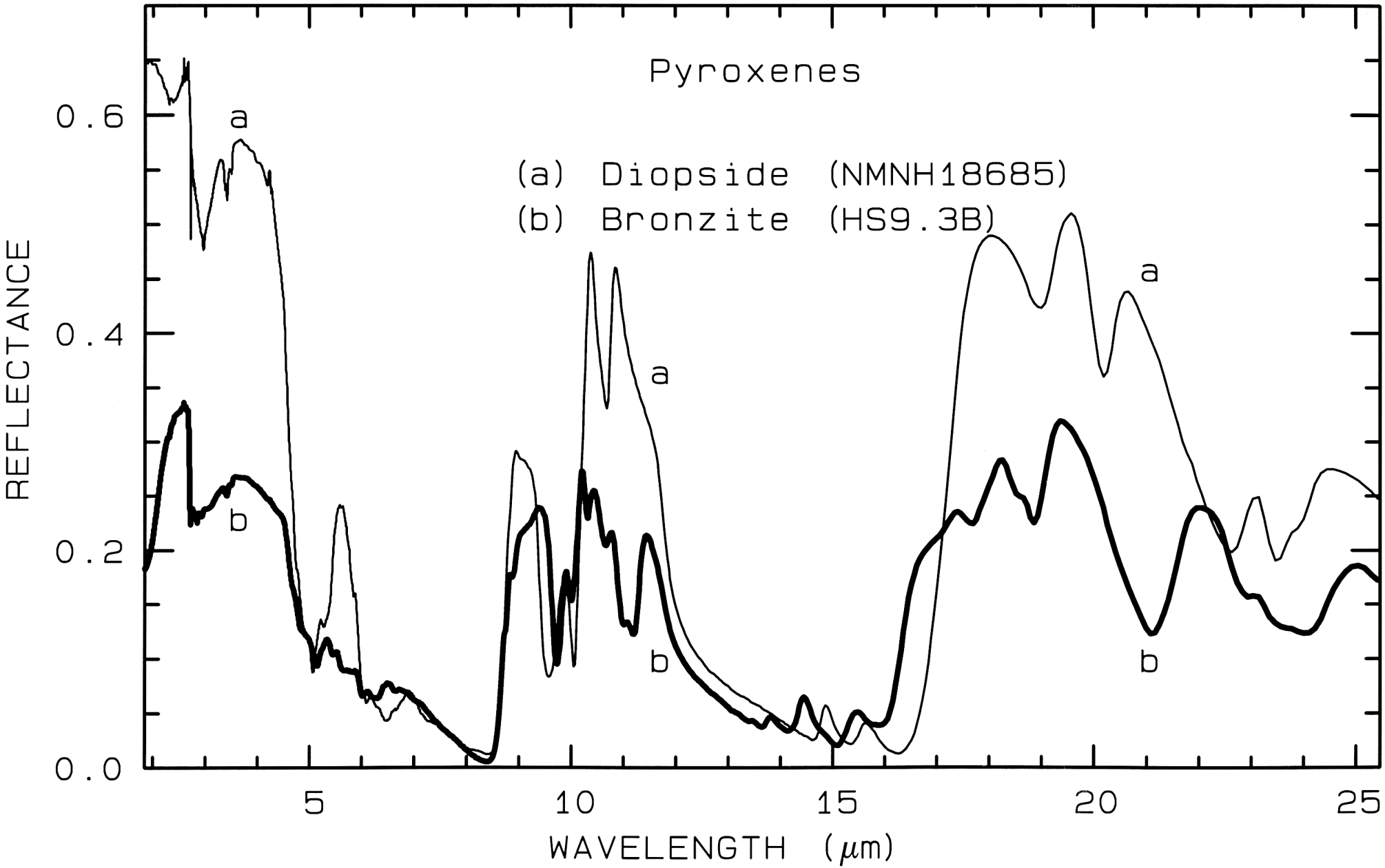
Pyroxenes
(a) Diopside (NMNH18685)
(b) Bronzite (HS9.3B)
REFLECTANCE
0.0
0.2
0.4
0.6
5
10
15
20
25
WAVELENGTH (μm)
a
b
a
b
a
b

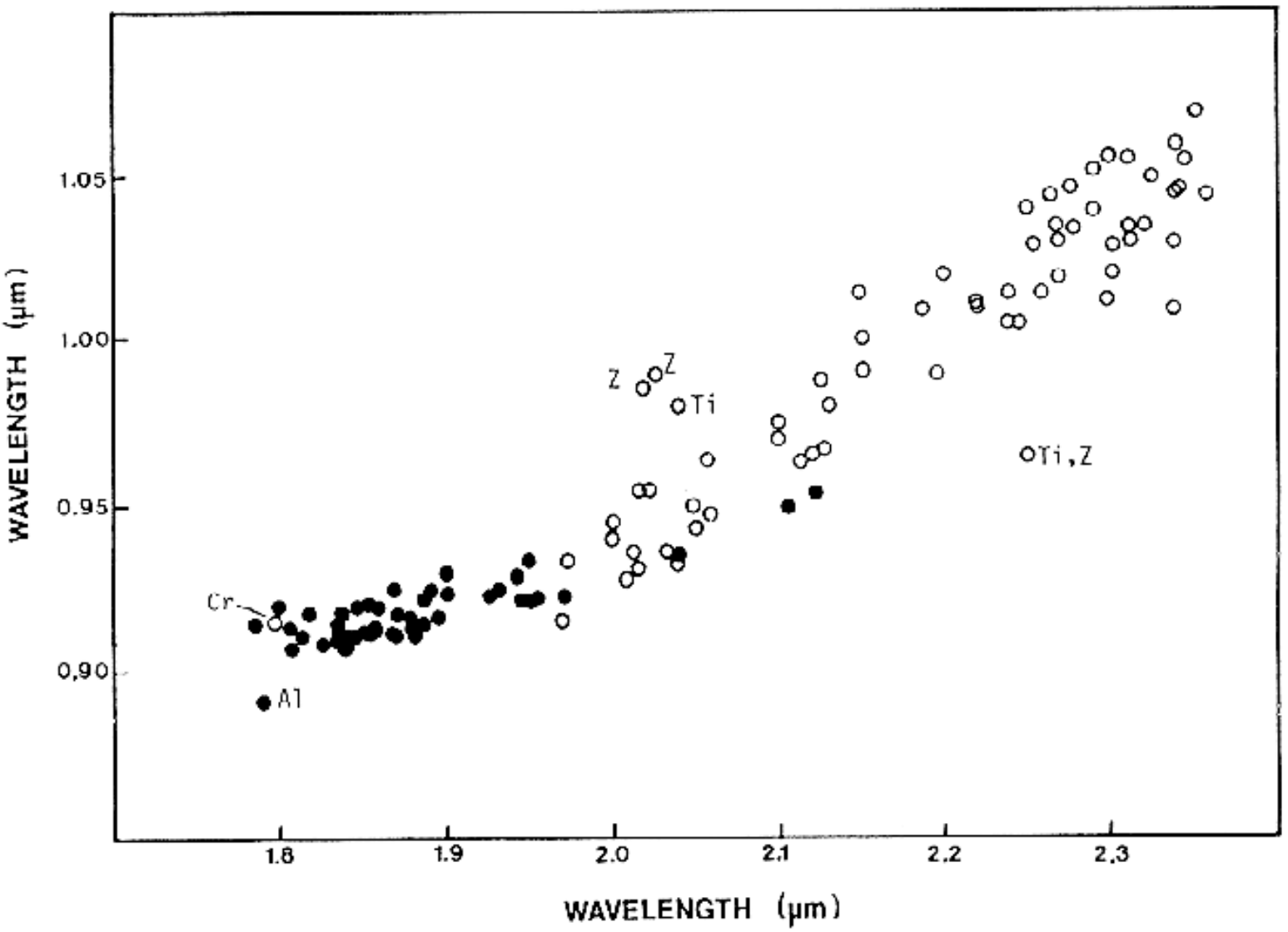
1.05
1.00
0.95
0.90
WAVELENGTH (μm)
Z
Z
Ti
Ti,Z
Cr
Al
1.8
1.9
2.0
2.1
2.2
2.3
WAVELENGTH (μm)

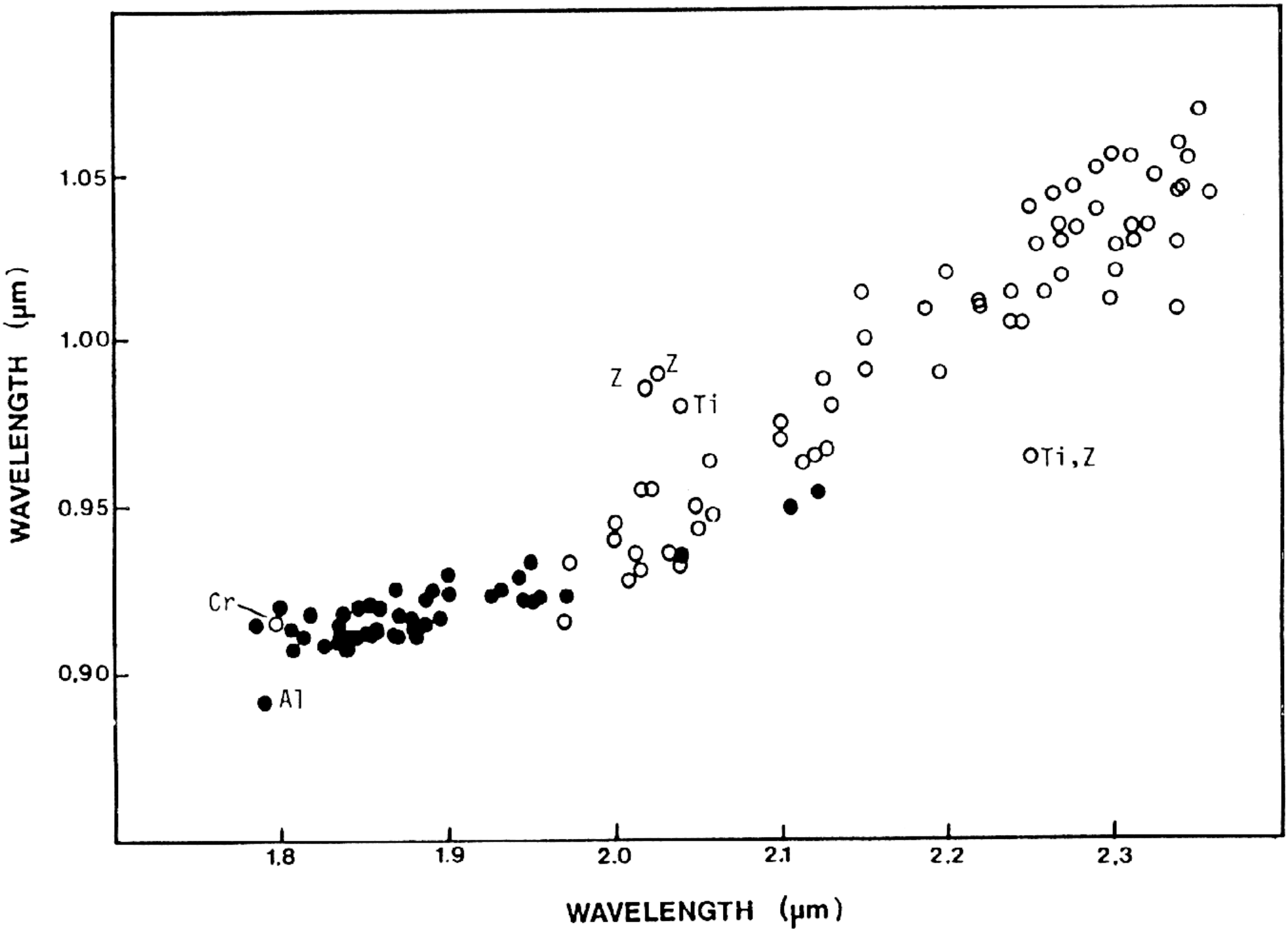
WAVELENGTH (μm)
1.05
1.00
0.95
0.90
Cr
Al
Z
Z
Ti
Ti,Z
1.8
1.9
2.0
2.1
2.2
2.3
WAVELENGTH (μm)

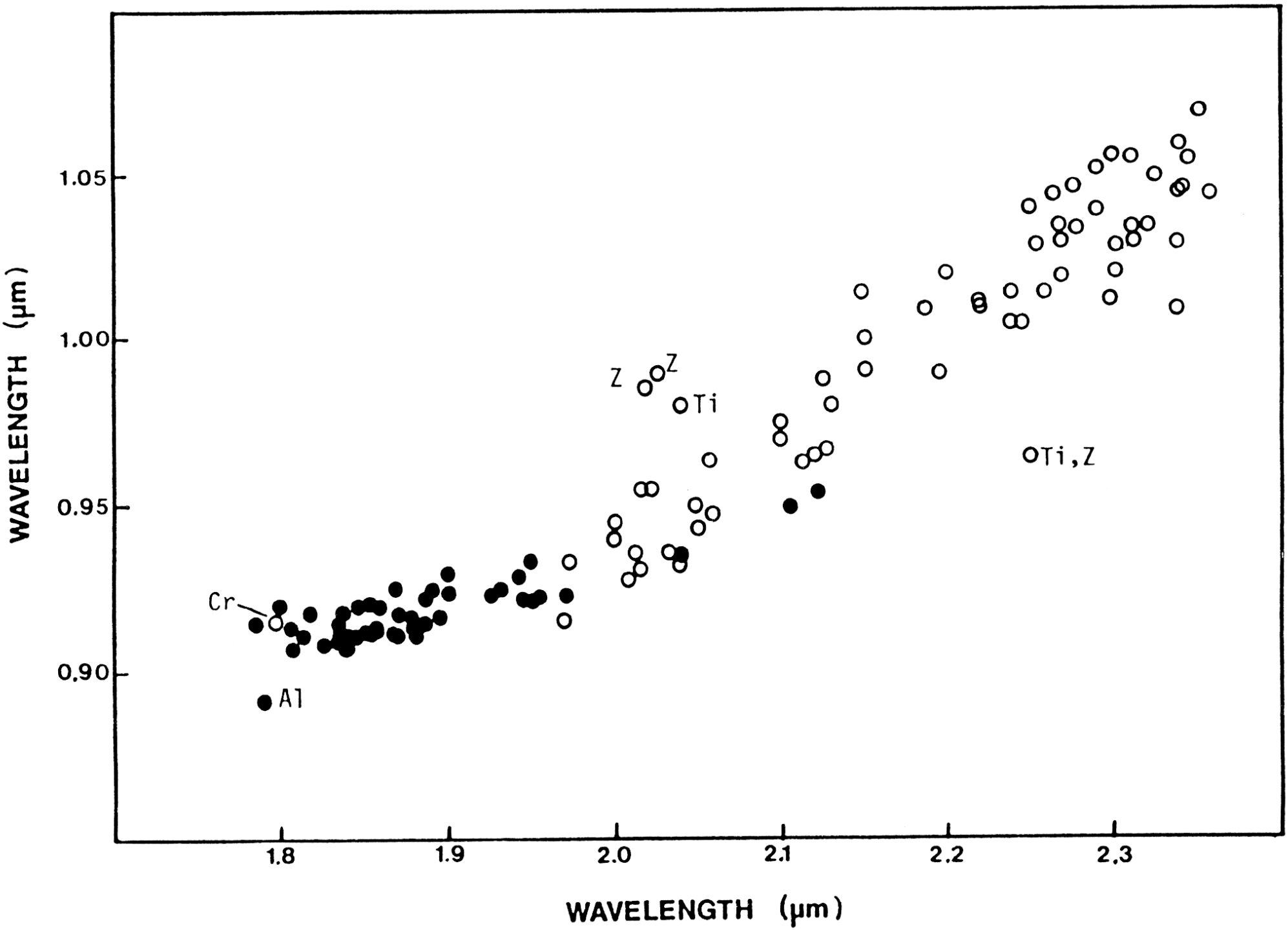
1.05
1.00
0.95
0.90
WAVELENGTH (μm)
Z
Z
Ti
Ti,Z
Cr
Al
1.8
1.9
2.0
2.1
2.2
2.3
WAVELENGTH (μm)

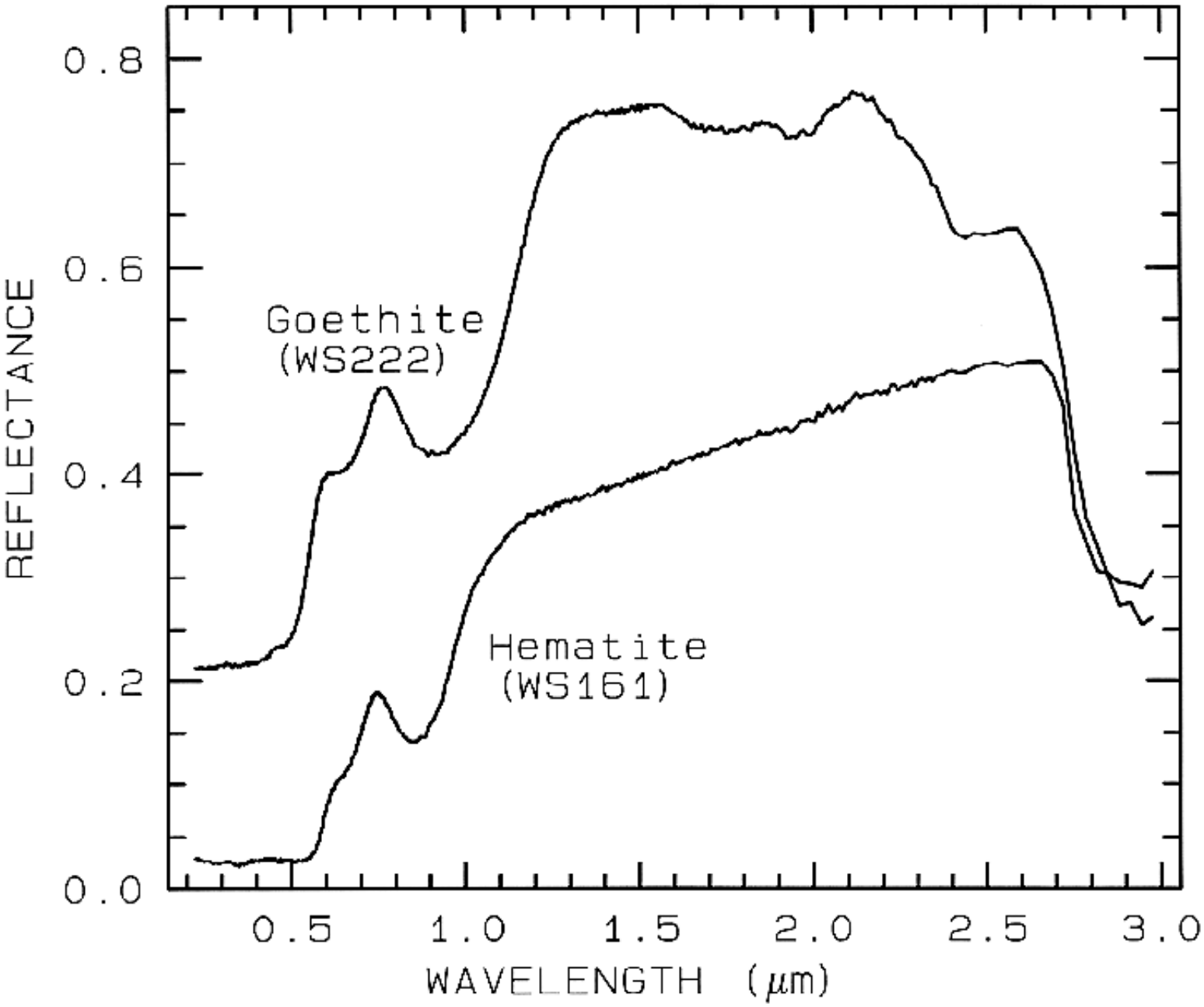
0.8
0.6
0.4
0.2
0.0
REFLECTANCE
Goethite
(WS222)
Hematite
(WS161)
0.5
1.0
1.5
2.0
2.5
3.0
WAVELENGTH (μm)

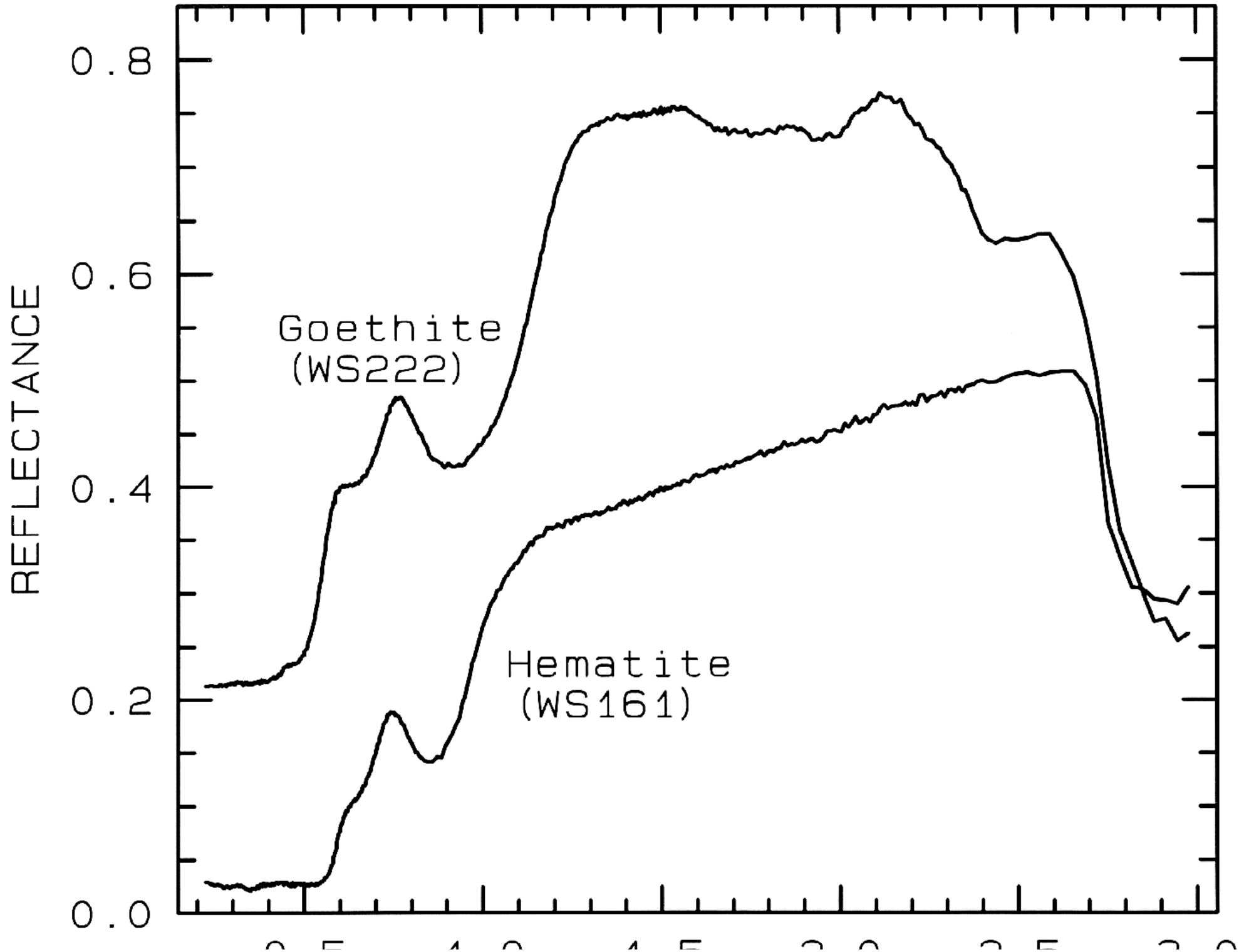
0.8
0.6
0.4
0.2
0.0
REFLECTANCE
Goethite
(WS222)
Hematite
(WS161)

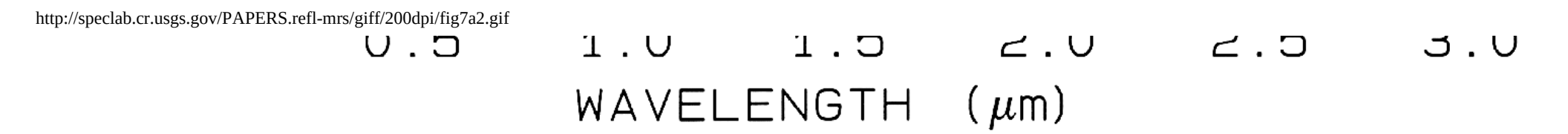
0.5
1.0
1.5
2.0
2.5
3.0
WAVELENGTH (μm)

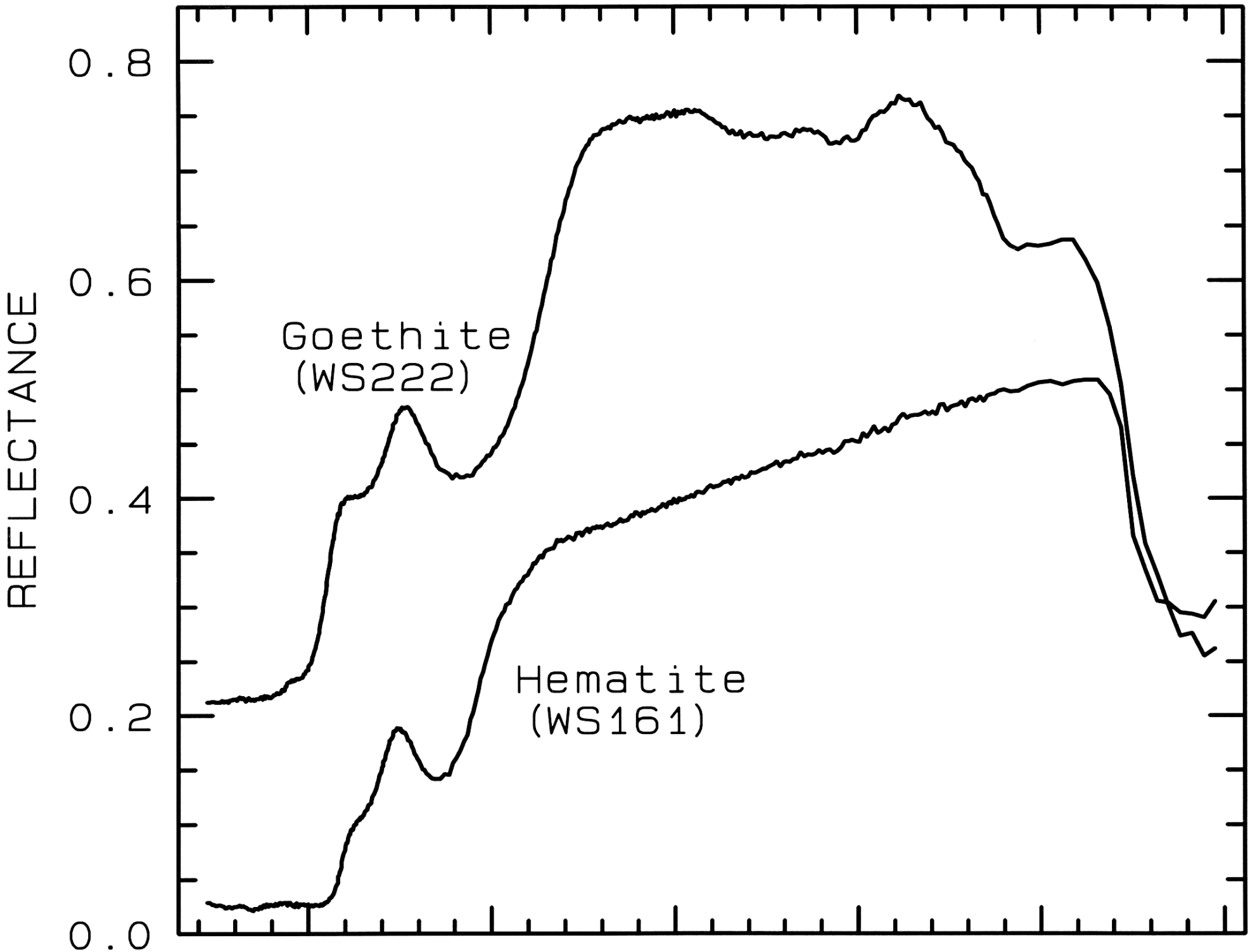
0.8
0.6
0.4
0.2
0.0
REFLECTANCE
Goethite
(WS222)
Hematite
(WS161)

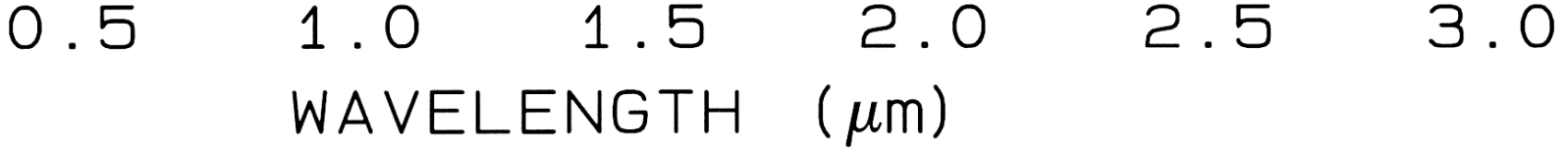
0.5
1.0
1.5
2.0
2.5
3.0
WAVELENGTH (μm)

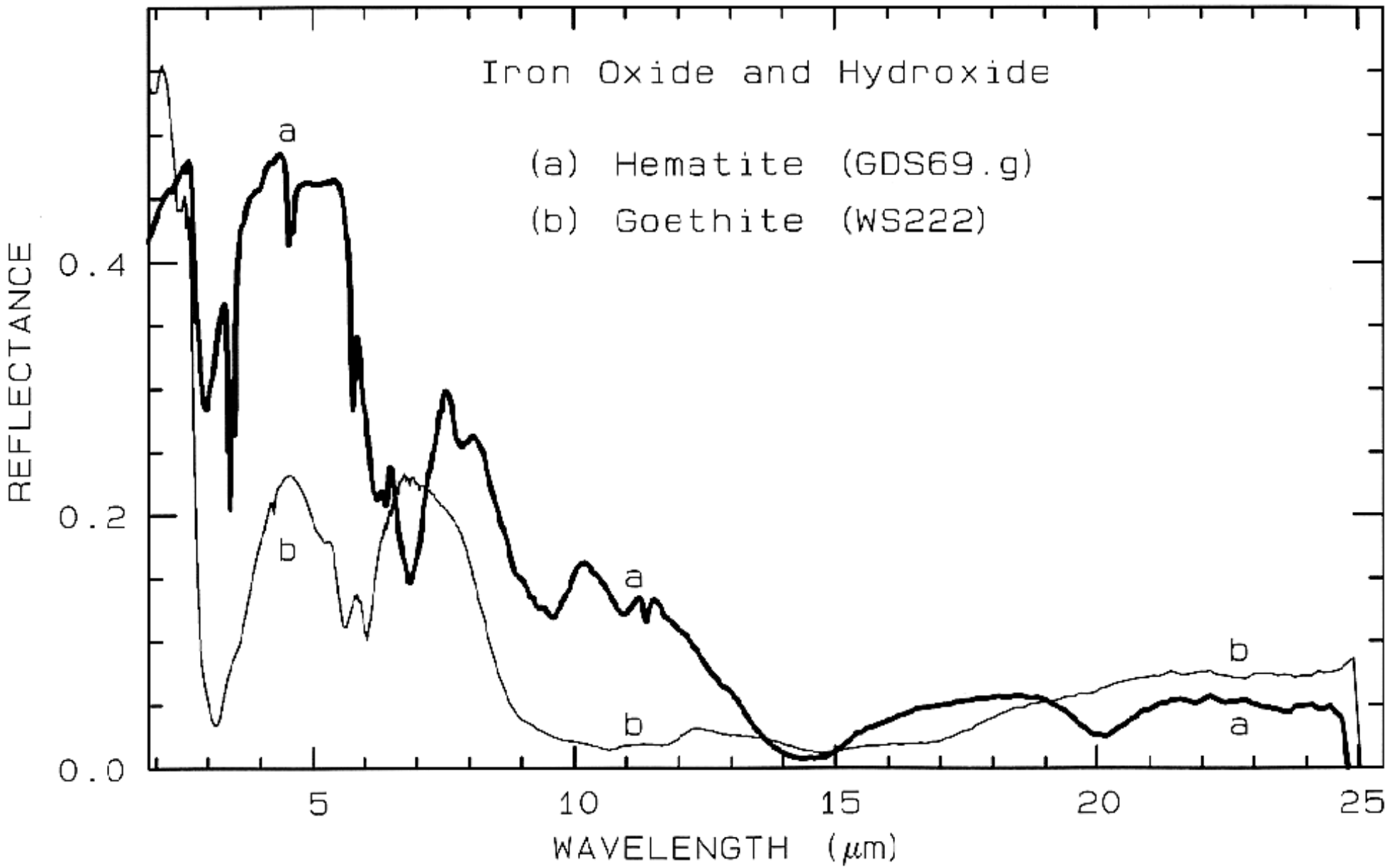
Iron Oxide and Hydroxide
(a) Hematite (GDS69.g)
(b) Goethite (WS222)
REFLECTANCE
0.0
0.2
0.4
5
10
15
20
25
WAVELENGTH (μm)
a
b
a
b
b
a

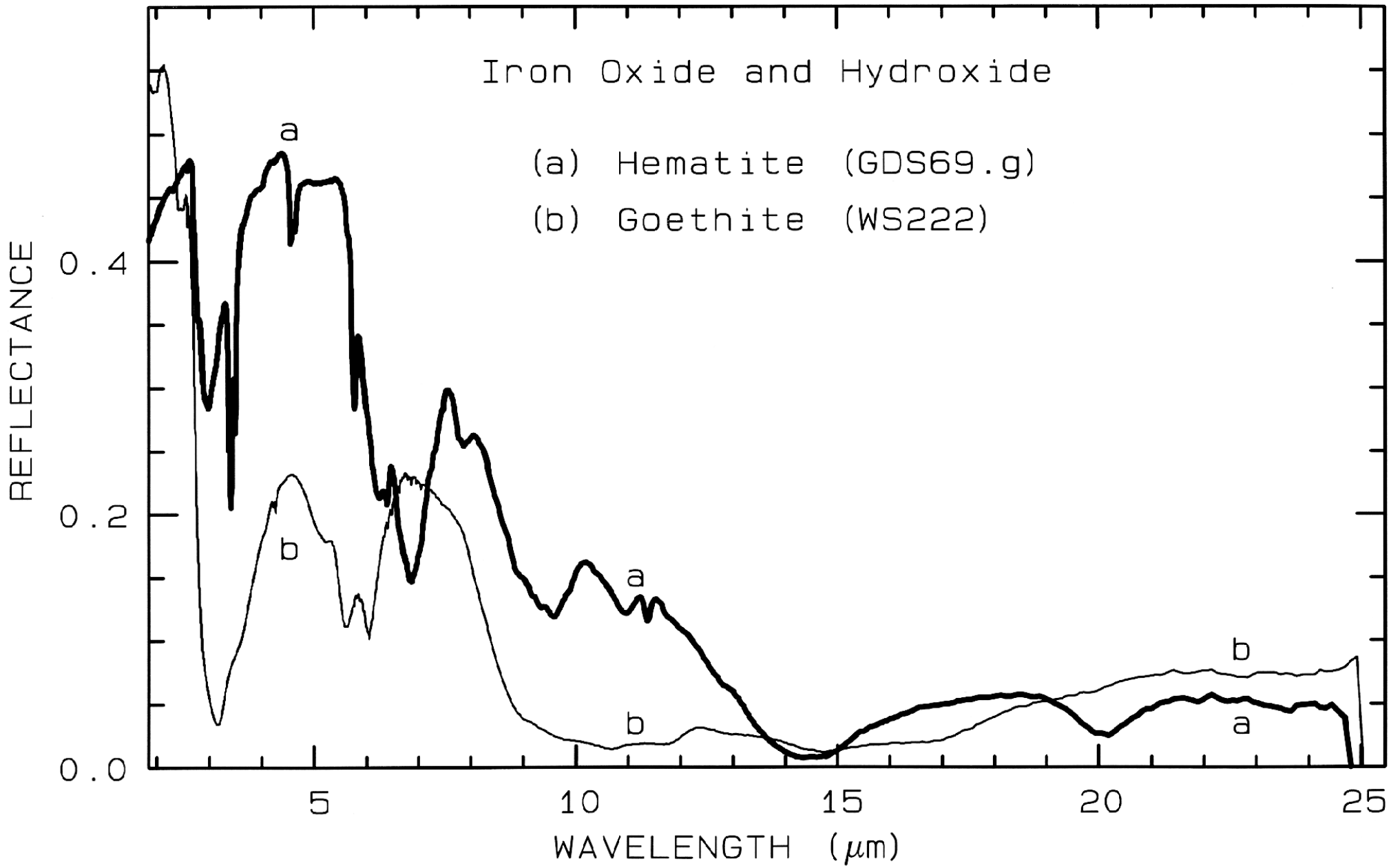
Iron Oxide and Hydroxide
(a) Hematite (GDS69.g)
(b) Goethite (WS222)
REFLECTANCE
0.0
0.2
0.4
5
10
15
20
25
WAVELENGTH (μm)
a
b
a
b
b
a

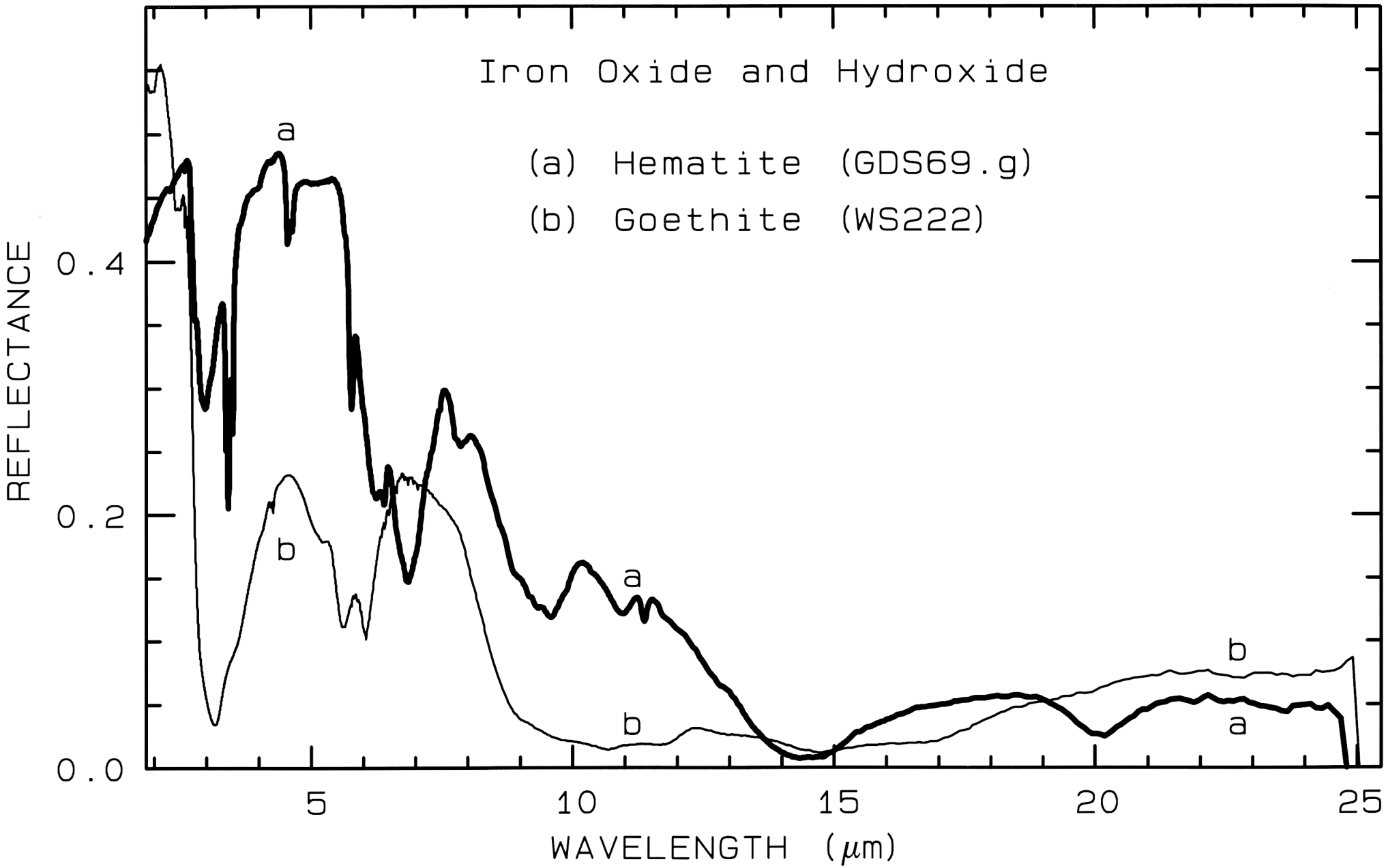
Iron Oxide and Hydroxide
(a) Hematite (GDS69.g)
(b) Goethite (WS222)
REFLECTANCE
0.0
0.2
0.4
5
10
15
20
25
WAVELENGTH (μm)
a
b
a
b
b
a

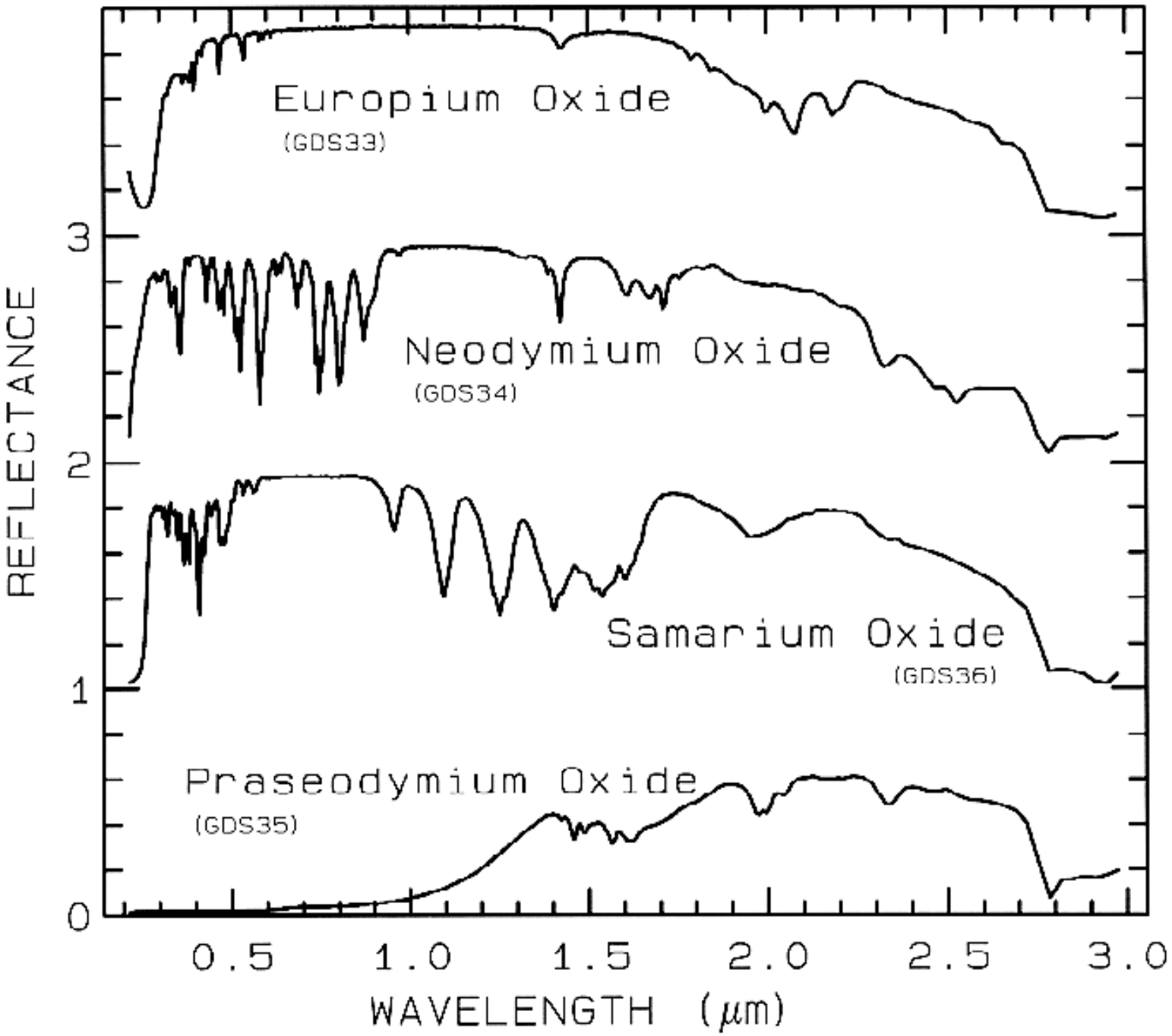
Europium Oxide
(GDS33)
Neodymium Oxide
(GDS34)
Samarium Oxide
(GDS36)
Praseodymium Oxide
(GDS35)
REFLECTANCE
0
1
2
3
0.5
1.0
1.5
2.0
2.5
3.0
WAVELENGTH (μm)

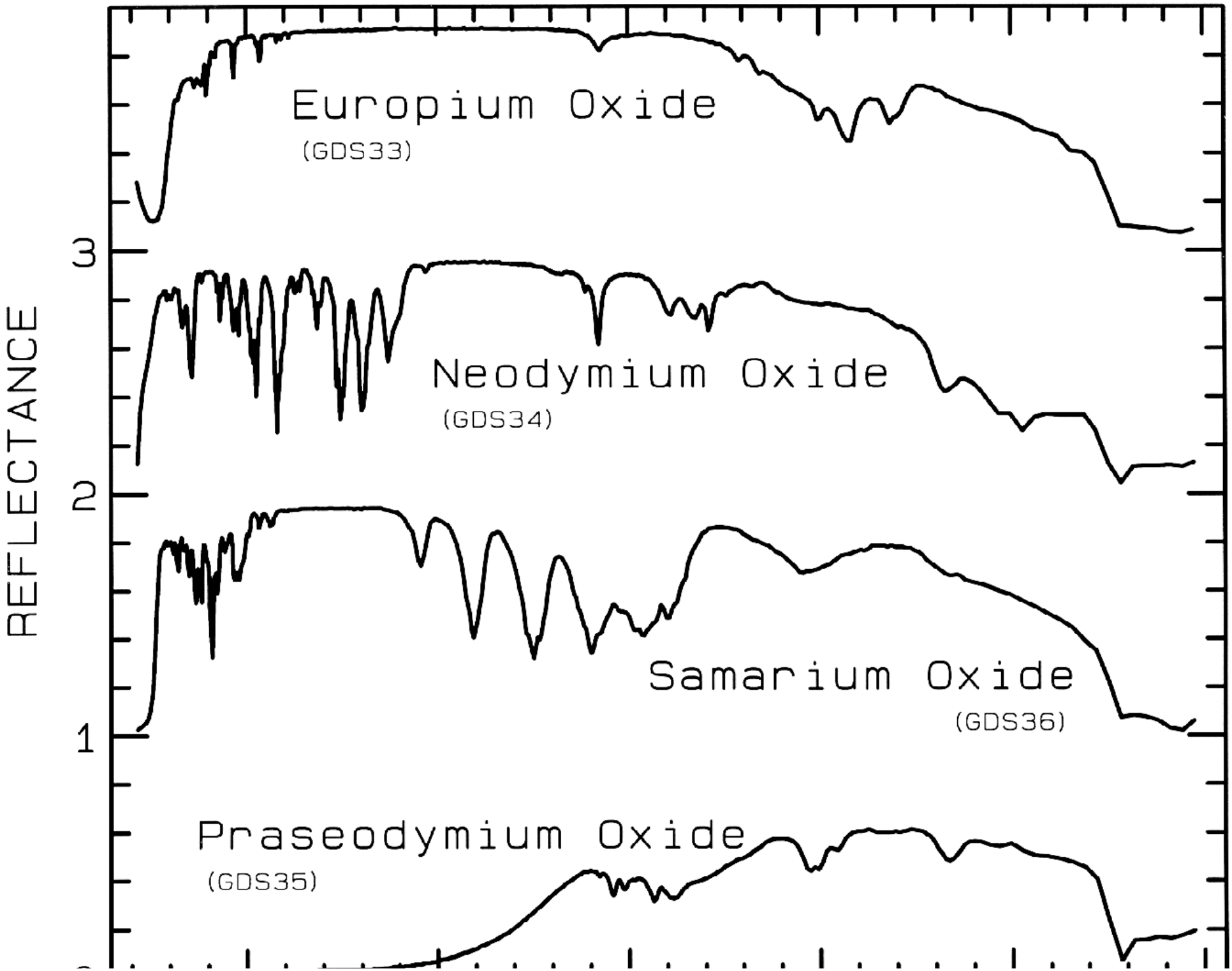
Europium Oxide
(GDS33)
Neodymium Oxide
(GDS34)
Samarium Oxide
(GDS36)
Praseodymium Oxide
(GDS35)
REFLECTANCE
3
2
1

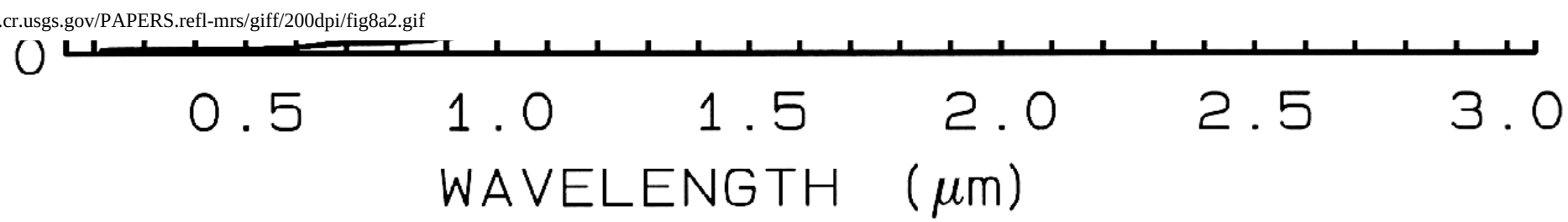
0
0.5
1.0
1.5
2.0
2.5
3.0
WAVELENGTH (μm)

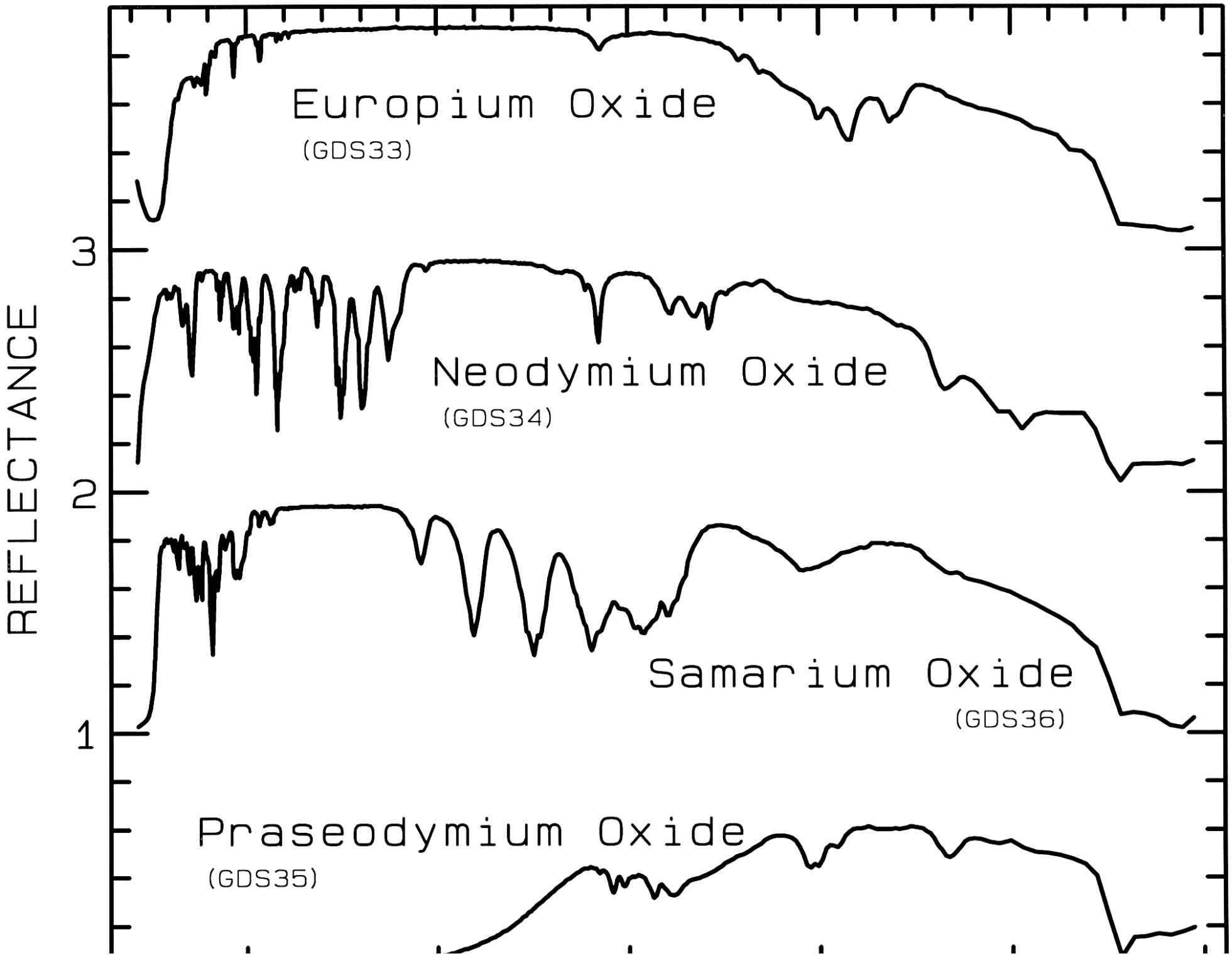
Europium Oxide
(GDS33)
Neodymium Oxide
(GDS34)
Samarium Oxide
(GDS36)
Praseodymium Oxide
(GDS35)
REFLECTANCE
3
2
1

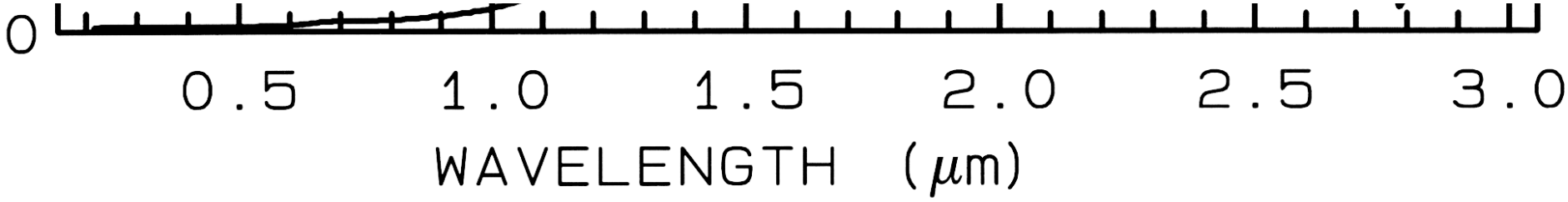
0
0.5
1.0
1.5
2.0
2.5
3.0
WAVELENGTH (μm)

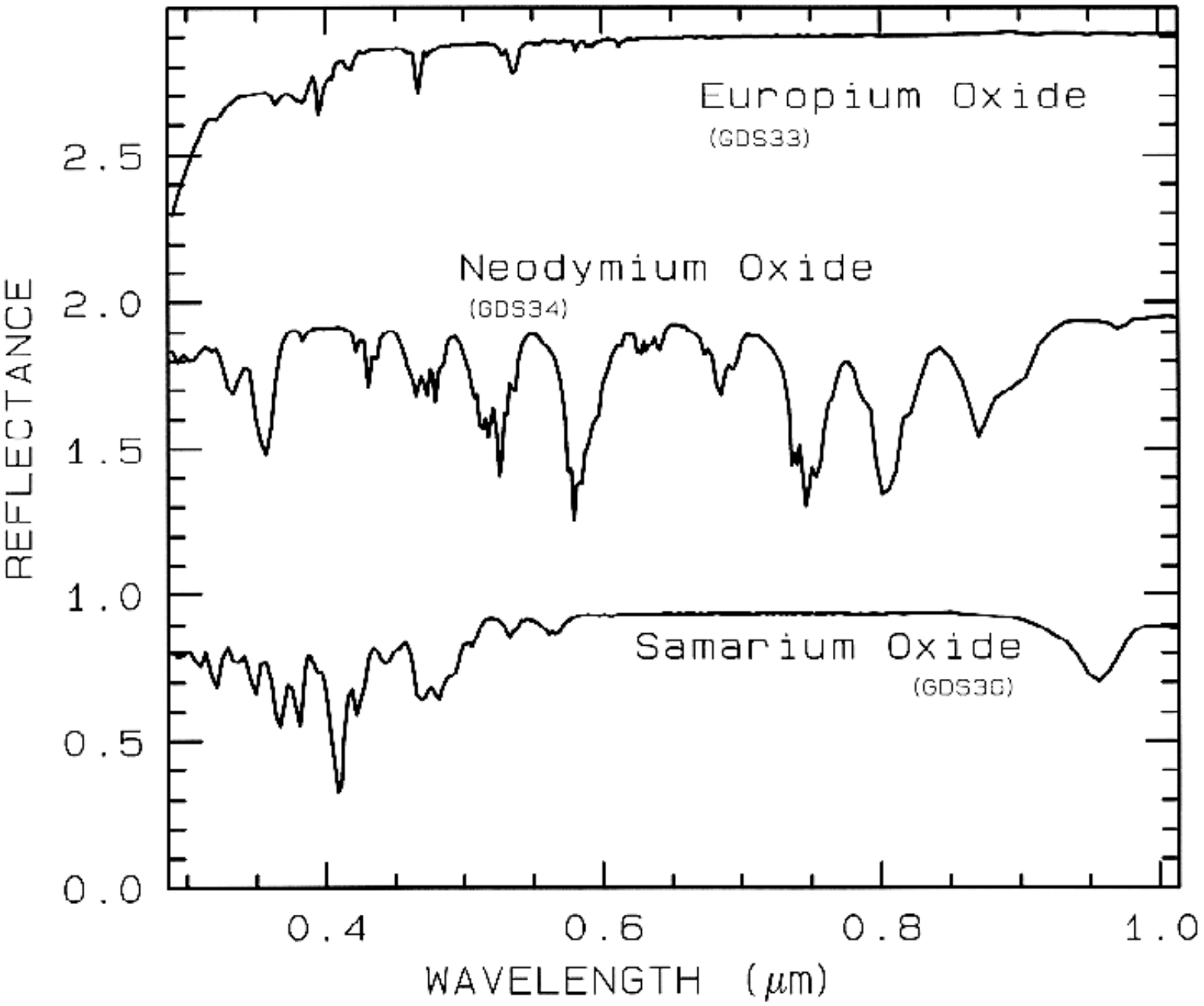
Europium Oxide
(GDS33)
Neodymium Oxide
(GDS34)
Samarium Oxide
(GDS30)
REFLECTANCE
2.5
2.0
1.5
1.0
0.5
0.0
0.4
0.6
0.8
1.0
WAVELENGTH (μm)

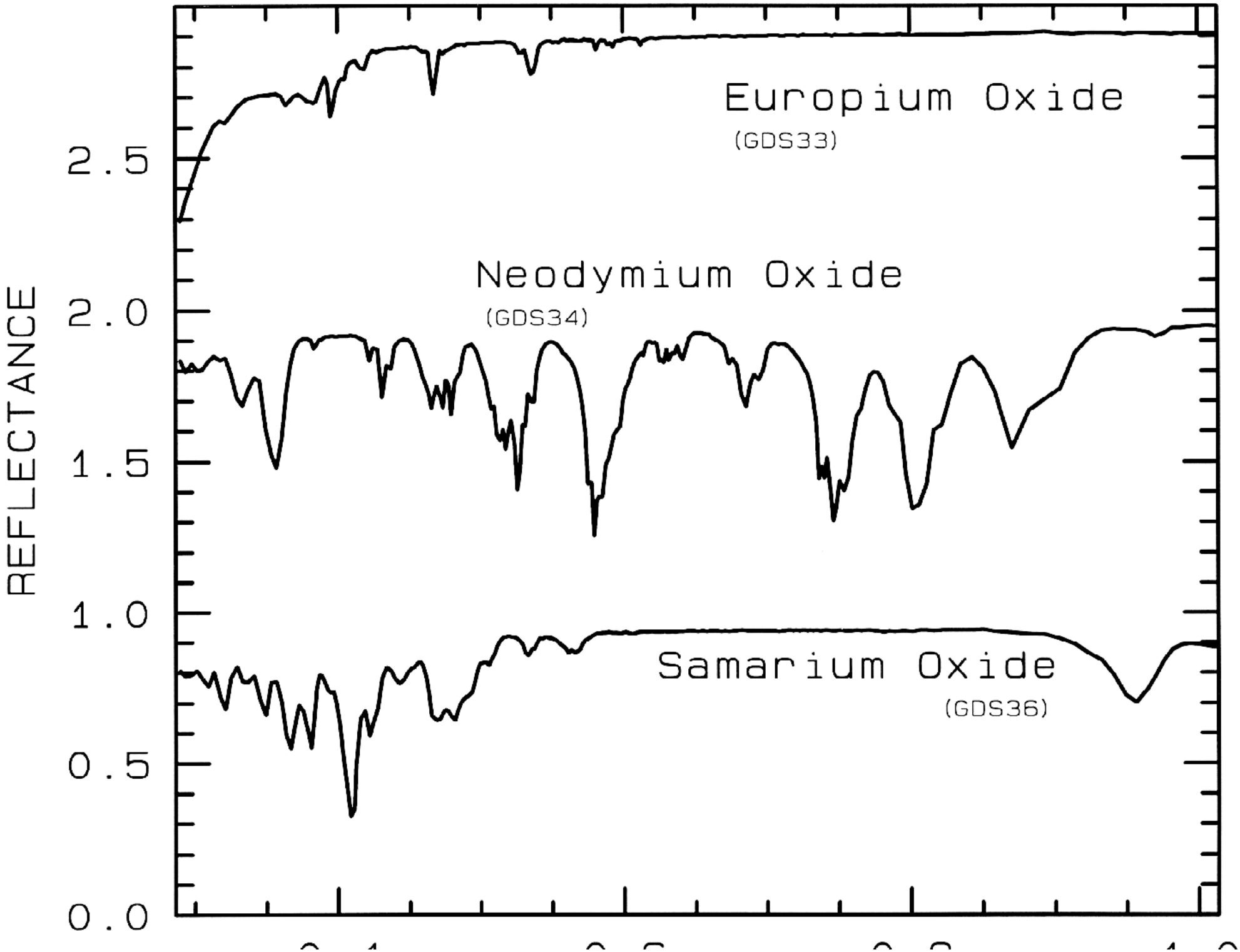
Europium Oxide
(GDS33)
Neodymium Oxide
(GDS34)
Samarium Oxide
(GDS36)
REFLECTANCE
2.5
2.0
1.5
1.0
0.5
0.0

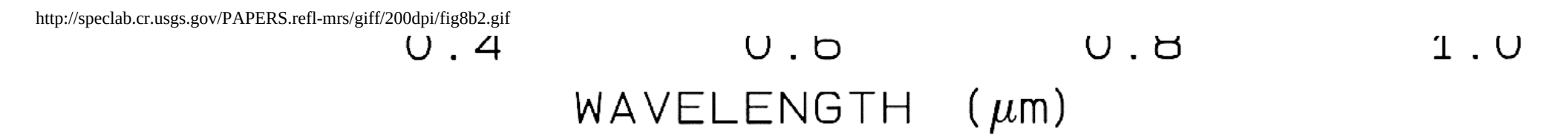
0.4
0.6
0.8
1.0
WAVELENGTH (μm)

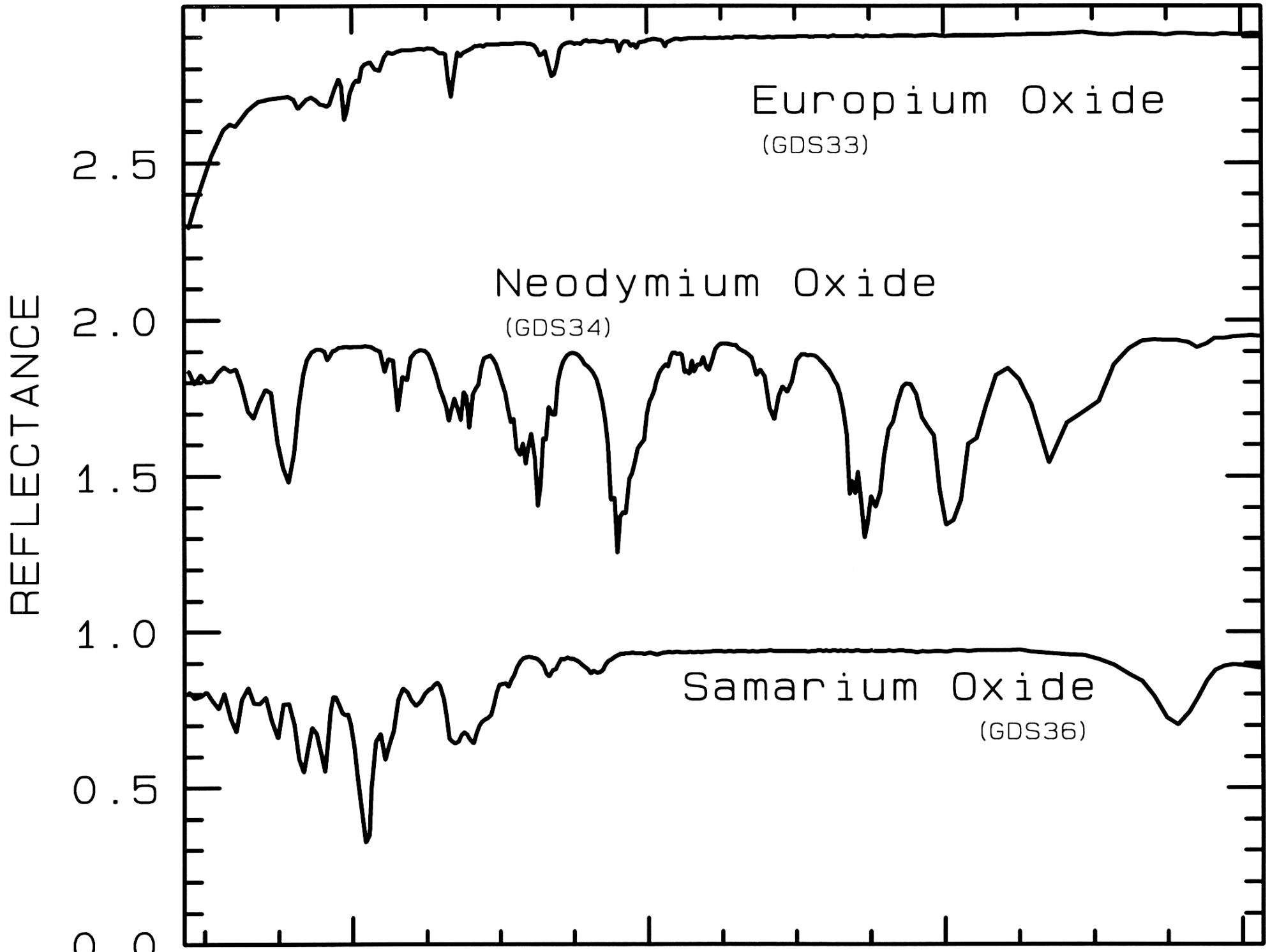
Europium Oxide
(GDS33)
Neodymium Oxide
(GDS34)
Samarium Oxide
(GDS36)
REFLECTANCE
2.5
2.0
1.5
1.0
0.5
0.0

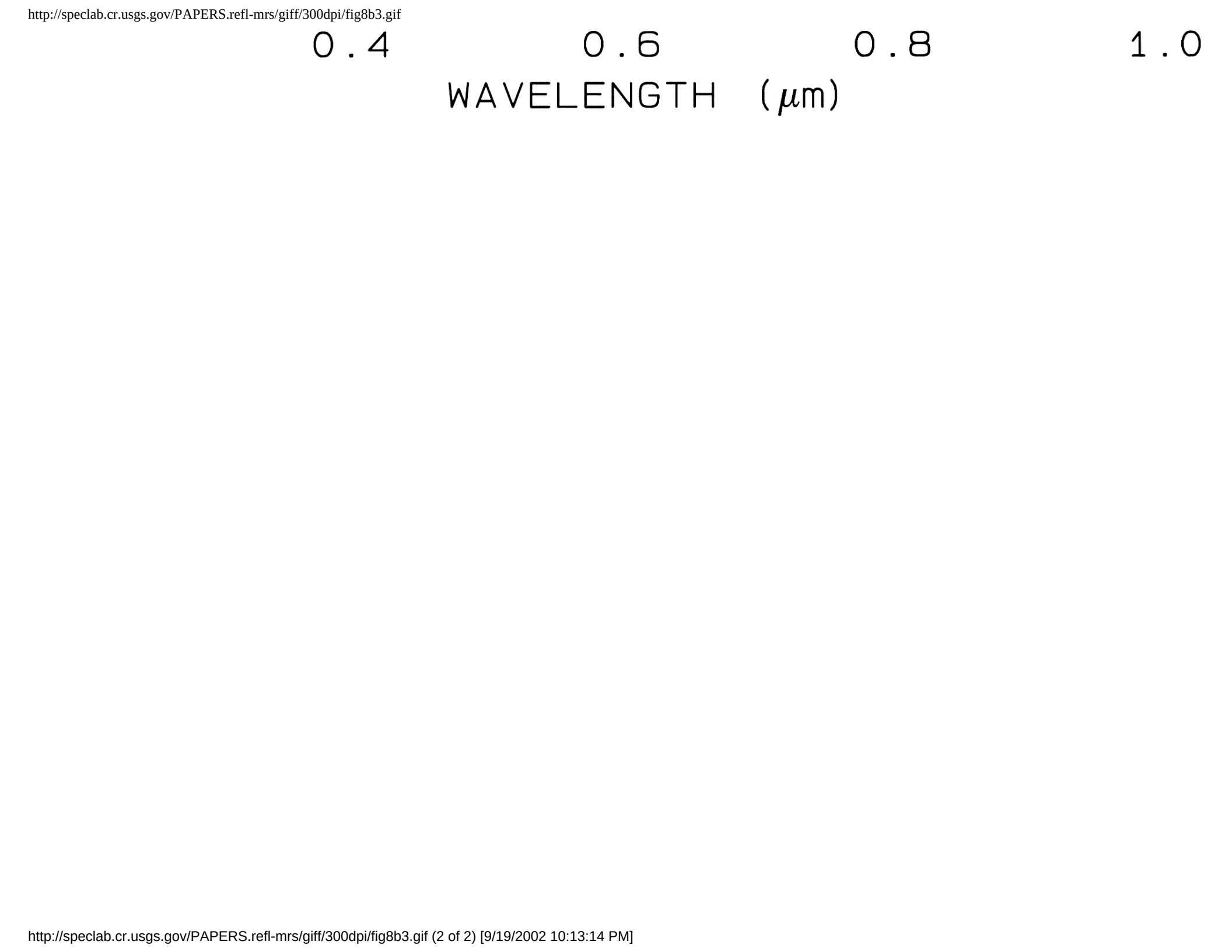
0.4
0.6
0.8
1.0
WAVELENGTH (μm)

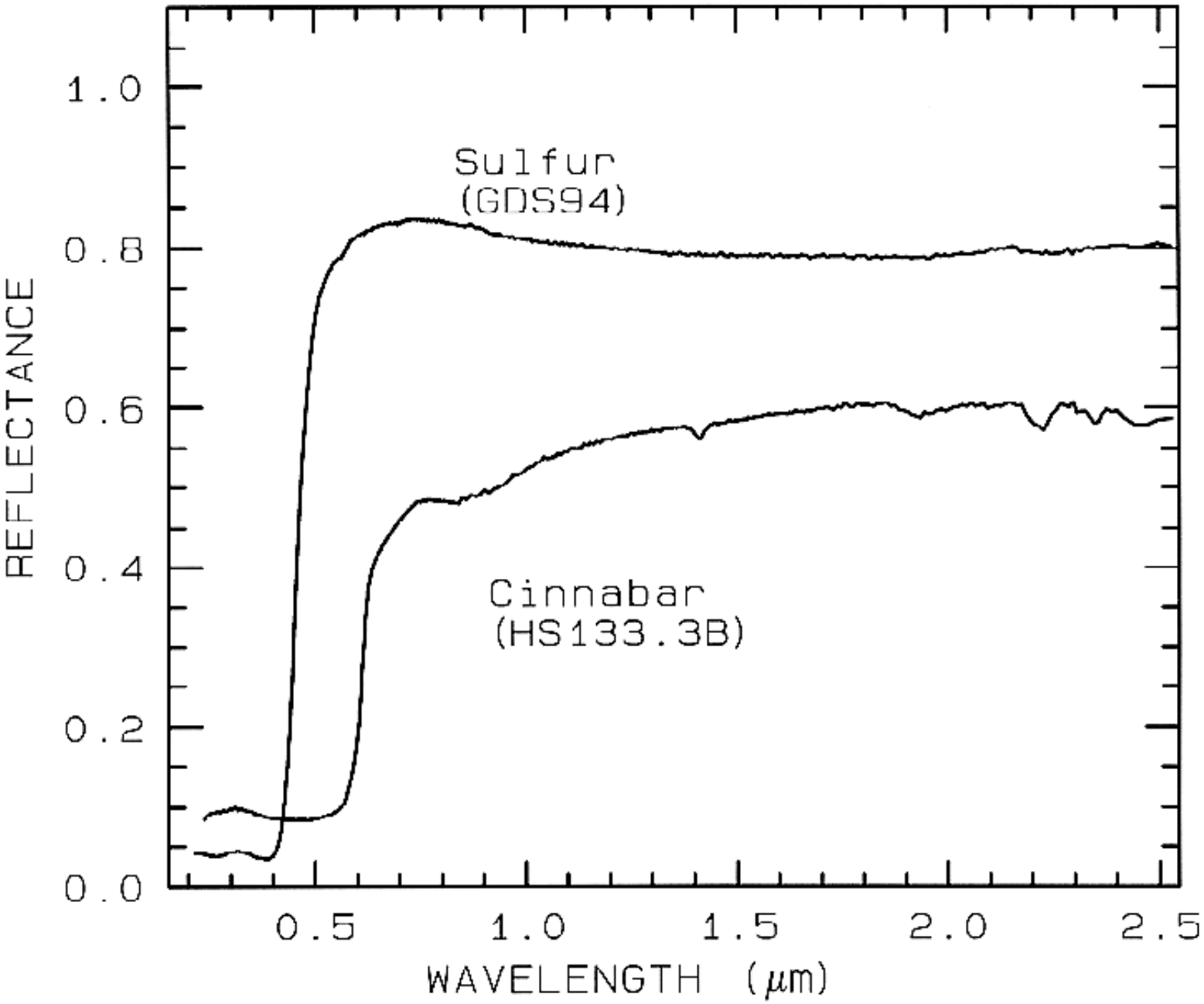
1.0
0.8
0.6
0.4
0.2
0.0
REFLECTANCE
Sulfur
(GDS94)
Cinnabar
(HS133.3B)
0.5
1.0
1.5
2.0
2.5
WAVELENGTH (μm)

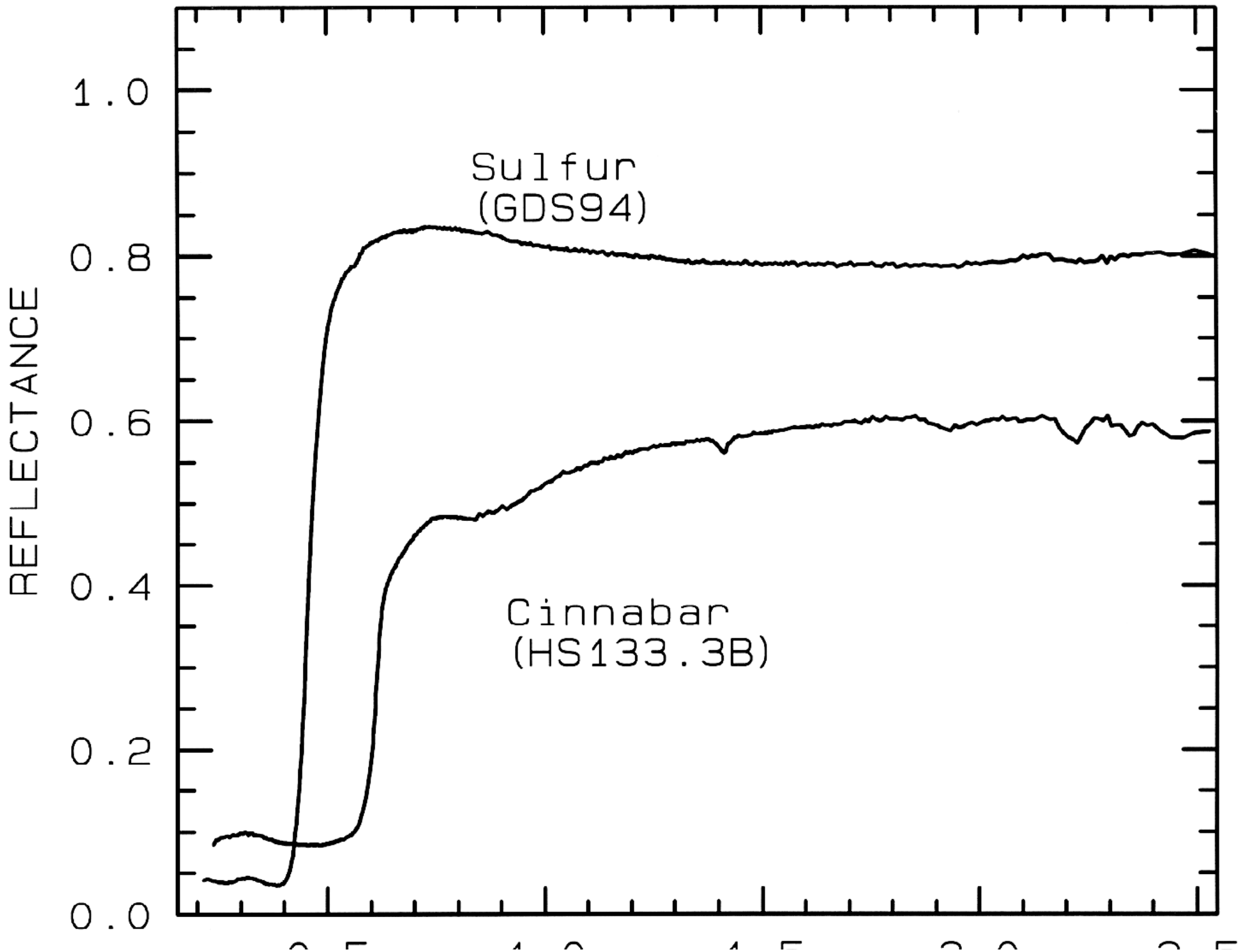
1.0
0.8
0.6
0.4
0.2
0.0
REFLECTANCE
Sulfur
(GDS94)
Cinnabar
(HS133.3B)

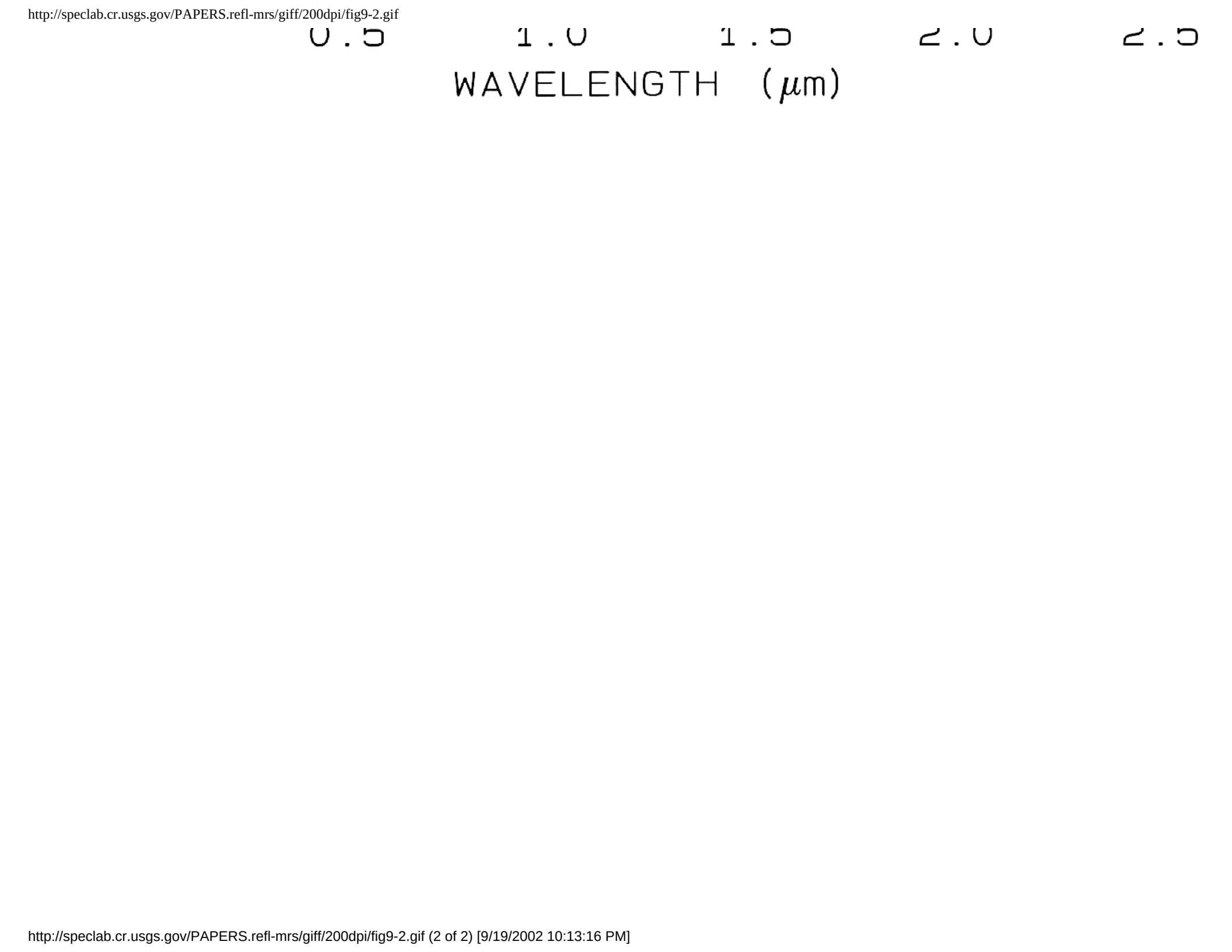
0.5
1.0
1.5
2.0
2.5
WAVELENGTH (μm)

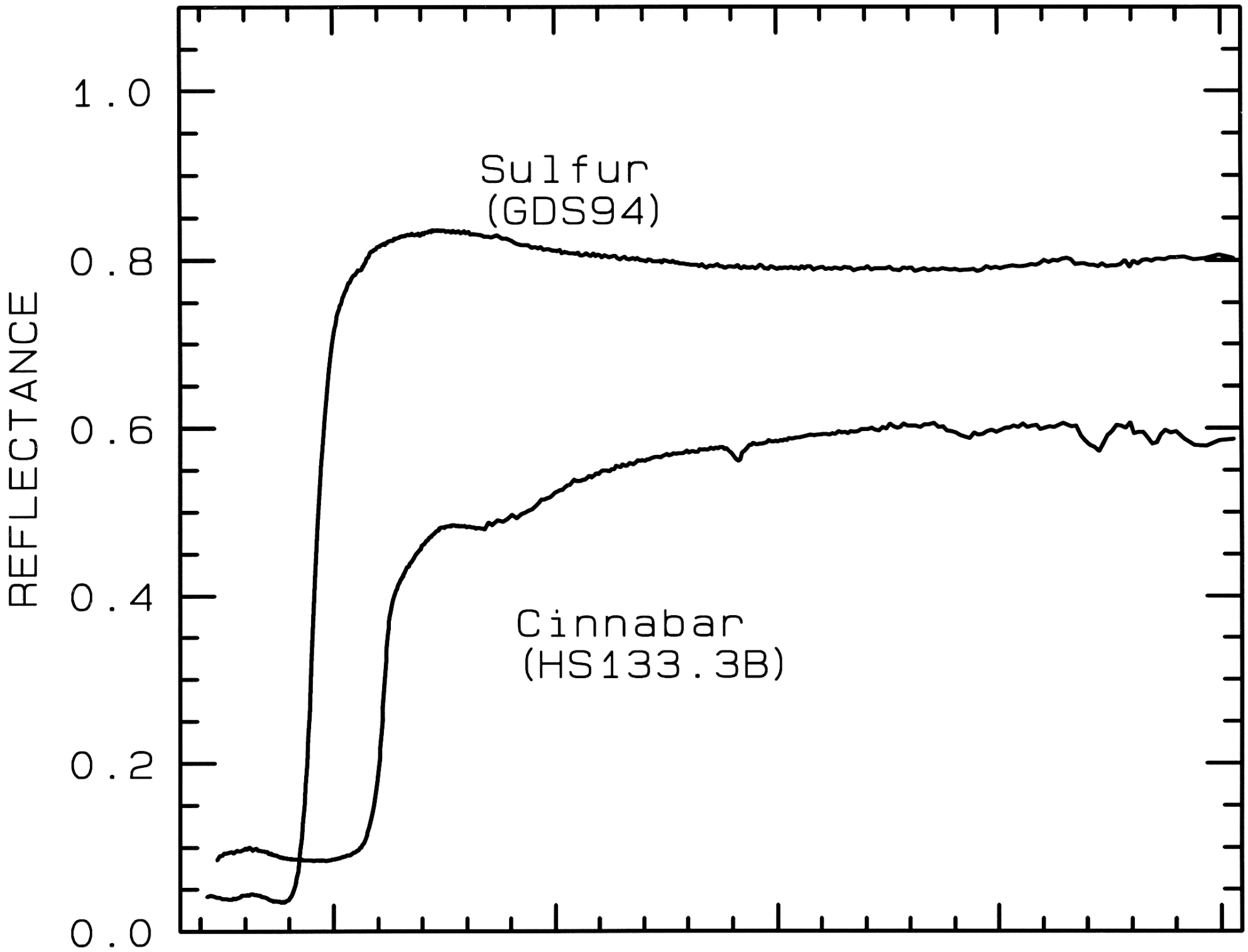
1.0
0.8
0.6
0.4
0.2
0.0
REFLECTANCE
Sulfur
(GDS94)
Cinnabar
(HS133.3B)

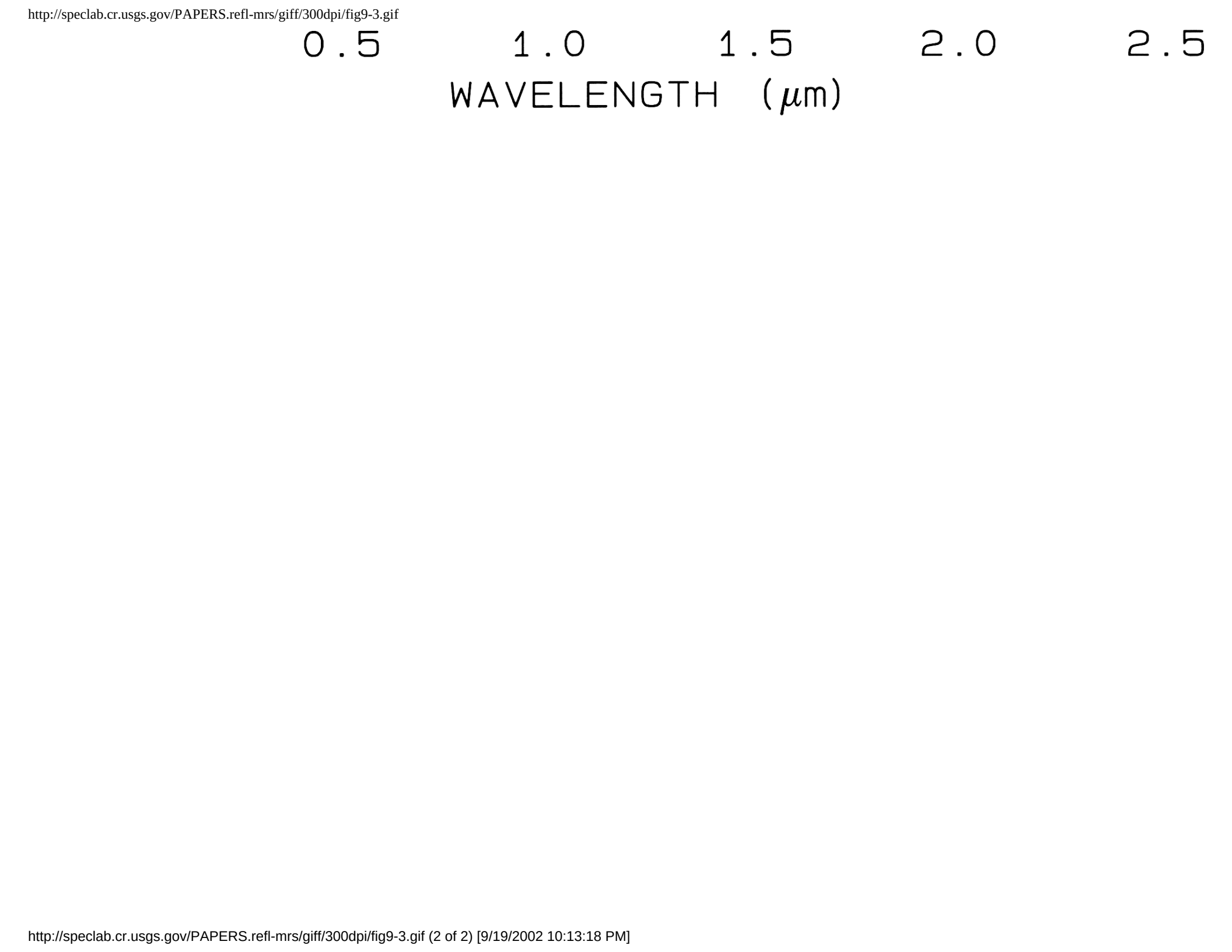
0.5
1.0
1.5
2.0
2.5
WAVELENGTH (μm)

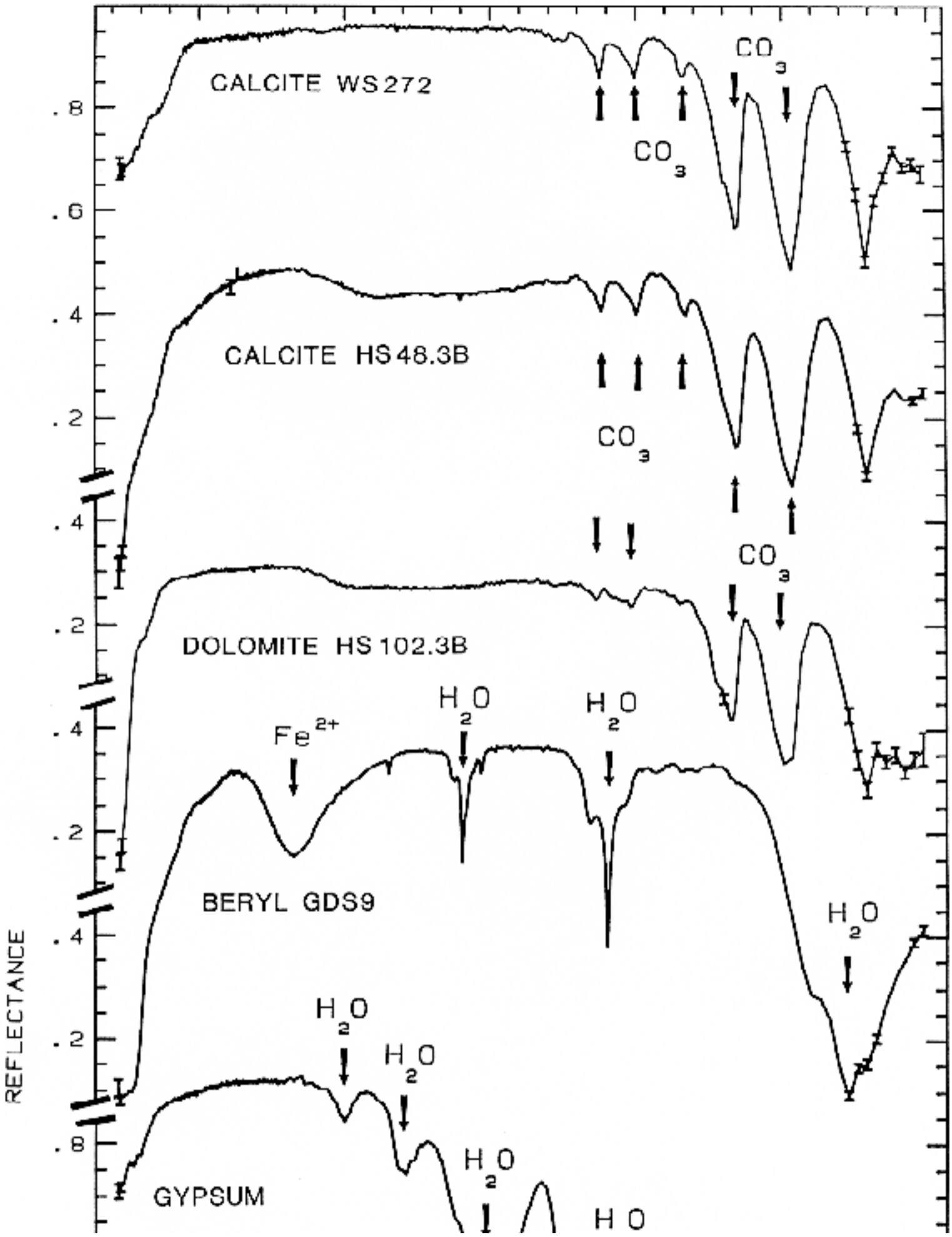
CALCITE WS272
CO3
CO3
CALCITE HS48.3B
CO3
CO3
DOLOMITE HS102.3B
Fe2+
H2O
H2O
BERYL GDS9
H2O
H2O
H2O
GYPSUM
H O
REFLECTANCE
.8
.6
.4
.2
.4
.2
.4
.2
.8

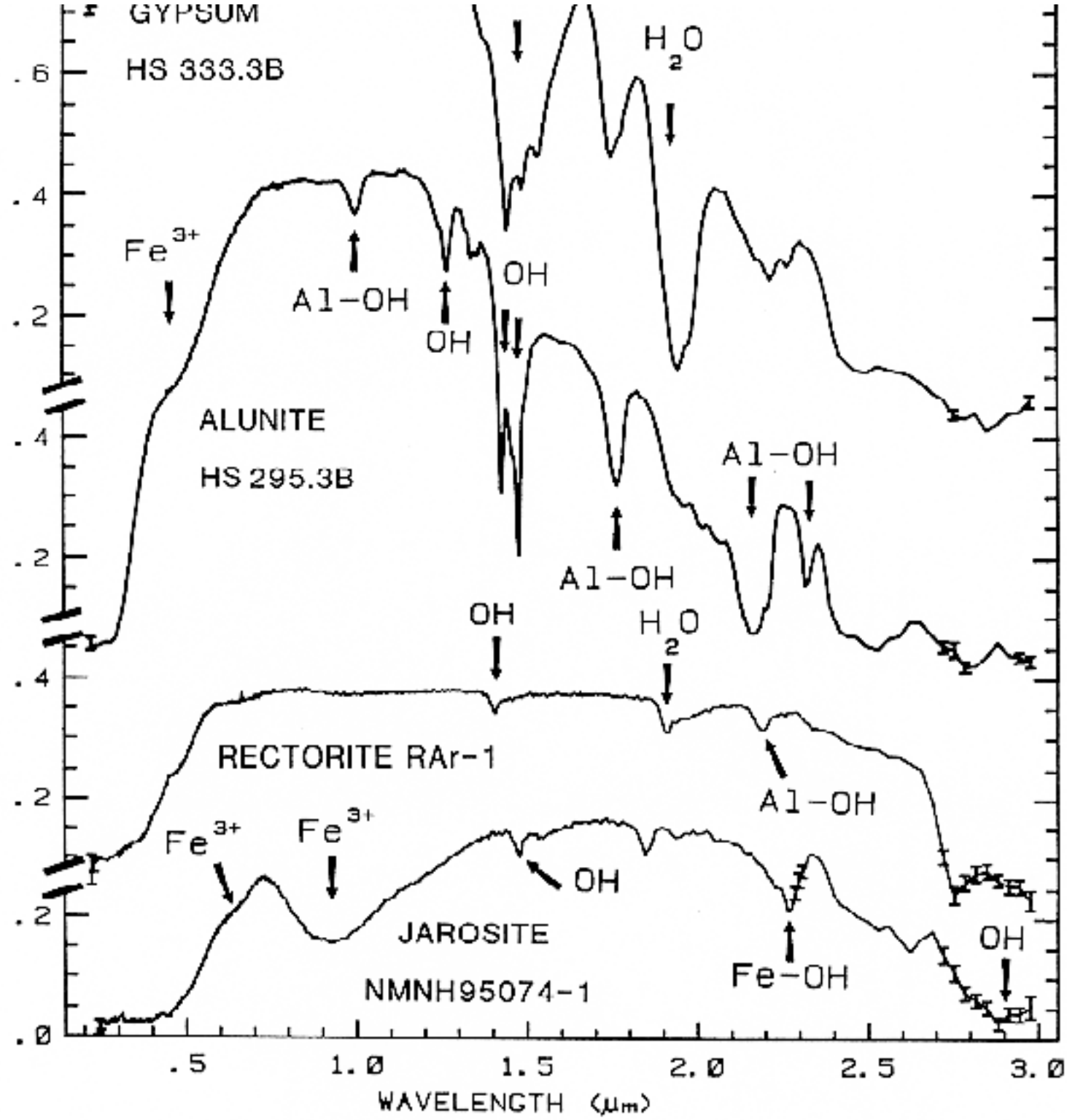
GYPSUM
HS 333.3B
H2O
Fe3+
Al-OH
OH
OH
ALUNITE
HS 295.3B
Al-OH
Al-OH
OH
H2O
RECTORITE RAr-1
Al-OH
Fe3+
Fe3+
OH
JAROSITE
NMNH95074-1
Fe-OH
OH
.6
.4
.2
.4
.2
.4
.2
.0
.5
1.0
1.5
2.0
2.5
3.0
WAVELENGTH (μm)

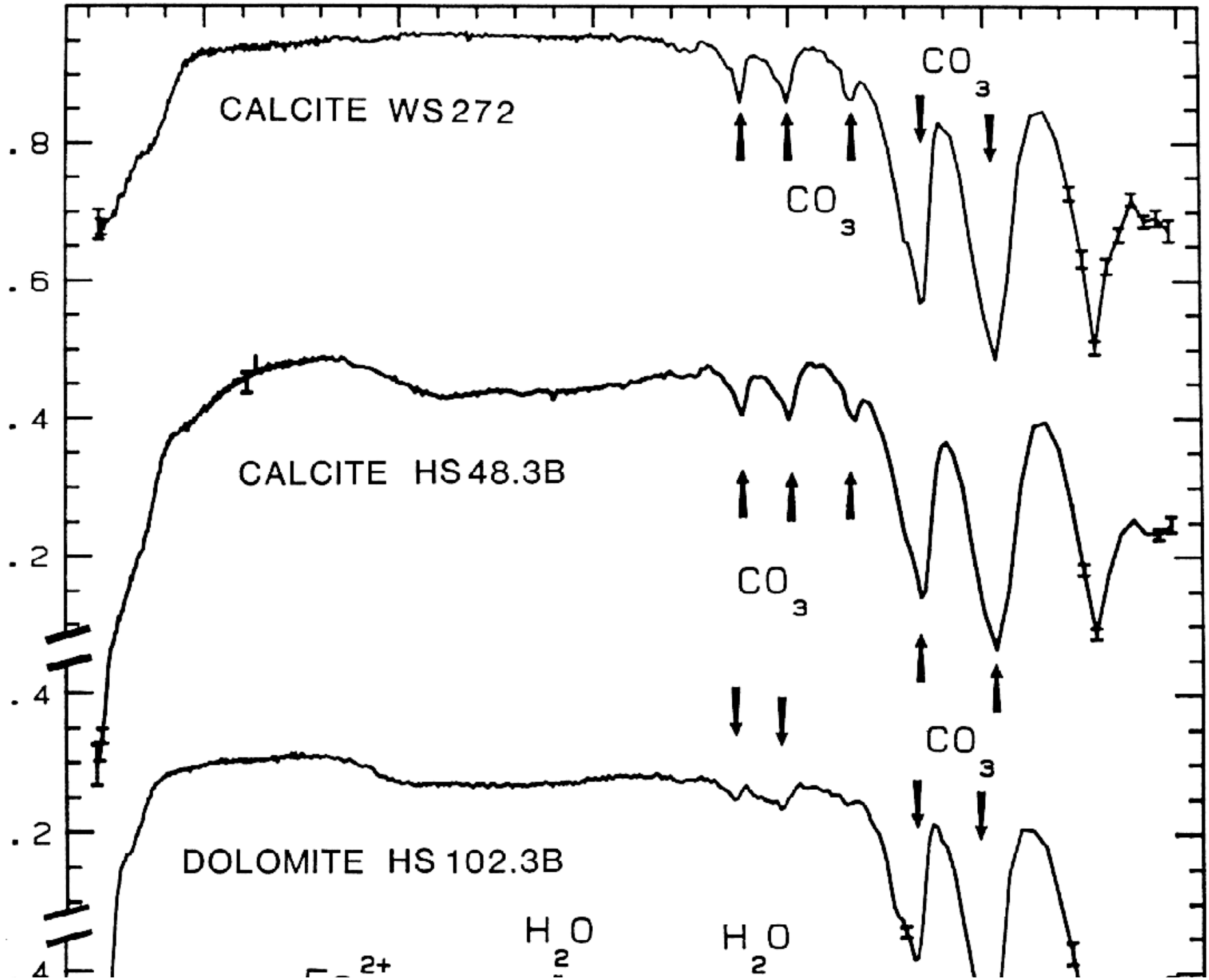
CALCITE WS272
CO3
CO3
CO3
.8
.6
.4
CALCITE HS48.3B
.2
CO3
.4
CO3
.2
DOLOMITE HS102.3B
H2O
H2O

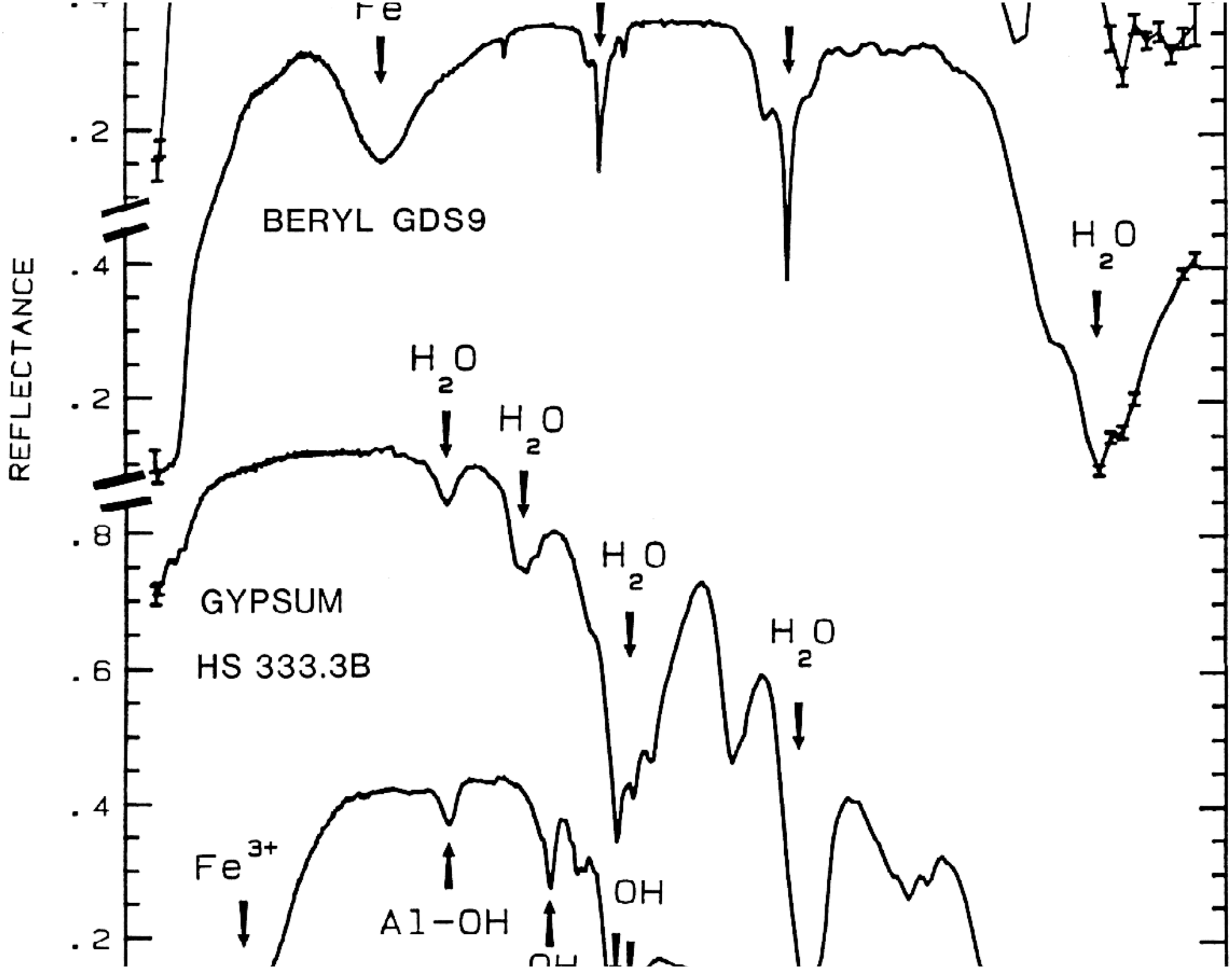
REFLECTANCE
.2
.4
.2
.8
.6
.4
.2
Fe
BERYL GDS9
H2O
H2O
H2O
GYPSUM
HS 333.3B
H2O
H2O
Fe3+
Al-OH
OH

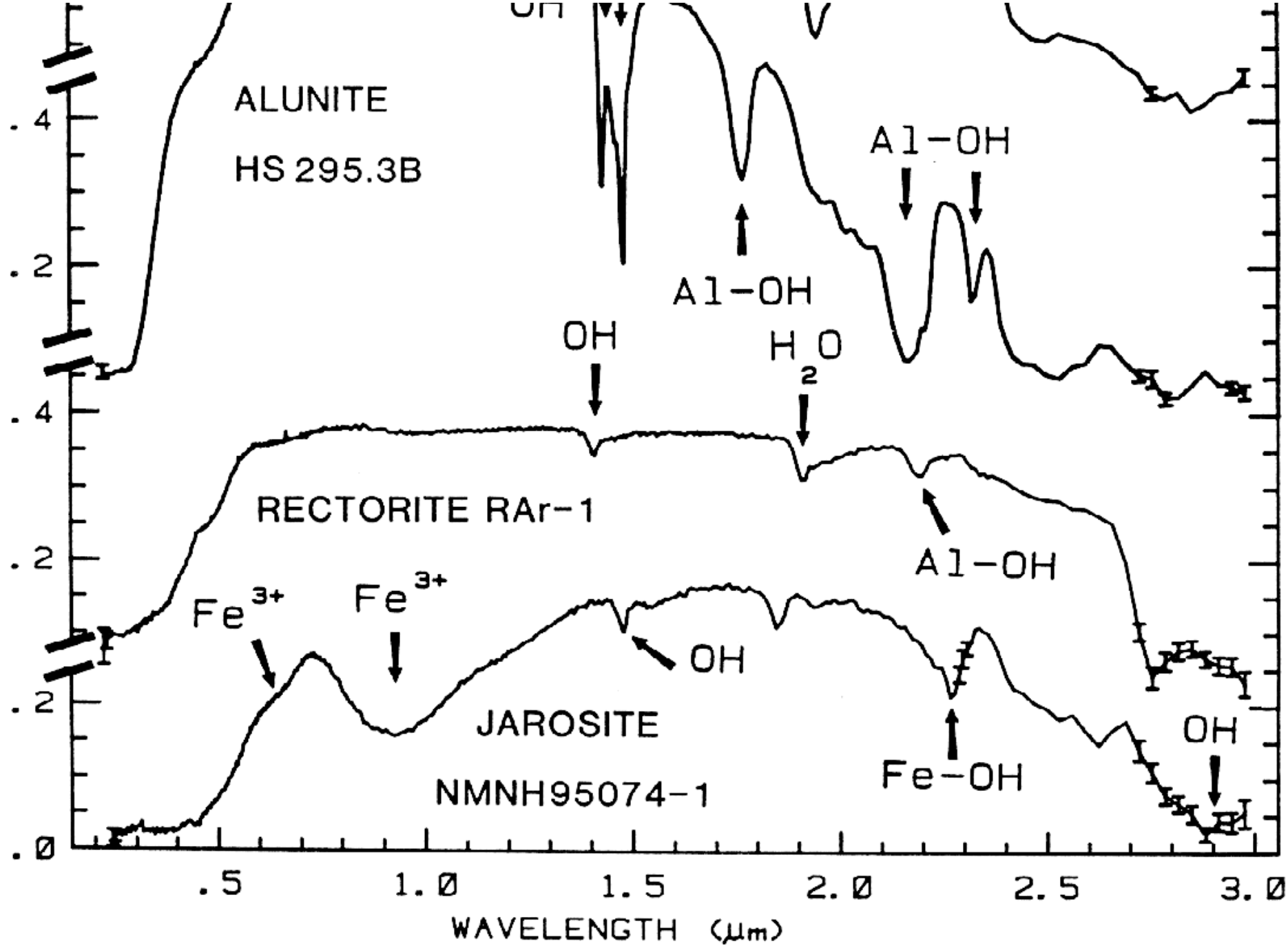
ALUNITE
HS 295.3B
Al-OH
Al-OH
OH
H2O
Al-OH
RECTORITE RAr-1
Fe3+
Fe3+
OH
JAROSITE
NMNH95074-1
Fe-OH
OH
.4
.2
.4
.2
.2
.0
.5
1.0
1.5
2.0
2.5
3.0
WAVELENGTH (μm)

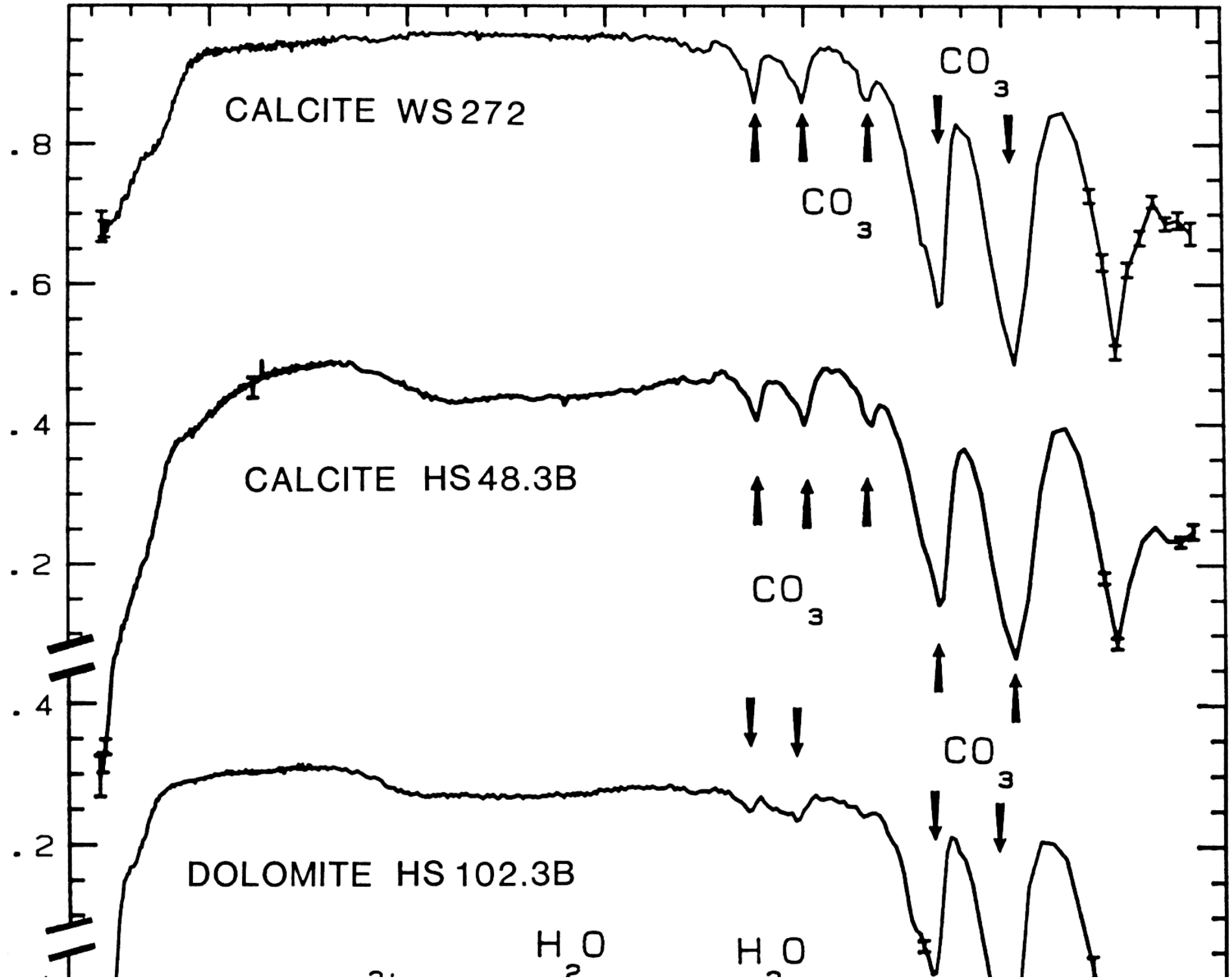
CALCITE WS272
CALCITE HS48.3B
DOLOMITE HS102.3B
CO3
CO3
CO3
CO3
CO3
H2O
H2O
.8
.6
.4
.2
.4
.2

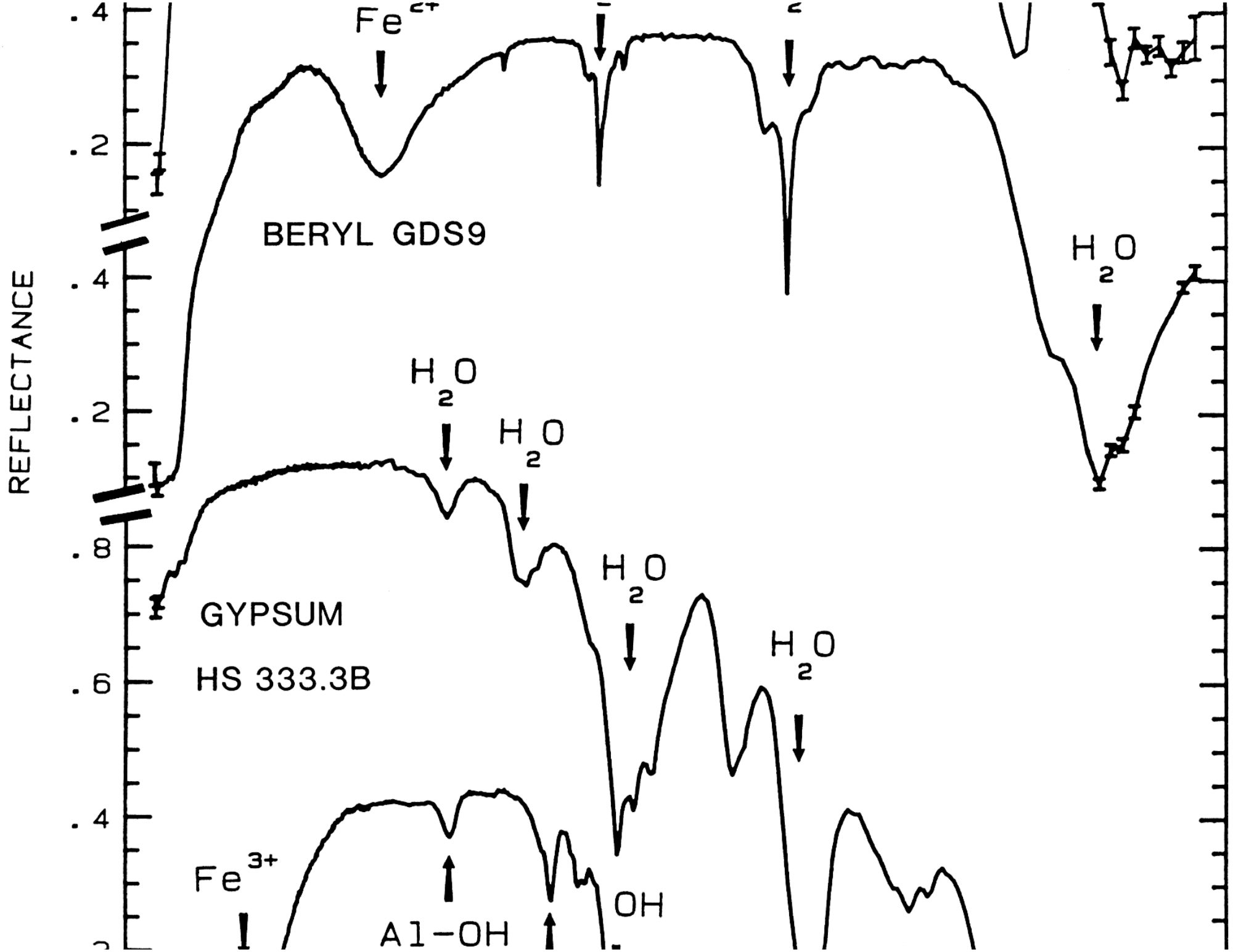

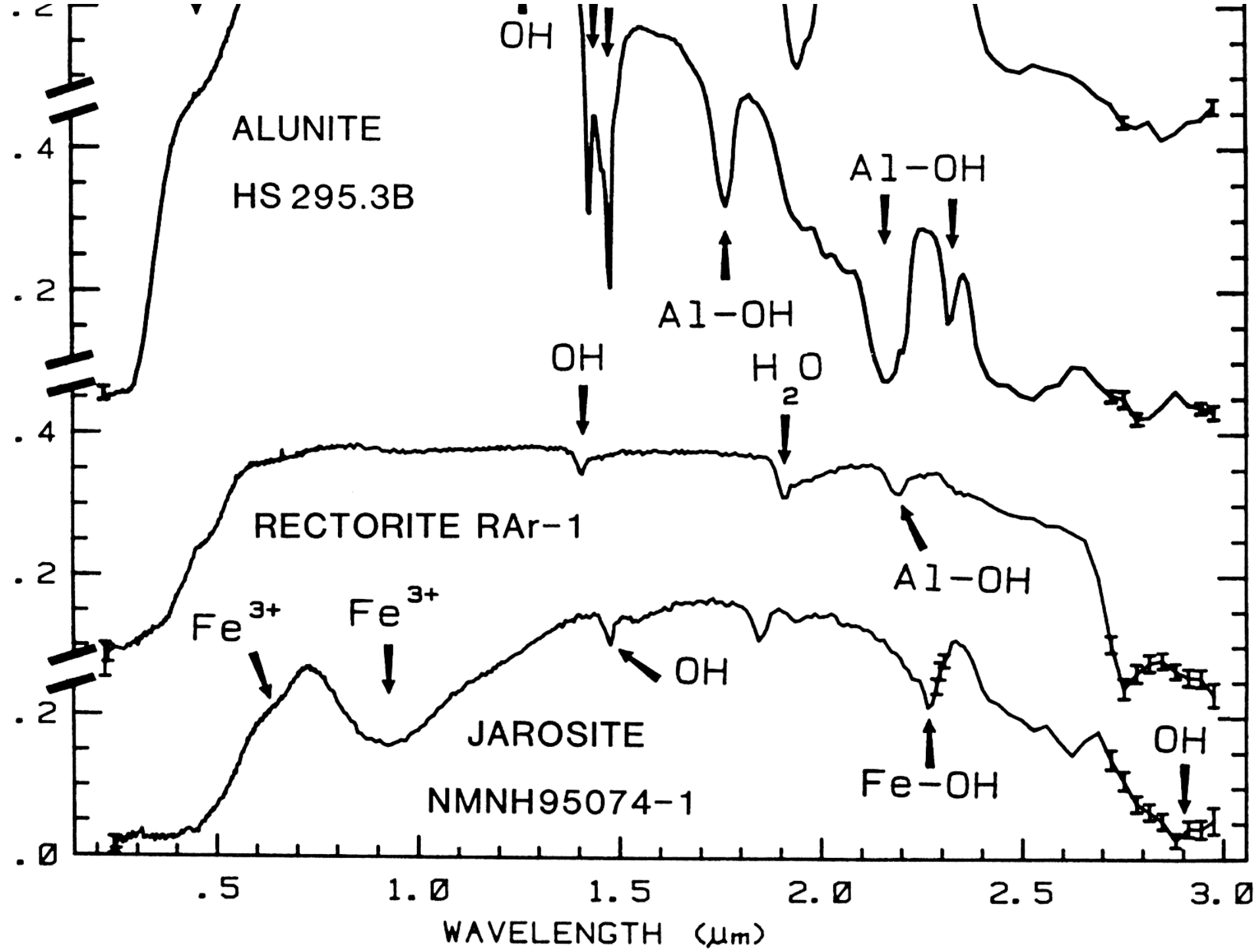
OH
ALUNITE
HS 295.3B
Al-OH
Al-OH
OH
H2O
RECTORITE RAr-1
Al-OH
Fe3+
Fe3+
OH
JAROSITE
NMNH95074-1
Fe-OH
OH
.4
.2
.4
.2
.2
.0
.5
1.0
1.5
2.0
2.5
3.0
WAVELENGTH (μm)

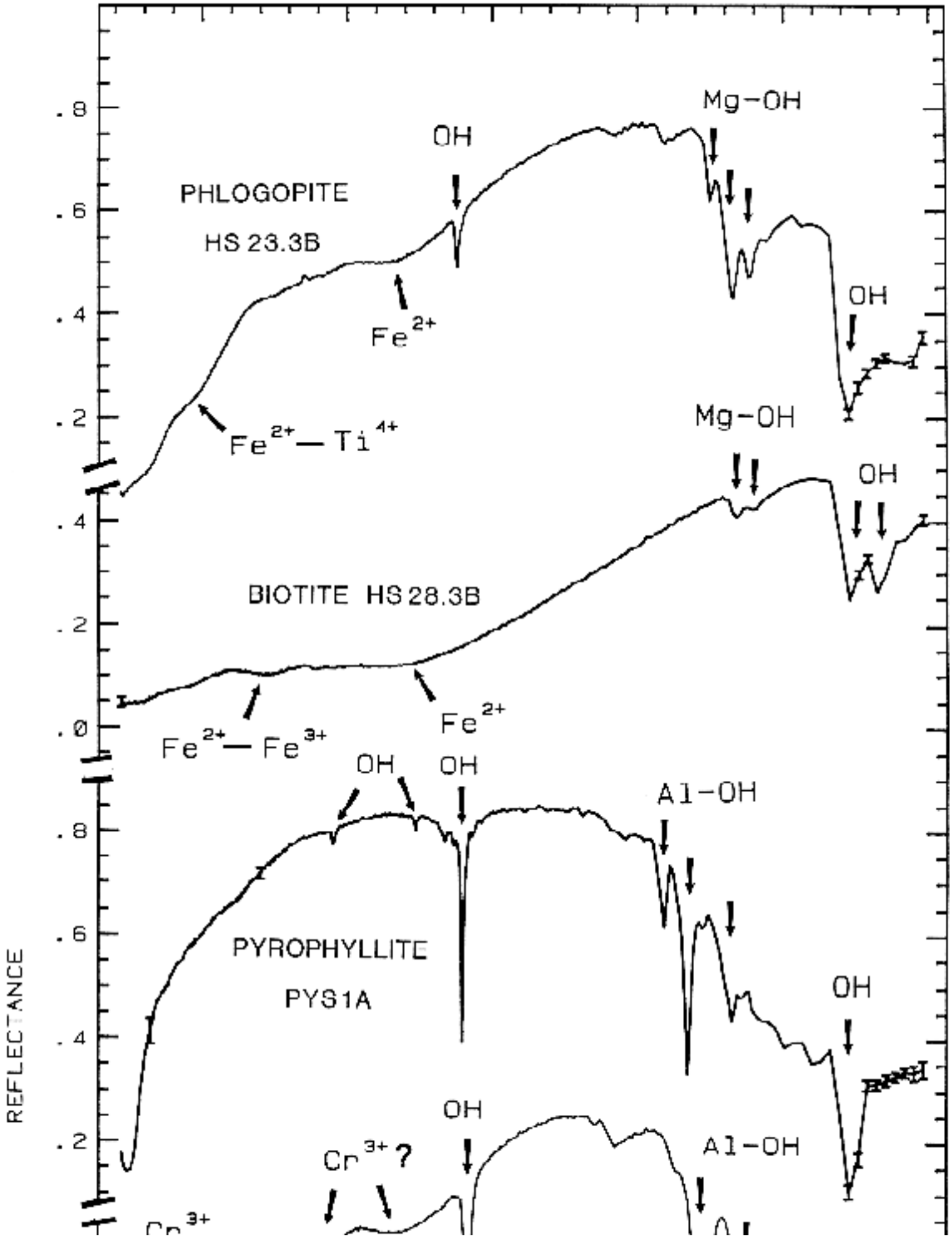
REFLECTANCE
.8
.6
.4
.2
.0
PHLOGOPITE
HS 23.3B
OH
Mg-OH
OH
Fe2+
Fe2+ — Ti4+
BIOTITE HS 28.3B
Mg-OH
OH
Fe2+ — Fe3+
Fe2+
PYROPHYLLITE
PYS1A
OH
OH
Al-OH
OH
Cr3+ ?
OH
Al-OH
Cr3+

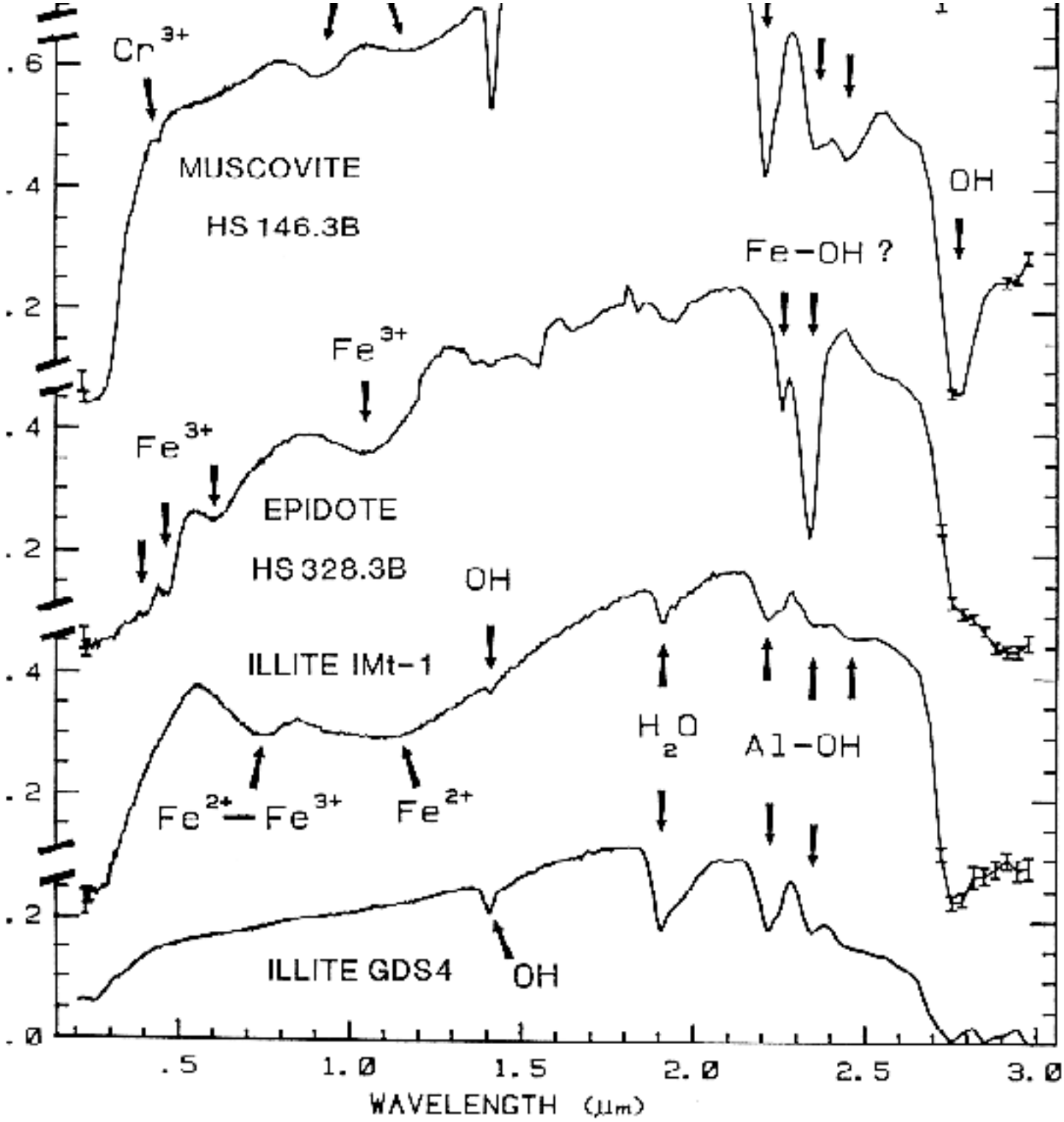
Cr 3+
MUSCOVITE
HS 146.3B
OH
Fe-OH ?
Fe 3+
Fe 3+
EPIDOTE
HS 328.3B
OH
ILLITE IMt-1
H2O
Al-OH
Fe 2+ — Fe 3+
Fe 2+
ILLITE GDS4
OH
.6
.4
.2
.4
.2
.4
.2
.0
.5
1.0
1.5
2.0
2.5
3.0
WAVELENGTH (μm)

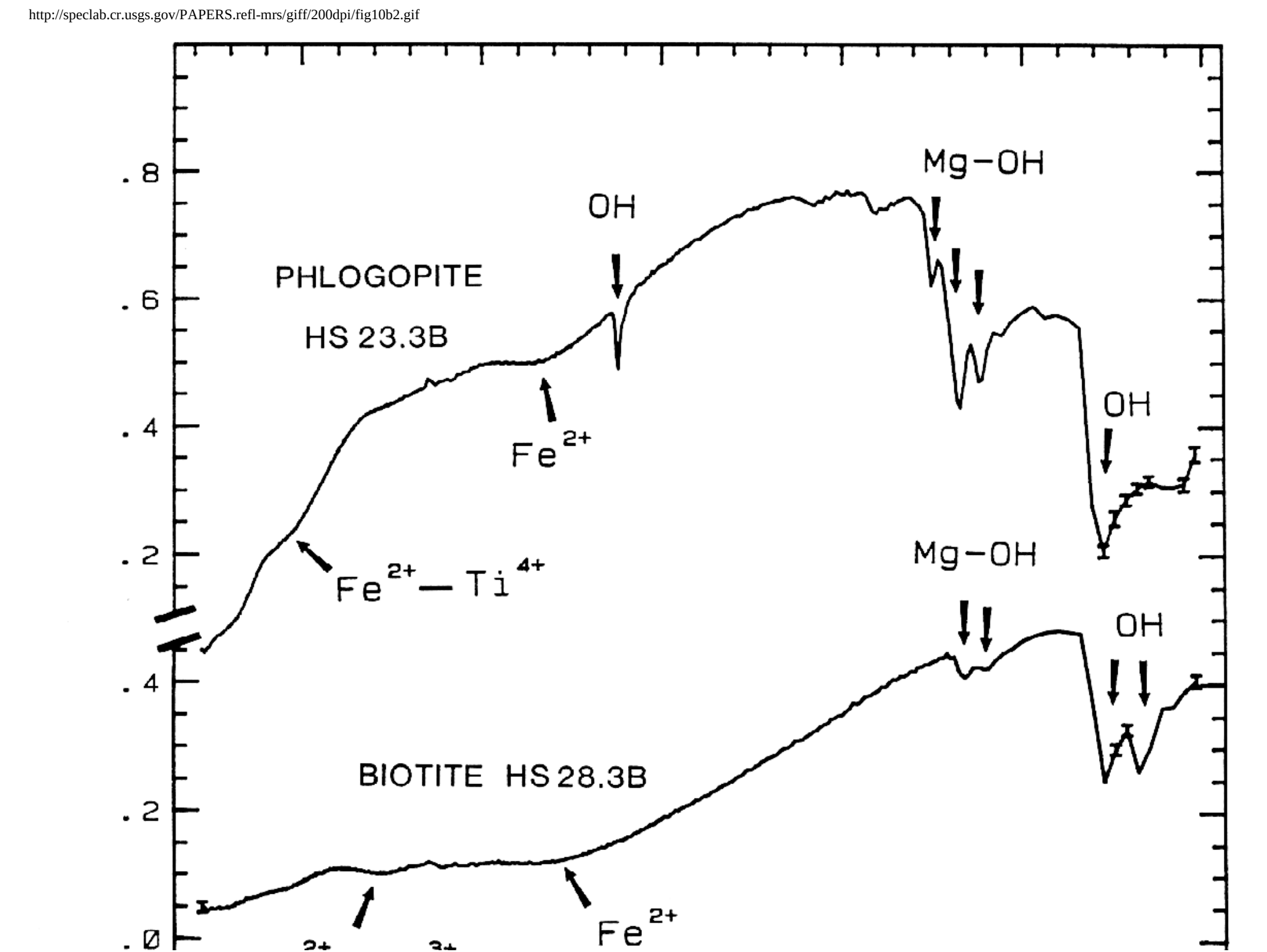
.8
.6
.4
.2
.4
.2
.0
PHLOGOPITE
HS 23.3B
OH
Mg-OH
OH
Fe2+
Fe2+ — Ti4+
Mg-OH
OH
BIOTITE HS 28.3B
Fe2+

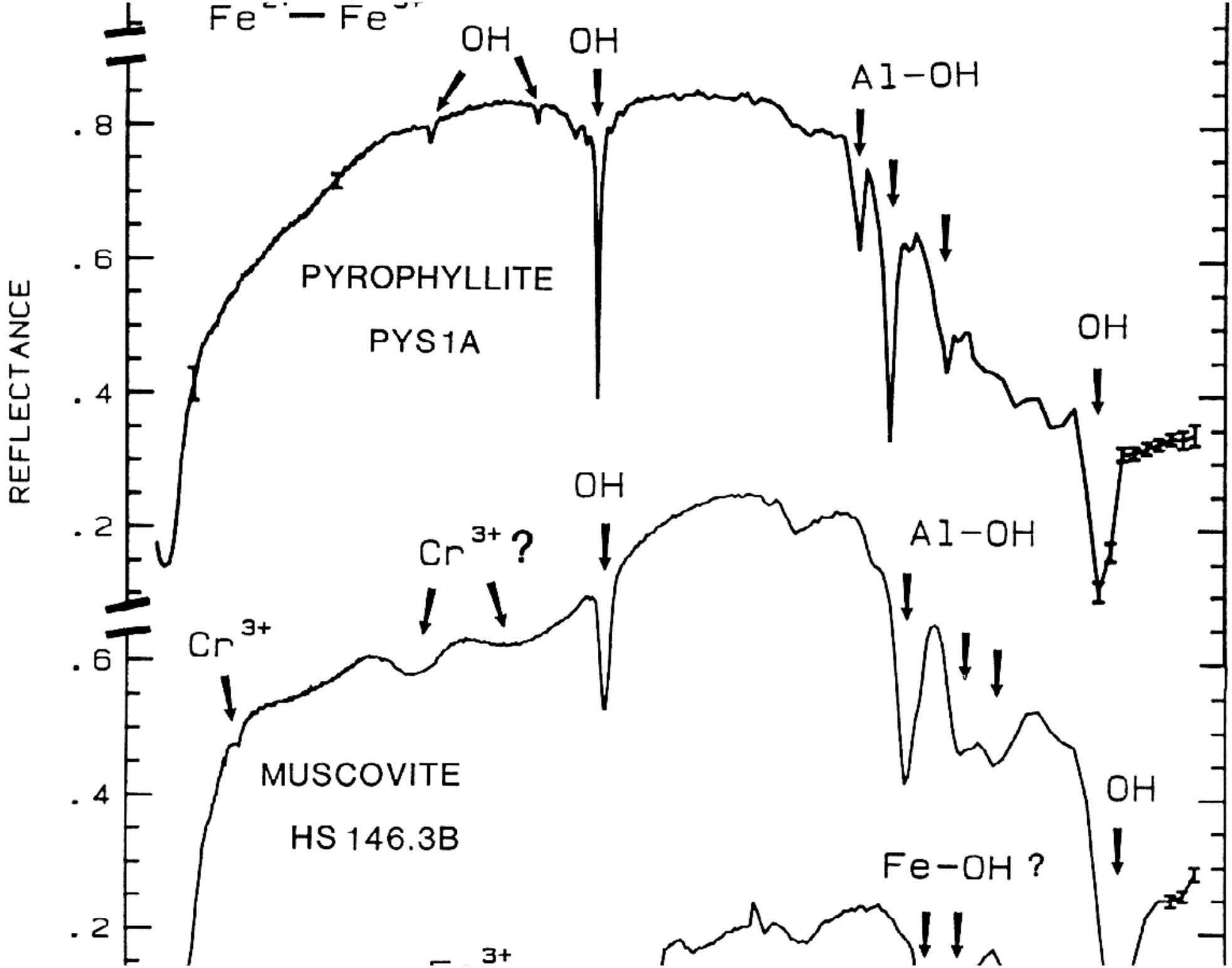
Fe — Fe
OH
OH
Al-OH
OH
PYROPHYLLITE
PYS1A
REFLECTANCE
.8
.6
.4
.2
OH
Cr 3+ ?
Al-OH
Cr 3+
MUSCOVITE
HS 146.3B
OH
Fe-OH ?
.6
.4
.2

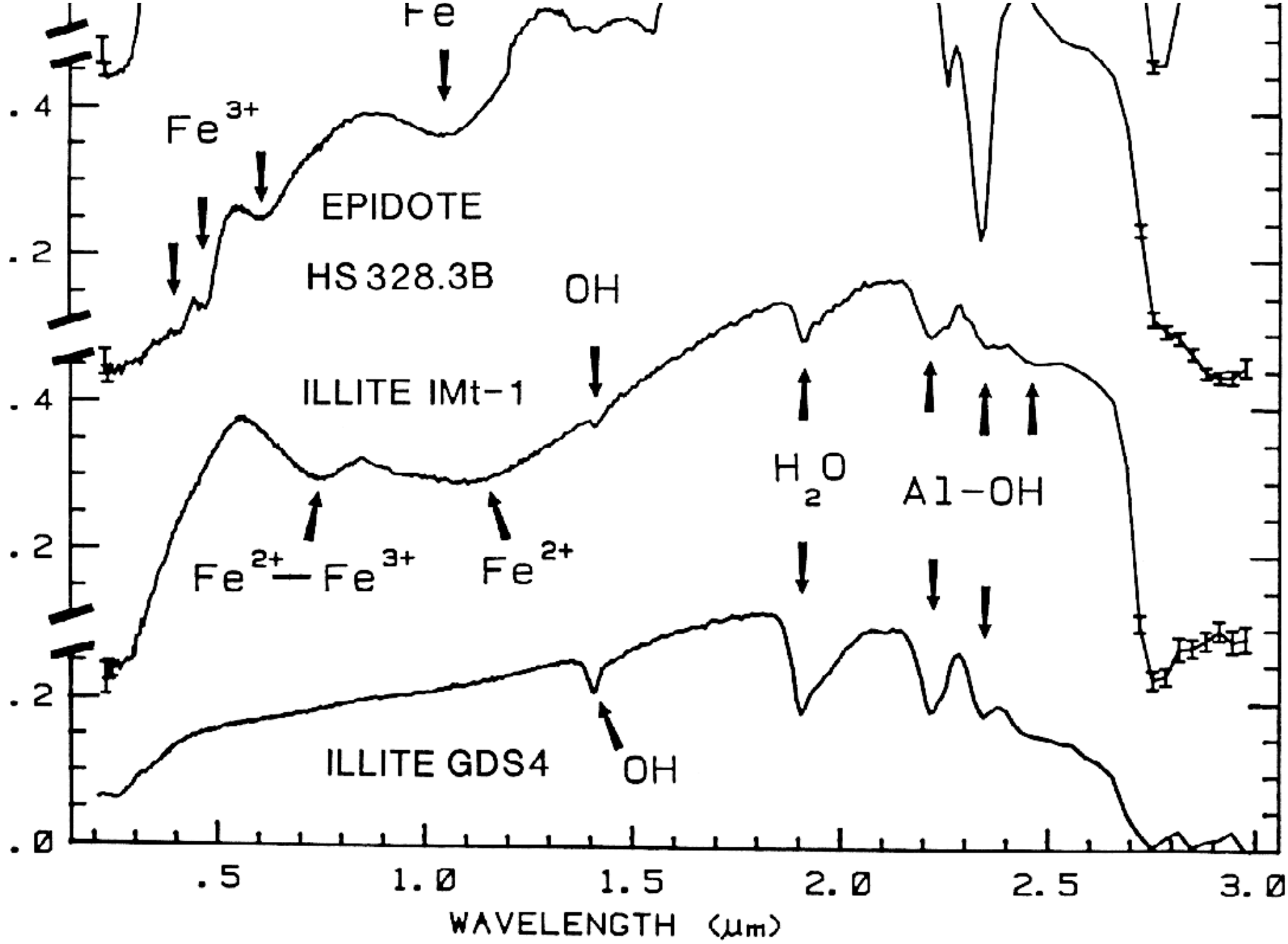
Fe
Fe3+
EPIDOTE
HS 328.3B
OH
ILLITE IMt-1
H2O
Al-OH
Fe2+—Fe3+
Fe2+
ILLITE GDS4
OH
.4
.2
.4
.2
.0
.5
1.0
1.5
2.0
2.5
3.0
WAVELENGTH (μm)

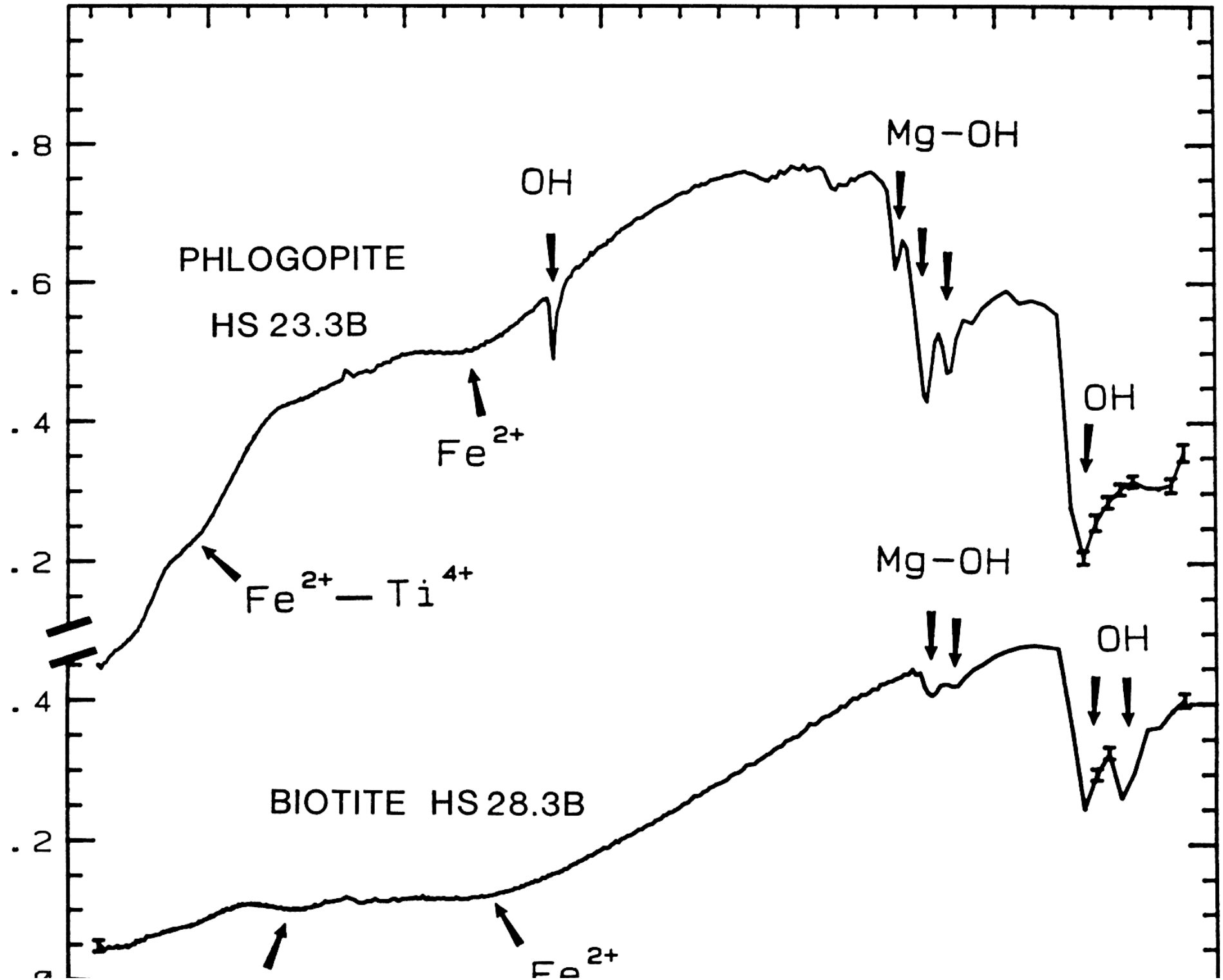
.8
.6
.4
.2
.4
.2
PHLOGOPITE
HS 23.3B
OH
Mg-OH
OH
Fe2+
Fe2+ — Ti4+
Mg-OH
OH
BIOTITE HS 28.3B
Fe2+

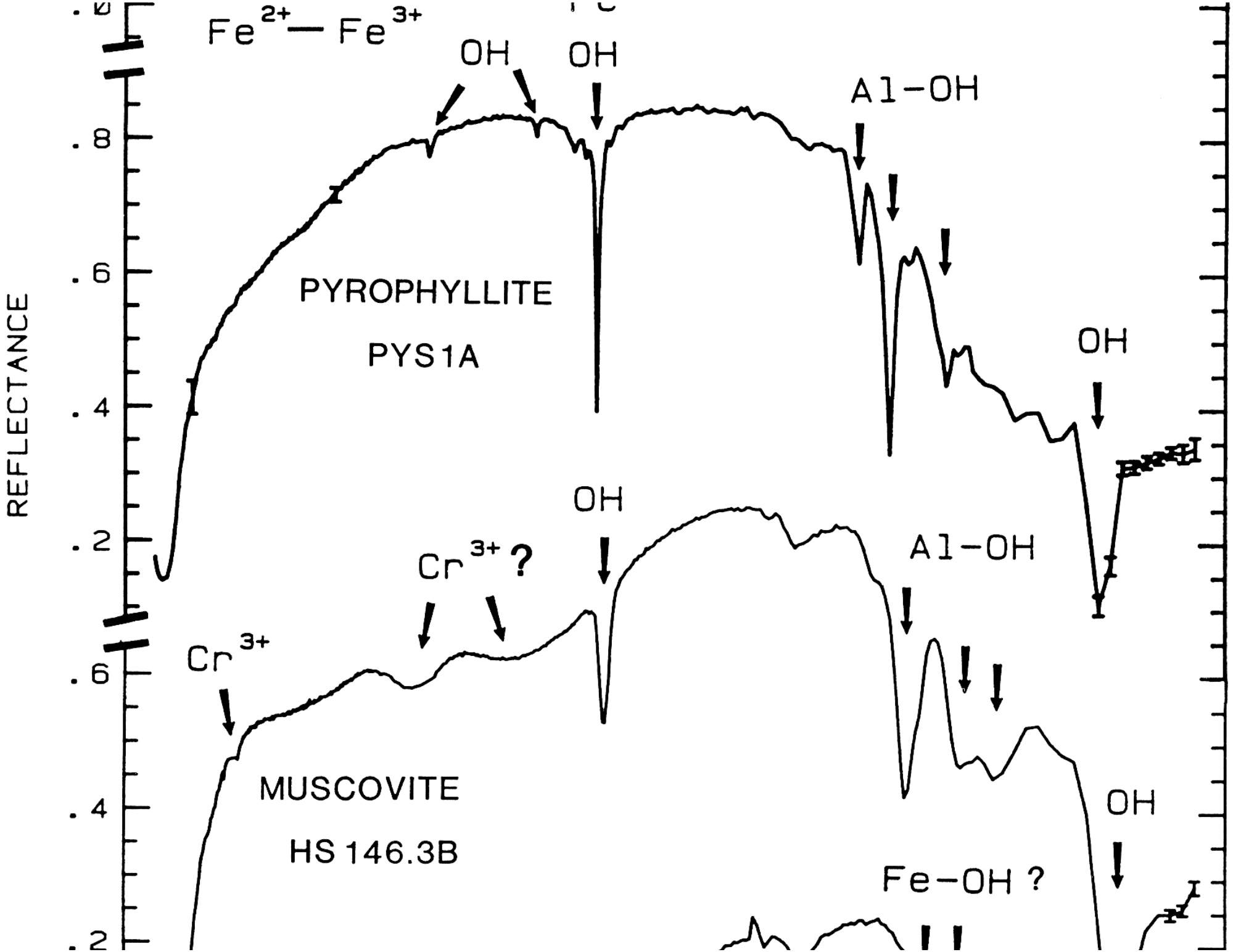
Fe2+— Fe3+
OH
OH
Al-OH
OH
PYROPHYLLITE
PYS1A
REFLECTANCE
.8
.6
.4
.2
OH
Cr3+?
Al-OH
Cr3+
MUSCOVITE
HS 146.3B
OH
Fe-OH ?
.6
.4
.2

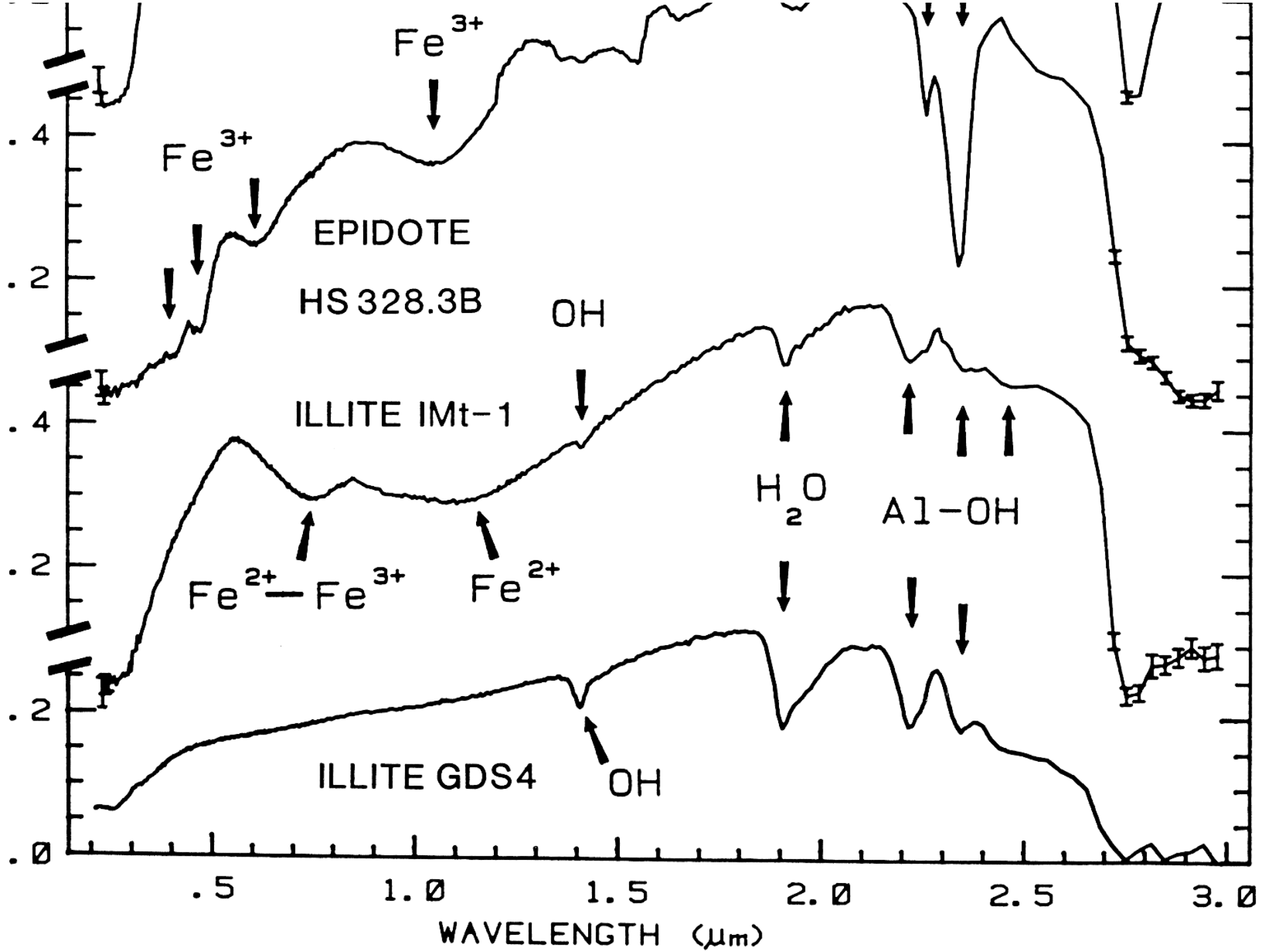
Fe 3+
Fe 3+
EPIDOTE
HS 328.3B
OH
ILLITE IMt-1
H2O
Al-OH
Fe 2+ — Fe 3+
Fe 2+
ILLITE GDS4
OH
.4
.2
.4
.2
.2
.0
.5
1.0
1.5
2.0
2.5
3.0
WAVELENGTH (μm)

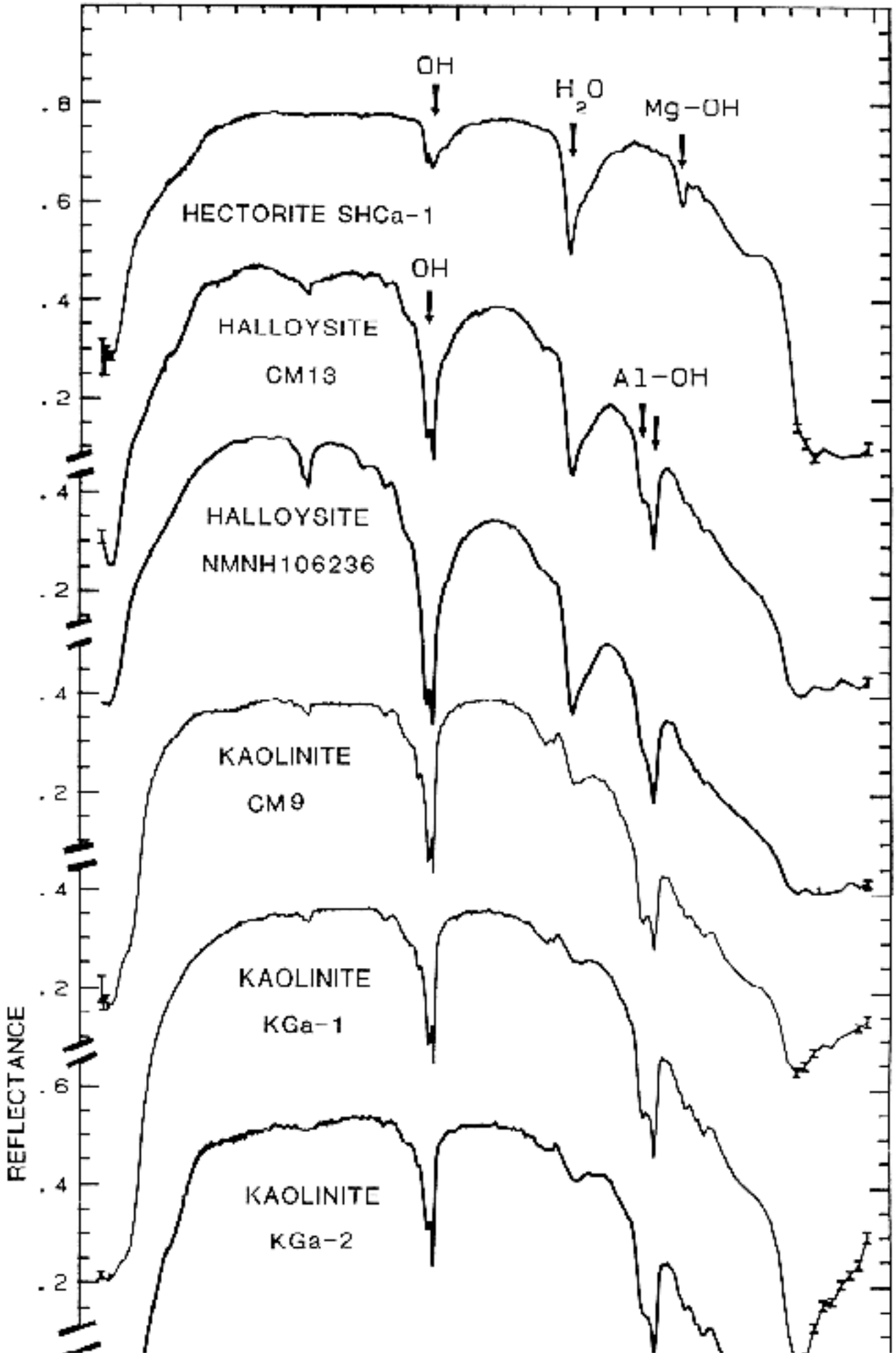
OH
H2O
Mg-OH
HECTORITE SHCa-1
OH
HALLOYSITE
CM13
Al-OH
HALLOYSITE
NMNH106236
KAOLINITE
CM9
KAOLINITE
KGa-1
KAOLINITE
KGa-2
REFLECTANCE
.8
.6
.4
.2
.4
.2
.4
.2
.4
.6
.4
.2

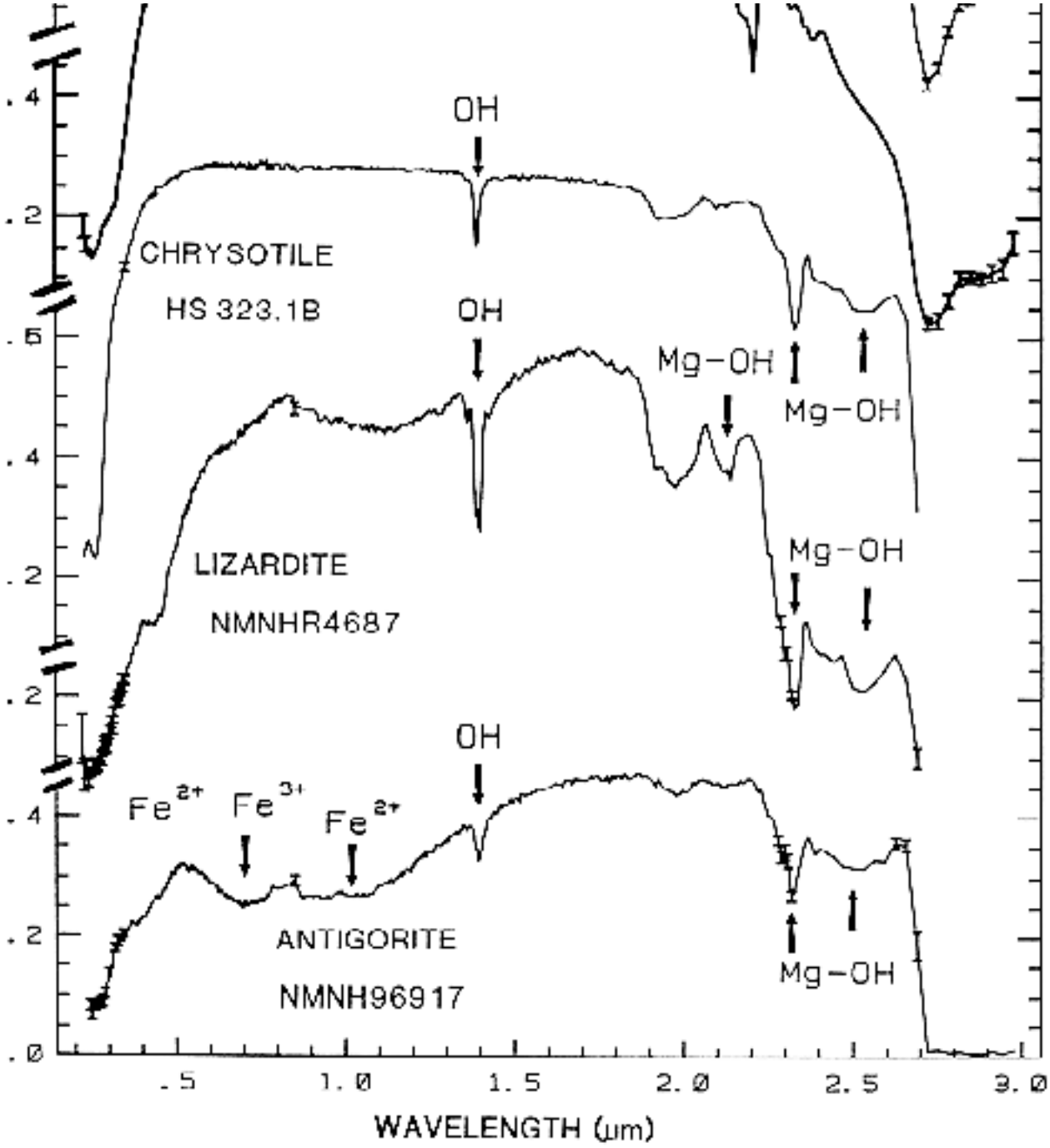
OH
CHRYSOTILE
HS 323.1B
OH
Mg-OH
Mg-OH
LIZARDITE
NMNHR4687
Mg-OH
OH
Fe2+
Fe3+
Fe2+
ANTIGORITE
NMNH96917
Mg-OH
.4
.2
.6
.4
.2
.2
.4
.2
.0
.5
1.0
1.5
2.0
2.5
3.0
WAVELENGTH (μm)

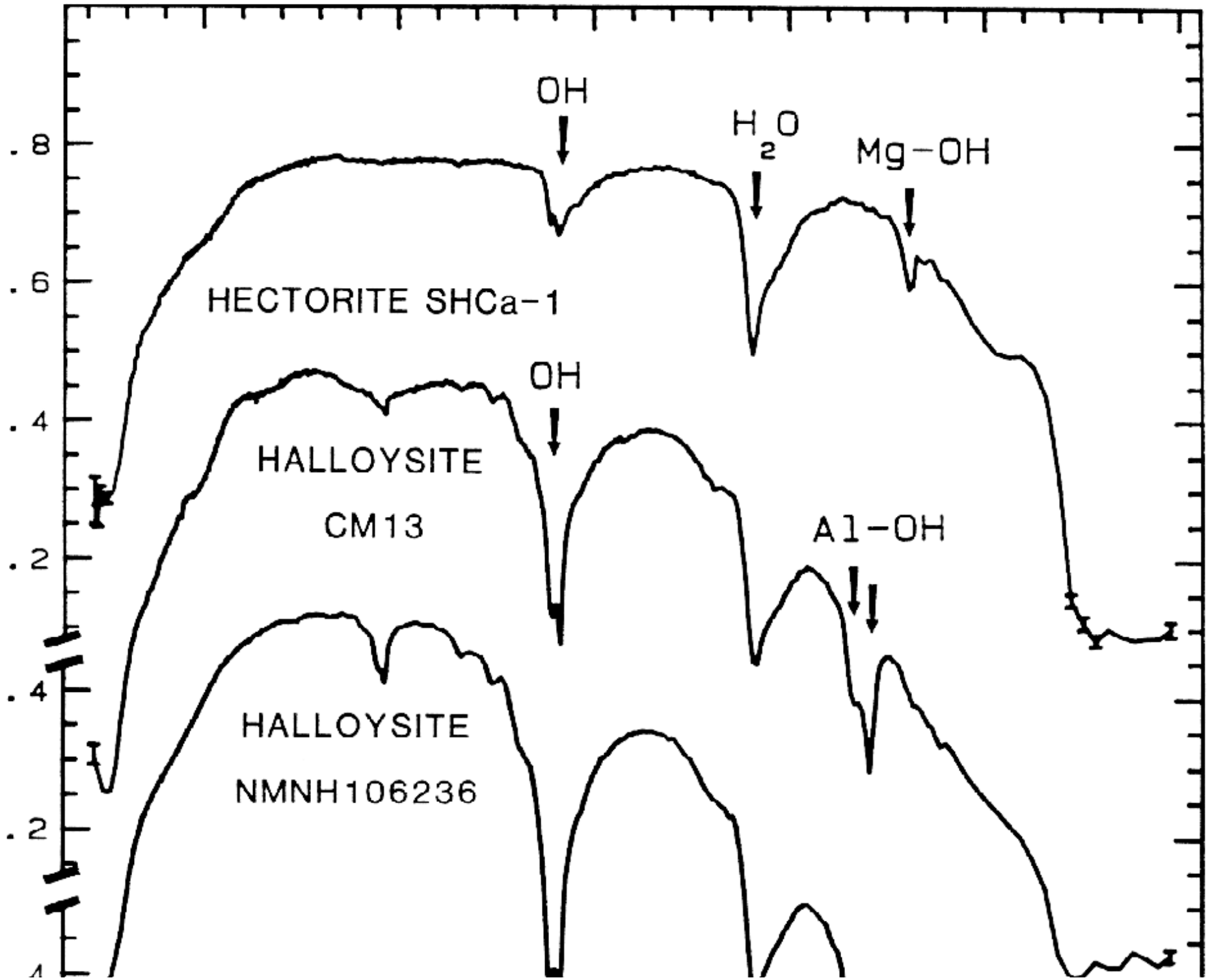
OH
H2O
Mg-OH
.8
.6
HECTORITE SHCa-1
OH
.4
HALLOYSITE
CM13
Al-OH
.2
.4
HALLOYSITE
NMNH106236
.2

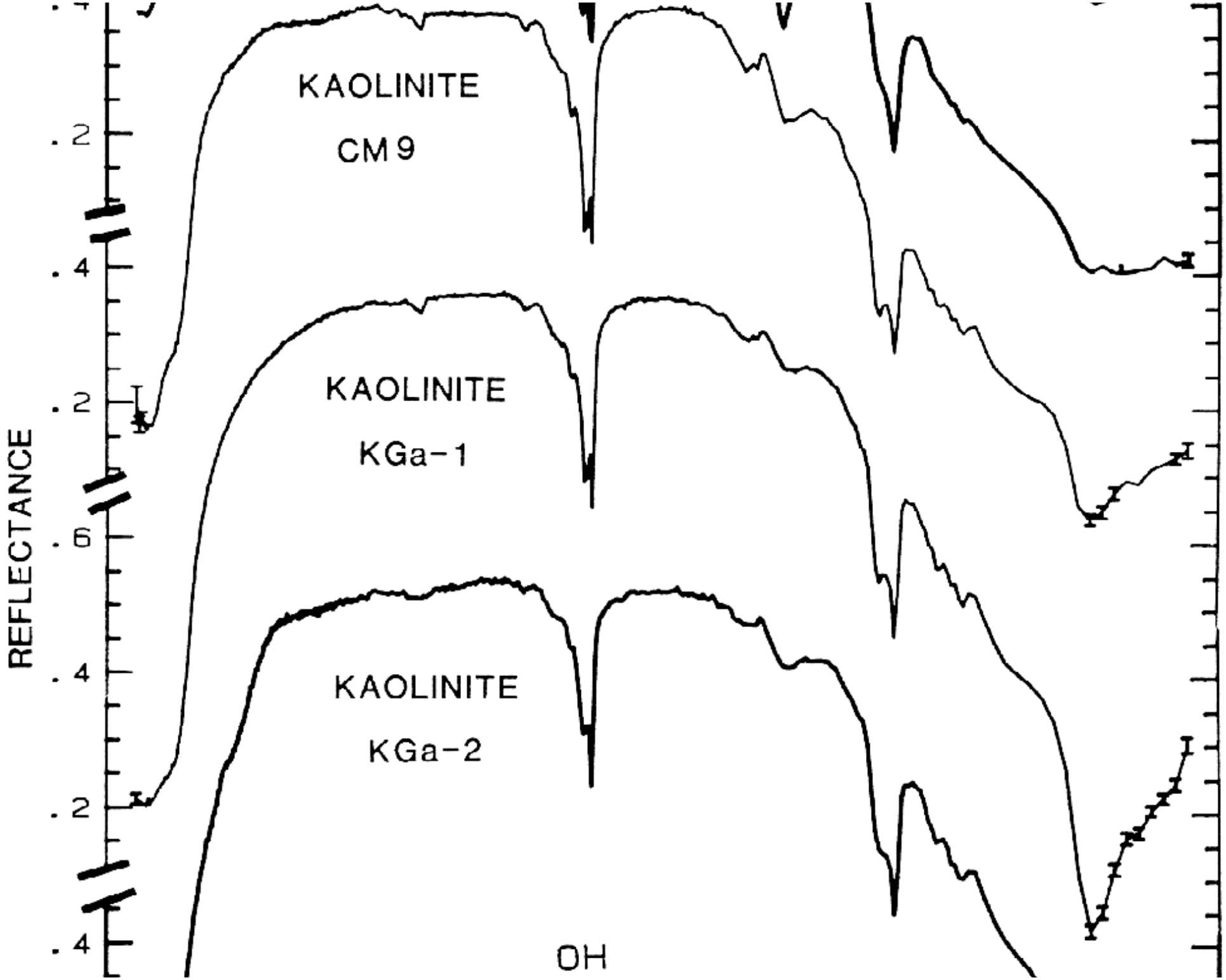
KAOLINITE
CM 9
KAOLINITE
KGa-1
KAOLINITE
KGa-2
OH
REFLECTANCE
.2
.4
.2
.6
.4
.2
.4

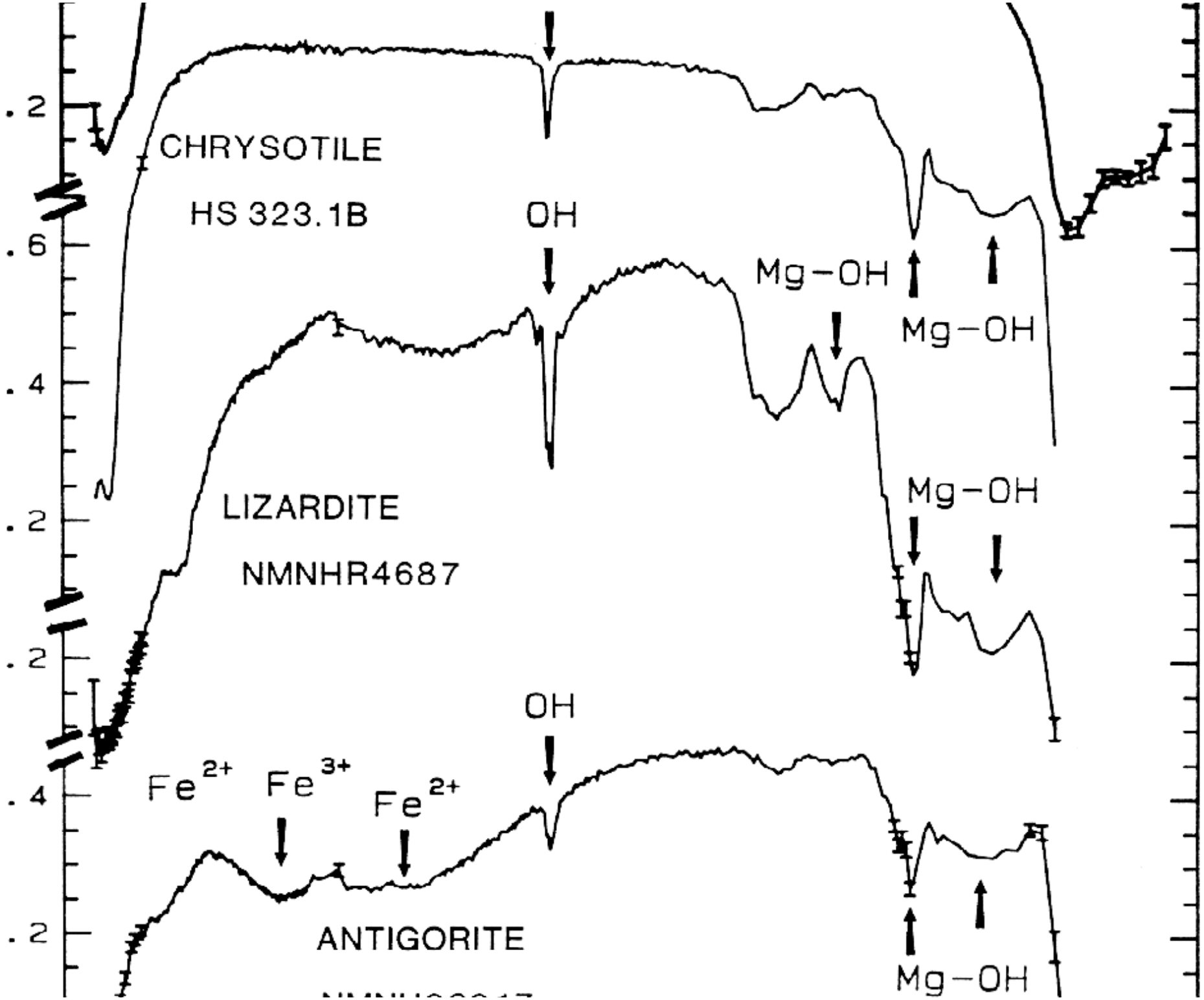
.2
.6
.4
.2
.2
.4
.2
CHRYSOTILE
HS 323.1B
OH
Mg-OH
Mg-OH
LIZARDITE
NMNHR4687
Mg-OH
OH
Fe2+
Fe3+
Fe2+
ANTIGORITE
Mg-OH

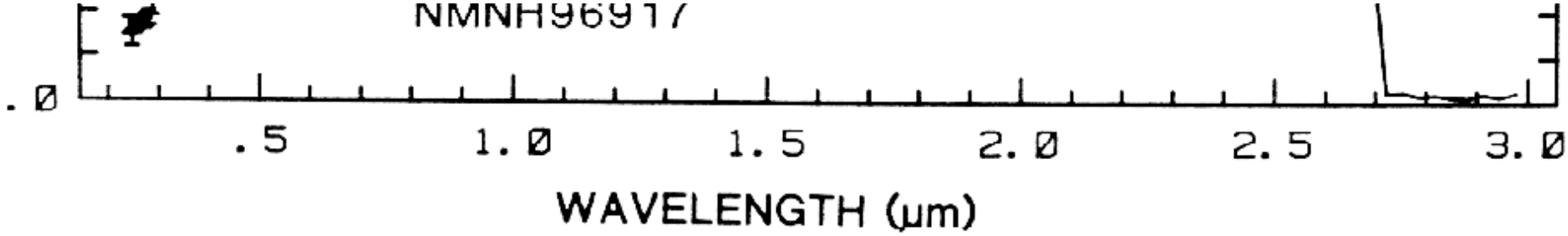
NMNH96917
.0
.5
1.0
1.5
2.0
2.5
3.0
WAVELENGTH (μm)

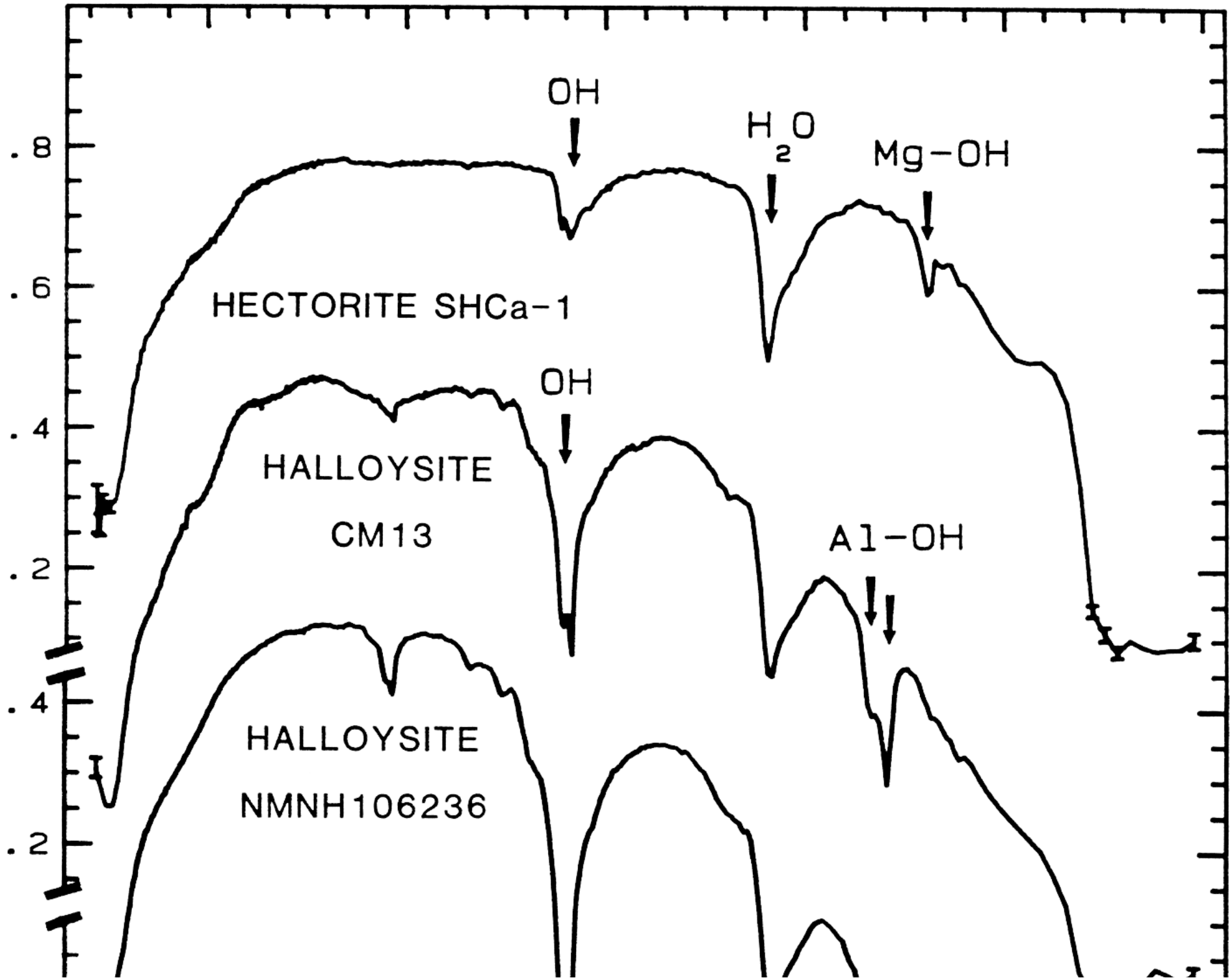
OH
H2O
Mg-OH
.8
.6
HECTORITE SHCa-1
OH
.4
HALLOYSITE
CM13
Al-OH
.2
.4
HALLOYSITE
NMNH106236
.2

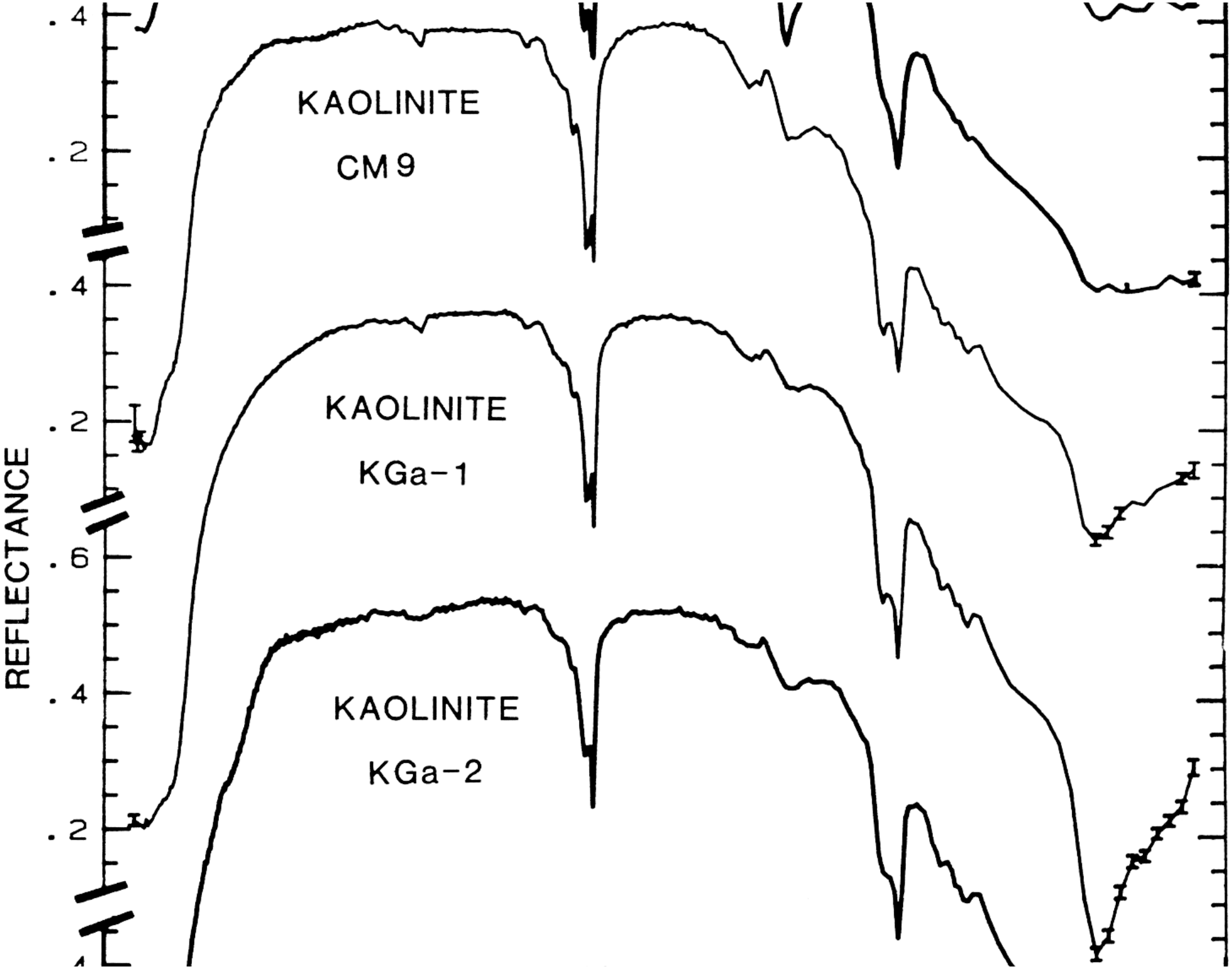
KAOLINITE
CM 9
KAOLINITE
KGa-1
KAOLINITE
KGa-2
REFLECTANCE
.4
.2
.4
.2
.6
.4
.2

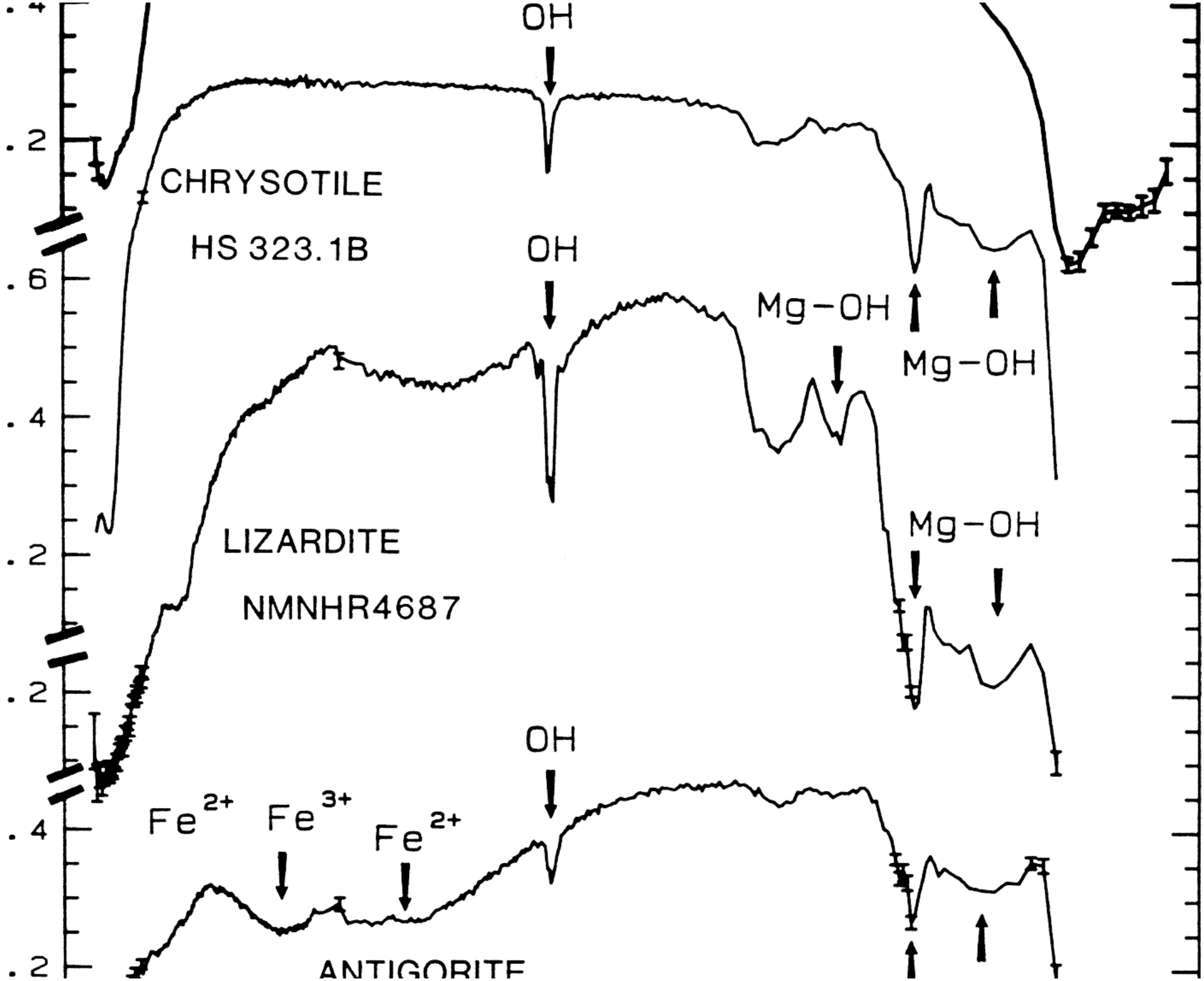
OH
CHRYSOTILE
HS 323.1B
OH
Mg-OH
Mg-OH
Mg-OH
LIZARDITE
NMNHR4687
OH
Fe2+
Fe3+
Fe2+
ANTIGORITE

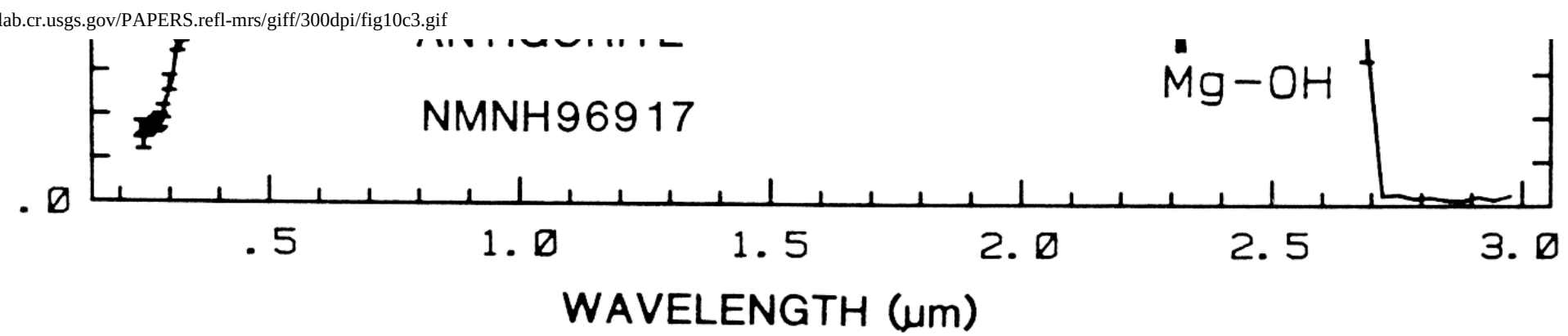
NMNH96917
Mg-OH
.0
.5
1.0
1.5
2.0
2.5
3.0
WAVELENGTH (μm)

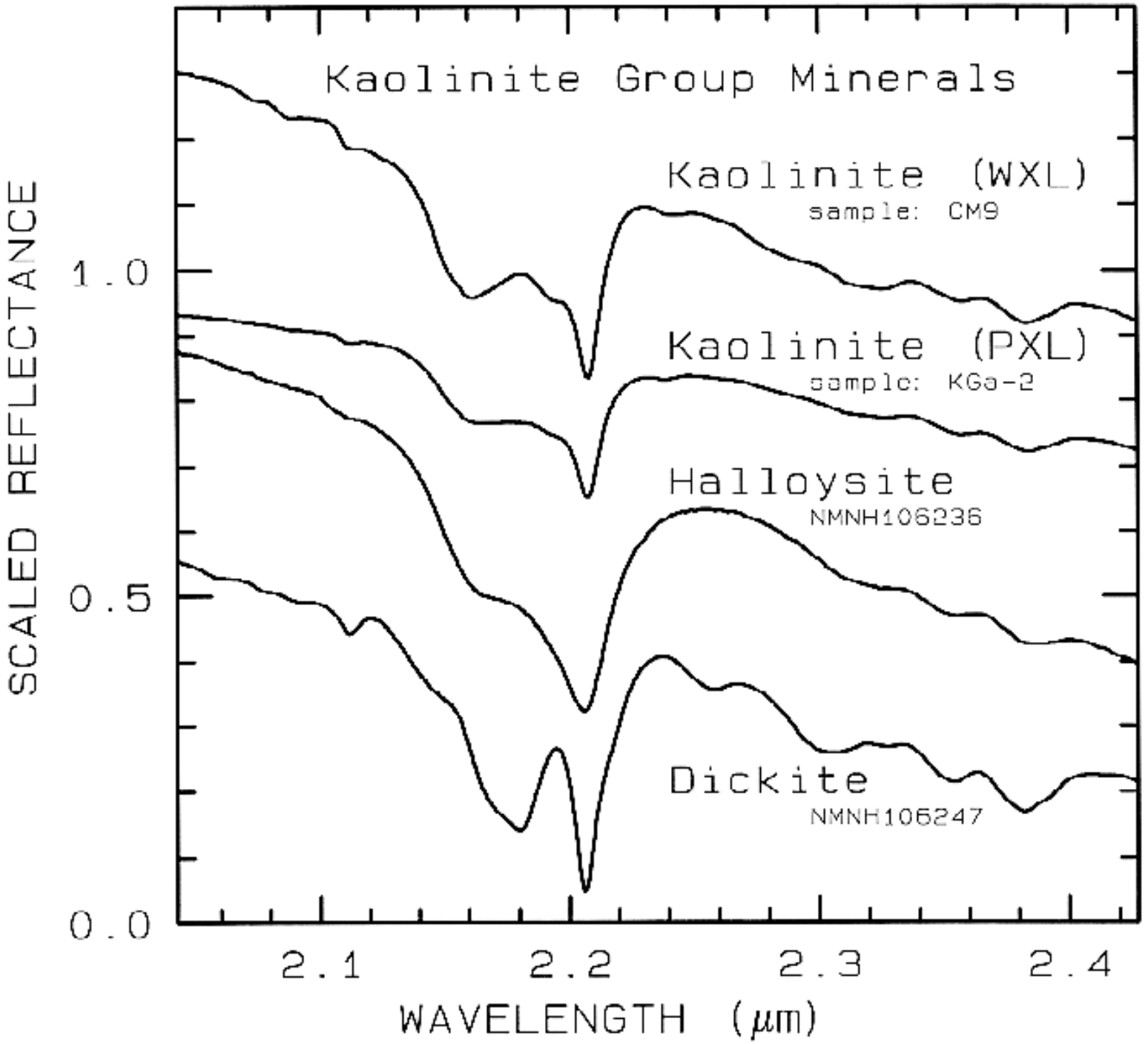
Kaolinite Group Minerals
Kaolinite (WXL)
sample: CM9
Kaolinite (PXL)
sample: KGa-2
Halloysite
NMNH106236
Dickite
NMNH106247
SCALED REFLECTANCE
1.0
0.5
0.0
2.1
2.2
2.3
2.4
WAVELENGTH (μm)

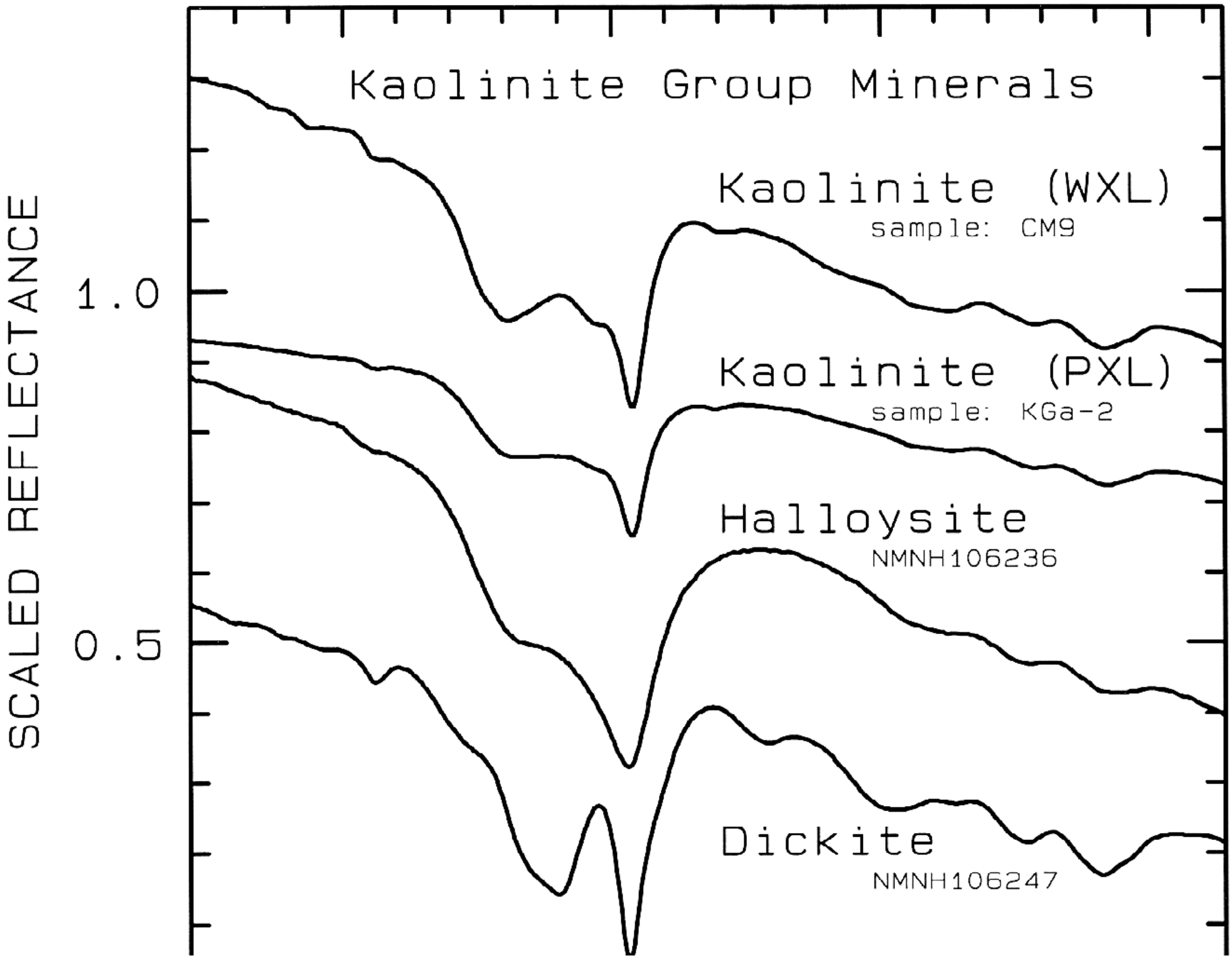
Kaolinite Group Minerals
Kaolinite (WXL)
sample: CM9
Kaolinite (PXL)
sample: KGa-2
Halloysite
NMNH106236
Dickite
NMNH106247
SCALED REFLECTANCE
1.0
0.5

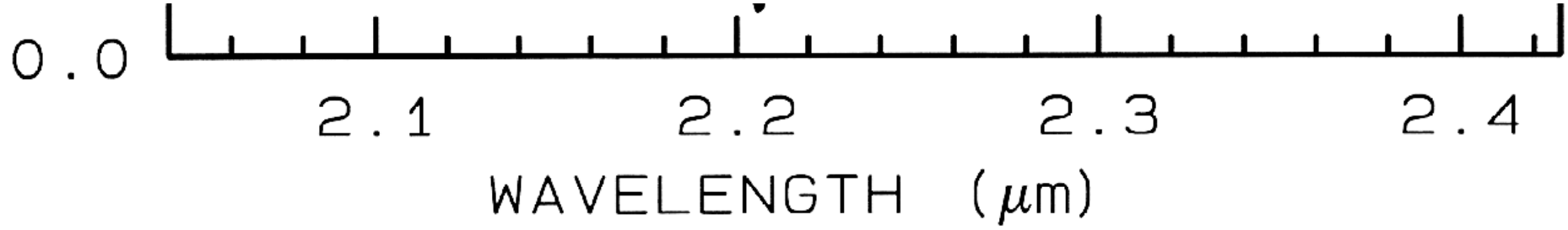
0.0
2.1
2.2
2.3
2.4
WAVELENGTH (μm)

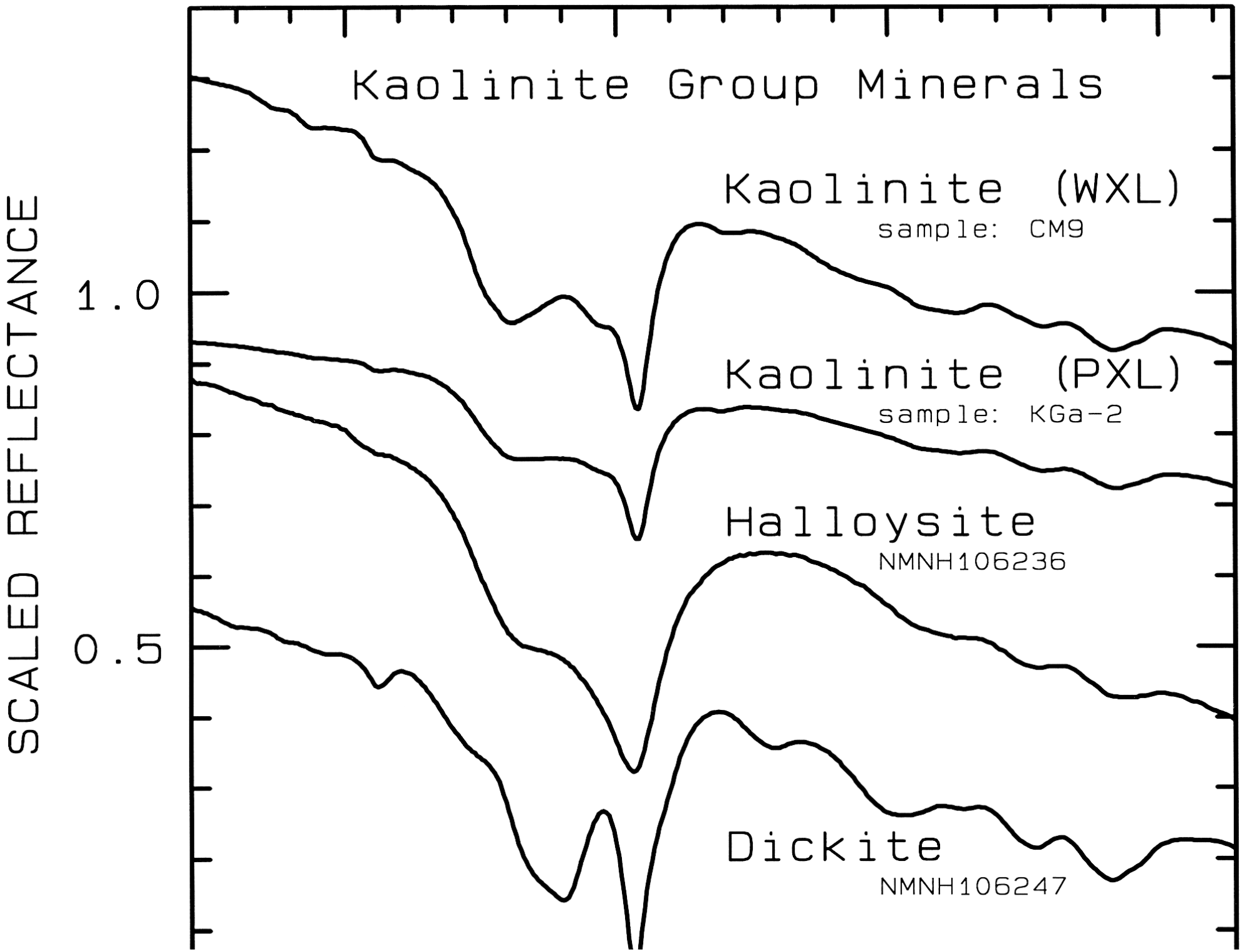
Kaolinite Group Minerals
Kaolinite (WXL)
sample: CM9
Kaolinite (PXL)
sample: KGa-2
Halloysite
NMNH106236
Dickite
NMNH106247
SCALED REFLECTANCE
1.0
0.5

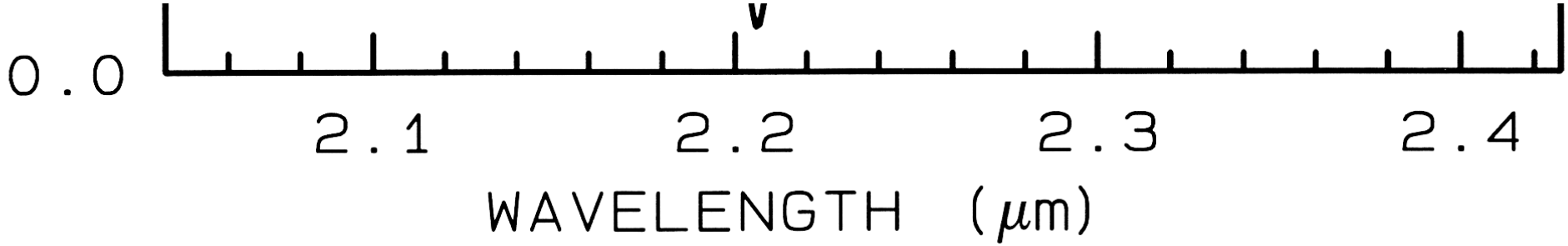
0.0
2.1
2.2
2.3
2.4
WAVELENGTH (μm)

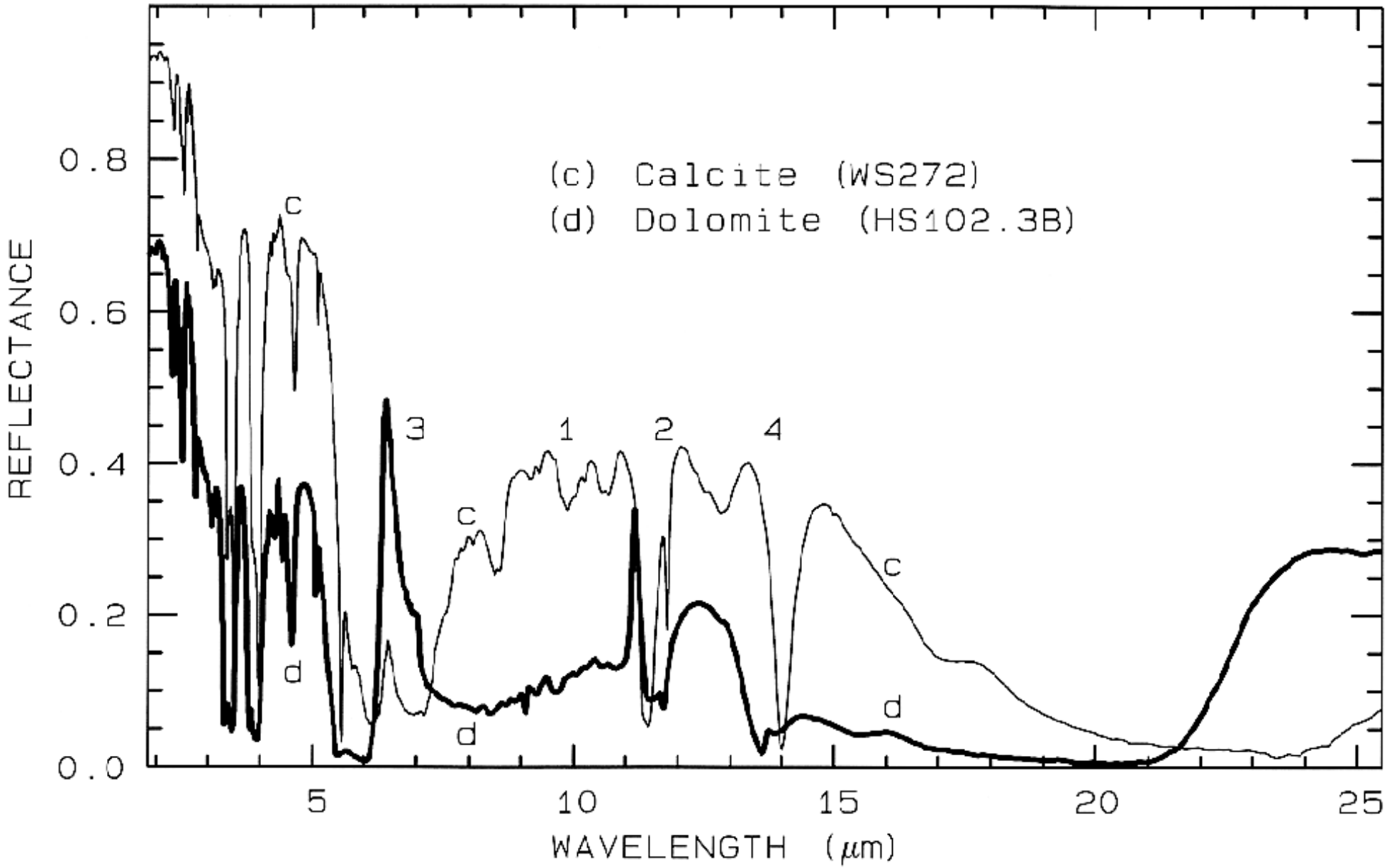
(c) Calcite (WS272)
(d) Dolomite (HS102.3B)
REFLECTANCE
0.0
0.2
0.4
0.6
0.8
5
10
15
20
25
WAVELENGTH (μm)
c
d
1
2
3
4

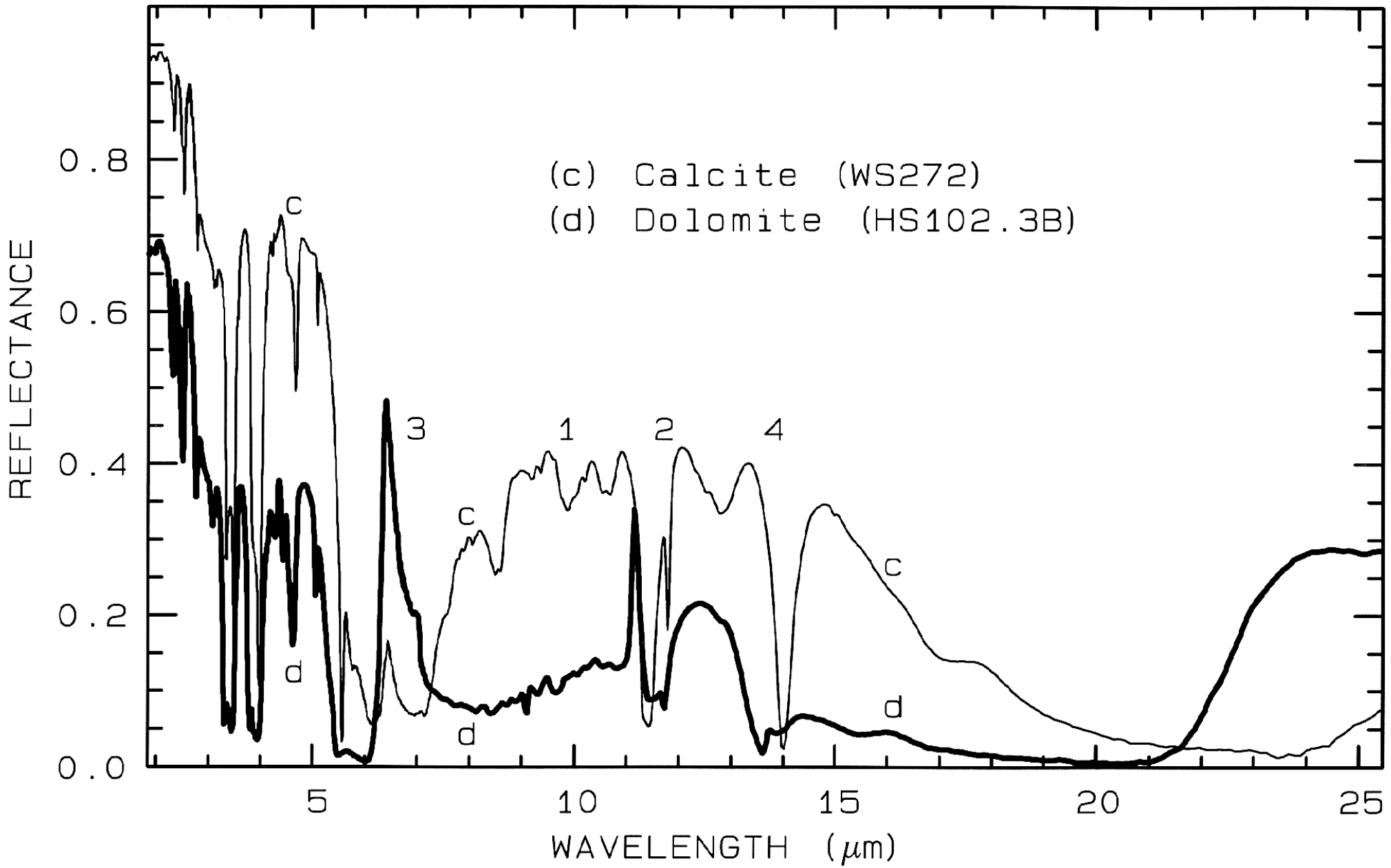
(c) Calcite (WS272)
(d) Dolomite (HS102.3B)
REFLECTANCE
0.0
0.2
0.4
0.6
0.8
5
10
15
20
25
WAVELENGTH (μm)
1
2
3
4
c
d

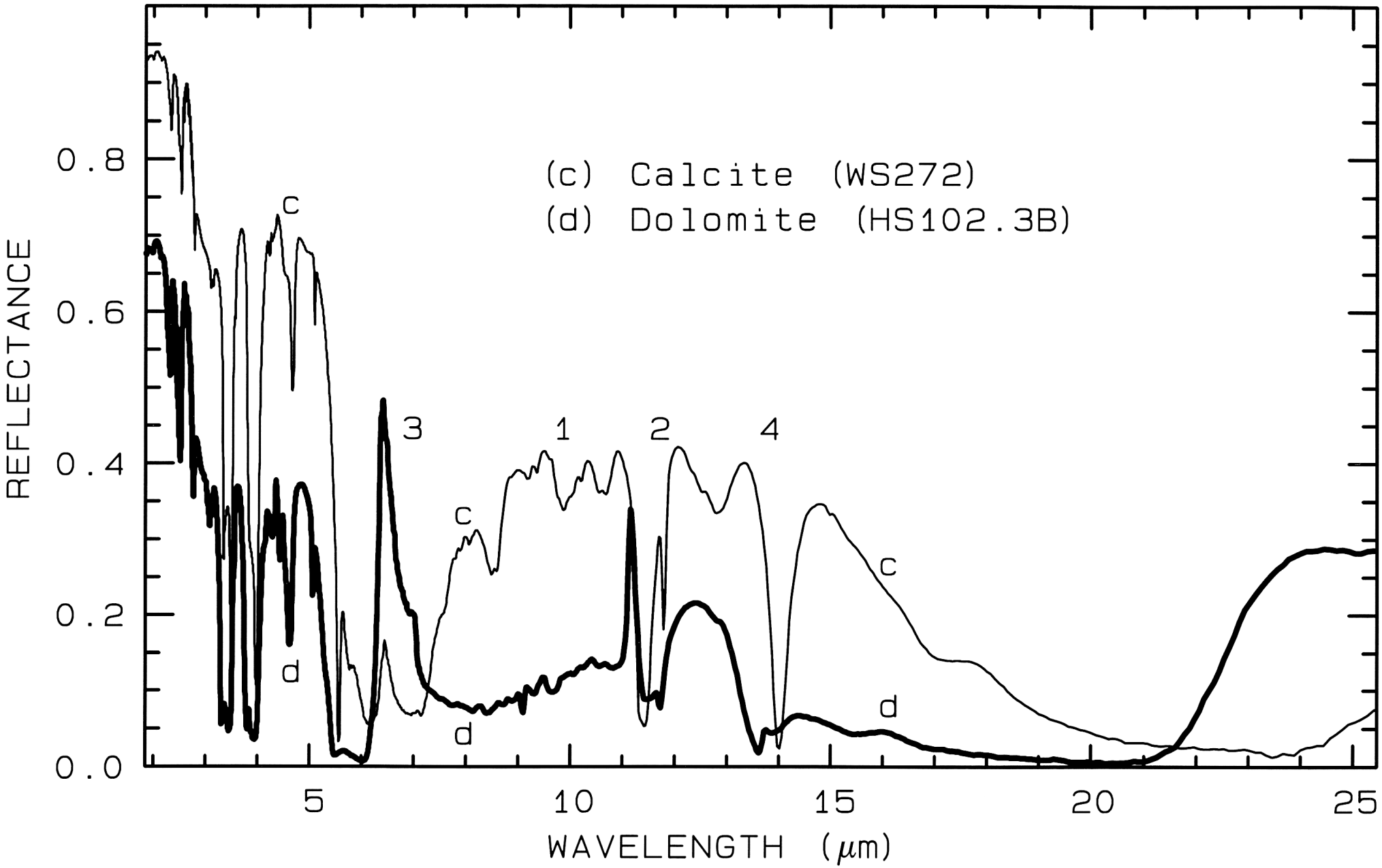
(c) Calcite (WS272)
(d) Dolomite (HS102.3B)
REFLECTANCE
0.0
0.2
0.4
0.6
0.8
5
10
15
20
25
WAVELENGTH (μm)
c
d
1
2
3
4

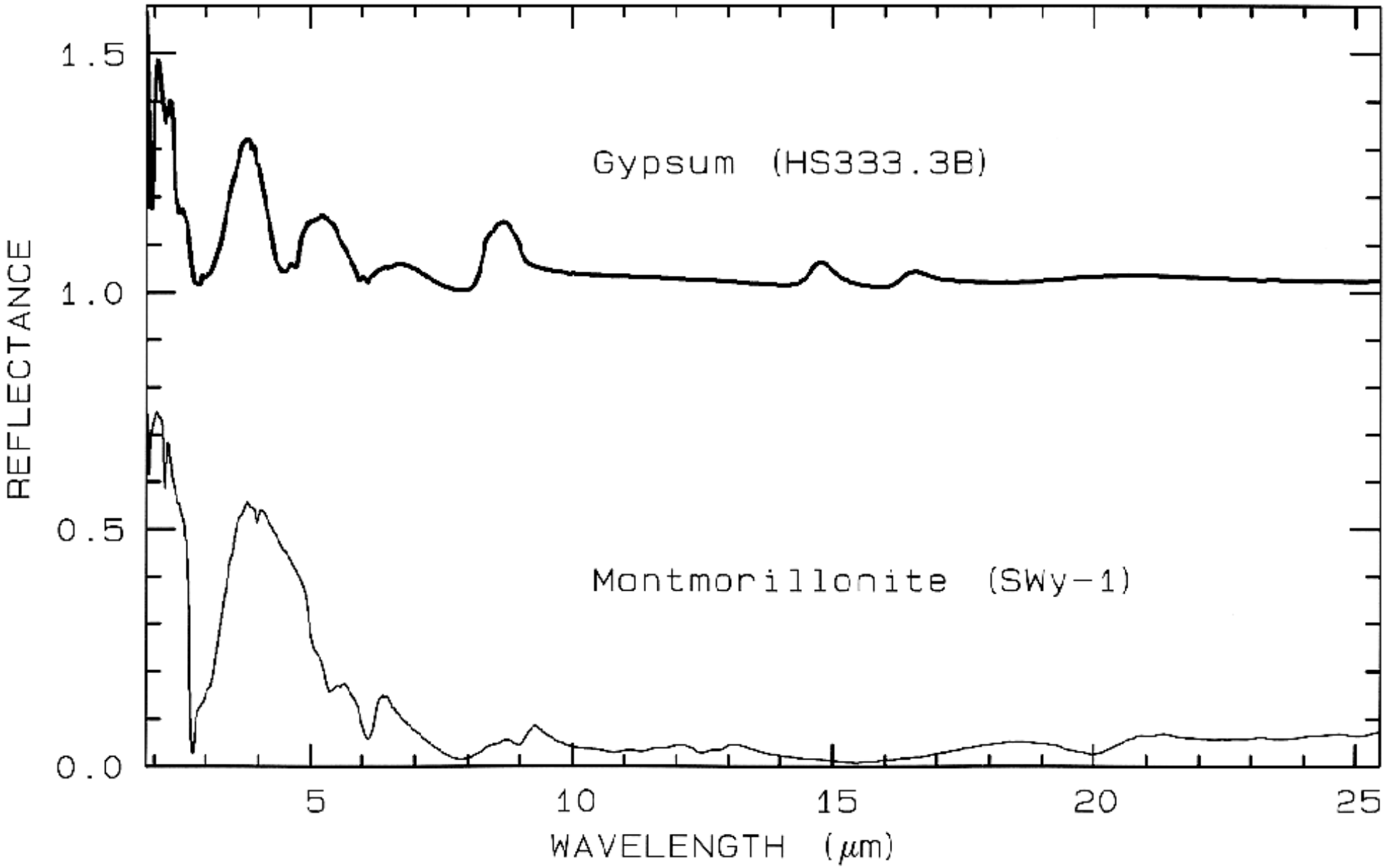
1.5
1.0
0.5
0.0
REFLECTANCE
Gypsum (HS333.3B)
Montmorillonite (SWy-1)
5
10
15
20
25
WAVELENGTH (μm)

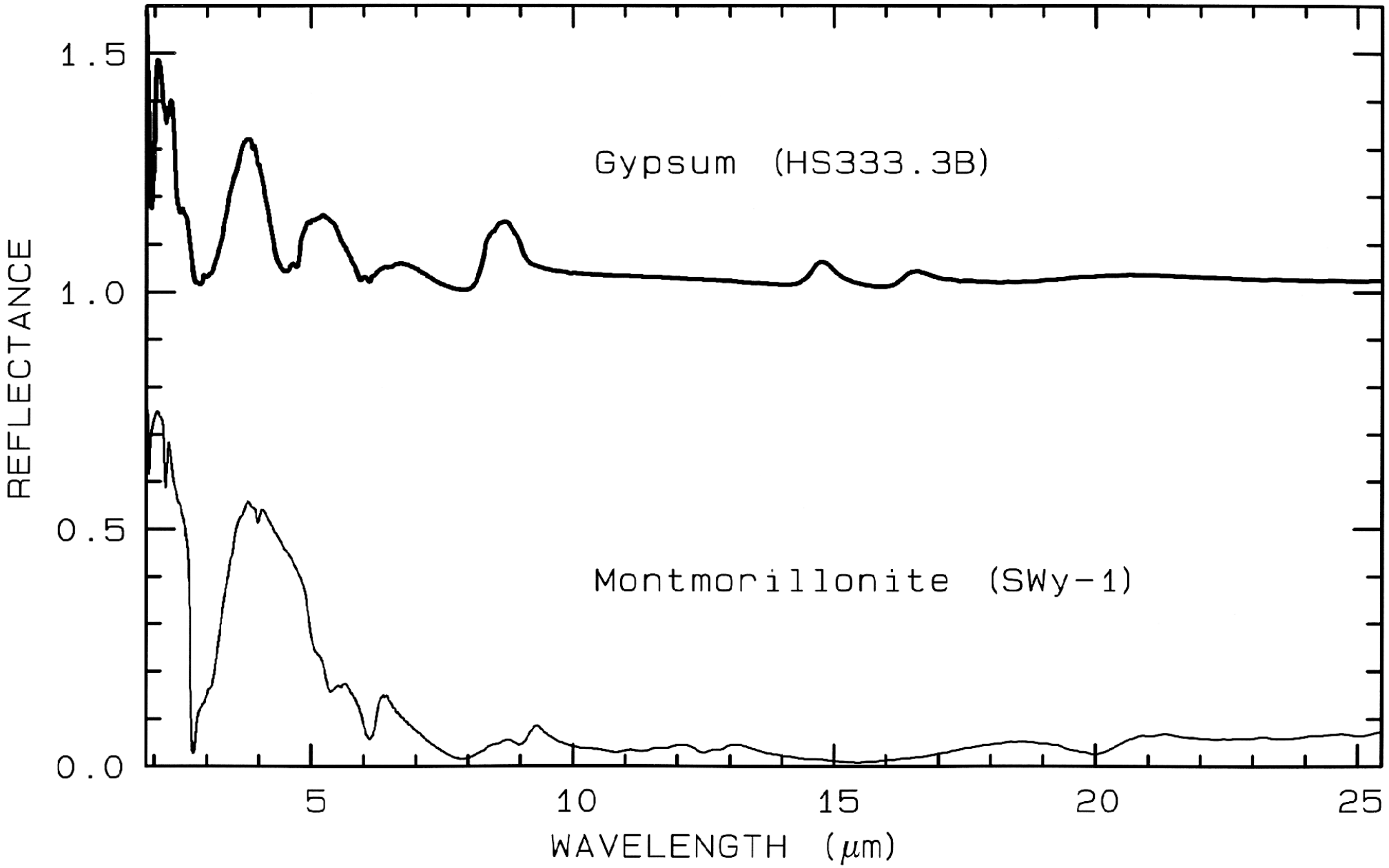
1.5
1.0
0.5
0.0
REFLECTANCE
Gypsum (HS333.3B)
Montmorillonite (SWy-1)
5
10
15
20
25
WAVELENGTH (μm)

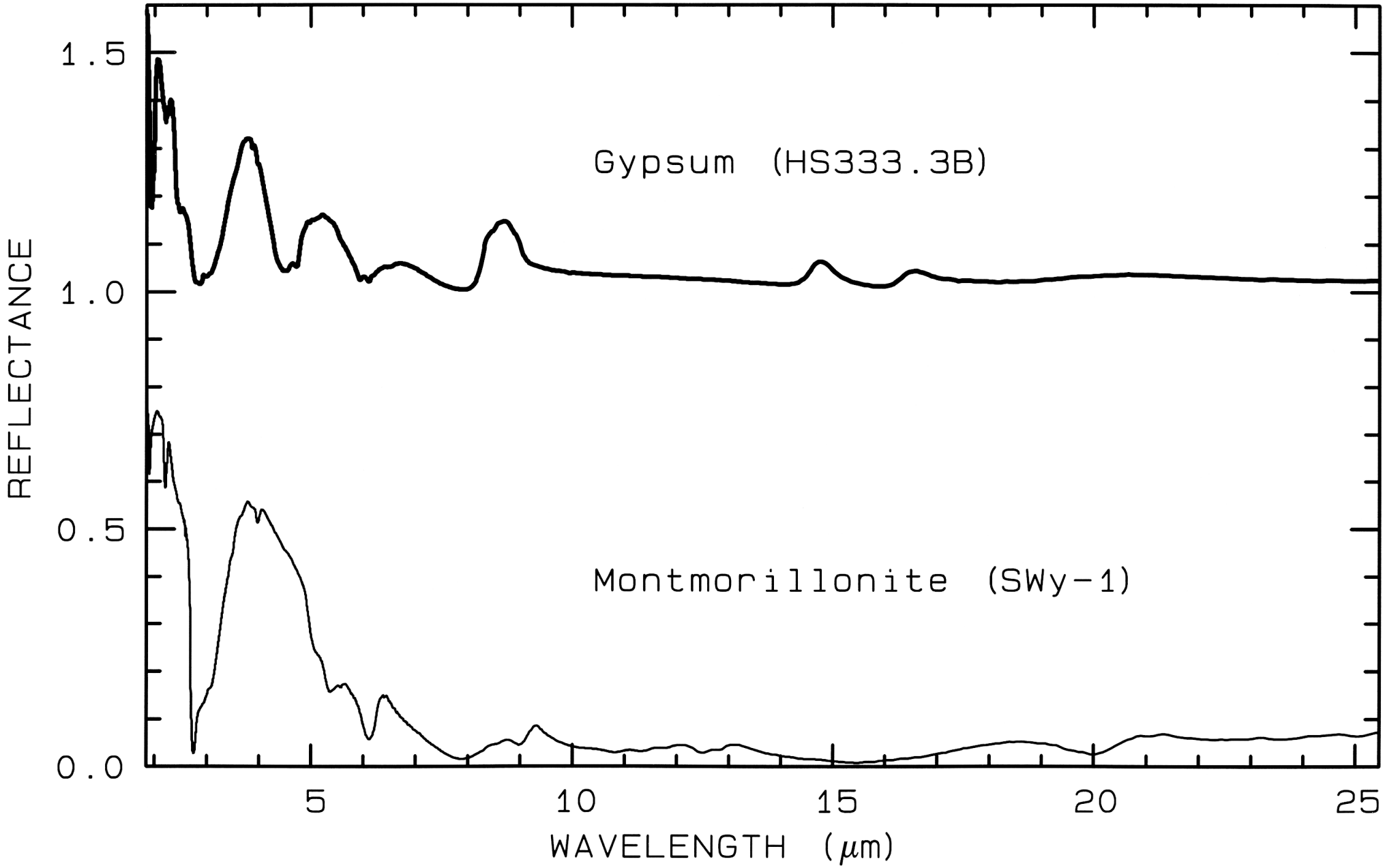
1.5
1.0
0.5
0.0
REFLECTANCE
Gypsum (HS333.3B)
Montmorillonite (SWy-1)
5
10
15
20
25
WAVELENGTH (μm)

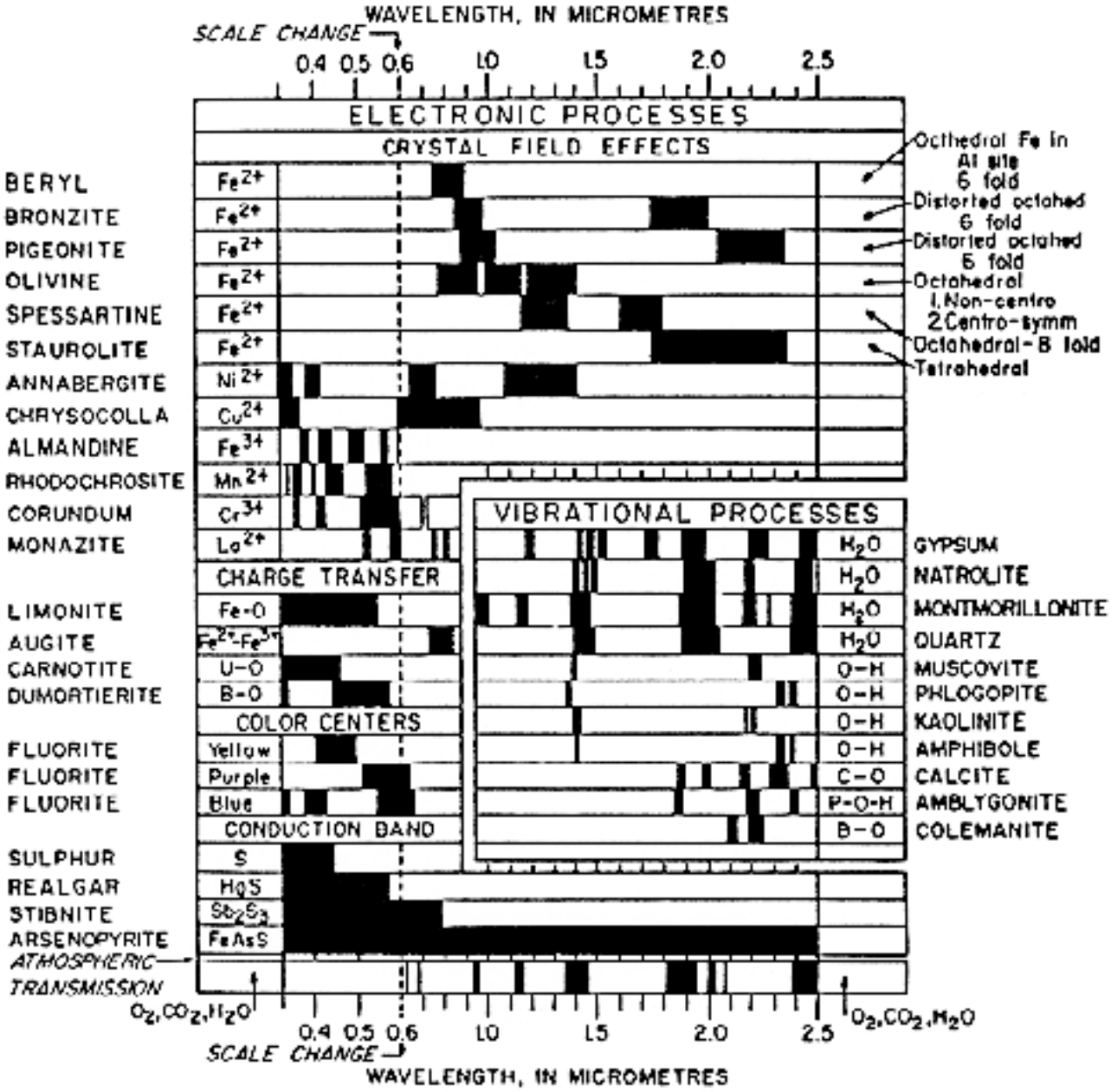
WAVELENGTH, IN MICROMETRES
SCALE CHANGE
0.4 0.5 0.6 1.0 1.5 2.0 2.5
ELECTRONIC PROCESSES
CRYSTAL FIELD EFFECTS
Octhedral Fe in Al site 6 fold
Distorted octahed 6 fold
Distorted octahed 6 fold
Octahedral
1.Non-centro
2.Centro-symm
Octahedral-8 fold
Tetrahedral
BERYL
BRONZITE
PIGEONITE
OLIVINE
SPESSARTINE
STAUROLITE
ANNABERGITE
CHRYSOCOLLA
ALMANDINE
RHODOCHROSITE
CORUNDUM
MONAZITE
LIMONITE
AUGITE
CARNOTITE
DUMORTIERITE
FLUORITE
FLUORITE
FLUORITE
SULPHUR
REALGAR
STIBNITE
ARSENOPYRITE
ATMOSPHERIC TRANSMISSION
Fe^{2+}
Ni^{2+}
Cu^{2+}
Fe^{3+}
Mn^{2+}
Cr^{3+}
La^{3+}
CHARGE TRANSFER
Fe-O
Fe^{2+}-Fe^{3+}
U-O
B-O
COLOR CENTERS
Yellow
Purple
Blue
CONDUCTION BAND
S
HgS
Sb_2S_3
FeAsS
VIBRATIONAL PROCESSES
H_2O
H_2O
H_2O
H_2O
O-H
O-H
O-H
O-H
C-O
P-O-H
B-O
GYPSUM
NATROLITE
MONTMORILLONITE
QUARTZ
MUSCOVITE
PHLOGOPITE
KAOLINITE
AMPHIBOLE
CALCITE
AMBLYGONITE
COLEMANITE
O_2, CO_2, H_2O
O_2, CO_2, H_2O
0.4 0.5 0.6 1.0 1.5 2.0 2.5
SCALE CHANGE
WAVELENGTH, IN MICROMETRES

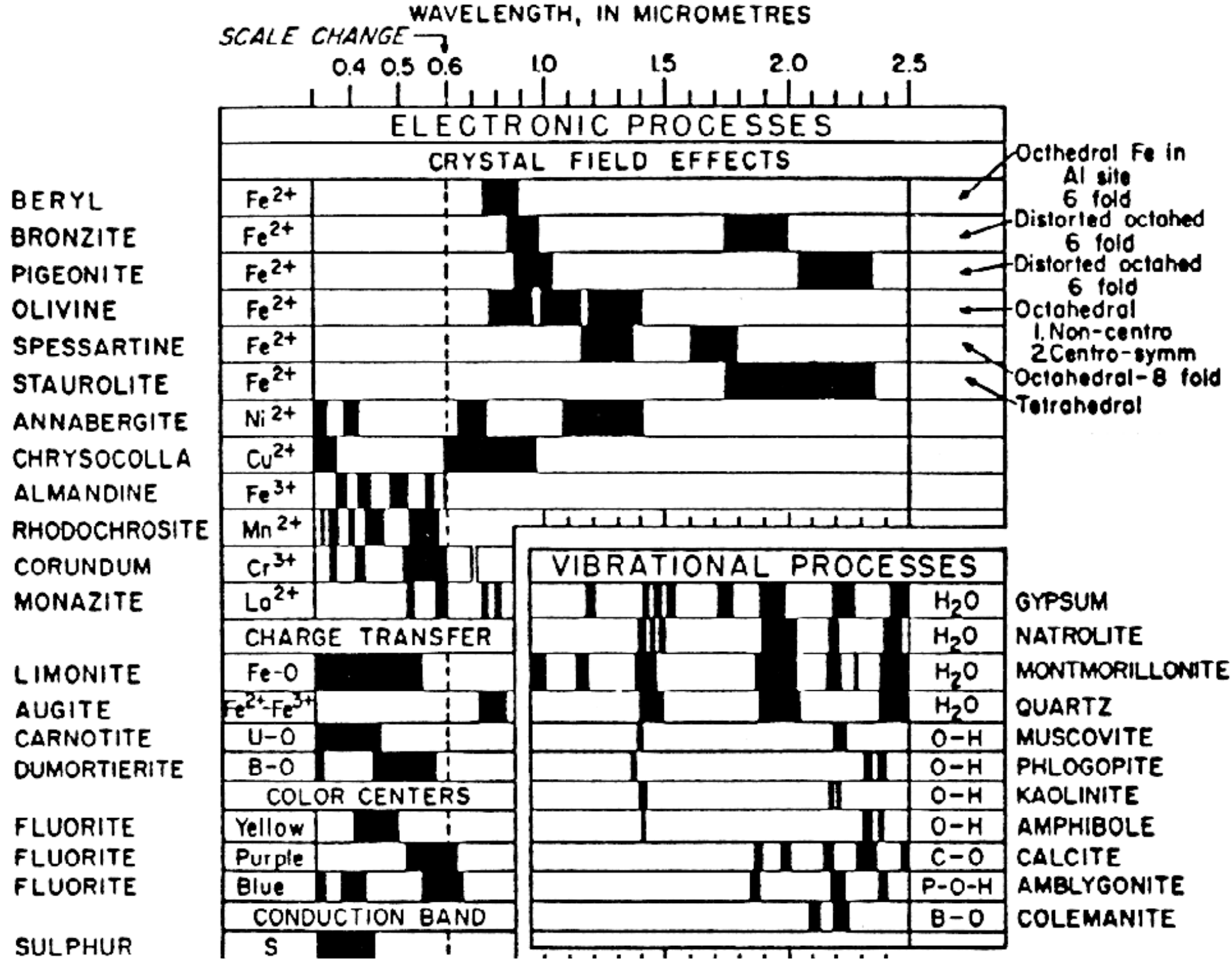
WAVELENGTH, IN MICROMETRES
SCALE CHANGE
0.4 0.5 0.6 1.0 1.5 2.0 2.5
ELECTRONIC PROCESSES
CRYSTAL FIELD EFFECTS
BERYL Fe2+
BRONZITE Fe2+
PIGEONITE Fe2+
OLIVINE Fe2+
SPESSARTINE Fe2+
STAUROLITE Fe2+
ANNABERGITE Ni2+
CHRYSOCOLLA Cu2+
ALMANDINE Fe3+
RHODOCHROSITE Mn2+
CORUNDUM Cr3+
MONAZITE Lo2+
CHARGE TRANSFER
LIMONITE Fe-O
AUGITE Fe2+-Fe3+
CARNOTITE U-O
DUMORTIERITE B-O
COLOR CENTERS
FLUORITE Yellow
FLUORITE Purple
FLUORITE Blue
CONDUCTION BAND
SULPHUR S
Octhedral Fe in Al site 6 fold
Distorted octahed 6 fold
Distorted octahed 6 fold
Octahedral
1. Non-centro
2 Centro-symm
Octahedral-8 fold
Tetrahedral
VIBRATIONAL PROCESSES
H2O GYPSUM
H2O NATROLITE
H2O MONTMORILLONITE
H2O QUARTZ
O-H MUSCOVITE
O-H PHLOGOPITE
O-H KAOLINITE
O-H AMPHIBOLE
C-O CALCITE
P-O-H AMBLYGONITE
B-O COLEMANITE

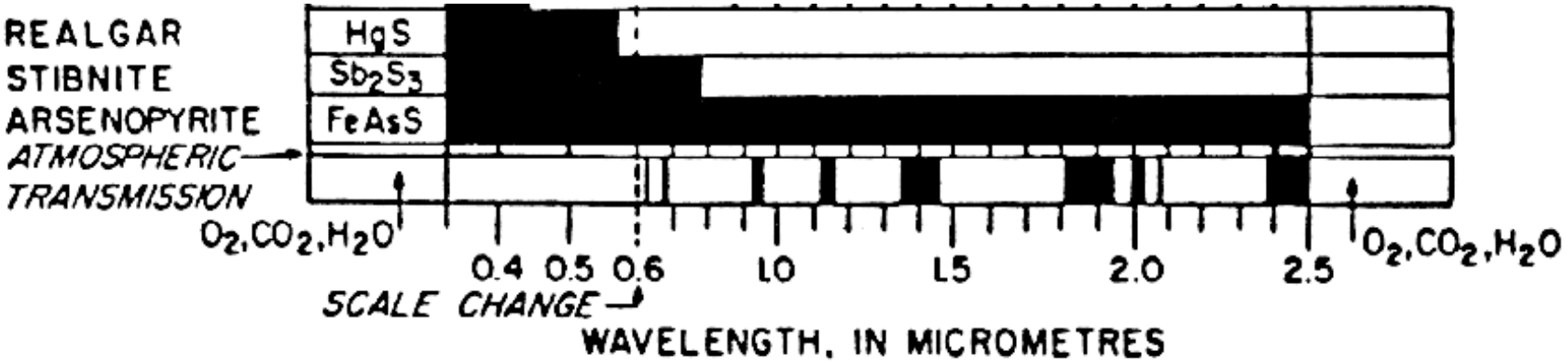
REALGAR
HgS
STIBNITE
Sb2S3
ARSENOPYRITE
FeAsS
ATMOSPHERIC
TRANSMISSION
O2,CO2,H2O
0.4 0.5 0.6 1.0 1.5 2.0 2.5
O2,CO2,H2O
SCALE CHANGE
WAVELENGTH, IN MICROMETRES

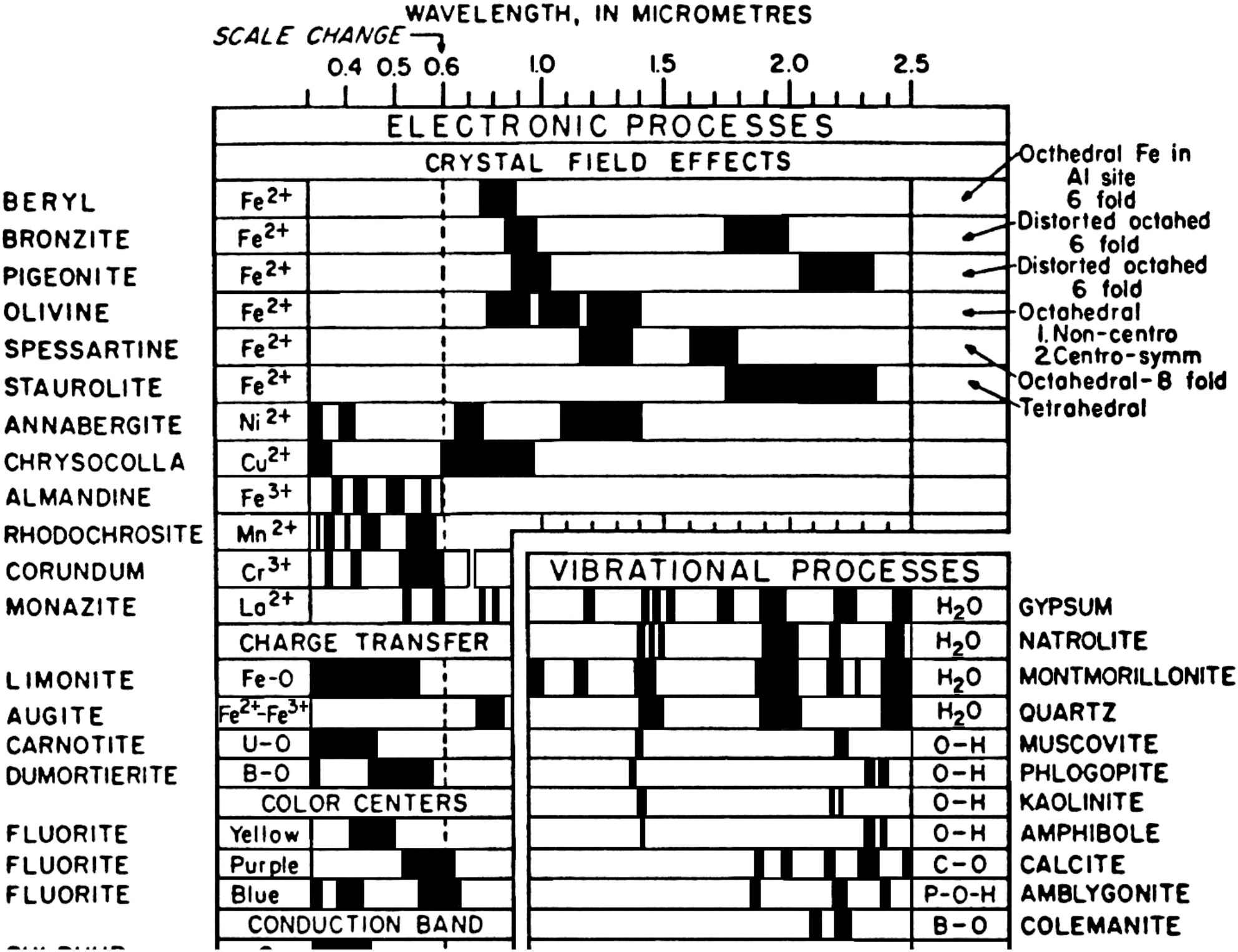
WAVELENGTH, IN MICROMETRES
SCALE CHANGE
0.4 0.5 0.6 1.0 1.5 2.0 2.5
ELECTRONIC PROCESSES
CRYSTAL FIELD EFFECTS
BERYL Fe2+
BRONZITE Fe2+
PIGEONITE Fe2+
OLIVINE Fe2+
SPESSARTINE Fe2+
STAUROLITE Fe2+
ANNABERGITE Ni2+
CHRYSOCOLLA Cu2+
ALMANDINE Fe3+
RHODOCHROSITE Mn2+
CORUNDUM Cr3+
MONAZITE Lo2+
CHARGE TRANSFER
LIMONITE Fe-O
AUGITE Fe2+-Fe3+
CARNOTITE U-O
DUMORTIERITE B-O
COLOR CENTERS
FLUORITE Yellow
FLUORITE Purple
FLUORITE Blue
CONDUCTION BAND
Octhedral Fe in Al site 6 fold
Distorted octahed 6 fold
Distorted octahed 6 fold
Octahedral 1. Non-centro 2. Centro-symm
Octahedral-8 fold
Tetrahedral
VIBRATIONAL PROCESSES
H2O GYPSUM
H2O NATROLITE
H2O MONTMORILLONITE
H2O QUARTZ
O-H MUSCOVITE
O-H PHLOGOPITE
O-H KAOLINITE
O-H AMPHIBOLE
C-O CALCITE
P-O-H AMBLYGONITE
B-O COLEMANITE

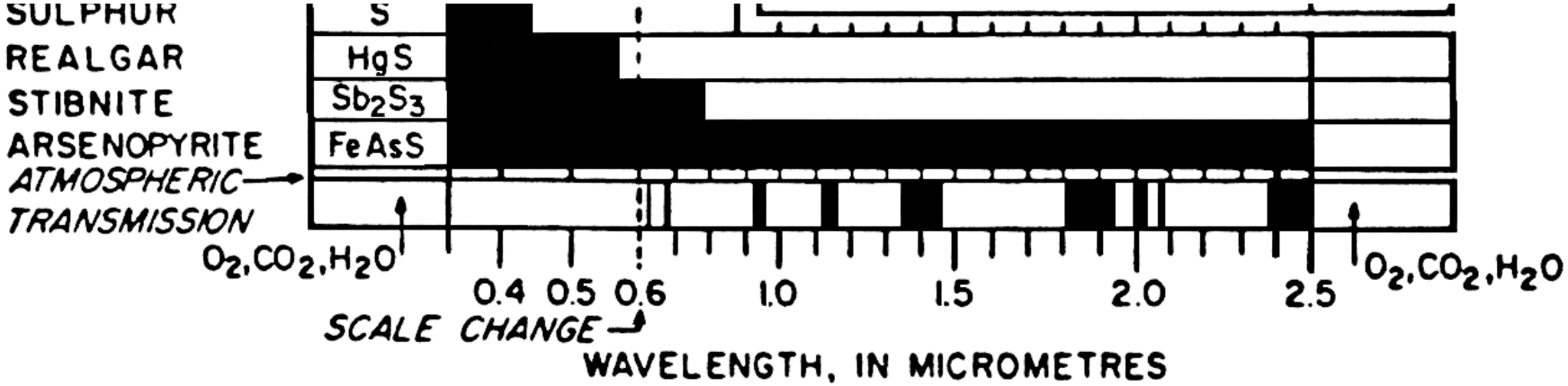
SULPHUR
S
REALGAR
HgS
STIBNITE
Sb2S3
ARSENOPYRITE
FeAsS
ATMOSPHERIC
TRANSMISSION
O2,CO2,H2O
0.4 0.5 0.6 1.0 1.5 2.0 2.5
O2,CO2,H2O
SCALE CHANGE
WAVELENGTH, IN MICROMETRES

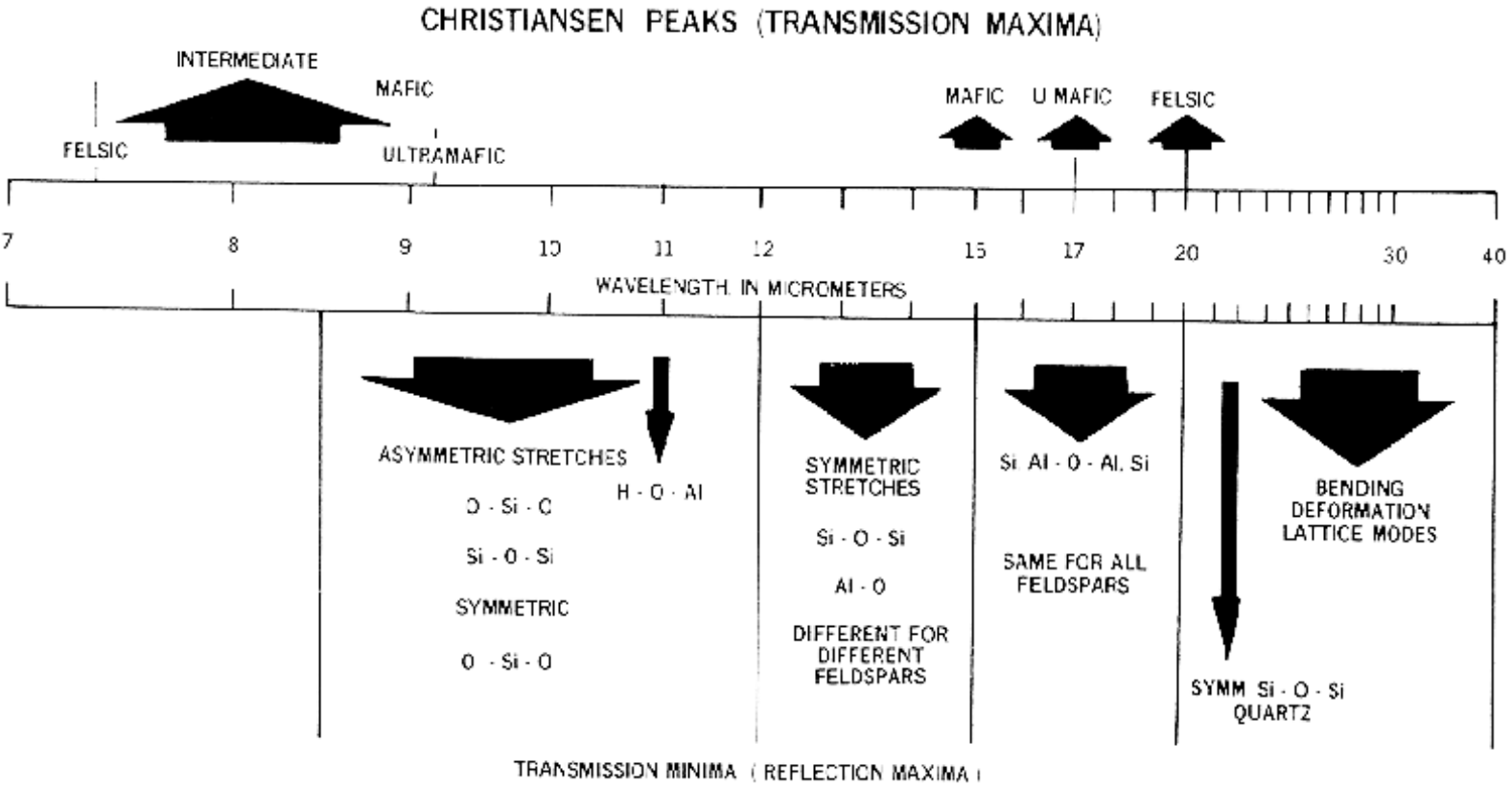
CHRISTIANSEN PEAKS (TRANSMISSION MAXIMA)
INTERMEDIATE
MAFIC
FELSIC
ULTRAMAFIC
MAFIC
U MAFIC
FELSIC
7
8
9
10
11
12
15
17
20
30
40
WAVELENGTH IN MICROMETERS
ASYMMETRIC STRETCHES
H - O - Al
O - Si - O
Si - O - Si
SYMMETRIC
O - Si - O
SYMMETRIC STRETCHES
Si - O - Si
Al - O
DIFFERENT FOR DIFFERENT FELDSPARS
Si, Al - O - Al, Si
SAME FOR ALL FELDSPARS
BENDING DEFORMATION LATTICE MODES
SYMM Si - O - Si
QUARTZ
TRANSMISSION MINIMA (REFLECTION MAXIMA)

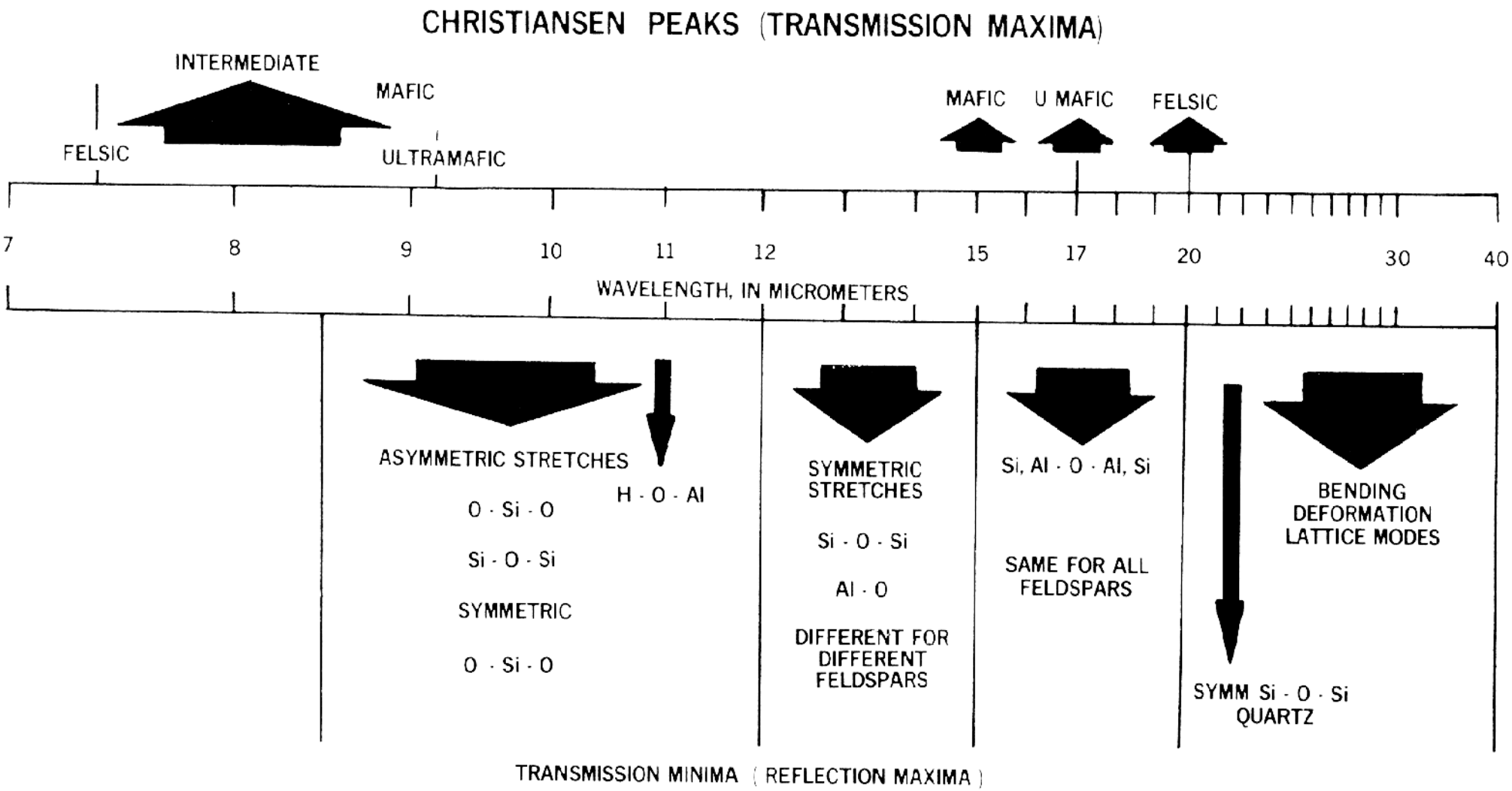
CHRISTIANSEN PEAKS (TRANSMISSION MAXIMA)
INTERMEDIATE
MAFIC
FELSIC
ULTRAMAFIC
MAFIC
U MAFIC
FELSIC
7
8
9
10
11
12
15
17
20
30
40
WAVELENGTH, IN MICROMETERS
ASYMMETRIC STRETCHES
O · Si · O
Si · O · Si
SYMMETRIC
O · Si · O
H · O · Al
SYMMETRIC STRETCHES
Si · O · Si
Al · O
DIFFERENT FOR DIFFERENT FELDSPARS
Si, Al · O · Al, Si
SAME FOR ALL FELDSPARS
SYMM Si · O · Si
QUARTZ
BENDING DEFORMATION LATTICE MODES
TRANSMISSION MINIMA (REFLECTION MAXIMA)

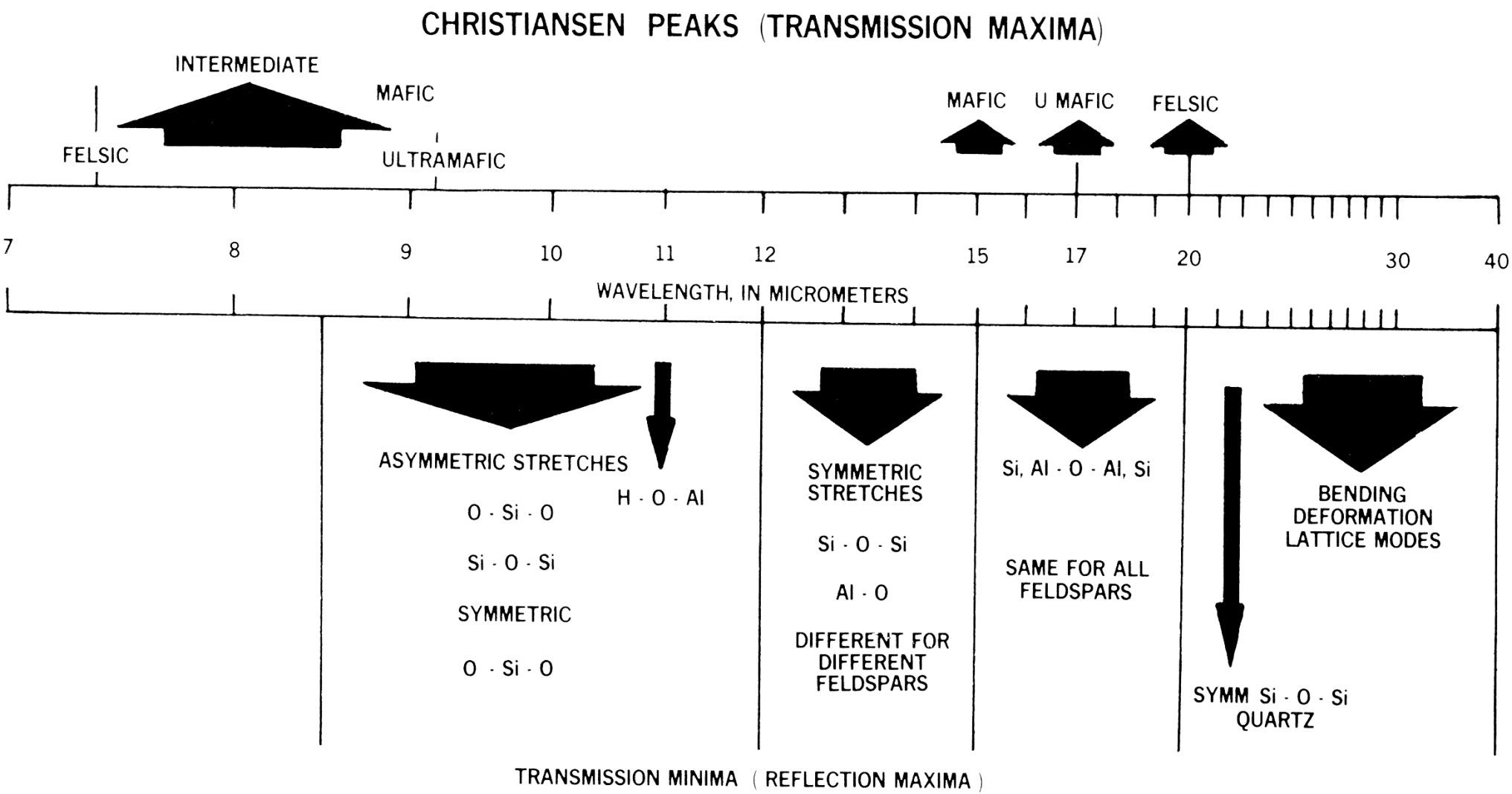
CHRISTIANSEN PEAKS (TRANSMISSION MAXIMA)
INTERMEDIATE
MAFIC
FELSIC
ULTRAMAFIC
MAFIC
U MAFIC
FELSIC
7
8
9
10
11
12
15
17
20
30
40
WAVELENGTH, IN MICROMETERS
ASYMMETRIC STRETCHES
O - Si - O
Si - O - Si
SYMMETRIC
O - Si - O
H - O - Al
SYMMETRIC STRETCHES
Si - O - Si
Al - O
DIFFERENT FOR DIFFERENT FELDSPARS
Si, Al - O - Al, Si
SAME FOR ALL FELDSPARS
SYMM Si - O - Si
QUARTZ
BENDING DEFORMATION LATTICE MODES
TRANSMISSION MINIMA (REFLECTION MAXIMA)

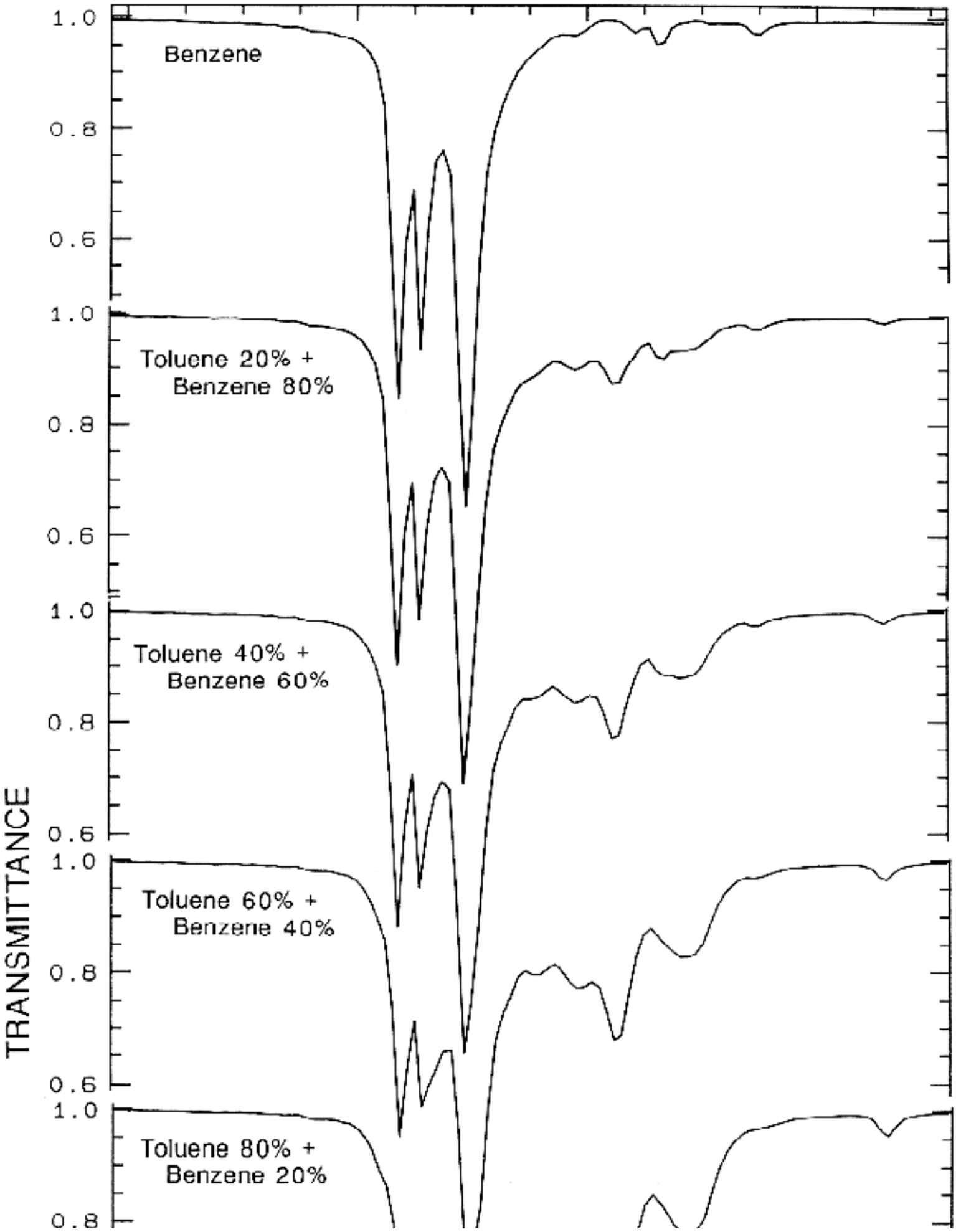
1.0
Benzene
0.8
0.6
1.0
Toluene 20% +
Benzene 80%
0.8
0.6
1.0
Toluene 40% +
Benzene 60%
0.8
0.6
1.0
Toluene 60% +
Benzene 40%
0.8
0.6
1.0
Toluene 80% +
Benzene 20%
0.8
TRANSMITTANCE

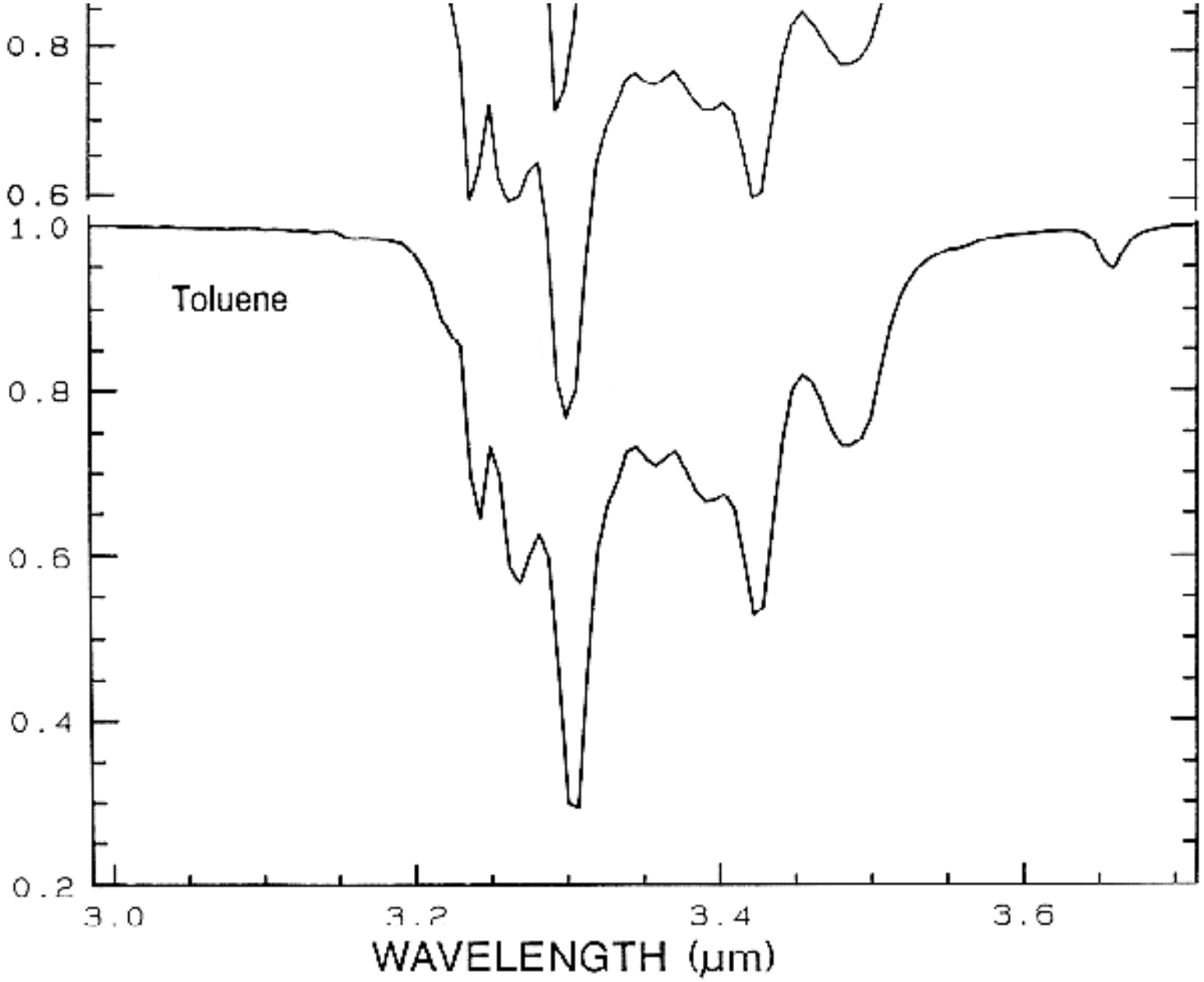
0.8
0.6
1.0
Toluene
0.8
0.6
0.4
0.2
3.0
3.2
3.4
3.6
WAVELENGTH (μm)

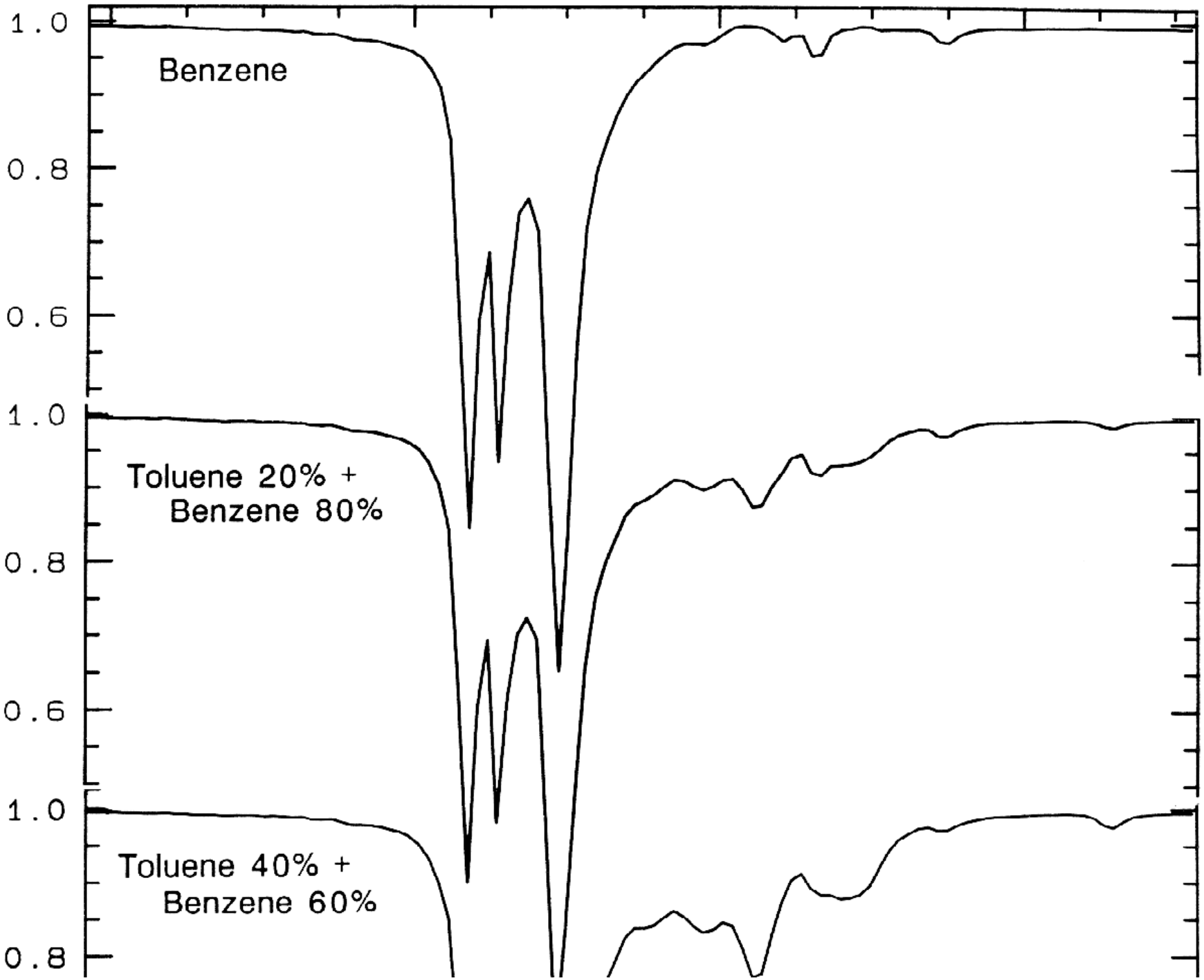
1.0
Benzene
0.8
0.6
1.0
Toluene 20% +
Benzene 80%
0.8
0.6
1.0
Toluene 40% +
Benzene 60%
0.8

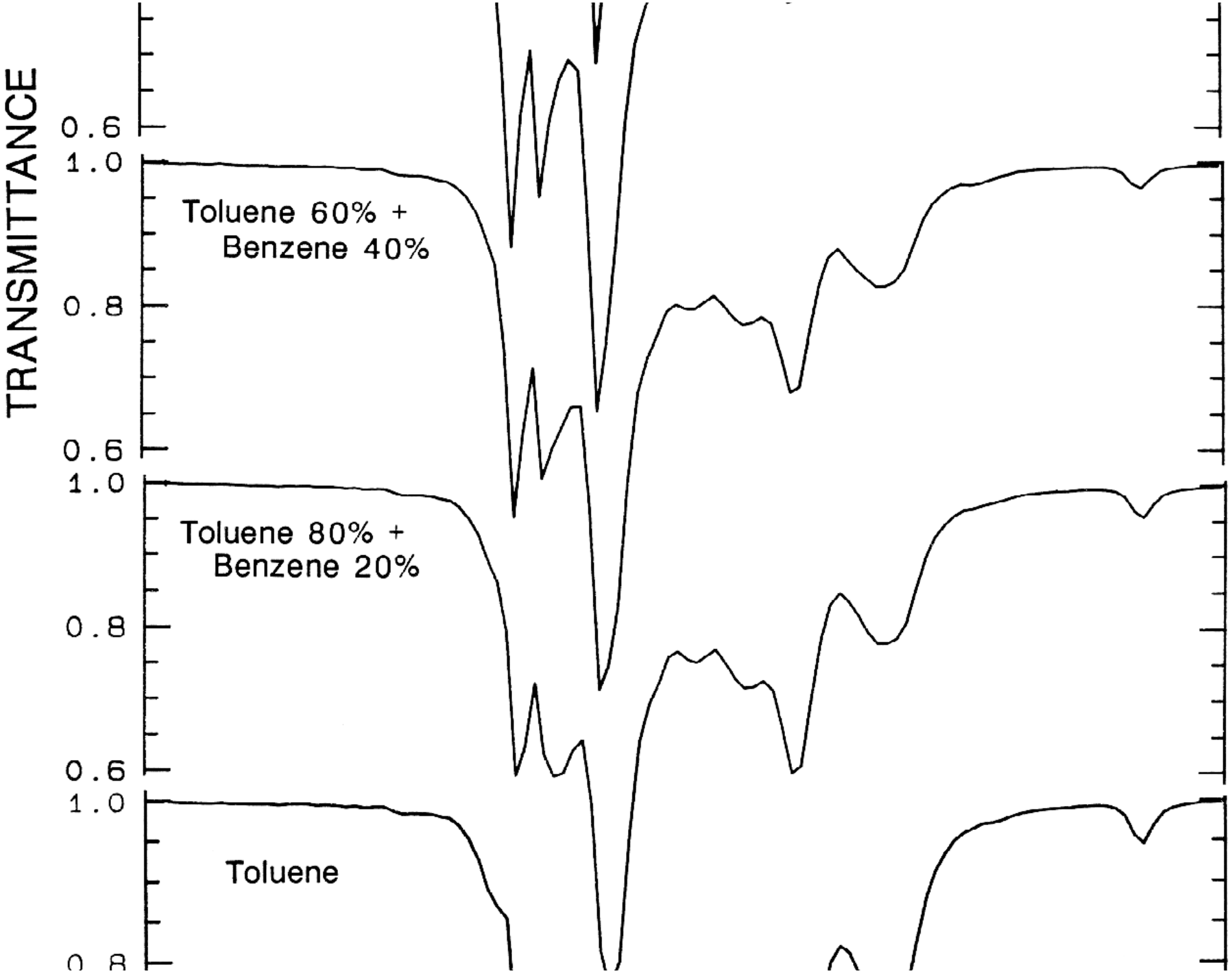
TRANSMITTANCE
0.6
1.0
Toluene 60% +
Benzene 40%
0.8
0.6
1.0
Toluene 80% +
Benzene 20%
0.8
0.6
1.0
Toluene
0.8

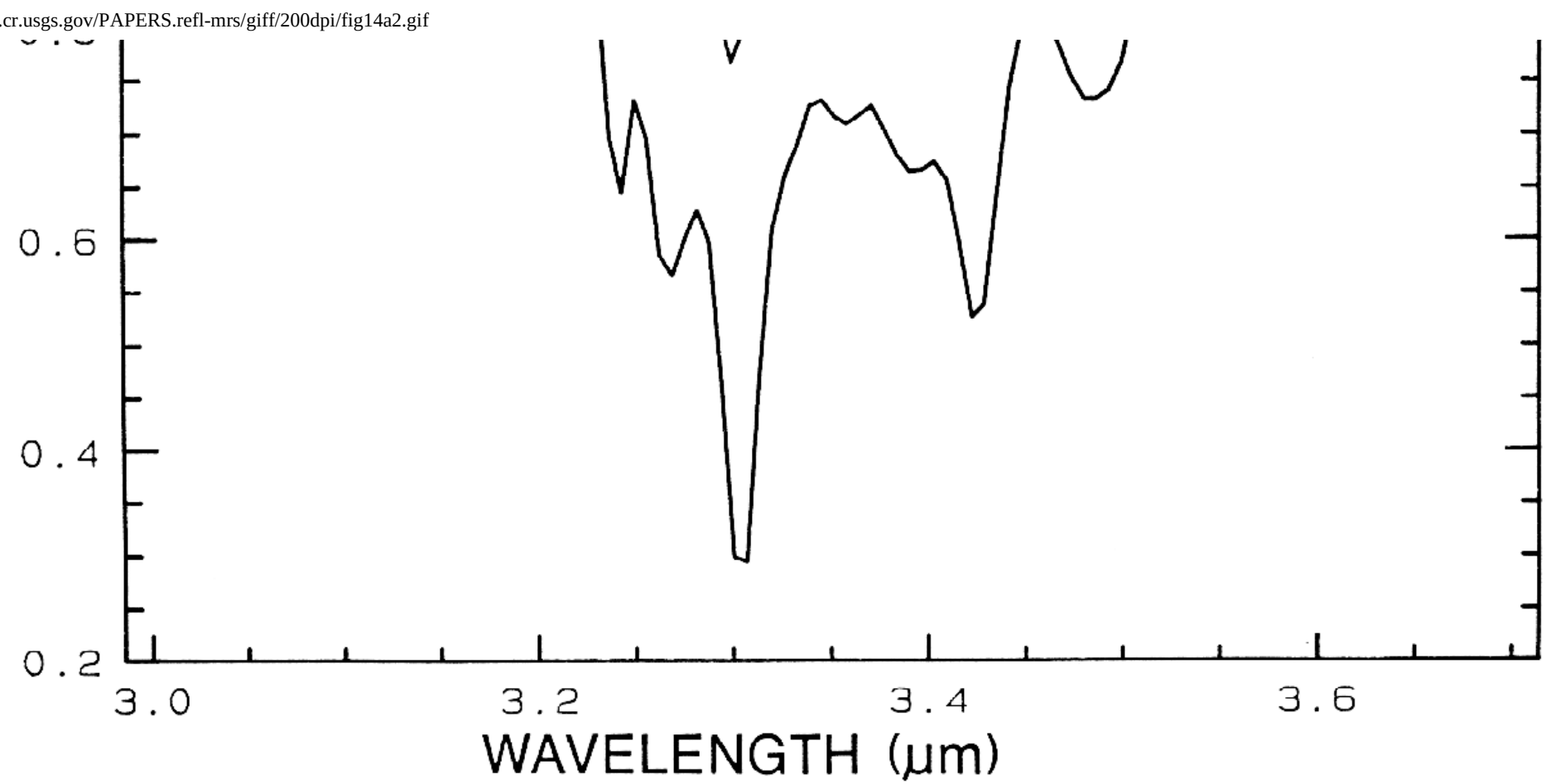
0.6
0.4
0.2
3.0
3.2
3.4
3.6
WAVELENGTH (μm)

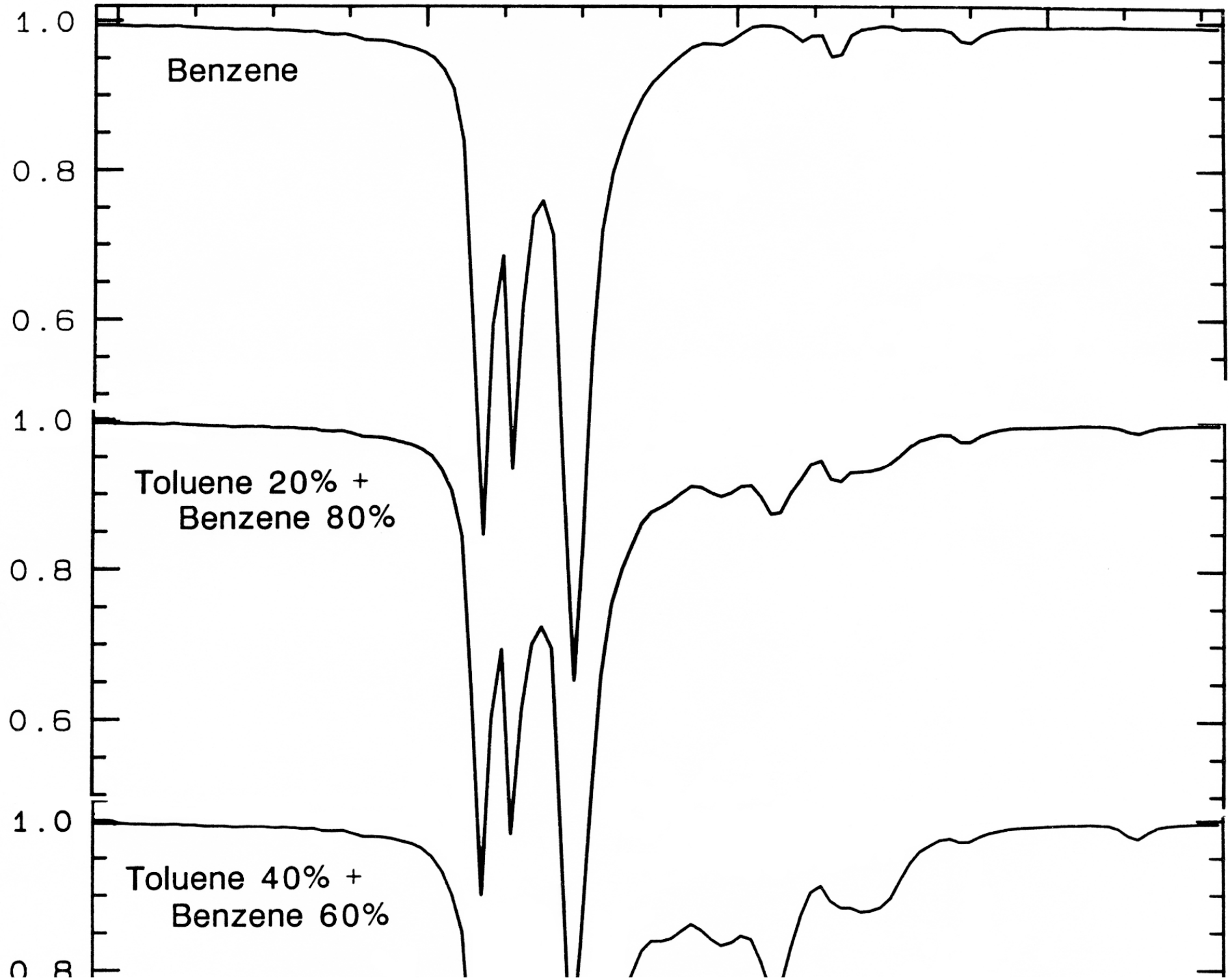
1.0
Benzene
0.8
0.6
1.0
Toluene 20% +
Benzene 80%
0.8
0.6
1.0
Toluene 40% +
Benzene 60%
0.8

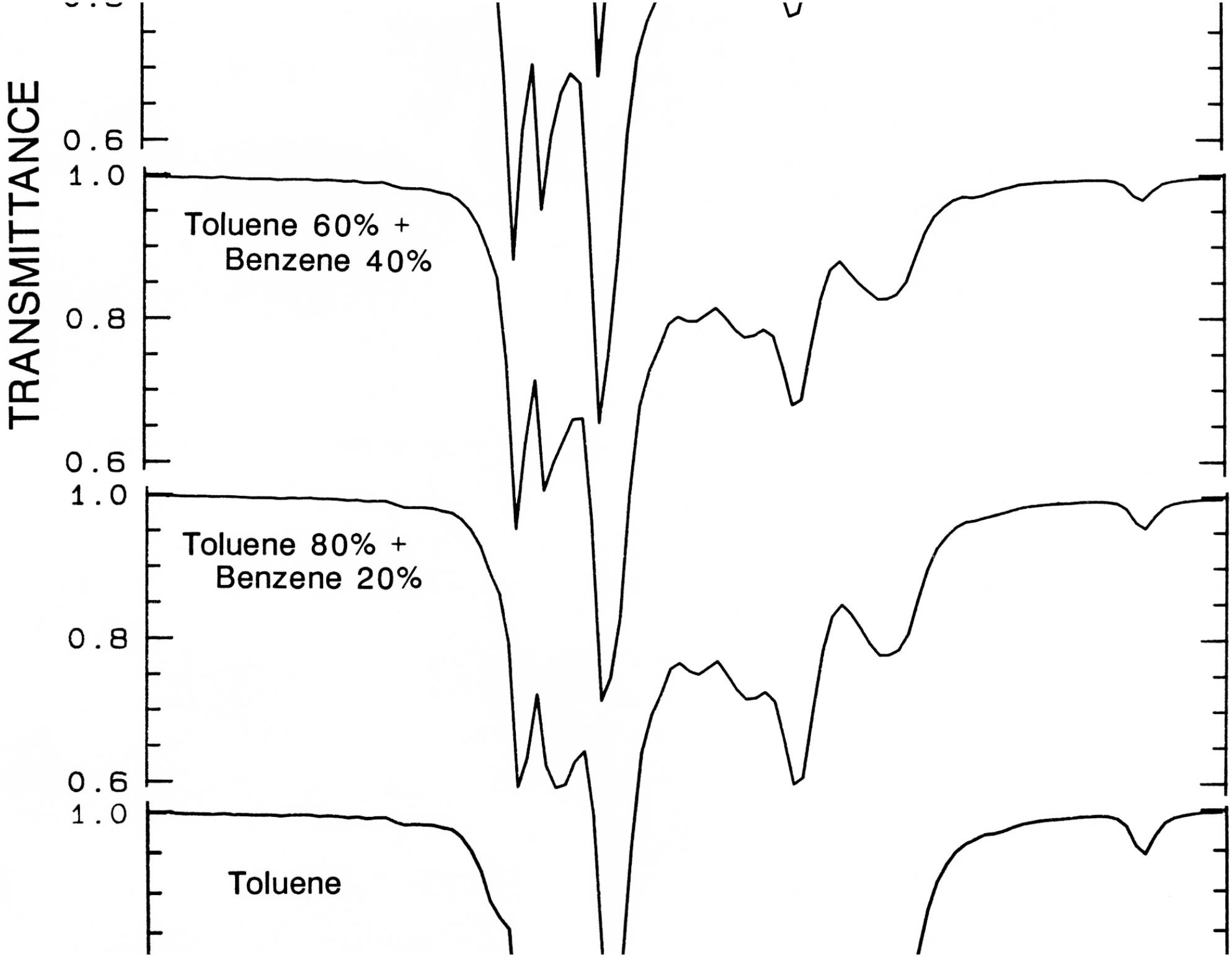
TRANSMITTANCE
0.6
1.0
Toluene 60% +
Benzene 40%
0.8
0.6
1.0
Toluene 80% +
Benzene 20%
0.8
0.6
1.0
Toluene

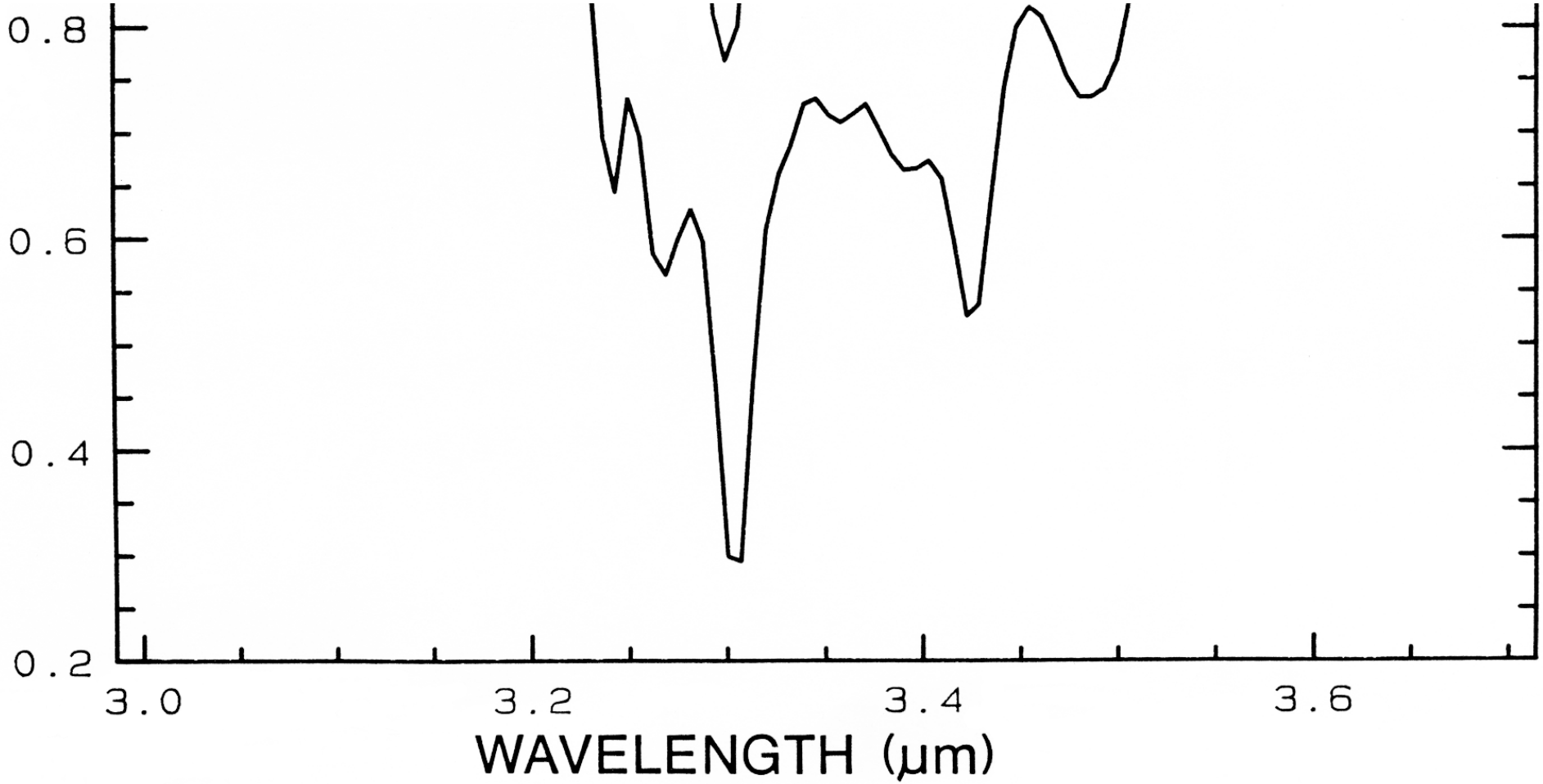
0.8
0.6
0.4
0.2
3.0
3.2
3.4
3.6
WAVELENGTH (μm)

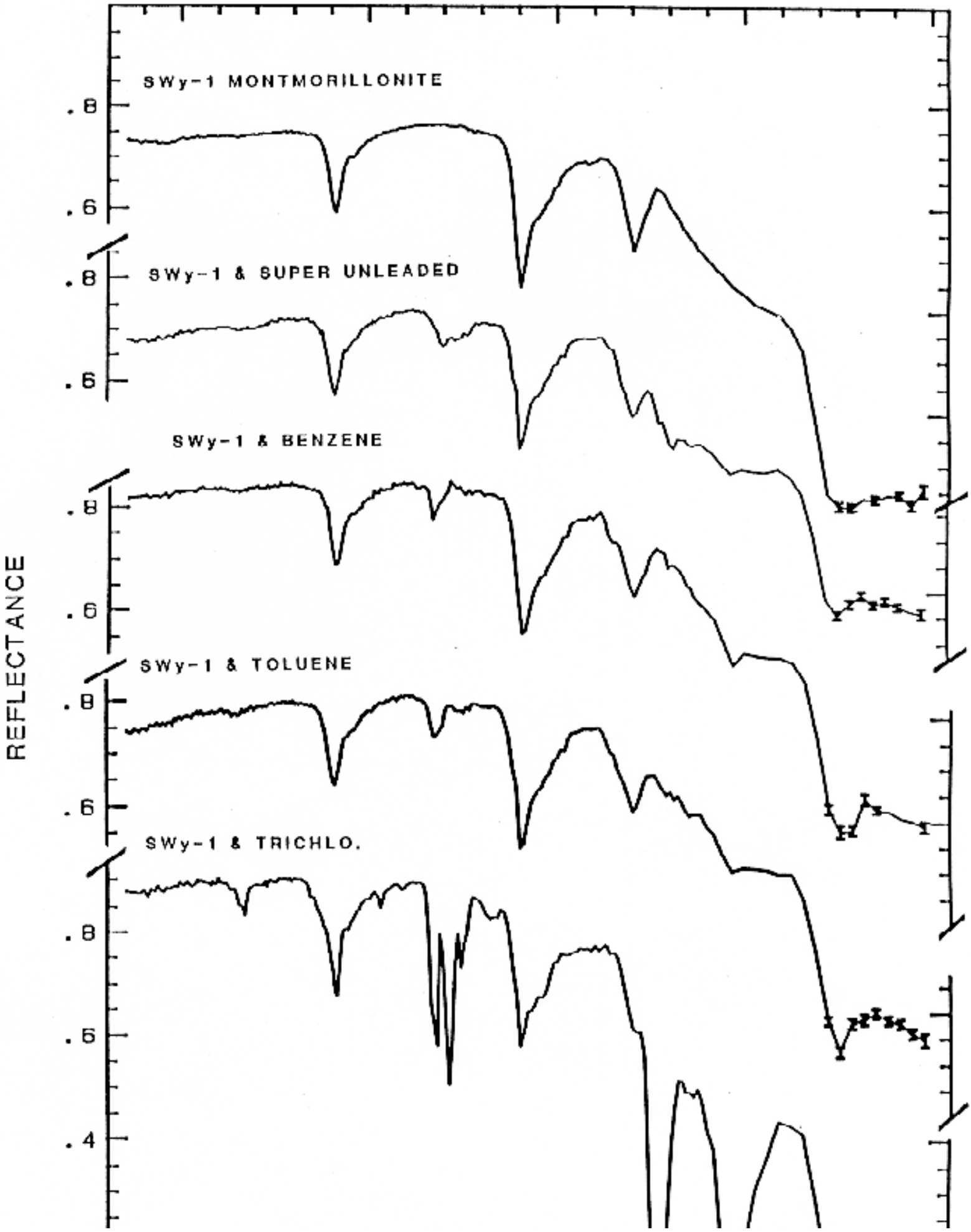
SWy-1 MONTMORILLONITE
SWy-1 & SUPER UNLEADED
SWy-1 & BENZENE
SWy-1 & TOLUENE
SWy-1 & TRICHLO.
REFLECTANCE
.8
.6
.4

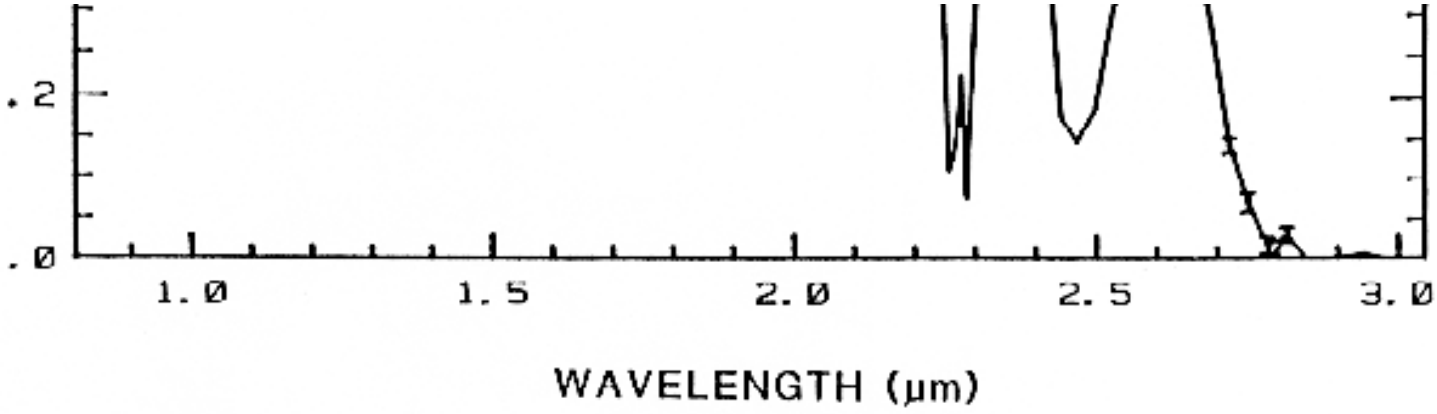

WAVELENGTH (μm)

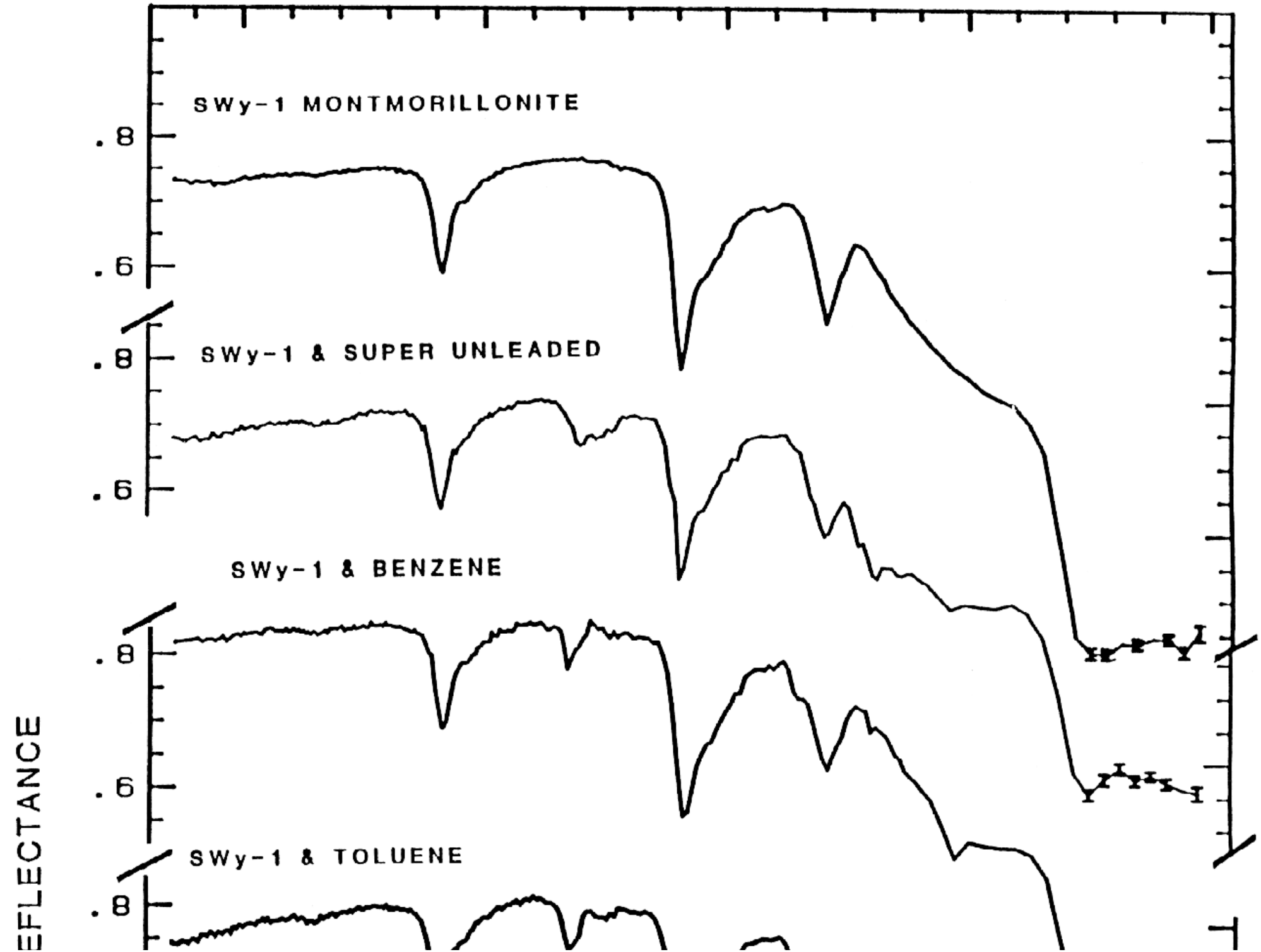
SWy-1 MONTMORILLONITE
.8
.6
SWy-1 & SUPER UNLEADED
.8
.6
SWy-1 & BENZENE
.8
.6
SWy-1 & TOLUENE
.8
EFLECTANCE

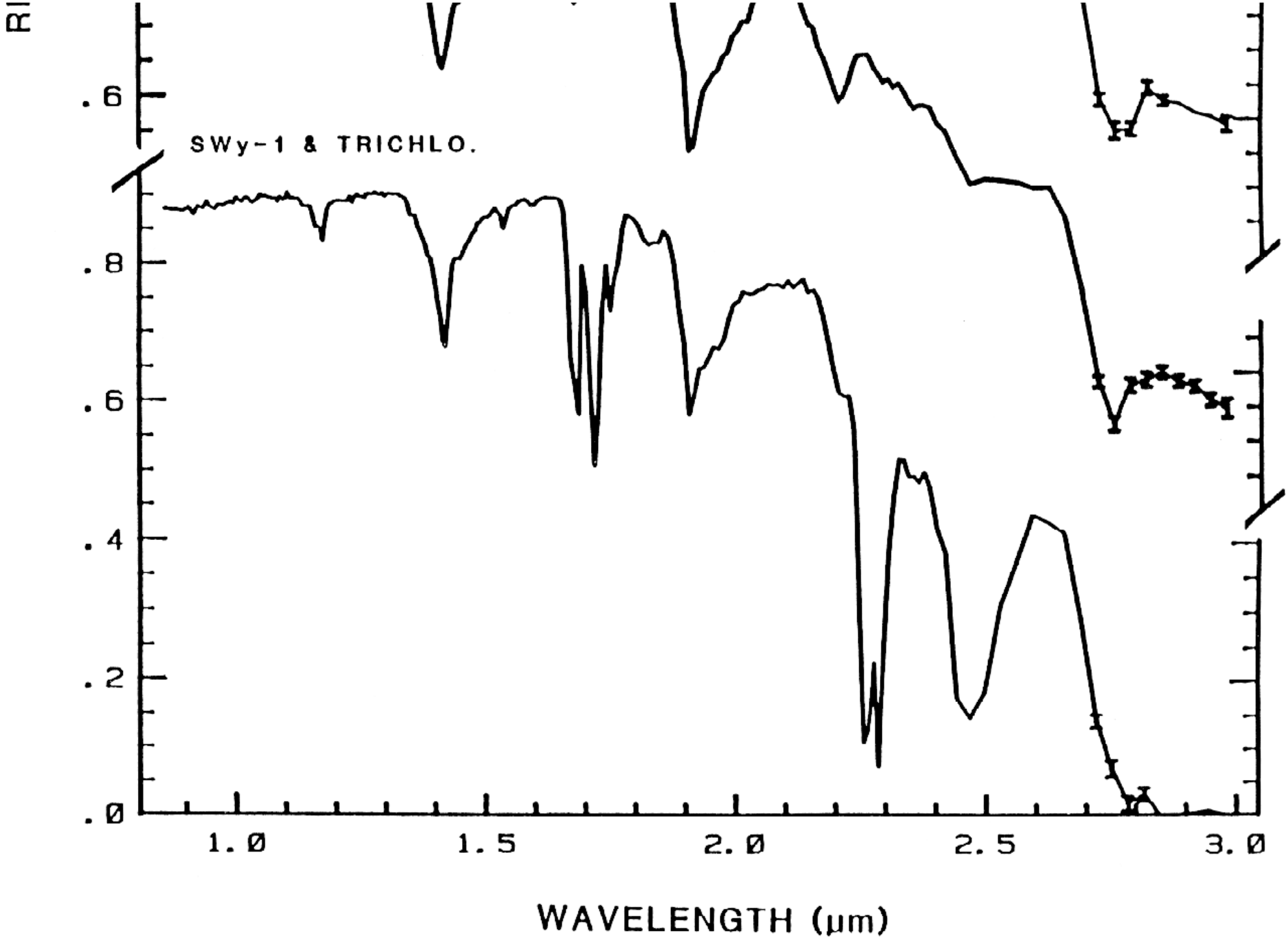
SWy-1 & TRICHLO.
.6
.8
.6
.4
.2
.0
1.0
1.5
2.0
2.5
3.0
WAVELENGTH (μm)

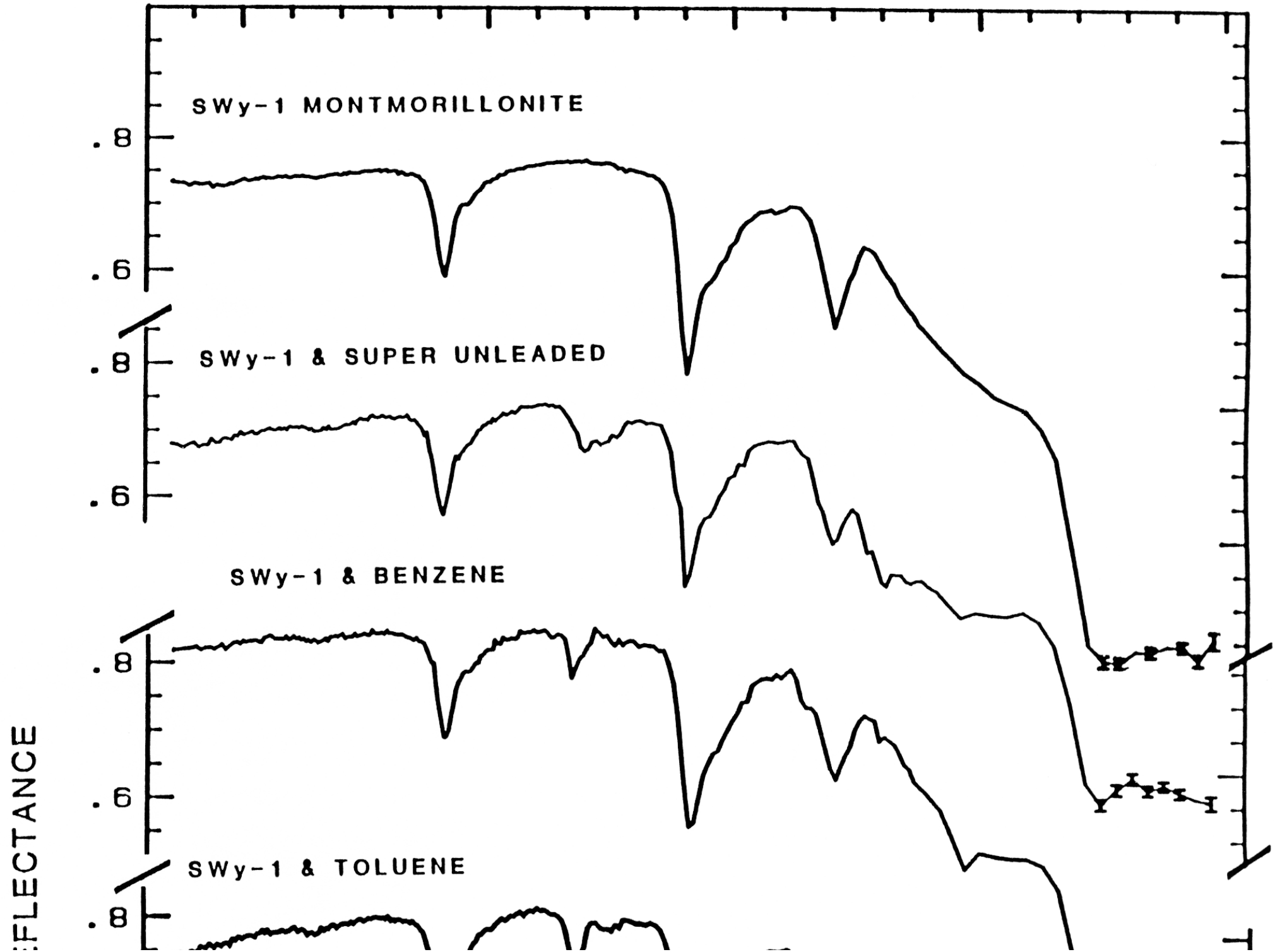
SWy-1 MONTMORILLONITE
.8
.6
SWy-1 & SUPER UNLEADED
.8
.6
SWy-1 & BENZENE
.8
.6
SWy-1 & TOLUENE
.8
FLECTANCE

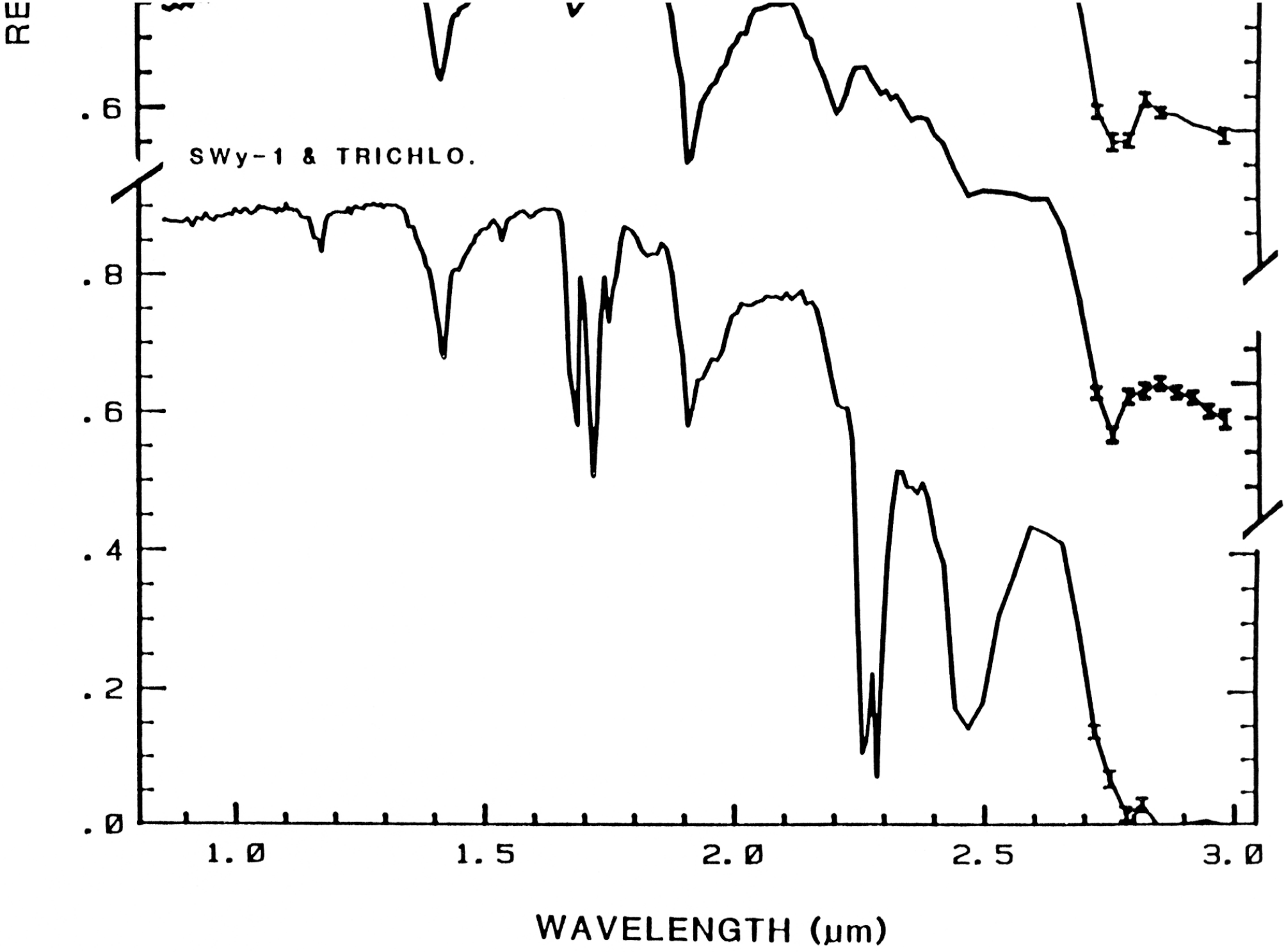
RE
.6
SWy-1 & TRICHLO.
.8
.6
.4
.2
.0
1.0
1.5
2.0
2.5
3.0
WAVELENGTH (µm)

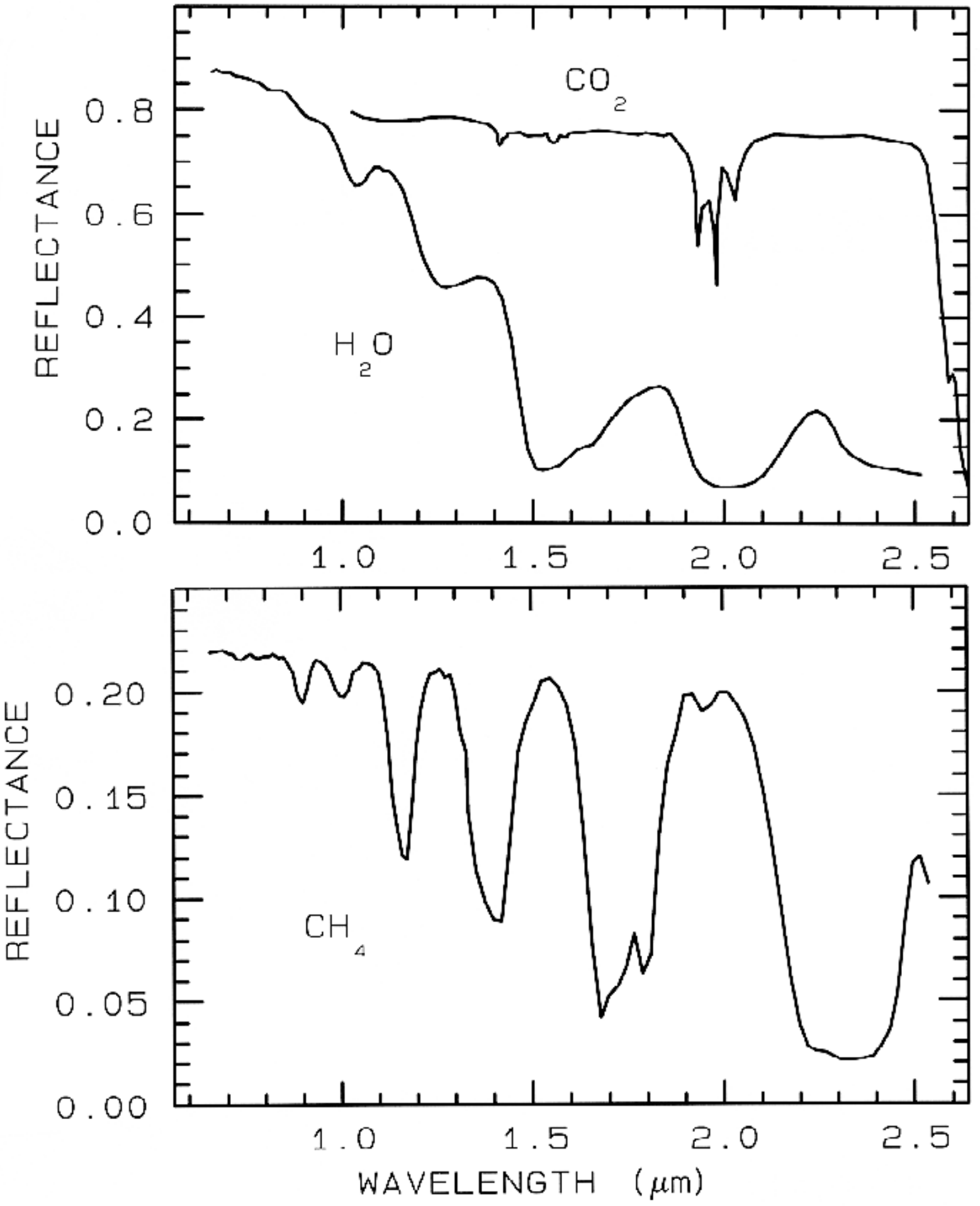
REFLECTANCE
0.0
0.2
0.4
0.6
0.8
CO2
H2O
1.0
1.5
2.0
2.5
REFLECTANCE
0.00
0.05
0.10
0.15
0.20
CH4
1.0
1.5
2.0
2.5
WAVELENGTH (μm)

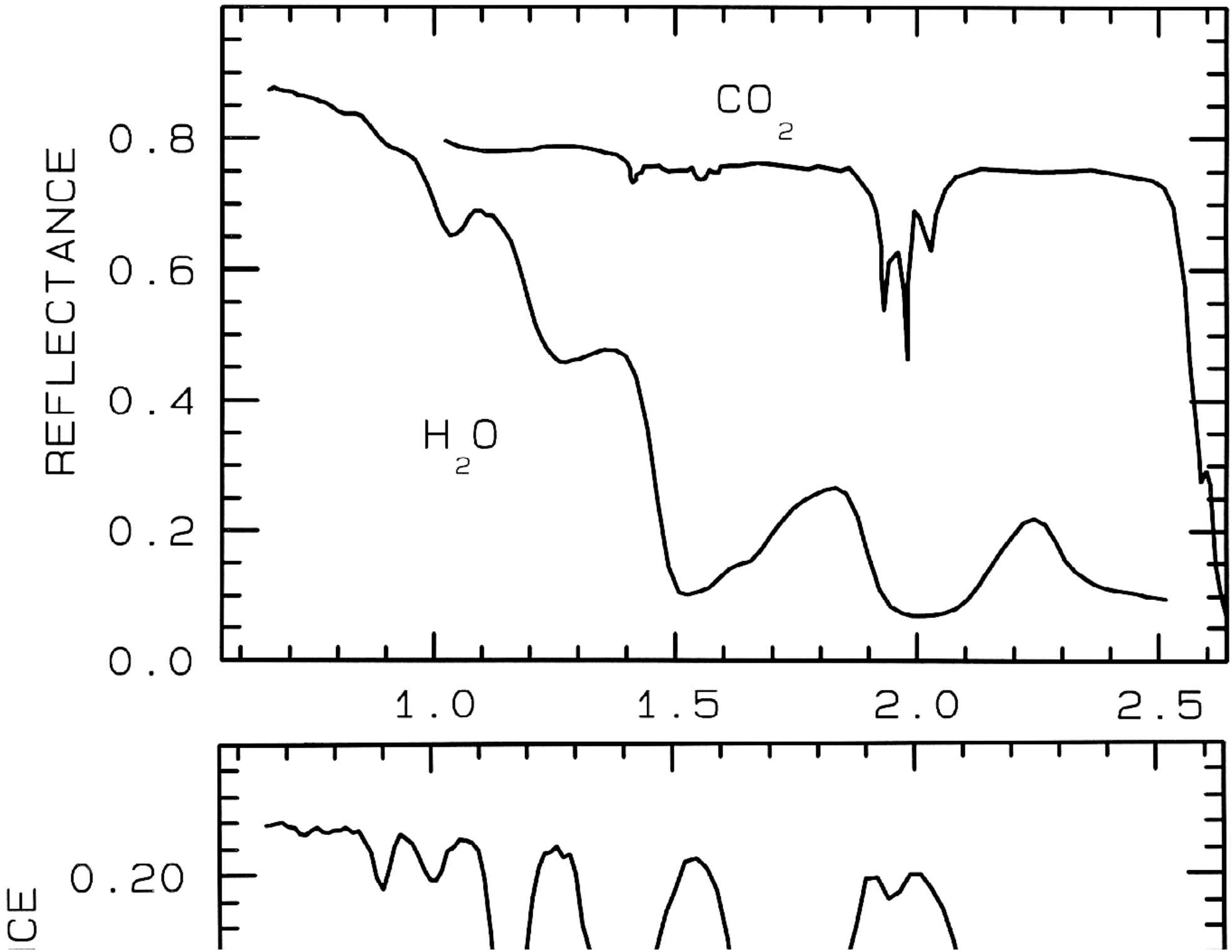
REFLECTANCE
0.8
0.6
0.4
0.2
0.0
CO2
H2O
1.0
1.5
2.0
2.5
0.20

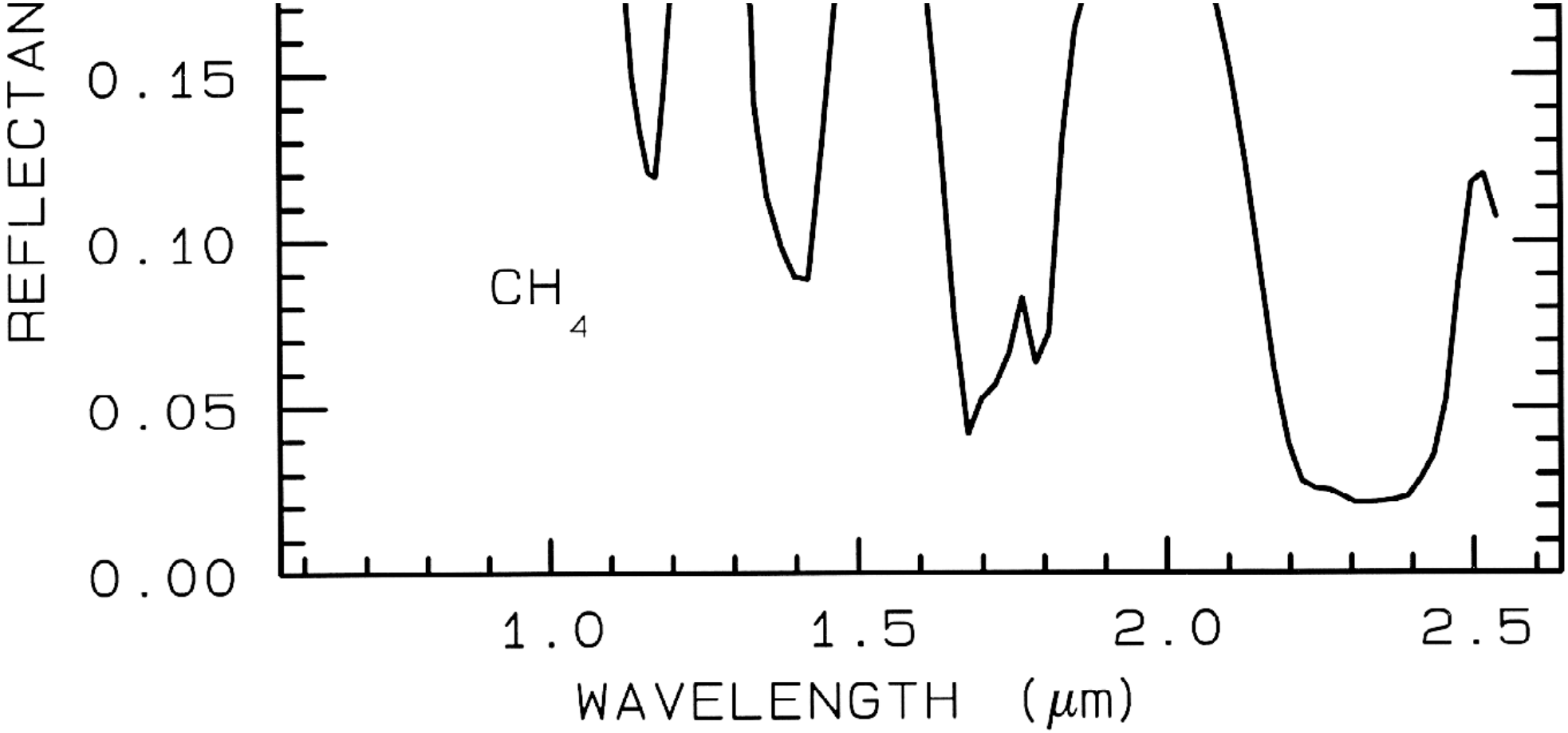
REFLECTAN
0.15
0.10
0.05
0.00
CH4
1.0
1.5
2.0
2.5
WAVELENGTH (μm)

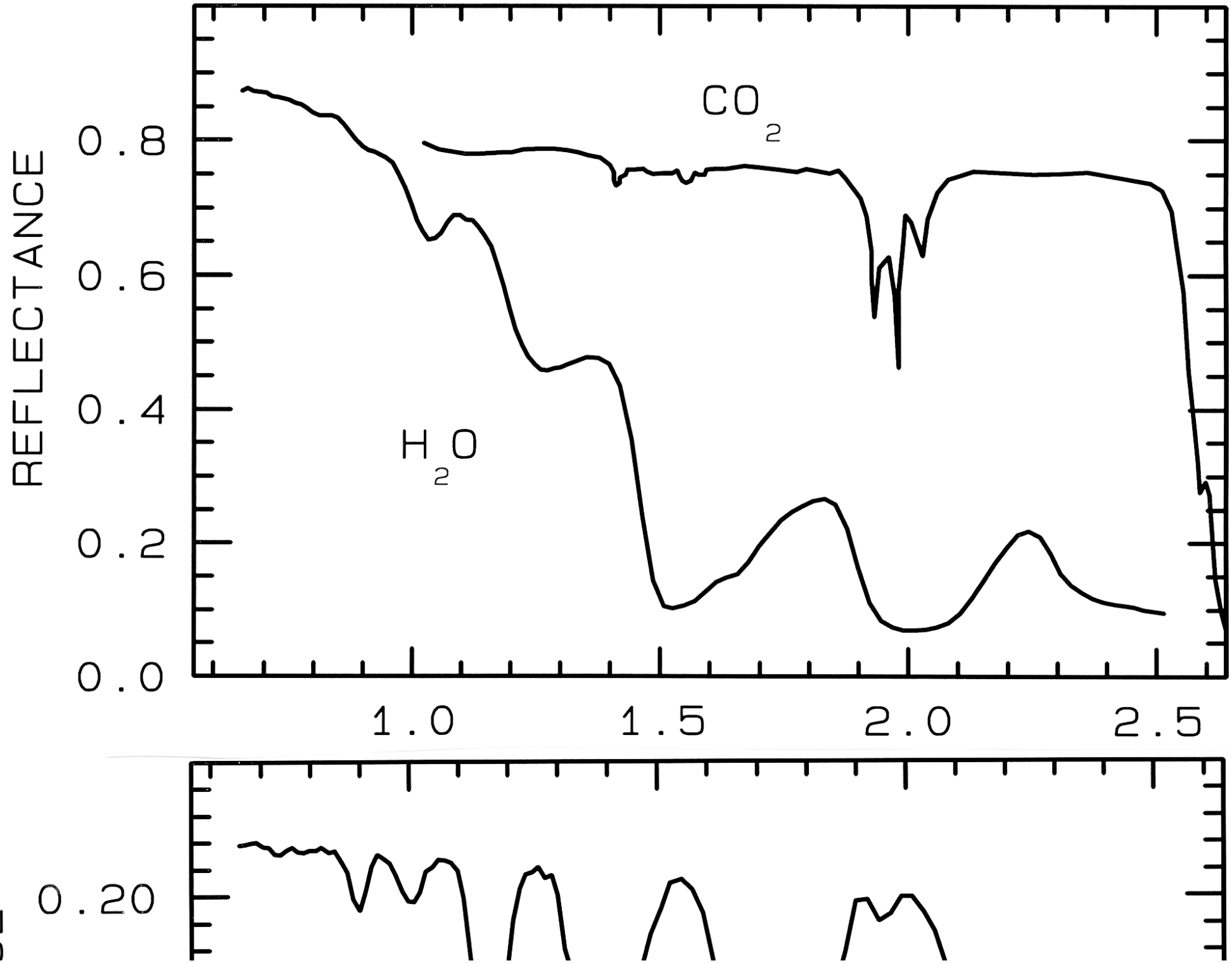
REFLECTANCE
0.0
0.2
0.4
0.6
0.8
1.0
1.5
2.0
2.5
CO_2
H_2O
0.20

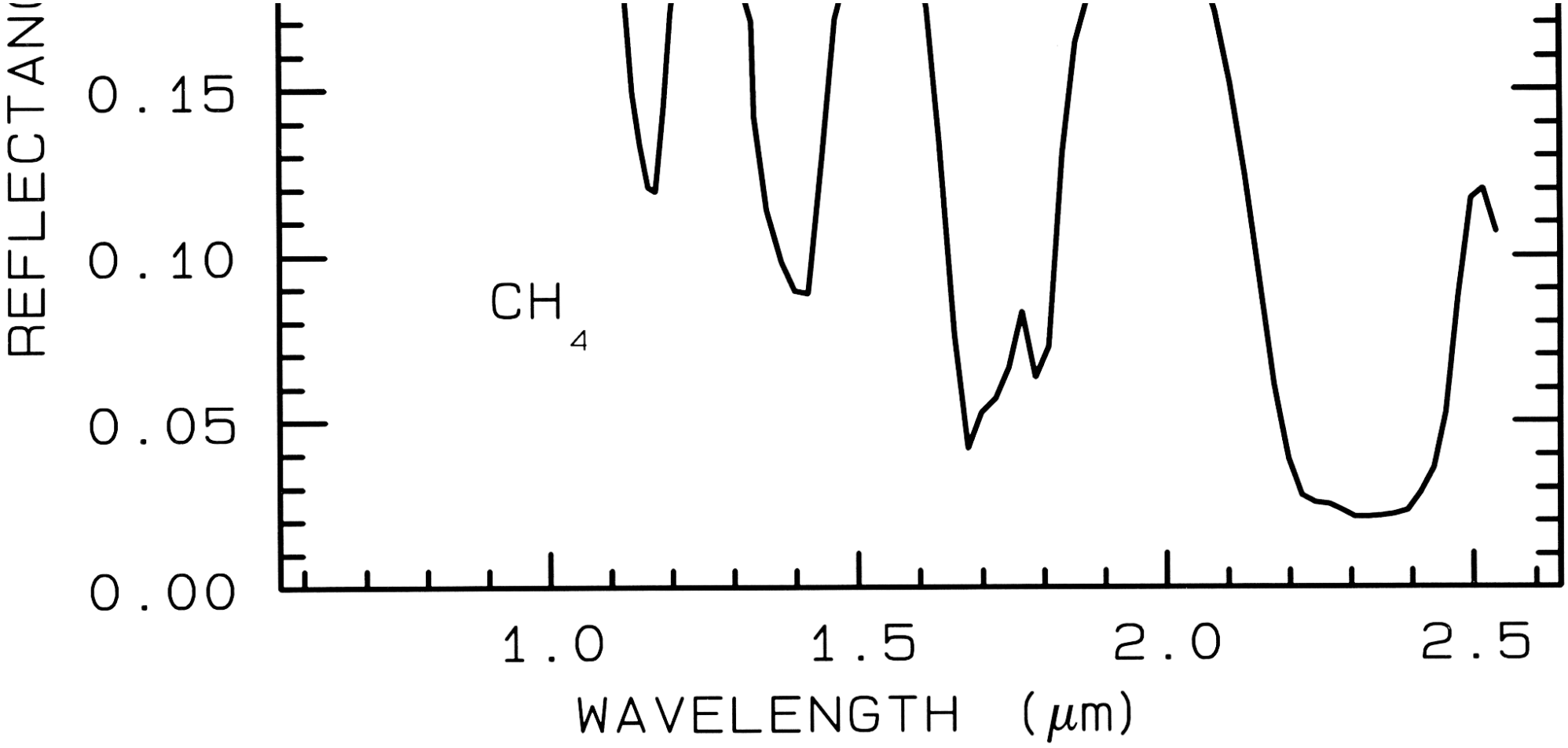
REFLECTANC
0.15
0.10
0.05
0.00
CH4
1.0
1.5
2.0
2.5
WAVELENGTH (μm)

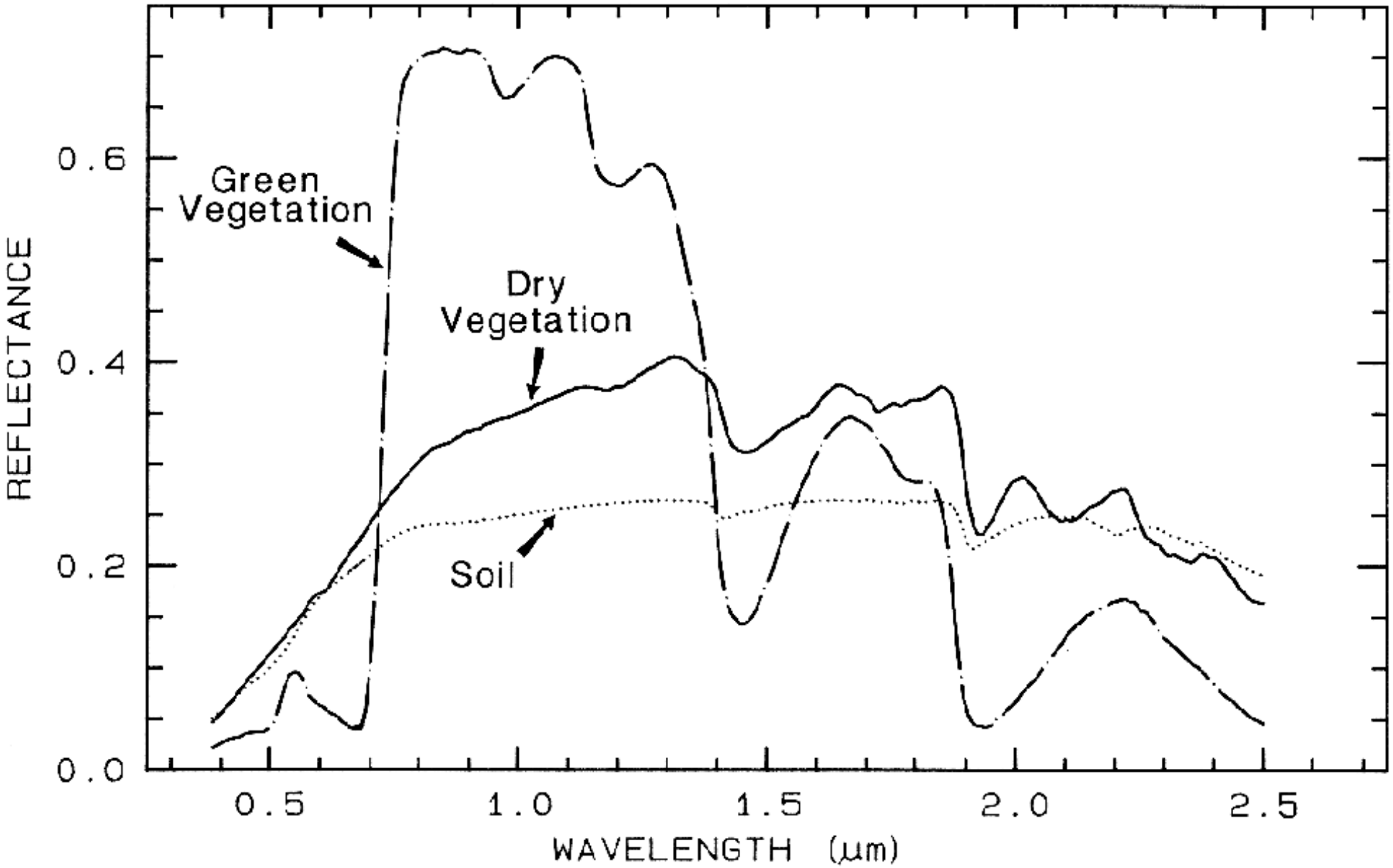
Green
Vegetation
Dry
Vegetation
Soil
REFLECTANCE
0.0
0.2
0.4
0.6
0.5
1.0
1.5
2.0
2.5
WAVELENGTH (μm)

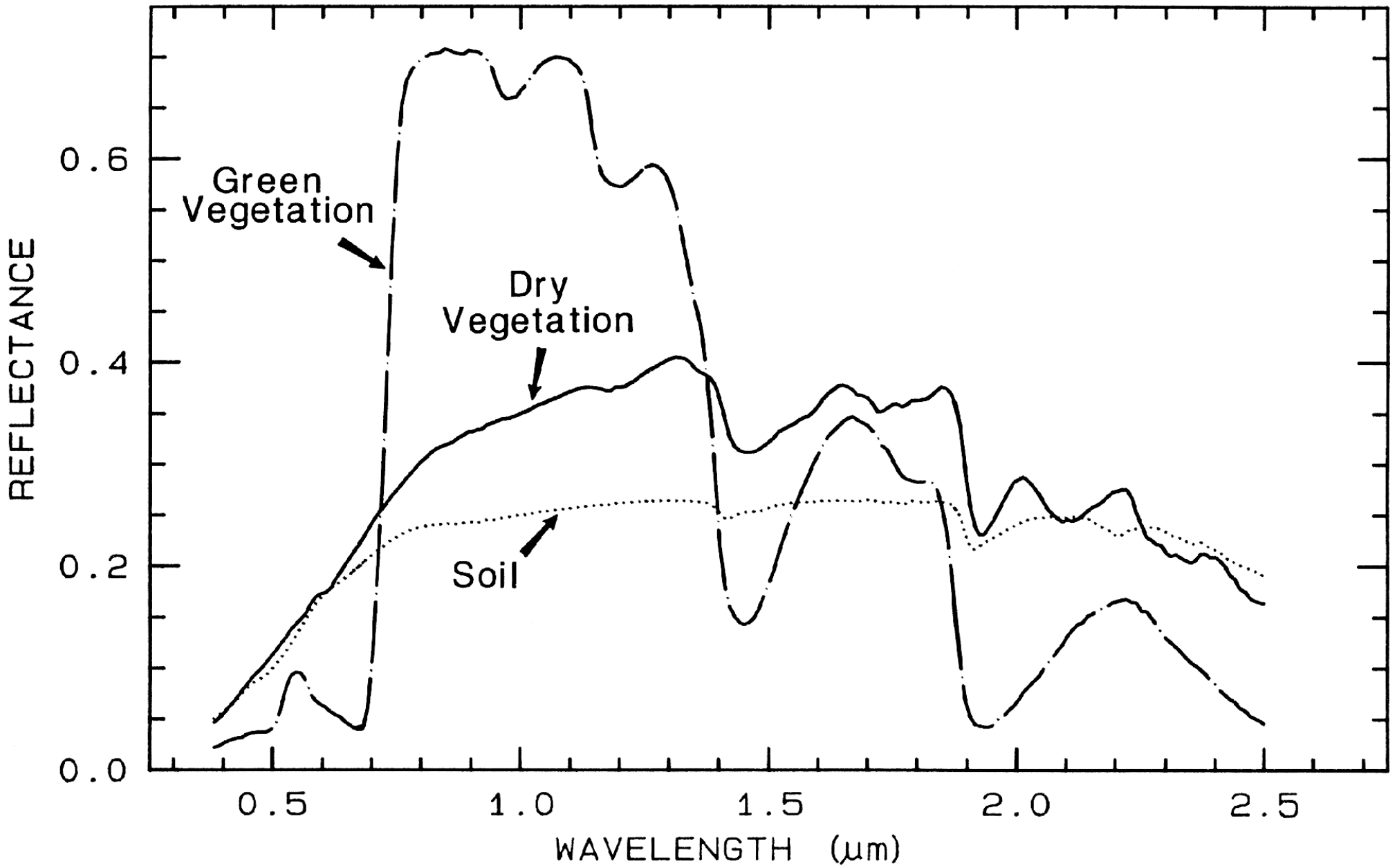
Green
Vegetation
Dry
Vegetation
Soil
REFLECTANCE
0.0
0.2
0.4
0.6
0.5
1.0
1.5
2.0
2.5
WAVELENGTH (μm)

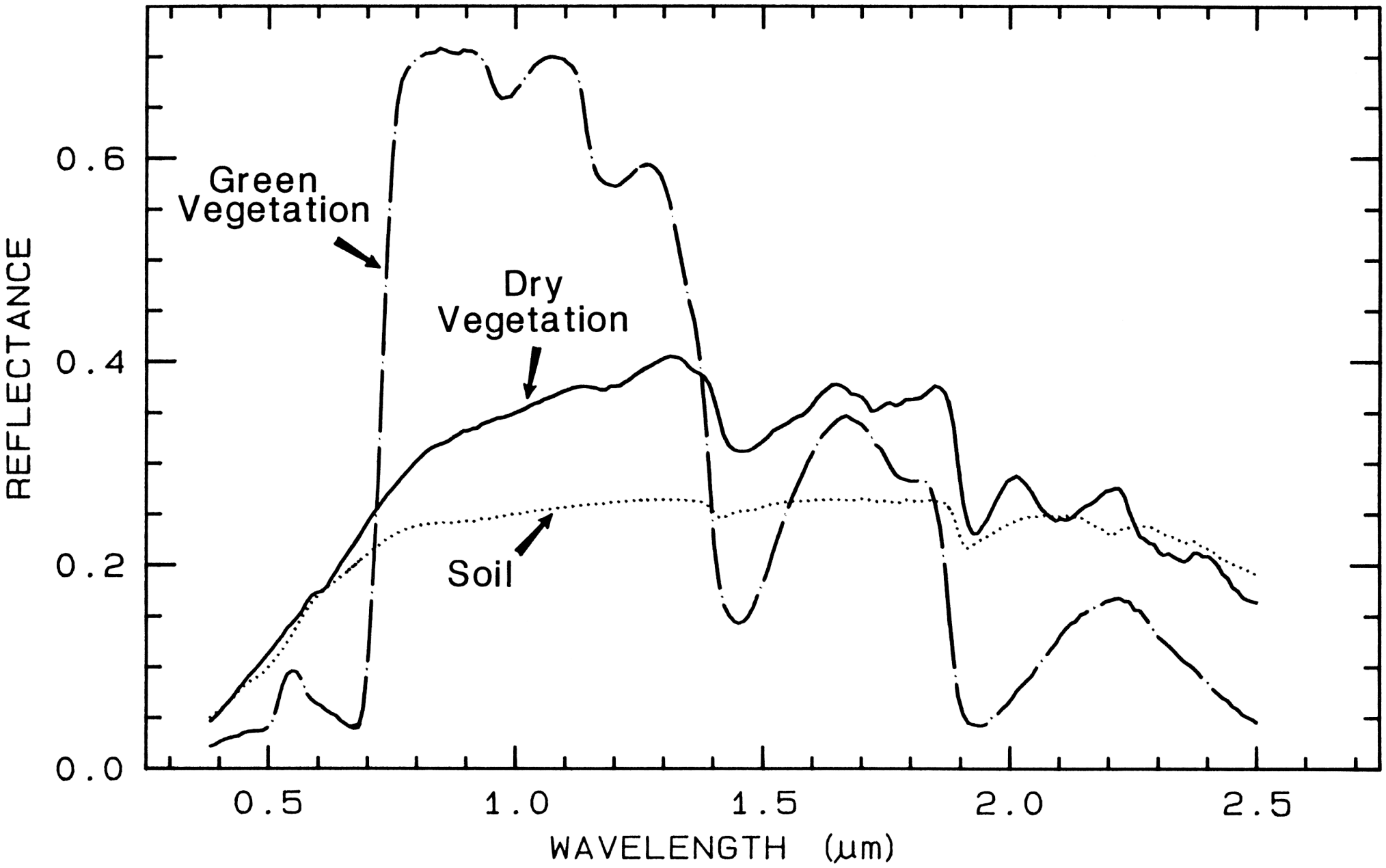
Green
Vegetation
Dry
Vegetation
Soil
REFLECTANCE
0.0
0.2
0.4
0.6
0.5
1.0
1.5
2.0
2.5
WAVELENGTH (μm)

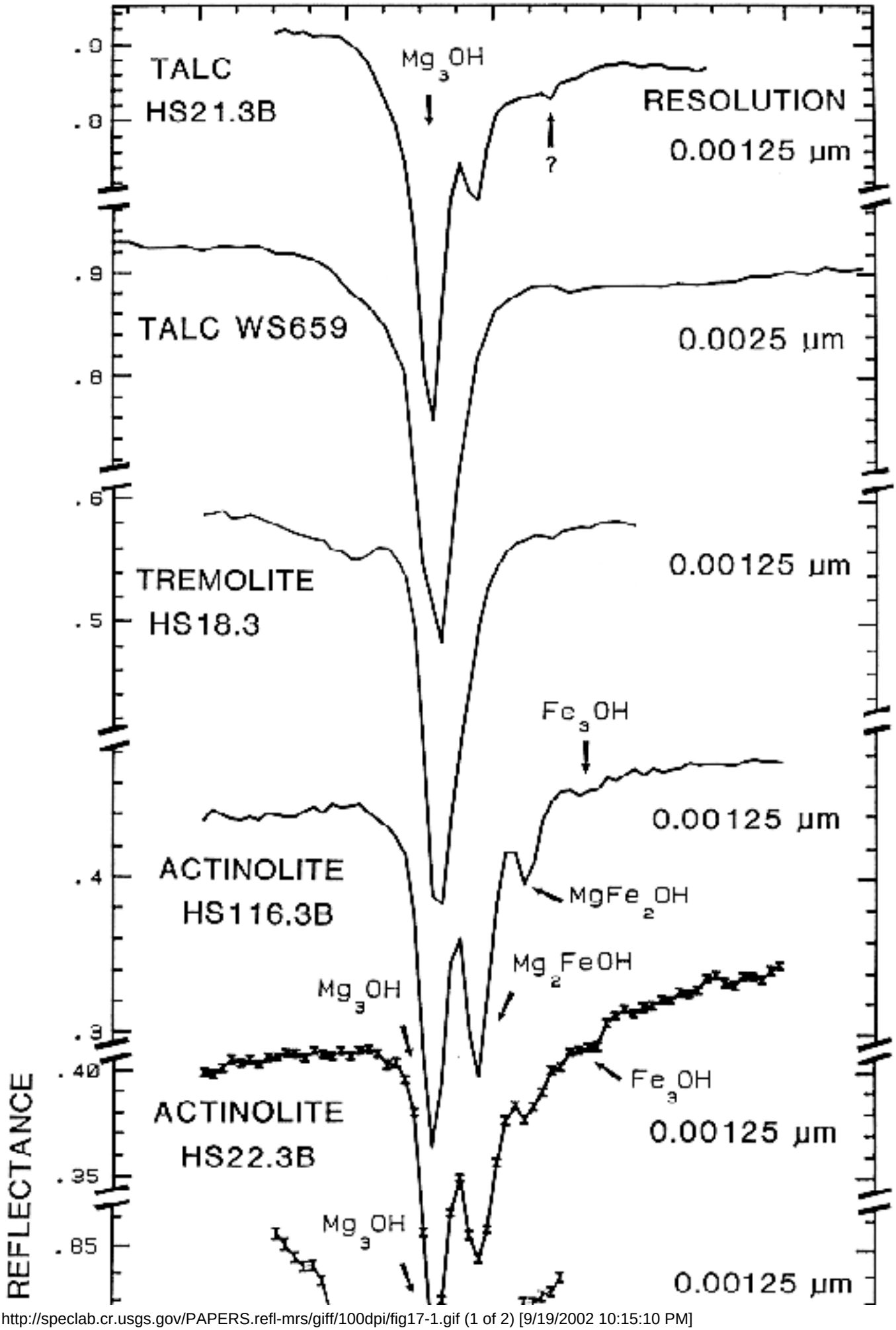
TALC
HS21.3B
Mg3OH
?
RESOLUTION
0.00125 µm
TALC WS659
0.0025 µm
TREMOLITE
HS18.3
0.00125 µm
Fe3OH
ACTINOLITE
HS116.3B
0.00125 µm
MgFe2OH
Mg2FeOH
Mg3OH
Fe3OH
ACTINOLITE
HS22.3B
0.00125 µm
Mg3OH
0.00125 µm
REFLECTANCE
.9
.8
.9
.8
.6
.5
.4
.3
.40
.35
.85

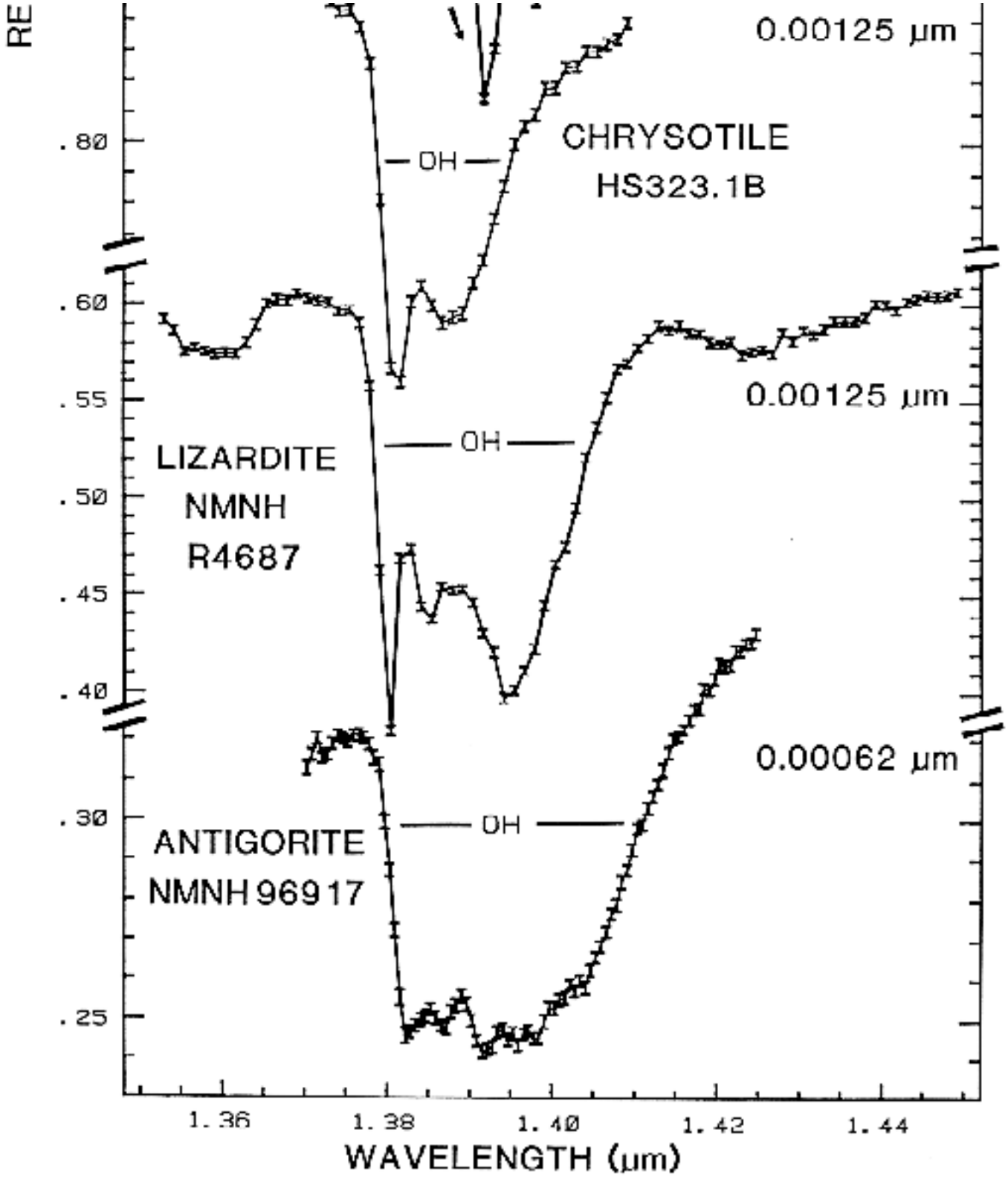
RE
.80
.60
.55
.50
.45
.40
.30
.25
0.00125 µm
CHRYSOTILE
HS323.1B
OH
0.00125 µm
LIZARDITE
NMNH
R4687
OH
0.00062 µm
ANTIGORITE
NMNH 96917
OH
1.36
1.38
1.40
1.42
1.44
WAVELENGTH (µm)

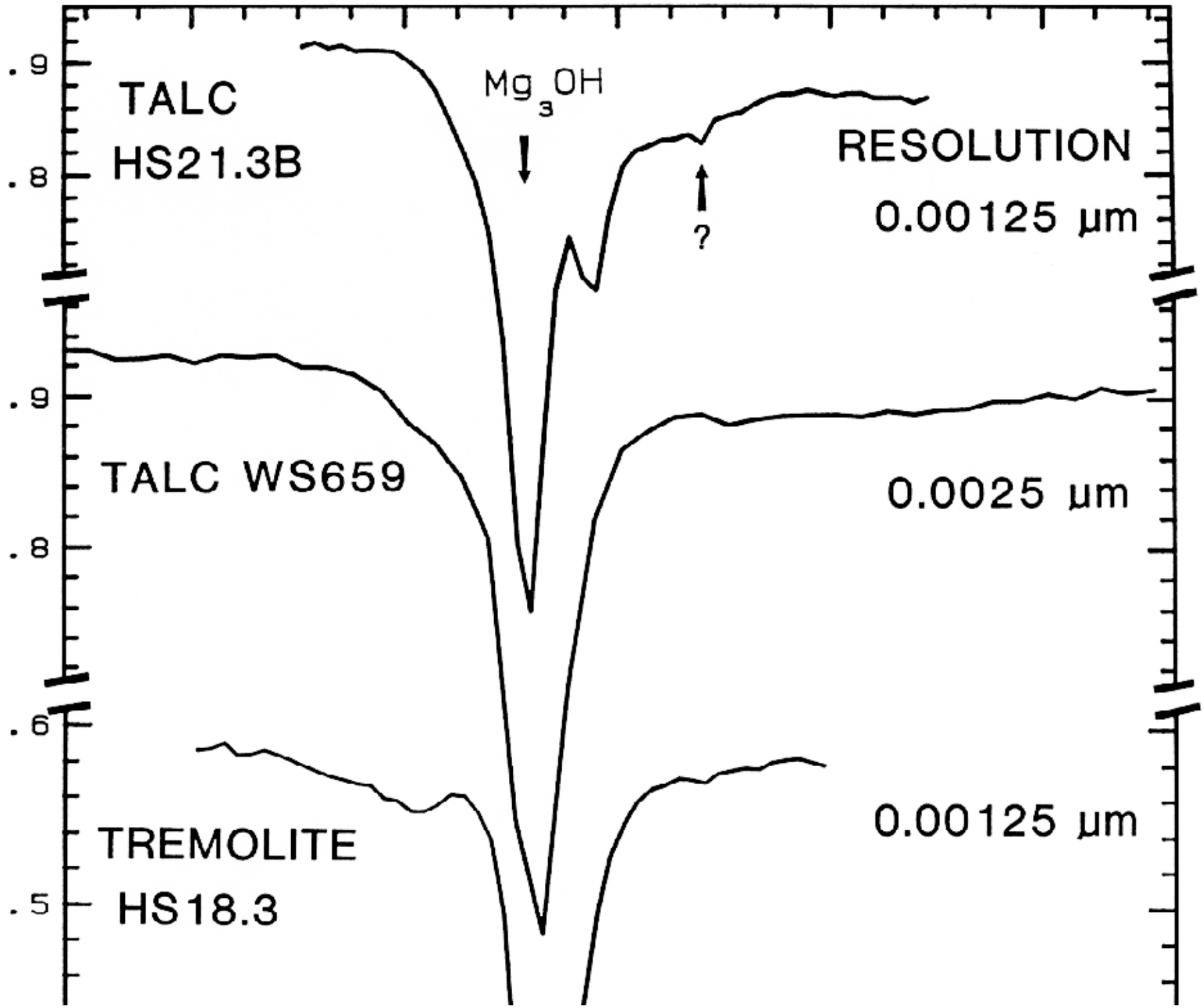
.9
.8
TALC
HS21.3B
Mg3OH
?
RESOLUTION
0.00125 µm
.9
.8
TALC WS659
0.0025 µm
.6
.5
TREMOLITE
HS18.3
0.00125 µm

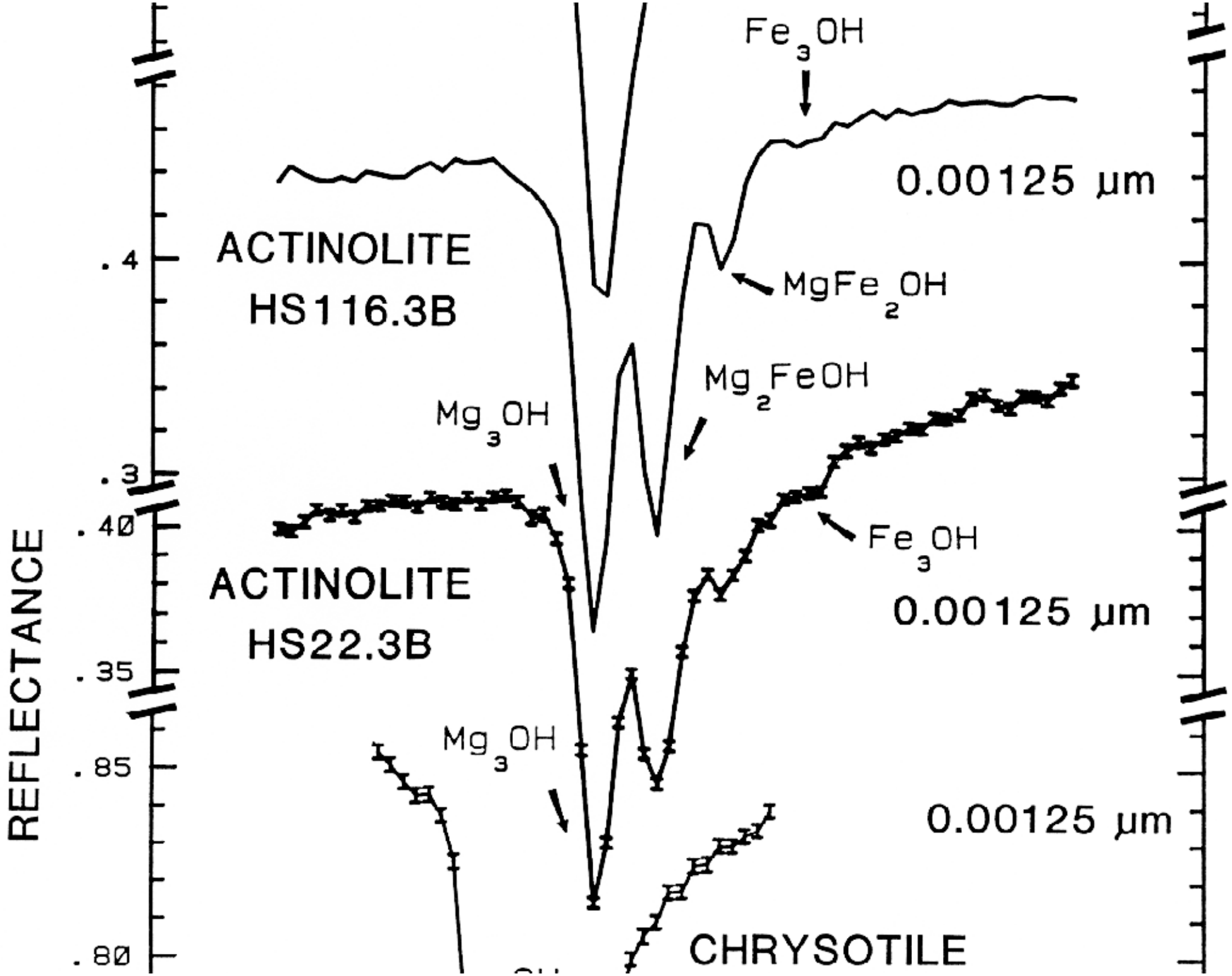
Fe3OH
0.00125 µm
ACTINOLITE
HS116.3B
MgFe2OH
Mg2FeOH
Mg3OH
Fe3OH
ACTINOLITE
HS22.3B
0.00125 µm
Mg3OH
0.00125 µm
CHRYSOTILE
REFLECTANCE
.4
.3
.40
.35
.85
.80

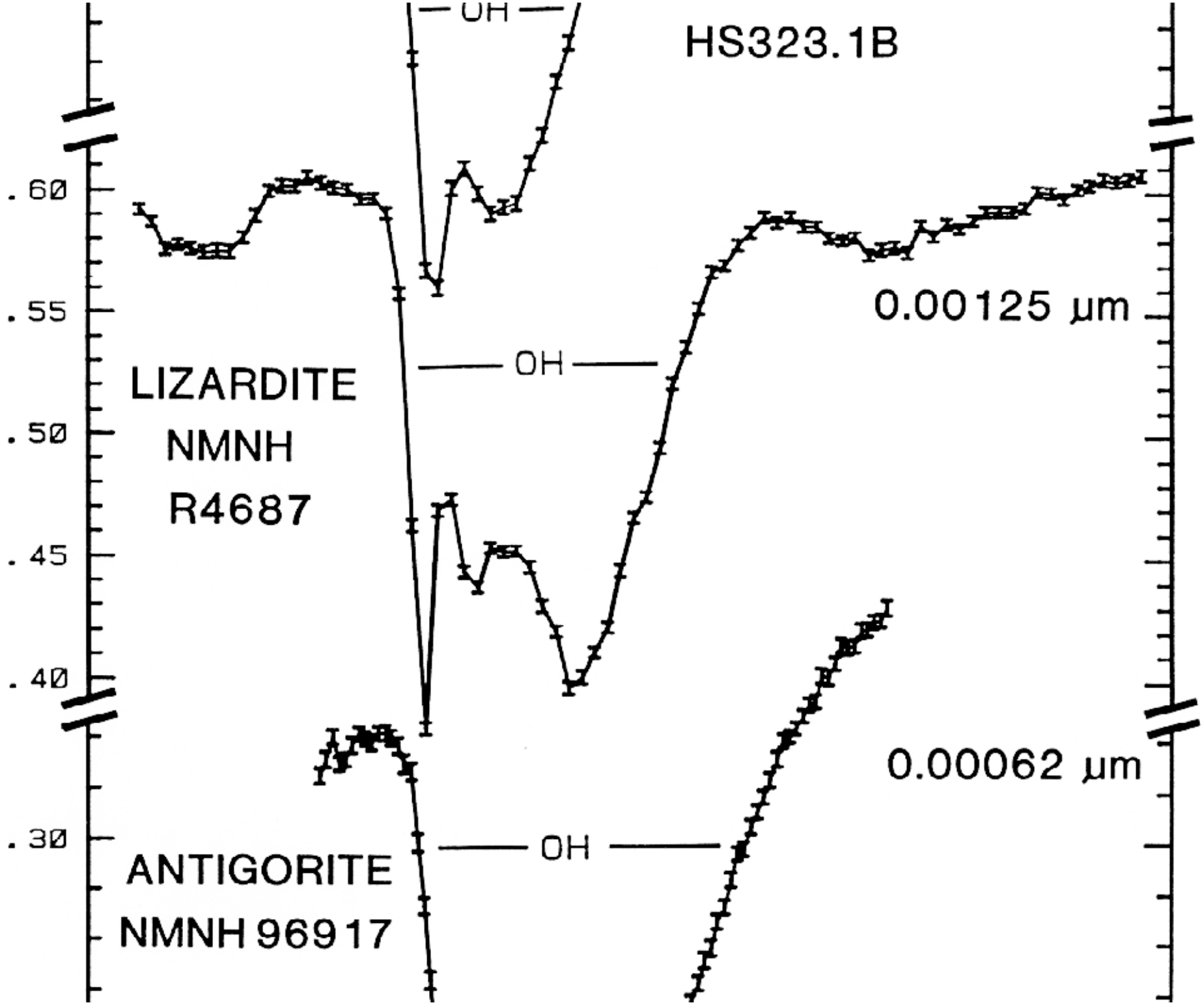
OH
HS323.1B
.60
.55
.50
.45
.40
.30
0.00125 µm
OH
LIZARDITE
NMNH
R4687
0.00062 µm
OH
ANTIGORITE
NMNH 96917

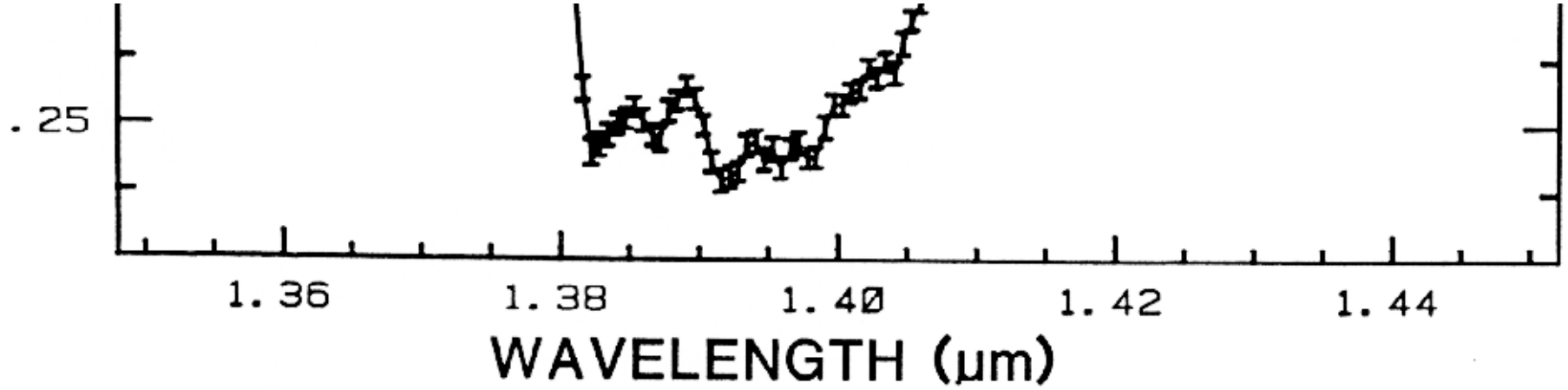
.25
1.36
1.38
1.40
1.42
1.44
WAVELENGTH (µm)

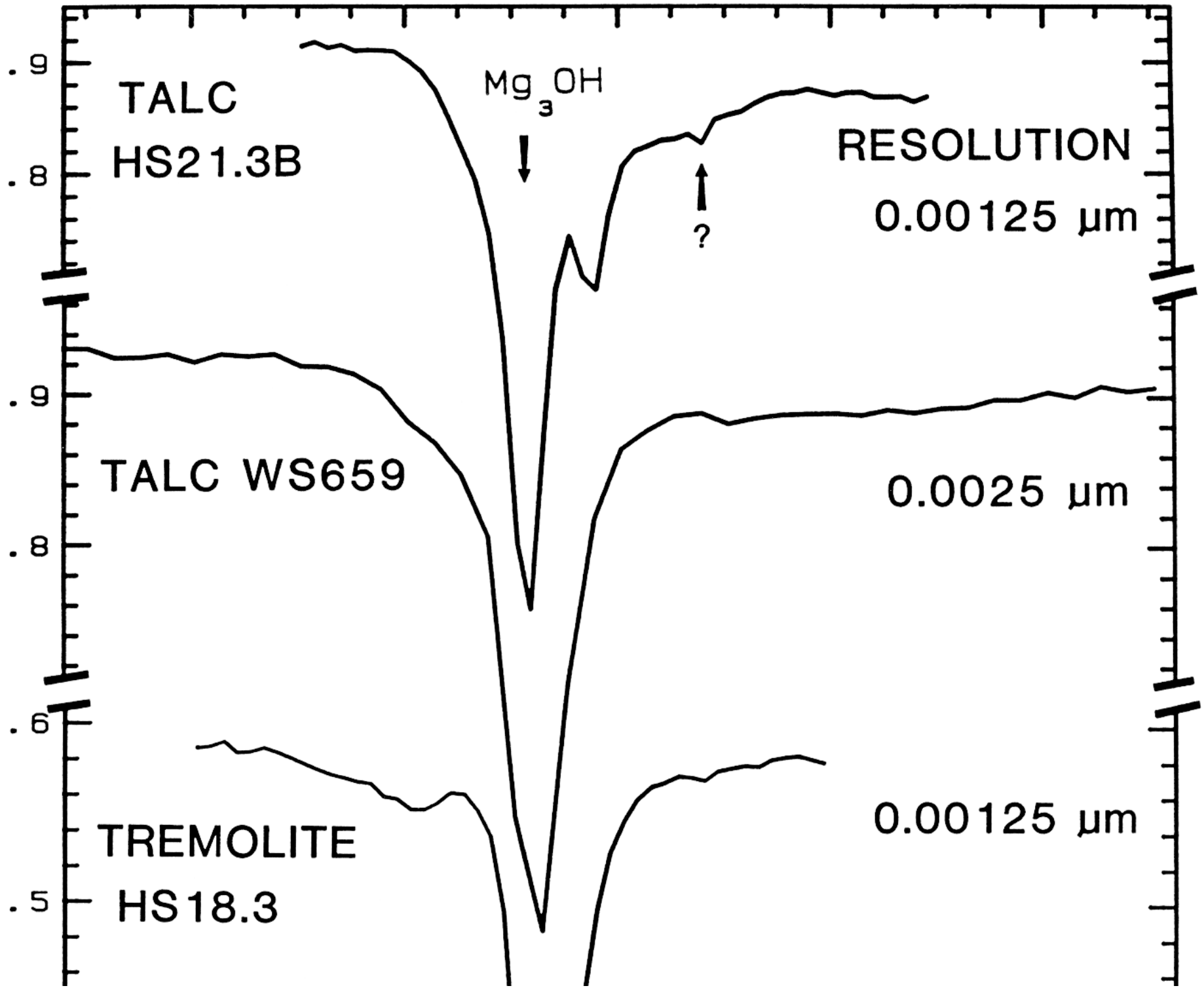
.9
.8
TALC
HS21.3B
Mg3OH
?
RESOLUTION
0.00125 µm
.9
.8
TALC WS659
0.0025 µm
.6
.5
TREMOLITE
HS18.3
0.00125 µm

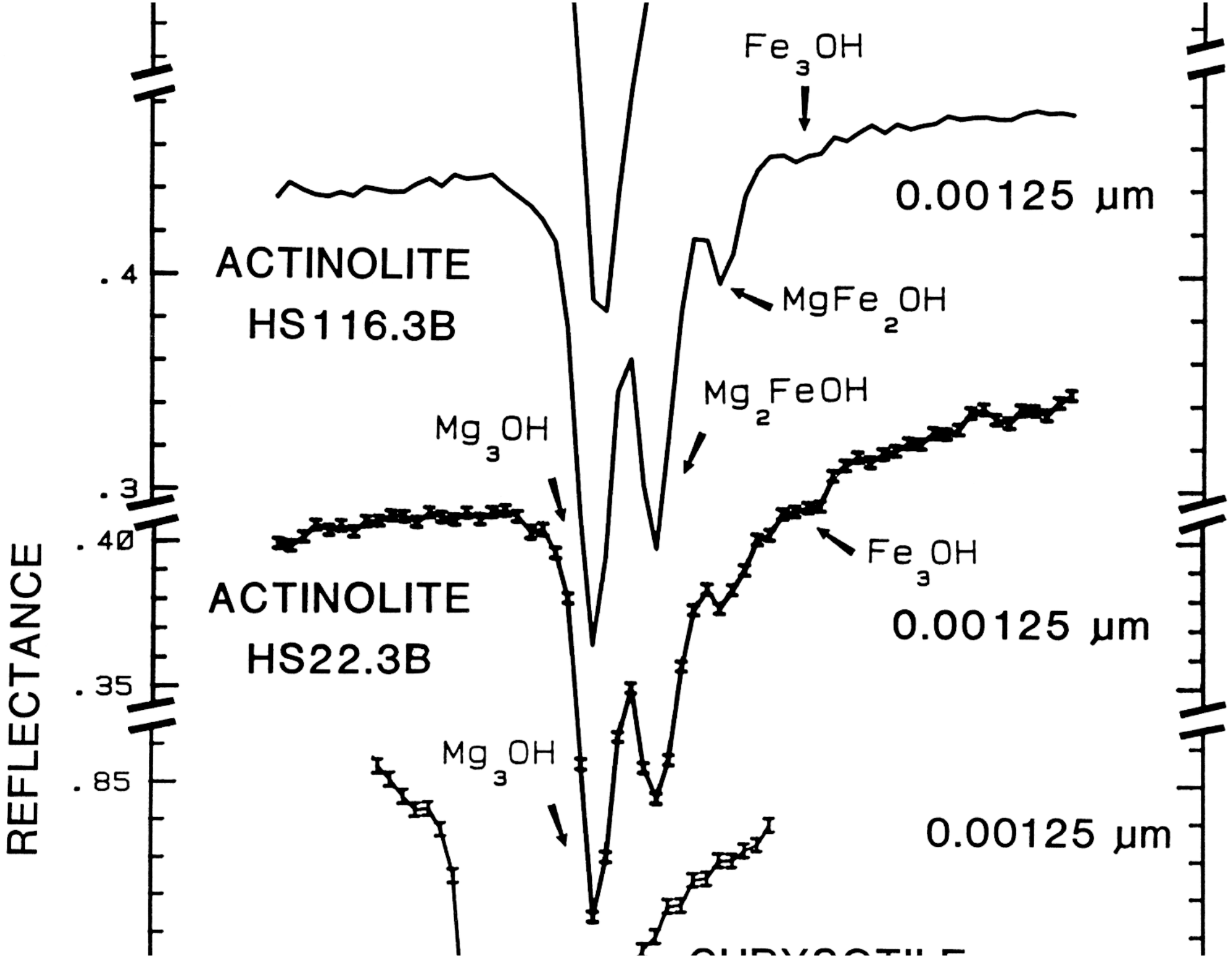
Fe3OH
0.00125 µm
ACTINOLITE
HS116.3B
MgFe2OH
Mg2FeOH
Mg3OH
Fe3OH
ACTINOLITE
HS22.3B
0.00125 µm
Mg3OH
0.00125 µm
REFLECTANCE
.4
.3
.40
.35
.85

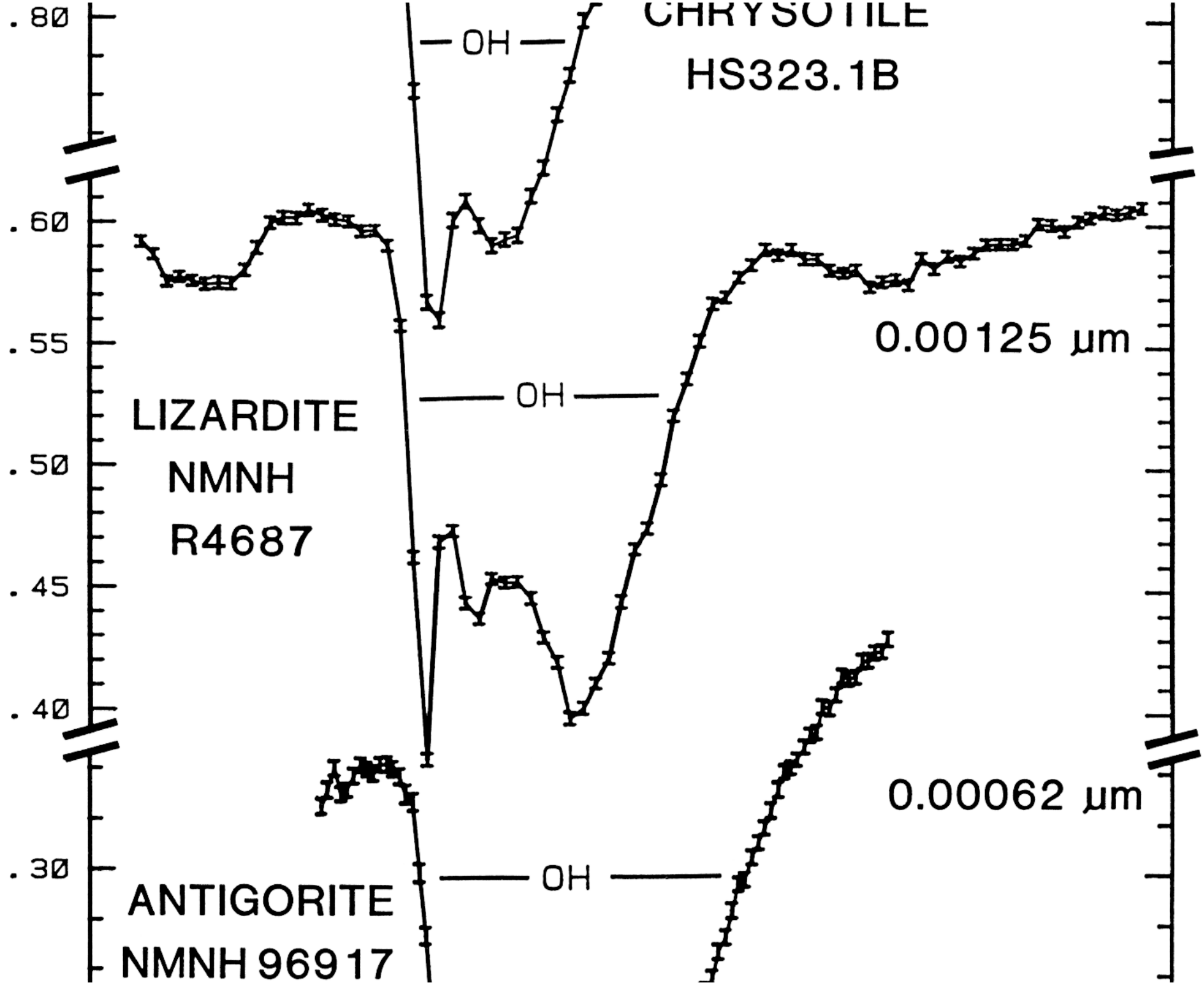
.80
.60
.55
.50
.45
.40
.30
OH
OH
OH
CHRYSOTILE
HS323.1B
0.00125 µm
LIZARDITE
NMNH
R4687
0.00062 µm
ANTIGORITE
NMNH 96917

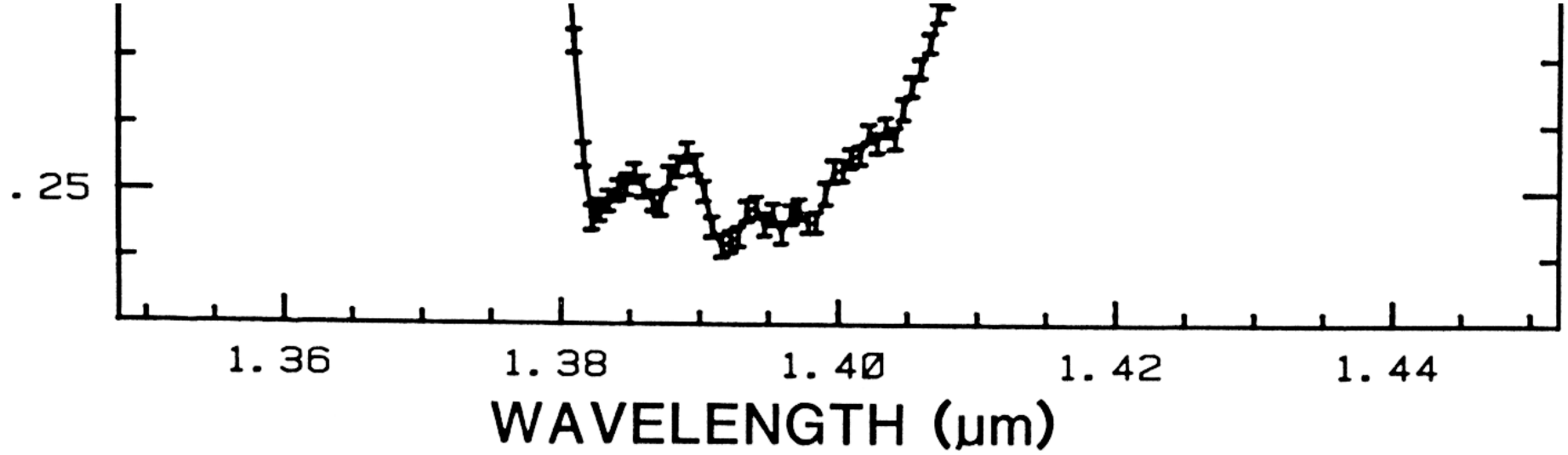
.25
1.36
1.38
1.40
1.42
1.44
WAVELENGTH (μm)

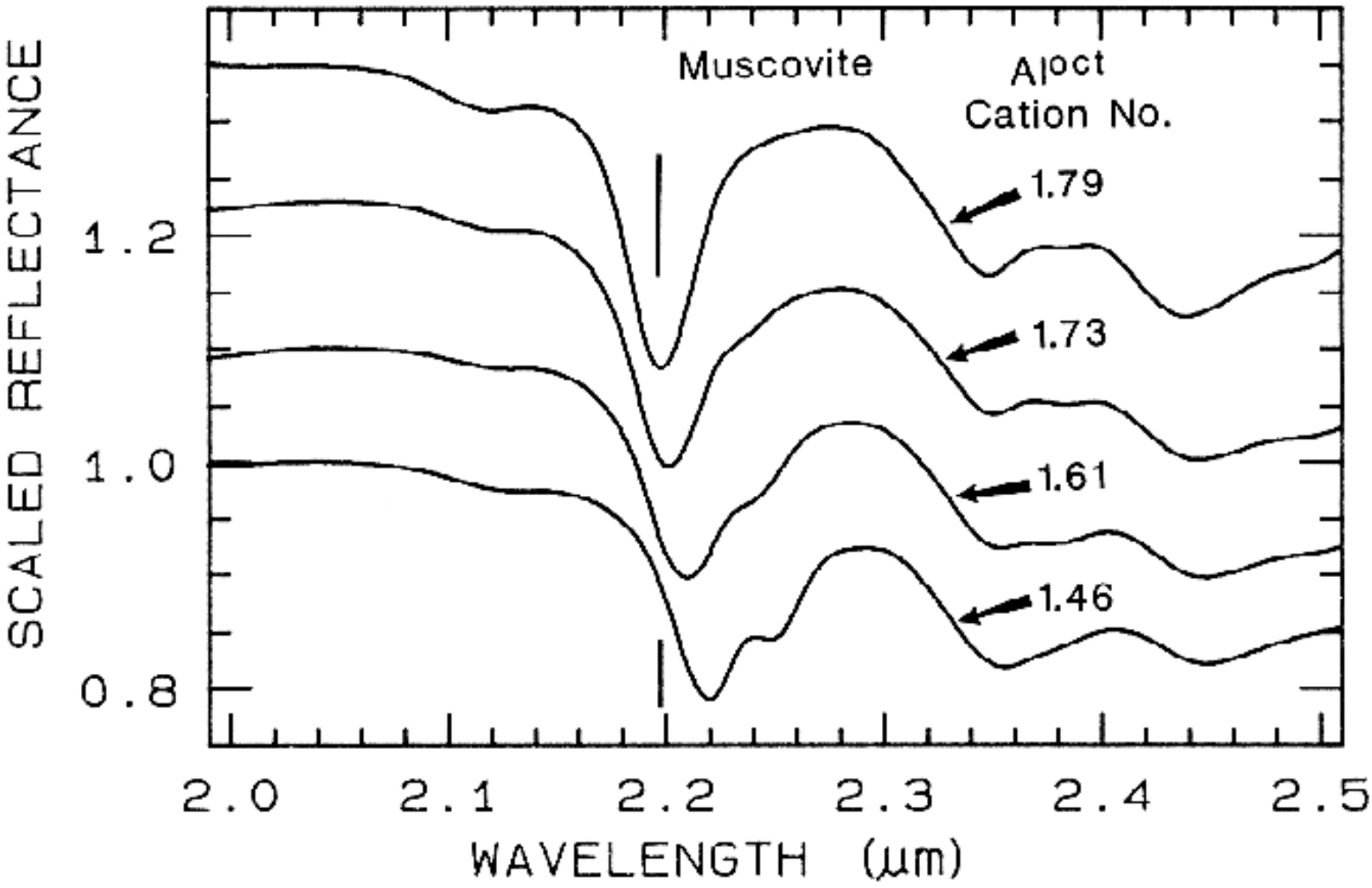
Muscovite
Al oct
Cation No.
1.79
1.73
1.61
1.46
SCALED REFLECTANCE
1.2
1.0
0.8
2.0
2.1
2.2
2.3
2.4
2.5
WAVELENGTH (μm)

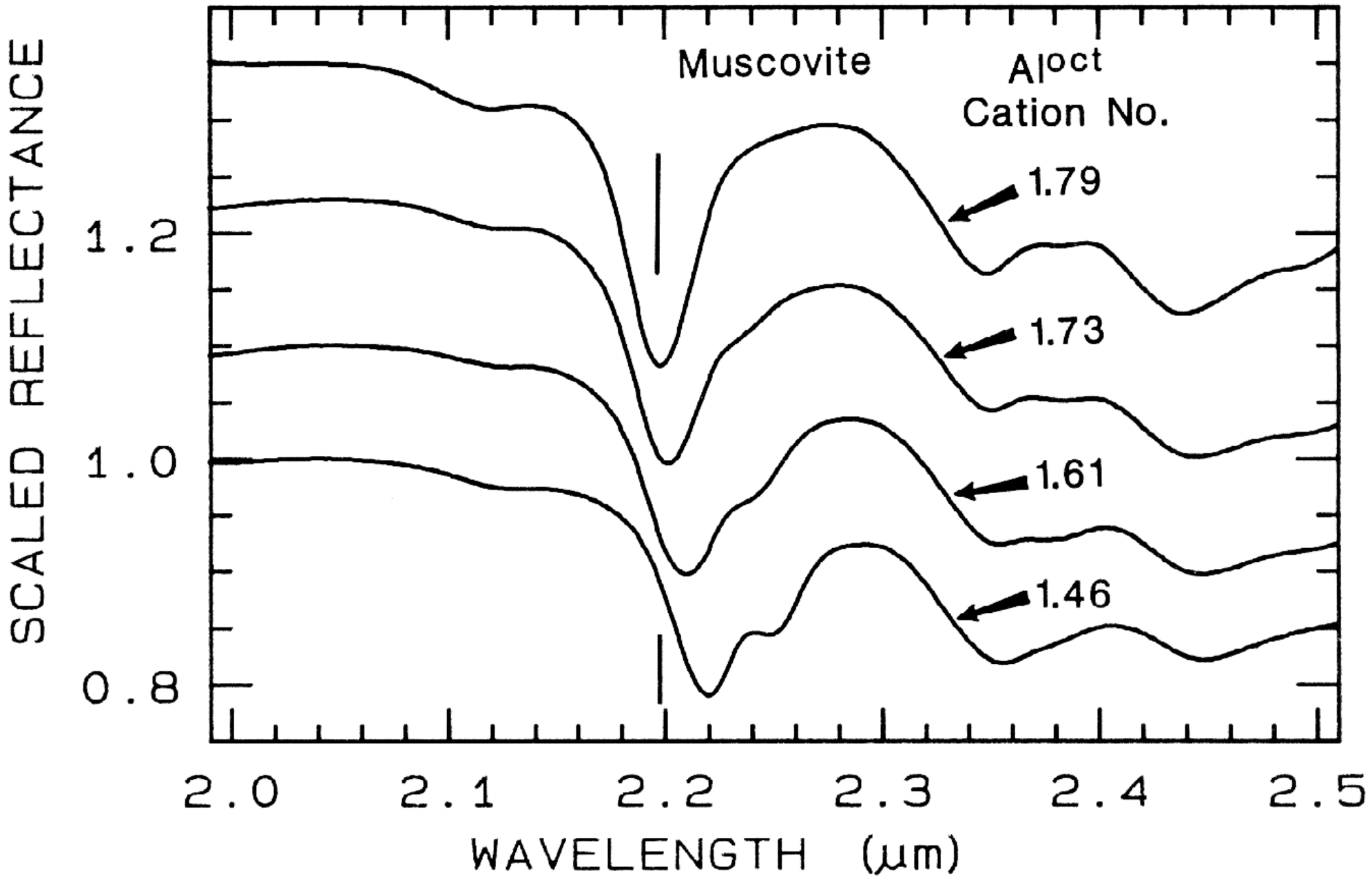
Muscovite
Al oct
Cation No.
1.79
1.73
1.61
1.46
SCALED REFLECTANCE
1.2
1.0
0.8
2.0
2.1
2.2
2.3
2.4
2.5
WAVELENGTH (μm)

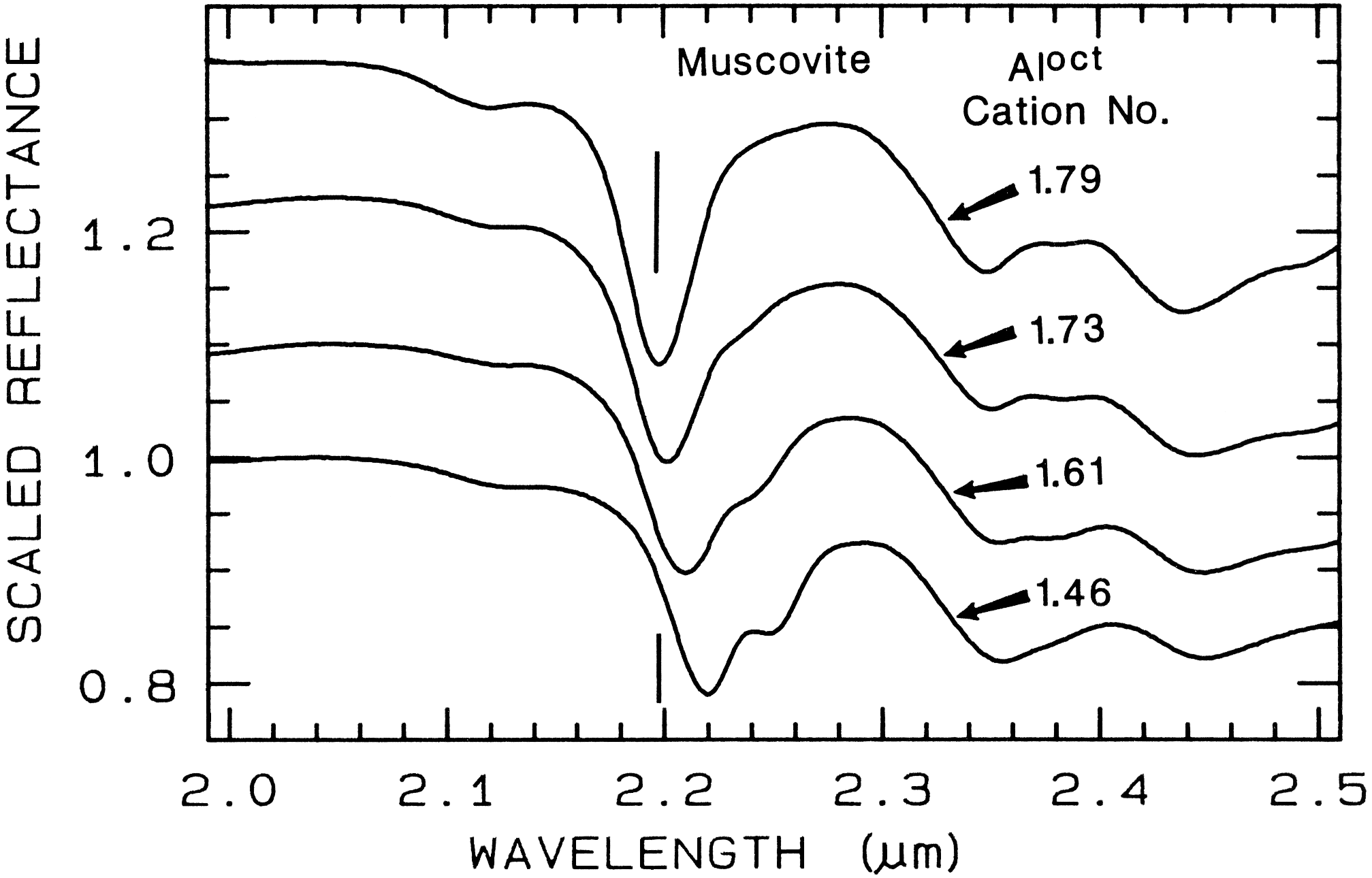
Muscovite
Al oct
Cation No.
1.79
1.73
1.61
1.46
SCALED REFLECTANCE
1.2
1.0
0.8
2.0
2.1
2.2
2.3
2.4
2.5
WAVELENGTH (μm)

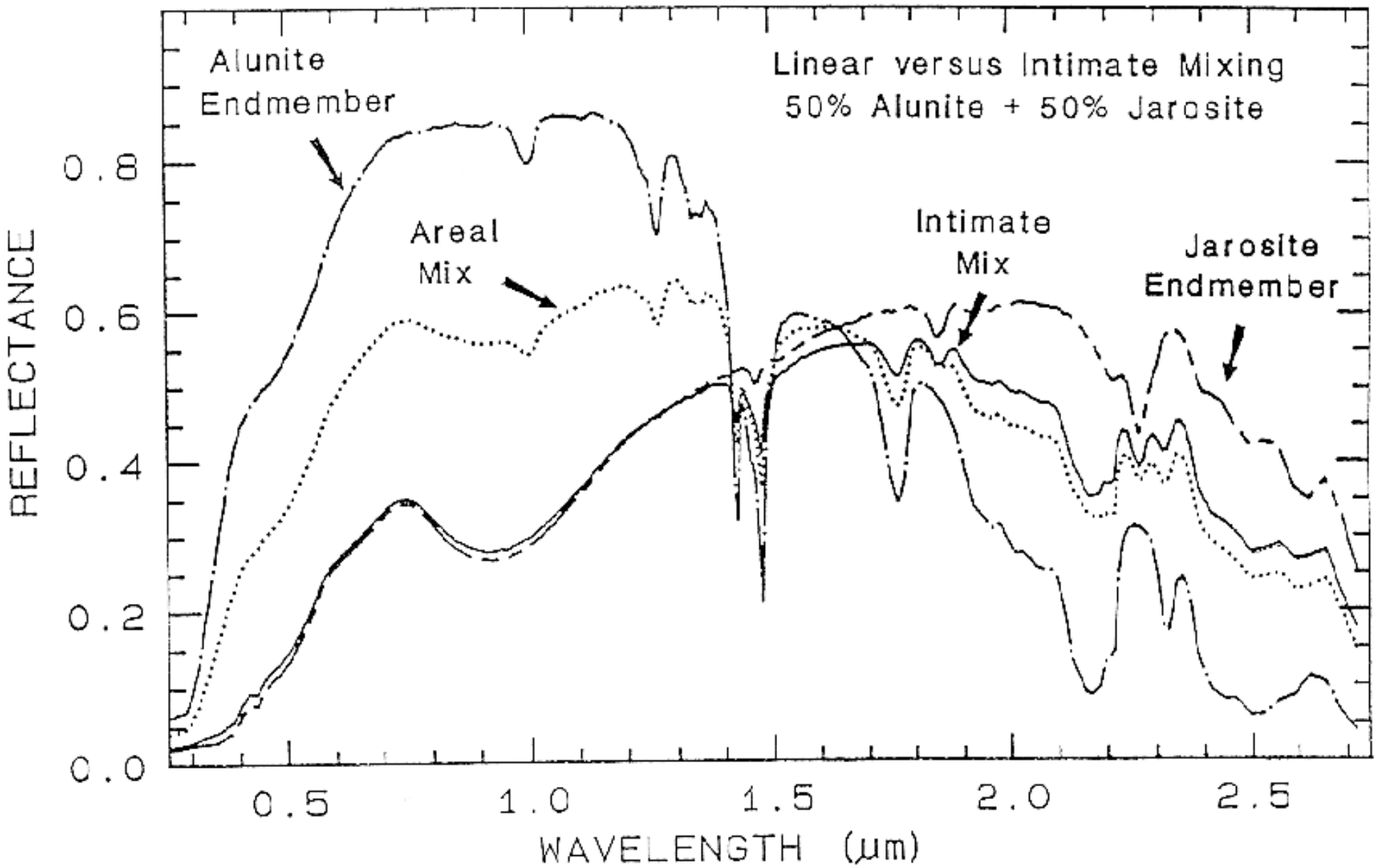
Linear versus Intimate Mixing
50% Alunite + 50% Jarosite
Alunite
Endmember
Areal
Mix
Intimate
Mix
Jarosite
Endmember
REFLECTANCE
0.0
0.2
0.4
0.6
0.8
0.5
1.0
1.5
2.0
2.5
WAVELENGTH (μm)

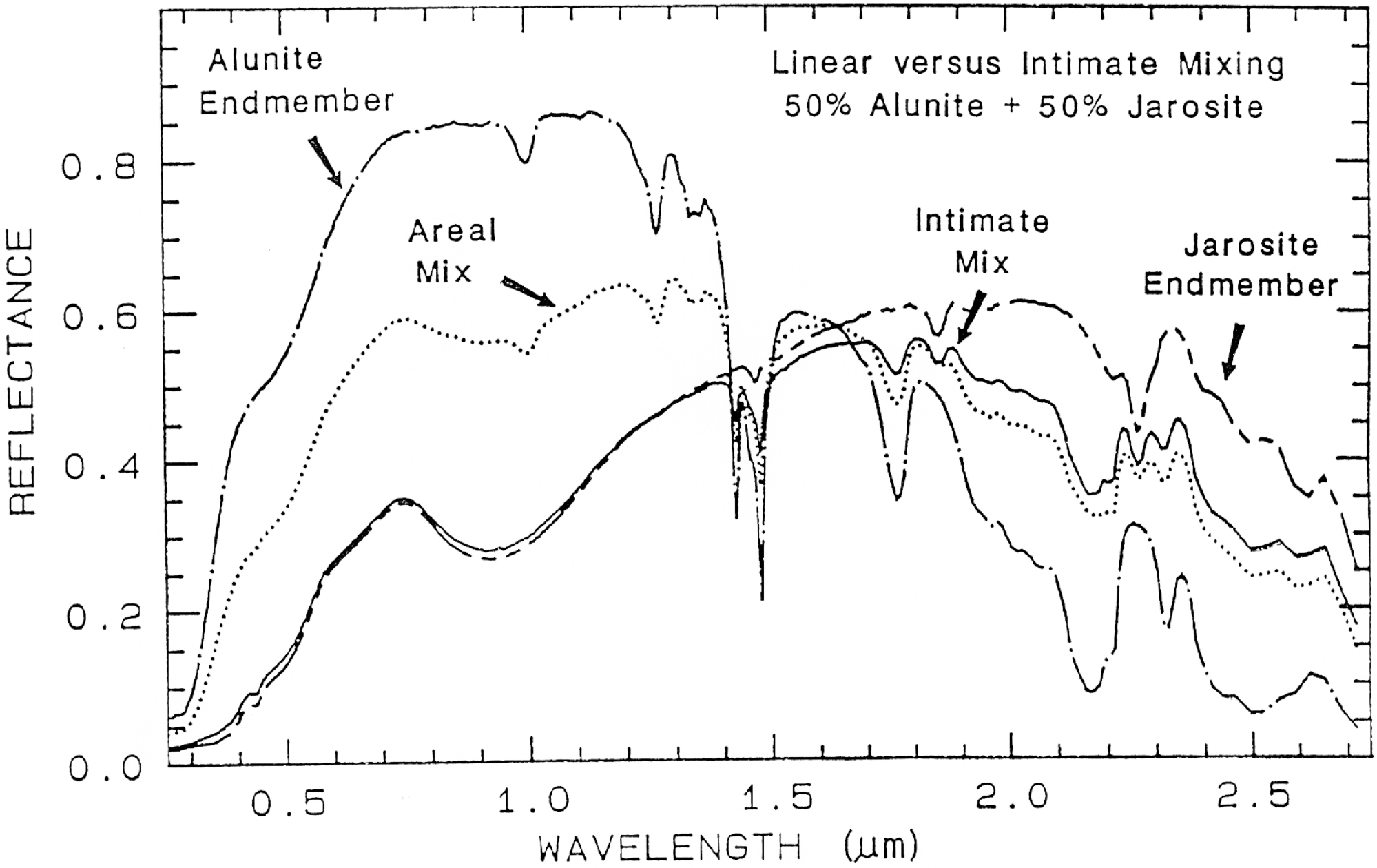
Alunite
Endmember
Linear versus Intimate Mixing
50% Alunite + 50% Jarosite
Areal
Mix
Intimate
Mix
Jarosite
Endmember
REFLECTANCE
0.0
0.2
0.4
0.6
0.8
0.5
1.0
1.5
2.0
2.5
WAVELENGTH (μm)

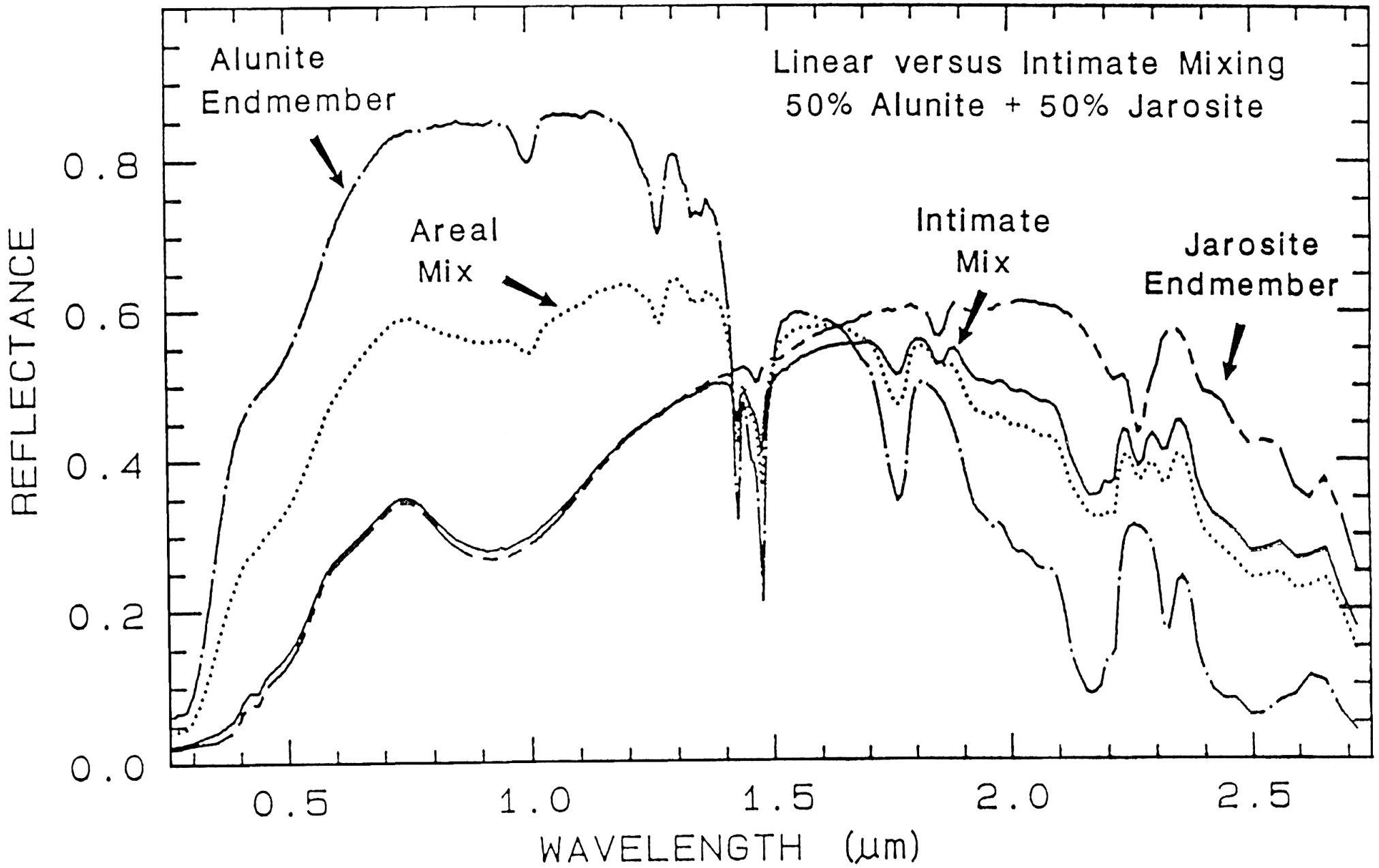
Alunite
Endmember
Linear versus Intimate Mixing
50% Alunite + 50% Jarosite
Areal
Mix
Intimate
Mix
Jarosite
Endmember
REFLECTANCE
0.0
0.2
0.4
0.6
0.8
0.5
1.0
1.5
2.0
2.5
WAVELENGTH (μm)

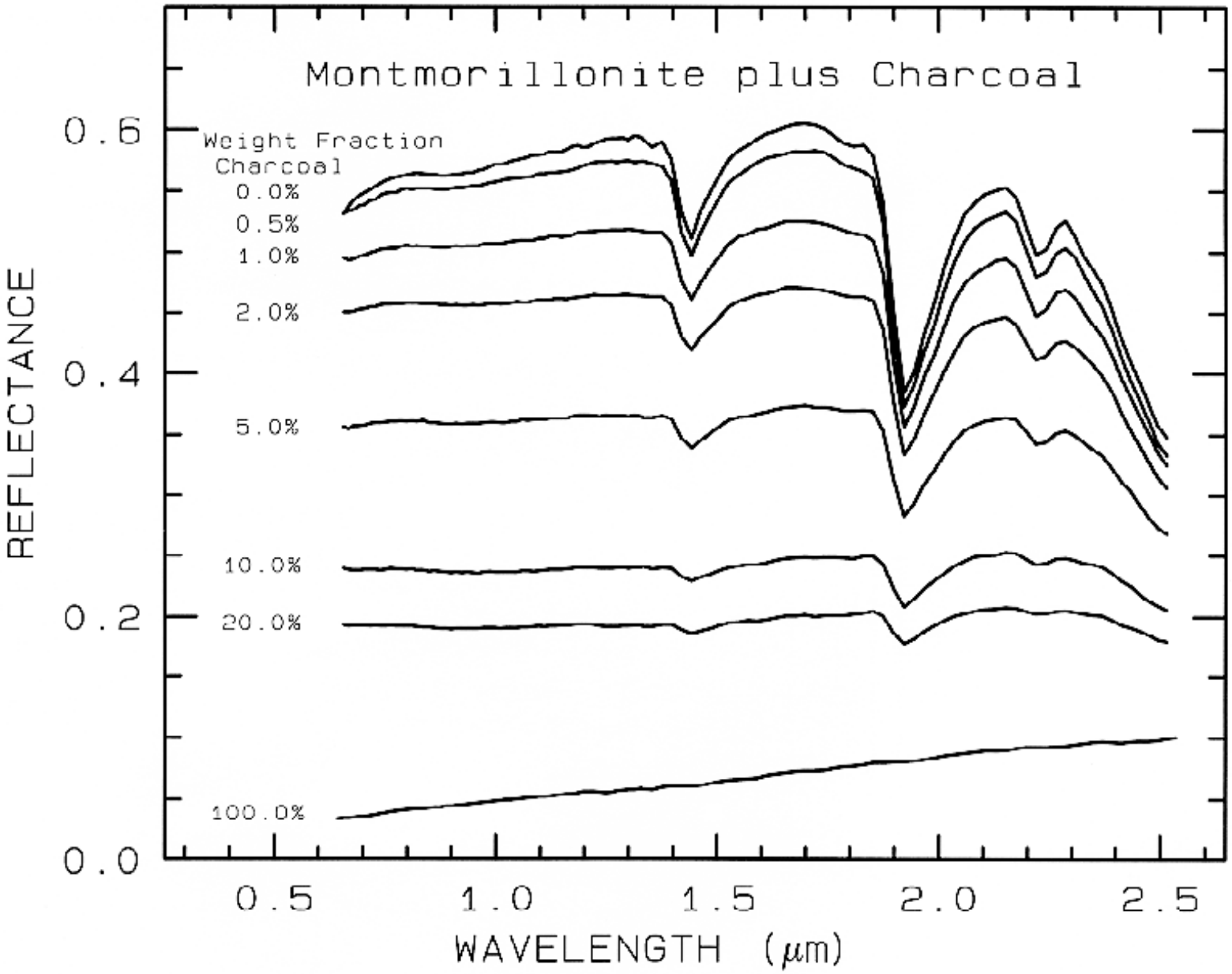
Montmorillonite plus Charcoal
Weight Fraction Charcoal
0.0%
0.5%
1.0%
2.0%
5.0%
10.0%
20.0%
100.0%
REFLECTANCE
0.0
0.2
0.4
0.6
0.5
1.0
1.5
2.0
2.5
WAVELENGTH (μm)

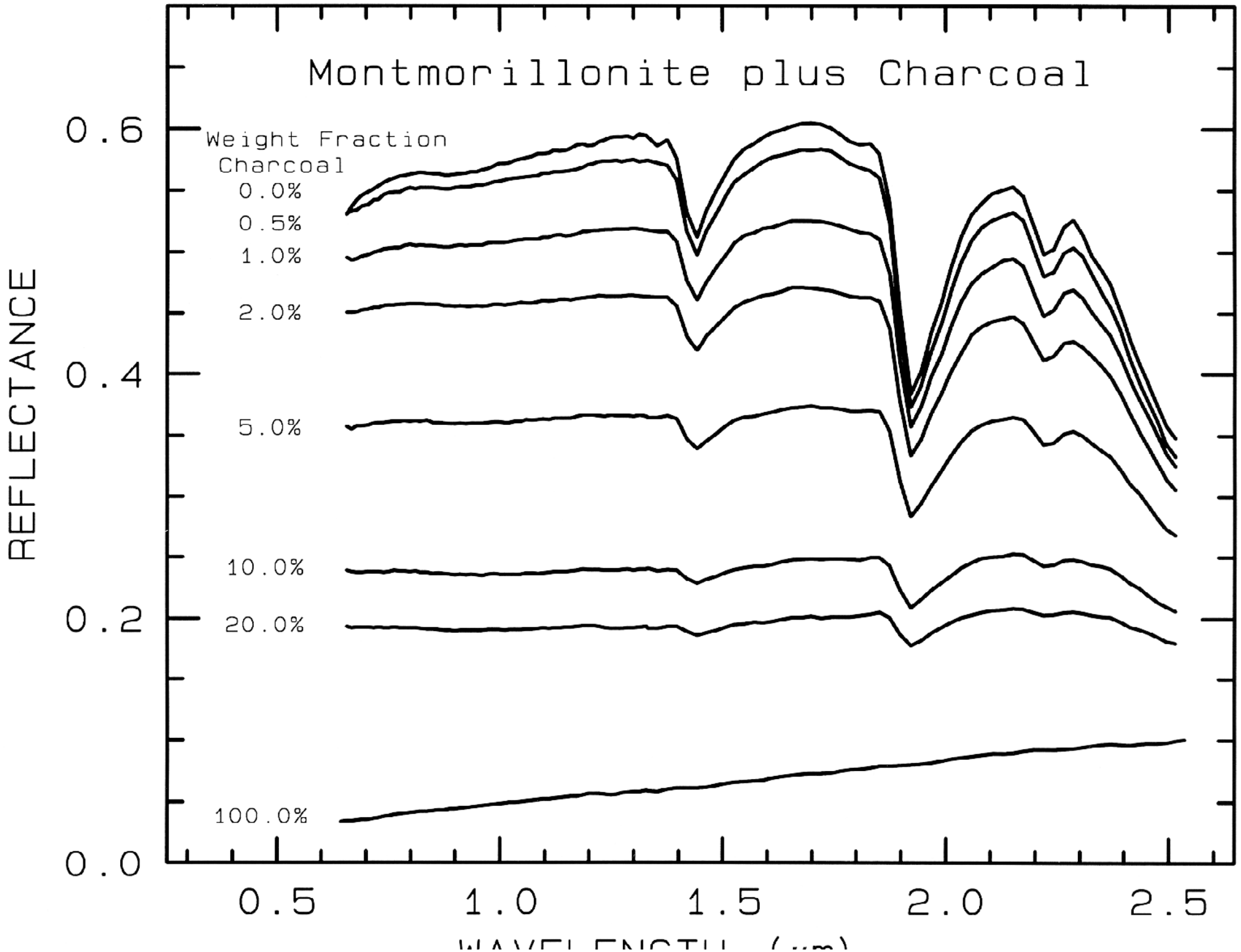
Montmorillonite plus Charcoal
Weight Fraction Charcoal
0.0%
0.5%
1.0%
2.0%
5.0%
10.0%
20.0%
100.0%
REFLECTANCE
0.0
0.2
0.4
0.6
0.5
1.0
1.5
2.0
2.5

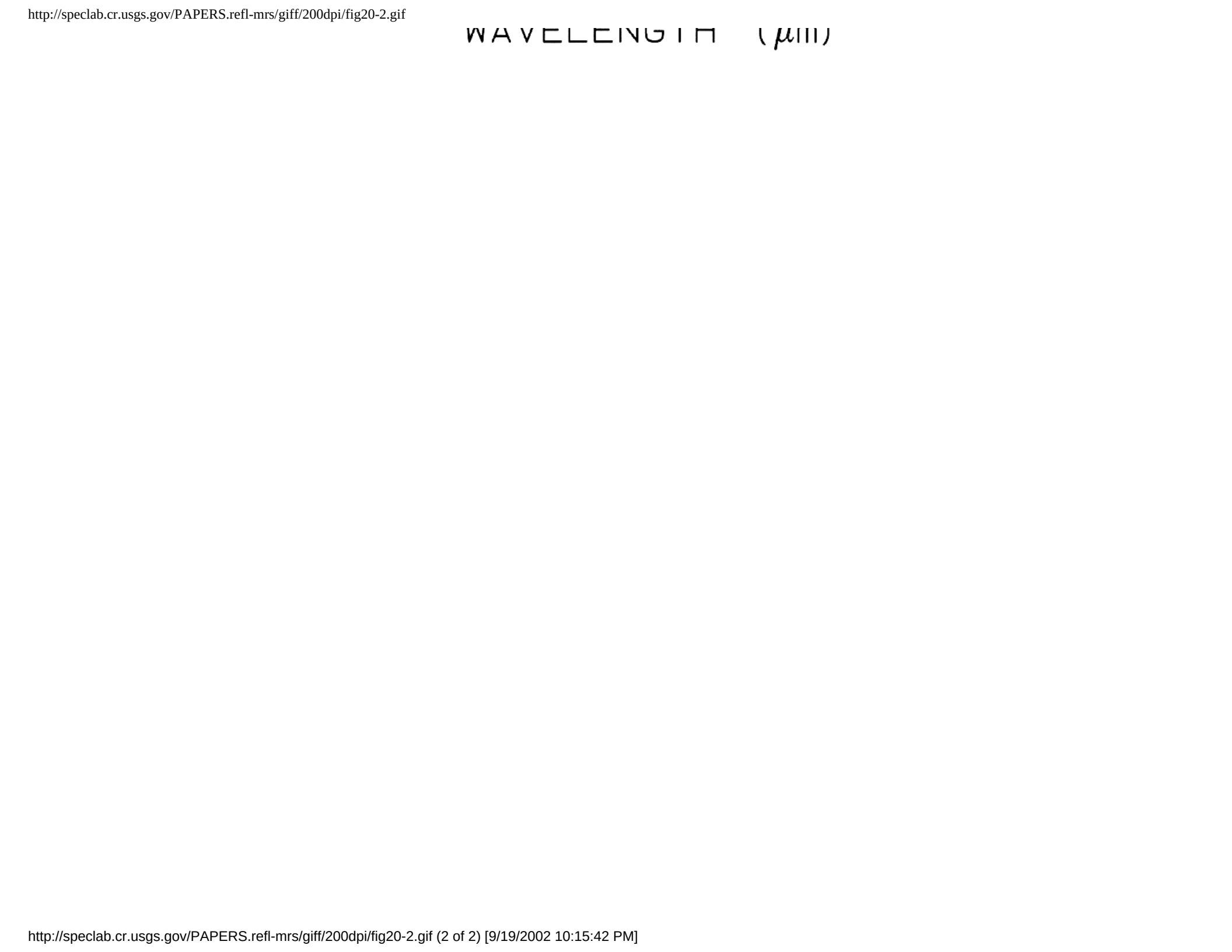
WAVELENGTH (μm)

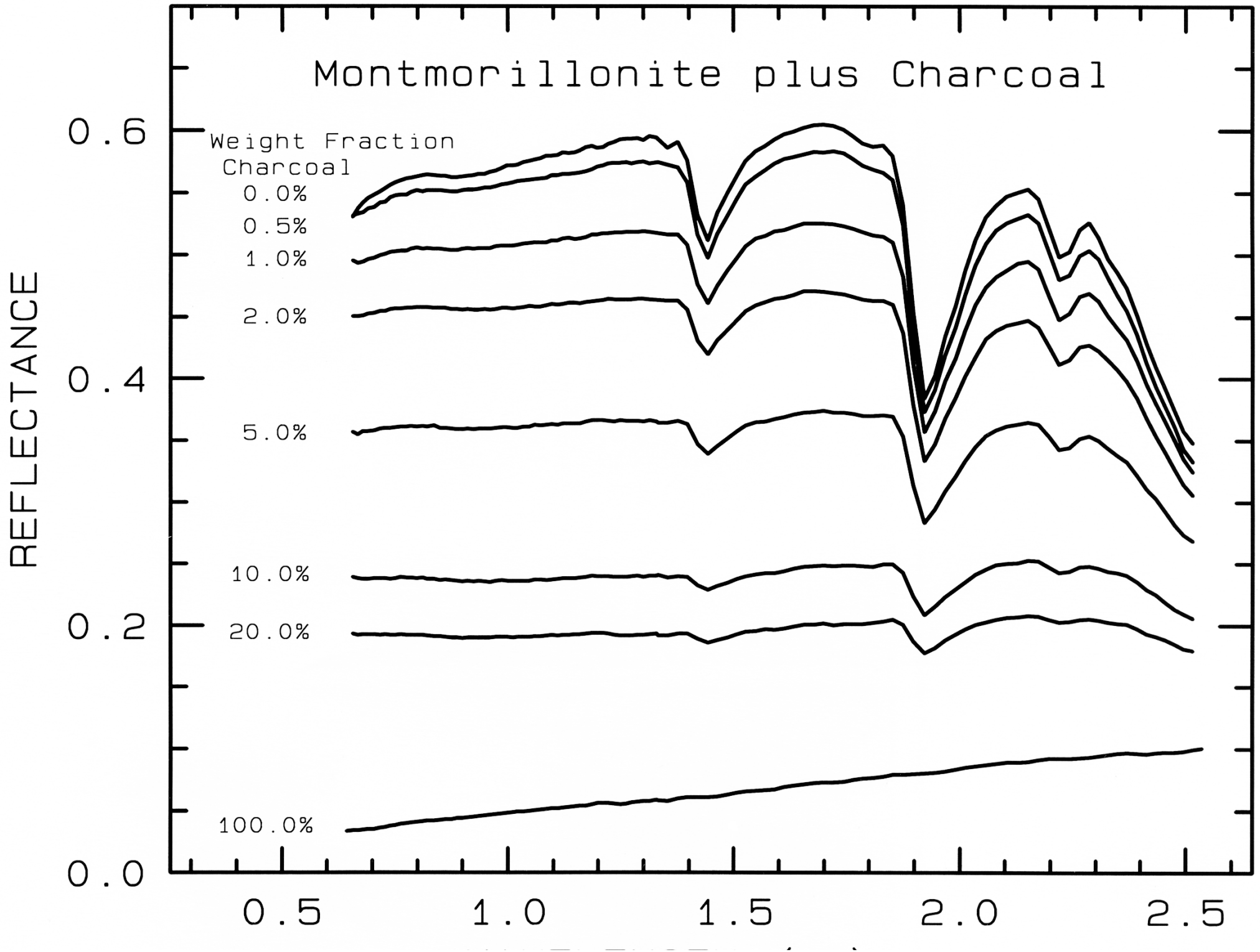
Montmorillonite plus Charcoal
Weight Fraction Charcoal
0.0%
0.5%
1.0%
2.0%
5.0%
10.0%
20.0%
100.0%
REFLECTANCE
0.0
0.2
0.4
0.6
0.5
1.0
1.5
2.0
2.5

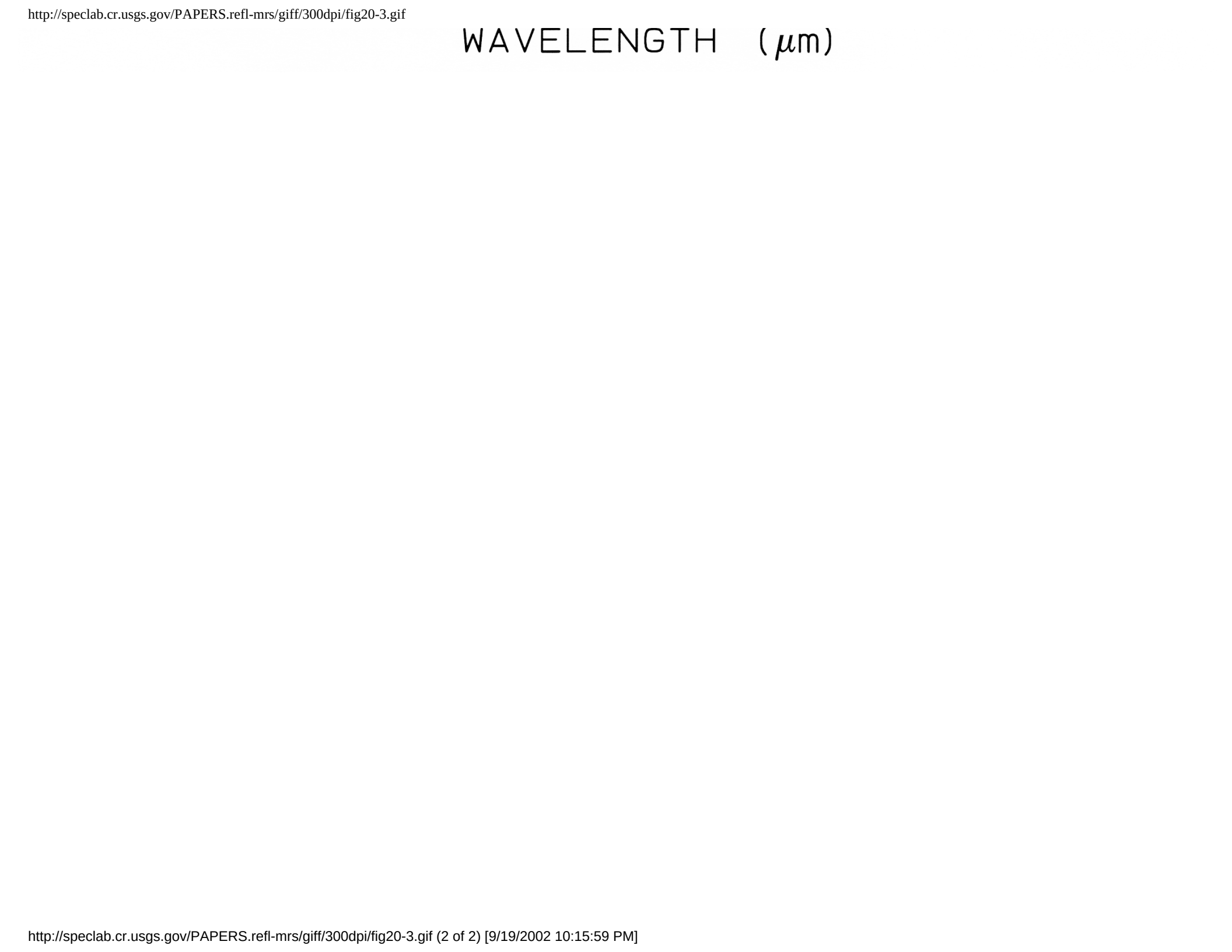
WAVELENGTH (μm)

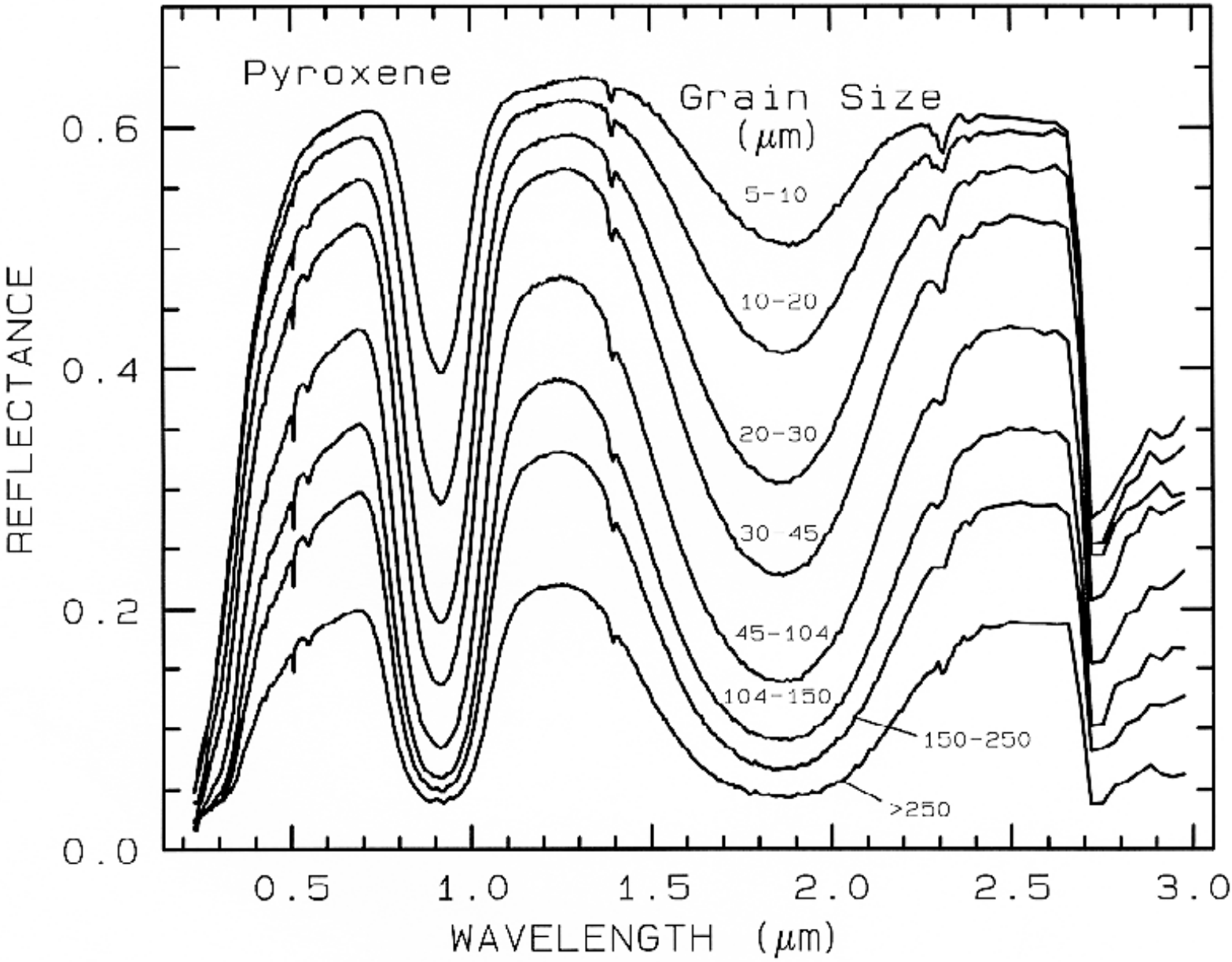
Pyroxene
Grain Size
(μm)
5-10
10-20
20-30
30-45
45-104
104-150
150-250
>250
REFLECTANCE
0.0
0.2
0.4
0.6
0.5
1.0
1.5
2.0
2.5
3.0
WAVELENGTH (μm)

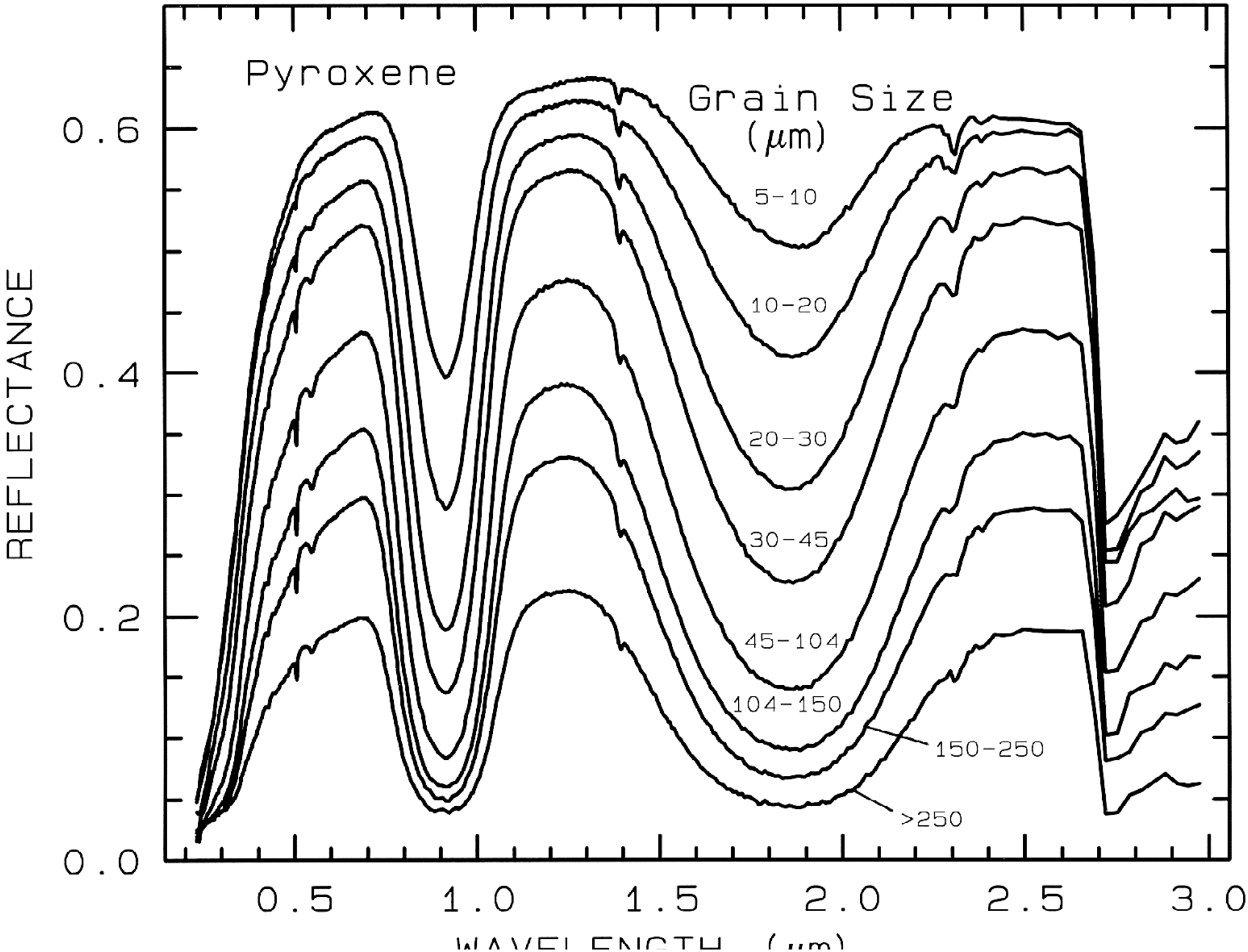
Pyroxene
Grain Size
(μm)
5-10
10-20
20-30
30-45
45-104
104-150
150-250
>250
REFLECTANCE
0.0
0.2
0.4
0.6
0.5
1.0
1.5
2.0
2.5
3.0


WAVELENGTH (μm)

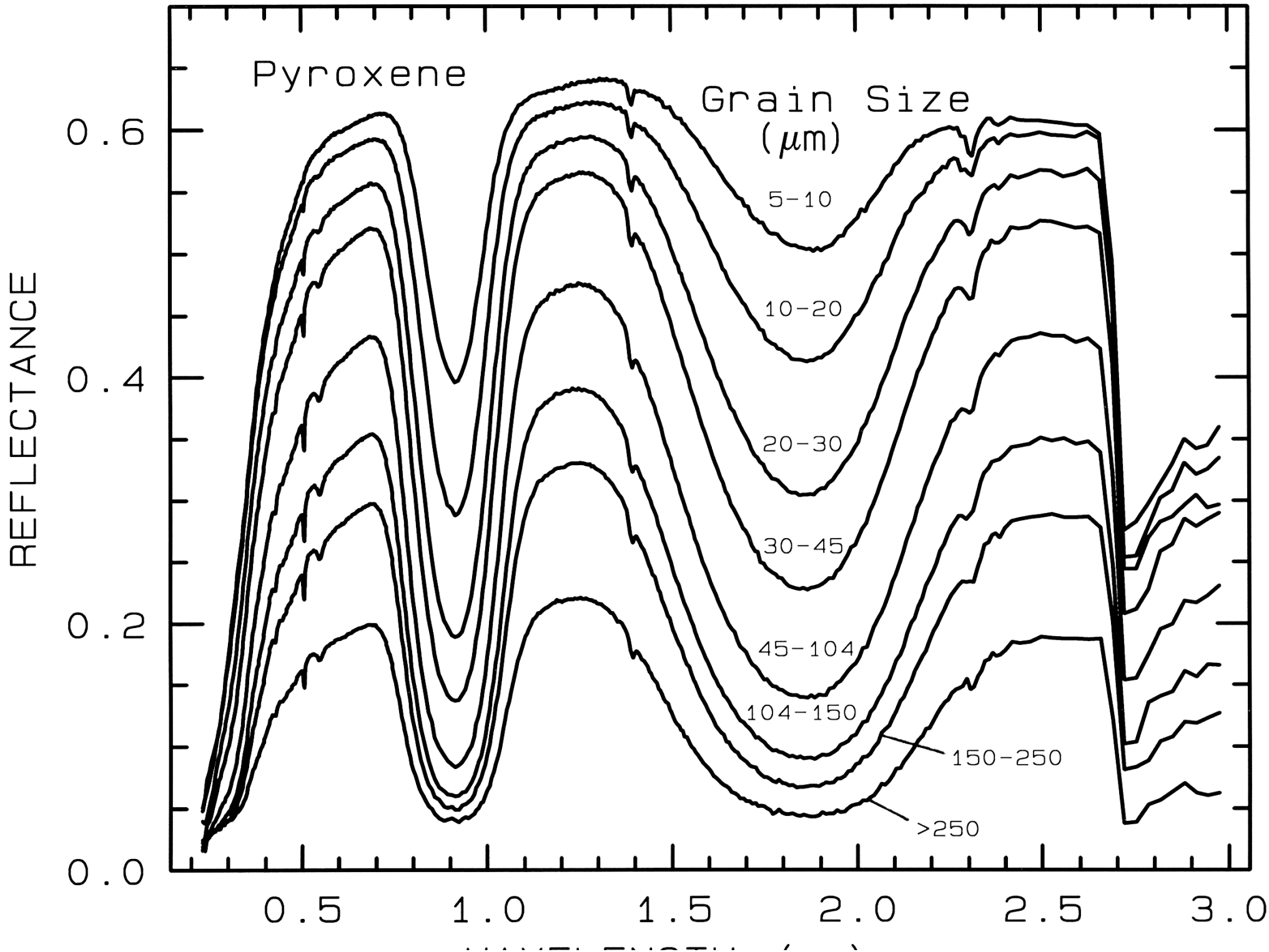
Pyroxene
Grain Size
(μm)
5-10
10-20
20-30
30-45
45-104
104-150
150-250
>250
REFLECTANCE
0.0
0.2
0.4
0.6
0.5
1.0
1.5
2.0
2.5
3.0

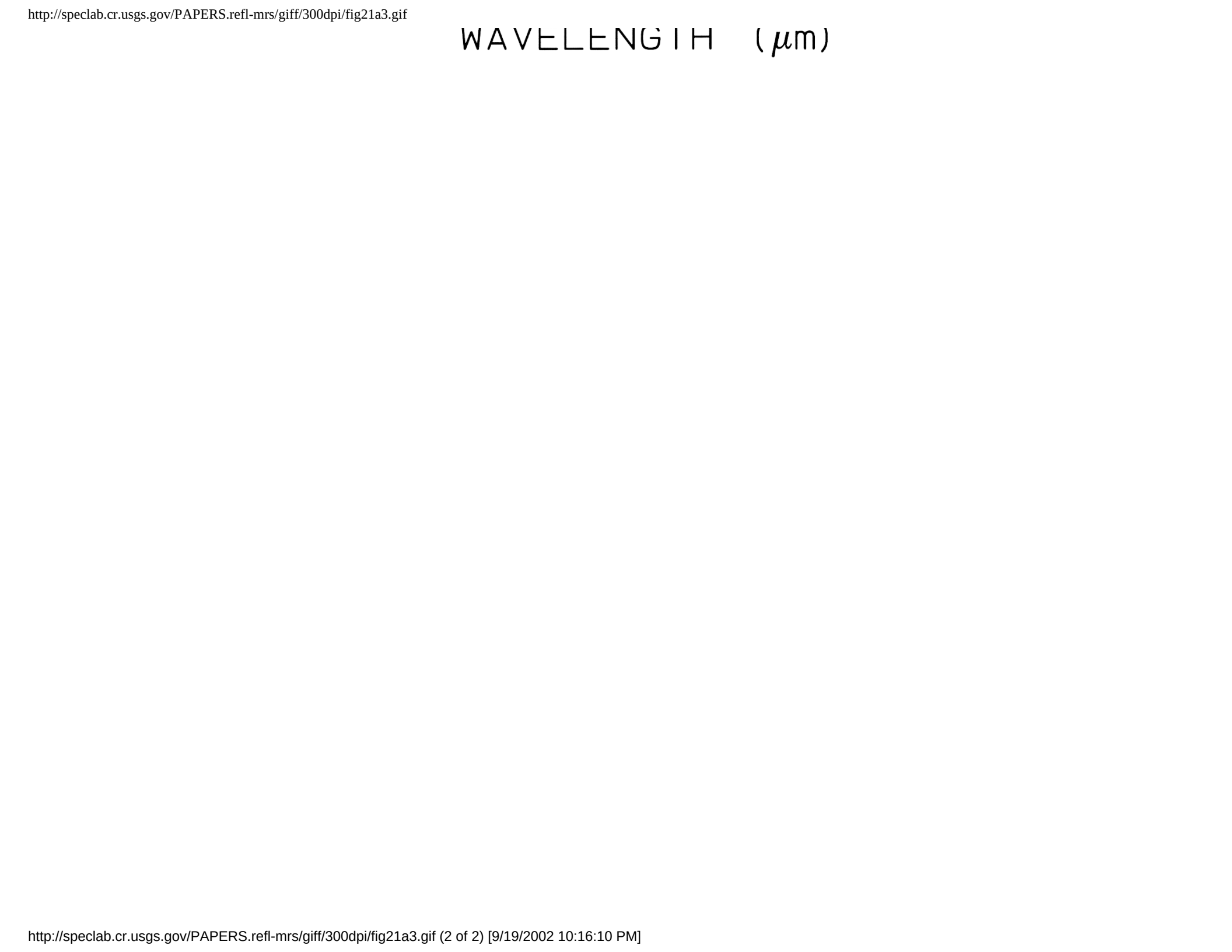
WAVELENGTH (μm)

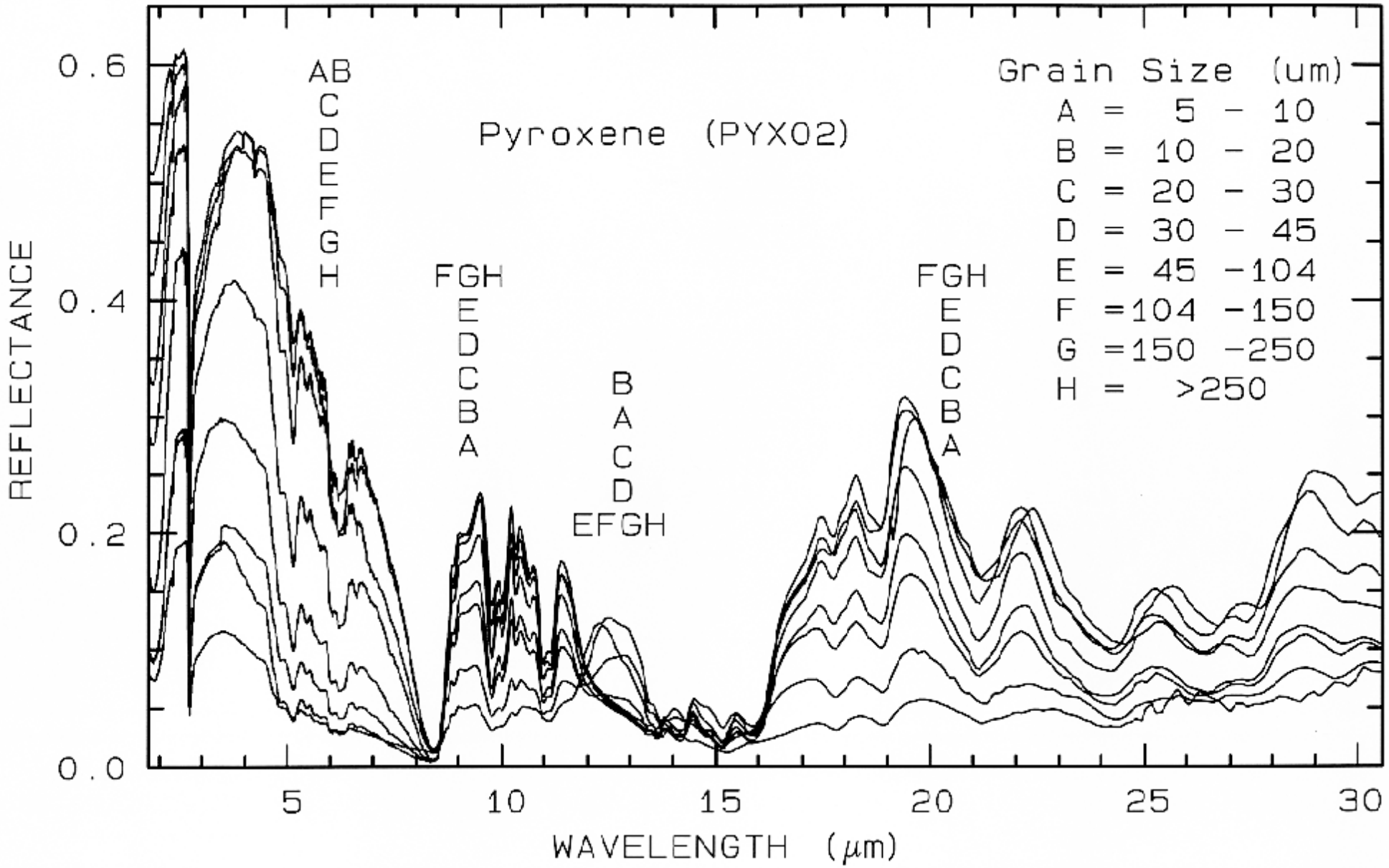
Pyroxene (PYX02)
Grain Size (um)
A = 5 - 10
B = 10 - 20
C = 20 - 30
D = 30 - 45
E = 45 -104
F =104 -150
G =150 -250
H = >250
AB
C
D
E
F
G
H
FGH
E
D
C
B
A
B
A
C
D
EFGH
FGH
E
D
C
B
A
REFLECTANCE
0.0
0.2
0.4
0.6
5
10
15
20
25
30
WAVELENGTH (μm)

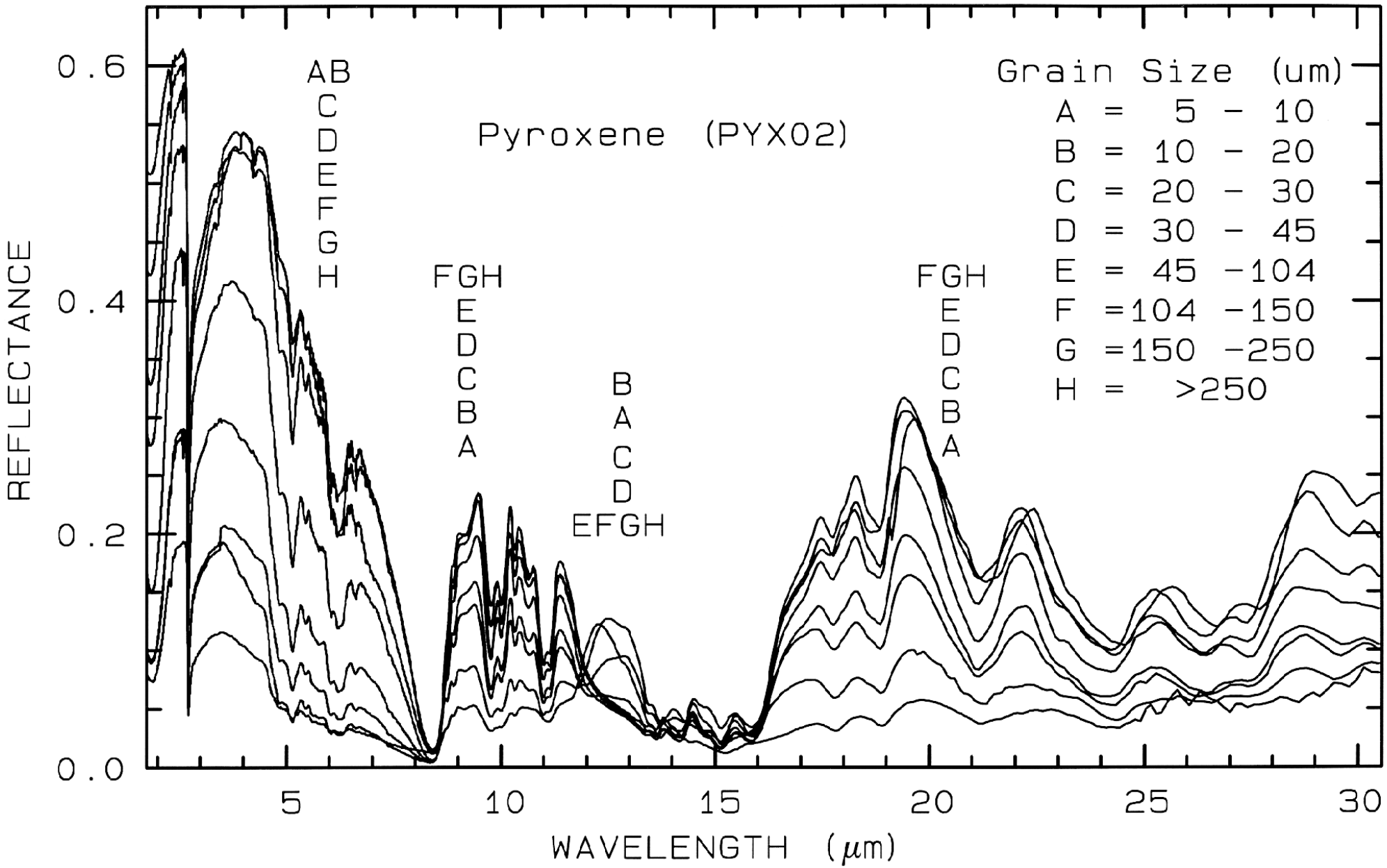
Pyroxene (PYX02)
Grain Size (um)
A = 5 - 10
B = 10 - 20
C = 20 - 30
D = 30 - 45
E = 45 -104
F =104 -150
G =150 -250
H = >250
AB
C
D
E
F
G
H
FGH
E
D
C
B
A
B
A
C
D
EFGH
FGH
E
D
C
B
A
REFLECTANCE
0.0
0.2
0.4
0.6
5
10
15
20
25
30
WAVELENGTH (μm)

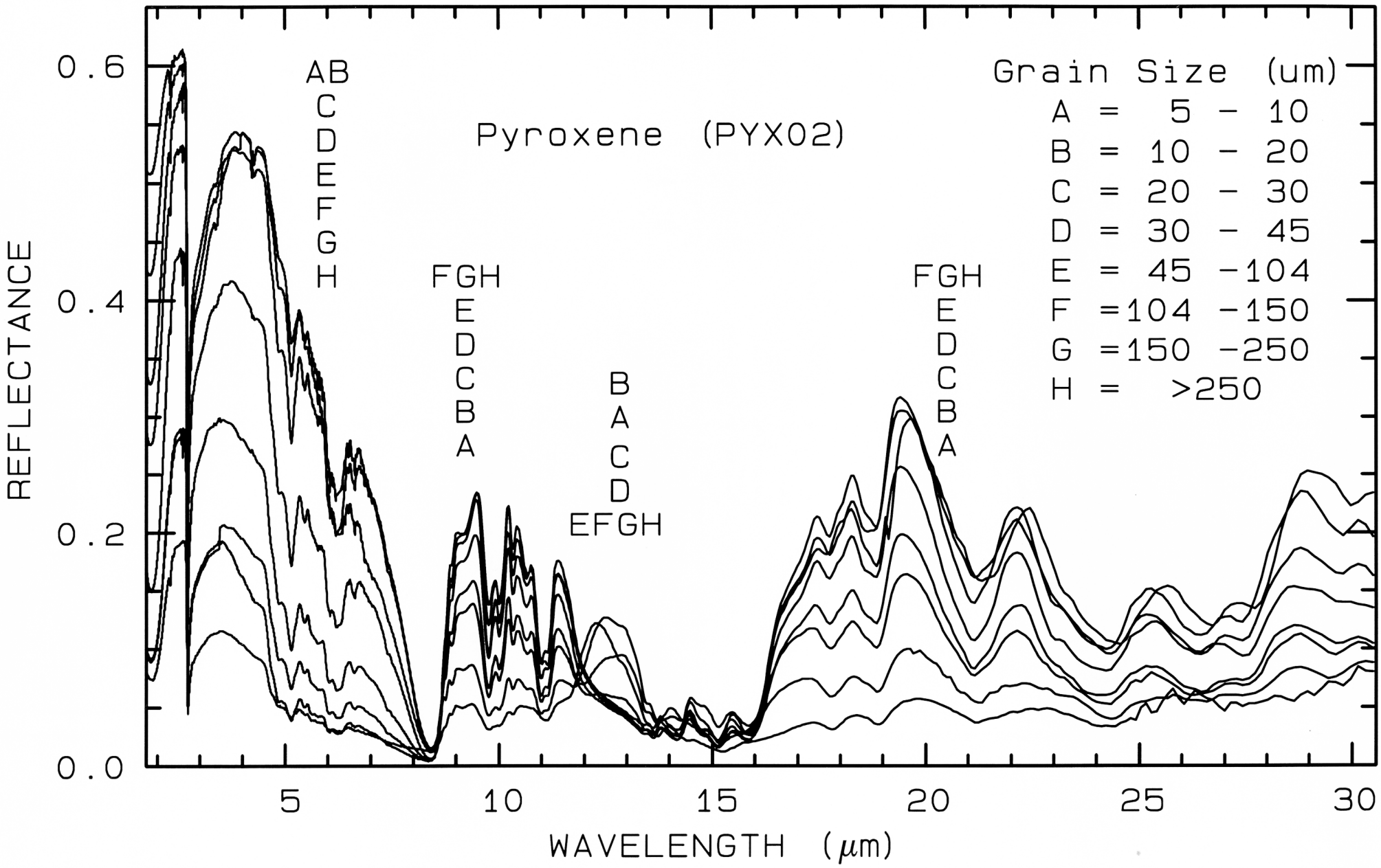
Pyroxene (PYX02)
Grain Size (um)
A = 5 - 10
B = 10 - 20
C = 20 - 30
D = 30 - 45
E = 45 -104
F =104 -150
G =150 -250
H = >250
AB
C
D
E
F
G
H
FGH
E
D
C
B
A
B
A
C
D
EFGH
FGH
E
D
C
B
A
REFLECTANCE
0.0
0.2
0.4
0.6
5
10
15
20
25
30
WAVELENGTH (μm)

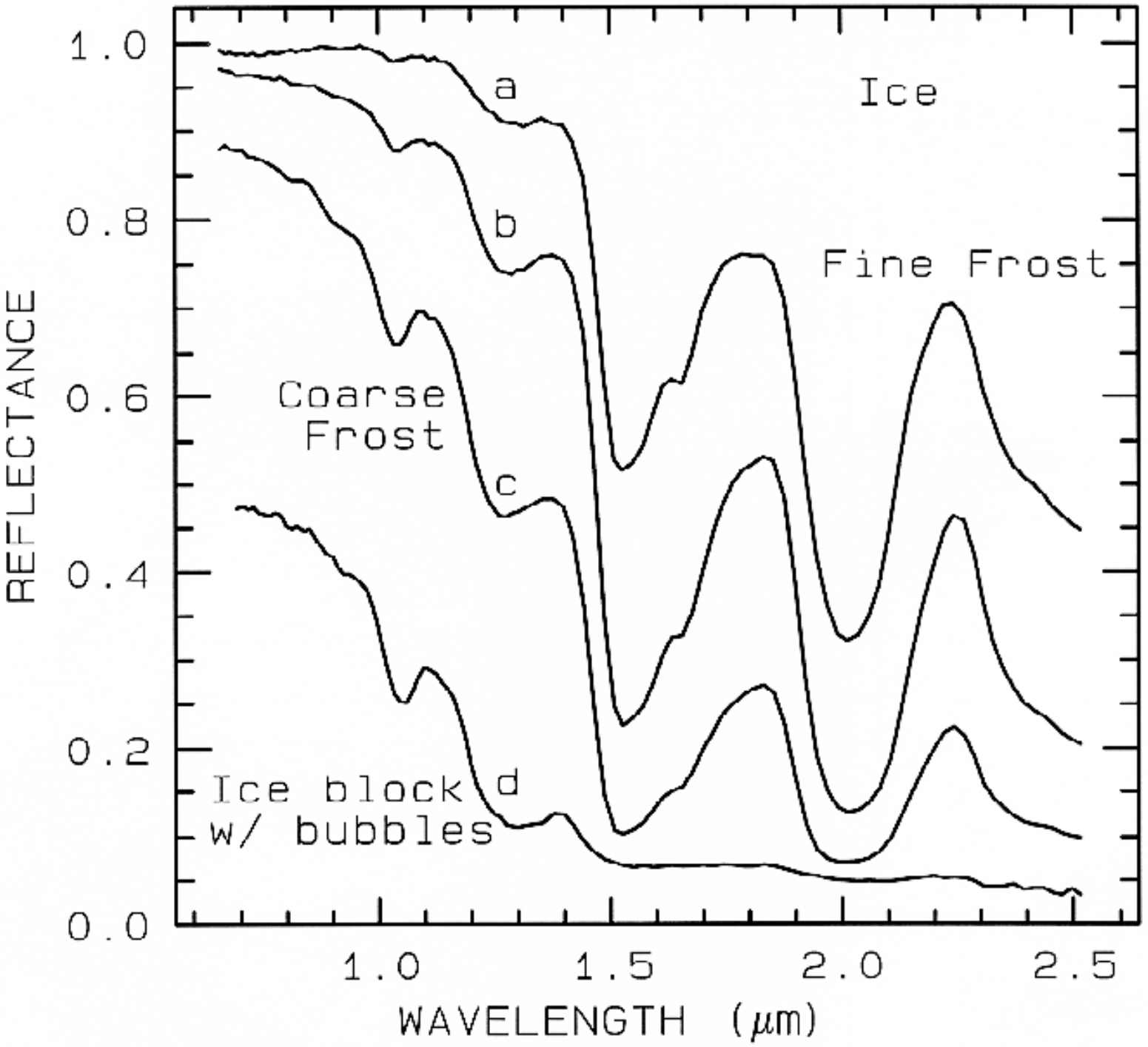
1.0
0.8
0.6
0.4
0.2
0.0
REFLECTANCE
a
Ice
b
Fine Frost
Coarse
Frost
c
Ice block
w/ bubbles
d
1.0
1.5
2.0
2.5
WAVELENGTH (μm)

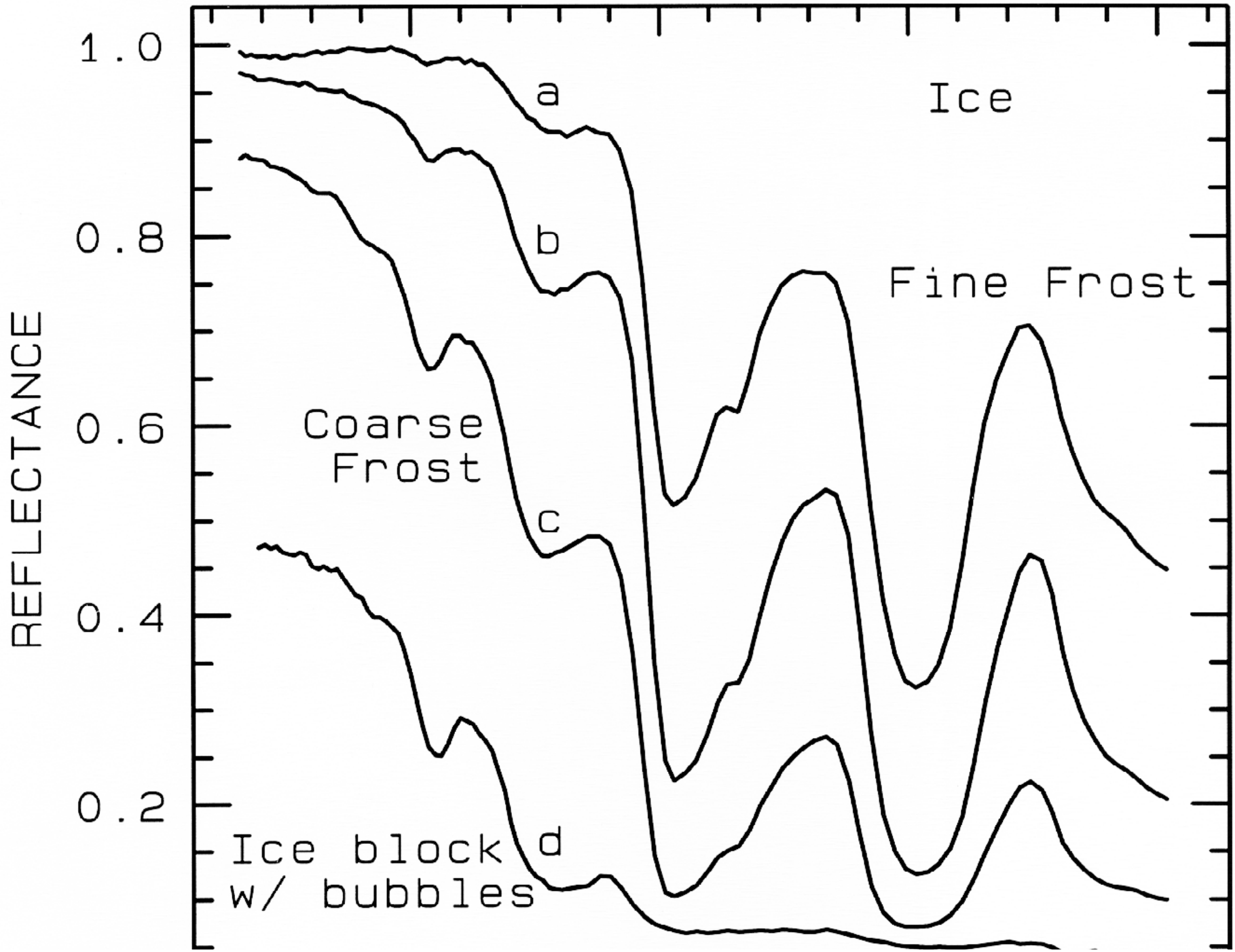
1.0
0.8
0.6
0.4
0.2
REFLECTANCE
a
Ice
b
Fine Frost
Coarse
Frost
c
Ice block
w/ bubbles
d

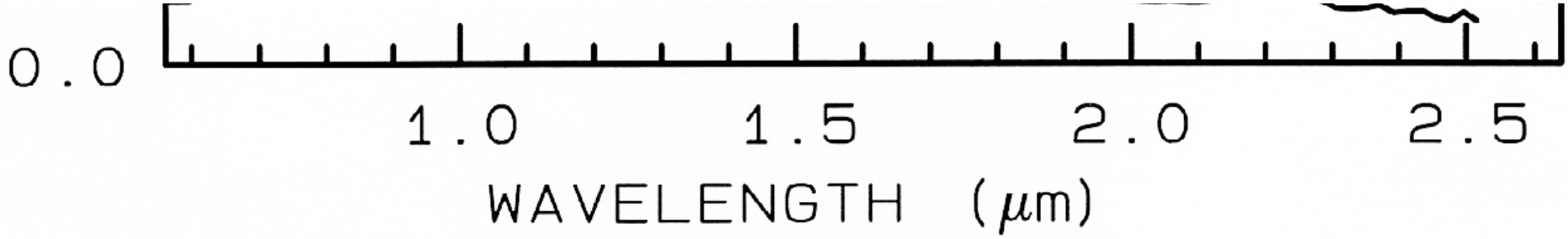
0.0
1.0
1.5
2.0
2.5
WAVELENGTH (μm)

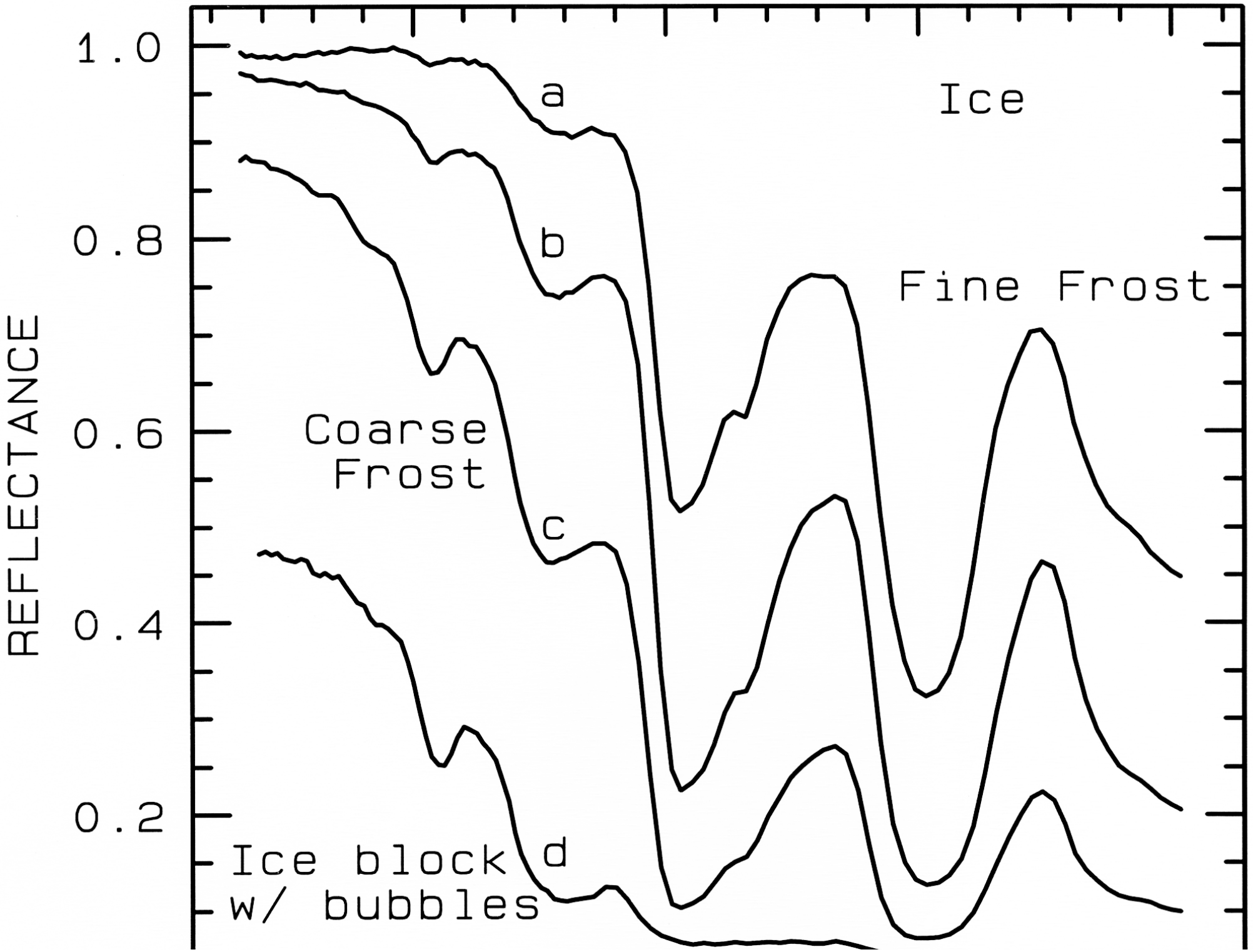
1.0
0.8
0.6
0.4
0.2
REFLECTANCE
a
Ice
b
Fine Frost
Coarse
Frost
c
d
Ice block
w/ bubbles

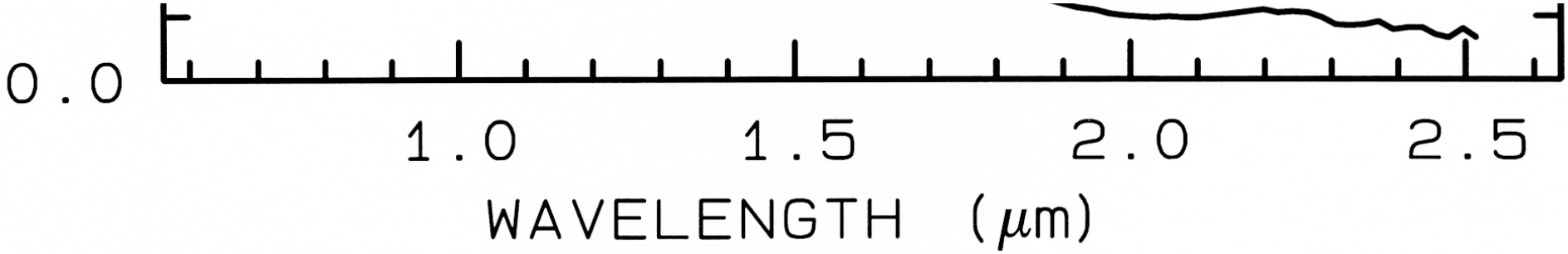
0.0
1.0
1.5
2.0
2.5
WAVELENGTH (μm)

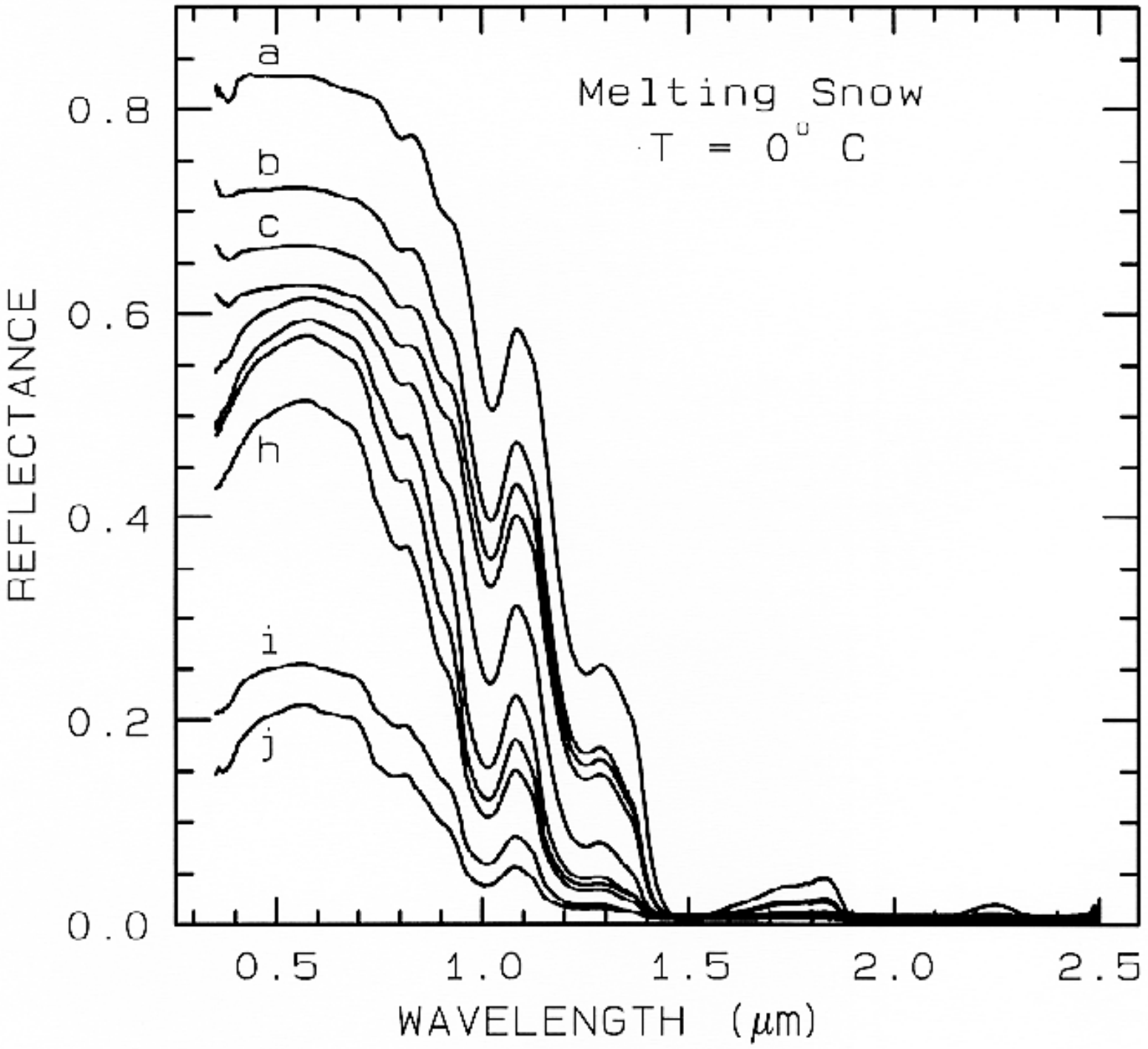
Melting Snow
T = 0° C
a
b
c
h
i
j
REFLECTANCE
0.0
0.2
0.4
0.6
0.8
0.5
1.0
1.5
2.0
2.5
WAVELENGTH (μm)

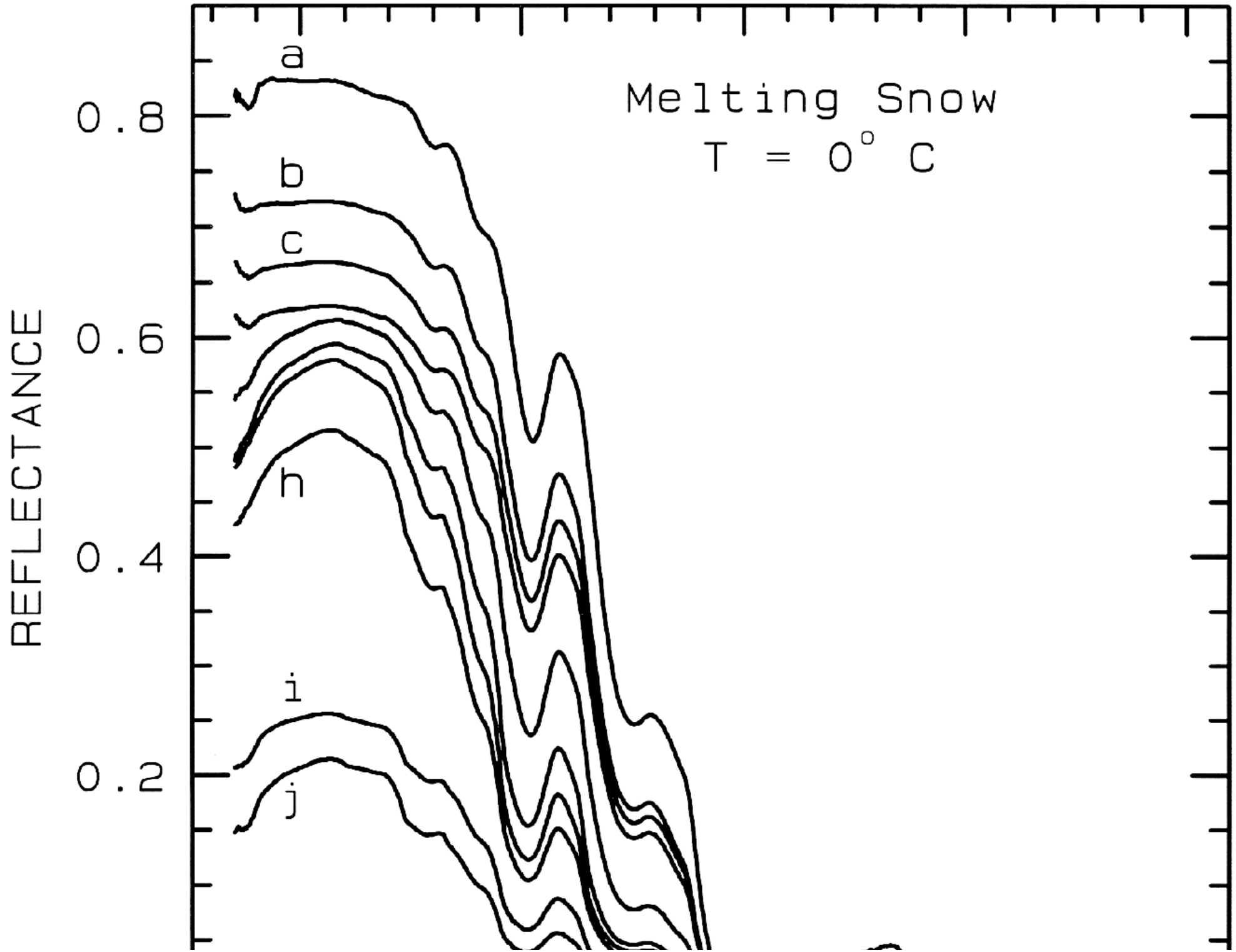
Melting Snow
T = 0° C
REFLECTANCE
0.8
0.6
0.4
0.2
a
b
c
h
i
j


0.0
0.5
1.0
1.5
2.0
2.5
WAVELENGTH (μm)

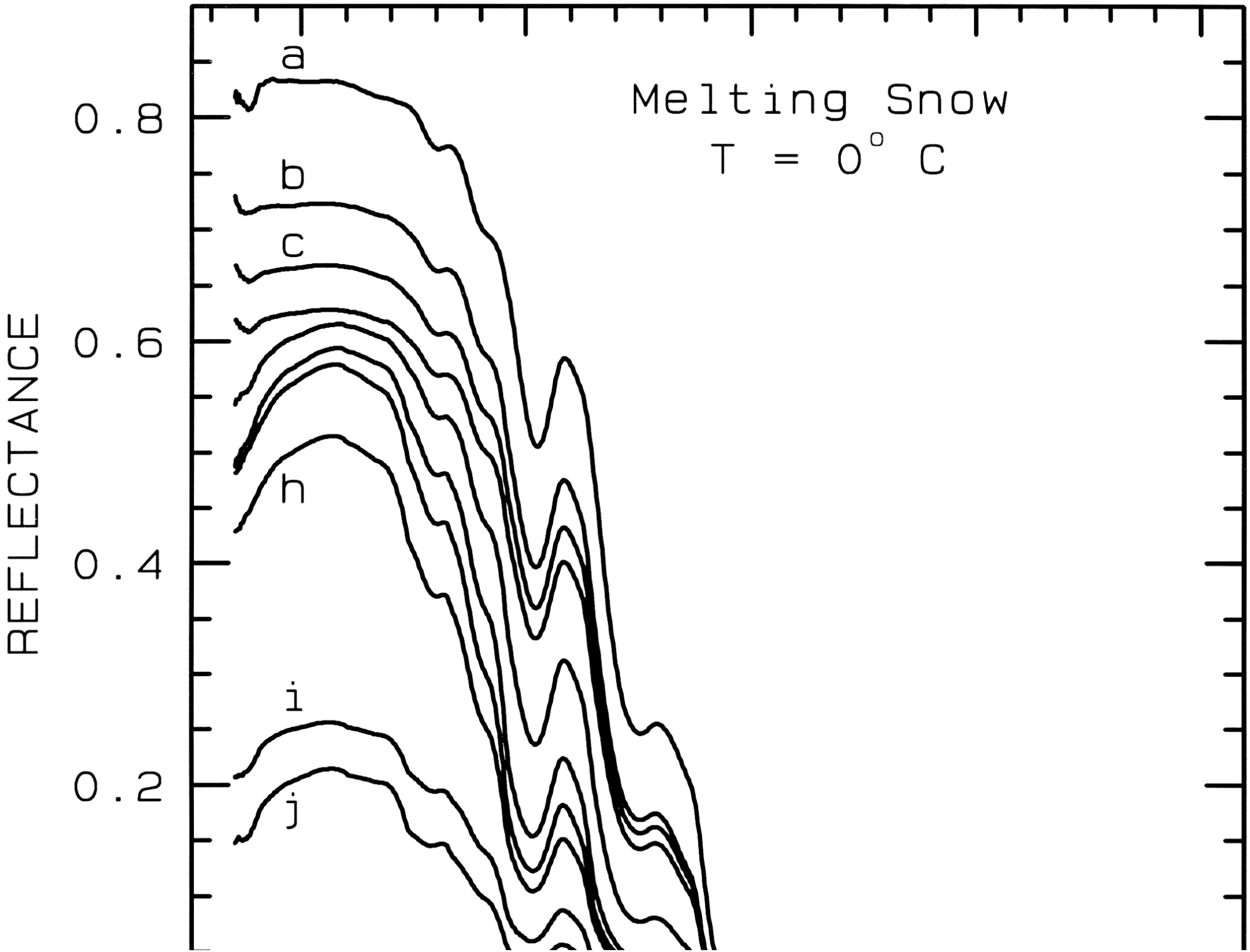
Melting Snow
T = 0° C
REFLECTANCE
0.8
0.6
0.4
0.2
a
b
c
h
i
j


0.0
0.5
1.0
1.5
2.0
2.5
WAVELENGTH (μm)

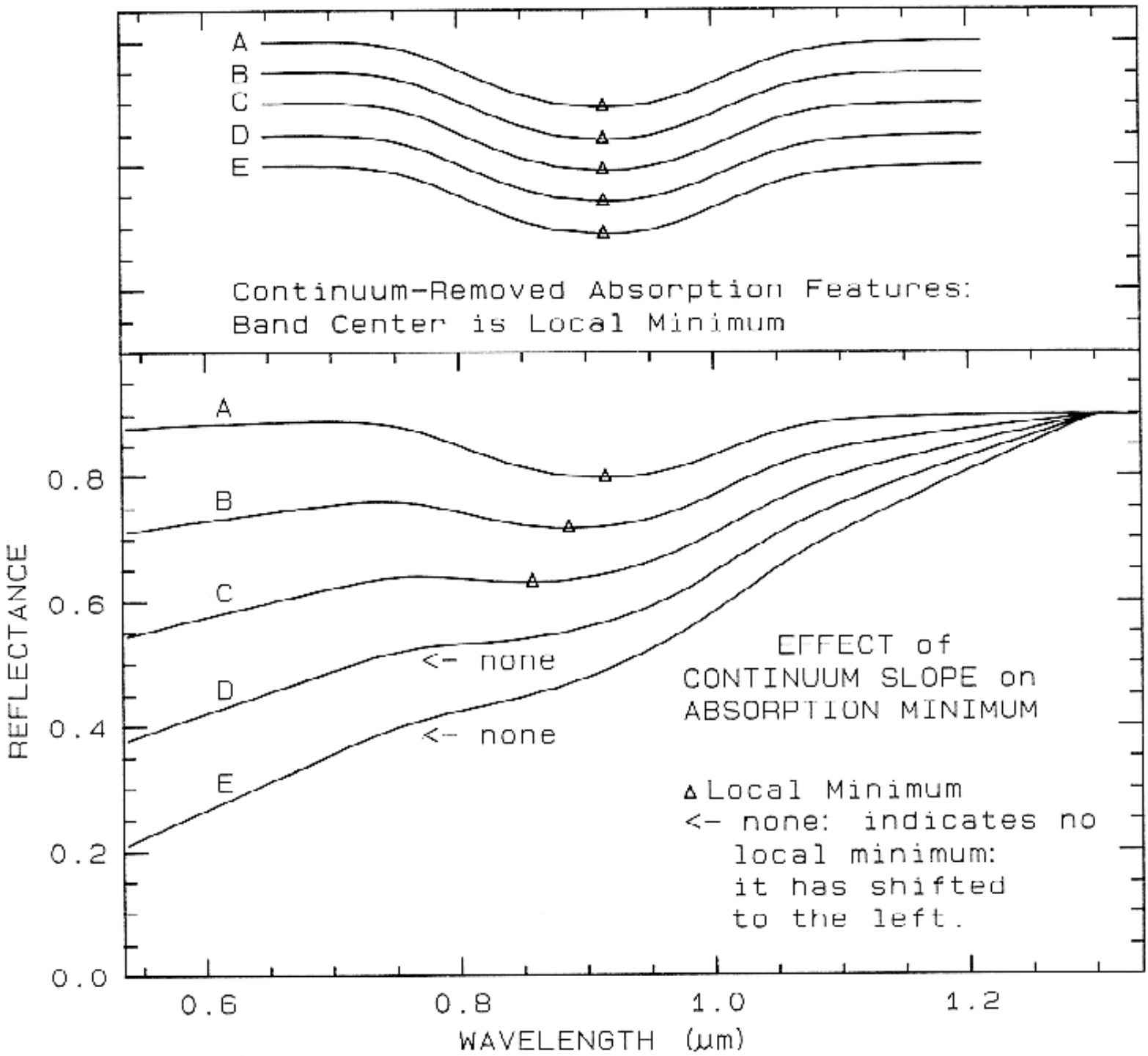
A
B
C
D
E
Continuum-Removed Absorption Features:
Band Center is Local Minimum
A
B
C
D
E
<- none
<- none
EFFECT of
CONTINUUM SLOPE on
ABSORPTION MINIMUM
Δ Local Minimum
<- none: indicates no
local minimum:
it has shifted
to the left.
REFLECTANCE
0.0
0.2
0.4
0.6
0.8
0.6
0.8
1.0
1.2
WAVELENGTH (μm)

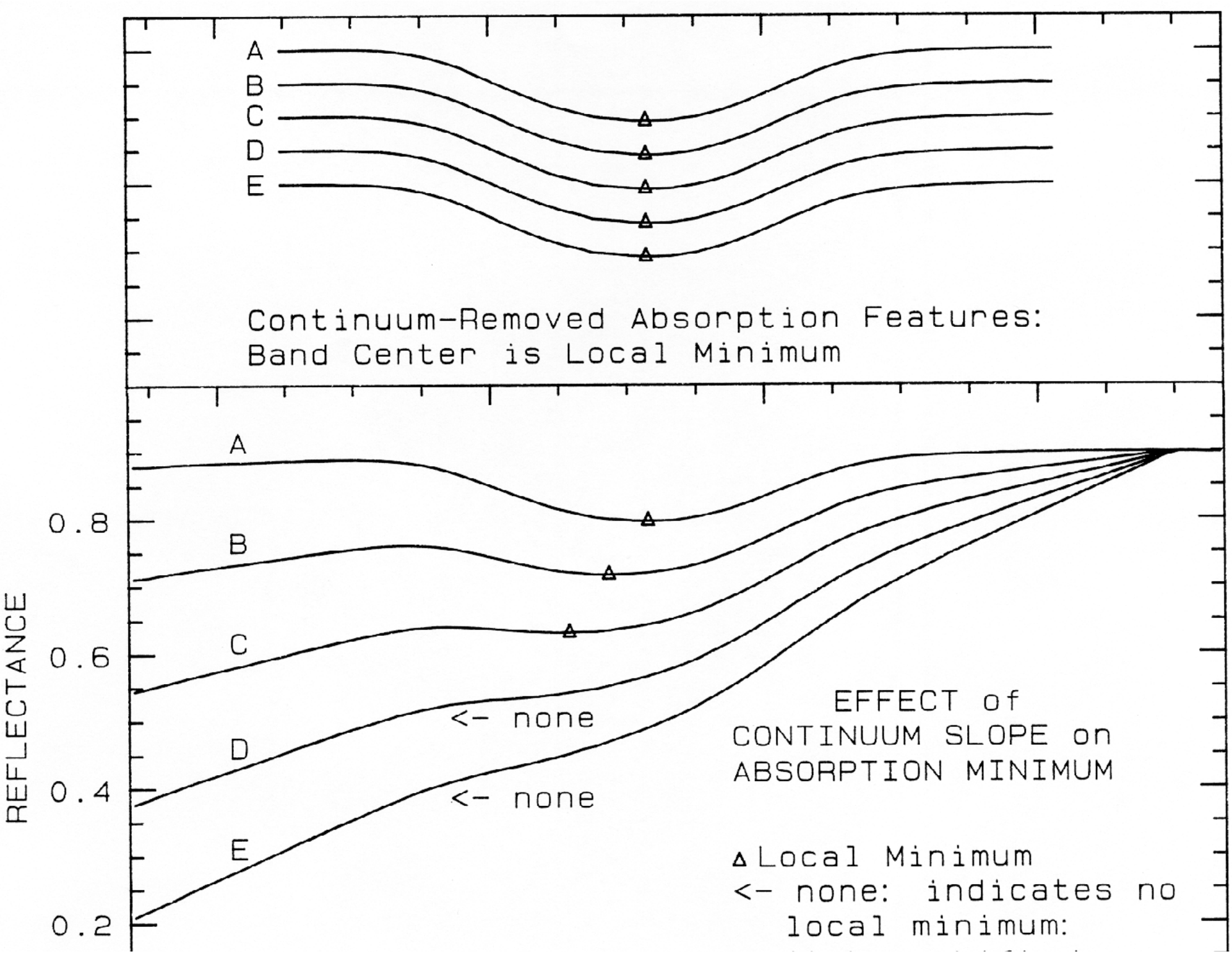
A
B
C
D
E
Continuum-Removed Absorption Features:
Band Center is Local Minimum
A
B
C
D
E
0.8
0.6
0.4
0.2
REFLECTANCE
<- none
<- none
EFFECT of
CONTINUUM SLOPE on
ABSORPTION MINIMUM
Δ Local Minimum
<- none: indicates no
local minimum:

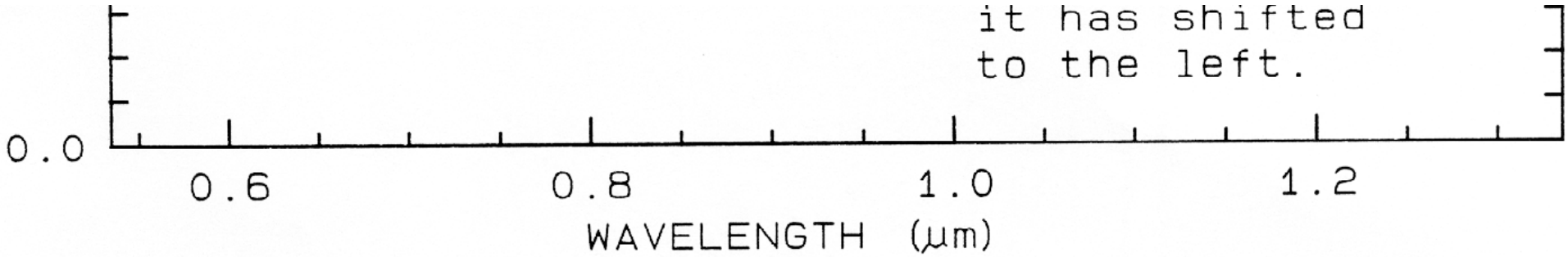
it has shifted
to the left.
0.0
0.6
0.8
1.0
1.2
WAVELENGTH (μm)

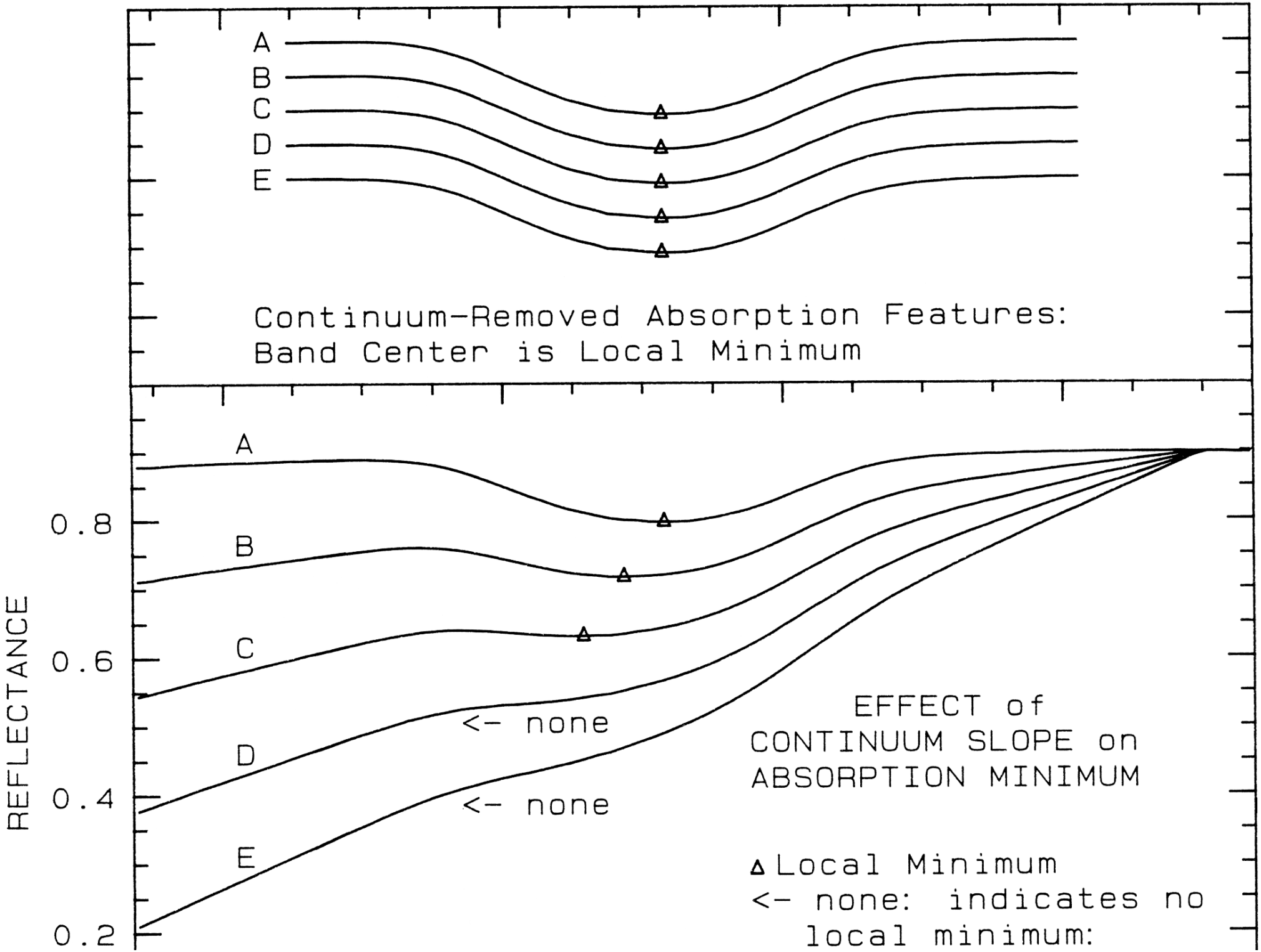
A
B
C
D
E
Continuum-Removed Absorption Features:
Band Center is Local Minimum
A
B
C
D
E
0.8
0.6
0.4
0.2
REFLECTANCE
<- none
<- none
EFFECT of
CONTINUUM SLOPE on
ABSORPTION MINIMUM
Δ Local Minimum
<- none: indicates no
local minimum:

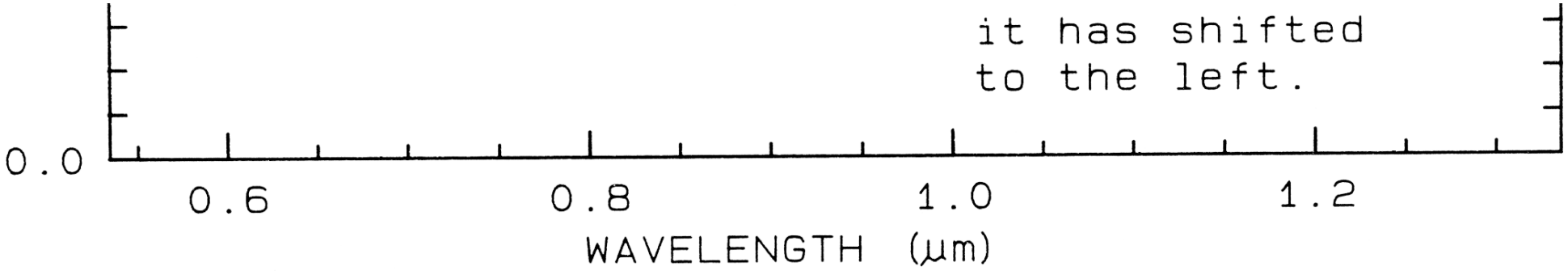
it has shifted
to the left.
0.0
0.6
0.8
1.0
1.2
WAVELENGTH (μm)

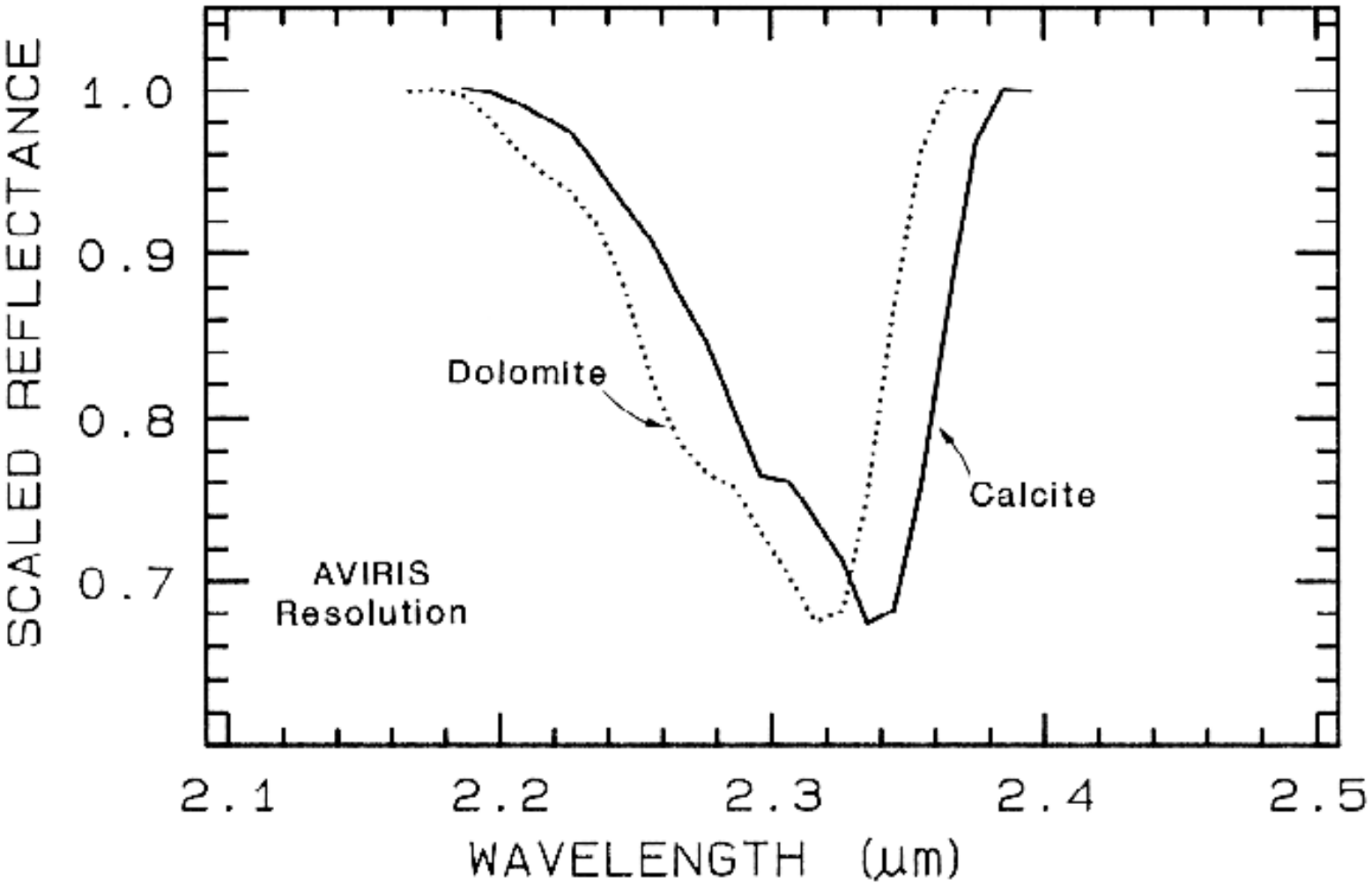
SCALED REFLECTANCE
1.0
0.9
0.8
0.7
Dolomite
Calcite
AVIRIS
Resolution
2.1
2.2
2.3
2.4
2.5
WAVELENGTH (μm)

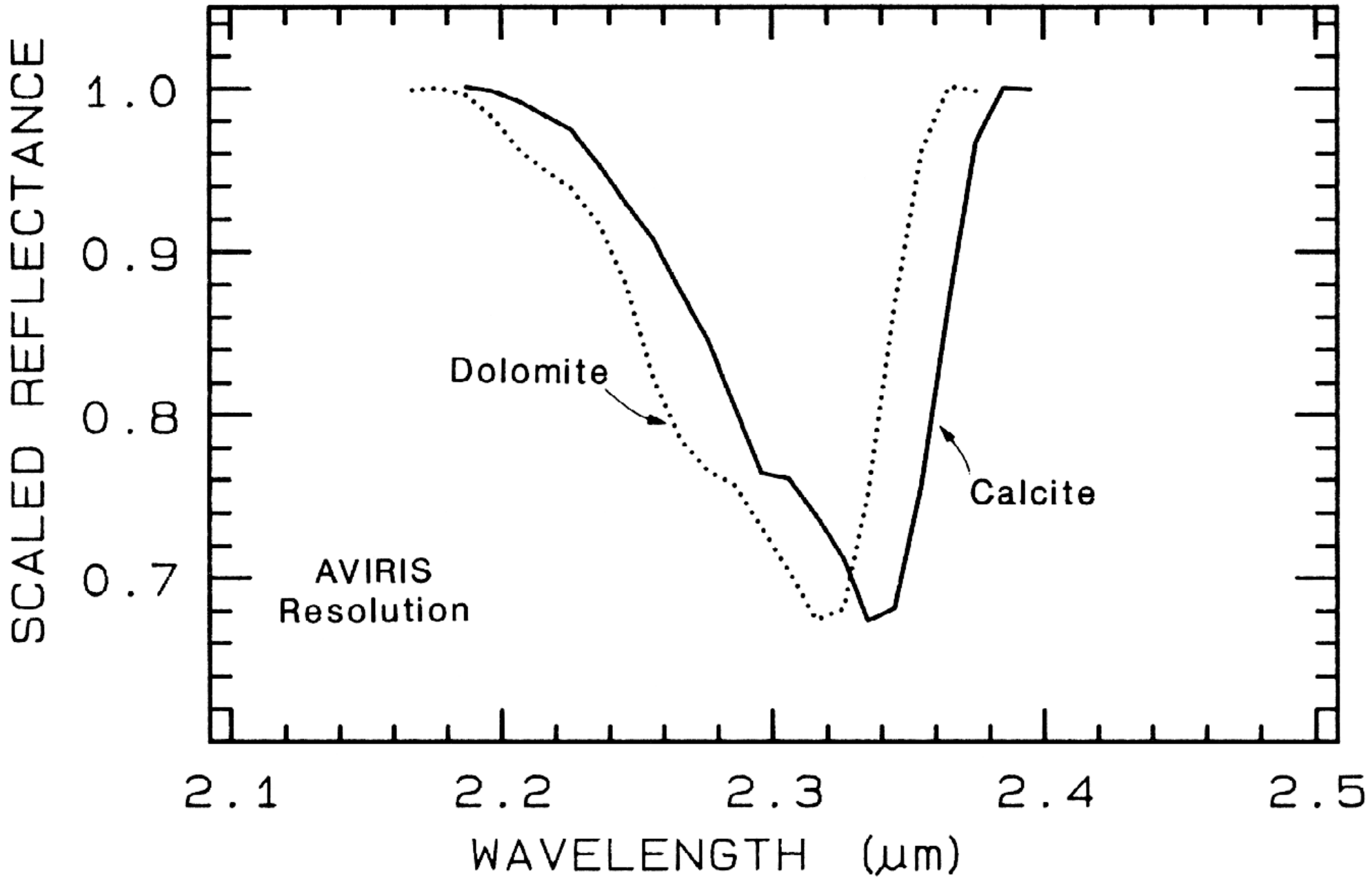
SCALED REFLECTANCE
1.0
0.9
0.8
0.7
Dolomite
Calcite
AVIRIS
Resolution
2.1
2.2
2.3
2.4
2.5
WAVELENGTH (μm)

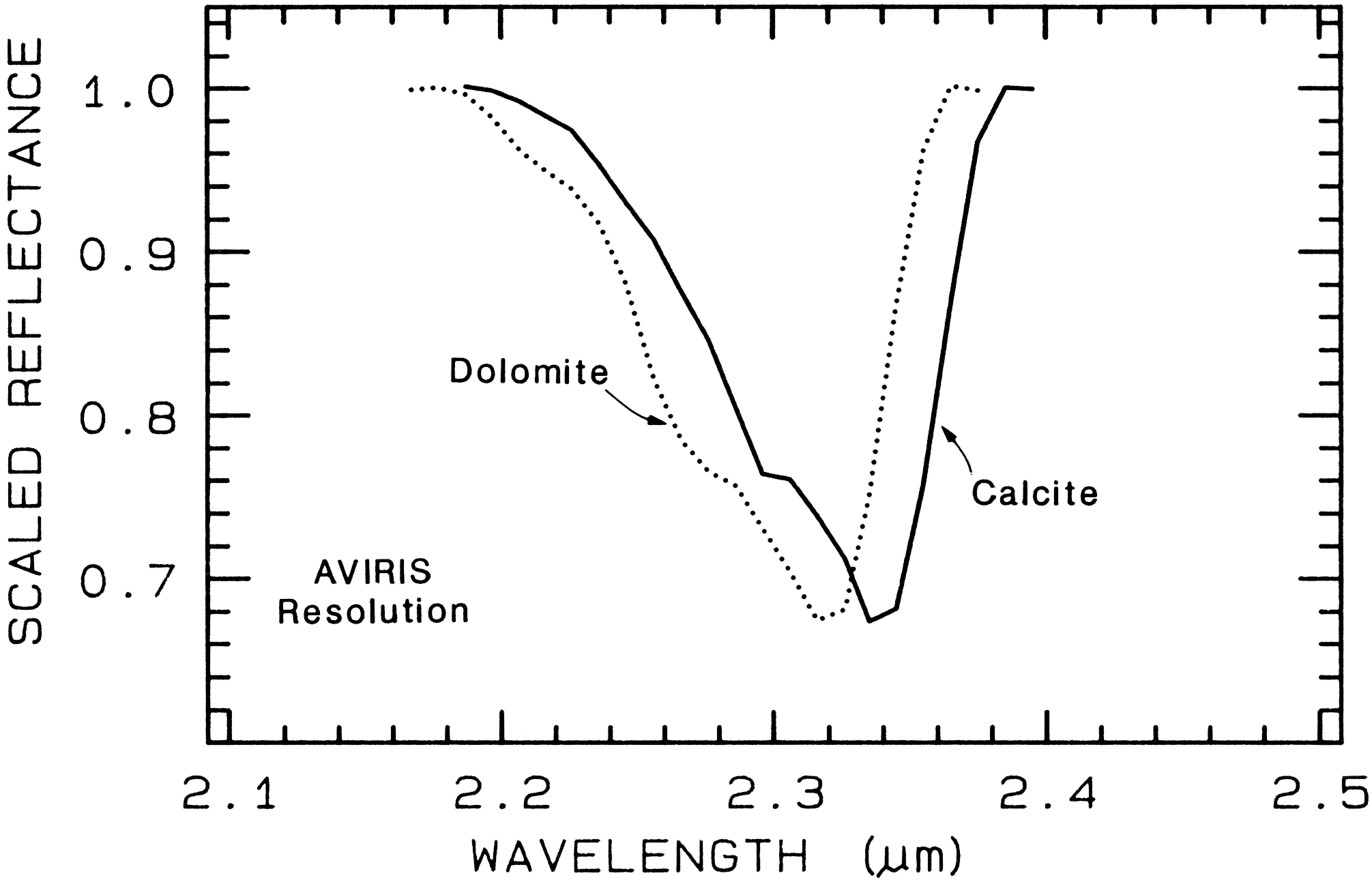
SCALED REFLECTANCE
1.0
0.9
0.8
0.7
Dolomite
Calcite
AVIRIS
Resolution
2.1
2.2
2.3
2.4
2.5
WAVELENGTH (μm)

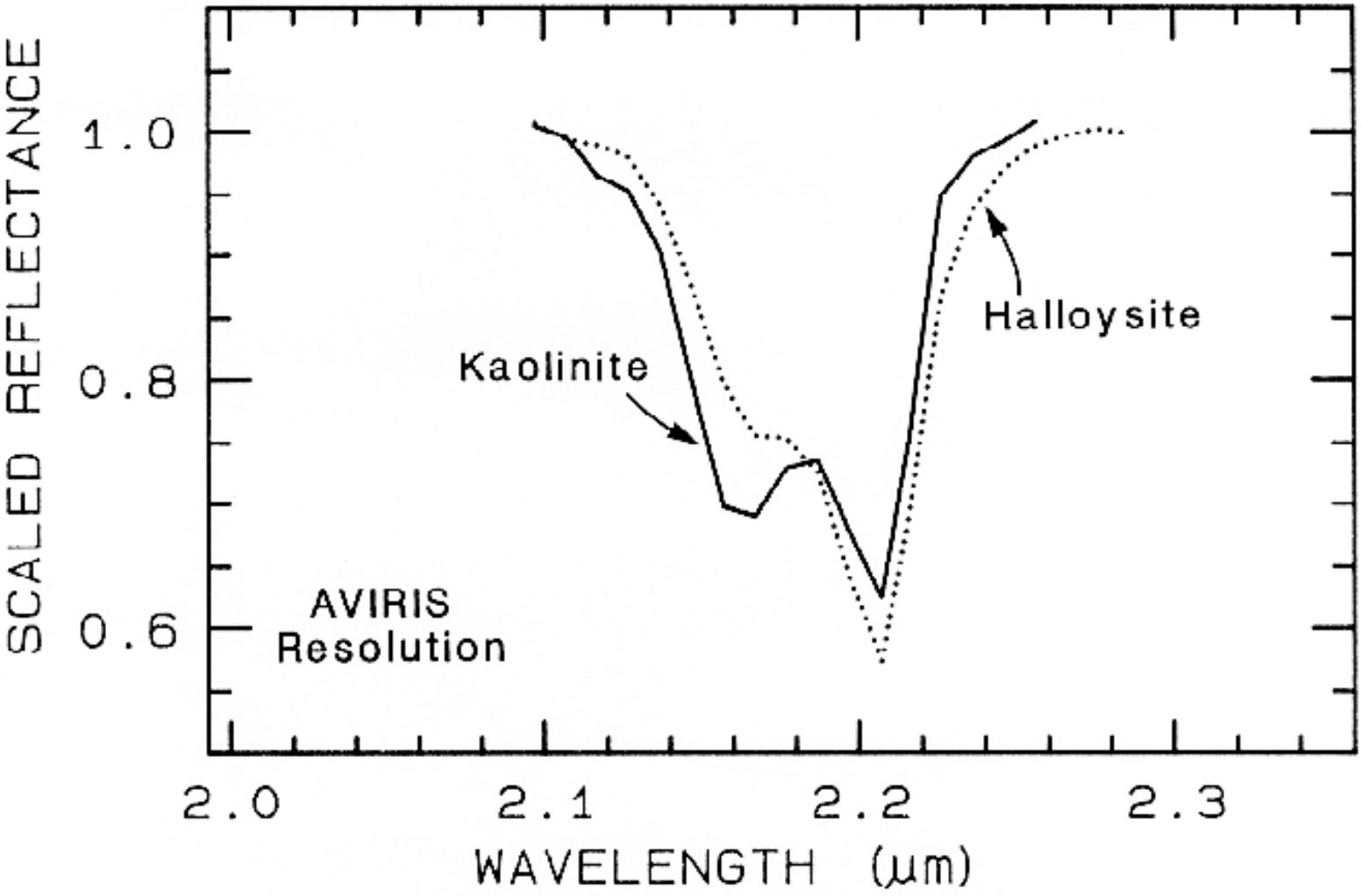
SCALED REFLECTANCE
1.0
0.8
0.6
Kaolinite
Halloysite
AVIRIS
Resolution
2.0
2.1
2.2
2.3
WAVELENGTH (μm)

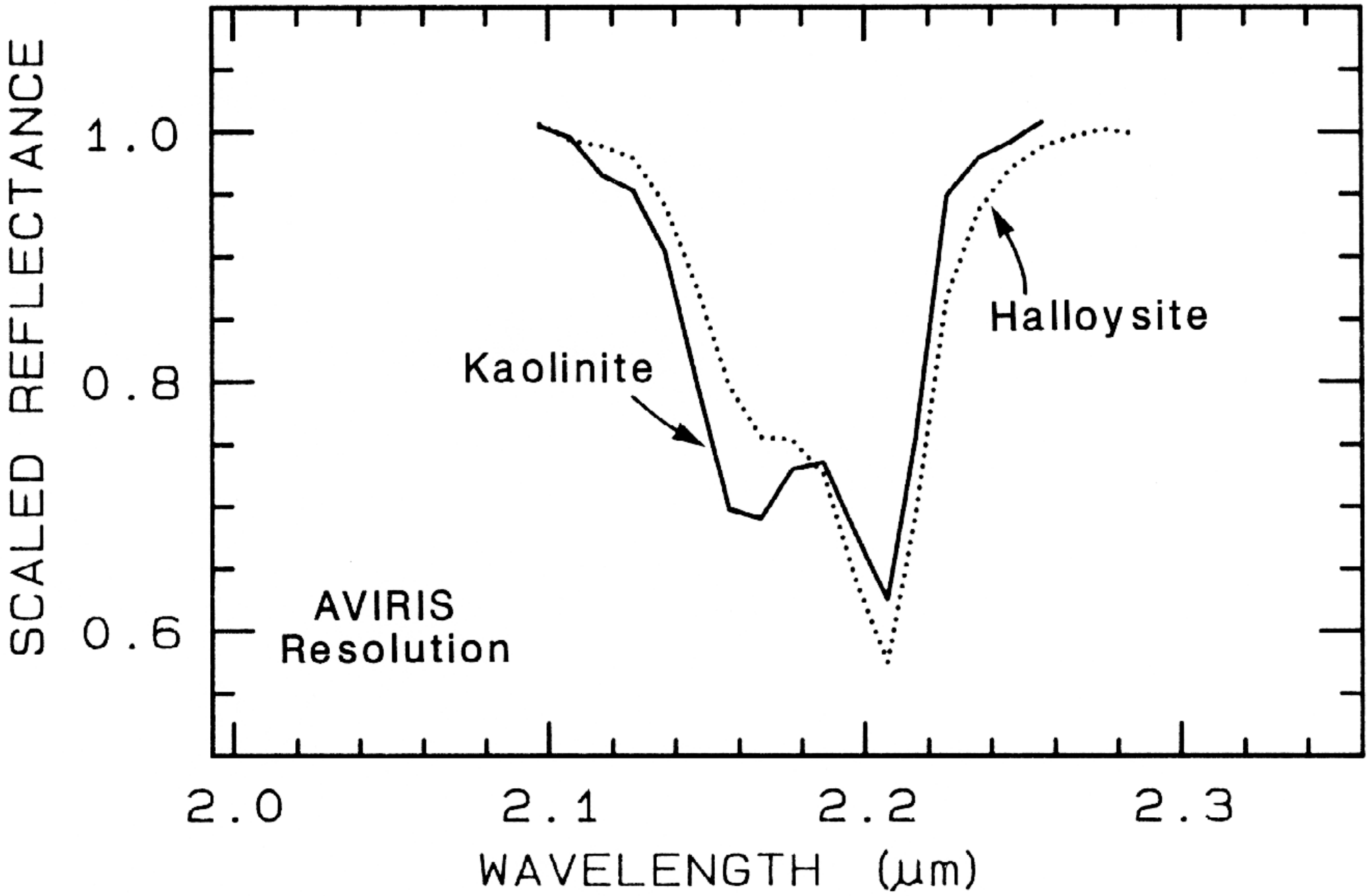
SCALED REFLECTANCE
1.0
0.8
0.6
Kaolinite
Halloysite
AVIRIS
Resolution
2.0
2.1
2.2
2.3
WAVELENGTH (μm)

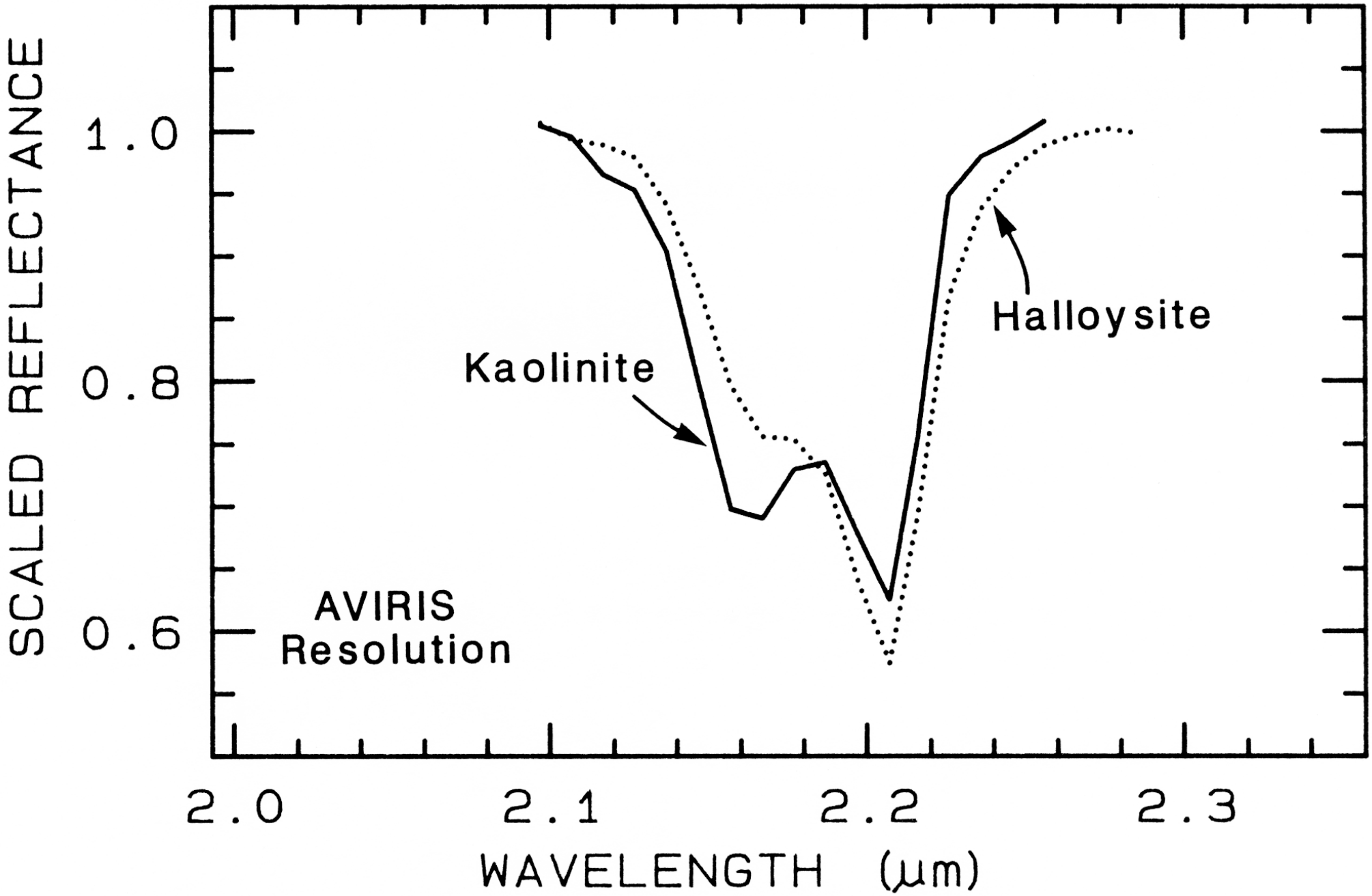
SCALED REFLECTANCE
1.0
0.8
0.6
Kaolinite
Halloysite
AVIRIS
Resolution
2.0
2.1
2.2
2.3
WAVELENGTH (μm)

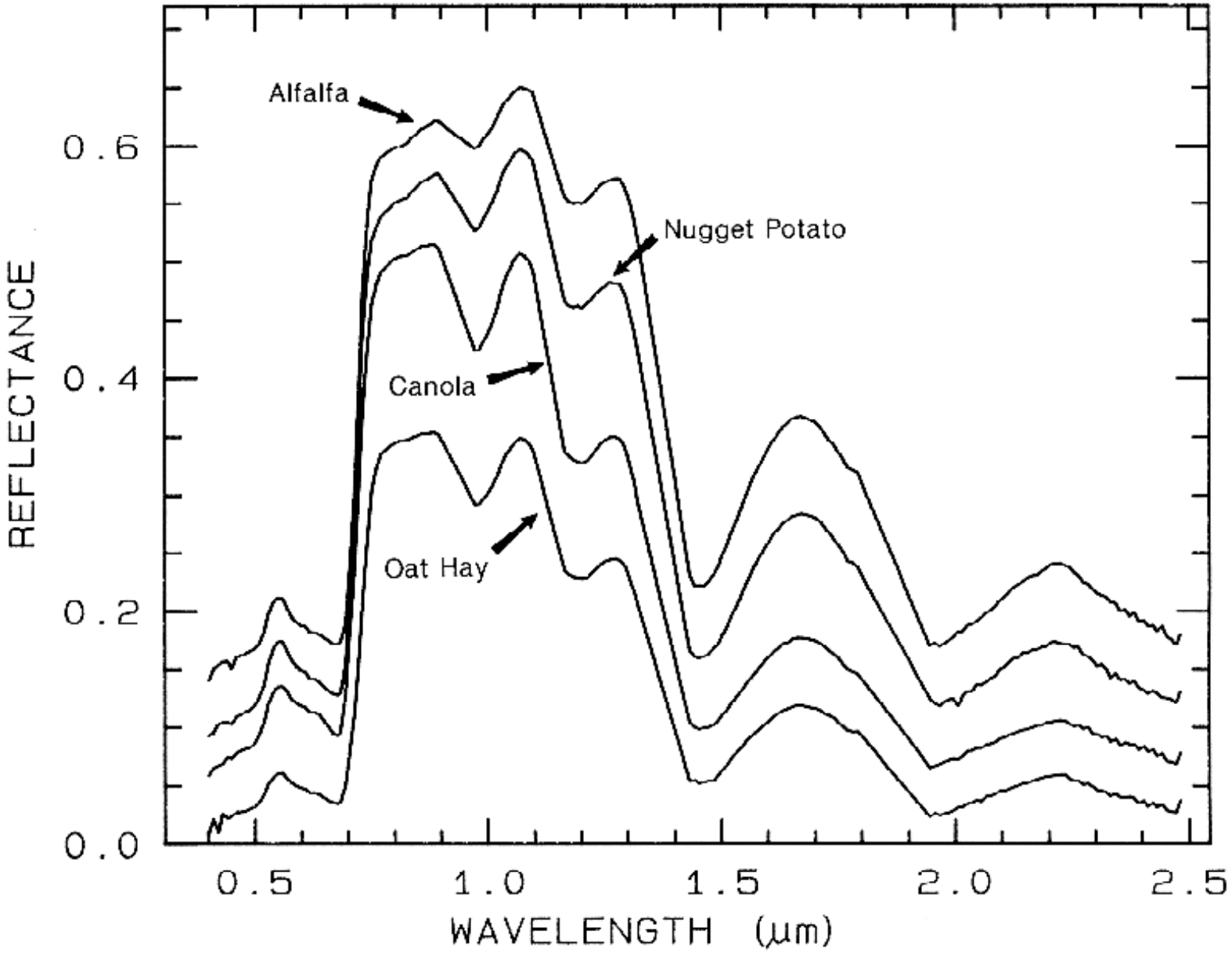
Alfalfa
Nugget Potato
Canola
Oat Hay
REFLECTANCE
0.0
0.2
0.4
0.6
0.5
1.0
1.5
2.0
2.5
WAVELENGTH (μm)

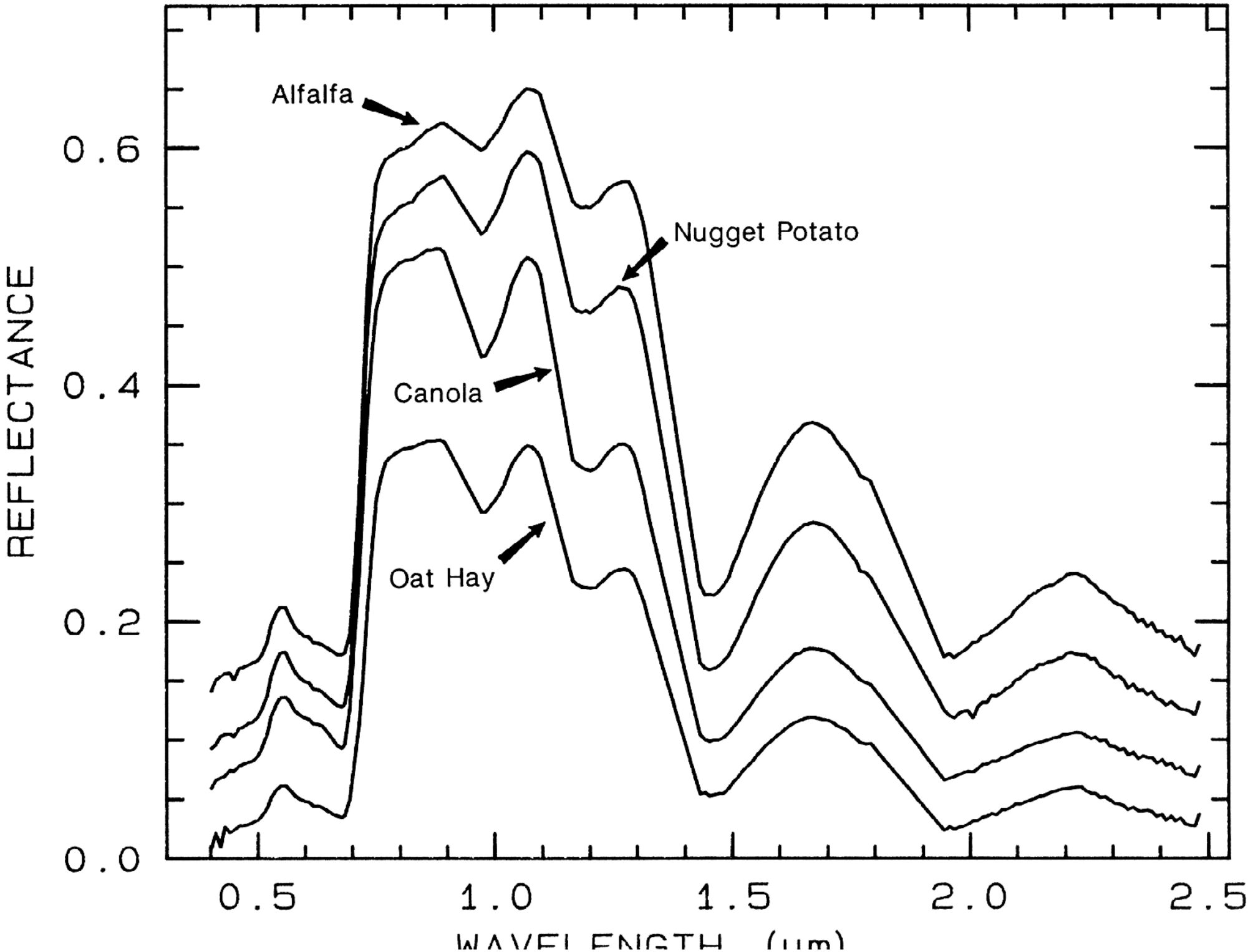
Alfalfa
Nugget Potato
Canola
Oat Hay
REFLECTANCE
0.0
0.2
0.4
0.6
0.5
1.0
1.5
2.0
2.5
WAVELENGTH (µm)


WAVELENGTH (μm)

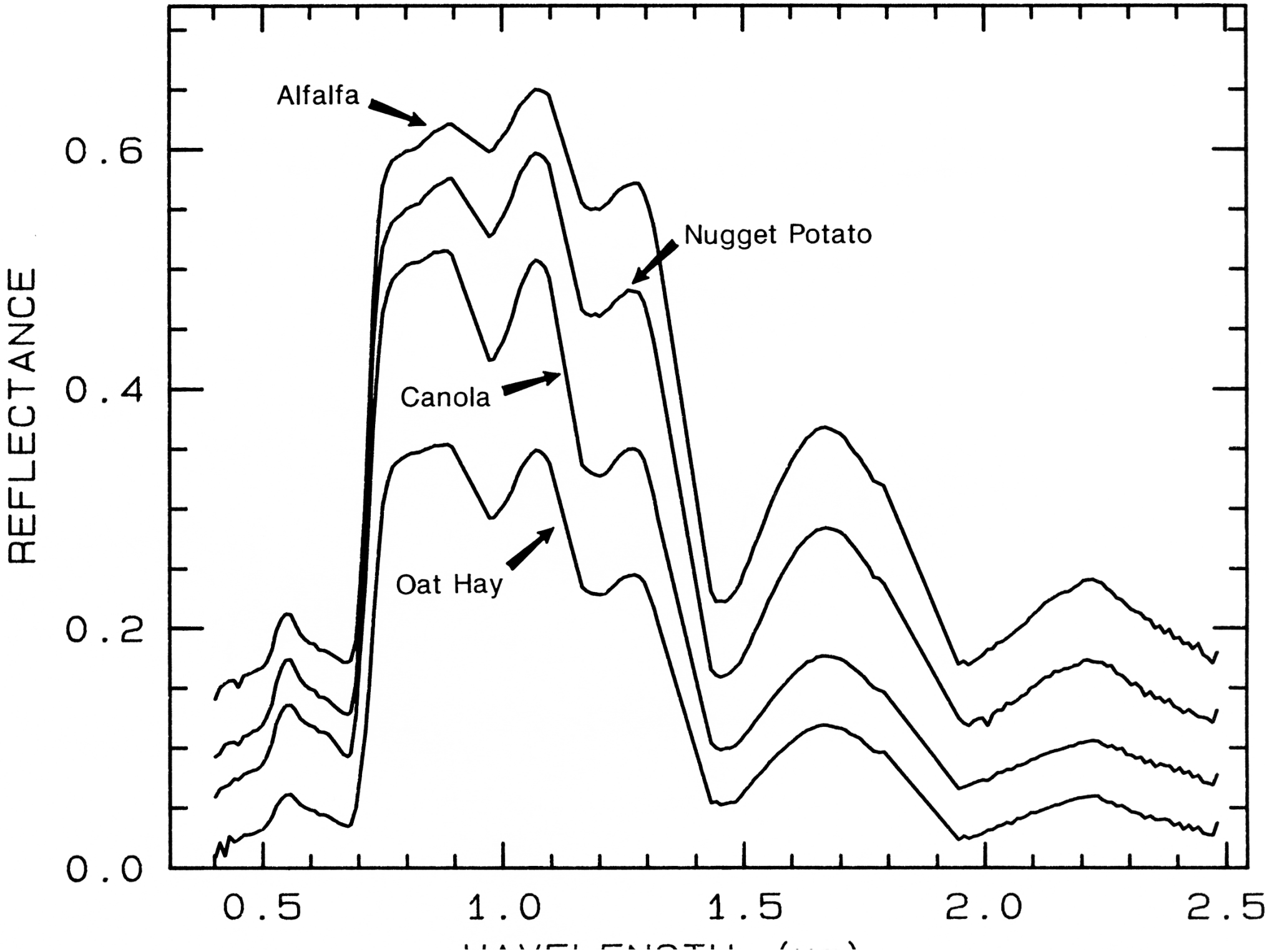
Alfalfa
Nugget Potato
Canola
Oat Hay
REFLECTANCE
0.0
0.2
0.4
0.6
0.5
1.0
1.5
2.0
2.5

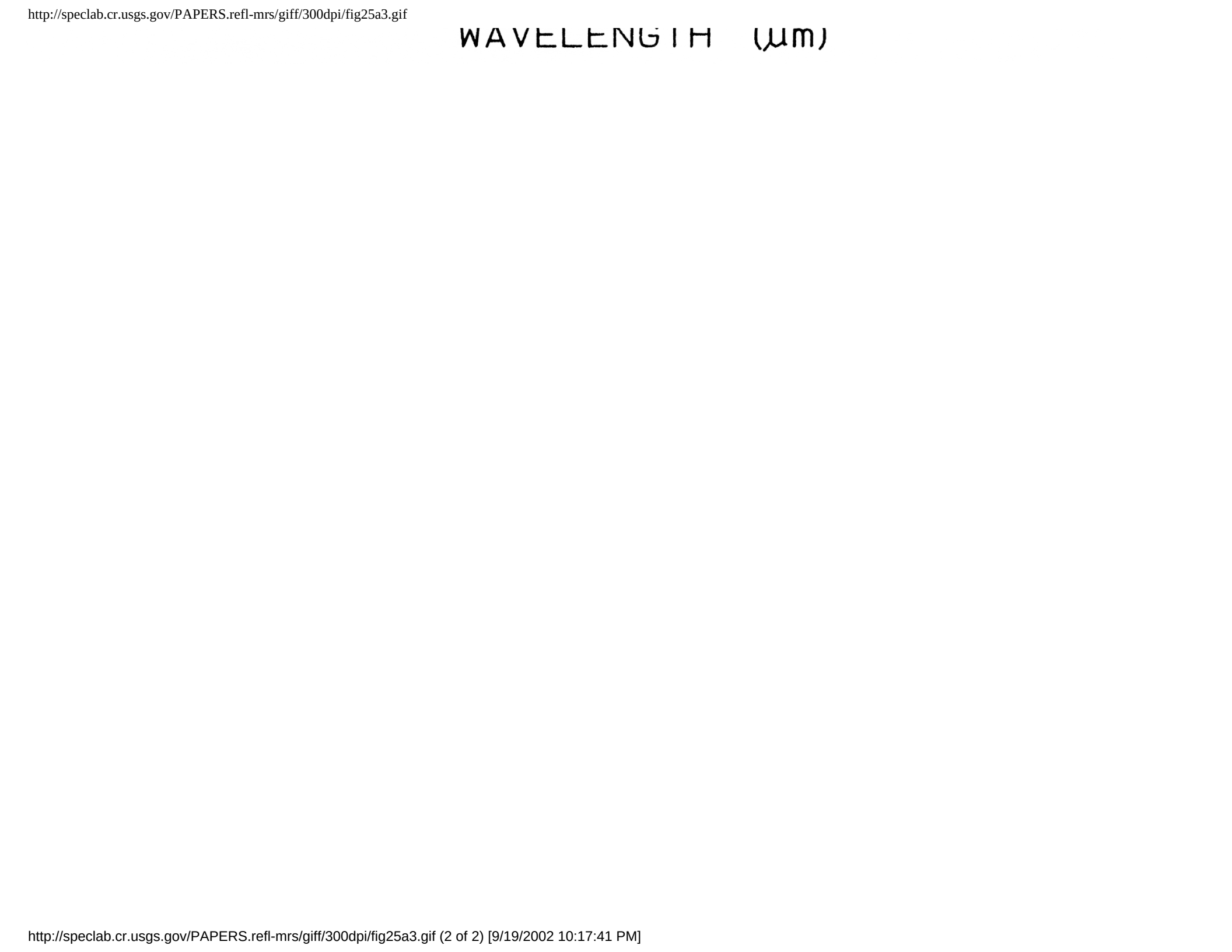
WAVELENGTH (µm)

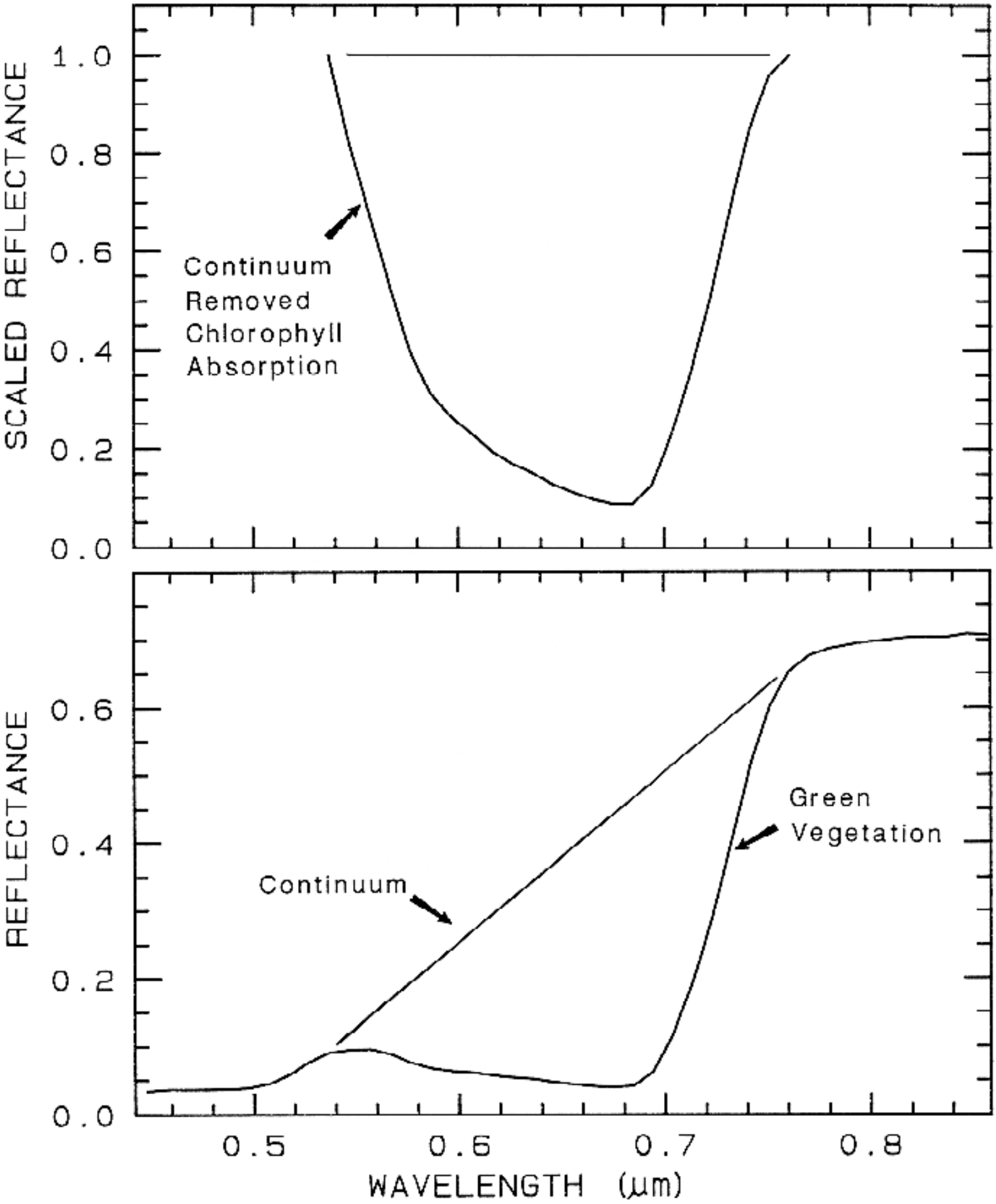
SCALED REFLECTANCE
1.0
0.8
0.6
0.4
0.2
0.0
Continuum
Removed
Chlorophyll
Absorption
REFLECTANCE
0.6
0.4
0.2
0.0
Green
Vegetation
Continuum
0.5
0.6
0.7
0.8
WAVELENGTH (μm)

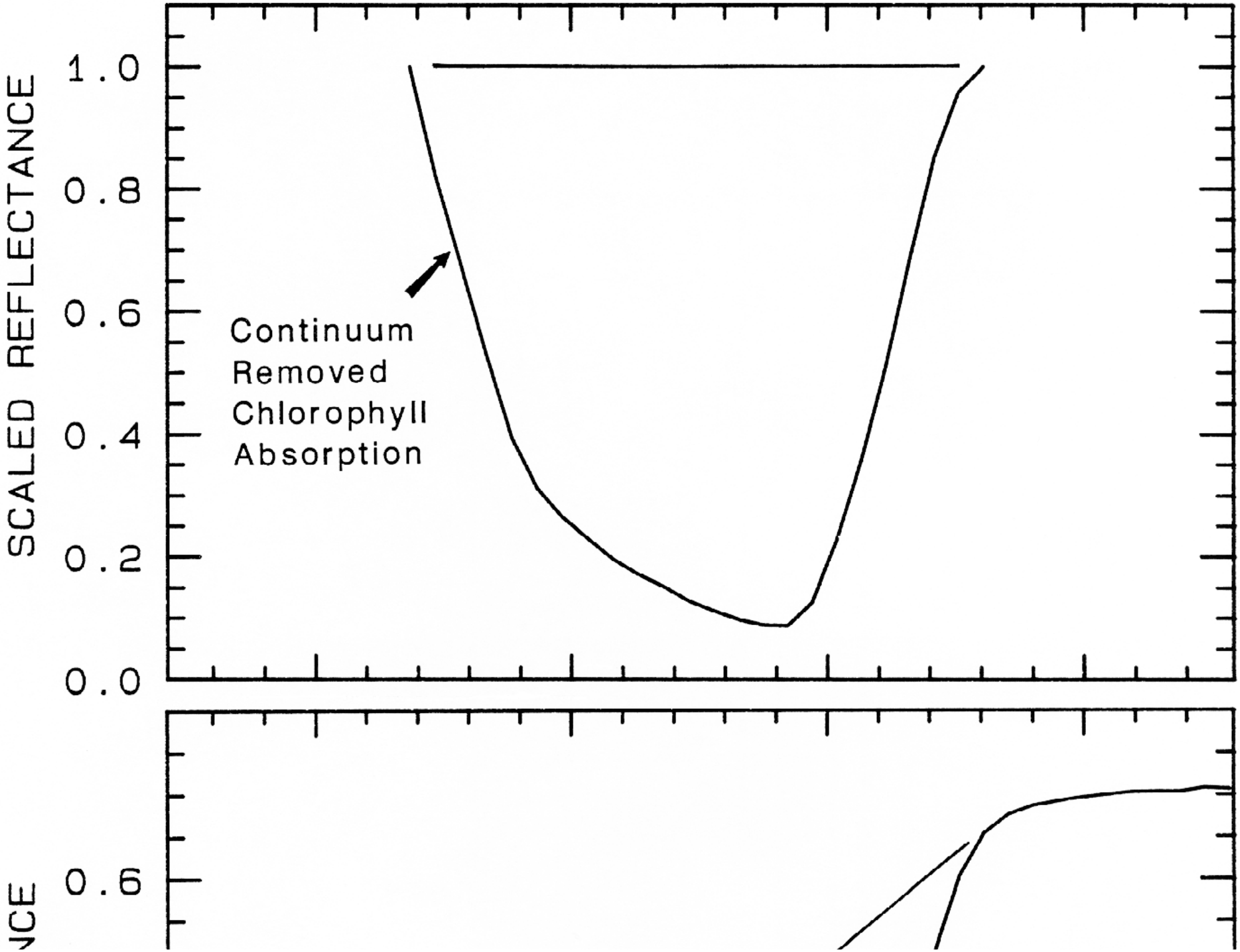
SCALED REFLECTANCE
1.0
0.8
0.6
0.4
0.2
0.0
Continuum
Removed
Chlorophyll
Absorption
0.6

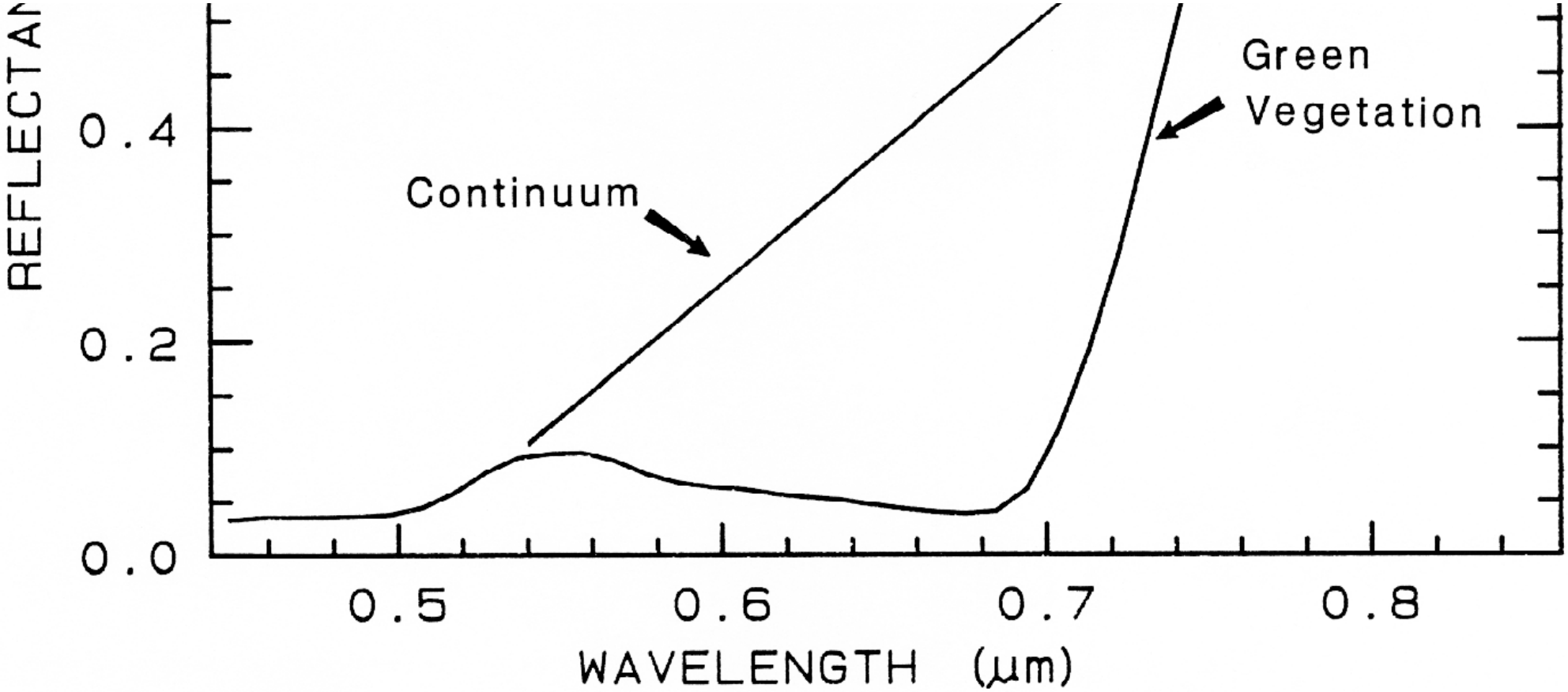
REFLECTAN
0.4
0.2
0.0
Continuum
Green
Vegetation
0.5
0.6
0.7
0.8
WAVELENGTH (μm)

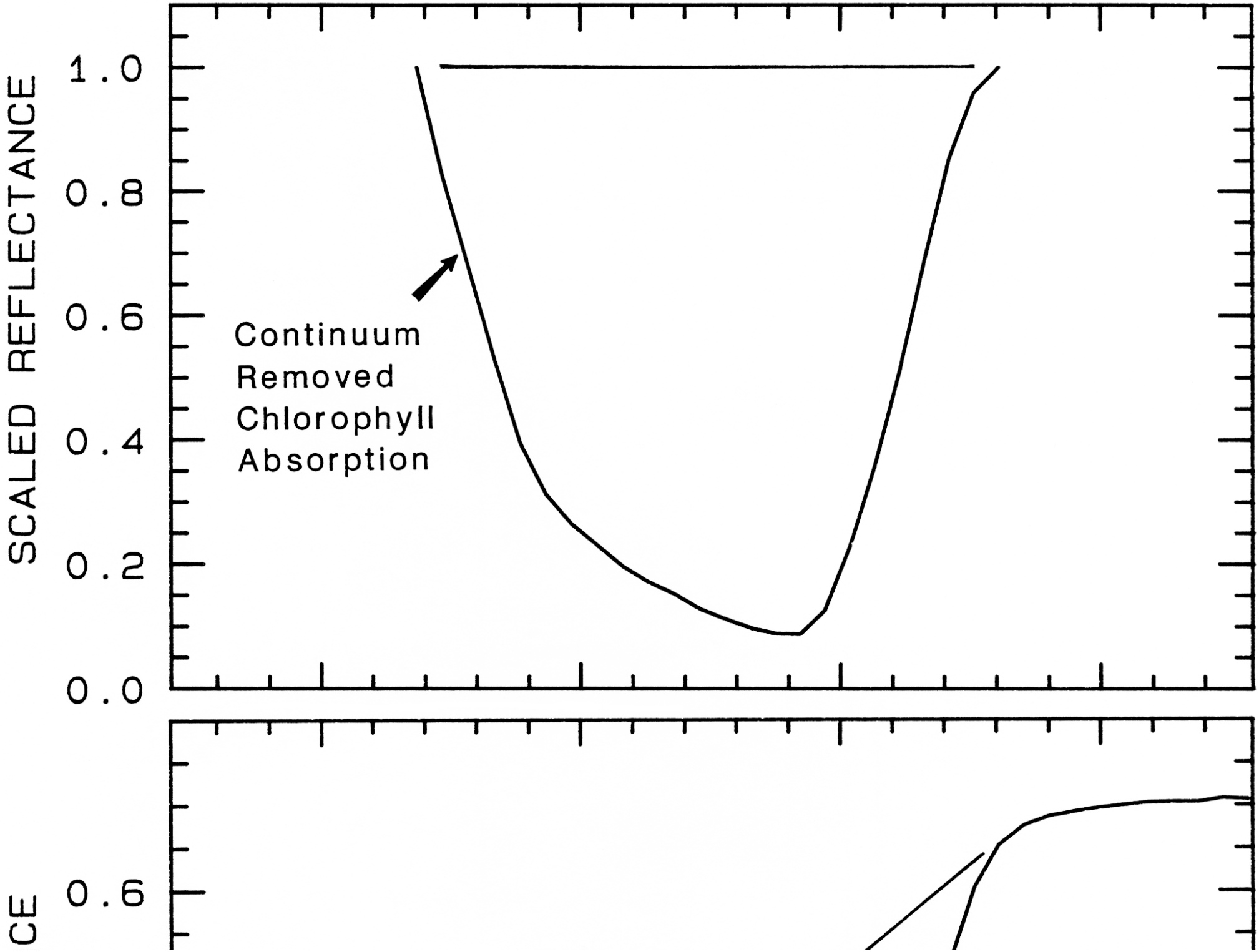
SCALED REFLECTANCE
1.0
0.8
0.6
0.4
0.2
0.0
Continuum
Removed
Chlorophyll
Absorption
0.6

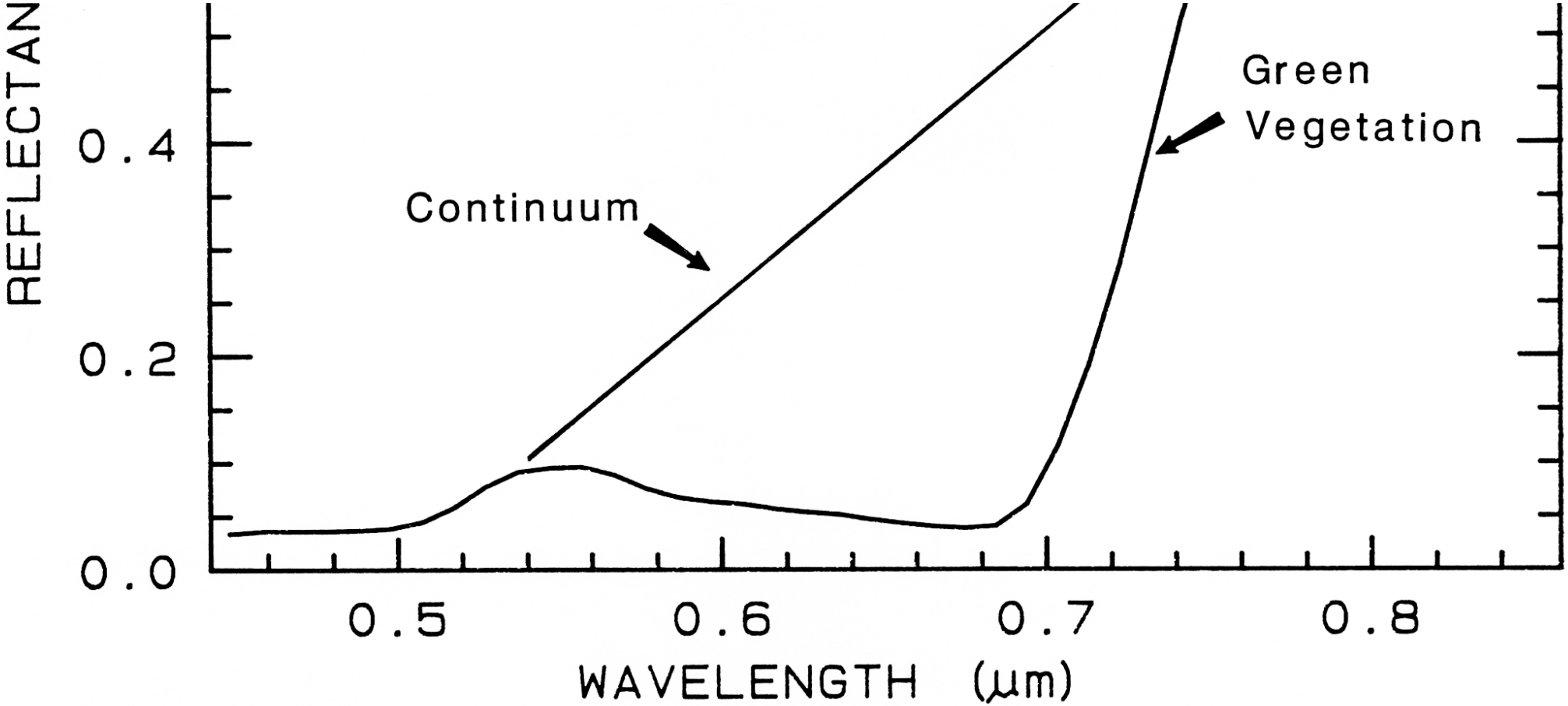
REFLECTAN
0.4
0.2
0.0
Continuum
Green
Vegetation
0.5
0.6
0.7
0.8
WAVELENGTH (μm)

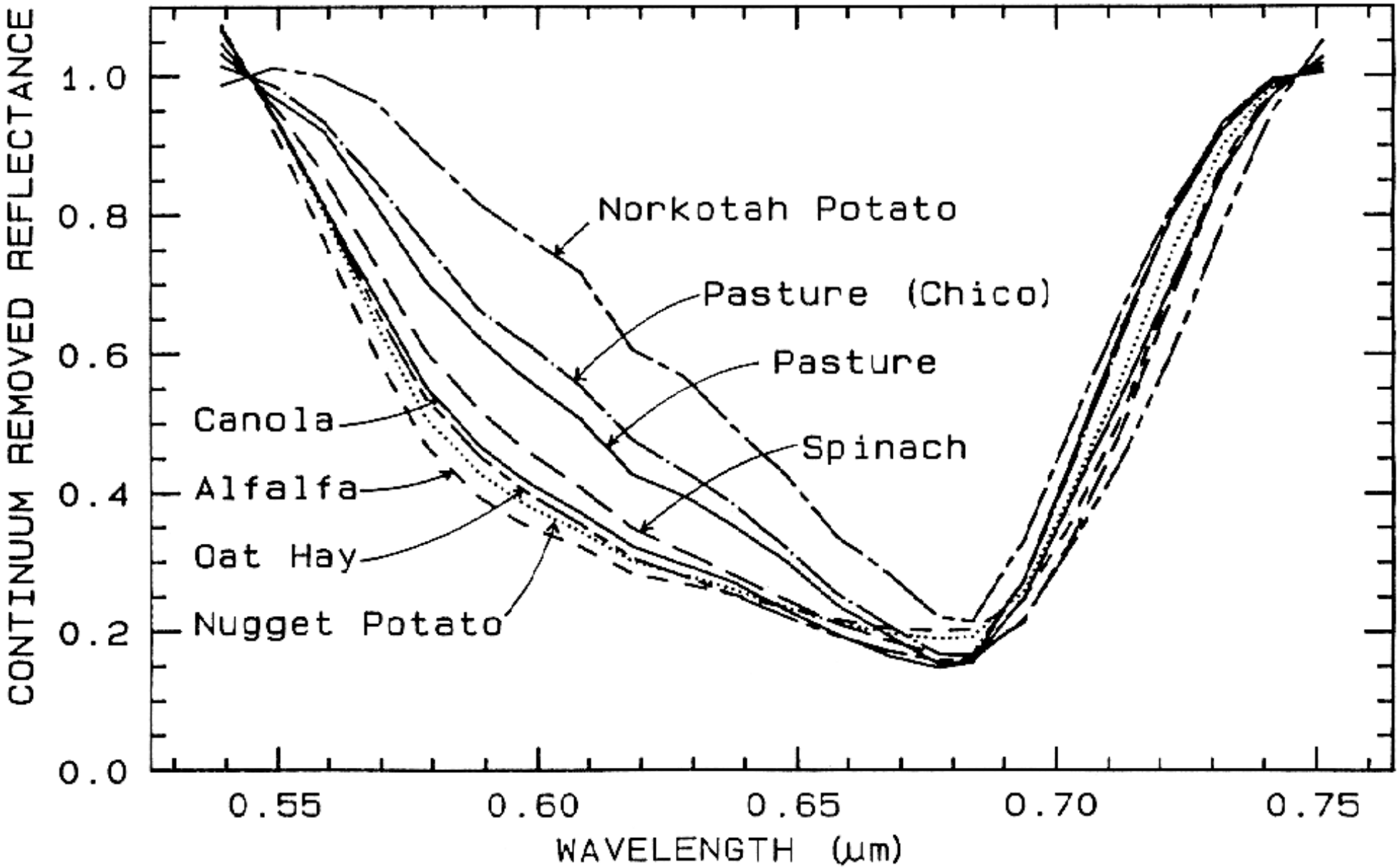
CONTINUUM REMOVED REFLECTANCE
1.0
0.8
0.6
0.4
0.2
0.0
0.55
0.60
0.65
0.70
0.75
WAVELENGTH (μm)
Norkotah Potato
Pasture (Chico)
Pasture
Spinach
Canola
Alfalfa
Oat Hay
Nugget Potato

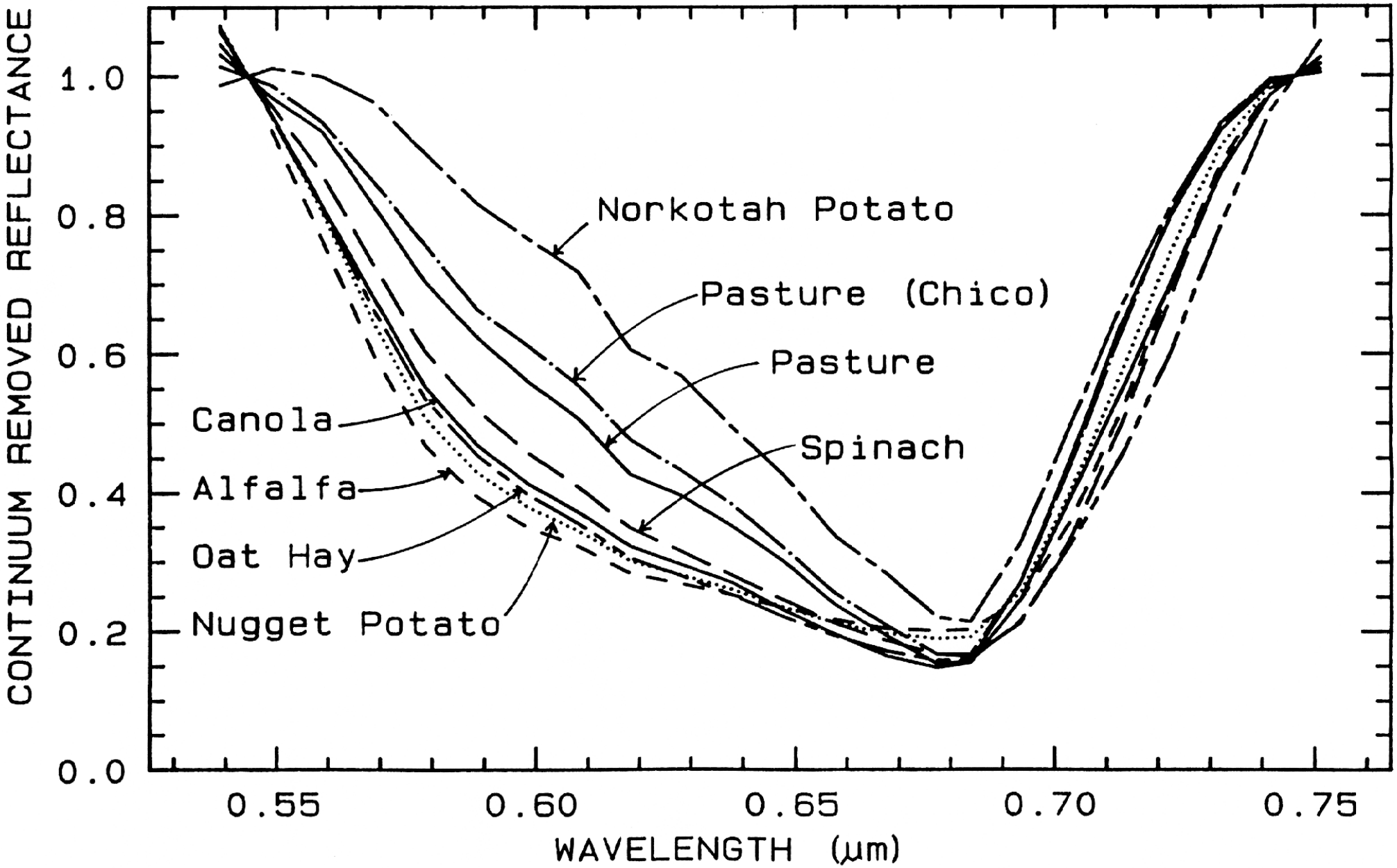
CONTINUUM REMOVED REFLECTANCE
1.0
0.8
0.6
0.4
0.2
0.0
0.55
0.60
0.65
0.70
0.75
WAVELENGTH (μm)
Norkotah Potato
Pasture (Chico)
Pasture
Spinach
Canola
Alfalfa
Oat Hay
Nugget Potato

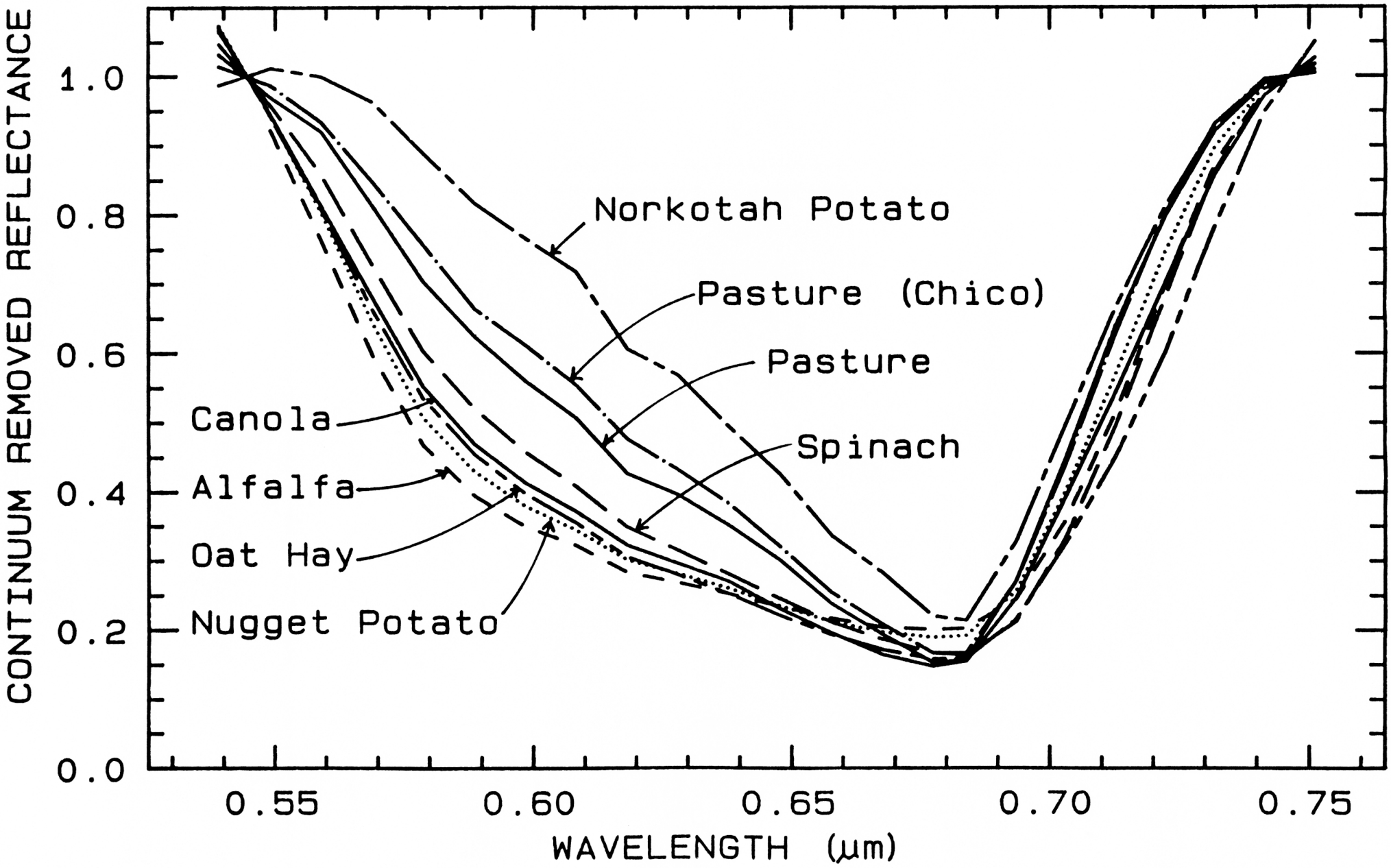
CONTINUUM REMOVED REFLECTANCE
1.0
0.8
0.6
0.4
0.2
0.0
0.55
0.60
0.65
0.70
0.75
WAVELENGTH (μm)
Norkotah Potato
Pasture (Chico)
Pasture
Spinach
Canola
Alfalfa
Oat Hay
Nugget Potato

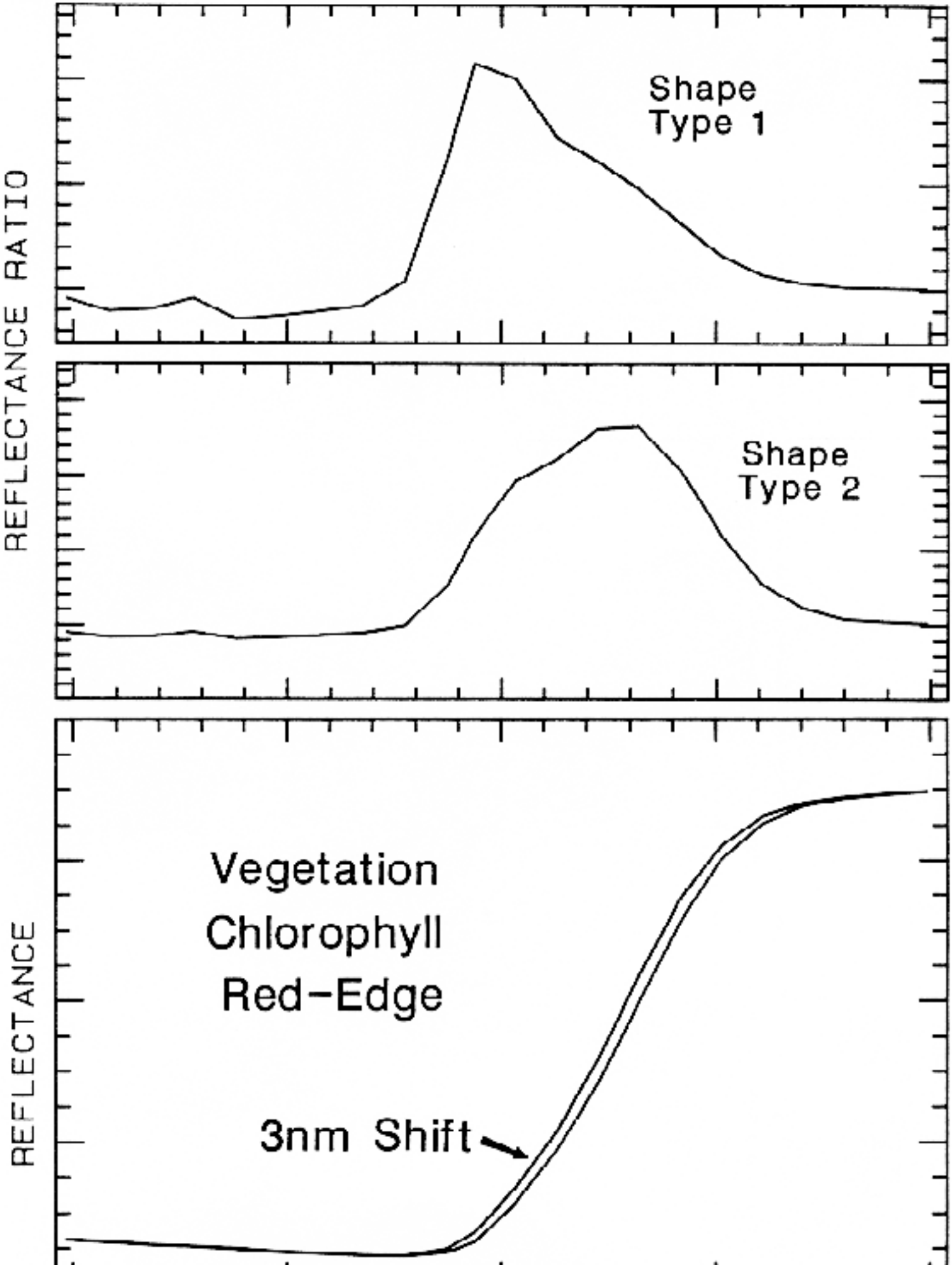
REFLECTANCE RATIO
Shape
Type 1
Shape
Type 2
REFLECTANCE
Vegetation
Chlorophyll
Red-Edge
3nm Shift

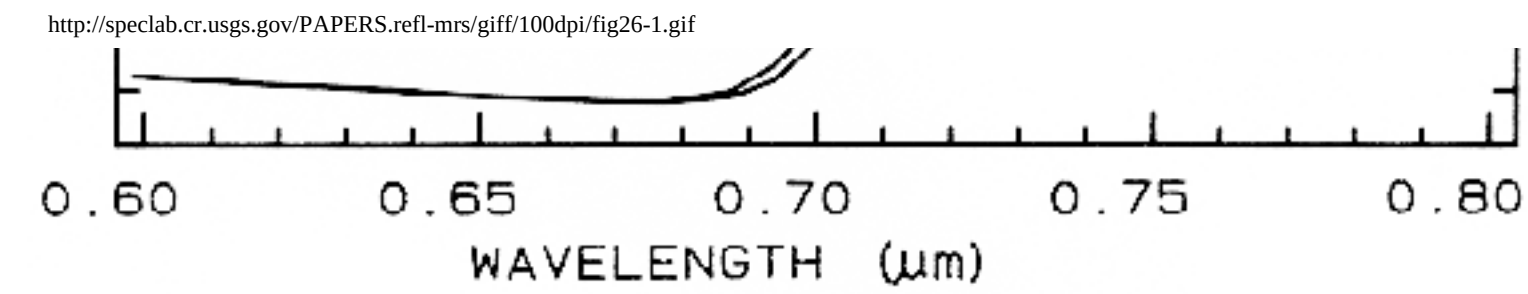
0.60
0.65
0.70
0.75
0.80
WAVELENGTH (μm)

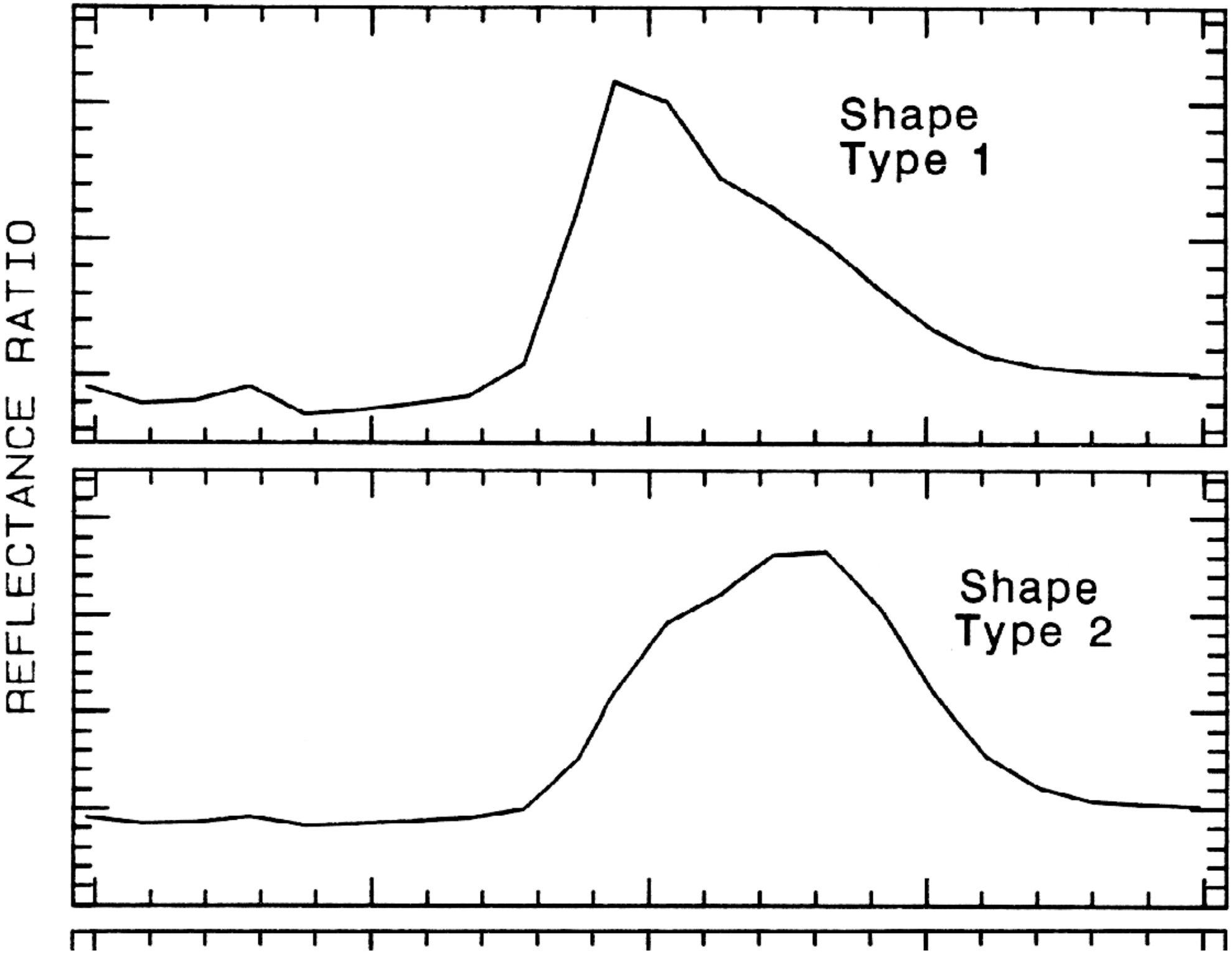
REFLECTANCE RATIO
Shape
Type 1
Shape
Type 2

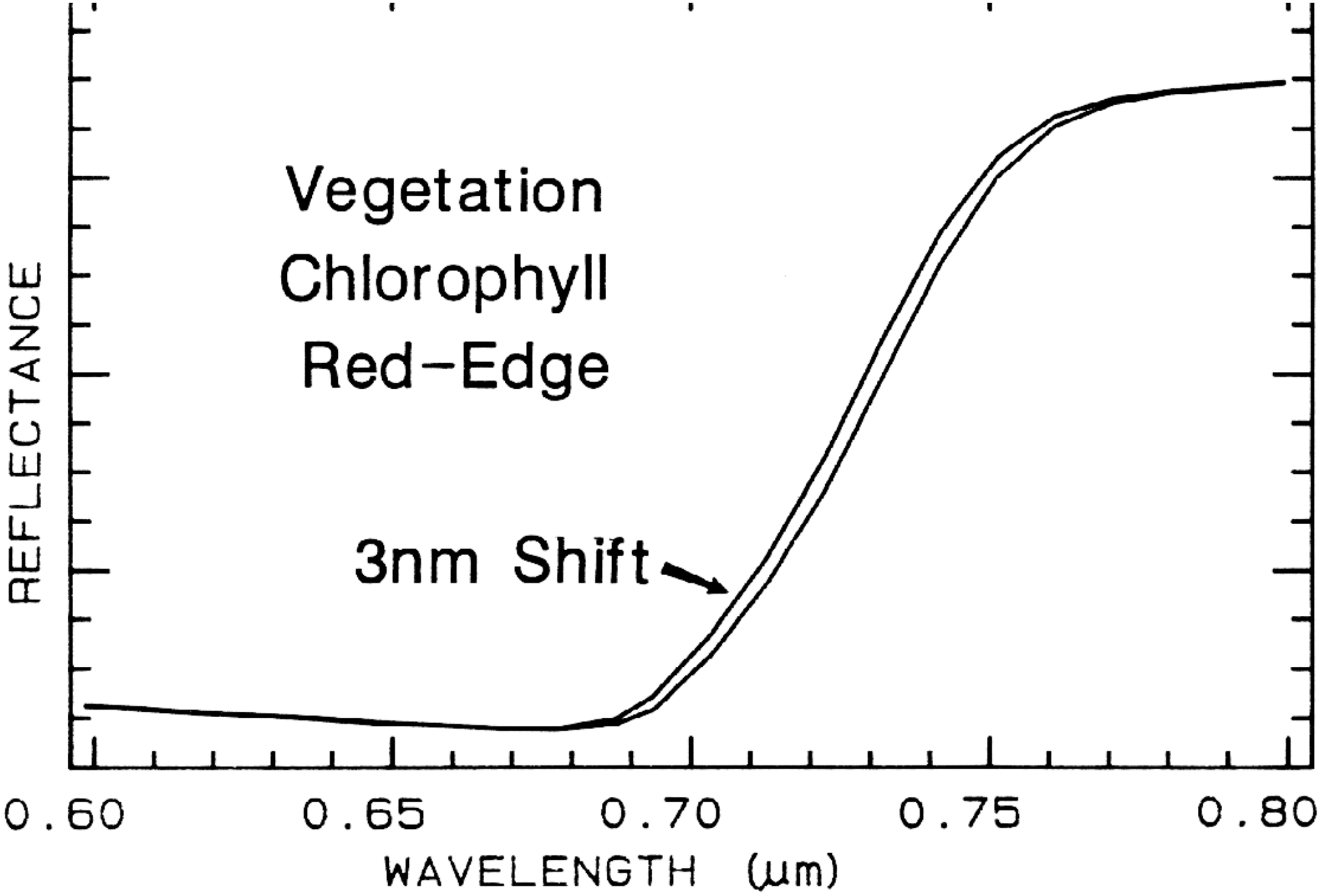
Vegetation
Chlorophyll
Red-Edge
3nm Shift
REFLECTANCE
0.60
0.65
0.70
0.75
0.80
WAVELENGTH (μm)

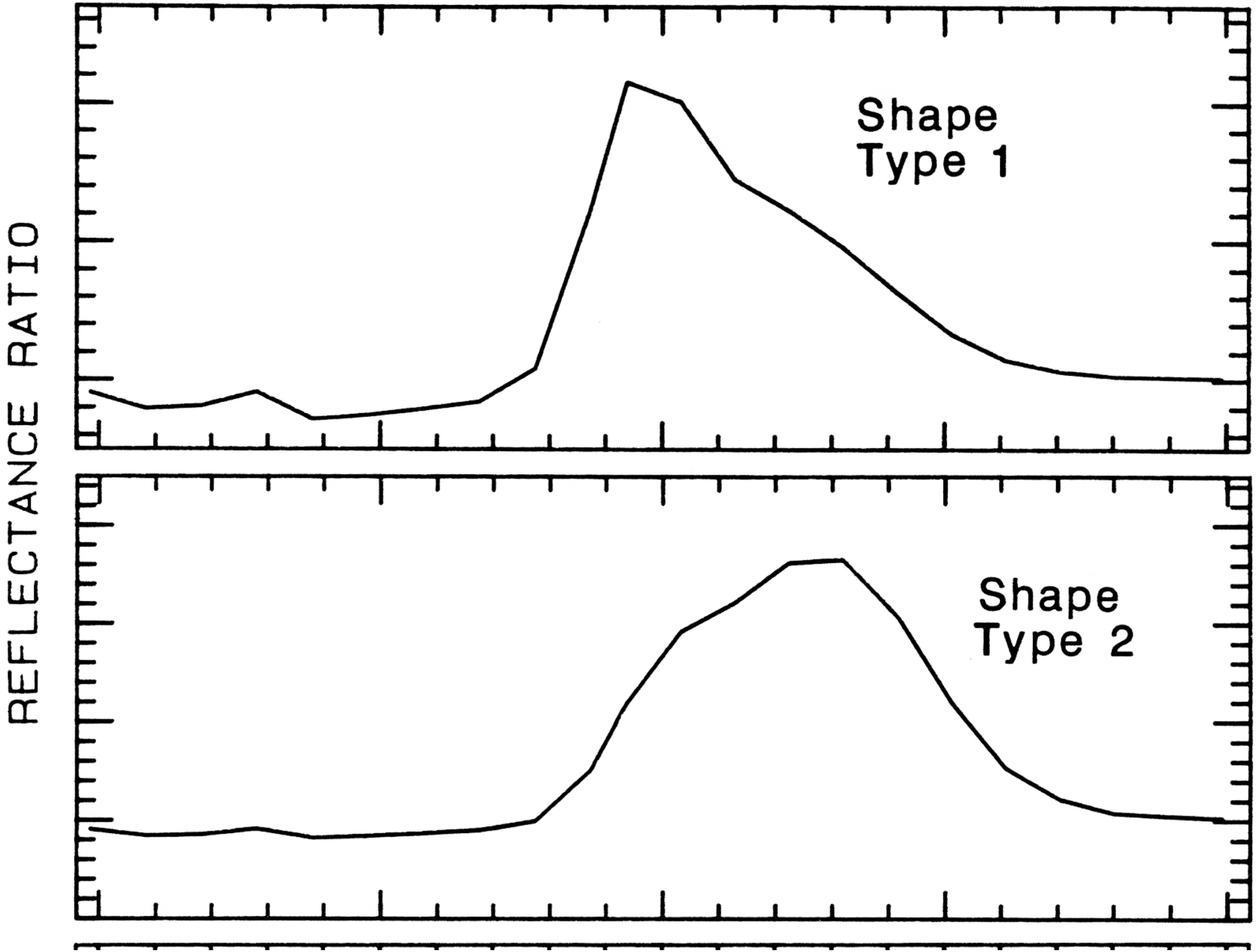
REFLECTANCE RATIO
Shape
Type 1
Shape
Type 2

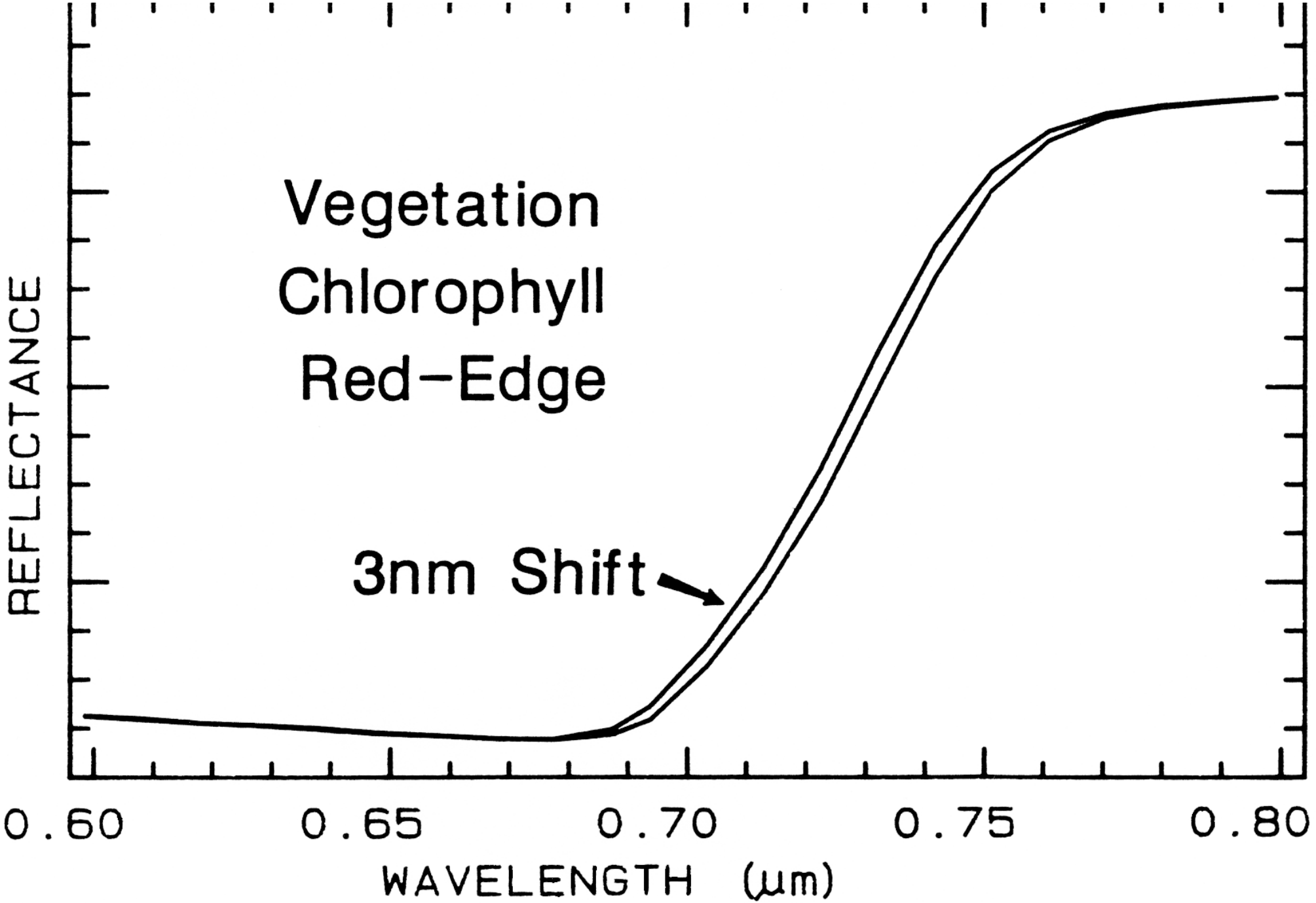
Vegetation
Chlorophyll
Red-Edge
3nm Shift
REFLECTANCE
0.60
0.65
0.70
0.75
0.80
WAVELENGTH (μm)

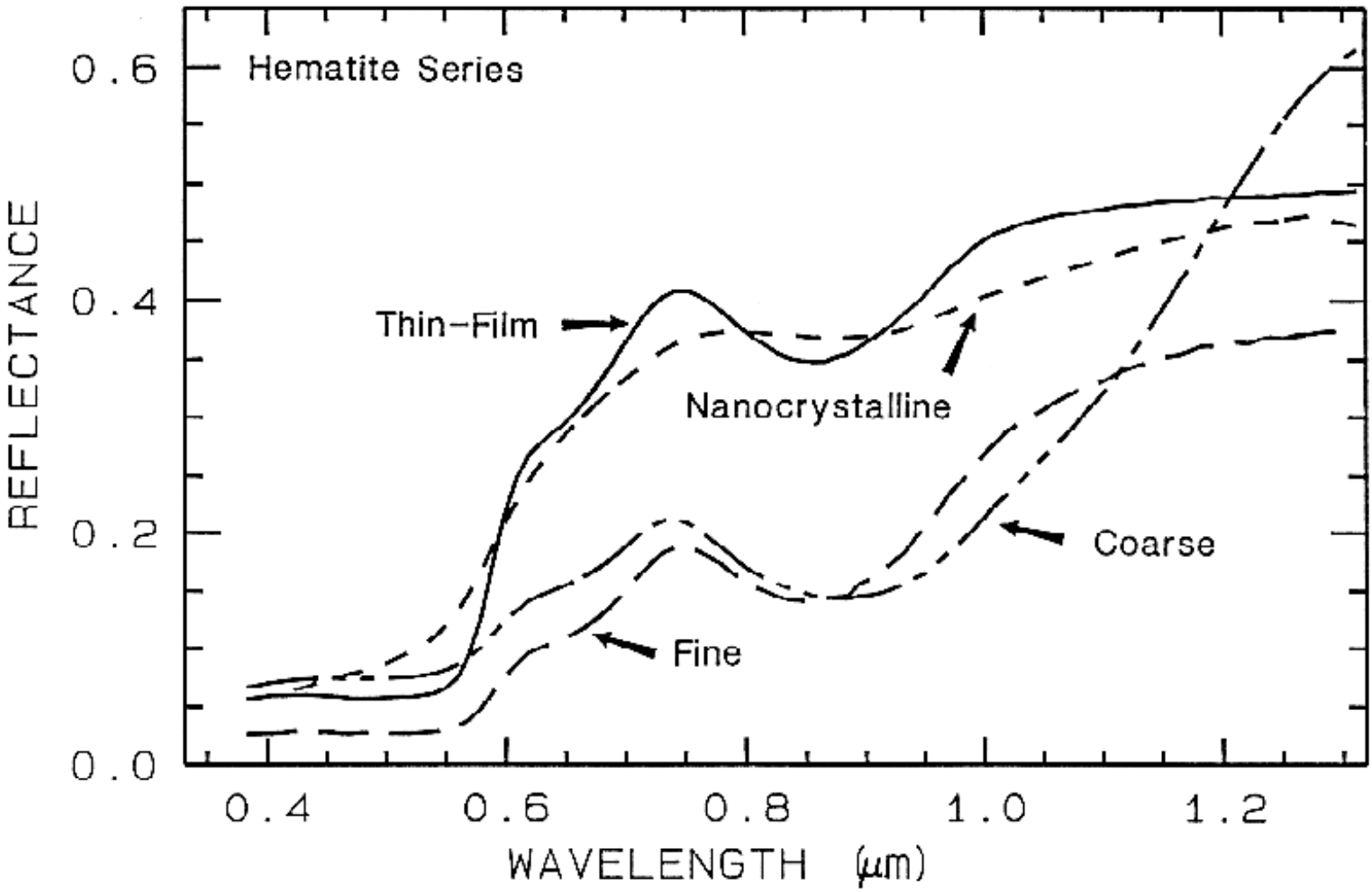
Hematite Series
Thin-Film
Nanocrystalline
Coarse
Fine
REFLECTANCE
0.0
0.2
0.4
0.6
0.4
0.6
0.8
1.0
1.2
WAVELENGTH (μm)

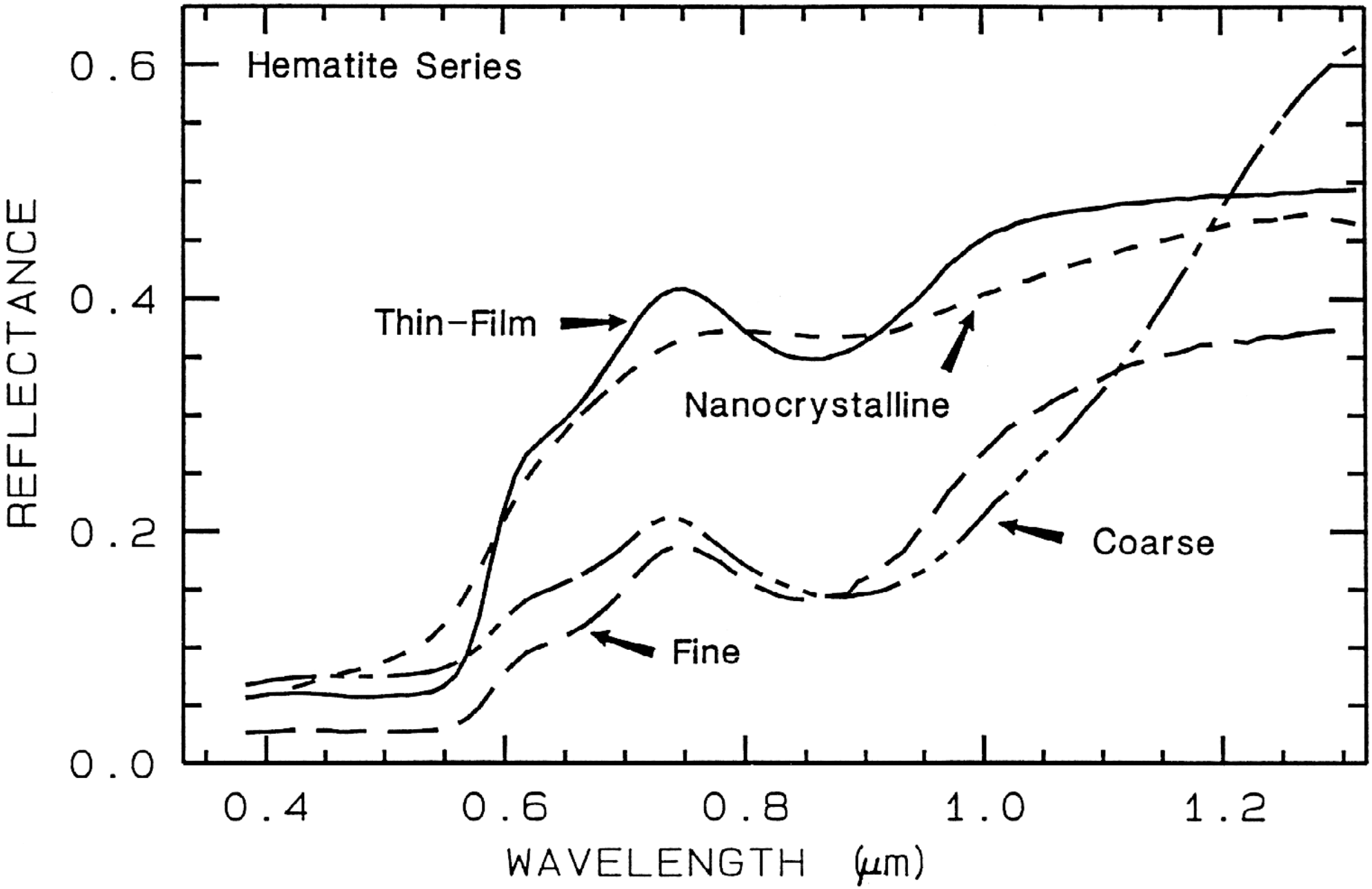
Hematite Series
REFLECTANCE
0.0
0.2
0.4
0.6
0.4
0.6
0.8
1.0
1.2
WAVELENGTH (μm)
Thin-Film
Nanocrystalline
Coarse
Fine

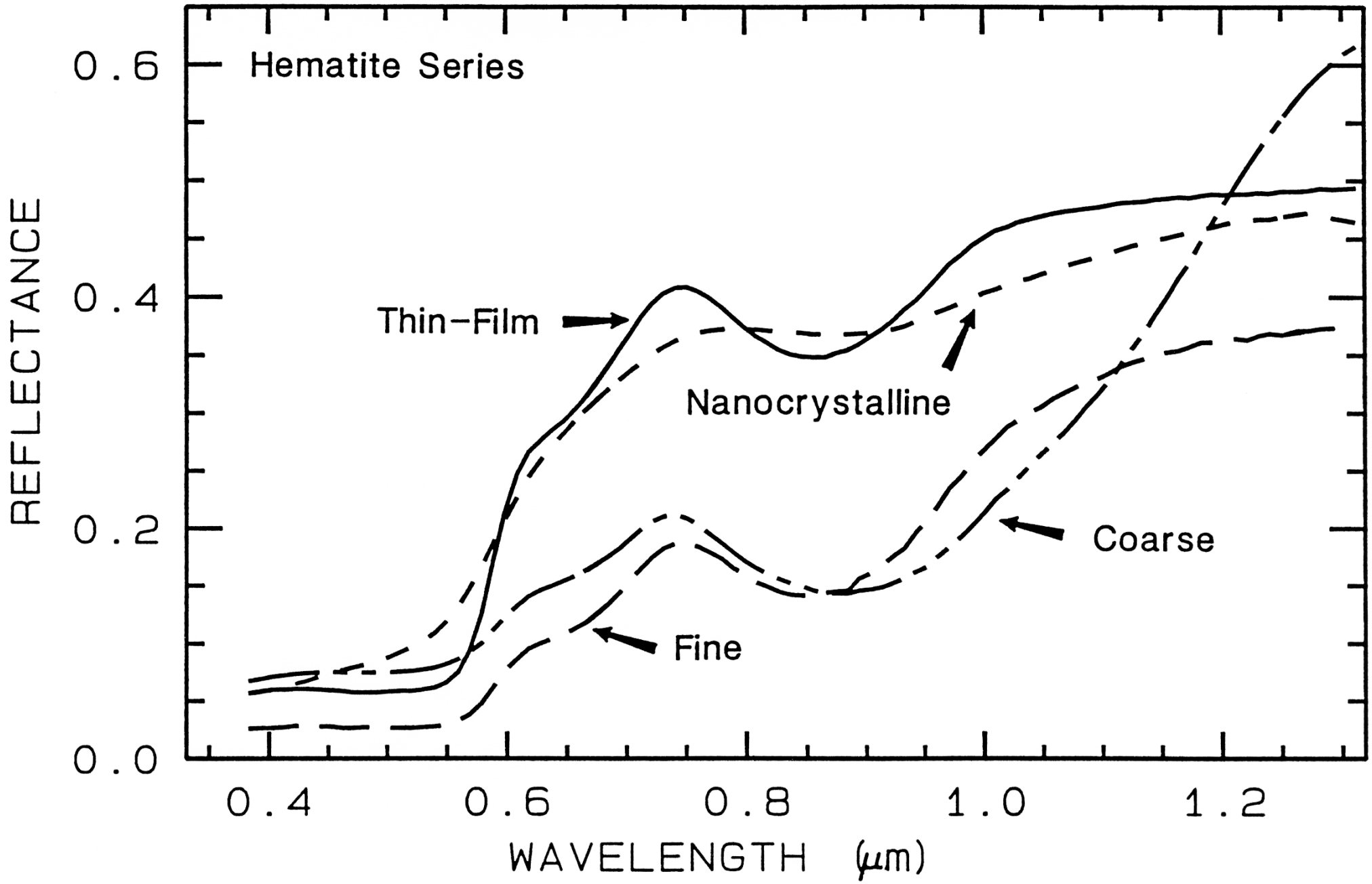
Hematite Series
Thin-Film
Nanocrystalline
Coarse
Fine
REFLECTANCE
0.0
0.2
0.4
0.6
0.4
0.6
0.8
1.0
1.2
WAVELENGTH (μm)

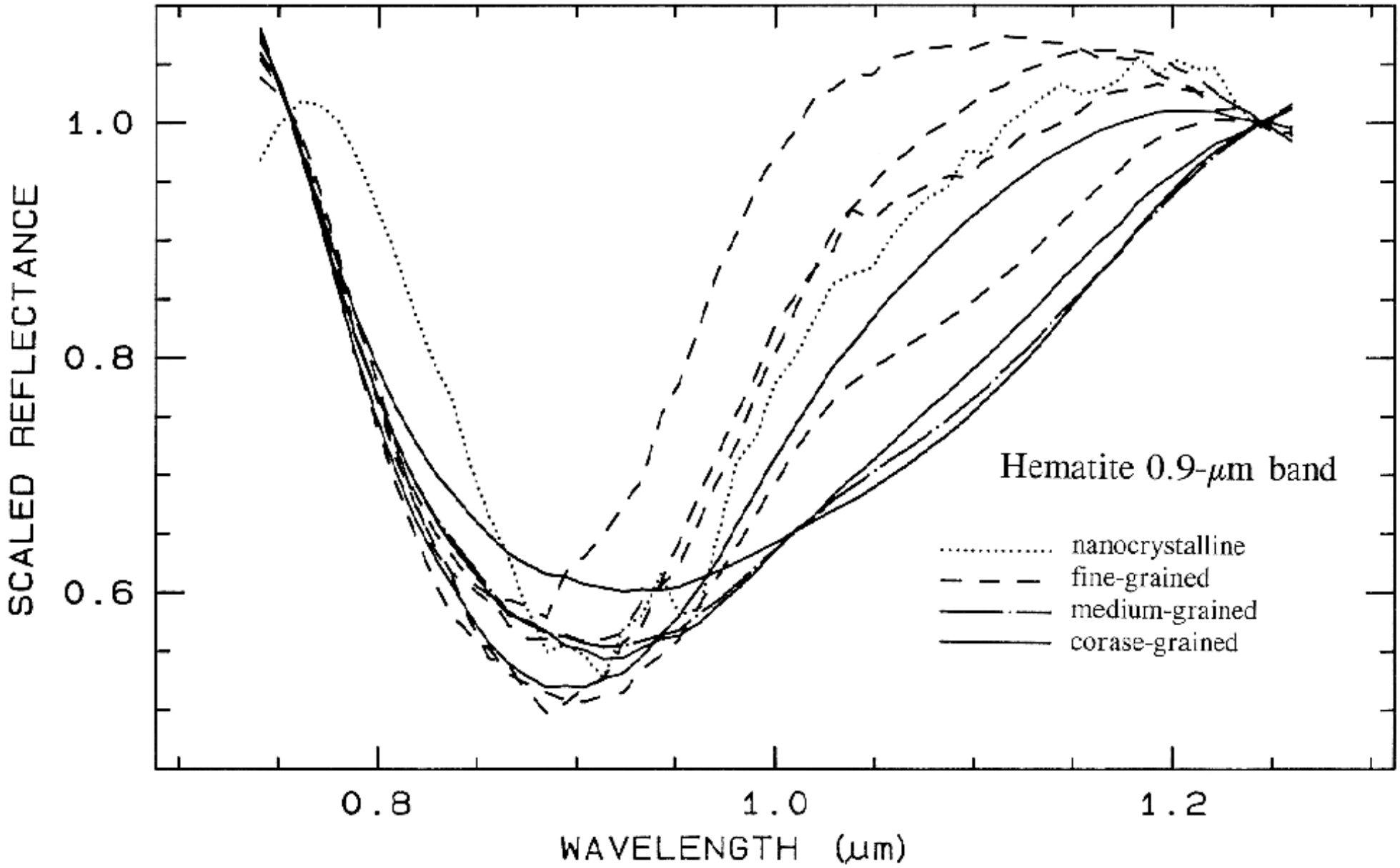
SCALED REFLECTANCE
1.0
0.8
0.6
0.8
1.0
1.2
WAVELENGTH (μm)
Hematite 0.9-μm band
nanocrystalline
fine-grained
medium-grained
corase-grained

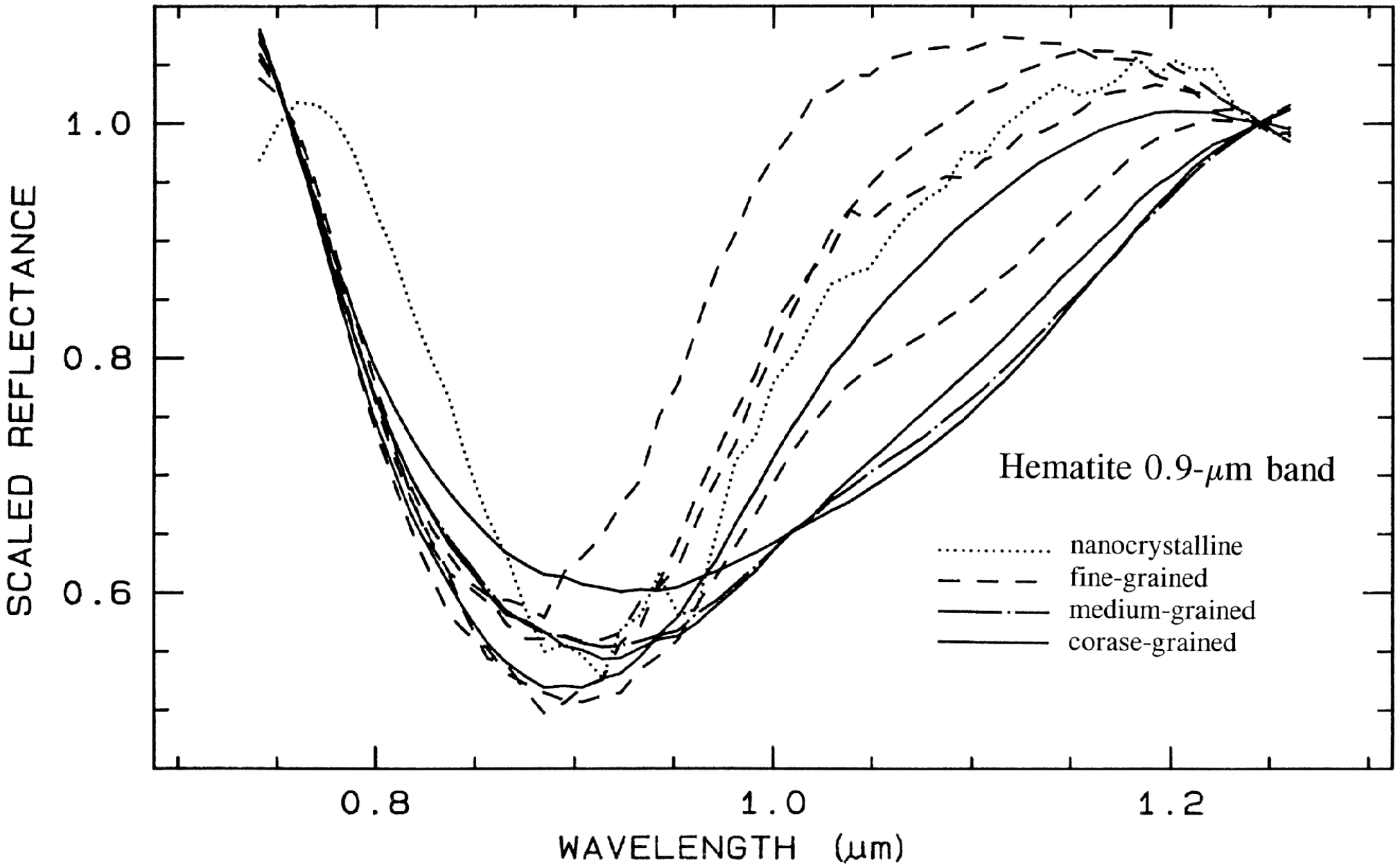
SCALED REFLECTANCE
1.0
0.8
0.6
0.8
1.0
1.2
WAVELENGTH (μm)
Hematite 0.9-μm band
nanocrystalline
fine-grained
medium-grained
corase-grained

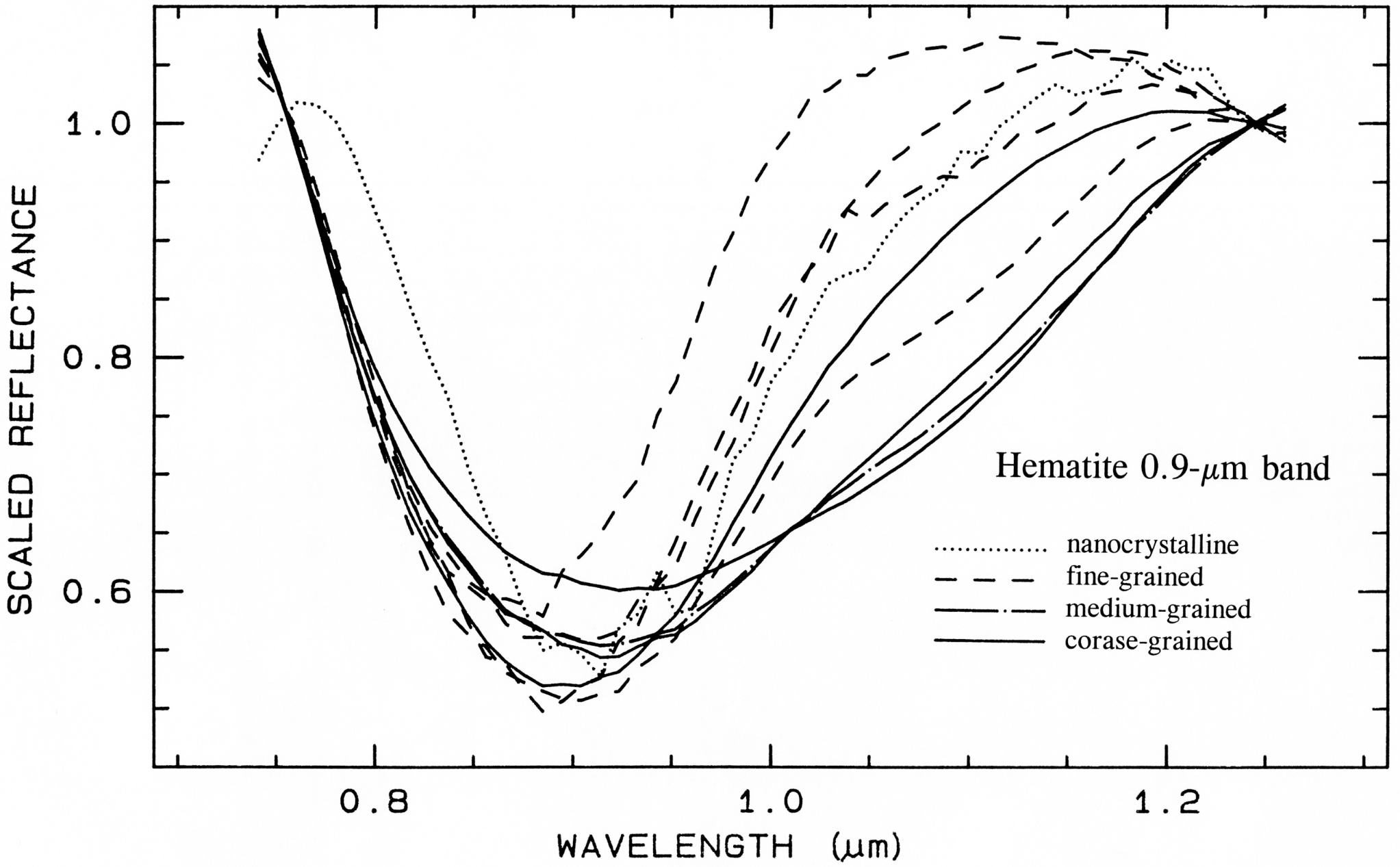
SCALED REFLECTANCE
1.0
0.8
0.6
0.8
1.0
1.2
WAVELENGTH (μm)
Hematite 0.9-μm band
nanocrystalline
fine-grained
medium-grained
corase-grained

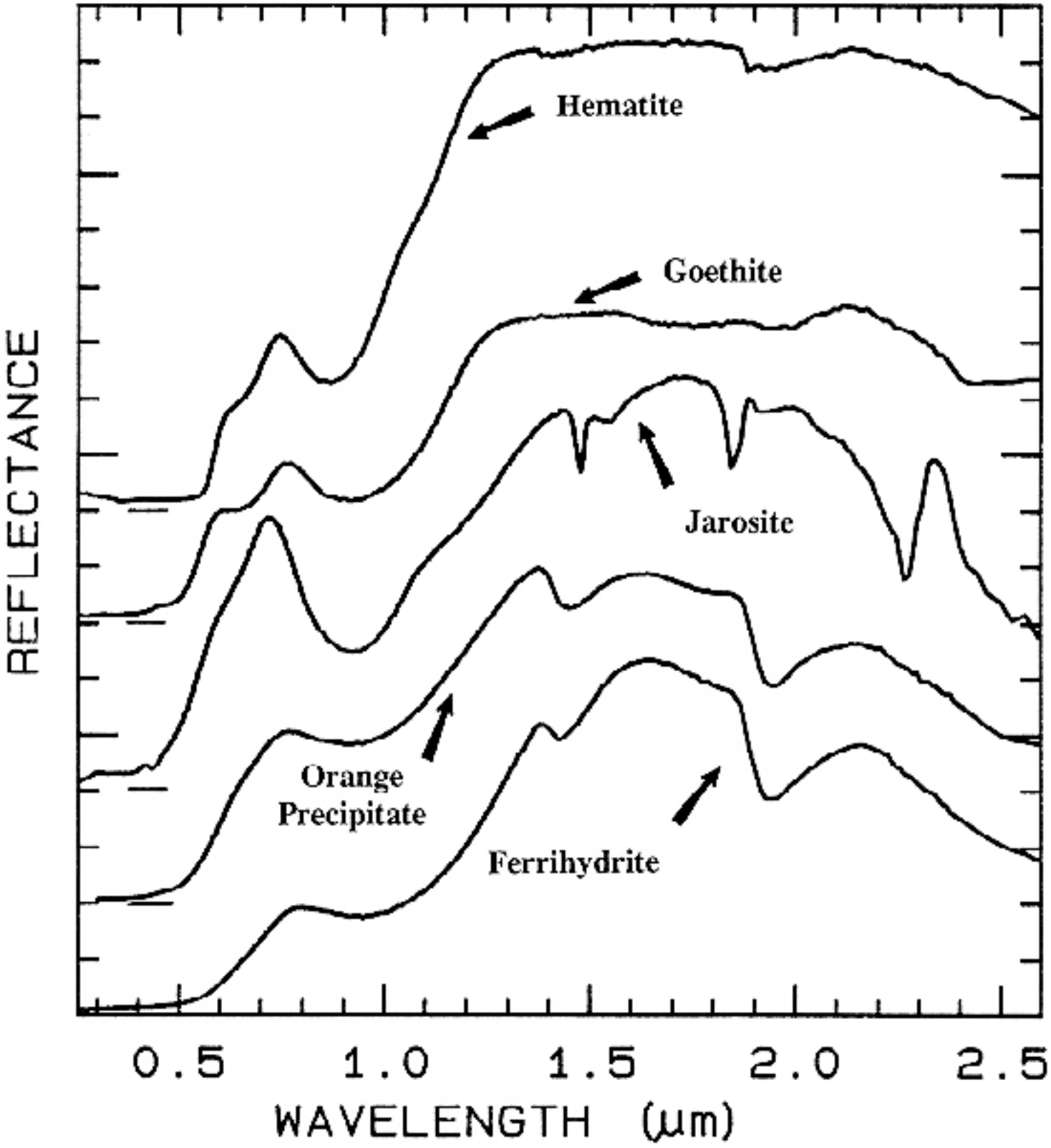
Hematite
Goethite
Jarosite
Orange
Precipitate
Ferrihydrite
REFLECTANCE
0.5
1.0
1.5
2.0
2.5
WAVELENGTH (μm)

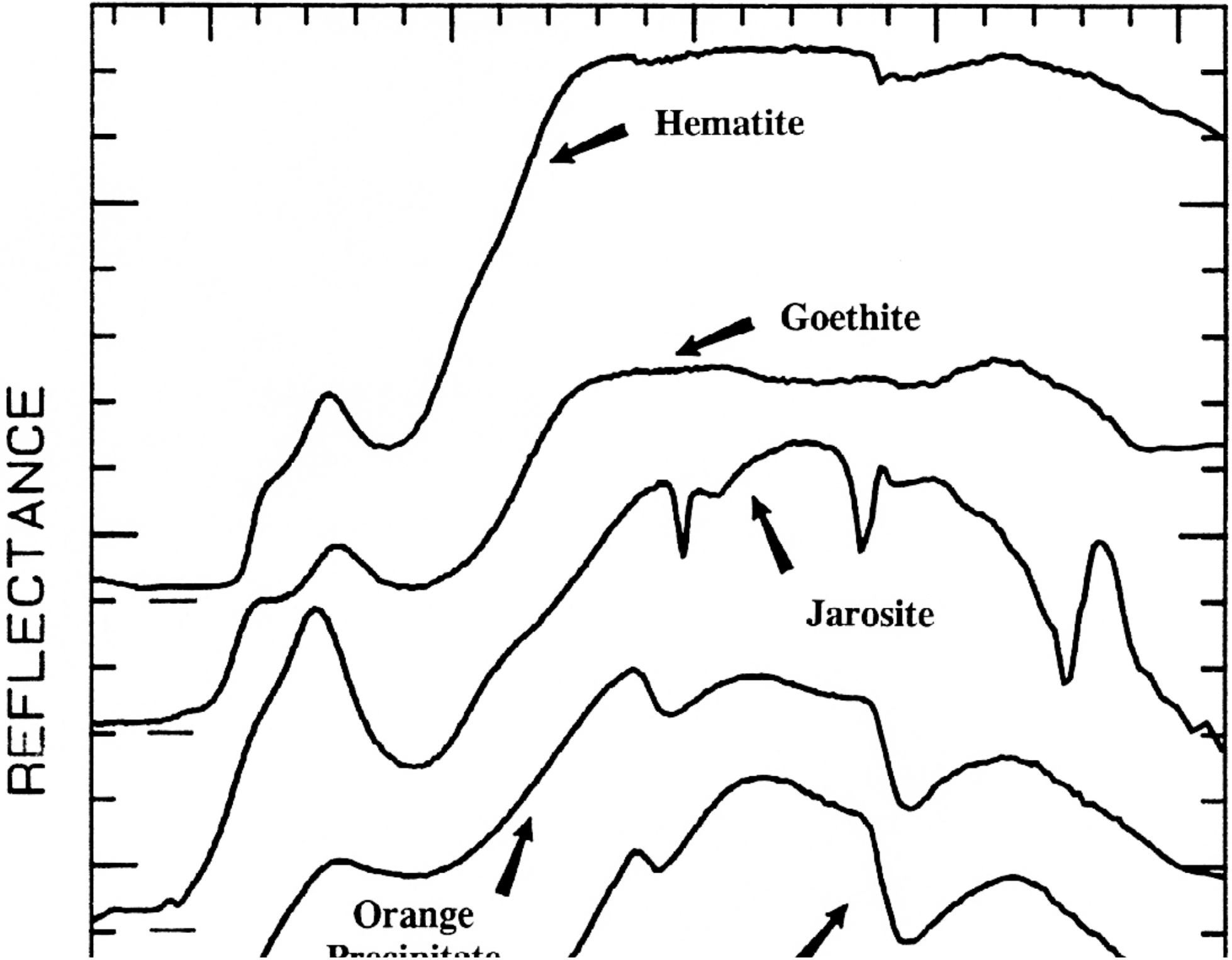
Hematite
Goethite
Jarosite
Orange
REFLECTANCE

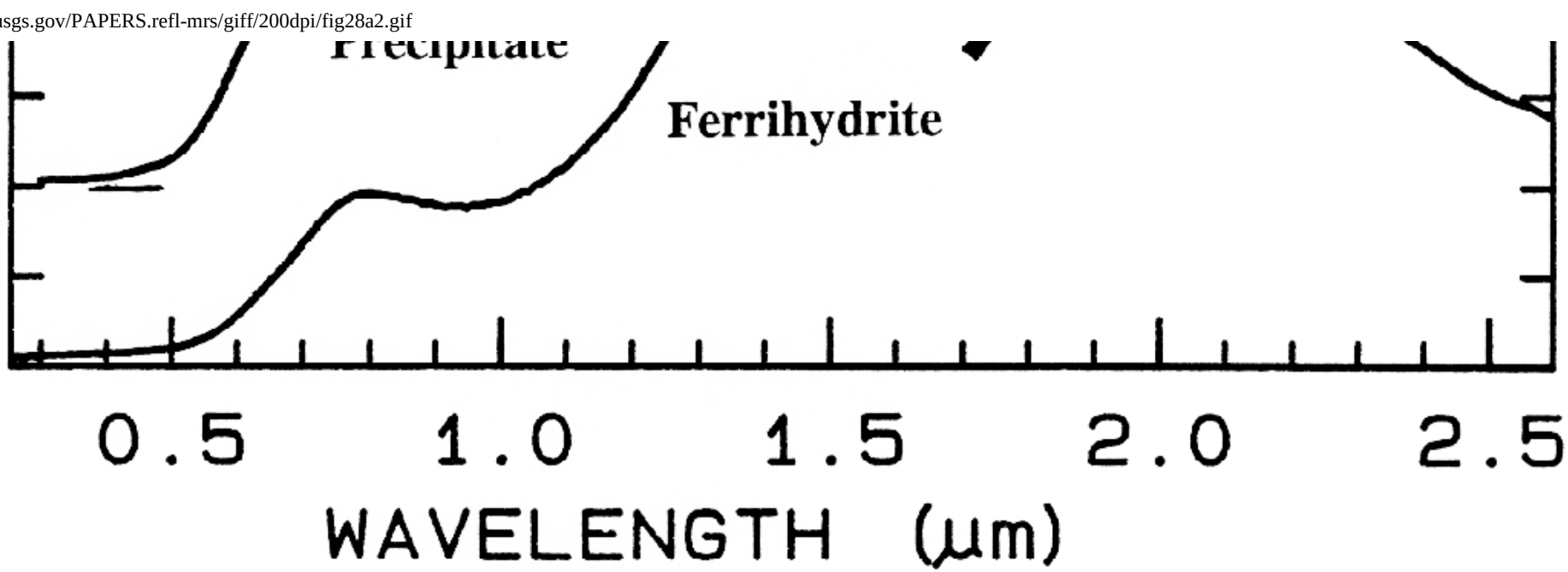
Precipitate
Ferrihydrite
0.5
1.0
1.5
2.0
2.5
WAVELENGTH (μm)

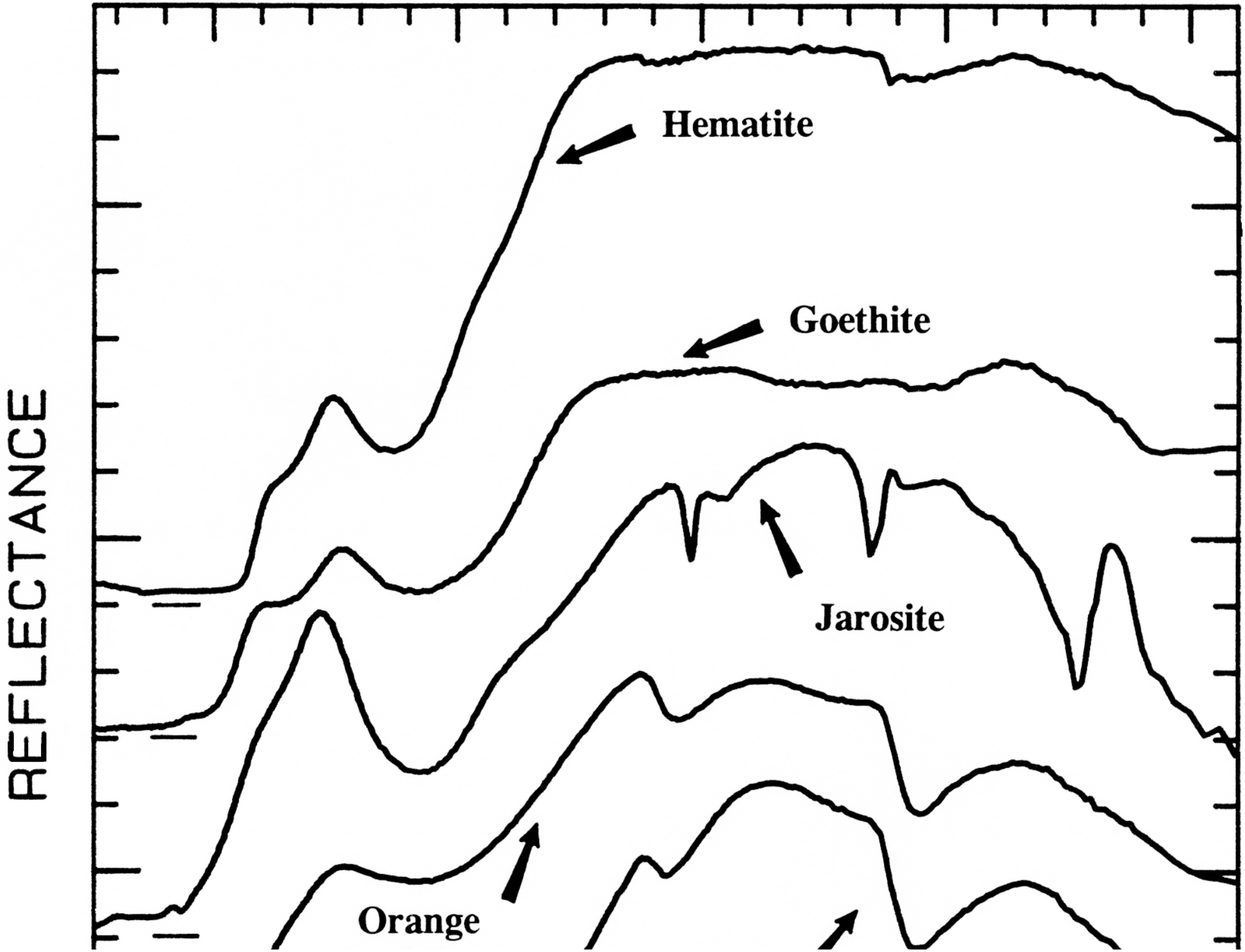
Hematite
Goethite
Jarosite
Orange
REFLECTANCE

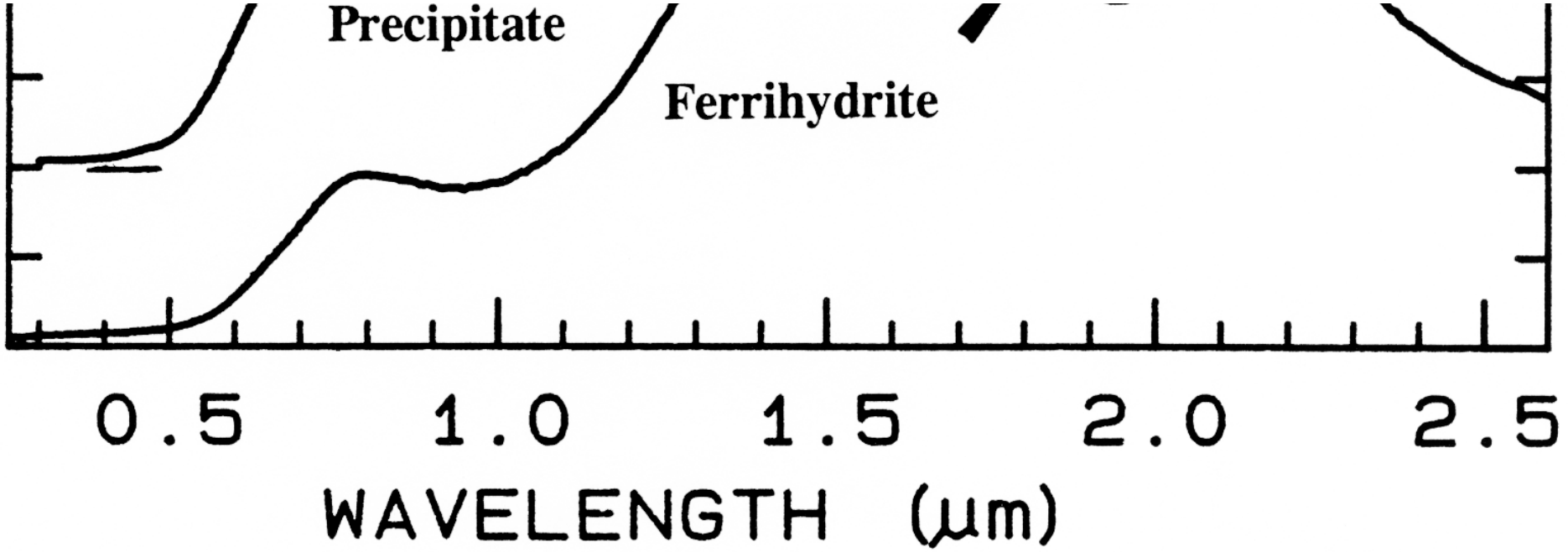
Precipitate
Ferrihydrite
0.5
1.0
1.5
2.0
2.5
WAVELENGTH (μm)

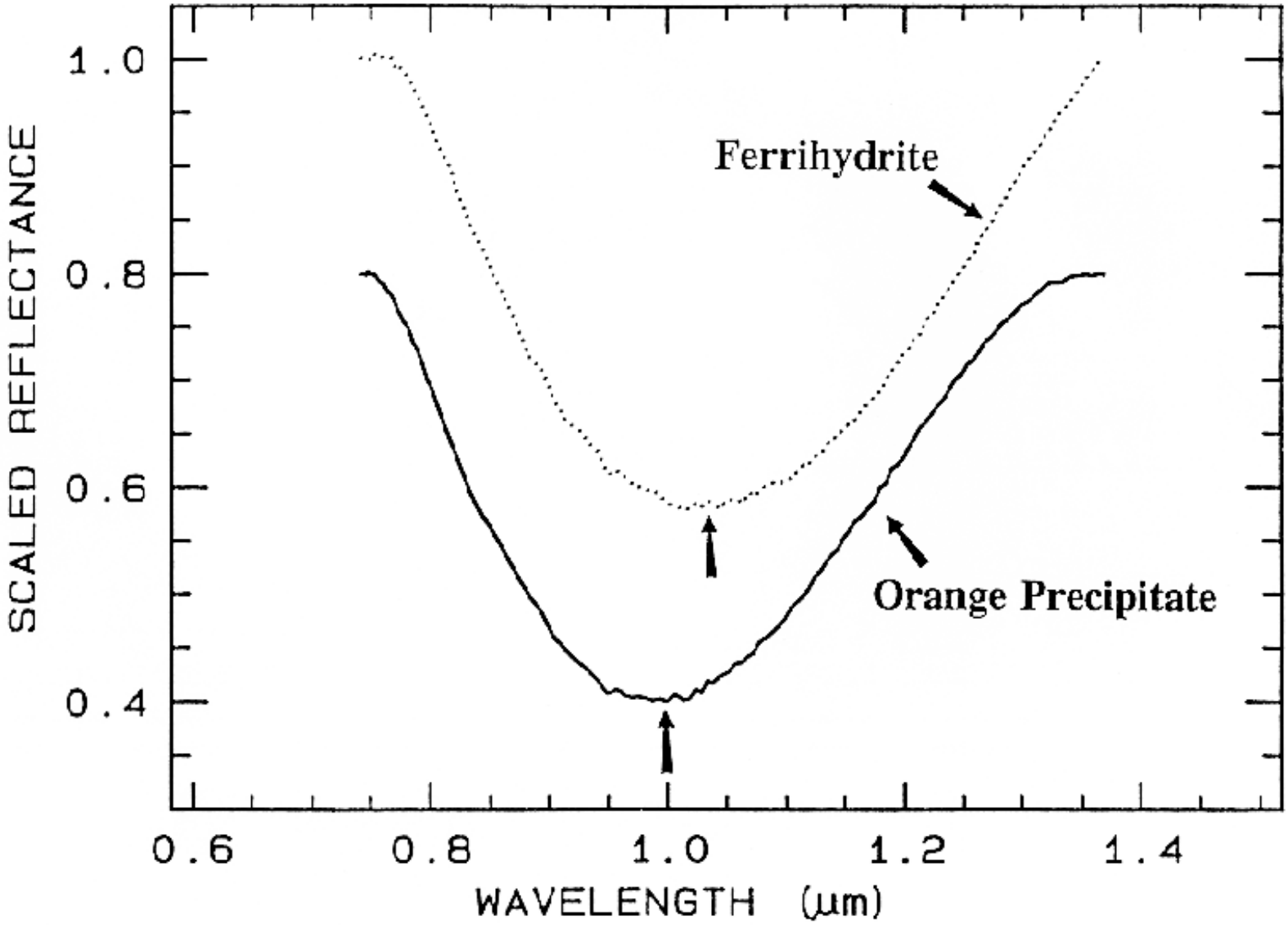
1.0
0.8
0.6
0.4
SCALED REFLECTANCE
Ferrihydrite
Orange Precipitate
0.6
0.8
1.0
1.2
1.4
WAVELENGTH (μm)

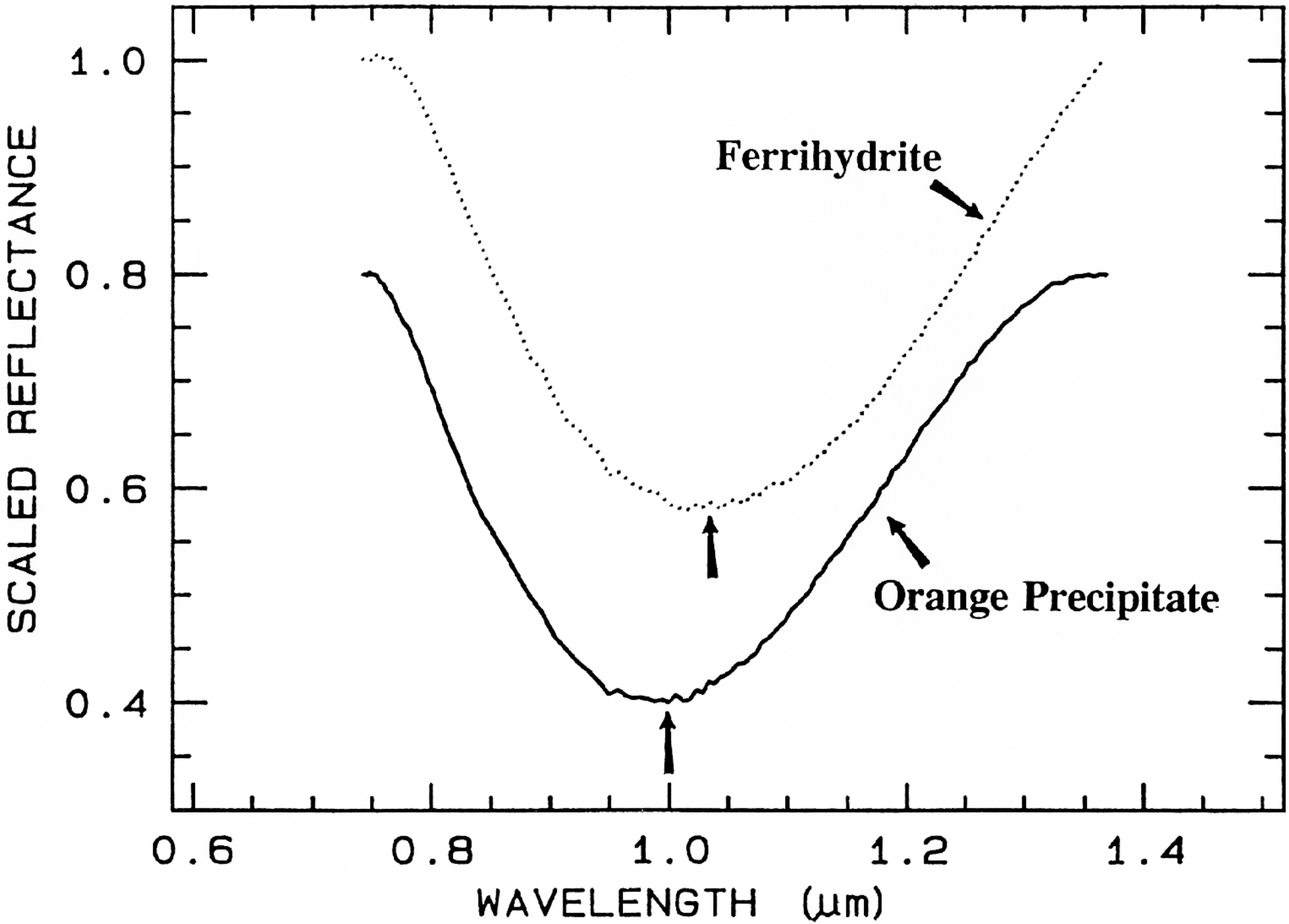
1.0
0.8
0.6
0.4
SCALED REFLECTANCE
Ferrihydrite
Orange Precipitate
0.6
0.8
1.0
1.2
1.4
WAVELENGTH (μm)

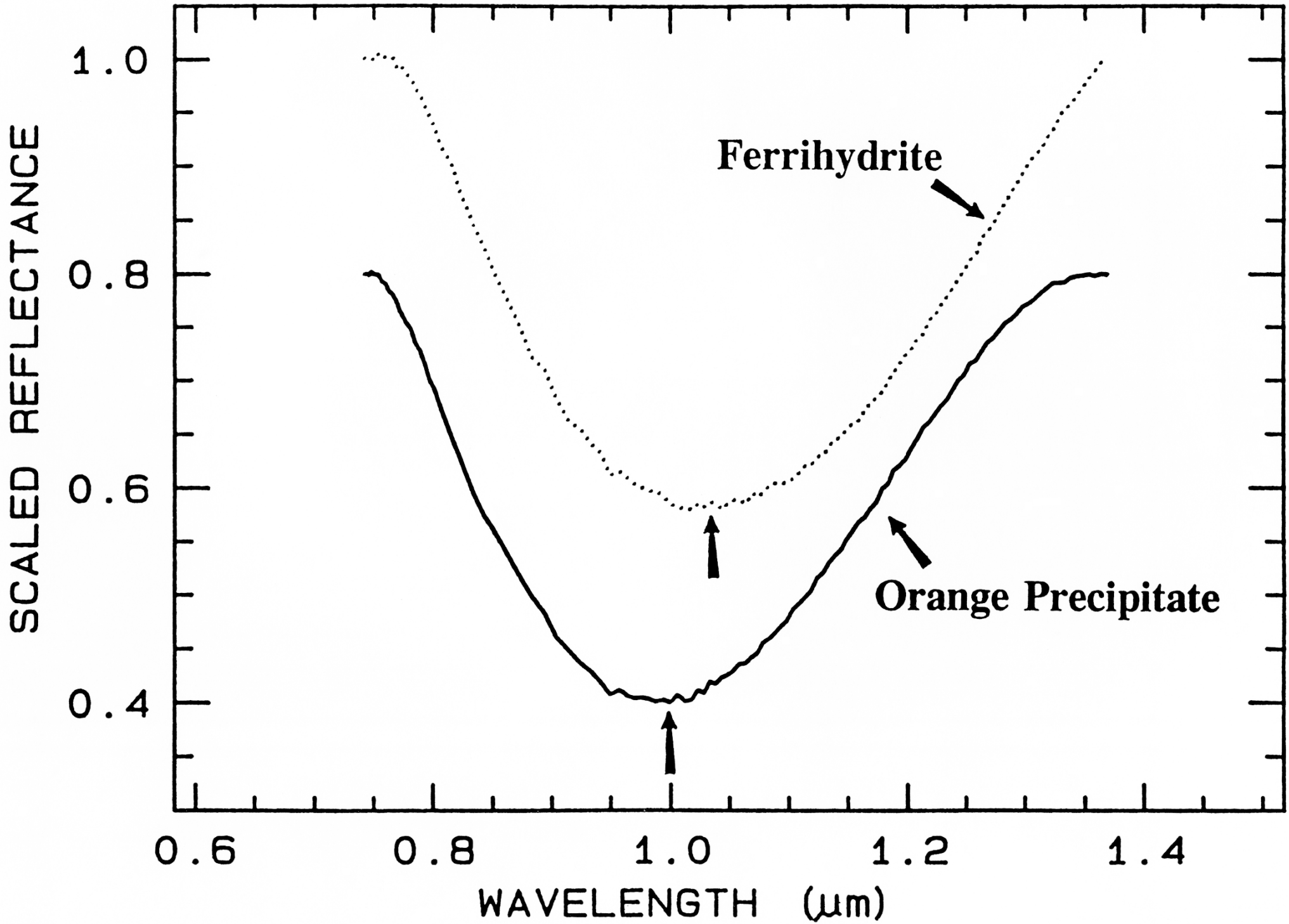
1.0
0.8
0.6
0.4
SCALED REFLECTANCE
Ferrihydrite
Orange Precipitate
0.6
0.8
1.0
1.2
1.4
WAVELENGTH (μm)